UNIVERSITY OF
NEWCASTLE UPON TYNE

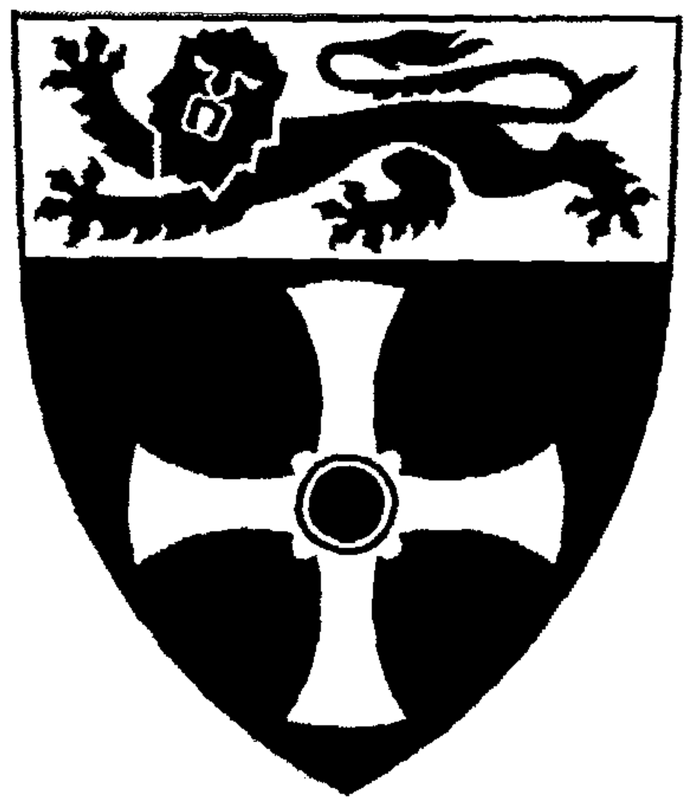

DEPARTMENT OF CHEMISTRY

"New Insights Into Micellar Structural Evolution And Interaction Using Voltammetric Methods"

Ian David Charlton BSc. G.R.S.C.

Ph.D. Thesis

June 1999

Abstract :

The development of electrochemical techniques as applied to self-assembled supramolecular systems (e.g. micelles) has advanced over the past decade. The main properties that have been elucidated by these techniques have been micellar self-diffusion and size. Although there are reports that have paid attention to the qualitative influence of intermicellar interactions on the behaviour of the micellar system, quantitative assessments of interaction are very limited. In this thesis, the application of rotating disk voltammetry, primarily, has led to a quantitative rationalisation of intermicellar interactions in cationic and nonionic micellar systems over a range of surfactant and electrolyte concentrations.

Two 'normal' micellar systems are studied with aggregates formed from cationic (CTAC) and nonionic (Triton X-100) surfactants. Initial measurements and analysis yields micellar sizes that are consistent with published values, demonstrating the validity and the ease of application of electrochemical techniques. Measuring self-diffusion coefficients over a range of electrolytes provides a comprehensive assessment of micellar phase behaviour and yields further structural parameters which are conventionally determined using a variety of methods.
The first reported study of electrochemistry in a reverse micelle 'nanoemulsion' is presented. The growth in micellar size on the addition of a solubilised probe gives important inferences for the careful control of particle growth in a reverse micelle 'nano-reactor'.

In summary, the thesis, as the title states, gives new insights pertaining to micellar structural evolution and interaction. The thesis will examine the benefits of applying electrochemical techniques to study micellar systems and concentrate, predominately, on the wealth of information that can be obtained by the resultant analysis. The work forms an excellent basis for not only further quantitative analysis but also as a phenomenological template for employment in the study of a diversity of self-assembled supramolecular species.

Acknowledgements :

My supervisor, Dr. Andrew Doherty (now of Queens University of Belfast), for his continued support and assistance.

Jim Hambledon and Graeme Bentley from Sycopel Scientific Ltd. for technical support throughout my PhD.

John Marshall (glassblowing workshops) for the construction and maintenance of the electrochemical cells.

In memory of my late father, David, who died during the first year of my Ph.D.

With love to my mother, Carole and sister, Susan.

Contents Page

Chapter 3A : Triton X-100 (RDV)

Chapter 4A : CTAC (RDV)

Chapter 4B : Rheology of CTAC

List of Tables :

Chapter 3C Tables

Chapter 4A Tables

Chapter 4B Tables

Chapter 4C Tables

Chapter 5 Tables

List of Illustrations :

Chapter 5 Illustrations

List of Appendices :

Chapter 3B Appendices

Chapter 3C Appendices

Chapter 4A Appendices

Chapter 4B Appendices

Chapter 4C Appendices

Chapter 5 Appendices

List of Symbols:

Roman Symbols

Symbol	Meaning	Usual Dimensions
a_O	Surfactant chain cross sectional area	nm^2
a	Long dimension semi axis	nm
A	Electrode area	cm^2
b	Short dimension semi axis	nm
C_{dl}	Double layer capacitance	F, μF
C_O	Electroactive probe concentration	mol dm^{-3}
C_S	Surfactant Concentration	mol dm^{-3}
D	Self diffusion coefficient	cm^2 s^{-1}
$E_{1/2}$	Half wave potential	V, mV
E_A	Activation energy	KJ mol^{-1}
E^O	Formal potential	V, mV
F	Faraday constant	C mol^{-1}
f_{aq}	Fraction of probe in aqueous phase	none
i_{app}	Apparent current	A, μA
i_{aq}	Aqueous phase current	A, μA
i_C	Capacitance current	A, μA
i_{Lim}	Limiting current	A, μA
i_P	Peak current	A, μA
i(t)	Current at time t	A, μA
k_B	Boltzmann constant	J K^{-1}
k^O	Heterogeneous rate constant	cm s^{-1}
k_D	Interaction parameter (diffusion)	dm^3 mol^{-1}
k_V	Interaction parameter (viscosity)	dm^3 mol^{-1}
l_{max}	Max. surfactant chain length	nm
n	No. of electrons	none
N_{agg}	Aggregation number	none

r	Centre - centre distance	nm
Re	Reynolds number	none
R_H^O	Hydrodynamic radius	nm
R_{HS}	Hard sphere radius	nm
R_U	Uncompensated solution resistance	Ω
T_C	Cloud point temperature	^oC
U(r)	Coulombic potential	J
V_{hc}	Vol. of hydrocarbon core	nm^3
V_{HG}	Vol. of micellar headgroup	nm^3
V_{CI}	Vol. of micellar counterion	nm^3
V_S	Vol. of water	nm^3
V_θ	Rotational velocity	$cm\ s^{-1}$
V_r	Velocity of radial flow	$cm\ s^{-1}$
V_z	Velocity of laminar flow	$cm\ s^{-1}$
W	Ratio of $[H_2O]$ / [AOT]	none

Greek Symbols

Symbol	Meaning	Usual Dimensions
δ	Degree of dissociation	none
δ_D	Diffusion layer thickness	nm
ΔE	Peak - peak separation	V, mV
ε	Molar extinction coefficient	$dm^3\ mol^{-1}\ cm^{-1}$
ϕ	Micellar volume fraction	none
[η]	Intrinsic viscosity	$cm^3\ g^{-1}$
η	Static viscosity	$g\ cm^{-1}\ s^{-1}$
η_r	Relative viscosity	none
η_{SP}	Specific viscosity	none
κ^{-1}	Debye screening length	nm
l	Shear plane distance	nm
σ	Particle diameter	nm
τ_1	Micelle - solution surfactant exchange rate	s, μs

τ_2	Micelle lifetime	s, ms
υ	Potential sweep rate	V s^{-1}, mV s^{-1}
ω	Electrode rotation rate	Hz
ω_{HG}	Degree of headgroup hydration	none
ψ_O	Micellar surface potential	V, mV

Chapter 1: Introduction

Writing an introduction to give a brief overview of surfactants, micelles and their characteristic properties is a rather thankless task. An abundance of literature exists[1,2,3,4] describing micellar and surfactant structure, industrial applications, interfacial adsorption and liquid crystal formation to name but a few. Rather than expending the time and effort of both the author and reader, this introduction will only briefly touch on the aforementioned topics. Instead, attention will be paid to the methods which have been used to determine micellar structural parameters. Although, all the techniques that will be referred to are very powerful, many have inherent complications, namely assumptions, regarding the state of the micellar system. Though this does not compromise the validity of each method and subsequent analysis it does, however, encourage the utilisation of methods needing no such assumptions. The development of electrochemical techniques as applied to micellar systems has expanded over the last decade. The use of an electroactive probe solubilised within the micellar interior has allowed the precise and accurate determination of micellar self-diffusion coefficients. A review of these studies will be presented along with profiles of each method used for the forthcoming experimentation. The fundamental purpose of this thesis is to show that micellar properties such as size, shape, growth, interaction and structural evolution can be elucidated by the application of different electrochemical techniques.

1.1 Micelles : A Background Review

The word surfactant derives from the phrase 'surface active agent', where a surfactant can adsorb at a surface, altering interfacial properties that result from a change in the free energy of the system. They are generally described as amphiphilic, meaning that the molecule contains both hydrophobic and hydrophilic groups. It is essentially the amphiphilic nature of surfactants that has made them integral constituents for a number of industrial applications. Surfactants exist not only as

chemically synthesised products but also are widespread in nature. Natural surfactants are generally referred to as polar lipids which are abundant in all living organisms. Lecithin, for example, can be acquired without any chemical transformation from phospholipid-rich sources such as soybean. Surfactants are divided into four main classes, defined by the nature of the polar headgroup. These are anionic, cationic, nonionic and zwitterionic, each of which have physical and chemical properties that are distinctive of that class.

Anionic surfactants are the most frequently used surfactant class, they have a negatively charged headgroup balanced by a positively charged counterion. They are easy and inexpensive to manufacture and are commonly used as emulsifiers and in detergent formulations. The most popular sub-classes of anionic surfactant are, amongst others, sulfates, phosphates and carboxylates and these are illustrated below.

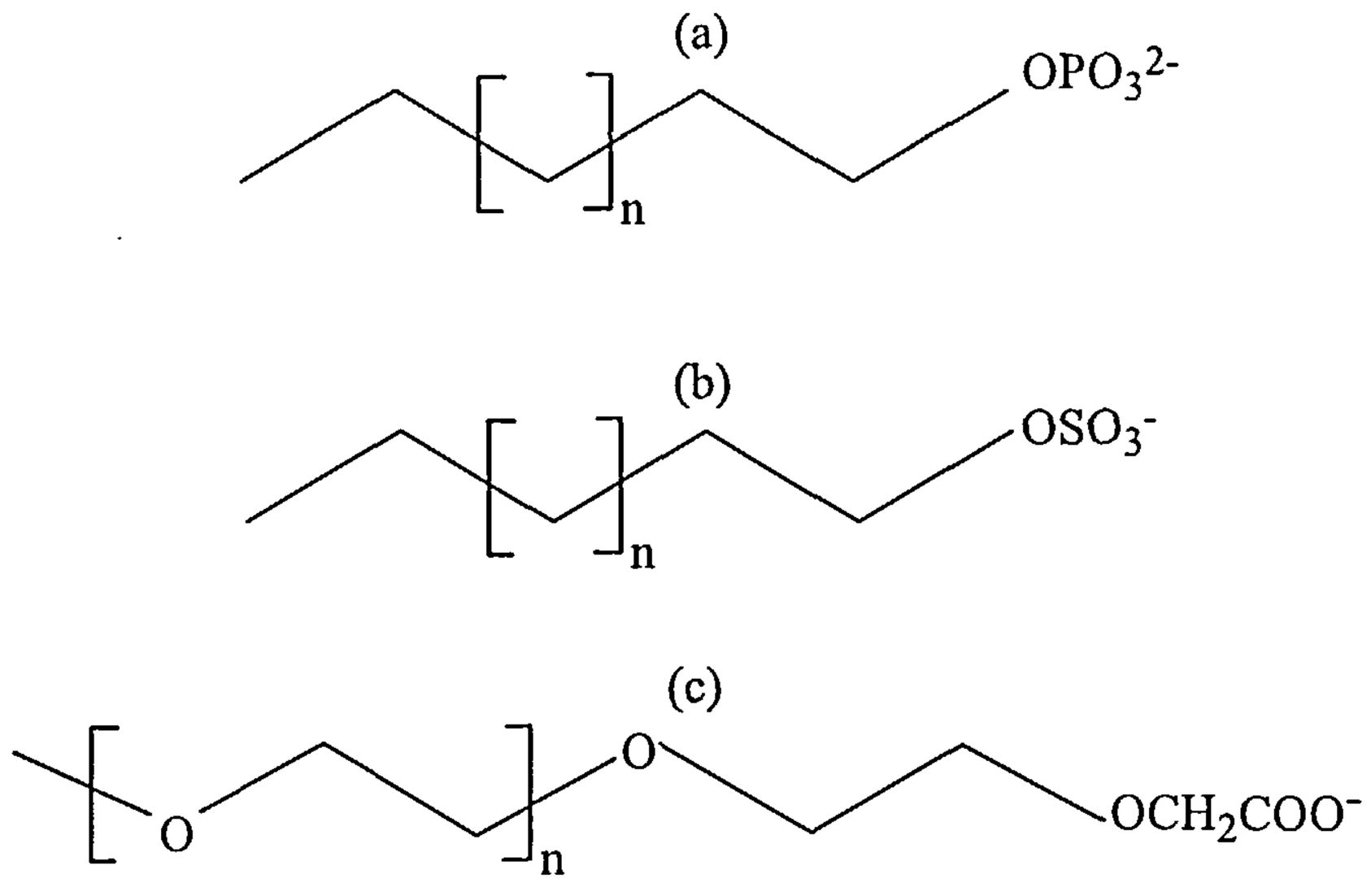

Figure 1.1: Examples of anionic surfactants (a) alkyl phosphate, (b) alkyl sulfate, (c) alkyl ethercarboxylate.

Cationics are the second most common surfactant class and contain positively charged headgroups and negatively charged counterions. Most cationic surfactants are based on nitrogen containing headgroups as illustrated in Fig. 1.2.

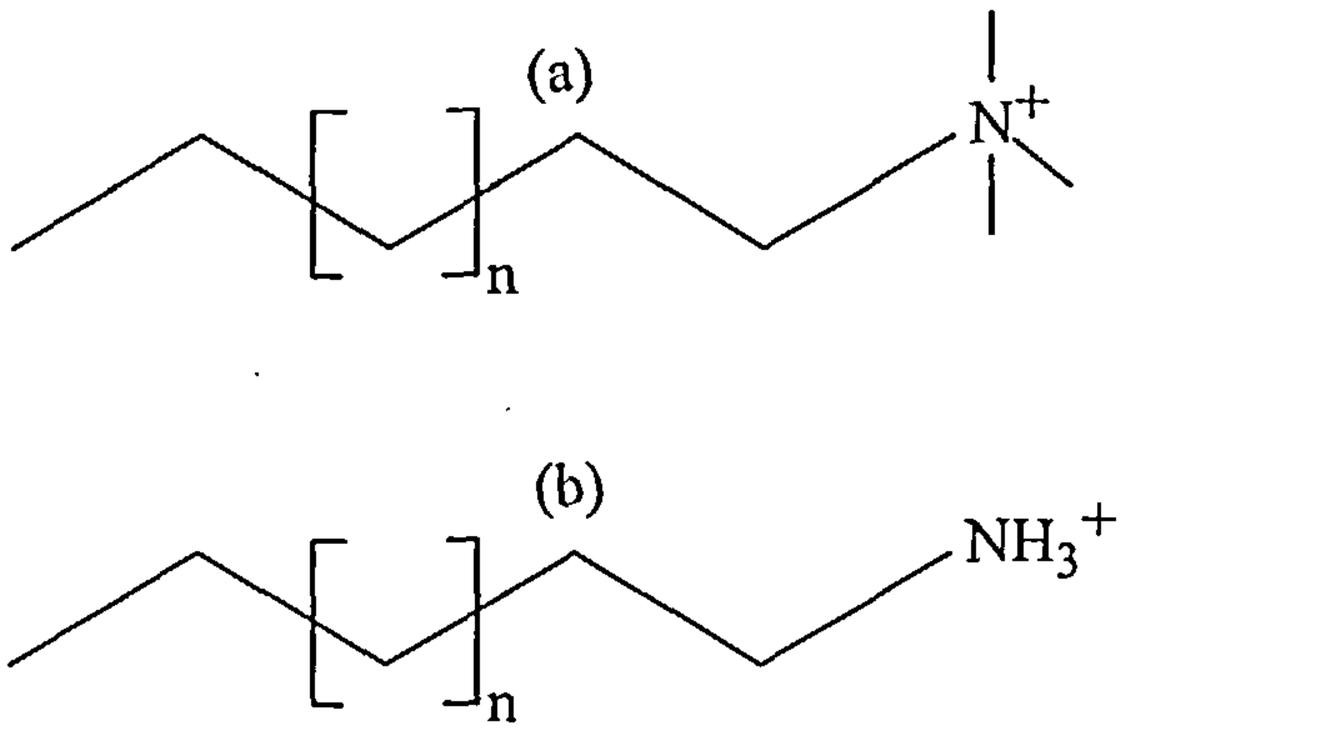

Figure 1.2: Examples of cationic surfactants (a) alkyl quaternary, (b) fatty amine.

Most natural surfaces are negatively charged and therefore allow cationic surfactants to adsorb easily forming hydrophobic surfaces. This explains why cationic surfactants are used as anti-corrosion and anti-static agents (plastics and fibres), they are also used in herbicides and fabric softeners.

The use of nonionic surfactants is less widespread than anionic and cationic. The convenience of nonionic surfactants is that because of their uncharged nature they are compatible with all other surfactant types. The tendency is to use these nonionic species as co-surfactants in detergency formulations and as emulsifying agents. An illustration of two nonionic surfactants is shown below.

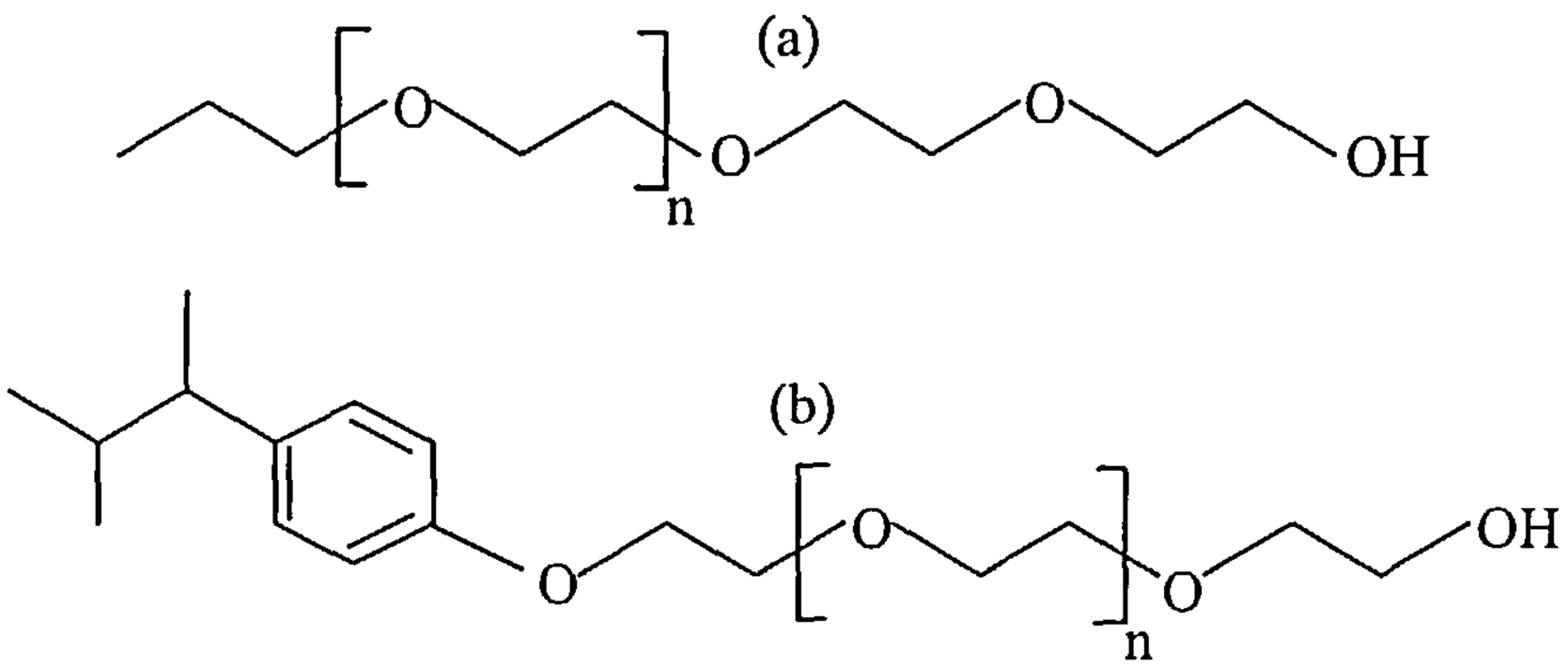

Figure 1.3: Examples of nonionic surfactants (a) fatty alcohol ethoxylate, (b) alkyl phenol ethoxylate.

Zwitterionic surfactants are generally referred to as amphoteric and are the least commonly used class. They contain two charged headgroups of opposite sign and this property results in the compatibility with all other surfactant types. The lack of skin / eye irritation that they exhibit makes them popular in personal care products.

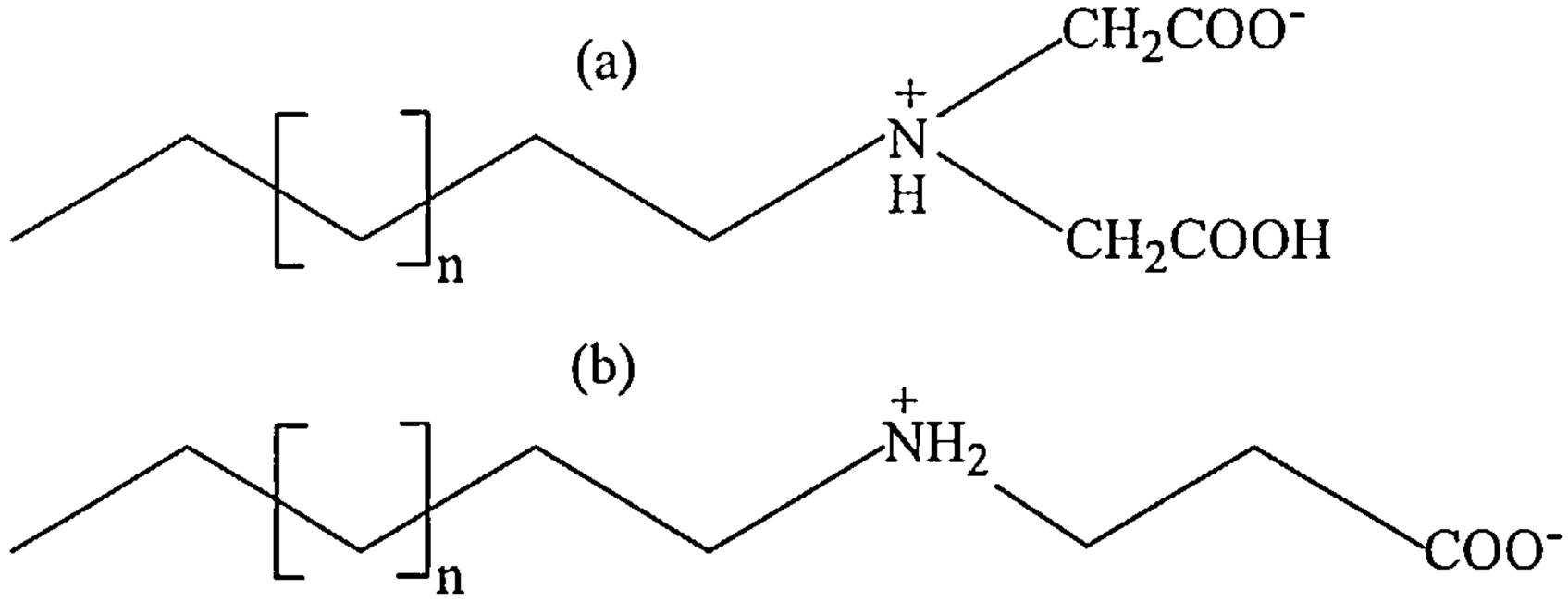

Figure 1.4: Examples of Zwitterionic surfactants (a) N-alkyl-β-iminodipropionic acid, (b) β-N-alkylaminopropionic acid.

At low surfactant concentrations in solution most physical properties are analogous to those of a simple electrolyte. However, at certain higher concentrations abrupt changes are noted for almost all measurable physical properties. Results from each experimental method that observes the change infer that there is a transition from a solution containing monomer to one containing the surfactant in a more aggregated state. The point at which the abrupt changes are evident is termed the critical micelle concentration (c.m.c.), as an example, a sharp reduction in solution molar conductivity is observed. This is evidence of the formation of supramolecular structures from unassociated surfactant chains. The similarity between micelles, membranes and globular proteins explains the use of micelles in a number of biotechnological applications. Figure 1.5 illustrates how selected physical properties are substantially altered at the c.m.c.

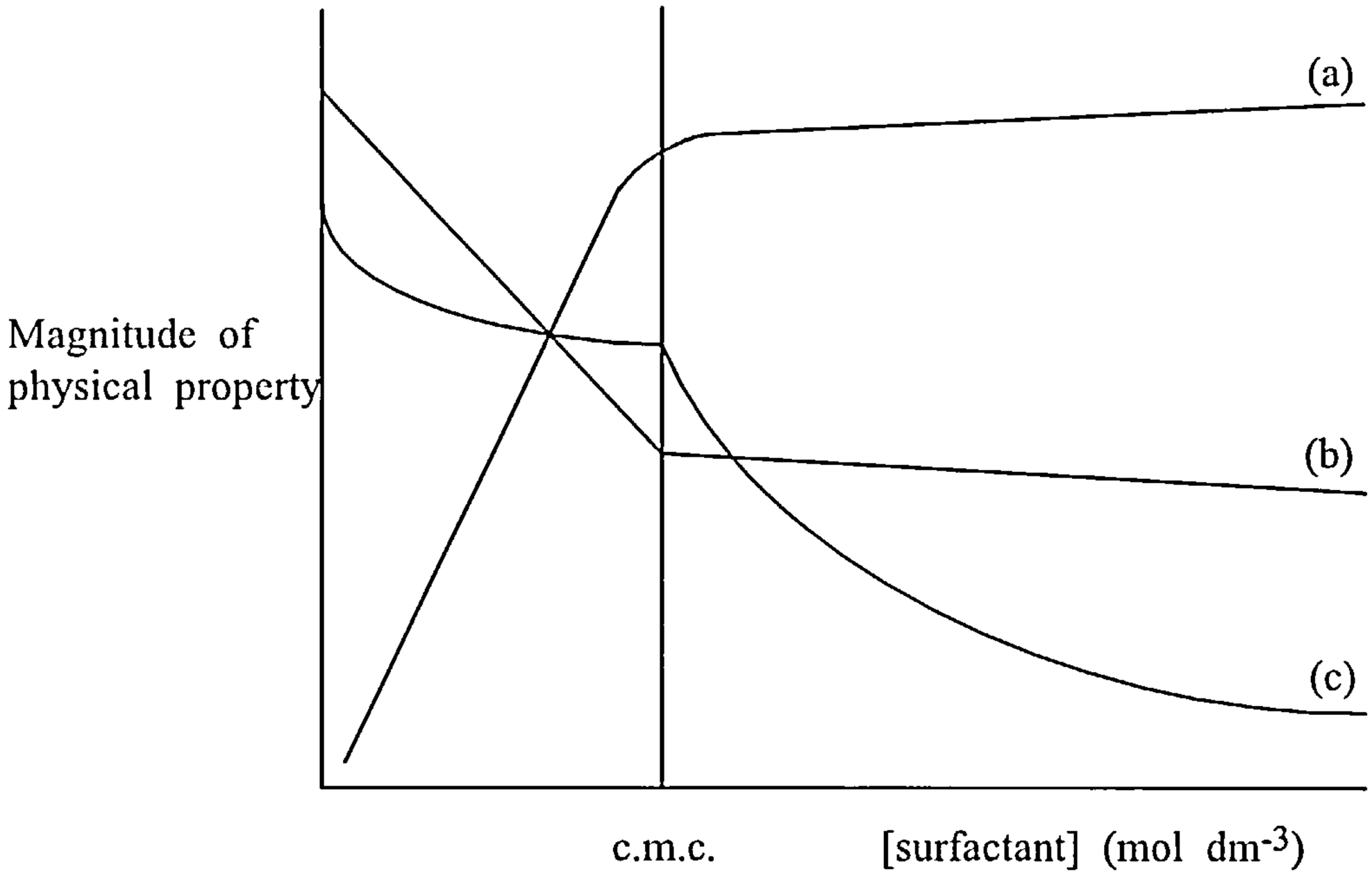

Figure 1.5: An illustration of how micelle formation at the c.m.c. affects certain physical properties; (a) osmotic pressure, (b) surface tension, (c) molar conductivity.

The amphiphilic nature of a surfactant chain is instrumental in determining the c.m.c. in aqueous solution. The driving force for the micellisation process is essentially governed by the elimination of contact between the hydrophobic group and the solvent. On aggregation, the surfactant headgroups arrange themselves to not only act as a barrier between the solvent and hydrophobic group but also to minimise repulsion between themselves. The free energy (ΔG_{MIC}) associated with the surfactant to micelle transformation is therefore a subtle balance between the two surfactant components. ΔG_{MIC} can be expressed as a function of individual free energies[1]:-

$$\Delta G_{MIC} = \Delta G_{MIC}(CH_3) + n.\Delta G_{MIC}(CH_2) + \Delta G_{MIC}(W) \qquad (1.1)$$

where n is the number of carbon atoms in the hydrophobic group and W represents the hydrophilic group. A negative free energy change, $\Delta G_{MIC}(CH_2)$, is related in the transference of a methylene group from the aqueous phase to micellar interior, which therefore encourages micellisation. This is countered by a positive free energy,

$\Delta G_{MIC}(W)$, on transition of hydrophilic headgroup from solvent to form the exterior of the micelle, and therefore opposes micellisation. The overall negative values for ΔG_{MIC} for the process are controlled by the large positive values for the associated entropy change (ΔS_{MIC}). The large entropy increase can essentially be described in two ways, firstly that the structured water around the hydrophobic group is broken when the group is transferred to a micelle. Secondly, that there is increased freedom of the hydrocarbon chain in the micelle in comparison to the aqueous phase.

The free energy of micellisation (ΔG_{MIC}) is quantitatively related to the critical micelle concentration by the expression[1,5,6,7]:-

$$\Delta G_{MIC} = 2.3RT\ (\log_{10}\text{c.m.c.} - \log \omega) \qquad (1.2)$$

where ω is the molar concentration of water (55.3 mol dm^{-3} @ 20 ^{O}C).

The c.m.c. of a surfactant system is affected by a number of factors including chain length, temperature, electrolyte and the presence of any organic additives. An increase of electrolyte concentration in an ionic surfactant system leads to a decrease in repulsion between headgroups effectively reducing the c.m.c. as described[8] by Equation 1.3. Equation 1.4 expresses the decrease in c.m.c. for nonionic and zwitterionic systems[9,10,11].

$$\log_{10}\text{c.m.c.} = -a.\log_{10}C_i + b \qquad (1.3)$$

$$\log_{10}\text{c.m.c.} = -KC_i + \text{constant} \qquad (1.4)$$

where a, b and K are constants and C_i represents the counter ion concentration.

A decrease in the c.m.c. is also observed when there is an increase in hydrocarbon chain length i.e. the number of carbons (n_C)[12].

$$\log_{10}\text{c.m.c.} = A - B.n_C \qquad (1.5)$$

A is a constant for a specified ionic headgroup at a given temperature and B $\approx$ 0.3 for ionic surfactants and B $\approx$ 0.5 for nonionic / zwitterionic surfactants at 35 ^{O}C.

Short chain alcohols increase the c.m.c. by virtue of the increased headgroup repulsion in ionic surfactants thus opposing the micellisation process. The effect of temperature, however, is less well defined. There is an increase in the dehydration of the hydrophilic groups (c.m.c.↓), but this is balanced by a disruption of the structured water around the hydrocarbon chain (c.m.c.↑). Therefore the effect of temperature is difficult to predict clearly.

The formation of micellar aggregates results in a significant increase in the solute solubilisation ability of the solution. The hydrocarbon core allows the encapsulation of molecules that are either partially or totally insoluble in the aqueous phase. It is this property that is of great use and interest to industries as diverse as pharmaceutical (controlled drug release) and petrochemical (enhanced oil recovery). It also allows the solubilisation of electroactive probes which are essential for the use of electrochemical techniques which will be discussed in Ch. 1.2.2.

From the periphery it may appear that micelles are static, rigid structures when they are actually dynamic entities, continually exchanging monomer chains between themselves and the bulk solution. This process can be expressed in the form[3]:-

$$A_n + A_1 \underset{k-}{\overset{k+}{\leftrightarrow}} A_{n+1} \qquad (1.6)$$

A_n represents the micellar aggregate, A_1 is a surfactant chain and A_{n+1} is the resultant aggregate. k_+ is the forward rate constant and is diffusion controlled, k_- is the reverse rate constant and depends on such factors as alkyl chain length and micelle size. A micelle exhibits two different relaxation times, τ_1 and τ_2. τ_1^{-1} is the rate at which the surfactant molecules exchange between micelles or the solution and is in the order of 10 μs. τ_2^{-1} is the rate at which micelles form and disintegrate (micelle lifetime), but is of a longer timescale, > 1 ms.

The sizes, shapes and growth patterns of micellar aggregates are parameters which can be substantially affected by the nature of the solution. At moderate temperatures, surfactant and electrolyte concentrations micelles tend to be spherical

and are described by a crystal packing parameter (CPP) < $^1/_3$. The CPP relates the volume of the hydrocarbon core (V_{HC}) to the maximum chain length (l_{max}) and cross sectional area of a surfactant molecule (a_O) where[4]:-

$$l_{max} = 1.5 + 1.265.n_C \qquad (1.7.a)$$

$$V_{HC} = 27.4 + 26.9.n_C \qquad (1.7.b)$$

$$CPP = V_{HC} / l_{max}.a_O \qquad (1.7.c)$$

Micelles can undergo a number of phase changes and these are best illustrated by an increase in surfactant concentration. An illustration of possible structural evolution is shown below:-

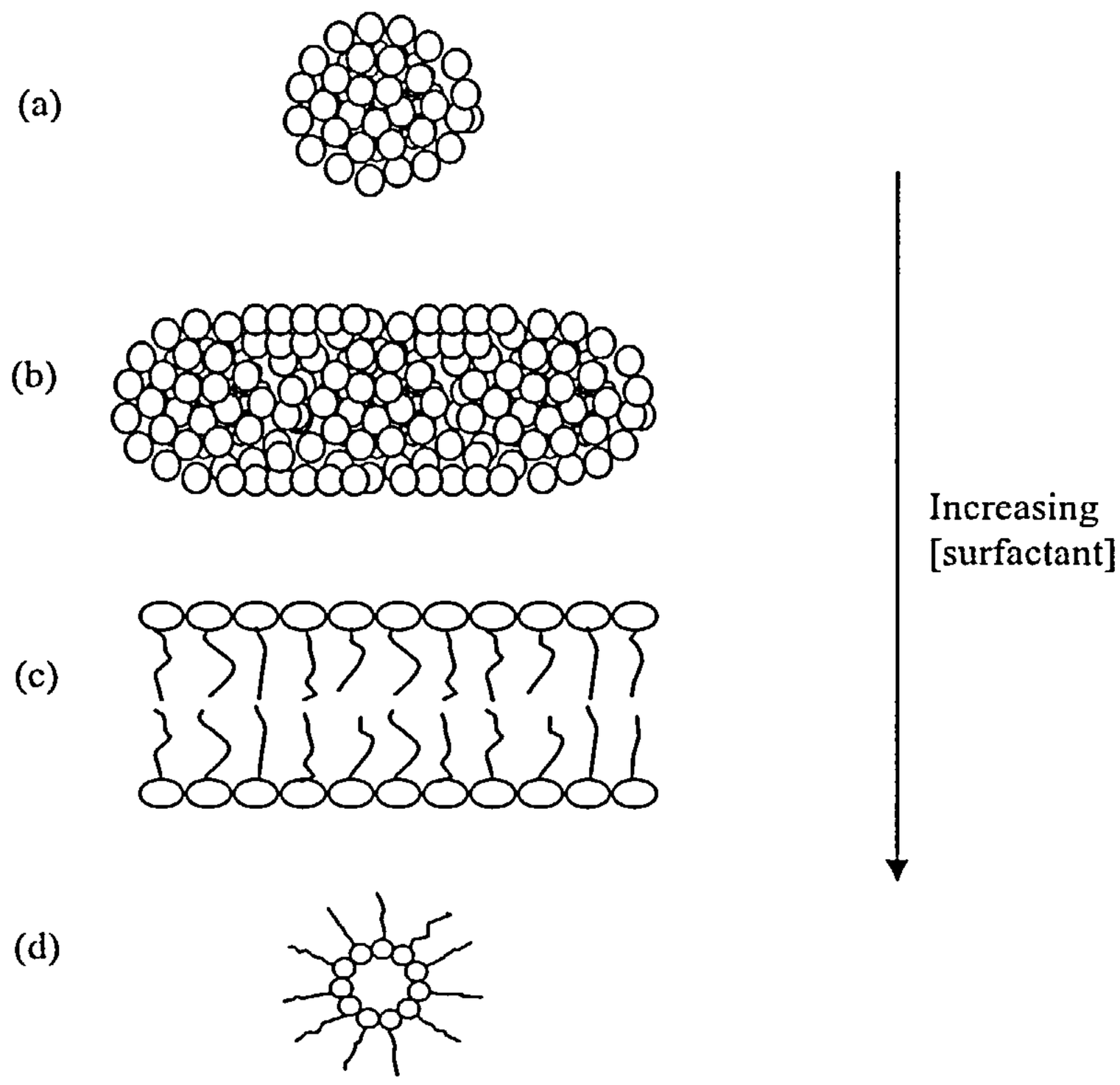

Figure 1.6: Example of possible structural transitions with an increase in surfactant concentration; (a) spherical, (b) rod-like, (c) lamellar, (d) reverse.

The structural transitions are mirrored by a corresponding increase in the crystal packing parameter as defined in Table 1.1

Table 1.1 : Variation in crystal packing parameter with structural evolution

Micellar structure	CPP
spherical	$< {}^{1}/_{3}$
rod-like	${}^{1}/_{3}$ - ${}^{1}/_{2}$
liquid crystal	${}^{1}/_{2}$ - 1
reverse (inverse)	>1

The structural transformations not only have importance in industrial applications but also form the basis of phenomenological understanding for a number of related systems e.g. in membrane mimetics[13,14]. It is the elucidation of the sphere to rod-like transition and the related interaction that is of interest in this thesis.

1.2 Why Electrochemical Methods?

This section aims to give a brief review of the experimental techniques that have been used in the past for the study of micellar systems. Attention will be paid to the application of electrochemical techniques over the last decade and suggest why these methods are such powerful tools for the elucidation of such factors as size, structure and interaction.

1.2.1 Techniques Used To Study Micellar Systems

The number of techniques that have been used to study the properties of supramolecular systems are too numerous to mention individually. By far the most popular techniques are those that involve scattering, whether of light or neutrons. Light scattering results were reported as much as 50 years ago with inferences made with regard to micellar molecular weight and aggregation number[15,16]. Debye first used classical light scattering (CLS) to determine the critical micelle concentration (c.m.c.)[16]. In monomer form (< c.m.c.) the surfactant chains were observed to scatter the incident light weakly, however, in the aggregate state the intensity (I) was seen to

increase substantially. The dependence of scattered light intensity on surfactant concentration (C_S) was shown to be[16]:-

$$(C_S - \text{c.m.c.}) / (I(C_S) - I(\text{c.m.c.})) = \alpha [1/M + 2A_2 (C_S - \text{c.m.c.})] \quad (1.8)$$

where M is the micellar molecular weight and α and A_2 are constants. However, although a powerful method there are inherent assumptions that severely restrict the application of the technique. Of greatest note is that M and A_2 remain constant above the c.m.c., which has been noted as been untrue[17]. It follows that CLS has been unable to provide consistent data on micellar systems at concentrations significantly above the c.m.c. Combining CLS with dynamic light scattering (DLS), in which diffusion coefficients are obtained, leads to inferences of micellar shape, molecular weight and interaction. There still remain a number of assumptions that are needed in DLS experiments, in particular that micellar interactions are regarded as hard sphere effects[18]. Nevertheless, DLS / CLS still remain powerful tools and along with quasi-elastic light scattering (QELS) are the authoritative methods for the probing of micellar properties[19,20,21,22,23,24].

Another prevalent technique that is widely used is small angle neutron scattering (SANS), which rather than measuring diffusion coefficients, directly determines time averaged micellar structure[25]. The fact that neutrons interact weakly with matter means that concentrated dispersions can be studied with no problems due to multiple scattering[25]. As for light scattering, assumptions are an integral part of the mathematical modelling of the SANS data. The major property that is of concern is the polydispersity which can affect the inferences made from the structural factor [25]. SANS remains an effective technique for determining micellar structural parameters and has great importance in the analysis of rod-like systems[26,27,28,29] and has recently been used to probe intermicellar interactions[30,31].

The use of assumptions, such as the degree of polydispersity, and mathematical modelling used in scattering experiments opened the door for techniques that could determine micellar diffusion coefficients directly[32,33]. Over the

past two decades electrochemical techniques have developed into very powerful methods for the elucidation of a number of micellar properties. Not only has micellar size and interaction been considered[32,34,35,36] but also factors such as surfactant adsorption[37,38] and electron transfer[39]. Despite the advantages of electrochemical methods (faster, less expensive, no assumptions) when compared to scattering techniques, they are still, in the authors opinion, vastly underused. The diffusion coefficients obtained differ from those deduced from light scattering methods in one major respect. Light scattering yields mutual-diffusion coefficients (D_M) as compared to self-diffusion coefficients (D_S) from electrochemical methods. D_S represents the independent motion of single molecules, whereas D_M results from the correlated motion of distinct molecules associated with a concentration gradient (a concentration gradient of micelles does not occur at an electrode surface)[25,40]. The self diffusion coefficients are termed 'long time' as the mean micellar displacement is greater than the mean intermicellar spacing. Though interaction is an integral part of the D_S analysis, relatively little work has been carried out on rationalising intermicellar interactions. The majority of self-diffusion data has been obtained over a range of surfactant concentrations thus yielding the hydrodynamic radius[32,34,35,36]. However, the effect of electrolyte on size and interaction has not been fully considered by electrochemical techniques though some attention has been paid using D_M values from light scattering data[21,22,23,24]. Therefore, the opportunity exists for a comprehensive study of micellar interaction and size over a range of electrolyte and surfactant concentrations.

1.2.2 The Electroactive Probe

Electrochemical techniques rely on the solubilising ability of micelles to incorporate an electroactive probe. The probe and micelle effectively act as a single entity during mass transport processes and therefore by observing changes in the probe diffusion directly leads to the micellar diffusion coefficient.

The choice of electroactive probe is of paramount importance when conducting electrochemical self-diffusion (D_S) measurements in micellar media[32,34,35,41,42]. There are a number of important criteria that need to be satisfied if the probe is to be effective. These requirements were indicated by Chokshi et al.[42]:-

- Diffusion controlled charge transfer.
- Low solubility in aqueous phase.
- Half wave potentials ($E_{1/2}$) are within the potential range for the system.
- Little or no adsorption on the electrode.
- No affect on the properties of the system.

Chokshi et al. suggested that ferrocene (fc) was an ideal probe for their chosen microemulsion system of CTAB/NaCl/n-Butanol[42].

Other authors have considered different probes for micellar systems. Mandal et al. used a cobalt probe, ($Co(en)_3(ClO_4)_3$: en = ethylenediamine)[35], ferrocyanide ($K_4Fe(CN)_6$)[41] as well as ferrocene[32]. For both $Co(en)_3(ClO_4)_3$ and $K_4Fe(CN)_6$ it was clear that both probes had a degree of solubility in the aqueous phase which leads to complications in determining the diffusion coefficients of micelles[32,35,41]. However, if partition coefficient behaviour is needed to be studied then these probes are ideal[35]. Hence, if the probe is completely solubilised within the micellar interior the diffusion coefficient is purely due to the diffusion of the micelle towards the electrode surface[32]. Ferrocene has a low solubility in water ($1x10^{-5}$ mol dm^{-3}) and therefore satisfies the criterion[32,43,44]. Ferrocene has been shown to exhibit a simple one electron reversible reaction in micellar media even at high surfactant concentrations[32]. For a rotating disk electrode (RDE)[34], a limiting current is reached at >0.32 mV vs. Ag/AgCl, with half-wave potentials ($E_{1/2}$) between 230-250 mV[32,34,43,44,45]. Each voltammogram displays the characteristics of diffusion controlled behaviour i.e. a straight line plot of peak or limiting current (i_p or i_{lim}) against the square root of sweep rate or rotation speed ($\nu^{1/2}$ or $\omega^{1/2}$) with a (0,0) intercept[32,34,35,41,44].

The half wave potentials of the fc/fc^+ redox couple have been shown to be reasonably stable when there is a change in the surfactant system[32,43]. The only factor that seems to greatly affect $E_{1/2}$ in micellar media is the concentration of the

surfactant (C_S)[34]. It has also been recorded that the peak to peak separations in cyclic voltammetry (CV) experiments remain constant with values varying from 59-63 mV[32,34,43,44], essentially indicating fast reversible electrochemical behaviour.

Another important factor to consider when choosing a redox probe is whether or not it will adsorb onto the electrode surface. It is known that probes such as ferricyanide adsorb on platinum electrodes leading to surface blocking and a subsequent change in the heterogeneous rate constant[46]. Ferrocene, however does not present a major problem in this respect. Although it has been observed using FTIR that ferricinium (fc^+) may form films on platinum, no such films were observed when ferrocene was oxidised in CTAB[47]. On glassy carbon, no significant adsorption exists[42].

The final point to be addressed is how, if at all, the probe affects the properties of the system. In this respect, the choice of probe must be careful so as not to interfere with the micellar media. Mandal et al.[41] demonstrated that for cationic micelles a neutral or cationic probe must be chosen as $K_4Fe(CN)_6$ (anionic) caused precipitation with CTAB micelles. Therefore, ferrocene in CTAC micelles should be inert with respects to the micellar solution.

The actual electron transfer rate for the redox couple can be affected by a number of factors including the blocking of the electrode surface and electrostatic interactions between the adsorbed surfactant and solute. Therefore, the nature of the probe-electrode interaction is of great importance and has been divided into four parts[48].

- Distance between electrode and probe.
- Environment surrounding probe at time of transfer.
- Structure / dynamics of surfactant aggregates on the surface.
- Dynamics of interactions of probe with structures on electrode.

It is widely known that in micellar solutions there will be a degree of surfactant adsorption onto electrode surfaces[37,45,48,49]. The extent of adsorption depends on a number of factors including the surfactant type, electrode material and electrode potential. The majority of studies have considered how the electrode potential

influences the degree of adsorption with techniques such as fluorescence[49], surface-enhanced raman spectroscopy (SERS)[50] and atomic force microscopy (AFM)[51]. It is generally accepted that adsorption is strongest at extreme potentials of opposite polarity to that of the surfactant and it is possible that multilayers are formed[42]. Evidence for hemimicelle or bilayer formation exists for CTAC[49] and CTAB[51], though the distinction between a bilayer and a monolayer can be difficult[50]. Data presented in Ch. 4A.2.1 will show that there is no appreciable change in the double layer capacitance between a solution of pure water to a solution of 5% CTAC. Conversely, increases in the half wave potentials ($E_{1/2}$) are seen as the concentration of surfactant is increased (Ch. 3A.2.1, 4A.2.1). It can therefore be suggested that there is a degree of surfactant adsorbed at the electrode surface, though the exact nature of the layer is difficult to establish from the data presented.

1.2.3 The Electrode Interface

At an interface between two phases a partition of positive and negative charges may exist and this is especially apparent at an electrode - solution interface. Charge separation can occur, amongst other mechanisms, by the adsorption of one charge type on the electrode preferentially to the other and charge transfer across the liquid - liquid interface[52,53]. Although the solution will be electrically neutral, charged species will migrate to the interfacial region to oppose the charge on the electrode surface to give a double layer. There are a number of theories describing the charged interface which involves charge on the surface balanced by opposite charge on the solution side of the interface. The Helmholtz model assumes that the solvated ions in solution are rigidly structured on the electrode surface. Conversely, the Gouy - Chapman model assumes that the structure is diffuse in nature. Neither of these models adequately describe the structure of the double layer, but combining both models leads to the more acceptable Stern model[54].

In the Stern model the electrode double layer is described by a number of conceptual layers adjacent to the electrode surface, and is illustrated in Appendix 1.i a. The layer closest to the electrode consists of specifically adsorbed solvent molecules and ions

and is termed the Stern or Helmholtz layer. The centre of these charged species represent the inner Helmholtz plane (IHP) which occurs at a distance x_1 from the electrode surface. The next layer contains solvated cations held in place by electrostatic forces and are represented by the outer Helmholtz plane (OHP) occurring at a distance x_2. These ions are non-specifically adsorbed and are distributed out into the bulk solution forming a diffuse electrical double layer. The potential between the electrode and solution decays in an exponential fashion which leads to a high potential drop across the interfacial region leading to a high electric field (Appendix 1.i b). The potential profile across the interface can be expressed by the following equation[55]:-

$$[\tanh (z.e.\psi / 4.k_B.T)] / [\tanh (z.e.\psi_O / 4.k_B.T)] = \exp (-\kappa x) \qquad (1.9)$$

where z is the valency on the ion, e is the electronic charge, ψ is the potential at some distance x, ψ_O is the potential at the surface and κ is the inverse of the Debye screening length. It is this potential profile expression which will be utilised for the determination of shear plane potential (Ch. 4A.2.3.3).

As the interfacial region is essentially described as two layers of equal and opposite charge separated by dielectric material, it can be considered a capacitor. The current response of the electrode to the applied potential can be described as an RC circuit i.e. the solution resistance (R_u) is in series with the double layer capacitance (C_{dl}). The R_uC_{dl} constant is designated the time constant of the system and determines how quickly the electrode responds to a change in applied potential (assuming that the potentiostat is faster). Obviously, a fast response time is advantageous so that the true potential is close to the applied potential. For example, in a potential step experiment when a instantaneous potential (E_{inst}) is applied to the electrode, the true potential (E_{true}) will lag behind in an exponential fashion, governed by the R_uC_{dl} constant. This can be expressed in the form[55] :-

$$E_{true} = E_{inst} (1-e^{-t/RuCdl}) \qquad (1.10)$$

The current response of the electrode is therefore vital when conducting electrochemical experiments. It is therefore prudent to investigate whether surfactant or electrolyte adsorption would have a detrimental effect on the electrode response. In Ch. 4A.2.1, data from a series of background scans will be presented indicating that electrolyte concentration predominates over surfactant in determining the electrode capacitance.

1.3 Experimental Techniques

This section of the introduction will give an overview of each of the electrochemical methods used for the determination of micellar self-diffusion coefficients. Attention will be paid to the shape of the voltammetric waves resulting from the Faradaic response of the oxidation of the ferrocene probe. A brief summary of the rheological method will also be presented.

1.3.1 Hydrodynamic Method - Rotating Disk Voltammetry

Rotating disk voltammetry (RDV) is a hydrodynamic technique in which forced convection is used to increase the overall rate of mass transport towards the electrode. In quiescent solutions the diffusion layer from the electrode surface extends into the solution to a significant distance (at long time scales) whereas with the rotating disk electrode (RDE) the diffusion layer is fixed and stagnant at a set rotation speed[52]. In both techniques mass transport to the electrode is by diffusion, but because the diffusion layer is of constant thickness (depending on ω) then the diffusion profile is reproducible and accurately variable. The nature of the stagnant diffusion layer allows any electroactive species to approach the electrode evenly across the electrode surface. This characteristic is referred to as uniform accessibility

which essentially ensures the properties of hydrodynamic flow and the constant concentration profile on the surface[56]. These are the fundamental properties which ensure a steady state response.

Steady state responses can be easily measured as they are not only independent of time and potential but are also of a greater magnitude than transient methods at long times. Whereas in the unstirred system the solution can be said to be of a uniform nature, hydrodynamics creates an environment in which the solution is divided into two distinct regions. Adjacent to the electrode is a stationary layer of liquid, termed the diffusion layer (δ_D), the thickness of which is primarily determined by the disk rotation rate. Across this layer the mass transport is purely diffusional due to the linear concentration gradient between the electrode surface and the bulk solution. The mass transport in the bulk solution is governed by convection due to the disk rotation. Spinning the disk at a frequency (f), creates layers of laminar flow perpendicular (z) to the disk surface. This has the effect of sucking solution towards the surface and forcing it out sideways (r) due to centrifugal forces. The system effectively acts as a pump with the laminar flow solution replacing the expelled solution, this mechanism is illustrated in Appendix 1.ii. The velocity of the laminar flow (V_z) is obviously highly dependent on the disk rotation rate and at distances close to the surface can be described by[52,55]:-

$$V_z = 0.51\ \omega^{3/2}.\nu^{-1/2}.z^2 \qquad (1.11)$$

where ω is the rotation rate (s^{-1}) and ν is the kinematic viscosity of the solution ($cm^2\ s^{-1}$). The limiting velocity in the z direction is given by[55]:-

$$U_0 = \lim_{z \to \infty} V_z = 0.88447\ (\omega.\nu)^{1/2} \qquad (1.12)$$

Also of interest is the velocity of the radial (centrifugal) flow close to the disk surface (V_r). V_r is zero at the surface and passes through a maximum close to the surface. This is described by the same terms used in Equation 1.11 and 1.12[55]:-

$$V_r = 0.51\ \omega^{3/2}.\nu^{-1/2}.r.z \qquad (1.13)$$

Assuming constant values for ω and ν, V_z is a function of only the perpendicular distance (z), V_r is a function of both z and the radial distance (r).

The final velocity component needed to fully characterise the system is the rotational velocity (V_θ). At the surface, V_θ will be equal to the rotation of the disk (ω), but will decrease rapidly with distance from the surface (z).

Velocity profiles for both V_z, V_r and V_θ are shown in Appendix 1.iii a,b,c.

The thickness of the diffusion layer is of great importance as it determines the rate of diffusional mass transport to the electrode. As the rotation rate increases the diffusion layer decreases in thickness according to Equation 1.14, where D is the diffusion coefficient.

$$\delta_D = 0.643.D^{1/3}.\nu^{1/6}.\omega^{-1/2} \qquad (1.14)$$

The thinner the layer, the greater the concentration gradient across the layer leading to a faster rate of diffusion (Appendix 1.iv). This results in proportionally higher currents than those obtained by transient methods at long times.

There are two limiting cases within which experimentation with the rotating disk must be carried. A very low rotation speed will result in a large diffusion layer, if this is of a similar dimension to the disk radius then approximations describing diffusional transport break down[55]. For a disk radius of 1 cm the approximations will become invalid at δ_D = 1 cm, and for a solution of D = $5x10^{-7}$ cm^2 s^{-1} and ν = $1.5x10^{-2}$ cm^2 s^{-1} a value for ω ~ $6.4x10^{-6}$ s^{-1} is obtained according to Equation 1.14. Therefore, for the approximations to be strictly valid this rotation speed must be exceeded which because of its small magnitude does not present a problem. Conversely, at high rotation speeds turbulent flow can occur leading to deviation from hydrodynamic conditions[55]. This upper limit is described by the Reynolds number (Re) using:-

$$Re = \omega.r_C^2 / \nu \qquad (1.15)$$

where r_C is the disk radius. A typical critical Reynolds number for turbulent flow is generally assumed[57] to be of the order $1x10^5$ which leads to $\omega_{crit} = 1200\ s^{-1}$. Therefore, laminar flow will be present as long as the rotation speed is between $\omega = 6.4x10^{-6}$ - $1200\ s^{-1}$. In all the RDV experiments carried out the rotation rate varies between 2 - 12 s^{-1}, well within the limiting cases.

Using RDV to study a redox couple, as in ferrocene / ferricinium (fc / fc^+), a slow potential scan rate is applied (5 mV s^{-1}) to ensure that the recorded current is at the steady state diffusion limit i.e. the system responds instantaneously to the applied potential. A deviation from this condition will result in a peak as in cyclic voltammetry at a stationary electrode. A typical sigmoidal plot from an RDV experiment is shown in Appendix 1.v along with the respective concentration profiles at different points. The shape of the plot is independent of the electrode rotation rate, which shows that the current at any point varies linearly with $\omega^{1/2}$. Deviation from linearity in a plot of i_{lim} against $\omega^{1/2}$ would suggest kinetic limitations, in other words the mass transport rate is too fast for the electron transfer process to keep up[58].

The height of the limiting current (i_{lim}) for a reversible process is given by.

$$i_{lim} = n.F.A.D.C_O/\delta_D \qquad (1.16)$$

where n is the number of electrons transferred, F is Faraday's constant, A is the electrode area and C_O is the bulk concentration of electroactive probe. If Equations 1.14 and 1.16 are combined the results is the well known Levich equation[57]:-

$$i_{lim} = 1.554.n.F.A.D^{2/3}.C_O.\nu^{-1/6}.\omega^{1/2} \qquad (1.17)$$

With a known probe concentration, electrode area and kinematic viscosity, the Levich equation allows the simple determination of the diffusion coefficient by measuring i_{lim} as a function of $\omega^{1/2}$.

Rotating disk voltammetry has a number of different advantages over transient methods. The slope of i_{lim} against $\omega^{1/2}$ is more sensitive to changes in the diffusion coefficient ($D^{2/3}$) than, for example, cyclic voltammetry ($D^{1/2}$) and is therefore the preferred method for measuring values precisely. The increased rate of mass transport relative to a stationary technique means that higher currents are obtained, hence higher precision. Also, at steady state there is freedom from double layer charging effects and any possible pre-concentration effects at the electrode surface[55,59].

1.3.2 Transient Method - Cyclic Voltammetry

Cyclic voltammetry is a stationary method that involves mass transfer purely by diffusion. It is a popular technique as it can easily determine the formal potential (E^O) of a redox couple and is useful in mechanistic and structural studies[60,61,62,63]. Cyclic voltammetry involves scanning the applied potential from a voltage at which no Faradaic process occurs (E_1) to one where electron transfer occurs (E_2) and back to E_1. This is represented by a triangular waveform (Appendix 1.vi), where the potential at any given time (E_t) is given by Equations 1.18a, 1.18b.

$$\text{Forward scan } E_t = E_1 + \upsilon t \qquad (1.18a)$$

$$\text{Reverse scan } E_t = E_2 - \upsilon t \qquad (1.18b)$$

The current response of the system is, amongst other factors, characteristic of the heterogeneous rate constant and the surface concentration of the electroactive species. As the potential is initially raised there is no appreciable oxidation of the ferrocene until the formal potential is approached. At this stage the current rises dramatically while the concentration of ferrocene at the surface is consumed due to oxidation ($fc \leftrightarrow fc^+ + e^-$) and only partly replaced by fc from the bulk solution. The peak in the current - voltage curve is representative of a balance between the increasing forward rate constant and the depleted fc concentration i.e. diffusional control. Following the peak the current is determined purely by the diffusion of the

fc from the bulk to the electrode. At this point the diffusion layer at the electrode will be large and therefore the rate of diffusion will be slower, this is characterised by a $t^{-1/2}$ dependence[58].

When the potential reaches E_2, also termed the switching potential (E_S), the scan continues in the reverse cathodic direction. As E_t is still larger than E^O the oxidation reaction will still occur until E^O is approached again. At a potential less than E^0 a negative current will be observed due to the reduction of $fc^+ + e^- \rightarrow fc$. The fc^+ created in the forward scan will be close to the electrode and therefore reduced quickly, leading to the observed reverse scan peak. Following the peak, the fc^+ will be depleted at the surface leading to diffusional behaviour and the observed $t^{-1/2}$ dependence. An illustration of the current - voltage relationship can be seen in Appendix 1.vii.

The concentration dependence of the potential for the reaction can be expressed by the Nernst equation:-

$$E = E^0 + (R.T/ n.F) \ln ([fc+] / [fc]) \qquad (1.19)$$

The formal potential (E^0) is therefore defined as the potential (E) at which there are equal concentrations of the of the fc^+ and fc. The half wave potential ($E_{1/2}$) is usually very close to the formal potential and is related to the diffusion coefficients of the fc^+ and fc[55,58] by the following expression:-

$$E_{1/2} = E^0 - (R.T / 2.n.F) \ln (D_{fc+} / D_{fc}) \qquad (1.20)$$

Measurements of the peak currents (i_{pa},i_{pc}) are very important when studying the nature and behaviour of the system. It follows that care must be taken to ensure that the current measured is purely Faradaic. At potentials where no Faradaic processes occur there will be some residual current due to the charging of the electrode double layer, so measurements must be made by extrapolating this out i.e. by using it as a baseline. This non-Faradaic current becomes more problematic at both lower probe concentrations, where the Faradaic current is smaller, and higher scan rates where the charging current is larger as explicated in Equation 1.21[55].

$$I_C = A.C_{dl}.\upsilon \qquad (1.21)$$

If the capacitance and solution resistance are large then the difference between the applied and actual potential is $E + iR_U$. The characteristic manifestation of this uncompensated resistance is distortion of the voltammetric wave, leading to large errors in the determination of peak currents. This effect can be reduced by using an iR compensation utility of a potentiostat, high electrolyte concentration and a luggin capillary.

Once accurate measurement of the peak current is attained it can be related to the potential sweep rate by the Randles - Sevcik[57] equation (Equation 1.22). Each of the terms have been defined previously.

$$i_{pa} = 2.71x10^5.n^{3/2}.A.D^{1/2}.C_O.\upsilon^{1/2} \quad (20\ ^oC) \qquad (1.22)$$

It is therefore possible to calculate the self diffusion coefficient by recording the peak current as a function of the potential sweep rate. For a reversible one electron transfer a plot of i_{pa} against $\upsilon^{1/2}$ will yield a straight line with a (0,0) intercept.
The reversibility can also be assessed by two other methods. Firstly, for a reversible redox couple the ratio of the cathodic to anodic peak currents will be ~1, but accurate baseline definition is required[58]. The second method is to consider the peak to peak separation (ΔE_p). A typical separation of 2.3RT/nF is expected for a reversible redox couple over a wide range of υ, and any deviation is either due to capacitive distortion, iR drop or limitations in the electron transfer rate. The heterogeneous rate (k^O) constant can be estimated from[55]:-

$$k^O = \psi\ [D_{fc}.\pi.\upsilon.(nF/RT)]^{1/2}.\ (D_{fc+}/D_{fc})^{\alpha/2} \qquad (1.23)$$

where ψ is a kinetic parameter relating to ΔE_P and α is the transfer coefficient (usually 0.5). With carefully designed electrochemical experiments, the

hetereogeneous rate constants may be obtained easily. Calculations of k^O will be shown in Ch. 4C.2.1.

1.3.3 Potential Step Method - Chronoamperometry

In both rotating disk voltammetry and cyclic voltammetry the applied voltage was swept between two limiting values and the resulting current response measured. Chronoamperometry differs from these techniques in the fact the applied voltage is 'stepped' rather than swept (Appendix 1.viii). In chronoamperometry the potential is stepped instantaneously from a point where no Faradaic processes occur (E_1) to a voltage where the mass transport is limiting (E_2).

At the time of the potential step (t = 0), the current will theoretically tend towards infinity (Equation 1.24). In practice, the response time of the potentiostat (~20 ms) determines the initial current or R_UC_{dl}. At t = 0 the concentration of ferrocene at the electrode surface is equal to that of the bulk solution and therefore the resulting current is high and at a maximum value (Appendix 1.ix). As the experiment proceeds the ferrocene in the layer adjacent to the electrode begins to be depleted. This has the effect of causing an increase in the diffusion layer thickness and hence a reduction in the concentration gradient (Appendix 1.x). The rate of diffusional flux from the bulk solution is controlled by the concentration gradient and this will result in the current decreasing, eventually to zero[57]. The decay of the current after the initial maximum value is dependent on $t^{-1/2}$ which is characteristic of a diffusion controlled process[58]. The current - time response is described by the well known Cottrell equation[57]:-

$$i(t) = n.F.A.D^{1/2}.C_O / \pi^{1/2}.t^{1/2} \qquad (1.24)$$

where i(t) is the current at time t after the application of the potential step. It is therefore apparent that for a known electrode area the current - time response can be used to determine the diffusion coefficient from a plot of i against $t^{-1/2}$. There are a

number of factors that need to be considered before an accurate value for D can be obtained. The two major factors are ensuring that the response is purely Faradaic and that the analysis range for the Cottrell plot is valid.

When a potential step is applied to the system there will be charging of the electrode double layer which will have the effect of causing a non-Faradaic current to flow[55]. This current decays in an exponential fashion after the potential step and is determined by the solution resistance and the double layer capacitance:-

$$i = i_0.e^{-t/Ru.Cdl} \qquad (1.25)$$

The initial non-Faradaic current (i_0) is a function of the applied potential and solution resistance ($i_0 = E_{APP}/R_U$). For a large RC constant of the system the current will decay slowly and therefore contribute to the total measured current to a large extent at short times. At a time $t = R_UC_{dl}$ the non-F

Faradaic current will have decayed to 37% of the initial current and at $t = 4\ R_UC_{dl}$, $i = 0.018.i_0$ (Appendix 1.xi). Typically the decay time of a non-Faradaic process will be much faster than that of the Faradaic[64]. It so happens that $i = 0.37\ i_0$ at ~100 ms and 130 ms for the non-Faradaic and Faradaic response respectively. However, for the non-Faradaic response $i = 0.018.i_0$ after ~6 s whereas for the Faradaic process it is much greater than 8 s (Ch. 3C.2.3, Ch. 4C.2.4).

In order to ensure that any experimental values for the diffusion coefficient are wholly due to the Faradaic current a background scan is obtained and subtracted from the measured chronoamperometric response although such a correction has recently been questioned[65].

Many authors have studied which time range is the best for the Cottrell analysis as it is well known that at short times there is a deviation from linearity[64,66,67,68]. At long times the diffusion layer adjacent to the electrode will become large and susceptible to disruption by convective mass transport. It may be such that convective effects are seen at times as short as 10 s[67,68]. Therefore, care must be taken to ensure that analysis of the current - time response is maintained within the two time limits. Ranges of $1.5\ s < t < 10\ s$[68] and $2\ s < t < 4\ s$[67] have been

found to give accurate values for the diffusion coefficient with excellent correlation coefficients. It will be shown that the best range is 2 s < t < 5 s for analysis of both the Triton X-100 (Ch. 3C.2.3) and the CTAC (Ch. 4C.2.4) systems.

1.3.4 Microelectrode Technique

Microelectrodes are generally classed as electrodes with radii in the order of micrometres though some as small as nanometres have been constructed[69]. A range of microelectrode configurations have been used, including wires[69,70,71], rings[69,70,71,72], bands[69,70,71,72], arrays[69,70,71,72] and interdigitated arrays[70,71,72]. The majority of the microelectrode studies have utilised a planar disk arrangement not only for the ease of construction but also for the simple mathematical models which apply.

Microelectrodes are leading the way forward for electrochemical techniques in a range of diverse fields. They have a number of properties that are attractive not only for chemistry but also for medical applications. The range of possible uses are massive, ranging from the study of complex / fast reactions[56,69,71] to *in vivo* measurements of biogenic neurotransmitters within the brain[73,74]. The main characteristic of a microelectrode that makes it different to 'conventional' electrodes is their size. A small electrode diameter leads to a much smaller current (~nA) than is observed with a macroelectrode (~μA).

A macroelectrode experiences planar / linear diffusion at all times[56,69,70,72]. A microelectrode, however, experiences planar diffusion at short times and (hemi) spherical diffusion at long times[56,69,70,72] (Appendix 1.xii). The diffusion field can be further described by the following relationship[56]:-

$$\partial[C]/\partial t = D_C (\partial^2[C]/\partial x^2 + \partial^2[C]/\partial y^2 + \partial^2[C]/\partial z^2) \qquad (1.26)$$

where [C] is the concentration of electroactive species, D_C is the diffusion coefficient and *x*,y,z are the cartesian co-ordinates.

The (hemi) spherical diffusion is a consequence of edge effects from the small electrode size[70]. Edge effects are a result of the very high current densities almost parallel to the electrode surface[72]. The result of the (hemi) spherical diffusion field is the sigmoidal waveform that is analogous to that from a RDV[56,69,70,72]. The size and shape of the sigmoidal waveform is retained until high potential sweep rates. Only at $\upsilon > 100$ mV s^{-1} does a deviation occur with the wave becoming similar to that observed in a cyclic voltammetry experiment[70].

Although the currents are small, the small diffusion layer at the electrode causes a large concentration gradient and hence a high mass transport rate[56,69,70,72,75]. An equivalent mass transport rate at a macroelectrode could only be achieved with a rotation rate in the order of 1000 rpm[69]. Another advantage over macroelectrodes is the short response time of a microelectrode which is essentially a consequence of a lower time constant. A change in the applied potential will be matched by an almost instantaneous change in the redox state of the system i.e. the current[69]. This allows the investigation into fast reactions which may involve unstable intermediates which microelectrodes are sufficiently sensitive to detect[70,76]. In addition, at very small microelectrodes the rate of transport of electroactive particles can be larger than the heterogeneous rate constant, which causes the current to be kinetically controlled, therefore kinetic data may be obtained[75].

One major disadvantage of macroelectrodes is the presence of ohmic or iR drop between the reference and working electrodes. It has been discussed previously (Ch. 1.3.2) that this can lead to distortion in voltammograms obtained from CV leading to ambiguous kinetic data and in extreme cases causing the real potential to deviate from the applied potential by a large amount. In microelectrodes, however, ohmic drop is almost totally eliminated by virtue of the small current. The elimination of effects due to charging current vastly increases the number of systems available for study voltammetrically.

With macroelectrodes supporting electrolyte is necessary to limit uncompensated solution resistance whereas microelectrodes have no such restriction[56,70,71]. The use of highly resistive media such as non-polar solvents, supercritical fluids and solids is therefore possible as well as low temperature studies[69,70,71]. However, it has been noted that migrationary effects need to be considered in the absence of supporting electrolyte[71]. This can result in reduced flux towards to the electrode and has been characterised by a reduced limiting current for tetrathiafulvalene in acetonitrile[77]. This will be discussed in more detail in Ch. 5.4.2.3.

The distinct advantages that a microelectrode offers over macroelectrodes allows the study of reverse micelles in isooctane (Ch. 5). In Ch. 5, it will be seen that a simple steady state response leads to the determination of the diffusion coefficient given by the relationship[69,70,71,72,76,78]:-

$$i_{SS} = 4.n.F.D_S.C_O.r \qquad (1.27)$$

where i_{SS} is the steady state limiting current and r is the microelectrode radius. The resulting voltammograms will be shown to exhibit reversible one electron electrochemistry characterised by adherence to the Nernst equation (Ch. 5.3).

1.3.5 Rheological Theory of Viscosity

Viscosity is essentially a measure of the internal friction of a liquid, the greater the viscosity the less mobile the liquid[54]. The friction is caused when two layers are forced to move in relation to each other. As the frictional force increases so does the applied forced needed to cause the movement. The applied force per unit area (F/A) needed to induce shear is termed the shear stress (F') and it follows that a high shear force is needed for a highly viscous liquid. The shear rate (S) is defined as the velocity gradient (dv/dx) occurring when two adjacent layers move relative to each other as shown in Figure 1.7[79].

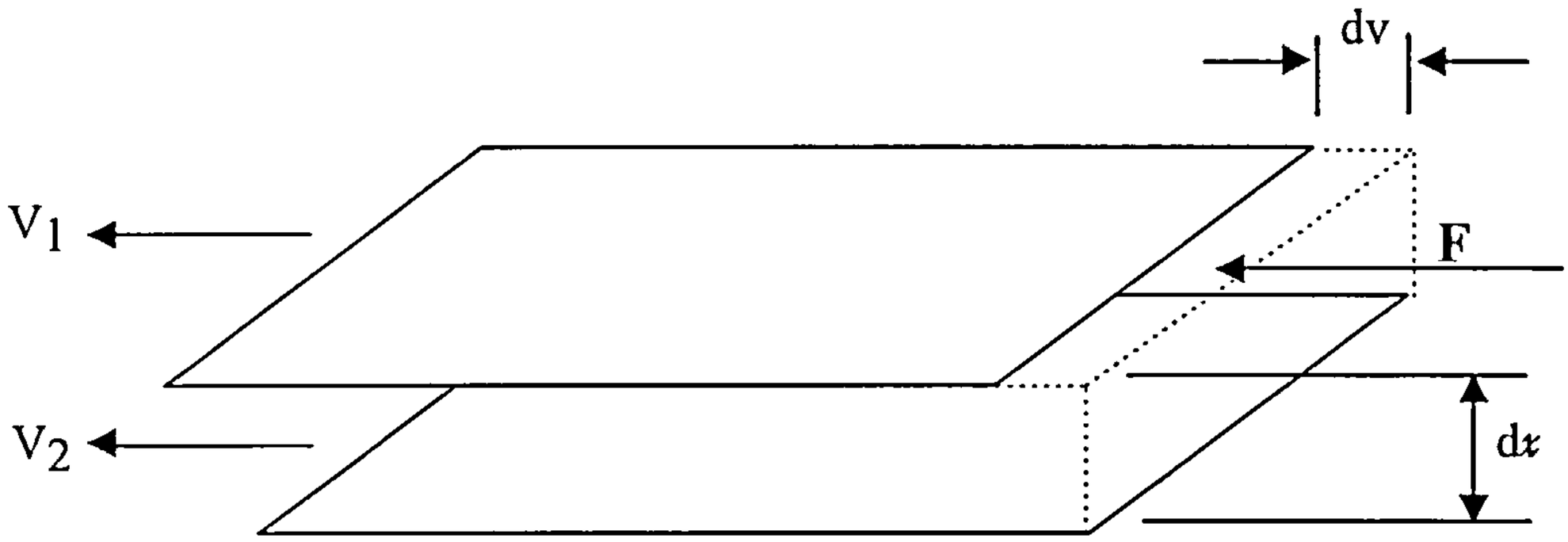

Figure 1.7 : Parallel plate model describing viscous shear flow

A cone and plate viscometer traps a thin layer of liquid between a spindle which rotates at a chosen speed and a plate under thermostatic control. The ratio of the shear stress to the shear rate (F' / S) defines the viscosity (η)[79].

Appendix 1.i : Representation of (a) electrode / solution interface and (b) potential profile from the electrode surface

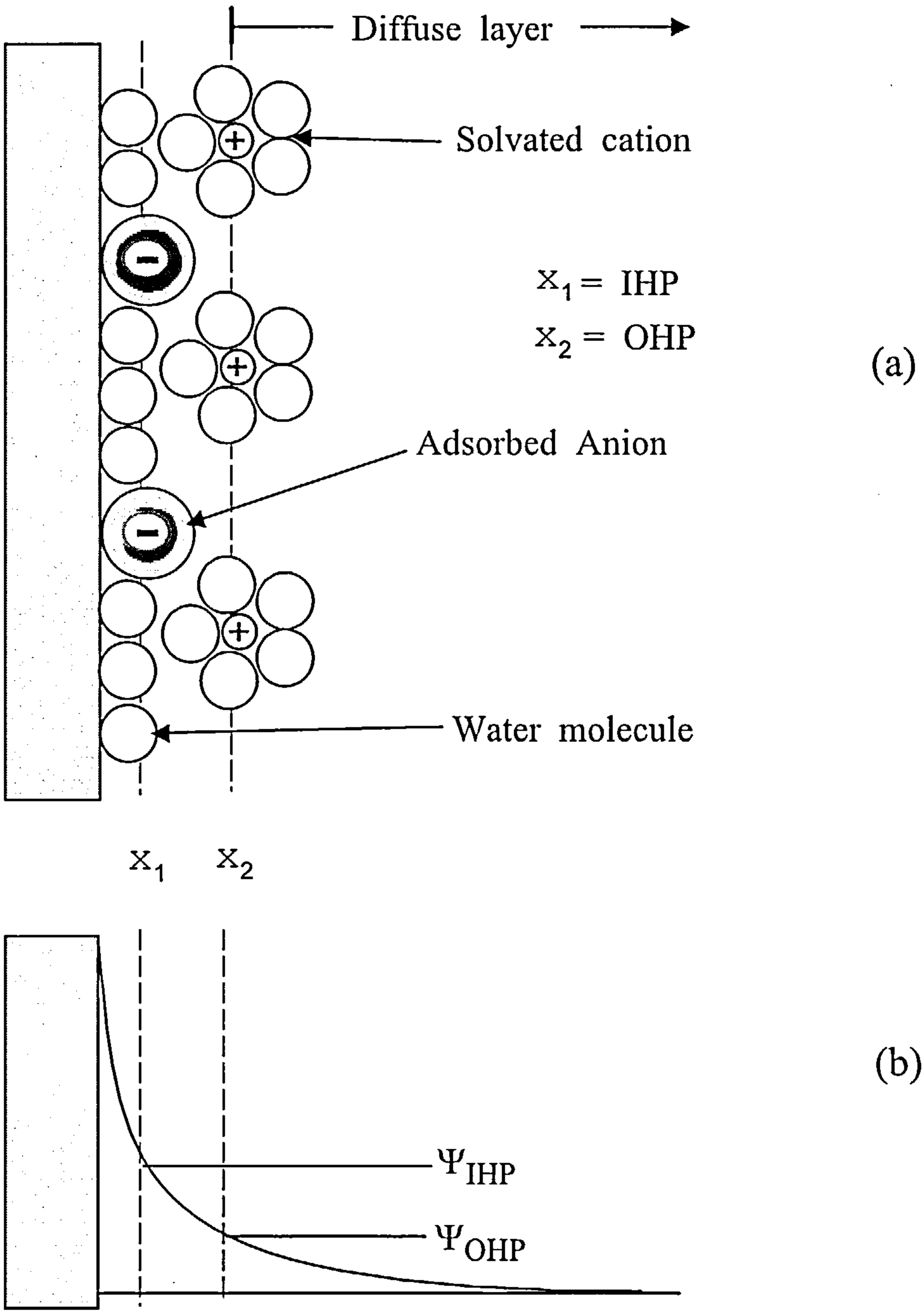

Appendix i.ii : Representation of the laminar flow at a rotating disk electrode (RDE)

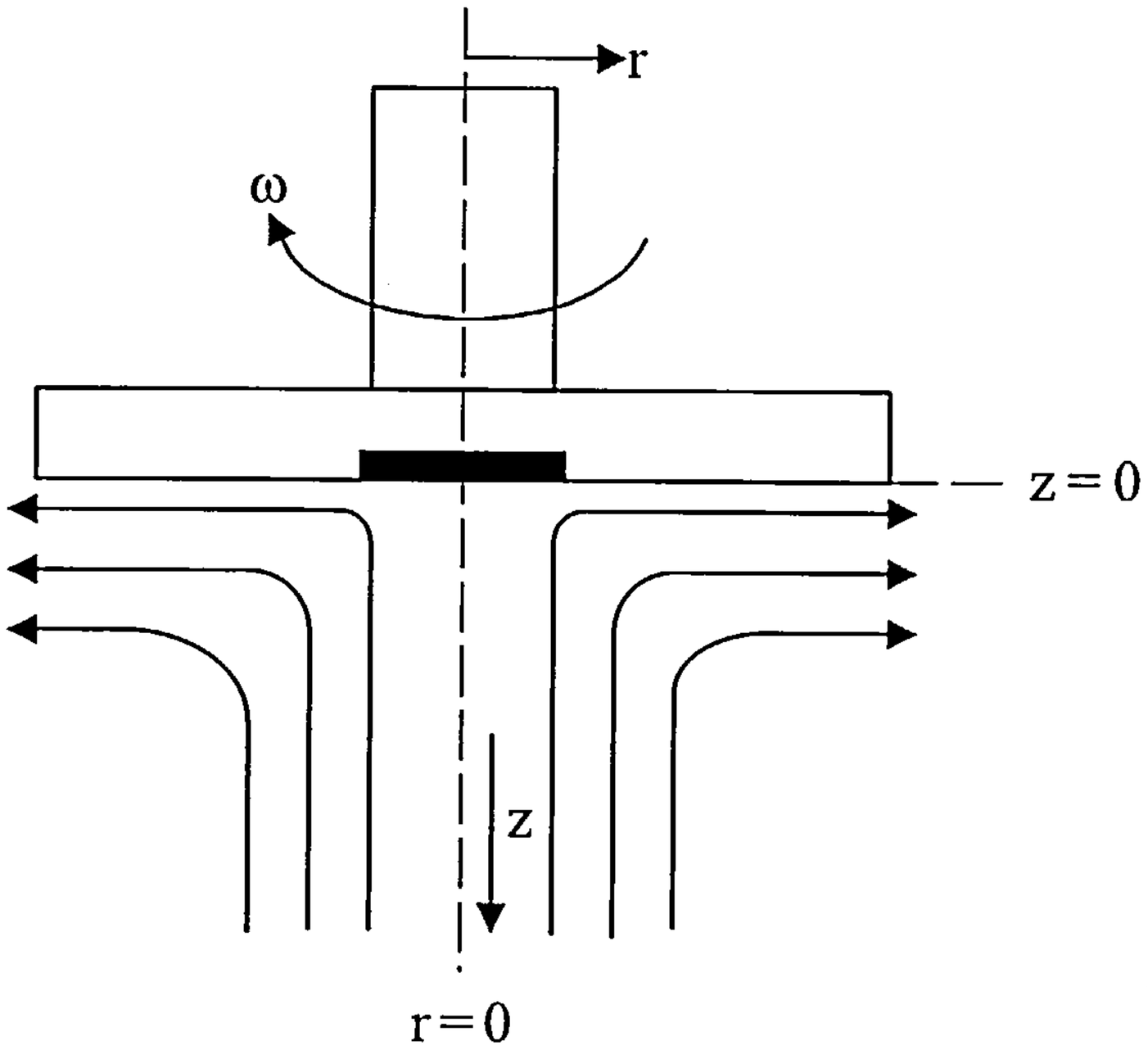

Appendix 1.iii : Variation of velocity with distance (z) for (a) V_z (b) V_r and (c) V_θ

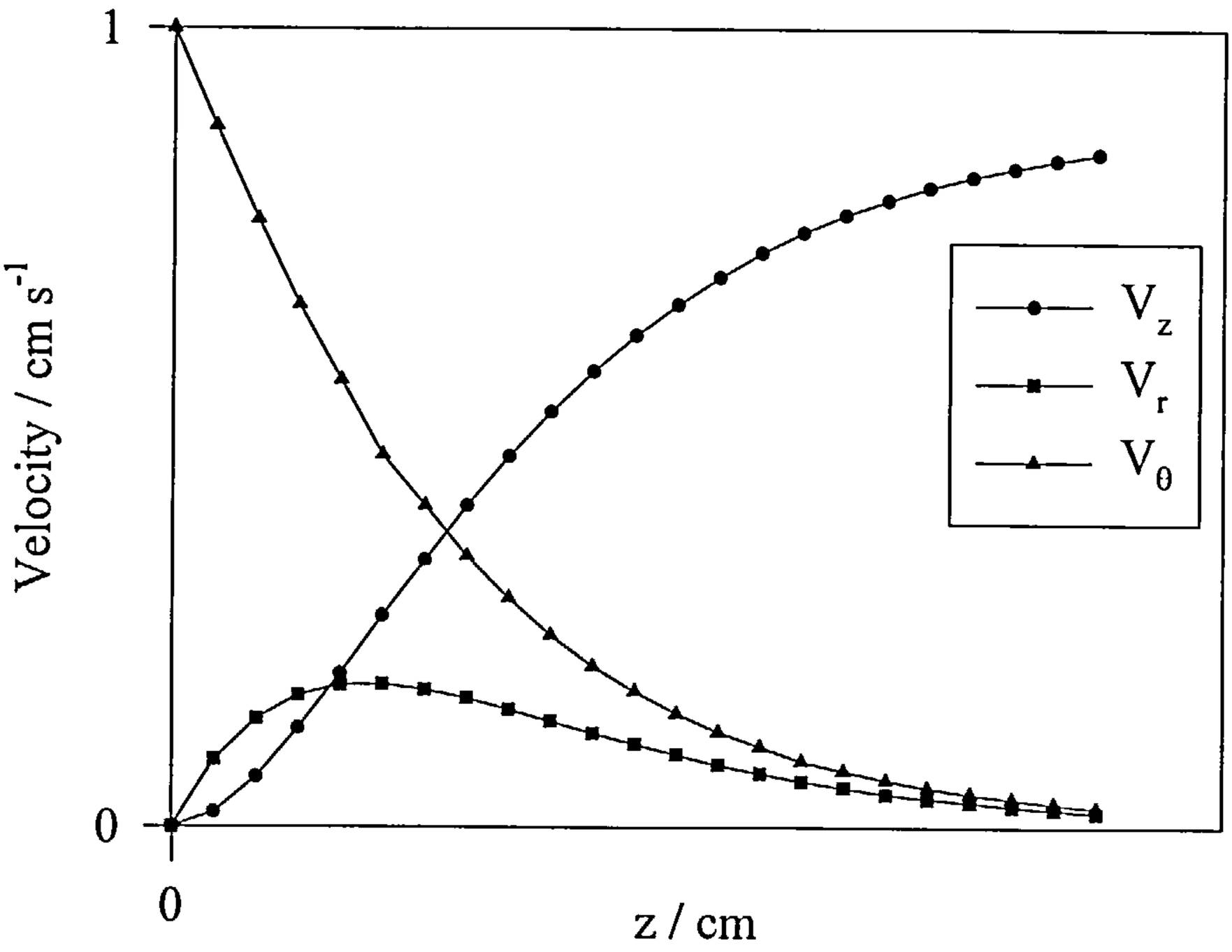

Appendix 1.iv : Schematic of concentration profile as a function of distance from the electrode: effect of electrode rotation rate

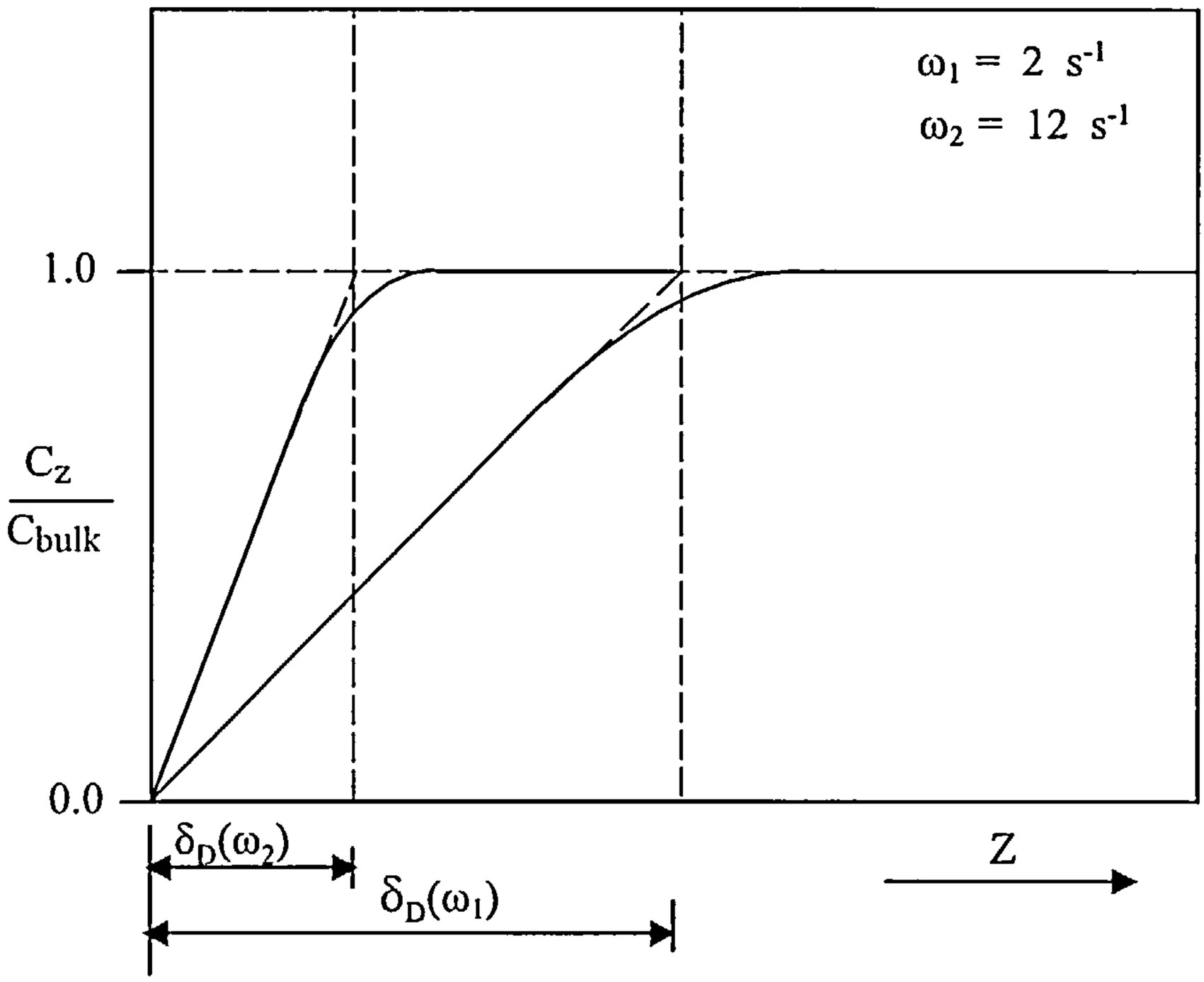

Appendix 1.v : A Typical rotating disk voltammogram : variation of concentration profile with potential

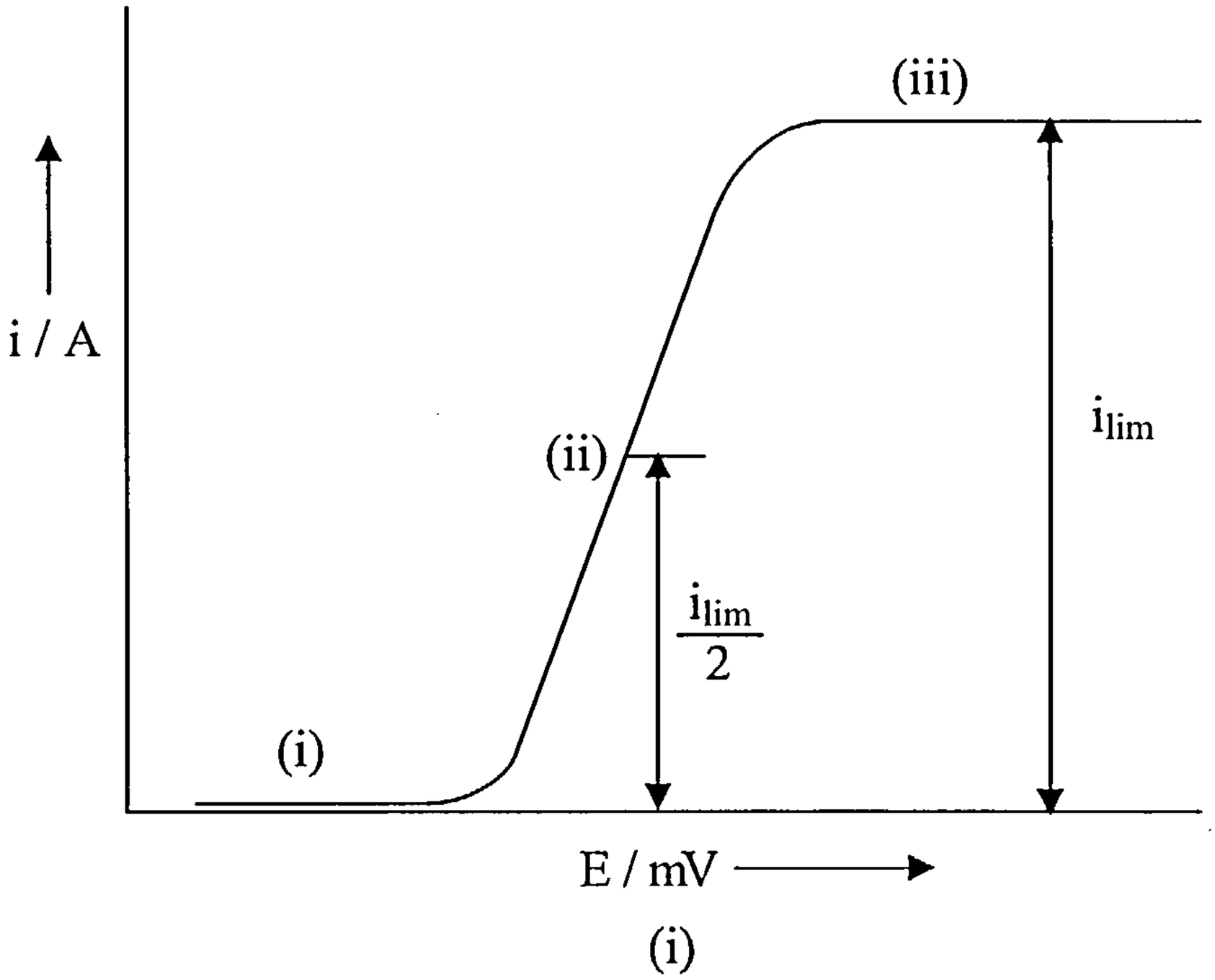

(i)

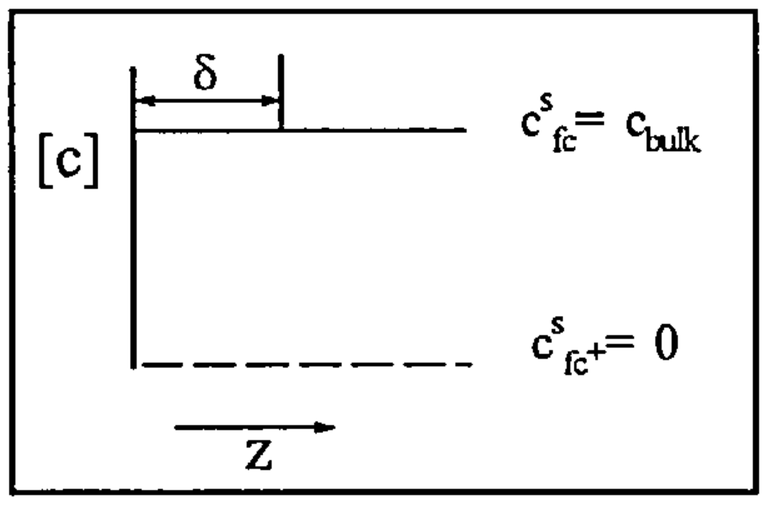

(ii)

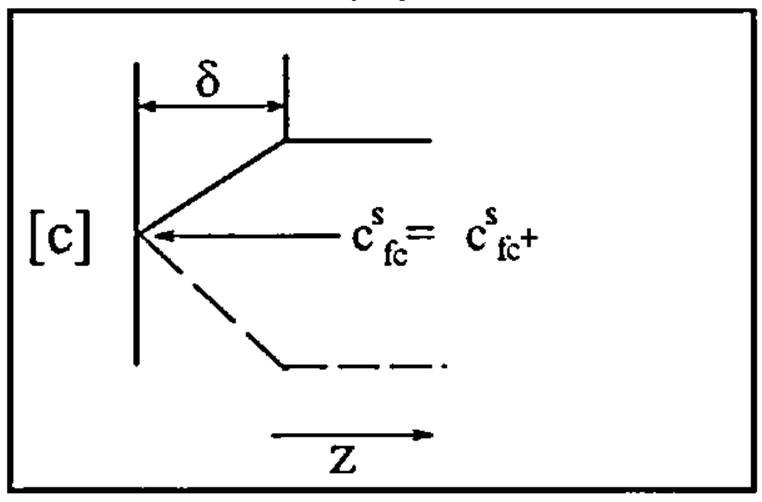

(iii)

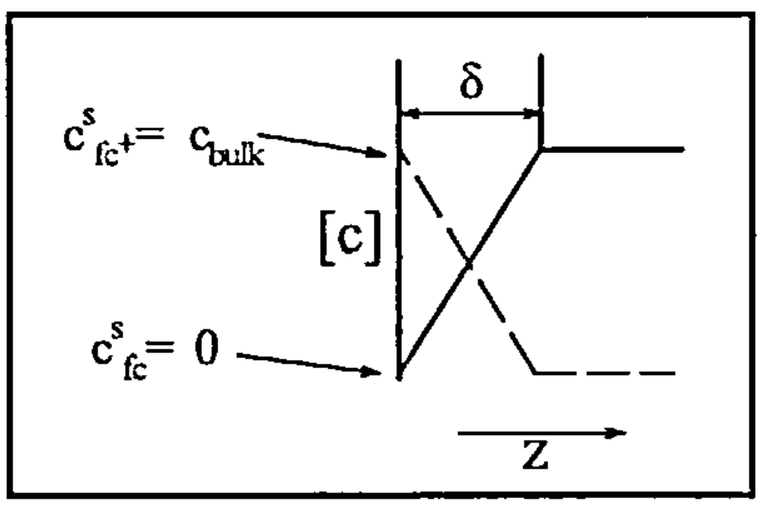

Appendix 1.vi : Variation of applied potential with time for cyclic voltammetry

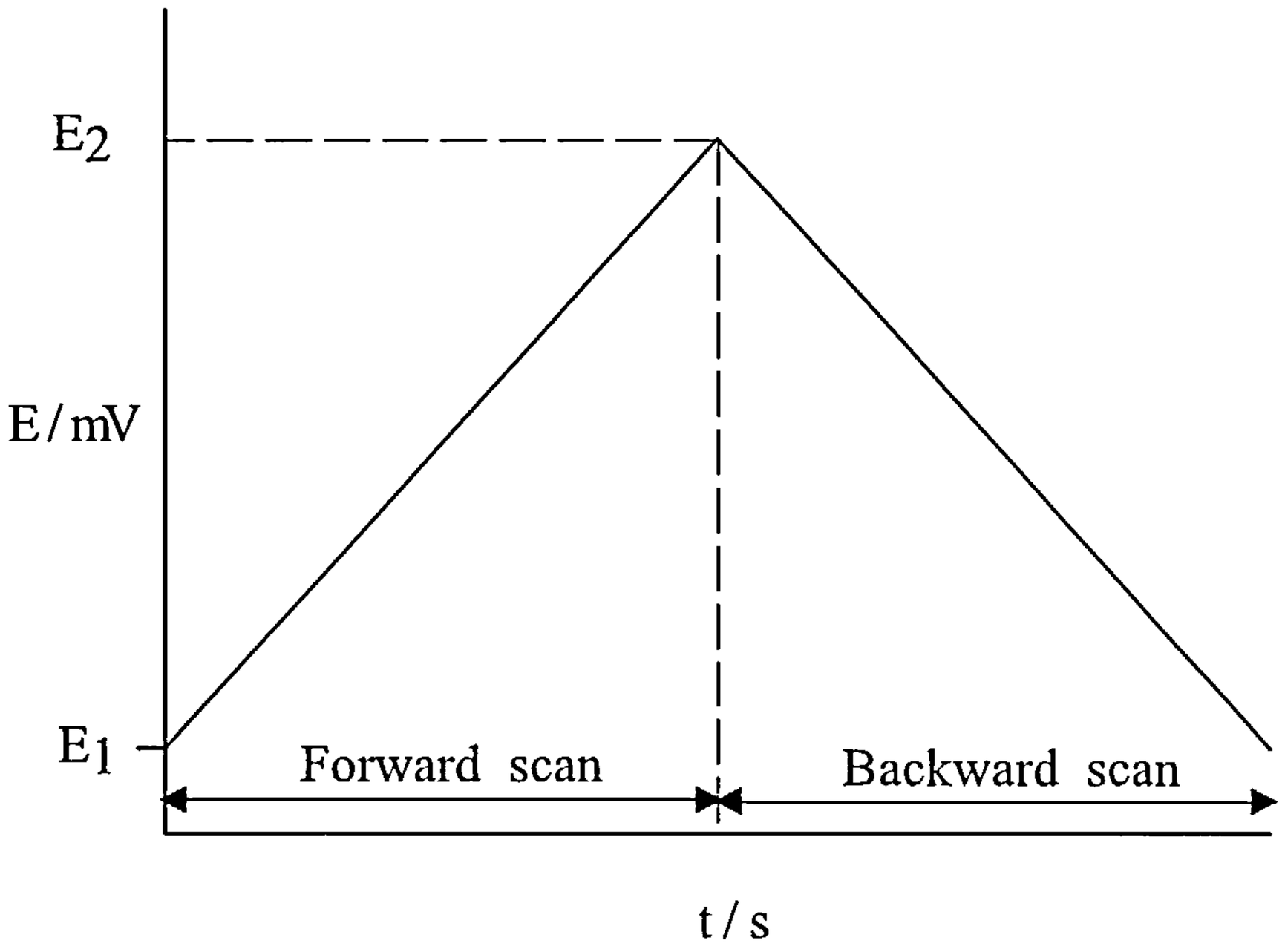

Appendix 1.vii : Typical current - potential voltammogram for CV

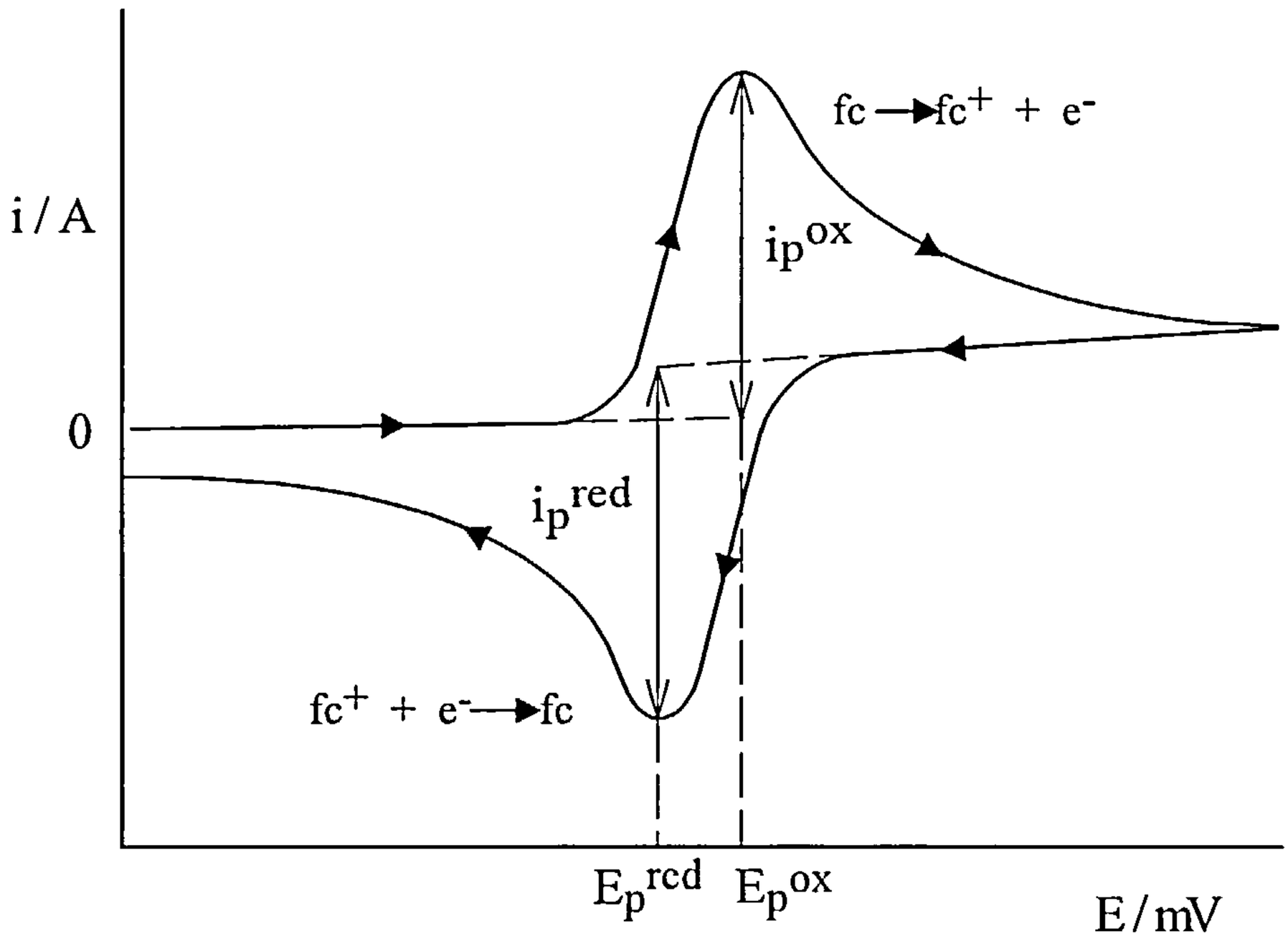

Appendix 1.viii : Potential waveform for a potential step experiment

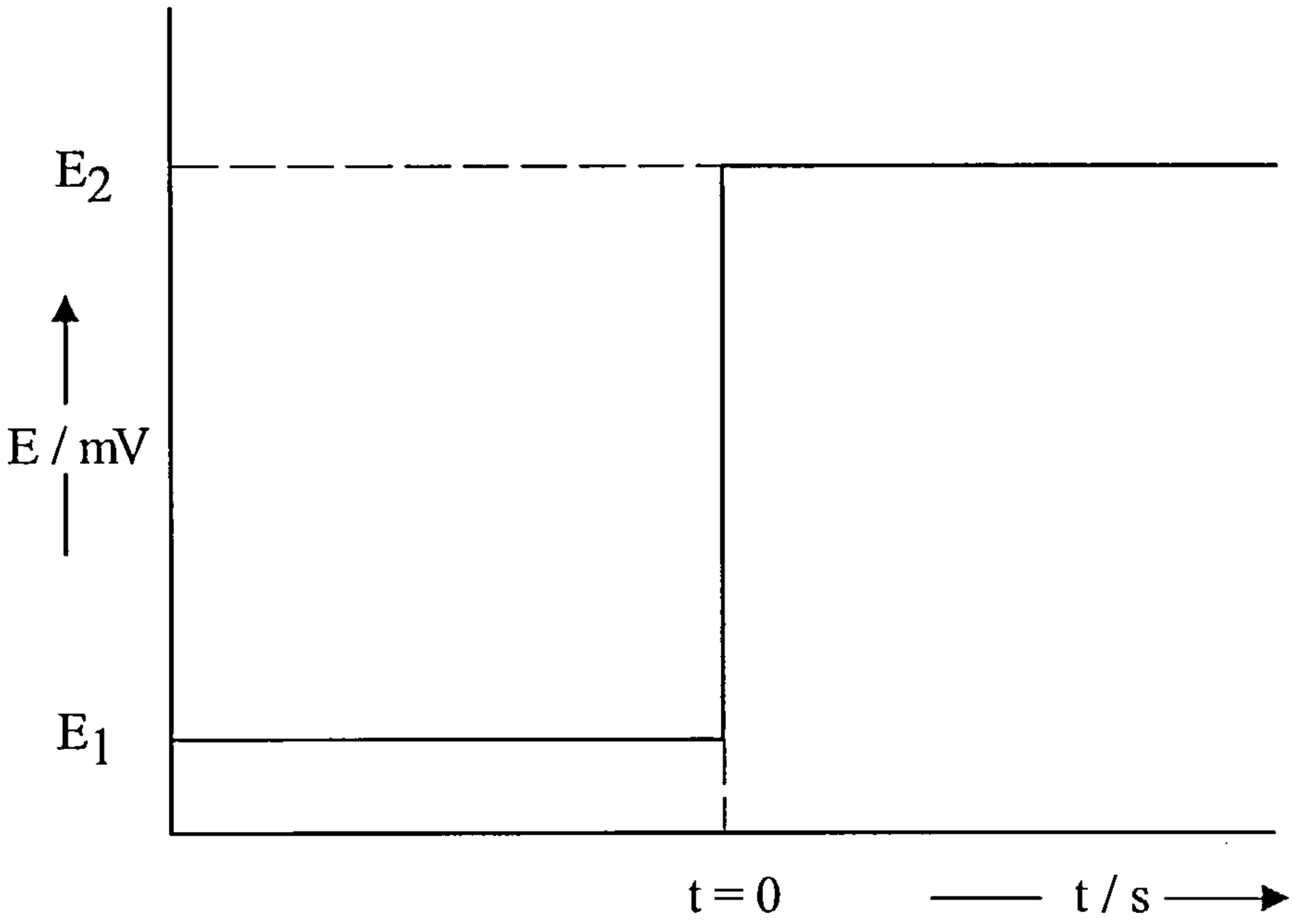

Appendix 1.ix : Variation of current response with time for a potential step experiment

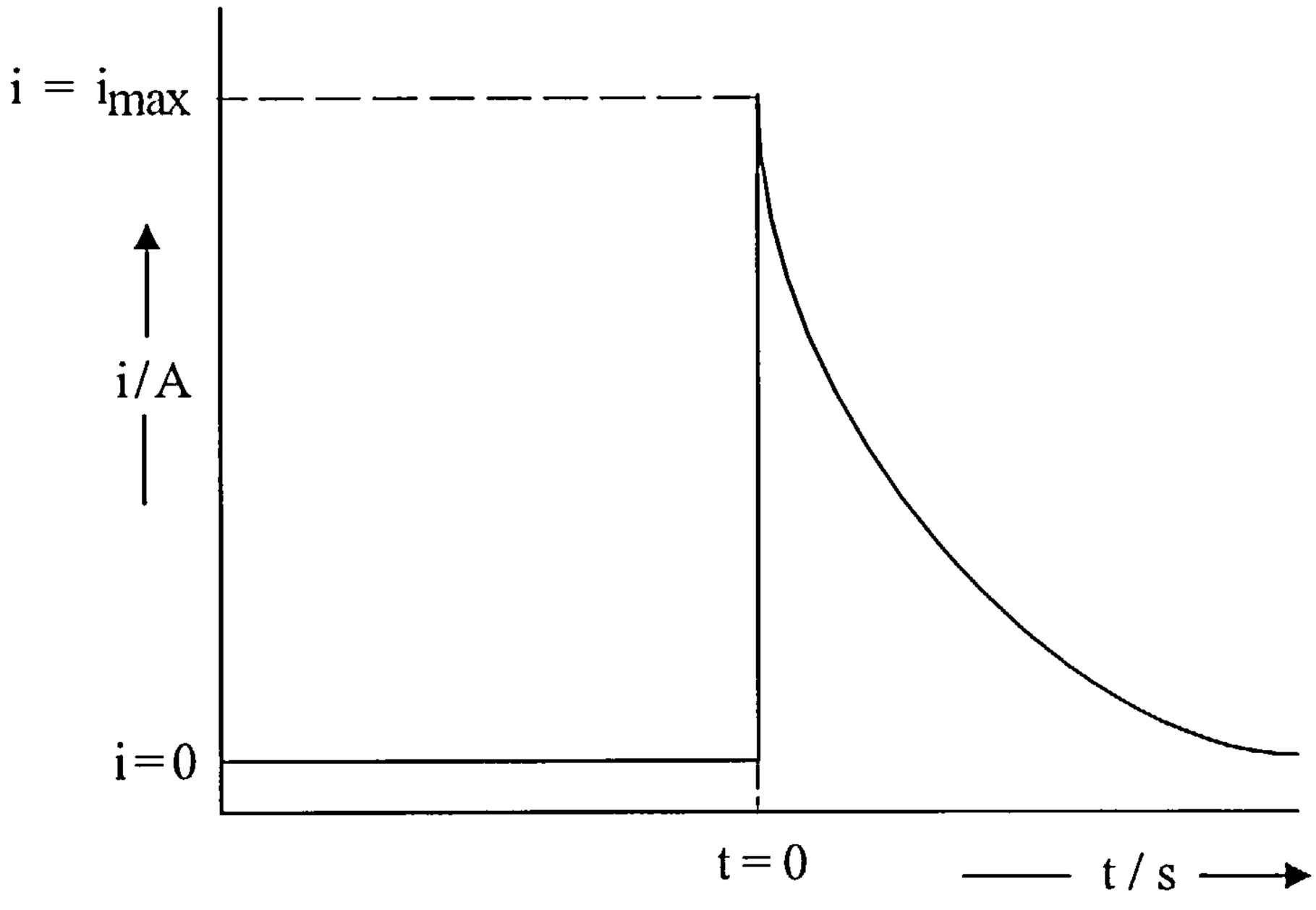

Appendix 1.x : Concentration profile and diffusion layer thickness after a potential step

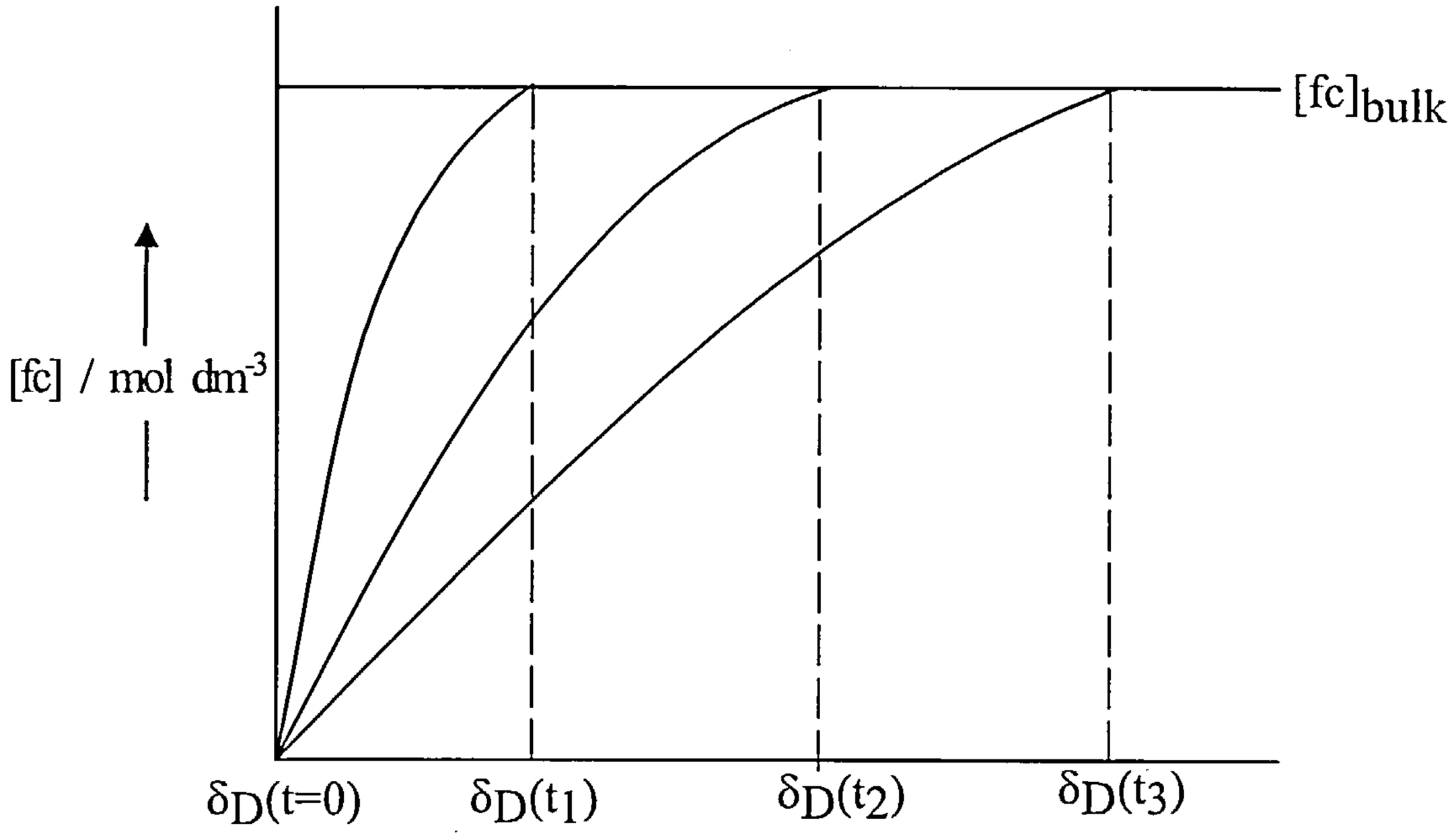

Appendix 1.xi : Variation of current with time after a potential step

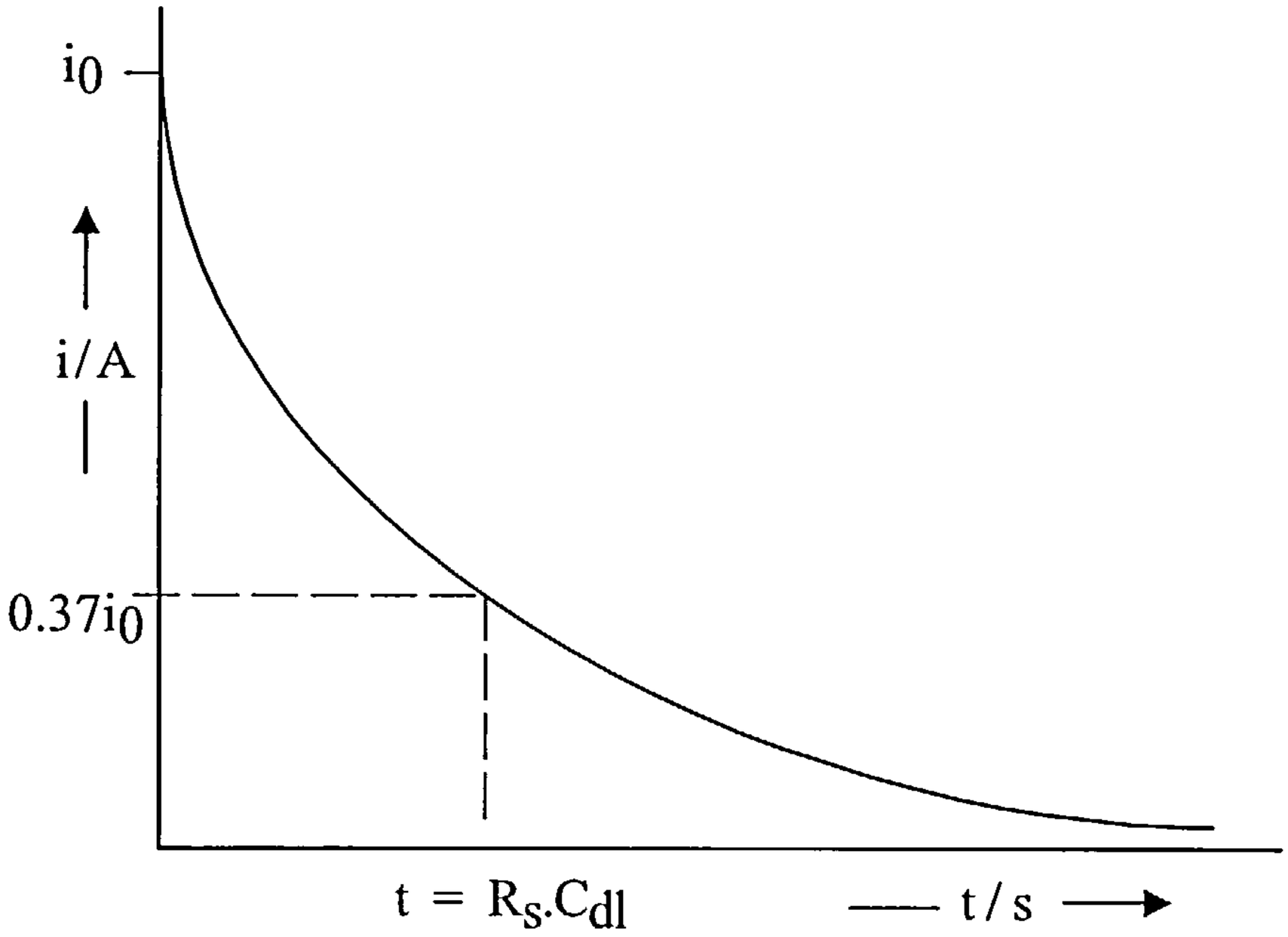

Appendix 1.xii : Transition from planar to (hemi) spherical diffusion at (a) short times and (b) long times for a microelectrode

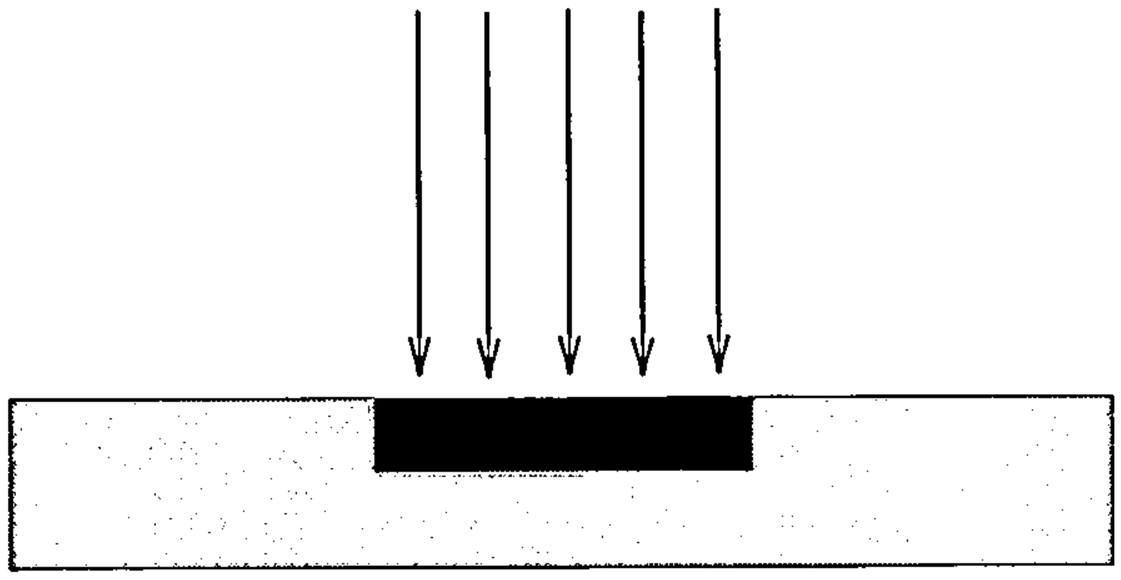

(a) Planar diffusion at short times

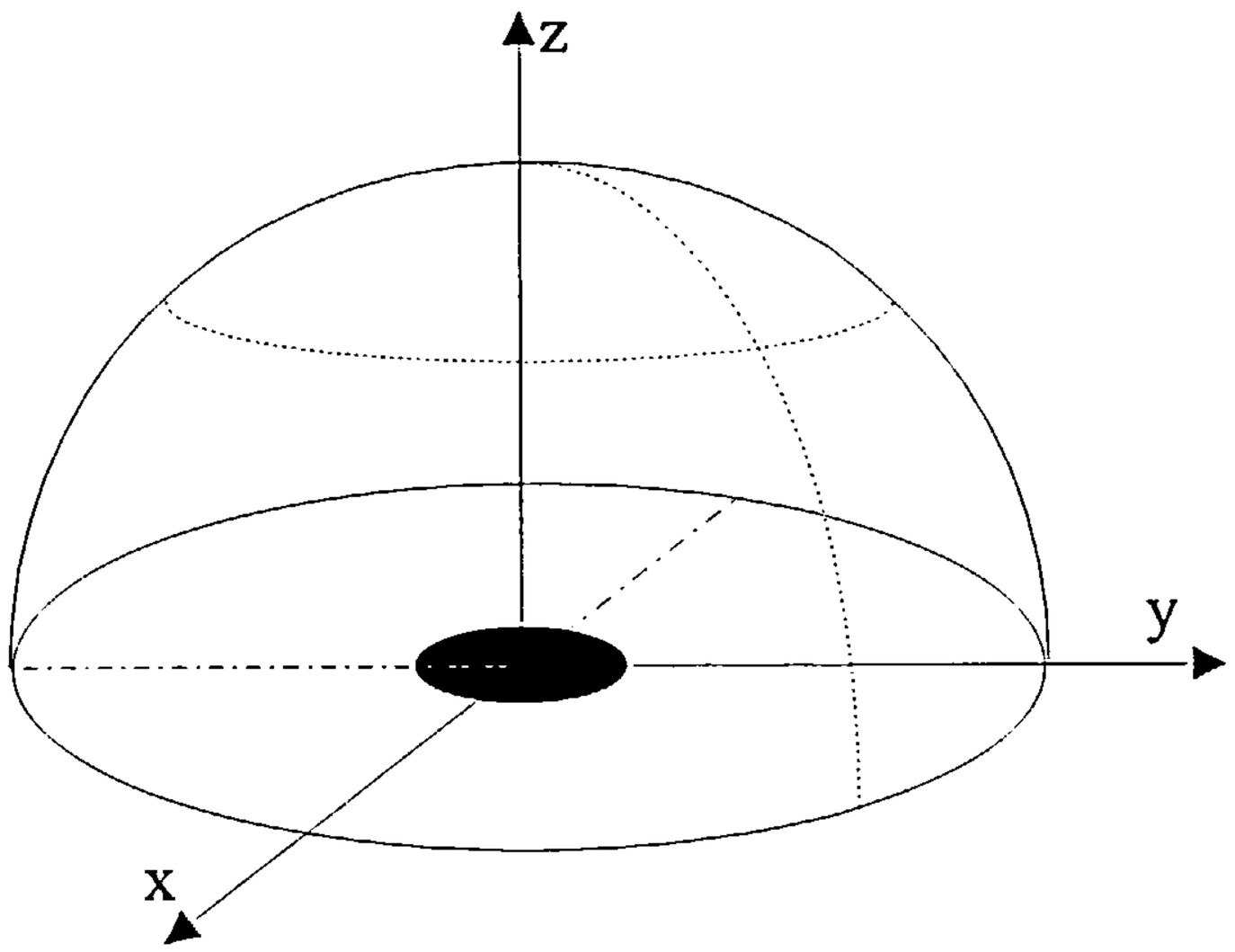

(b) (Hemi) spherical diffusion at long times

Introduction (Ch. 1) References :

1. M.J.Rosen, *Surfactants and Interfacial Phenomena*, J. Wiley & Sons, New York, 1989.

2. *Physics of Amphipiles: Micelles, Vesicles and Microemulsions,* (eds. V.Degiorgio, M.Corti), Societa Italiana di Fiscia, Bologna, 1985.

3. B.Jonsson, B.Lindman, K.Holmberg, B.Kronberg, *Surfactants and Polymers in Aqueous Solution*, J. Wiley & Sons, U.K., 1998.

4. C.Tanford, *The Hydrophobic Effect*, J. Wiley & Sons, New York, 1980.

5. P.Molyneux, C.T.Rhodes, J.Swarbrick, *Trans. Faraday Soc.*, 1965, vol. 61, p. 1043.

6. K.Shinoda, *Bull. Chem. Soc. Japan*, 1953, vol. 26, p. 101.

7. M.E.Hobbs, *J. Phys. Colloid Chem.*, 1951, vol. 55, p. 675.

8. M.L.Corrin, W.D.Harkin, *J. Am. Chem. Soc.,* 1947, vol. 69, p. 684.

9. K.Shinoda, T.Yamaguchi, R.Hori, *Bull. Chem. Soc. Japan*, 1965, vol. 38, p. 373.

10. K.Tori, T.Nakagawa, *Kolloid-Z. Z. Polym.*, 1963, vol. 189, p. 50.

11. A.Ray, G.Nemethy, *J. Am. Chem. Soc.*, 1971, vol. 93, p. 6787.

12. H.B.Klevens, *J. Am. Oil Chem. Soc.*, 1953, vol. 30, p. 74.

13. J.H.Fendler, *Chem. Rev.*, 1987, vol. 87, p. 877.

14. J.H.Fendler, *Membrane Mimetic Chemistry*, J. Wiley & Sons, New York, 1982.

15. L.M.Kushner, W.D.Hubbard, *J. Phys. Chem.*, 1954, vol. 58, p. 1163.

16. P.Debye, *Ann. N.Y. Acad. Sci.*, 1949, vol. 51, p. 755.

17. N.A.Mazer, *Dynamic Light Scattering, applications of photon correlation spectroscopy*, Ch. 5, R.Pecora (Ed.), Plenum Press, New York, 1985.

18. P.N.Pusey, R.J.Tough, *Dynamic Light Scattering, applications of photon correlation spectroscopy*, Ch. 4, R.Pecora (Ed.), Plenum Press, New York, 1985.

19. L.Cantu, M.Corti, V.Degiorgio, *Europhysics Letters*, 1986, vol. 2, p. 673.

20. V.Degiorgio, L.Cantu, M.Corti, R.Piazza, A.Rennie, *Colloids and Surfaces*, 1989, vol. 38, p. 169.

21. D.F.Nicoli, R.B.Dorshow, *Physics of Amphipiles: Micelles, Vesicles and Microemulsions,* (eds. V.Degiorgio, M.Corti), Societa Italiana di Fiscia, Bologna, 1985, p. 429.

22. A.Rohde, E.Sackmann, *J. Phys. Chem.,* 1980, vol. 84, p. 1598.

23. M.Corti, V.Degiorgio, *J. Phys. Chem.,* 1981, vol. 85, p. 711.

24. R.B.Dorshow, C.A.Bunton, D.F.Nicoli, *J. Phys. Chem.*, 1983, vol. 87, p. 1409.

25. E.Dickinson, *Ann. Rev. Prog. Chem.*, 1983, (c), p. 3.

26. M.Y.Lin, H.J.M.Hanley, S.K.Sinha, G.C.Straty, D.G.Peiffer, M.W.Kim, *Physica B*, 1995, vol. 213&214, p. 617.

27. P.G.Cummins, E.Staples, J.B.Hayter, J.Penfold, *J. Chem. Soc. Faraday Trans. 1*, 1987, vol. 83, p. 2773.

28. J.Penfold, E.Staples, A.K.Lhodi, I.Tucker, *Int. Journal of Thermophys.*, 1995, vol. 6, p. 1109.

29. J.Penfold, E. Staples, P.G.Cummins, *Adv. In Colloid and Int. Sci.*, 1991, vol. 34, p. 451.

30. P.S.Goyal, S.V.G.Menon, B.A.Dasannacharya, V.Rajagopalan, *Chem. Phys. Letters*, 1993, vol. 211, p. 559.

31. V.K.Aswal, P.S.Goyal, S.V.G.Menon, B.A.Dasannacharya, *Physica B*, 1995, vol. 213&214, p. 607.

32. A.B.Mandal, *Langmuir*, 1993, vol. 9, p. 1932.

33. R.Zana, R.A.Mackay, *Langmuir*, 1986, vol. 2, p. 109.

34. A.P.Doherty, K.Scott, *J. Chem. Soc. Faraday Trans.*, 1996, vol. 92, p. 4551

35. A.B.Mandal, B.U.Nair, *J. Phys. Chem.*, 1991, vol. 95, p. 9008.

36. T.Tominaga, M.Nishinaka, *J. Chem. Soc. Faraday Trans.*, 1993, vol. 89, p. 3459.

37. R.E.Verrall, S.Milioto, A.Giraudeau, R.Zana, *Langmuir*, 1989, vol. 5, p. 1242

38. J.F.Rusling, *Electroanal. Chem, A Series of Advances*, A.J.Bard (Ed), vol. 18, Dekker, New York, 1993.

39. M.J.Eddowes, M.Gratzel, *J. Electroanal Chem.*, 1984, vol. 163, p. 31.

40. E.Hawlicka, *Chem. Soc. Reviews*, 1995, vol. 24, p. 367.

41. A.B.Mandal, B.U.Nair, D.Ramaswamy, *Langmuir*, 1988, vol. 4, p. 736.

42. K.Chokshi, S.Qutubuddin, A.Hussam, *J. Colloid and Int. Sci.*, 1989, vol. 129, p. 315.

43. Y.Ohsawa, A.Aoyagui, *J. Electroanal. Chem.*, 1982, vol. 136, p. 353.

44. J.Georges, S.Desmettre, *Electrochimica Acta*, 1984, vol. 29, p. 521.

45. A.P.Abbott, G.Gounili, J.M.Bobbitt, J.F.Rusling, T.F.Kumosinski, *J. Phys. Chem.*, 1992, vol. 96, p. 11091.

46. C.Beriet, D.Pletcher, *J. Electroanal. Chem.*, 1993, vol. 367, p. 93.

47. G.N.Kamau, T.M.Saccucci, G.Gounili, A-E.F.Nassar, J.F.Rusling, *Anal. Chem.*, 1994, vol. 66, p. 994.

48. J.F.Rusling, *Colloids and Surfaces A: Physicochemical and Engineering Aspects*, 1997, vol. 123-124, p. 81.

49. M.F.Ahmadi, J.F.Rusling, *Langmuir*, 1991, vol. 7, p. 1529.

50. S.Sun, R.L.Birke, J.R.Lombardi, *J. Phys. Chem.*, 1990, vol. 94, p. 2005.

51. S.Manne, J.P.Cleveland, H.E.Gaub, G.D.Stucky, P.K.Hansma, *Langmuir*, 1994, vol. 10, p. 4409.

52. Southampton Electrochemistry Group, *Instrumental Methods in Electrochemistry*, Ellis Horwood Ltd., Chichester, 1985.

53. M.J.Sparnaay, *The Electrical Double Layer*, Pergamon Press, 1972.

54. P.W.Atkins, *Physical Chemistry*, Oxford University Press, Oxford, 1985.

55. A.J.Bard, L.R.Faulkner, *Electrochemical Methods*, J. Wiley & Sons, New York, 1980.

56. Y.V.Pleskov, V.Y.Filinovski, *The Rotating Disk Electrode*, Plenum Publishing, New York, 1976.

57. A.C.Fisher, *Electrode Dynamics*, Oxford University Press, U.K., 1996.

58. J.L.Atwood, J.E.D.Davies, D.D.Macnicol, F.Vogtle, (Eds.), *Comprehensive Supramolecular Chemistry*, Pergamon, U.K., 1996.

59. *Electrochemistry: Principles, Methods and Applications*, 1995, vol.2, no. 42, BAS E'CHEM Electrochemical Products Group.

60. P.Lemoine, Coord. *Chem. Revs.*, 1982, vol. 47, p. 55.

61. N.G.Connelly, W.E.Geiger, *Adv. Organomet. Chem.*, 1984, vol. 23, p. 1.

62. B.Tulyham, W.E.Geiger, *J. Am. Chem. Soc.*, 1985, vol. 107, p. 5960.

63. A.M.Bond, R.Colton, J.J.Jackowski, *Inorg. Chem.*, 1975, vol. 14, p. 274.

64. D.E.Weisshaar, D.E.Tallman, *Anal. Chem.*, 1983, vol. 55, p. 382.

65. P.Birkin, Private Communication.

66. W.T.Yap, L.M.Doane, *Anal. Chem.*, 1982, vol. 54, p. 1437.

67. M.Kakihana, H.Ikeuchi, G.P.Sato, K.Tokuda, *J. Electroanal. Chem.*, 1981, vol. 117, p. 201.

68. A.S.Baranski, W.R.Fawcett, C.M.Gilbert, *Anal. Chem.*, 1985, vol. 57, p. 166.

69. R.J.Forster, *Chem. Soc. Reviews*, 1994, vol. 24, p. 289.

70. J.Heinze, Angew. *Chem. Ind. Ed. Engl.*, 1993, vol. 32, p. 1268.

71. A.M.Bond, *Analyst*, 1994, vol. 119, p. R1.

72. K.Aoki, *Electroanalysis*, 1993, vol. 5, p. 627.

73. J.C.Hoogvliet, C.M.B. Van Den Beld, C.J.Van Der Poel, W.P.Van Bennekom, *J. Electroanal. Chem.*, 1986, vol. 201, p. 11.

74. J-X.Feng, M.Brazell, K.Renner, R.Kasser, R.N.Adams, *Anal. Chem.*, 1987, vol. 59, p. 1863.

75. F.Magno, I.Lavagnini, *Analytica Chimica Acta*, 1995, vol. 305, p. 96.

76. A.Fitch, D.H.Evans, *J. Electroanal. Chem.*, 1986, vol. 202, p. 82.

77. J.D.Norton, H.S.White, B.D.Pendley, H.D.Abruna, *Anal. Chem.*, 1991, vol. 63, p. 1909.

78. T.Abe, K.Itaya, I.Uchida, K.Aoki, K.Tokuda, *Bull. Chem. Soc. Japan*, 1988, vol. 61, p. 3417.

79. "*More Solutions to Sticky Problems*", Brookfield Engineering Lab. Inc., MA, U.S.A.

Chapter 2: Experimental

This chapter will provide all the information needed for the accurate and reproducible experimental determination of micellar self-diffusion coefficients. This will include the experimental apparatus and conditions appropriate to each electrochemical technique. Although the procedures to obtain self-diffusion coefficients is relatively simple, care must be taken to adhere strictly to the same routine each time to ensure reproducibility. The analytical solution preparation will be described as well as the preliminary experiments that must be completed prior to the measurement of self-diffusion coefficients.

2.1 Electrochemical Techniques

2.1.1 The Three Electrode Cell

For both cyclic voltammetry and rotating disk voltammetry a standard three electrode cell is used. This consists of a working (WE), reference (RE) and counter (CE) electrode. The potential of the working electrode (E_W) is maintained relative to the reference electrode potential (E_R) so that $\Delta E = E_W - E_R$. It is this potential difference (ΔE) form which the current response is measured. The reference electrode is connected at a high resistance point in the potentiostat to reduce current flow through this electrode and divert it via the counter electrode.

The working electrode consists of a 7 mm diameter glassy carbon disk in an epoxy shroud (Sycopel). Prior to each experiment the electrode is polished with 0.015 μm alumina slurry on a felt disk and then rinsed with distilled water. This ensures that any surface impurities are removed before immersion in the test solution.

The reference electrode was a standard silver / silver chloride (Ag / AgCl) electrode obtained from S.H.Scientific. A silver wire is coated in AgCl and immersed in a saturated KCl solution leading to the reaction $AgCl + e^- \leftrightarrow Ag + Cl^-$ with a standard electrode potential (E^O) = 0.222mV vs. SHE @25 ^oC[1]. Silver / silver chloride is an excellent reference electrode as it is easy to maintain and has a low temperature coefficient[2] i.e. E^O varies by only a small extent with a change in temperature. When not in use, the electrode was stored in a 1.0 mol dm^{-3} KCl solution. The counter electrode was a strip of platinum gauze which was flamed prior to each experiment to remove any surface impurities.

As was mentioned earlier (Ch. 1.3.2) the effect of solution resistance can be reduced by using a high concentration of supporting electrolyte or by positioning the reference electrode close to the working electrode. This problem is overcome by using a luggin capillary, at a distance $\geq 2d$ away from the surface, where d is the capillary diameter. It has been shown that such an arrangement is sufficient for electrochemical measurements[3]. Nevertheless, for CV experiments it is advantageous to further reduce any residual uncompensated solution resistance and this is achieved by utilising the iR compensation method on the BAS CV-50W. This method has two separate stages, the measurement of the uncompensated resistance and then the compensation / circuit stability testing. The method assumes that the electrochemical cell is equivalent to an RC circuit, and a 50 mV potential step is applied around the test potential (0 ± 25 mV) where no Faradaic processes are occurring. The resultant exponential current decay leads to a value for R_U. This is compensated for by using positive feedback into the potentiostat[4].

Each voltammetric measurement is temperature controlled by surrounding the solution with thermostatically controlled water jacket. To prevent any unintentional oxidation of the ferrocene care was taken to ensure that there was a constant flow of N_2 across the solution surface ('N_2 blanket').
The full experimental arrangement is shown in Appendix 2.i.

2.1.2 Rotating Disk Voltammetry

The theory to rotating disk voltammetry has been described in detail in Ch. 1.3.1, and the electrochemical cell introduced in Ch 2.1.1.

The electrode potential was scanned from 0 - 500 mV and back to 0 mV with the resulting Faradaic current for the ferrocene / ferricinium redox couple recorded. This was carried out over a number of electrode rotation rates (ω = 2-12 Hz) and the apparent limiting current (i_{app}) from the sigmoidal plots measured. Each apparent limiting current measured was corrected for the finite amount of ferrocene in the aqueous phase. Using values[5] of $D = 10.5 \times 10^{-6}$ cm^2 s^{-1} and $C_O = 1 \times 10^{-5}$ mol dm^{-3} in the Levich equation gave values for the current due to aqueous phase ferrocene (i_{aq}). Subtracting i_{aq} these values from those of i_{app} gave values for the true limiting currents (i_{Lim}). Corrections of this sort have been carried out previously by Doherty et al.[6] and Mandal et al.[5]. The true limiting currents are then used in the Levich equation (Ch. 1.3.1, Equation 1.17)

It follows that for a reversible one electron reaction, a plot of the i_{Lim} against $\omega^{1/2}$ will yield a straight line with a (0,0) intercept. From the gradient of the line the diffusion coefficient (D_{RDV}) is determined.

2.1.3 Cyclic Voltammetry

The electrochemical cell system was the same as used for RDV (Ch 2.1.2) and has been previously described in Ch 2.1.1. In the hydrodynamic experiments the potentiostat used was a Sycopel AEW2, whereas in this case a BAS CV-50W was utilised. This allowed the use of the iR compensation function which ensured that the voltammograms were unaffected by uncompensated solution resistance, although this was already low due to the use of the luggin capillary.

The applied potential is ramped from 0 - 500 mV and back to 0 mV at a set potential sweep rate (υ). The resultant voltammogram allows the measurement of the apparent peak currents (i_{app}) for the ferrocene / ferricinium redox couple. As for RDV the

peak currents are corrected for aqueous phase ferrocene yielding the true peak currents (i_P) By monitoring the peak anodic current as a function of $\upsilon^{1/2}$ a plot can be constructed in accordance with the Randles - Sevcik equation (Ch. 1.3.2, Equation 1.22)

It follows that a graph of i_P against $\upsilon^{1/2}$ will yield a linear plot with a (0,0) intercept, characteristic of a diffusion controlled reversible one electron process, and from which the diffusion coefficient (D_{CV}) can be determined.

2.1.4 Chronoamperometry

In contrast to CV and RDV in which a 3-electrode cell was used, chronoamperometry (CA) utilised a 2-electrode cell. The working electrode was a 0.0707 cm^2 glassy carbon disk shrouded in a plastic rod from BAS Bioanalytical Systems Inc. A miniature Ag / AgCl reference electrode was constructed by using a silver wire immersed in a saturated AgCl solution with a porous ceramic frit. The electrochemical cell was contained inside a Faraday cage connected to a Sycopel AEW2 potentiostat. As was described earlier (Ch. 1.3.3), one of the most important factors in chronoamperometric measurements is the attainment of a consistent current response. Measurements immediately after the electrodes were immersed in the solution showed that the magnitude of the Faradaic current was gradually reduced until a consistent response was observed after 5 minutes. Therefore, immersing both electrodes in the solution for 5 minutes prior to experimentation ensured reproducible current profiles.

For each experiment the electrode is held at 0 mV for 10 s before the application of a potential step (0 - 500 mV) which causes the current to rise sharply (theoretically to an infinite value) and subsequently decay as a function of $t^{-1/2}$ according to the Cottrell equation (Ch. 1.3.3, equation 1.24).

For each electrolyte concentration considered a background trace was recorded for the micellar solution without ferrocene. This was then subtracted from the actual experimental trace (with ferrocene) to ensure that the difference was due

to the ferrocene oxidation alone. Correction using background currents was necessary since significant capacitance currents were evident in both CTAC and TX-100 solutions (vide infra). As for both RDV and CV the currents are corrected for aqueous phase ferrocene.

A plot of the resultant current (i_{tr}) against $t^{-1/2}$ yields a gradient from which the diffusion coefficient (D_{CA}) is determined. The gradient of this plot is only linear over a certain time window which will be shown to be 2 - 5 s (Ch. 3C.2.3, 4C.2.4)

A smaller electrode was used (A = 0.0707 cm^2) than that in RDV and CV (A = 0.3848 cm^2) due to the sensitive nature of the technique to capacitance. Electrical noise is also a large problem and for this reason a Faraday cage was used. This allowed the use of the 2-electrode cell.

2.1.5 Microelectrode

The small currents obtained from a microelectrode mean that the choice of electrochemical equipment is vital. A two electrode arrangement was used with both the working and reference electrode contained within a Faraday cage in conjunction with a Sycopel AEW 2 potentiostat.

The (quasi) reference electrode was a silver wire dip coated with $[Os(bipy)_2(PVP)_{10}Cl]Cl$ where bipy = 2,2'-bipyridyl and PVP = poly-4-vinylpyridine. This provided a reference potential of -150 mV vs. SCE in a test solution of 1.0 mol dm^{-3} KCl in water. A potential difference of ~0 mV between a $[Os(bipy)_2(PVP)_{10}Cl]Cl$ coated and uncoated silver wire indicates that the polymer is not actively involved in the electrode process but rather behaves as a protective layer. This will be discussed in more detail in Ch. 5.2.

The working electrode was a 11 μm diameter carbon fibre within a glass capillary obtained from BAS Analytical Ltd. The importance of preparing the working electrode surface will be discussed in Ch. 2.3.1. Prior to each experiment the electrode was polished using 0.015 μm alumina slurry on a glass plate, rinsed and sonicated in distilled water. This procedure was repeated twice and it was found that

this method gave reproducible voltammograms each time. In each case the electrochemical cell was thermostatically controlled at 25 ± 0.1 ^{O}C.

2.1.6 Rheology

A thermostatically (20 ^{O}C) controlled Brookfield DV-I cone and plate viscometer was used for each measurement. In accordance with the manufacturers guidelines[7] the viscometer was calibrated beforehand using distilled water and consistently gave η = 0.89 - 0.90 g cm^{-1} s^{-1} at 25 ^{O}C. Continuing calibration at regular intervals ensured that the integrity of the viscometer spindle was maintained i.e. was not distorted in any way. For each measurement a sample volume of 1.0 cm^3 was used and care taken to ensure the solution had reached equilibrium temperature before a reading was taken. The measurements were repeated twice using a fresh sample each time.

2.2 Solution Preparation

2.2.1 Triton X-100

For each of the electrochemical methods used the solutions were prepared in an identical fashion to ensure valid comparison of results. The Triton X-100 was obtained from Aldrich Chemicals and used without further purification. The electroactive probe, ferrocene, was from Koch-Light Laboratories Ltd.

Preparation was as follows:-

(1) The required amount of surfactant was pipetted into a 500.0 cm^3 volumetric flask. Due to the highly viscous nature of neat TX-100 a residual amount of surfactant remained on the inside of the pipette. Therefore, care was taken to ensure that all the TX-100 was added to the flask. This was achieved by pouring de-oxygenated deionised water into the pipette tube, placing a section of sealable

film over the top and allowing the tube to hang above the flask until such a time that the remaining surfactant had been dissolved. The sealable film was then removed and the solution allowed to drop into the flask. Double rinsing of the inside of the pipette further ensured that all TX-100 was transferred to the flask. This procedure vastly reduced any possible experimental errors due to concentration effects.

(2) The amount of ferrocene required to obtain a minimum ferrocene : micelle ratio of 1:1 was added. The reported values for aggregation numbers were used to determine the correct weight needed. An N_{agg} value of 100[8,9,10] was used although higher values of 140[11,12] have been cited. The lower value was used to ensure that a ratio ≥1:1 was obtained as a lower ratio has been found to result in statistically lower self-diffusion coefficients (CTAC - Ch. 4A.2.2.1).

(3) The volumetric flask was made up to 500.0 cm^3 with de-oxygenated doubly distilled water and left to magnetically stir in a darkened box overnight. The solutions were then used freshly for experimentation.

Table 2.1 : Quantities of solution components (in 500.0 cm^3 flask)

[TX-100] / mol dm^{-3}	Vol. TX-100 / cm^3	Vol. H_2O / cm^3	[fc] / mol dm^{-3}	Mass fc / g
0.033	10	490	$3.30x10^{-4}$	0.0311
0.100	30	470	$1.00x10^{-3}$	0.0932
0.167	50	450	$1.67x10^{-3}$	0.1553

2.2.2 CTAC

For each of the electrochemical methods solutions are prepared in a similar fashion to that of Triton X-100. CTAC was obtained from Aldrich Chemicals and used without further purification, ferrocene was from Koch-Light Laboratories Ltd. The lower viscosity of CTAC in comparison to Triton X-100 meant that preparation of each solution was easier. Whereas with TX-100 their was large residual amount of surfactant remaining in the inside of the pipette, this was not the case with CTAC. The required amount of CTAC was pipetted into a 500.0 cm^3 volumetric flask, with

the pipette rinsed with de-oxygenated distilled water to ensure that all the surfactant was transferred to the flask.

The required amount of ferrocene to ensure a ferrocene : micelle ratio of 1:1 was added., where [micelle] = [CTAC] / N_{agg}. A value for N_{agg} = 100 was used[13,14,15,16,17,18,19,20,21,22], any micellar growth leading to an increase in N_{agg} would ensure that the ratio was ≥ 1:1 as the [micelle] would drop proportionally. It will be shown in Ch. 4A.2.2.1 that if the ferrocene : micelle ration falls below unity, the diffusion coefficients will be lower. A ratio of ≥ 1:1 had no effect on the diffusion coefficient and therefore it is this region in which the CTAC experiments are carried out.

After the addition of ferrocene the volumetric flask was made up to 500.0 cm^3 with de-oxygenated doubly distilled water and left to magnetically stir in a darkened box overnight. The solutions were then used freshly for experimentation.

Table 2.2 : Quantities of solution components (in 500.0 cm^3 flask)

[CTAC] / mol dm^{-3})	Vol. CTAC / cm^3	Vol. H_2O / cm^3	[fc] / mol dm^{-3}	Mass fc / g
0.0313	20	480	$3.13x10^{-4}$	0.0291
0.0938	60	440	$9.38x10^{-4}$	0.0873
0.1563	100	400	$1.563x10^{-3}$	0.1455

2.2.3 Aerosol-OT

The system used for this study was AOT / iso-octane / H_2O, the reverse micelles of which contained ferricyanide $\{K_3Fe(CN)_6\}$ as an electroactive probe. Properties of iso-octane (2,2,4 - tri-methylpentane) have been shown to deviate only a small degree from those of n - alkanes[23,24]. This offered a greater range of references to which experimental data could be compared. Probe molecules such as ferrocyanide[25,26], methyl viologen[27], ferrocene[27] as well as ferricyanide[27,28] have

been used in microemulsions to obtain electrochemical data. Ferricyanide is selected in this case due to the high degree of reversibility and hydrophilicity such that no probe dissolves in the organic phase.

The reversed micellar system consisted of two component solutions; the aqueous and non-aqueous fractions. In the first solution, the required mass of AOT (BDH laboratory) was added to iso-octane (Sigma) and allowed to dissolve. The second solution contained the required amount of $K_3Fe(CN)_6$ (BDH analaR) in the known volume of distilled water in a separate 100.0 cm^3 flask. The AOT / iso-octane solution was then poured into the flask containing $K_3Fe(CN)_6$ / H_2O and made up to 100 cm^3 with iso-octane. The small volumes of water used (2.7 - 4.5 ml) meant that this procedure would eliminate any errors due to loss of water on transference. The resultant solution was shaken and sonicated until transparent which characterised a fully homogeneous mixture[29]. This method is often referred to as the phase transfer technique[30]. The solutions were always prepared freshly prior to experimentation.

Table 2.3 : Quantities of solution components (in 100.0 cm^3 flask)

Vol. Fraction (ϕ)	[AOT] / mol dm^{-3}	Mass AOT / g	[H_2O] / mol dm^{-3}	Vol. H_2O / cm^3
0.084	0.15	6.67	1.50	2.7
0.112	0.20	8.89	2.00	3.6
0.140	0.25	11.11	2.50	4.5

The mass of ferricyanide was varied at each volume fraction to allow the influence of probe concentration on micellar size to be assessed.

2.3 Considerations

2.3.1 Preparation of Working Electrode

The condition of the glassy carbon (GC) working electrode is of great importance when considering the current - voltage relationship in a voltammogram. In techniques such as RDV and CV the currents are generally in the micro-amp range due to the relatively large surface area (~0.3848 cm^2), whereas with both CA and microelectrode (μE) the electrode areas and hence the currents are smaller. Although it might be expected that the relative effects on the macro and microelectrode will be the same, it will be shown that the condition of the glassy carbon appears to influence CA and μE to a larger extent than RDV and CV.

There are two general approaches to the study of the electrode condition and activity. Firstly, to obtain consistent and reproducible voltammograms[26,31,32,33,34] and secondly to enhance the current response of the electrode[35,36,37,38,39,40]. So, it follows that the electrode surface must be treated in some way to ensure not only reproducible voltammograms but also stable hetereogeneous rate constants (k^O)[41]. k^O is affected by three main characteristics, surface roughness, surface cleanliness and the presence of surface functional groups[32,38]. Pre-treatment essentially alters the electrode by modifying the activity of the surface. Activation involves the removal of surface impurities such as metal oxides (from polishing material) and an increase in the number of surface groups that could be used for electron transfer[40].

A number of methods have been used for pre-treating electrodes including polishing[26,31,40], annealing[34] anodisation / cathodisation[37,41,42,43], and laser activation[38,39]. Each method has advantages and disadvantages[37], but for the ease of use it was decided that polishing would be the preferred method. A highly polished surface generally results in lower residual currents[32] and reduced noise levels[31]. Unfortunately many authors have seen that polishing leads to unstable surface behaviour and hence poorly defined voltammograms[31,32,33,34,38]. However, this is

likely to be due to adsorbed metal oxides on the surface which can significantly affect the electrochemical response of the electrode[32]. This problem can be overcome by ensuring that the electrode is sonicated in distilled water after polishing to remove any surface oxides[40]. Hu et al. obtained reproducible voltammograms using a series of polishing and rinsing steps[40] as follows:-

- Sonication in distilled water.
- Polishing with 0.015μm alumina slurry on a smooth glass plate.
- Sonication in distilled water.
- Repeat (x2).

It is this procedure which has been adopted for the experimental work with chronoamperometry (Ch. 3C.2.3, Ch. 4C.2.4) and microelectrode (Ch. 5). It must be noted, however, that the pre-treatment procedure may need to be modified for different system e.g. electrolyte, electroactive probe[31,35]. Studies in micellar systems using CA and μE are very limited and therefore comparisons between different systems cannot be made.

2.3.2 Calibration of Macroelectrode Area

For all electrochemical methods one of the most important variables that needs to be accurately known is the electrode area. A careful distinction must be made between the geometric and active surface area. The geometric area assumes that the surface is perfectly smooth and free of defects, but in reality a totally smooth surface is difficult to achieve. It is well established that increasing the roughness of the surface leads to a greater number of active sites on glassy carbon[32,38,40,44,45] which can be viewed as altering the effective surface area. It is therefore vital that this active surface area is determined prior to experimentation for highly accurate and reproducible results.

In order to determine the electrode area we need to calibrate the system with a well recognised redox couple with a known diffusion coefficient. For this purpose the ferricyanide / ferrocyanide couple ($K_3Fe(CN)_6$ / $K_4Fe(CN)_6$) was selected. This

species undergoes a simple reversible one electron reaction, with the diffusion coefficient of ferricyanide = 7.63×10^{-6} cm^2 s^{-1} in 1.0 mol dm^{-3} KCl ($25^{O}C$)[46,47,48].

A known mass of ferricyanide was dissolved in de-oxygenated distilled water containing 1.0 mol dm^{-3} KCl as the supporting electrolyte and made up to 200.0 cm^3. The concentration of ferricyanide (2.032×10^{-3} mol dm^{-3}) was such that a large measurable current would be obtained, thus increasing the experimental accuracy.

Rotating disk voltammetry was used to measure the limiting current (i_{lim}) as a function of electrode rotation rate (ω). The gradient of a plot of i_{lim} against $\omega^{1/2}$ is a function of, amongst other known terms, the electrode area and the diffusion coefficient. Therefore, using the known diffusion coefficient it is simple to determine the electrode area. Sigmoidal plots from RDV are shown in Appendix 2.ii and the resulting linear plot of i_{lim} against $\omega^{1/2}$ is shown in Appendix 2.iii.

Table 2.4 : Variation of limiting current with (electrode rotation rate)$^{1/2}$ for 2.032×10^{-3} mol dm^{-3} $K_3Fe(CN)_6$ + 1.0 mol dm^{-3} KCl

$\omega^{1/2}$ / $Hz^{1/2}$	10^4 i_{lim} / A
1.41	1.38
2.00	1.91
3.16	2.77
3.46	3.09
Gradient / $AHz^{-1/2}$	9.90×10^{-5}

From the Levich equation (Ch. 1.3.1, Equation 1.17), the gradient obtained from the above plot is:-

$$\text{Gradient} = 1.554.n.F.A.C_O.\nu^{-1/6}.D^{2/3} \qquad (2.1)$$

With the diffusion coefficient of ferricyanide = 7.63×10^{-6} cm^2 s^{-1}, and the kinematic viscosity (ν) of water = 1.005×10^{-2} cm^2 s^{-1} the electrode area (A) can be easily found.

$$\text{Gradient} = 2.560 \times 10^{-4}.A \qquad (2.2)$$

The electrode area is calculated as 0.3867 cm^2 which is in excellent agreement with that expected from a 7 mm diameter electrode i.e. 0.3848 cm^2. An error of less than 1% shows not only the precision of the glassy carbon electrode but also the ability of RDV to accurately determine diffusion coefficients. It also shows that the active surface area is very close to the geometric surface area.

2.3.3 Calibration of Microelectrode Area

It has been shown that for a macroelectrode the active surface area of a working electrode must be used in calculations rather than the geometric surface area. With a microelectrode the errors due to geometric area are more pronounced. For example, the microelectrode used in this study came with a manufacturers specification of diameter = 11 ± 2 μm, and so a difference between 9 - 13 μm is possible. Therefore, it was necessary to determine the real surface area from voltammetric measurements. It is known that the limiting current (i_{Lim}) of a microelectrode voltammogram varies linearly with probe concentration (C_O) by the well characterised equation where D_F is the calibrating ferricyanide probe diffusion coefficient[49,50,51]:-

$$i_{Lim} = 4.n.F.r.D_F.C_O \qquad (2.3)$$

Monitoring i_{Lim} as a function of C_O gave a linear plot the gradient of which led to the microelectrode radius (r). As for the macroelectrode calibration, ferricyanide was used the probe. A range of solutions in aqueous 1.0 mol dm^{-3} KCl were prepared with $[K_3Fe(CN)_6]$ = (0.528 - 3.031) x10^{-3} mol dm^{-3}. From knowledge of the ferricyanide diffusion coefficient[46,47,48] (D_F = 7.63x10^{-6} cm^2 s^{-1}) the radius is determined. Appendix 2.iv shows the voltammograms from which the limiting current is obtained, the resulting plot of i_{Lim} vs. $[K_3Fe(CN)_6]$ is shown in Appendix 2.v. From the gradient of Appendix 2.v, the radius was found to be 5.20 μm which was in excellent agreement with the manufacturers specification. The electrode area was tested throughout the range of experiments and was found to remain unchanged. Therefore, r = 5.20 μm was used for all further calculations.

Appendix 2.i : Electrochemical cell set-up for RDV and CV

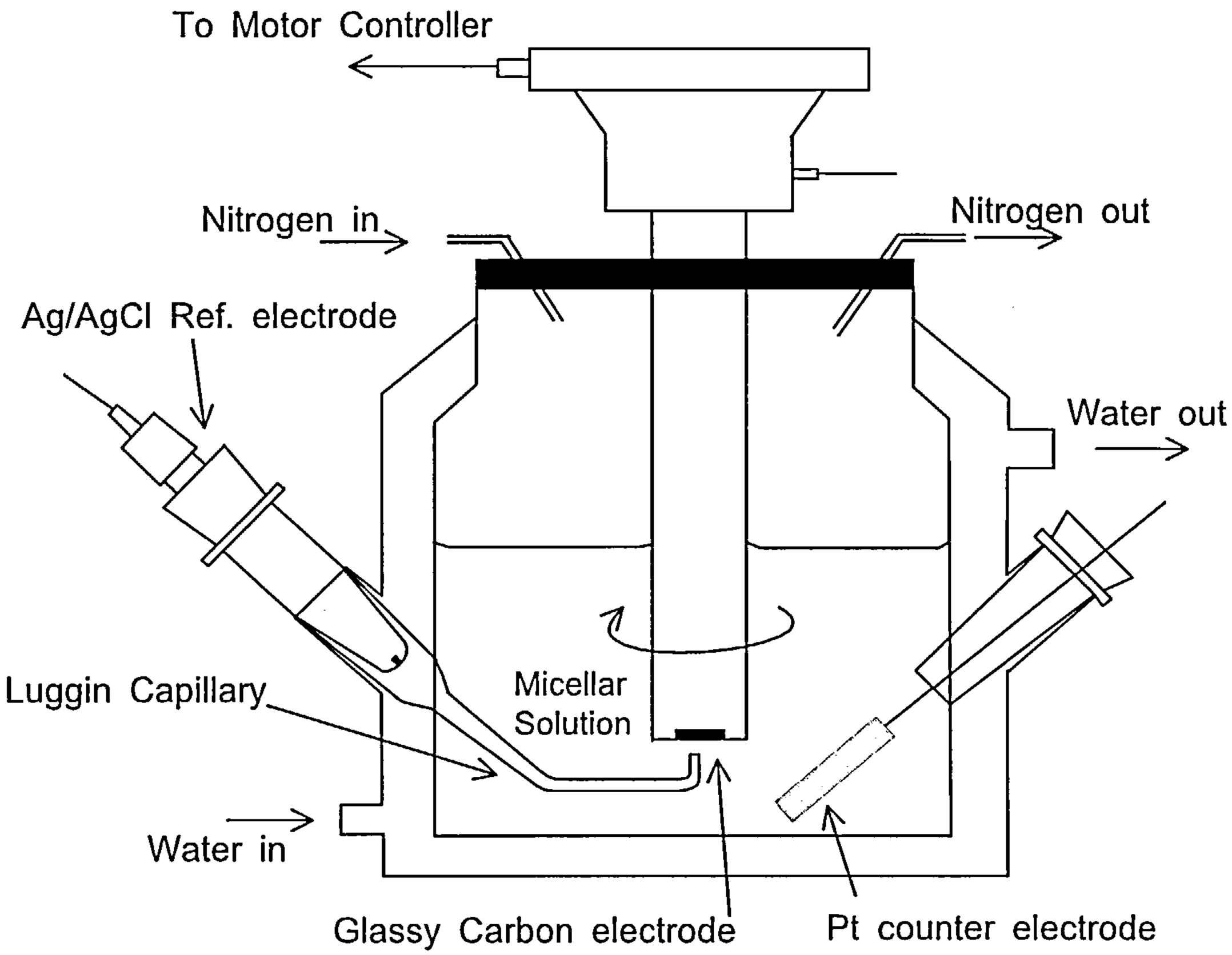

Appendix 2.ii : RDV plots of 2.032×10^{-3} mol dm^{-3} $K_3Fe(CN)_6$ + 1.0 mol dm^{-3} KCl for electrode area calibration

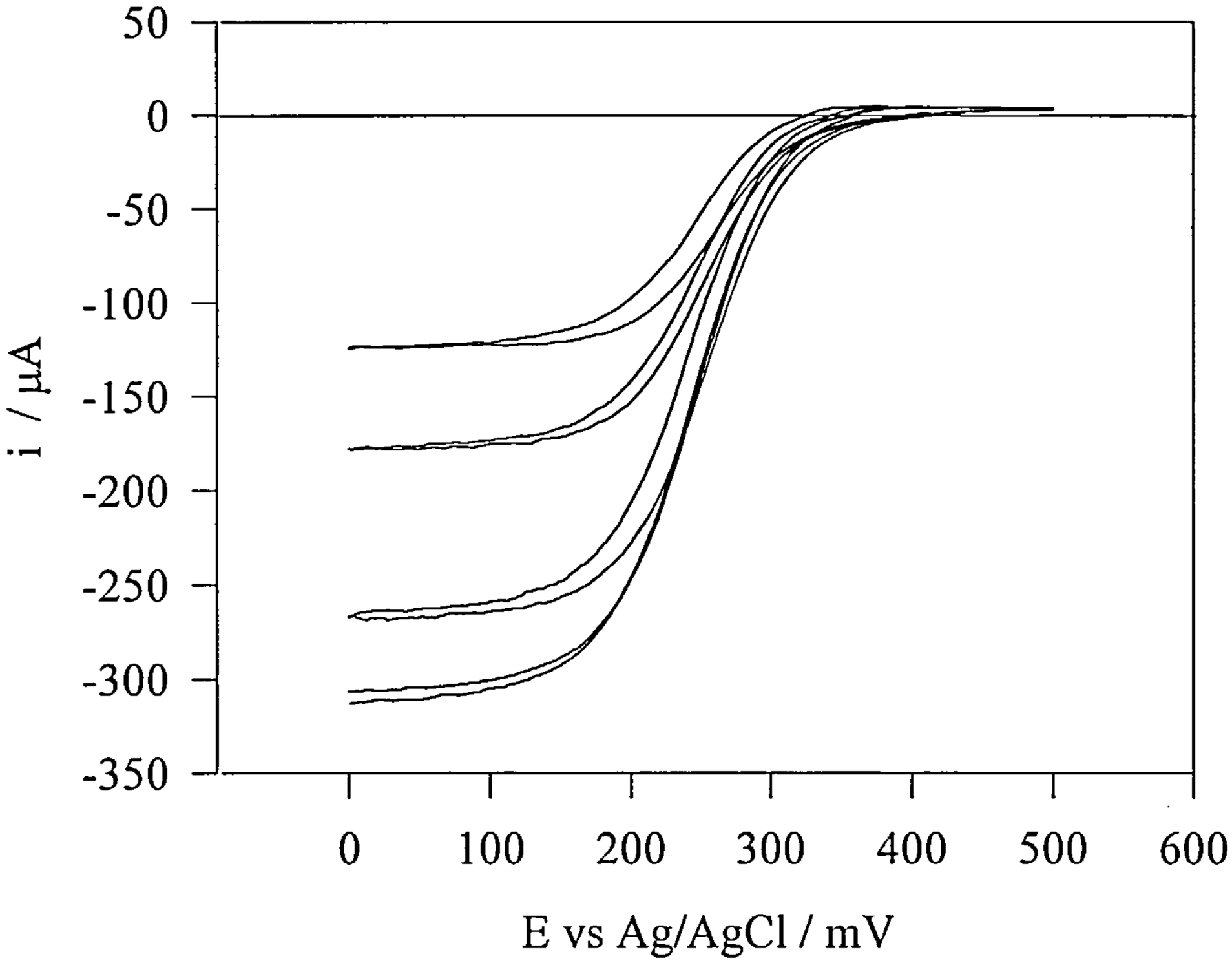

Appendix 2.iii : Variation of i_{Lim} with $\omega^{1/2}$ for RDV plots in Appendix 2.ii

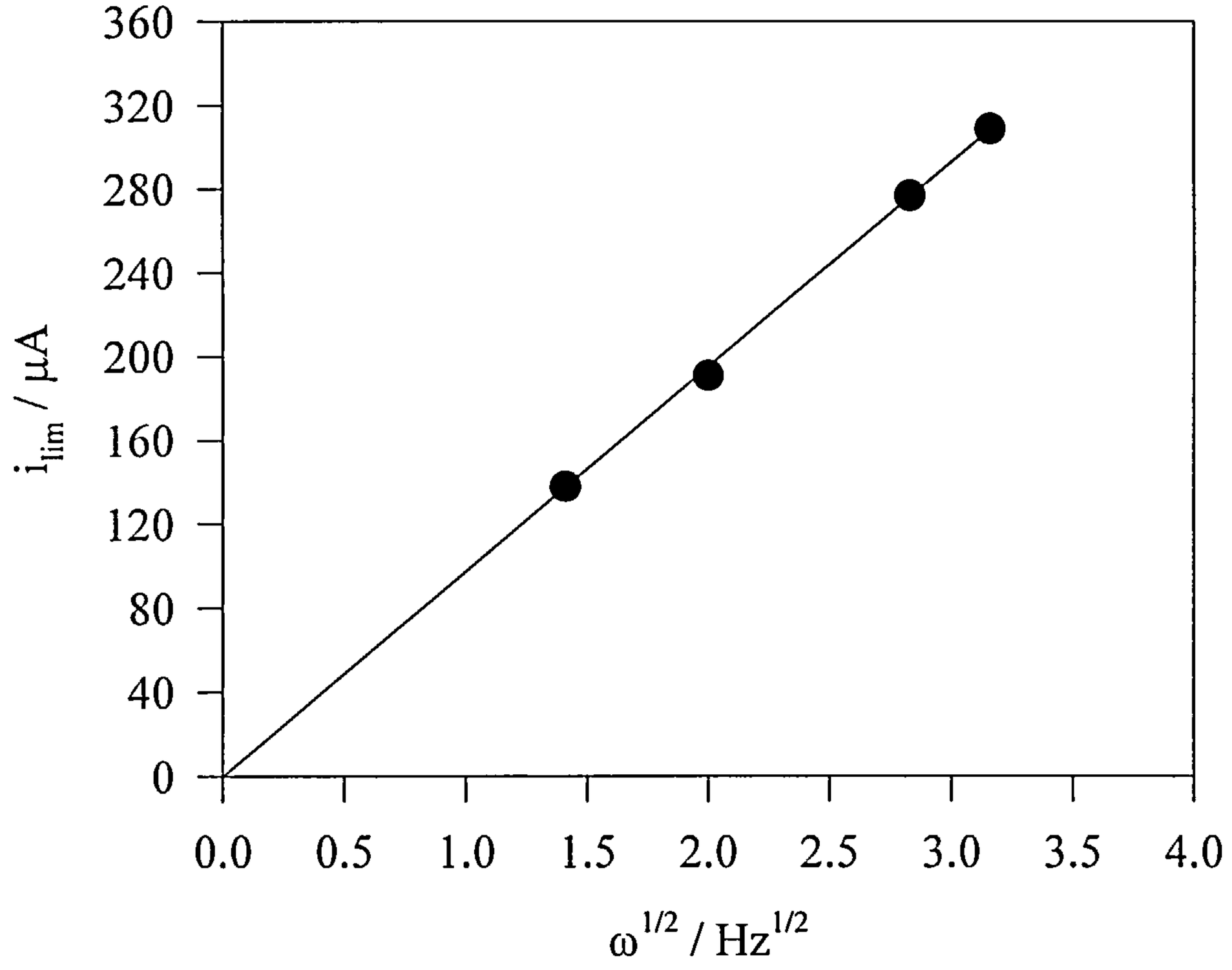

Appendix 2.iv : Voltammograms for calibration of microelectrode area

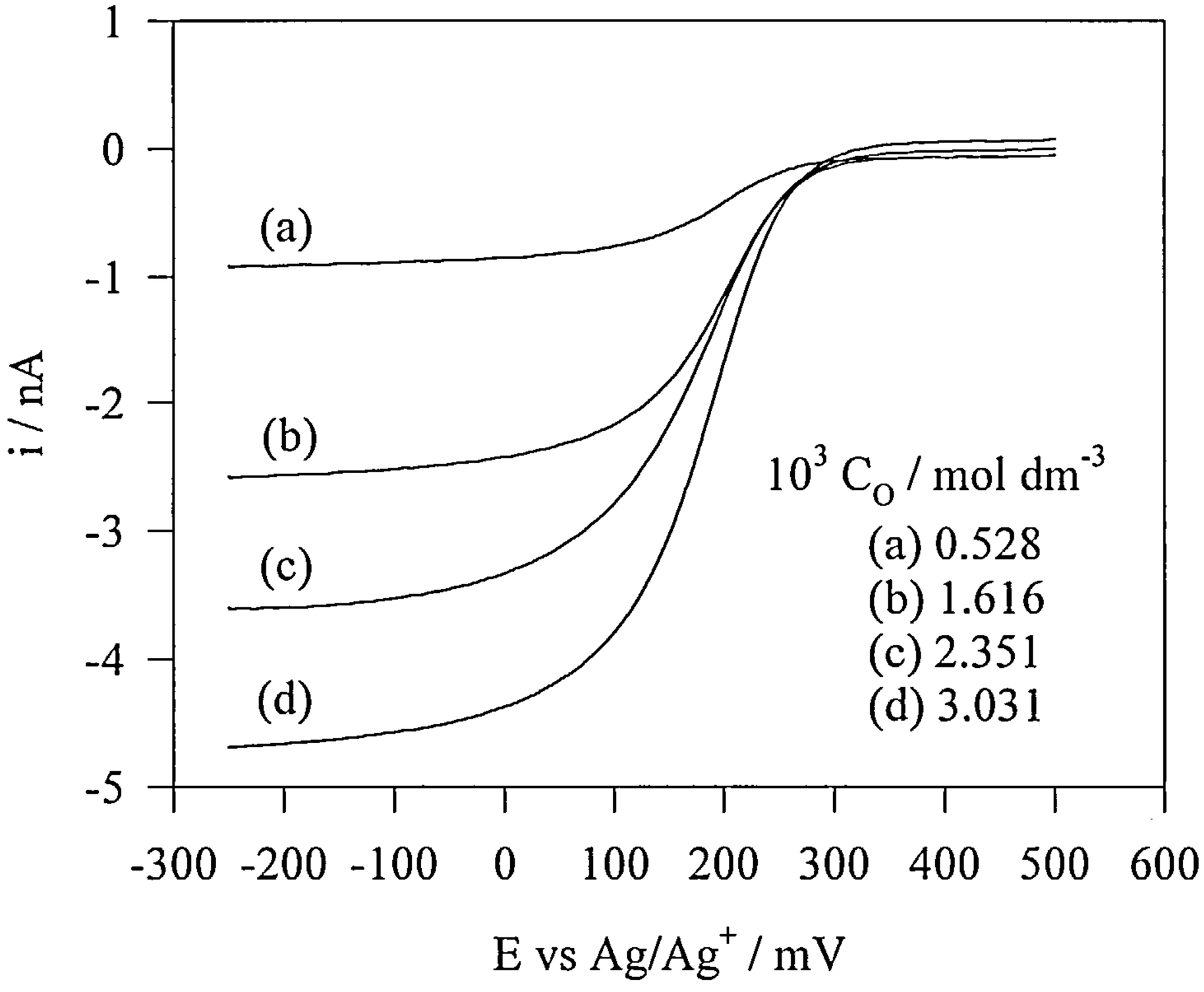

Appendix 2.v : Calibration graph for microelectrode area determination

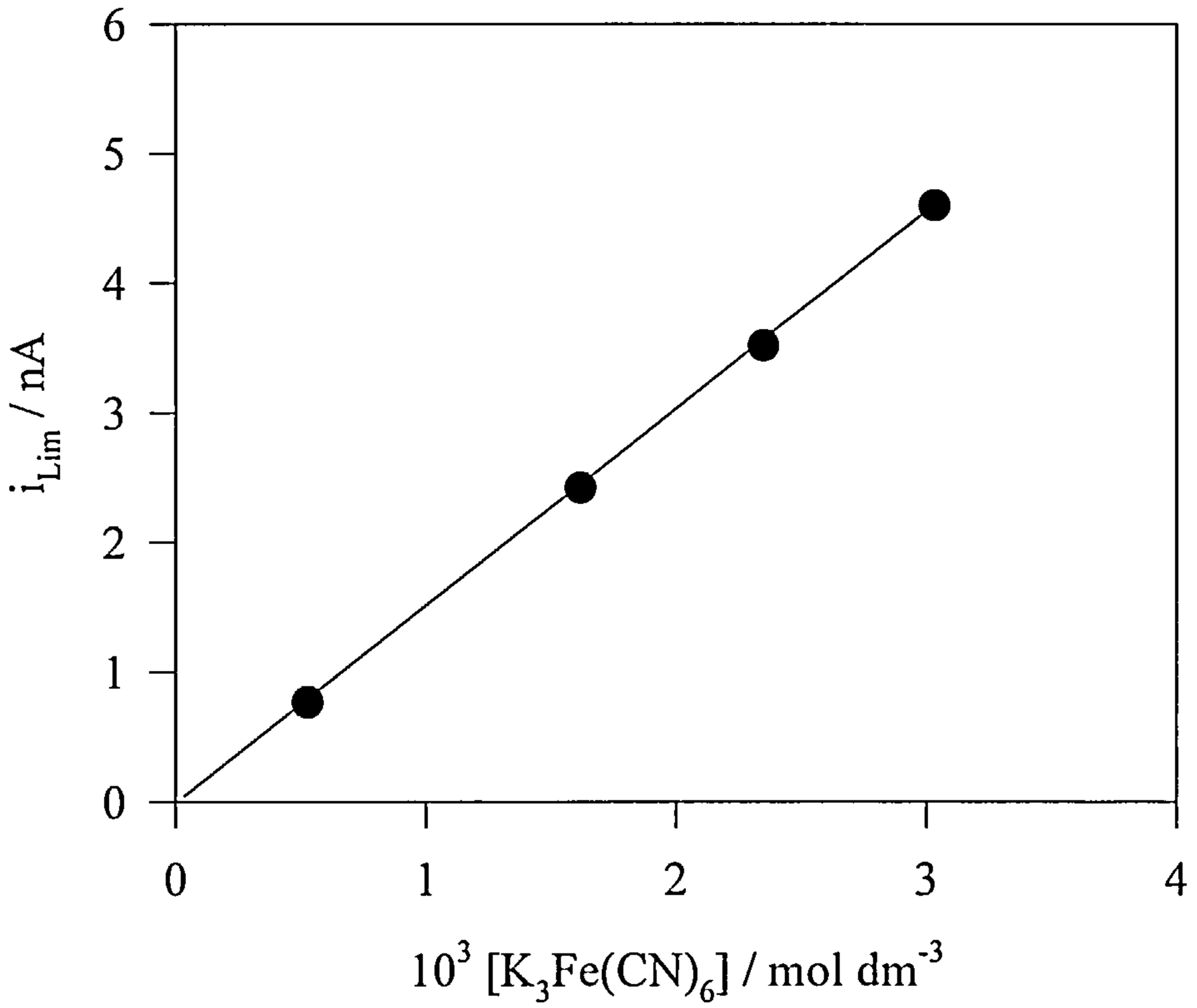

Experimental (Ch. 2) References :

1. J.L.Atwood, J.E.D.Davies, D.D.Macnicol, F.Vogtle, (Eds.), *Comprehensive Supramolecular Chemistry*, Pergamon, U.K., 1996.

2. A.J.Bard, L.R.Faulkner, *Electrochemical Methods*, J. Wiley & Sons, New York, 1980.

3. M.Sharp, *Electrochimica Acta*, 1983, vol. 28, p. 301.

4. BAS CV-50W Instruction Manual, Bioanalytical Systems Ltd., 1996.

5. A.B.Mandal, *Langmuir*, 1993, vol. 9, p. 1932.

6. A.P.Doherty, K.Scott, *J. Chem. Soc. Faraday Trans.*, 1996, vol. 92, p. 4551.

7. Brookfield Engineering Labs., *Operating Instructions*, Manual No. M/92-021-G895.

8. W.Brown, R.Rymden, J. van Stam, M.Almgren, G.Svensk, *J. Phys. Chem.*, 1989, vol. 93, p. 2512.

9. G.D.J.Phillies, J.Stott, S.Z.Ren, *J. Phys. Chem.*, 1993, vol. 97, p. 11563.

10. K.Streletzky, G.D.J.Phillies, *Langmuir*, 1995, vol. 11, p. 42.

11. L.M.Kushner, W.D.Hubbard, *J. Phys. Chem.*, 1954, vol. 58, p. 1163.

12. R.J.Robson, E.A.Dennis, *J. Phys. Chem.*, 1977, vol. 81, p. 1075

13. R.B.Dorshow, C.A.Bunton, D.F.Nicoli, *J. Phys. Chem.*, 1983, vol. 87, p. 1409.

14. A.Malliaris, J.Lang, R.Zana, *J. Phys. Chem.*, 1986, vol. 90, p. 655.

15. S.Reekmans, D.Bernik, M.Gehlen, J. van Stam, M. Van der Auweraer, F.C.De Schryver, *Langmuir,* 1993, vol. 9, p. 2289.

16. J.B.Hayter, J.Penfold, *Colloid and Polymer Sci.*, 1983, vol. 261, p. 1022.

17. D.F.Nicoli, R.B.Dorshow, *Physics of Amphipiles: Micelles, Vesicles and Microemulsions,* (eds. V.Degiorgio, M.Corti), Societa Italiana di Fiscia, Bologna, 1985, p. 429.

18. A.Malliaris, J.Le Moigne, J.Sturm, R.Zana, *J. Phys. Chem.*, 1985, vol. 89, p. 2709.

19. P.Lianos, M-L.Viriot, R.Zana, *J. Phys. Chem.*, 1984, vol. 88, p. 1098.

20. E.Roelants, F.C.De Schryver, *Langmuir*, 1987, vol. 3, p. 209.

21. A.Malliaris, J.Lang, R.Zana, *J. Chem. Soc. Faraday Trans.*, 1986, vol. 82, p. 109.

22. E.Roelants, E.Gelade, J.Smid, F.C.De Schryver, *J. Colloid and Int. Sci.,* 1985, vol. 7, p. 337.

23. E.Keh, B.Valeur, *J. Colloid and Polymer Sci.*, 1981, vol. 79, p. 465.

24. J.B.Peri, *J. Colloid and Int. Sci.*, 1969, vol. 29, p. 6.

25. A.B.Mandal, B.U.Nair, *J. Chem. Soc. Faraday Trans.*, 1991, vol. 87, p. 133.

26. K.Chokshi, S.Qutubuddin, A.Hussam, *J. Colloid and Int. Sci.*, 1989, vol. 129, p. 315.

27. R.A.Mackay, S.A.Myers, L.Bodalbhai, A.Brajter-Toth, *Anal. Chem.*, 1990, vol. 62, p. 1084.

28. R.A.Mackay in "*Microemulsions*", I.D.Robb (ed.), Plenum Press, 1982.

29. J.H.Fendler, *Acc. Chem. Res.*, 1976, vol. 9, p. 153.

30. P.L.Luisi, Angew. *Chem. Int. Ed. Engl.*, 1985, vol. 24, p. 439 and references therein.

31. M.Kakihana, H.Ikeuchi, G.P.Sato, K.Tokuda, *J. Electroanal. Chem.*, 1981, vol. 117, p. 201.

32. R.M.Wightman, M.R.Deakin, P.M.Kovach, W.G.Kuhr, K.J.Stutts, *J. Electrochem. Soc.,* 1984, vol. 131, p. 1578.

33. R.C.Engstrom, *Anal. Chem.*, 1982, vol. 54, p. 2310.

34. G.W.Hance, T.Kuwana, *Anal. Chem.*, 1987, vol. 59, p. 131.

35. R.J.Forster, *Chem. Soc. Reviews*, 1994, vol. 24, p. 289.

36. P.Tuzhi, L. Honghuan, L.Guoqing, C.Yuping, *Anal. Letters*, 1991, vol. 24, p. 935.

37. E.L.Goldstein, M.R. Van der Mark, *Electrochimica Acta*, 1982, vol. 27, p. 1079.

38. R.J.Rice, N.M.Pontikos, R.L.McCreery, *J. Am. Chem. Soc.*, 1990, vol. 112, p. 4617.

39. W.Huang, R.McCreery, *J. Electroanal. Chem.*, 1992, vol. 326, p. 1.

40. I-F.Hu, D.H.Karweik, T.Kuwana, *J. Electroanal. Chem.*, 1985, vol. 188, p. 59.

41. *Electrochemistry: Principles, Methods and Applications*, 1995, vol.2, no. 42, BAS E'CHEM Electrochemical Products Group.

42. K.Aoki, K.Akimoto, K.Tokuda, H.Matsuda, *J. Electroanal. Chem.*, 1984, vol. 171, p. 219.

43. L.Zhaohui, J.Zhenbin, G.Dengping, *J. Electroanal. Chem.*, 1989, vol. 259, p. 39.

44. J.C.Hoogvliet, C.M.B. Van Den Beld, C.J.Van Der Poel, W.P.Van Bennekom, *J. Electroanal. Chem.*, 1986, vol. 201, p. 11.

45. J-X. Feng, M.Brazell, K.Renner, R.Kasser, R.N.Adams, *Anal. Chem.*, 1987, vol. 59, p. 1863.

46. J. Heyrovsky and J. Kuta, *Principles of Polarography*, Academic Press, New York, 1966, p 106.

47. D.E. Weisshaar and D.E.Tallman, *Anal. Chem.*, 1983, vol. 55, p. 382.

48. W.T.Yap, L.M.Doane, Anal. Chem., vol. 54, p. 1439.

49. J.Heinze, *Angew. Chem. Int. Ed. Engl.*, 1993, vol. 32, p. 1268.

50. T.Abe, K.Itaya, I.Uchida, K.Aoki, K.Tokuda, *Bull. Chem. Soc. Japan.*, 1988, vol. 61, p. 3417.

51. K.Aoki, *Electroanalysis*, 1993, vol. 5, p. 627.

Chapters 3A, 3B, 3C- A nonionic micellar system

- Triton X-100 -

Chapter 3A: Triton X-100 Self-Diffusion Coefficients (RDV)

3A.1 Introduction

Triton X-100 (TX-100) [p-(1,1,3,3,-tetramethyl butyl) phenoxypoly (oxyethylene) glycol] is a nonionic surfactant that forms micellar aggregates above a critical micelle concentration (c.m.c.) of ~0.3 mM[1,2,3,4,5]. TX-100 contains a hydrophobic octylphenyl group which forms the micellar core and a hydrophilic polyethylene oxide (PEO) group which forms the outer micellar surface which is in contact with the solvent. It is widely utilised for biological applications such as separation of proteins from cell membranes[6,7] and subsequently in the solubilisation of membrane bound enzymes without inhibiting their biological activity[4]. TX-100 mixed with phospholipids, also produces effective substrates for studying enzymes of phospholipid metabolism[8,9,10,11], other mixed TX-100 micelles are used in the chemical industry[12,13].

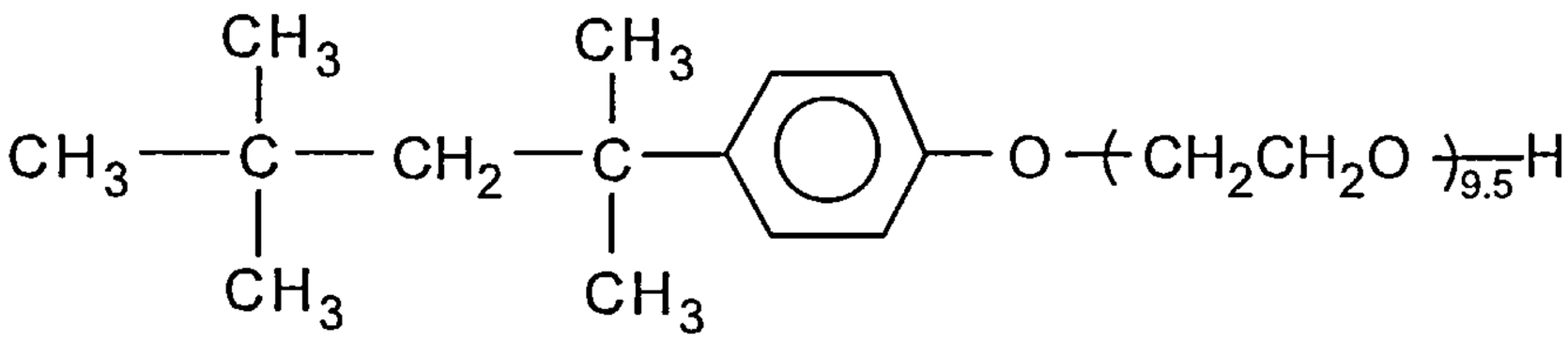

Figure 3A.1 : Structure of Triton X-100

A wide number of studies have been carried out on TX-100 micelles in an attempt to elucidate its physical properties (size, shape, aggregation number). One of the earliest cited and most referenced studies was in 1954 by Kushner and Hubbard[14] who used light scattering (LS) to determine micellar molecular weight and hence the aggregation number (N_{agg}). The same authors also studied TX-100 micelles in the presence of added electrolyte using viscometry, a technique which gives results from which size, shape and hydration values can be inferred.

The extent of TX-100 micelle hydration is one property which has received a great deal of attention, however, a lack of understanding still exists regarding the role of water in micelle formation. This can be explained by the fact that the solvent system and/or electrolyte type are often different. Electrolyte concentration is known to affect the degree of hydration quite considerably and therefore differences in results are generally due to the ternary system chosen. Brown et al.[15] have noted that there may be a difference in the molecular weight of the TX-100 surfactant from different sources. This is most likely due to the number of ethylene oxide chains (n) varying between 9-10 which may alter the aggregation number and size as well as calculated concentrations[14]. In this case an average value[3,4,16] of n = 9.5 gives a molecular weight of 624 g mol^{-1}.

The size of TX-100 micelles have been well reported and a great deal of agreement between authors using different methods have been noted. Techniques as diverse as quasi-elastic light scattering (QELS) and gel permeation chromatography (GPC) have determined radii of 4.50 nm and 4.00 nm respectively[15,16]. Other techniques including small angle neutron scattering (SANS), nuclear magnetic resonance (NMR) and Taylor dispersion (TD) gave values slightly lower, but considering the broad range of these methods this is not altogether unexpected[2,4,17,18]. It must also be noted that TX-100 is highly polydisperse, with the micelles acting as dynamic entities which are constantly and reversibly exchanging monomers[19]. This may further explain any variance between techniques as for example, NMR is known to be highly sensitive to free monomer in solution[15]. It follows that for an accurate description of micellar phase behaviour, results from a range of experimental methods would be advantageous.

The final and probably the most elusive property to elucidate is the micellar shape. It is known that nonionic micelles grow - and hence change shape - upon elevation of temperature and also with increases in surfactant and electrolyte concentration[20,21,22,23,24,25]. This results in the formation of rodlike micelles and further to lamellar phases[19,23,25,26]. As was mentioned earlier, the nature and degree of micelle hydration is somewhat unclear and it is this factor that essentially leads to difficulties in the evaluation of micellar geometry[16,20,27,28]. At present, the

unresolved issue regarding TX-100 micelles is whether the micelle is spherical or ellipsoidal at low concentrations of surfactant and electrolyte as well as moderate temperatures.

This chapter will present data from electrochemical studies of TX-100 micelles over a range of temperatures and electrolyte concentrations using rotating disk voltammetry (RDV). The results presented will enhance understanding of the TX-100 / water micellar system. Inferences from the data will lead to information on micellar shape, interaction and size. From the micellar size, the degree of extension for ethylene oxide chains will also be estimated. Temperature studies will show how the micellar growth characteristics are significantly altered by electrolyte concentrations. This will be illustrated by reference to the Arrhenius behaviour of the system.

3A.2 Results and Discussion

3A.2.1 General Electrochemistry

The micellar self-diffusion coefficients were measured on a series of TX-100 solutions, varying in concentration from 0.033 mol dm^{-3} to 0.167 mol dm^{-3}. This narrow range was selected as it is known that over a 1-15 wt% concentration range the volume of each micelle remains constant[1,2] and therefore any change in diffusion coefficient will be purely due to interactions[29]. An added electrolyte concentration range of 0.01-0.80 mol dm^{-3} KCl was chosen as some degree of micellar growth was expected over this range[21]. In contrast to CTAC (Ch. 4A) the self-diffusion coefficient was not measured at 0.00 mol dm^{-3} KCl, this was due to the fact that TX-100 is uncharged and has no dissociated counterions to contribute to the solution which leads to a large uncompensated solution resistance. This has the consequence of distorting the experimental current - voltage response. The current passing through a highly resistive solution implies therefore, that the true potential is not equal to the applied potential. The addition of electrolyte will reduce the iR allowing

a true Faradaic current - voltage relationship to be obtained[30]. This can be seen in Appendix 3A.i, where the addition of 0.01 mol dm^{-3} KCl significantly shifts the sigmoidal redox wave with only a slight change (~0.4μA) in the limiting current. The effect of electrolyte can be further analysed by constructing a Nernstian plot as described by Equation 3A.1 the values for which are shown in Table 3A.1 and illustrated in Appendix 3A.ii.

$$E = E_{1/2} + 2.3\ RT/nF\ \log_{10}[i / (i_{Lim} - i)] \qquad (3A.1)$$

Table 3A.1 : Nernstian data for 0.167 mol dm^{-3} TX-100 - effect of [KCl]

No KCl		+0.01 mol dm^{-3} KCl	
E / V	$\log_{10}[i /(i_{lim}-i)]$ / i in A	E / V	$\log_{10}[i /(i_{lim}-i)]$ / i in A
0.20	-0.926	0.20	-0.786
0.22	-0.704	0.21	-0.618
0.24	-0.512	0.22	-0.453
0.26	-0.328	0.23	-0.281
0.28	-0.162	0.24	-0.281
0.30	-2.4e-4	0.25	0.057
0.32	0.161	0.26	0.215
0.34	0.389	0.27	0.386
0.36	0.515	0.28	0.554

At 0.00 mol dm^{-3} KCl a gradient of 111 mV $decade^{-1}$ is obtained in contrast to 60 mV $decade^{-1}$ at 0.01 mol dm^{-3} KCl. Half wave potentials of 299 mV and 247 mV were observed for 0.00 and 0.01 mol dm^{-3} KCl respectively. So, the addition of only 0.01 mol dm^{-3} KCl produces a shift of ~50 mV in both the half wave potential and the Nernstian gradient. It also shows how data may be unreliable at 0.00 mol dm^{-3} KCl due to the non-Nernstian response of the system. If half wave potentials ($E_{1/2}$) from the RDV data are analysed fully over both the KCl and surfactant range then the following results are obtained (Table 3A.2).

Table 3A.2 : Nernstian data for surfactant and electrolyte range

[TX-100] / mol dm^{-3}	$E_{1/2}$ / mV	
	0.01 mol dm^{-3} KCl	0.80 mol dm^{-3} KCl
0.033	215.0	202.1
0.100	232.7	223.9
0.167	247.0	238.7

It can be seen that $E_{1/2}$ drops by ~10 mV over the KCl range and increases as the [TX-100] increases. Behaviour of this nature has been reported previously[5,31] and is concluded to be a function of TX-100 adsorption on the electrode surface[5,31,32,33] although there does not appear to be any concerted agreement as to the relationship between $E_{1/2}$ and surfactant concentration. Whilst Verrall et al.[32] and Munoz et al.[31] reported a decrease in $E_{1/2}$ with an increase in [TX-100], results from Mandal et al.[5] tend to concur with the findings presented here. This observed increase in $E_{1/2}$ over the [TX-100] range would tend to suggest that the electron transfer process occurs with greater difficulty[31,32,34].

At [TX-100] below the c.m.c. there is believed to be fragmented adsorption (individual aggregates) of micelles on a mercury electrode surface and as the concentration of TX-100 increases the micelles coalesce to form a continuous layer[34,35]. This adsorption process (< c.m.c.) has been modelled in terms of a modified Frumkin isotherm[31,33]. However, in these studies the surfactant concentrations were low (1 - 5) $x10^{-4}$ mol dm^{-3} and it is therefore likely that at the concentrations studied here (0.033 - 0.167 mol dm^{-3}) the adsorbed layer is of continuous a nature[34,35]. It follows that an increase in surfactant concentration may increase the adsorbed layer thickness on the electrode, thus hindering the electron transfer ($E_{1/2}$ increases). Levitz et al. showed that at low surface coverage close to the c.m.c. the adsorbed layer consists of micellar aggregates similar to those in the bulk solution[35]. However, if the surface coverage (θ) is high, as would be expected in this case, the adsorbed layer takes the form of a continuous bilayer structure[35]. This is corroborated somewhat by the observation that at low to medium θ the adsorbed layer density increases until it reaches a limiting density at high θ[35]. At this point, at constant density, it is the size of the surfactant aggregates that

predominates, increasing in size as surface coverage in increased further[35]. Therefore, because the [TX-100] is significantly larger than the c.m.c., it can be assumed that it is the adsorbed layer thickness increasing as opposed to the adsorbed layer density.

The addition of electrolyte is known to induce nonionic micellar growth and it has been noted that the addition of NaBr reduces surfactant adsorption on electrodes, in favour of micellar growth in the bulk solution[36]. Guidelli et al. reported a drop in $E_{1/2}$ as Br^- is added to a TX-100 micellar solution which is also assumed to be a reduction in the surfactant blocking effect on the electrode[33]. So, it can be proposed that the addition of electrolyte effectively 'forces out' surfactant from the electrode into the bulk solution. The surfactant chains are consequently utilised in thermodynamically driven growth of the micellar aggregates. This will have the effect of decreasing the adsorbed surfactant layer thickness and decreasing the half wave potential as observed here.

A representation of the possible effect of KCl and TX-100 and $E_{1/2}$ can be seen in Figure 3A.2

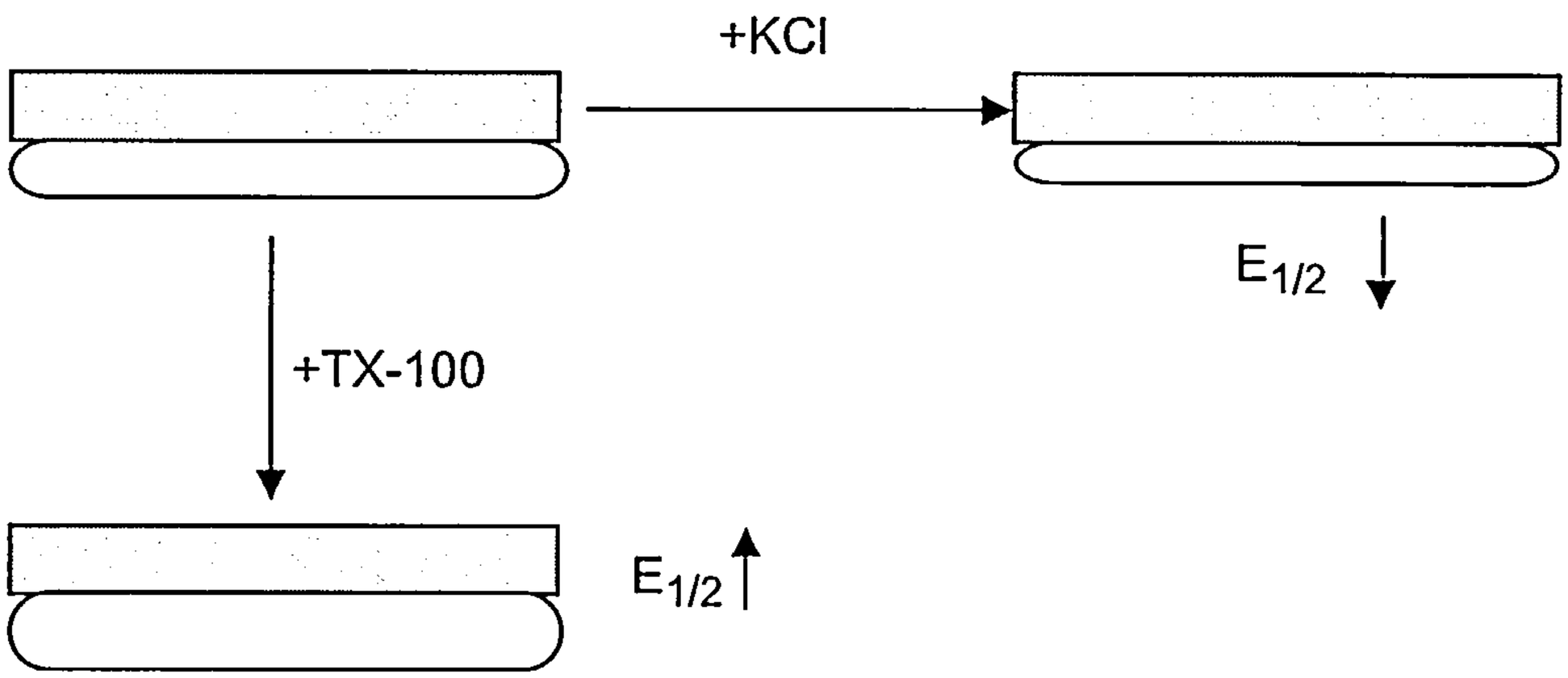

Figure 3A.2 : Mechanism of the possible effect of surfactant and electrolyte on an adsorbed TX-100 layer on electrode.

TX-100 is known to adsorb strongly and specifically on mercury[34,37], latex[36] and glassy carbon[38]. The actual mechanism of adsorption is believed to be due to the methyl groups interacting with the surface, PEO groups in solution and association

of the phenyl groups in face-face geometry[36]. Rather than the surfactant associating with adsorbed water on the electrode surface, it has been proposed that the surfactant displaces solvent molecules, even at low concentrations[33]. This results in the occupation of electrode surface sites by adsorbed TX-100[33].

A representation of possible TX-100 adsorption is shown in Figure 3A.3.

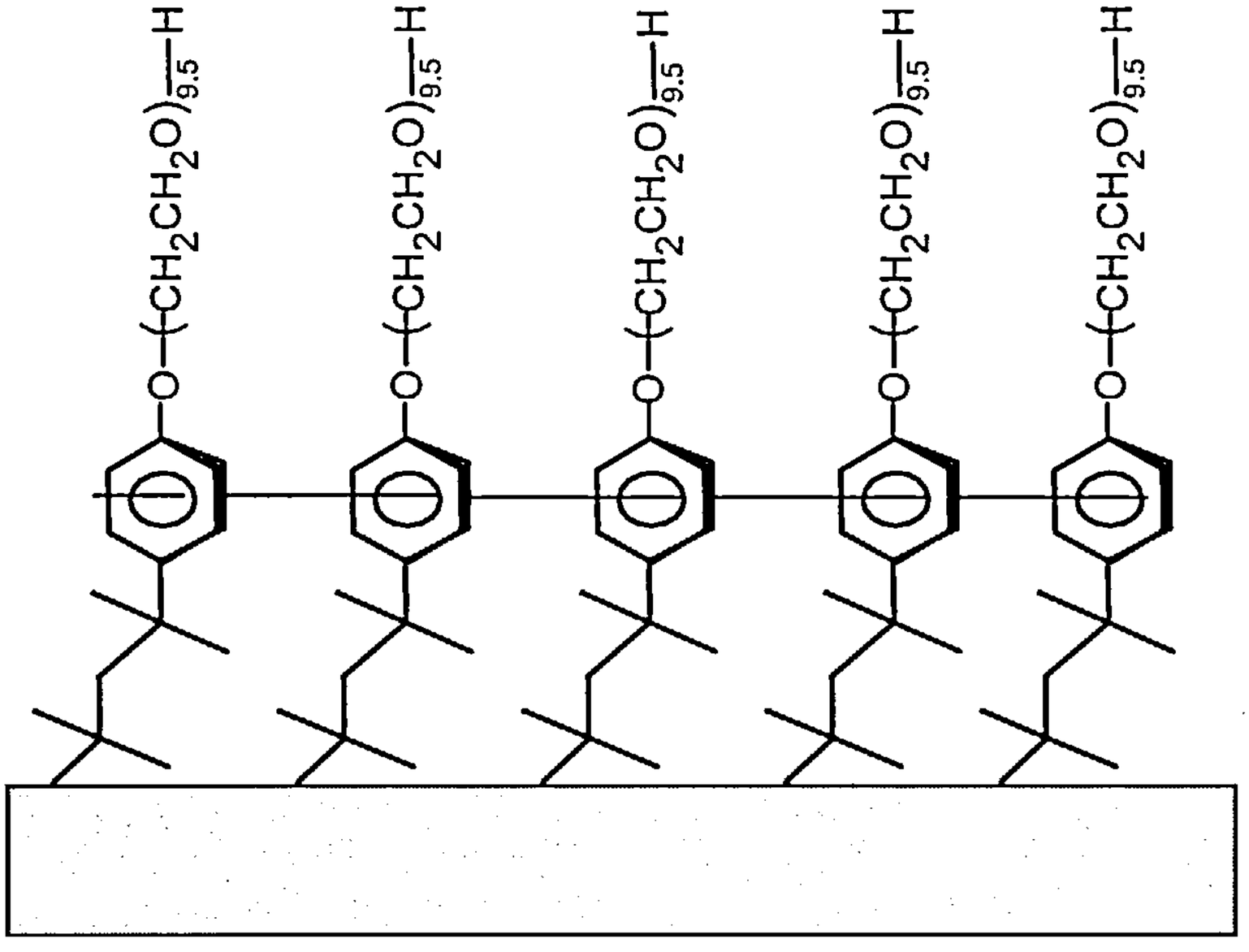

Figure 3A.3 : Possible mode of TX-100 surfactant chain adsorption on an electrode surface

Despite the obvious presence of adsorbed surfactant at the electrode surface accurate limiting currents may still be measured leading to the estimation of micellar self-diffusion coefficients.

3A.2.2 Diffusion Coefficient Results

A full set of typical RDV plots over a rotation rate range of 2-12 Hz for 0.167 mol dm^{-3} TX-100 + 0.10 mol dm^{-3} KCl can be seen in Appendix 3A.iii. Levich plots for different TX-100 concentrations are shown in Appendix 3A.iv. Initial measurements on 0.167 mol dm^{-3} TX-100 showed that the variation in D_{RDV} between 0.01 - 0.1 mol dm^{-3} KCl was ~$0.1x10^{-7}$ cm^2 s^{-1} which could be accounted for by experimental error.

It was therefore decided that measuring D_{RDV} at intermediate concentrations would not lead to any further characterisation of the system over this range. This was validated by the fact a perfectly linear relationship with increasing [KCl] was observed for all [TX-100] (Appendix 3A.v). The experimental diffusion coefficients (D_{RDV}) are shown in Table 3A.3.

Table 3A.3 : Experimental D_{RDV} results

[KCl] / mol dm^{-3}	$10^7 D_{RDV}$ / cm^2 s^{-1}		
	0.033 mol dm^{-3} TX-100	0.100 mol dm^{-3} TX-100	0.167 mol dm^{-3} TX-100
0.01	4.52	3.32	2.21
0.10	4.28	3.15	2.13
0.20	4.13	2.98	1.99
0.40	3.70	2.70	1.74
0.80	3.03	2.22	1.35

Note: standard error = ±0.06x10^{-7} cm^{2}s^{-1}, experiments repeated twice.

Plots of D_{RDV} against [KCl] for each [TX-100] are shown in Appendix 3A.v along with lines of best fit. Correlation coefficients >0.995 show that the relationship is perfectly linear and hence values for the fitted line are used for further calculations. These fitted values are shown below in Table 3A.4.

Table 3A.4 : Linearly fitted D_{RDV} results

[KCl] / mol dm^{-3}	$10^7 D_{RDV}$ / cm^2 s^{-1}		
	0.033 mol dm^{-3} TX-100	0.100 mol dm^{-3} TX-100	0.167 mol dm^{-3} TX-100
0.01	4.51	3.35	2.20
0.10	4.26	3.19	2.11
0.20	4.10	3.03	1.96
0.40	3.69	2.71	1.73
0.80	3.04	2.20	1.36

By comparing the fitted values in Table 3A.4 to the experimental data in Table 3A.3 it can be seen that the biggest deviation is 0.05x10^{-7} cm^{2}s^{-1} which is within experimental error showing that the linearly fitted values are valid.

3A.2.2.1 D_{RDV} - Results Analysis

The D_{RDV} values show the general trend of decreasing as the [TX-100] increases, this agrees with previously reported studies of self diffusion coefficients of non-ionic micelles[4,5,18,25,29]. The experimental results can be linked to the surfactant concentration via the linear relationship[39,40] (Equation 3A.2). Examples of these plots are shown in Appendix 3A.vi.

$$D_{RDV} = D^{O}_{RDV} \{1-k_D(C_S - c.m.c)\} \qquad (3A.2)$$

The critical micelle concentration (~0.3 mM)[1,2,3,4,5] had negligible effect on the outcome of the linear analysis and was therefore omitted from further calculations. In fact, as the concentration of KCl is increased the c.m.c drops[13]. A plot of D_{RDV} against [TX-100] yields an intercept of D^{O}_{RDV} (diffusion coefficient in the absence of interactions) and a gradient from which the intermicellar interaction parameter (k_D) can be determined. Values for the hydrodynamic radius (R_H^{O}) (based on a spherical model) can be easily calculated by the Stokes-Einstein equation[16,20,29,41] (3A.3).

$$R_H^{O} = (k_B.T) / (6.\pi.\eta.D^{O}_{RDV}) \qquad (3A.3)$$

Values for D^{O}_{RDV}, k_D and R_H^{O} are shown in Table 3A.5 and illustrated in Appendices 3A.vii, 3A.viii and 3A.ix.

Table 3A.5 : Linear extrapolation results

[KCl] / mol dm^{-3}	10^7 D^{O}_{RDV} / cm^2 s^{-1}	R_H^{O} / nm	k_D / dm^3 mol^{-1}
0.01	5.07	4.22	3.38
0.10	4.79	4.47	3.40
0.20	4.63	4.62	3.45
0.40	4.18	5.12	3.50
0.80	3.45	6.21	3.63

Note: Errors: $D^{O}_{RDV} \sim \pm 0.06x10^{-7}\ cm^2\ s^{-1}$, $R_H^{O} \sim \pm 0.05\ nm$, $k_D \sim \pm 0.05\ dm^3\ mol^{-1}$, $V_H \sim \pm 11\ nm^3$

3A.2.2.2 Micellar Interaction

In ionic micellar systems it is well known that the addition of electrolyte to a solution reduces electrostatic repulsion between micelles. However, for nonionic systems electrolyte has no such effect. TX-100 micelles are uncharged and therefore have no electrostatic interactions, which means that the micelles effectively act as hard spheres[2,15,17]. Brown et al. have shown using SLS that a hard sphere model is valid at surfactant concentrations below 5% (≡ to highest the [TX-100] used in this study) above which concentration-driven micellar growth may begin[15].

KCl has the ability to alter the cloud point (T_C) of the TX-100 micellar system demonstrating that strong thermodynamic interactions exist between small ions and TX-100 micelles[42], the major consequence being that the micelle will undergo dehydration[22,23,43]. Although the actual dehydration mechanism has not been fully elucidated, results have shown that the charge, size and polarisability of ions determine the ion - solvent interactions[42]. The greater the ability of an ion to disrupt the solvent structure, the greater its dehydrating capability[42].

Within the outer layer of TX-100 micelles a degree of interpenetrating water can exist[20,21,41] which is associated with ethylene oxide chains by virtue of hydrogen bonding[22,44]. Addition of electrolyte will cause disruption of this EO chain - water structure weakening interactions between water and ethylene oxygens in the EO chains[42]. The dissociated electrolyte then tends to be distributed in the outer micelle layer rather than in the bulk solution (i.e. amongst the EO chains)[23].

The nature of the interaction is of great importance. As there are no electrostatic forces there must be some repulsive interactions present or the system would immediately flocculate. From Appendix 3A.viii, it can be seen that the interaction parameter increases linearly with added KCl which suggests that excluded volumes interactions are dominant[29,45], and this is demonstrated in

Appendix 3A.x with a plot of hydrodynamic radius against the intermicellar interaction parameter. This demonstrates that an increase in interaction parameter is matched by a corresponding increase in micellar size. The linear relationship that exits between them suggests that both parameters are intrinsically related.

3A.2.2.3 Micellar Structure

It can be clearly seen from Appendix 3A.ix that there is a linear increase in R_H^O over the KCl range studied. The absence of any major inflection in the curve would tend to suggest that no sudden shape transition takes place but rather a gradual structural evolution[46]. Conversely, with CTAC a sudden change in viscosity (Ch. 4B.2.1) and diffusion coefficient (Ch. 4A.2.3) was seen at 1.00-1.20 mol dm^{-3} KCl indicating a sphere to rod transition. The value of R_H^O at 0.01 mol dm^{-3} KCl (4.22 nm) is in excellent agreement with previously reported values[2,15,16,17,20,41,47] where the micelles are assumed to be spherical. Phillies et al.[21] have used QELS to obtain almost identical radii at three different [NaCl]; 0.00 mol dm^{-3} = 4.2 nm, 0.30 mol dm^{-3} = 5.0 nm, 0.60 mol dm^{-3} = 5.6 nm. These values are plotted along with experimentally calculated values in Appendix 3A.ix and illustrates that the data obtained from rotating disk voltammetry is highly accurate.

A factor that has received a growing amount of attention and is still as yet unresolved is the degree of extension and the conformation of the ethylene oxide chains. This is important as the length of the EO chains effectively governs the size of the micelle and the resultant packing of these chains determines the growth and aggregation patterns[15]. It has been shown by others that the radius of the hydrophobic core is fairly constant at 2.5-2.7 nm[16] and therefore any changes in size are not only due to increases in aggregation number but also to variations in the EO chain extension[15,16,22]. Four possible conformations of chain extension have been proposed:-

Zig-Zag (Extended)[47,48] :- 3.2-3.5 nm

Helix[48] :- ~2.5 nm

Random Coil[47,48] :- 1.4-1.6 nm

Meander[47,48] :- 1.6-1.7 nm

An experimental value for R_H^O of 4.22 nm has been obtained at 0.01 mol dm^{-3} KCl (where any effects due to salt induced dehydration are small). From this radius an estimation for the EO chain extension can be made using $R_{EO} = R_H^O - R_{CORE}$, where R_{CORE} is between 2.5 and 2.7 nm[16]. This results in an ethylene oxide chain length (R_{EO}) of 1.52-1.72 nm. This fits in well with both random coil and meander dimensions[2,48] and it is possible that due to the disordered nature[49] of the PEO chains both conformations are present. The calculations effectively eliminate Zig-Zig and Helical models which is in agreement with Matsuura et al. who also suggested that the Zig-Zag conformation was unlikely to exist[49]. However, it may be the case that as the concentration of electrolyte and hence R_H^O increases, the conformation of the chain is altered and begins to extend. This would explain the difference in reported hydrophilic lengths with values ranging from 1.25 nm[1,2] to 2.5 nm[16]. Any alterations in chain extension cannot be stated implicitly as it is known that the attractive forces will be increasing leading to aggregation induced micellar growth[15], and any alterations in chain length may effectively be masked. Contraction of the ethylene oxide chains with increasing temperature has also been postulated[15,22,44]. This further shows that chains extension can only be accurately estimated at low electrolyte concentrations and moderate temperatures i.e. in the absence of significant micellar growth.

As was discussed earlier the greatest area of debate regarding TX-100 micelles is their shape. Interpretations from results presented here will not attempt to implicitly state the micellar shape, but rather to add weight to a quasi-spherical form. At present there are three possible alternatives; sphere, oblate ellipsoid and prolate ellipsoid. It is generally accepted that a prolate ellipsoid model does not fit hydration values and is therefore unlikely to explain the micelle shape[2,16,17,47]. This will be further confirmed by rheological measurements (Ch. 3B.2.1.2).

Focusing on the oblate model, it is obvious that the hydrodynamic volume (See Table 3A.5) will remain constant regardless of shape with only the actual dimensions changing[47]. Authors that incline towards a 'quasi-spherical' shape

suggest a ratio of the long dimension semi axis : short dimension semi axis of approximately 2 (a/b ~2)[16,47,50]. As the radius of a sphere of equal volume[47] for an oblate ellipsoid is $(a^2b)^{1/3}$, dimensions of a and b can be easily found (Table 3A.6) i.e. $R_H^O = (a^2b)^{1/3}$. Again, the values are in agreement with the literature[1,2,17,47]. The oblate dimensions assume that the a/b ratio remains constant with increasing [KCl]. Analysis of viscosity data (Ch. 3B.2.1) suggests that this may not be the case, but this cannot be substantiated by the presented diffusion coefficient results. Accurate hydrodynamic radii can be determined, however, the shape of micelles can only be proposed from electrochemical measurements.

Table 3A.6 : Dimensions for oblate ellipsoid model

[KCl] / mol dm^{-3}	a / nm	b / nm
0.01	5.32	2.66
0.10	5.63	2.82
0.20	5.82	2.91
0.40	6.45	3.23
0.80	7.82	3.91

Further weighting to the oblate shape can be gained by considering surfactant chain packing. Studies have shown that for a spherical shape to be possible, some of the ethylene oxide chains must be embedded in the hydrophobic core[15,41,47,50,51]. For example, raman spectroscopy (RS) has shown that clear distinct polar and apolar regions do not occur which supports spherical geometry[51]. The octylphenyl groups are relatively large with a terminal $(CH_3)_3$ group and it follows that for $N_{agg} \geq 100$, the chains cannot be placed radially around the same point due to steric effects[41]. Also, the polydispersity of the EO chains may result in a non-uniform distribution around the micelle leading to a closer spherical nature than calculated[16,47]. A further point that must be made is that due to the polydispersity of TX-100[5,52], a broad size distribution is present that could lead to the conclusion that the micelle shape is non-spherical[29]. It follows, that if a micelle is spherical it must possess a narrow size distribution and hence the system must be assumed to be monodisperse[16,26,29,52]. A study by Wright showed that TX-100 micelles exhibit electric birefringence and by definition an isotropic sphere would show no such effect, therefore an ellipsoidal

shape was indicated[53]. For the present, the best solution is to assume a 'quasi-spherical' micelle as the "ellipsoidal model is valid regardless of precise shape" [48].

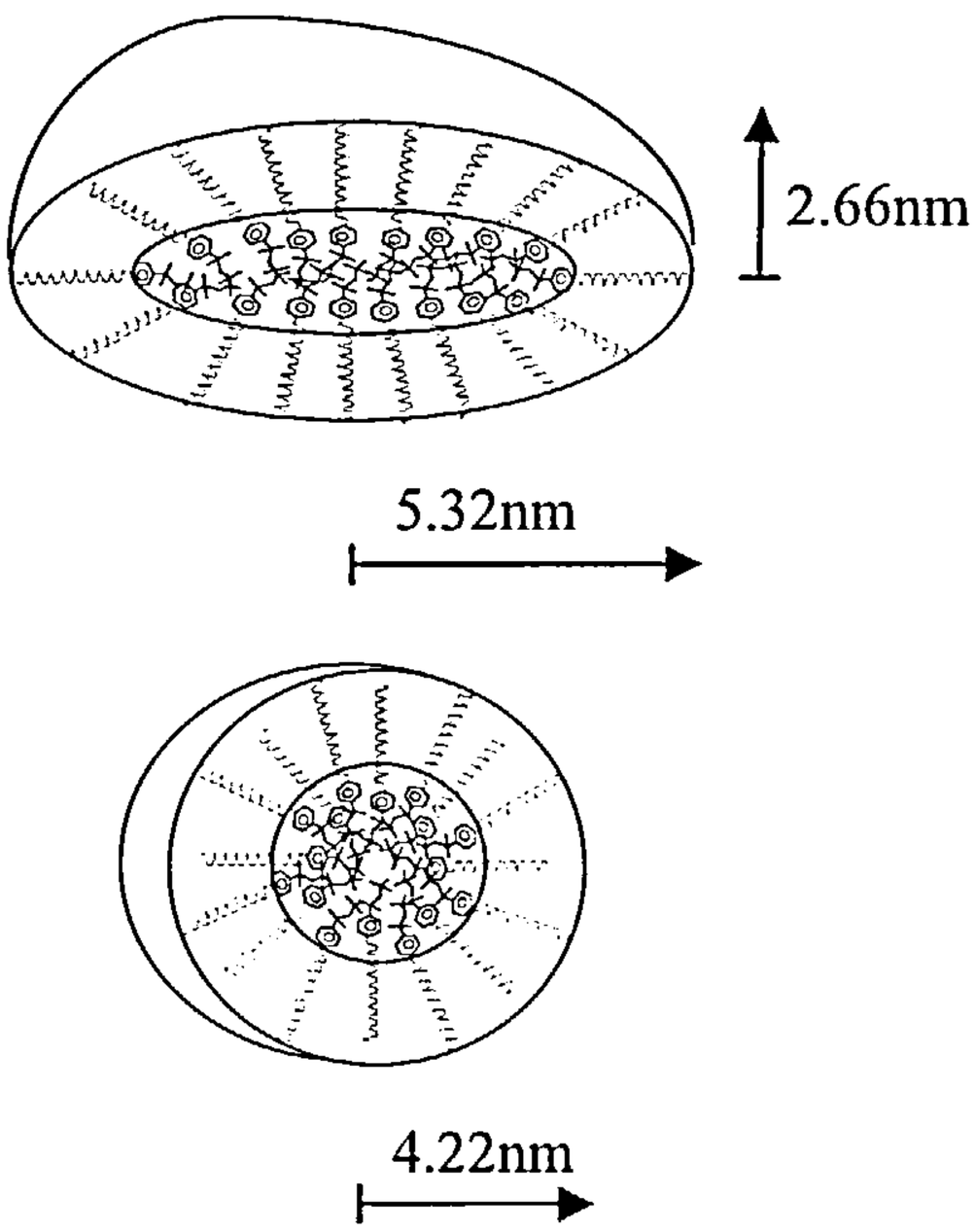

Figure 3A.4 : Comparison between oblate and spherical model (note that the spherical model has a degree of EO chain embedded in the hydrophobic core)

As was mentioned earlier, the observation of a gradual increase in the micellar size, as opposed to a precipitous change, is indicative of gradual micellar structural evolution. This is confirmed somewhat by Ikeda who suggested that rodlike micelles have two hemispherical endcaps and growth is achieved by the insertion of surfactant chains into the central part[26]. The actual cause of micellar growth with increasing the electrolyte concentration is explained by the nature of the micellar dehydration. The EO-EO repulsive interaction between adjacent chains will decrease with increasing dehydration, reducing the effective headgroup surface area[44]. This will increase the attractive potential which will subsequently lead to micellar aggregation[15]. Figure 3A.5 illustrates possible structural evolution from the data earlier presented in Table 3A.6.

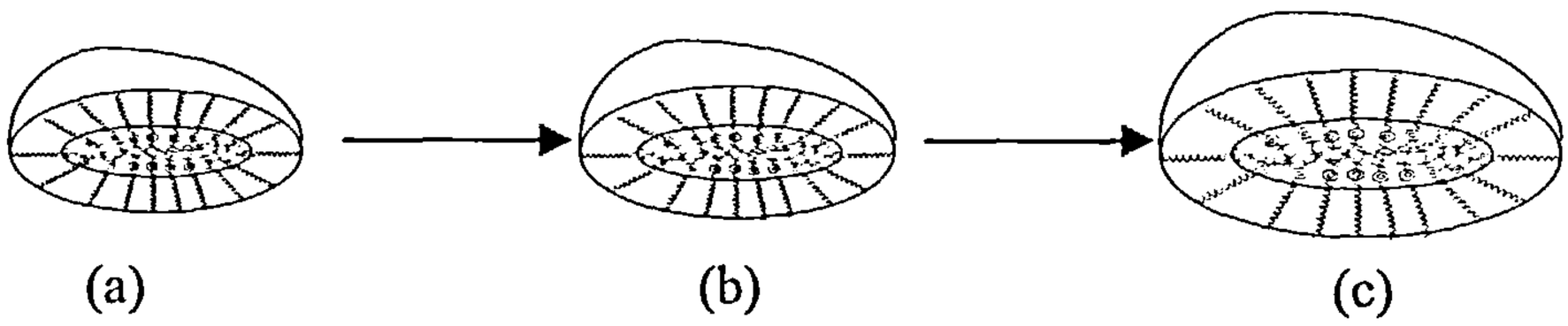

Figure 3A.5 : Electrolyte induced micellar growth assuming a constant dimension ratio i.e. a / b = 2 at (a) 0.01, (b) 0.20 and (c) 0.80 mol dm^{-3} KCl

3A.2.3 Effect of Temperature

A number of authors have paid attention to the variation of TX-100 micellar properties at different temperatures[3,15,20,22,54], though few have combined the effect of both temperature and electrolyte concentration. This set of experiments intend to show how the phase behaviour of TX-100/water system can be altered by the collective effect of both temperature and the concentration of added electrolyte. In addition to the D_{RDV} measurements at 20 ^{O}C, further results were obtained at 15,25,30,35 and 40 ^{O}C. Streletzky et al. have noted a linear increase in the hydrodynamic radius below 40 ^{O}C due to a slow growth in the aggregation number[20]. At temperatures greater than 40 ^{O}C, a rapid rise in the aggregation number was observed due to the onset of significant micellar growth[20].

So, with reference to this data, diffusion coefficient measurements were confined to temperatures at or below 40 ^{O}C. This ensured that any interpretation need not consider large scale micellar aggregation but rather gradual micellar growth..

3A.2.3.1 Results

All of the diffusion coefficients were measured using a surfactant concentration of 0.10 mol dm^{-3} TX-100. This concentration is the mid-point of the range studied previously and therefore as all solutions behave in an identical fashion, any analysis of the phase behaviour will likely be valid for both 0.033 mol dm^{-3} and 0.167 mol dm^{-3} TX-100.

Table 3A.7 : Diffusion coefficient variation with temperature and [KCl]

T / ^{O}C	10^7 D_{RDV} / cm^2 s^{-1}; with [KCl] / mol dm^{-3}				
	0.01	0.10	0.20	0.40	0.80
15	3.13	3.00	2.85	2.71	2.31
20	3.34	3.15	2.98	2.70	2.22
25	3.49	3.20	3.15	2.79	2.14
30	3.60	3.27	3.13	2.70	2.05
35	3.66	3.36	3.26	2.79	1.97
40	3.80	3.40	3.40	2.83	1.91

Note: standard error = ±0.06x10^{-7} cm^{2}s^{-1}

The data in Table 3A.7 is plotted in Appendix 3A.xi along with lines of best fit at each temperature. Excellent correlation coefficients were obtained for the linear fit (>0.996), which is not altogether surprising considering the precision of the measurements and hence values for the fitted line are used for further calculations. These values are shown below in Table 3A.8.

Table 3A.8 : Linearly fitted D_{RDV} results

T / ^{O}C	10^7 D_{RDV} / cm^2 s^{-1}; with [KCl] / mol dm^{-3}				
	0.01	0.10	0.20	0.40	0.80
15	3.09	3.00	2.90	2.70	2.30
20	3.28	3.15	3.02	2.74	2.19
25	3.44	3.29	3.13	2.79	2.13
30	3.50	3.33	3.14	2.76	2.01
35	3.62	3.43	3.22	2.80	1.96
40	3.75	3.54	3.31	2.84	1.91

The average shift in experimental results to the linearly fitted values is less than 0.04x10^{-7} cm^{2}s^{-1}. This falls within the boundary of experimental error and therefore shows that the fitted values are valid for use in further calculations.

3A.2.3.2 Results Analysis

From Appendix 3A.xi, it is apparent that the D_{RDV} values decrease in a linear fashion with an increase in [KCl] at all temperatures. Increasing the temperature can

be seen to alter the rate at which the diffusion coefficient drops i.e. the slope of D_{RDV} vs. [KCl] becomes steeper as the temperature rises.

It can also be seen that from Appendix 3A.xi that there is a common crossover point at ~0.50 mol dm^{-3} KCl. At < 0.50 mol dm^{-3} the diffusion coefficient increases with temperature as would be expected from kinetic considerations i.e. Arrhenius behaviour. Conversely, at [KCl] > 0.50 mol dm^{-3}, an increase in the temperature is actually causing a decrease in the motion of the micelle which is counter-intuitive i.e. anti-Arrhenius behaviour.

It has been reported that for complete hydration of a TX-100 micelle approximately two water molecules per EO unit (~20 H_2O per chain)[25] are required resulting in structured water around the EO groups. It is well established that when the temperature of the system increases, dehydration of the hydrophilic ethylene oxide chains occurs[2,17,22,23,43,44,45,54,55,56]. This will cause a break down of directional hydrogen bonding between ether oxygens[44,50,55], effectively decreasing the EO-EO chain repulsion[19,44]. Consequently, this will cause some degree of micellar growth and change in asymmetry of the micelle[15,20], which will have the effect of lowering the diffusion coefficient.

At low electrolyte concentrations there maybe insufficient ions to remove water from the ethylene oxide groups, whereas at higher [KCl] dehydration will be more favourable[43]. As mentioned in Ch. 3A.2.2, the mechanism of electrolyte induced dehydration is not fully understood. However, it is believed that as the concentration of electrolyte increases the K^+ and Cl^- ions displace the water from the hydrophilic layer[23]. Komaromy-Hiller et al. observed dissociated electrolyte residing in the hydrophilic region of Triton X-114 micelles[23].

It is apparent that both the addition of electrolyte and increase in temperature promote dehydration of the micellar outer layer by disrupting any structured water around the EO chains[44,50,55]. It is well established that the continued dehydration of nonionic micelles will induce a transition from a uniphasic to a biphasic mixture[2,17,23,25,43] and it is therefore prudent to assess the diffusion coefficient data with reference to this property.

Binary liquid mixtures that have the property of partial miscibility exhibit critical solution / consolute temperatures. There are two kinds of consolute temperatures, upper critical temperatures (UCT), above which both components are totally miscible and below which phase separation occurs, and lower critical temperatures (LCT) where the opposite is true.

An example of LCT and UCT are shown in Figure 3A.6.

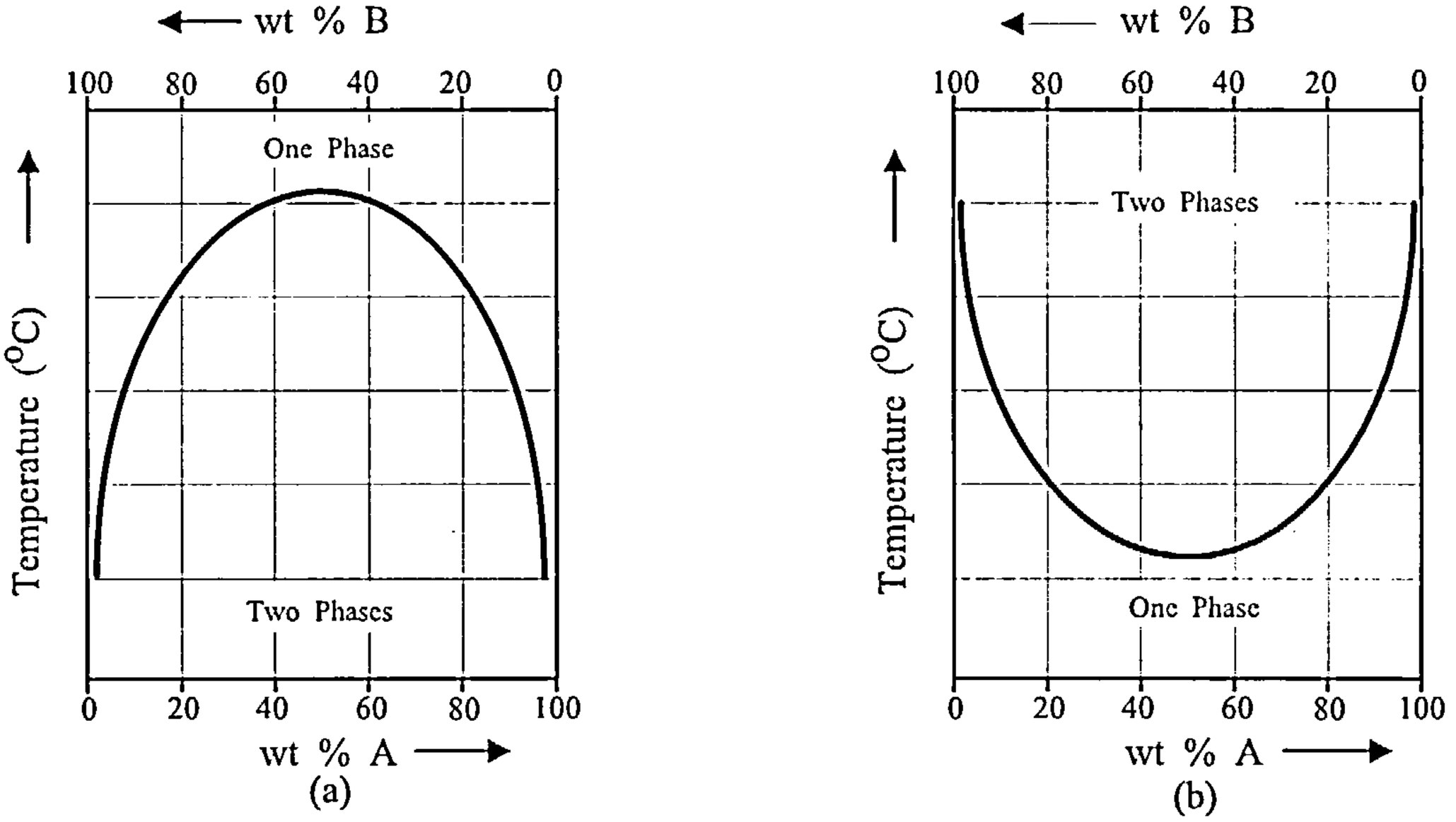

Figure 3A.6 : Examples of critical solution temperatures; (a) Upper consolute temperature (UCT), (b) Lower consolute temperature (LCT).

It has been well established that nonionic micelles exhibit a lower consolute or coexistence curve above which phase separation into micellar and solvent rich regions occurs[2,17,25,43]. The cloud point (T_C) is the temperature at which phase separation occurs and is known to be influenced by a number of competing factors[1,2,55]:-

a) EO-EO interaction
b) EO-H_2O interaction
c) Van der Waals attraction (water mediated interactions)
d) Micellar size and shape
e) Excluded volume interactions

It is the careful balancing of these parameters that determines the position of the cloud point and the phase behaviour of the system[15]. The cloud point has been

observed at temperatures (60-65 ^{O}C)[1,23,43] higher than those considered here (15-40 ^{O}C), and is generally described by a very significant increase in the micellar aggregation number[23]. In general, the phase behaviour is described by the temperature difference between the lower consolute curve and the experimental temperature and therefore it is the position of the lower consolute curve that determines the system properties[21,46].

As the cloud point is approached the system becomes more sensitive to increases in temperature and this is even more apparent when electrolyte is added to the system[21]. In addition to the dehydrating nature of electrolytes, they also have the effect of raising or lowering T_C by modifying the thermodynamic interactions between small ions and the micelles[21]. A decrease in T_C effectively brings the system closer to the lower consolute curve which has the effect of inducing micellar growth at lower temperatures[21,23]. Balasubramanian et al. have investigated the effects of different additives on the cloud temperature, and showed that both the cation and anion play a major role[42]. Table 3A.9 shows how increasing the concentration of KCl will depress the cloud point (Data taken from graph of T_C against salt concentration in Reference 42).

Table 3A.9 : Effect of KCl concentration on the cloud point temperature

[KCl] / mol dm^{-3}	T_C / ^{O}C
0.01	65.0
0.10	63.5
0.20	61.8
0.40	58.7
0.80	52.1

These values can be subsequently used to calculate the temperature difference ('distance') from the lower consolute curve at each KCl concentration (Table 3A.10). No benefit was seen by plotting the diffusion coefficient relative to these revised values. It will be seen later that these values for the cloud temperature are important when studying the onset of micellar growth from rheological measurements (Ch. 3B.2.2).

Table 3A.10 : Temperature 'distance' from cloud point - effect of KCl

[KCl] / mol dm^{-3}	'Distance' from lower consolute curve (T_C -T)					
	T=15 ^{O}C	T=20 ^{O}C	T=25 ^{O}C	T=30 ^{O}C	T=35 ^{O}C	T=40 ^{O}C
0.01	50.0	45.0	40.0	35.0	30.0	25.0
0.10	48.5	43.5	38.5	33.5	28.5	23.5
0.20	46.8	41.8	36.8	31.8	26.8	21.8
0.40	43.7	38.7	33.7	28.7	23.7	18.7
0.80	37.1	32.1	27.1	22.1	17.1	12.1

3A.2.3.3 Arrhenius Behaviour

From Appendix 3A.xi, it was seen that the diffusion coefficients decreased in a linear fashion with increasing [KCl] and that they are temperature dependent. It therefore follows that an Arrhenius plot can be constructed and hence the activation energy for diffusion (E_{AD}) of the system determined.

$$D_{RDV} = A.\exp(-E_{AD}/RT) \qquad (3A.4)$$

E_{AD} can be found by plotting a graph of ln D_{RDV} against 1/T, giving a gradient of -E_{AD} / R. Arrhenius data is shown in Table 3A.11 along with the resultant activation energies and are illustrated in Appendix 3A.xii and 3A.xiii respectively.

Table 3A.11 : Arrhenius data for temperature dependent diffusion coefficient

10^3 1/T / K^{-1}	ln D_{RDV} variation at different [KCl]				
	0.01 (mol dm^{-3})	0.10 (mol dm^{-3})	0.20 (mol dm^{-3})	0.40 (mol dm^{-3})	0.80 (mol dm^{-3})
3.195	-14.796	-14.854	-14.921	-15.074	-15.471
3.247	-14.832	-14.886	-14.949	-15.088	-15.445
3.300	-14.865	-14.915	-14.974	-15.103	-15.420
3.356	-14.883	-14.927	-14.977	-15.092	-15.362
3.413	-14.930	-14.971	-15.013	-15.110	-15.334
3.472	-14.990	-15.019	-15.053	-15.125	-15.285
E_{AD} / kJ mol^{-1}	5.51	4.69	3.67	1.33	-5.67
lnA	-12.68	-13.05	-13.51	-14.57	-17.66

Note: To make the Arrhenius equation dimensionally correct, the units of A must be equivalent to those of D_{RDV} (i.e. cm^2s^{-1}).

Although the correlation coefficients for each of the plots (0.40 mol dm^{-3}: R^2= 0.924) are not as high as may be expected the linear fit was still the best relationship. However, the actual values of E_{AD} are not the most important factor, but rather the trend that is apparent. From Appendix 3A.xiii, it is obvious that as the concentration of electrolyte increases the activation energy drops quite dramatically. Zhizhen et al.[43] have studied the effect of salt concentration on the temperature dependence of viscosity and related E_{AD} to the activation free energy of viscous flow (ΔG^*). If a similar analogy is made in this case, E_{AD} can correspond to the activation free energy of diffusion (also termed ΔG^*). Zhizhen et al.[43] interpreted ΔG^* as a function of the system to translate a spherical micelle into a cylindrical one. A negative value for the free energy term means that the reaction proceeds spontaneously and therefore a negative ΔG^* would suggest a favourable sphere-rod transition. So, it can be perceived that at electrolyte concentrations below 0.50 mol dm^{-3} KCl a sphere-rod transition is unfavourable i.e. positive E_{AD}. Although diffusion coefficient data can accurately determine micellar size, detecting shape changes appears to be beyond the scope of the technique. This is due to micellar growth being the cause of a shape change due to geometrical constraints of the surfactant chain packing. Above 0.50 mol dm^{-3} KCl, the free energy becomes negative indicating that micellar growth or a change in shape is spontaneous. An increase in the negative free energy of the system with increasing electrolyte concentration has been attributed to the more favourable separation of water molecules from the ethylene oxide groups[43]. Conversely, a lower negative free energy at low electrolyte concentrations is believed to be due to electrolyte ions adhering to the micelle instead[43].

3A.3 Summary

Rotating disk voltammetry has been used to accurately and precisely determine the self-diffusion coefficients (D_{RDV}) of TX-100 micelles over a range of surfactant (0.033 - 0.167 mol dm^{-3}) and electrolyte concentrations (0.01 - 0.80 mol dm^{-3}). Data at 0.00 mol dm^{-3} KCl was unreliable due large uncompensated solution resistance leading to distortion of the current - voltage response. A linear relationship was observed between D_{RDV} and [TX-100] which allowed the application of linear interaction theory. The resultant analysis of this extrapolation led to values of the apparent hydrodynamic radius (R_H^O) and interaction parameter (k_D).

The hydrodynamic radius as obtained from the linear extrapolation theory increased linearly with [KCl] indicating gradual structural evolution rather than significant changes in micellar aggregation parameters. The increase in R_H^O over the [KCl] range studied was attributed to electrolyte induced dehydration of the ethylene oxide (EO) chains in the hydrophilic layer. The calculated values for R_H^O over 0.01 - 0.80 mol dm^{-3} KCl were in excellent agreement with those reported in the literature by various other methods (QELS, SANS, NMR)[2,4,15,16,17,18]. A value of R_H^O of 4.22 nm at 0.01 mol dm^{-3} KCl indicated that for a core radius of 2.5-2.7 nm a meander / random coil conformation for the EO chains is likely to exist. Although, no concerted agreement exists regarding the micellar shape, the experimental results tended to suggest that the micelles are likely to be 'quasi-spherical' with a preference of oblate over prolate ellipsoid.

The interaction parameter (k_D) has been seen to increase in a linear fashion with [KCl], which suggested that electrolyte induced dehydration was the governing factor[22,23,43]. The relationship between the hydrodynamic radius and the interaction parameter indicated that although attractive interactions determine the growth characteristics[23,46], some excluded volume interactions exist to prevent the system immediately flocculating[15,20]. It is a careful balance between the attractive and repulsive forces that essentially determines the cloud point of the system, a property of interest when considering the influence of temperature[15,20].

The phase behaviour of the TX-100/water micellar system has been studied here over a range of temperatures (15 - 40 ^{O}C) and electrolyte concentrations (0.01 - 0.80 mol dm^{-3}). It was found that both temperature and electrolyte operated collectively to considerably modify the micellar phase behaviour. The temperature dependence of the diffusion coefficient was found to exhibit two regions of behaviour. At [KCl] < 0.50 mol dm^{-3} D_{RDV} increased with temperature as expected from kinetic theory, whereas at [KCl] > 0.50 mol dm^{-3} D_{RDV} decreased with temperature which is counter intuitive. This resulted in an 'isobestic' point, at which the diffusion coefficient was unaffected by a change in temperature. Activation energies have been measured by Arrhenius analysis as a function of increasing electrolyte concentration and have found to decrease in a quadratic fashion. Assuming the activation energy equivalent to the free energy of diffusion (ΔG^*), then it is seen that the spontaneity of micellar growth or of a shape change increases, with $\Delta G^* = 0$ at 0.50 mol dm^{-3} KCl.

Appendix 3A.i : Effect of electrolyte on RDE sigmoidal redox wave (0.167 mol dm^{-3} TX-100)

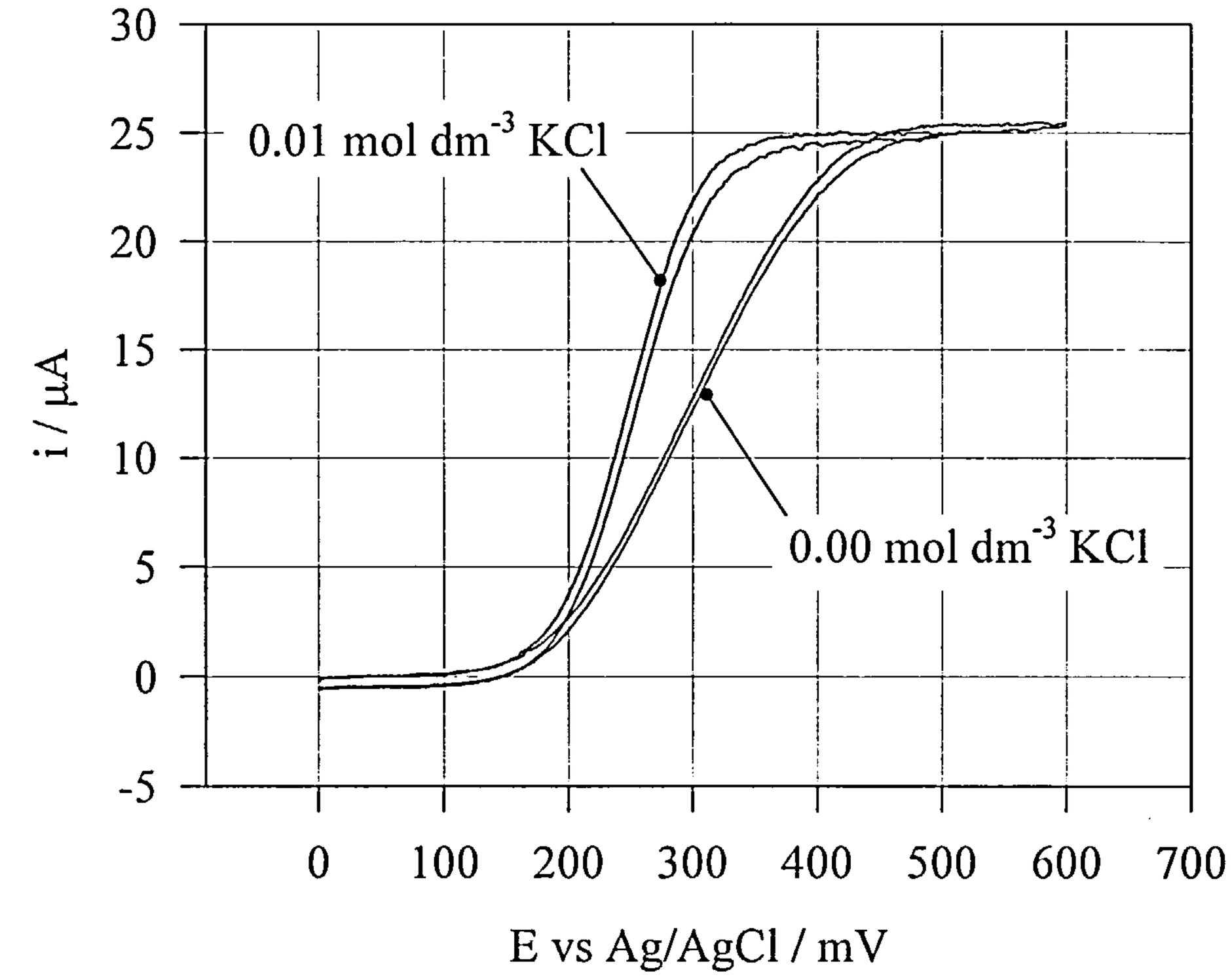

Appendix 3A.ii : Effect of electrolyte on Nernstian plots (0.167 mol dm^{-3} TX-100)

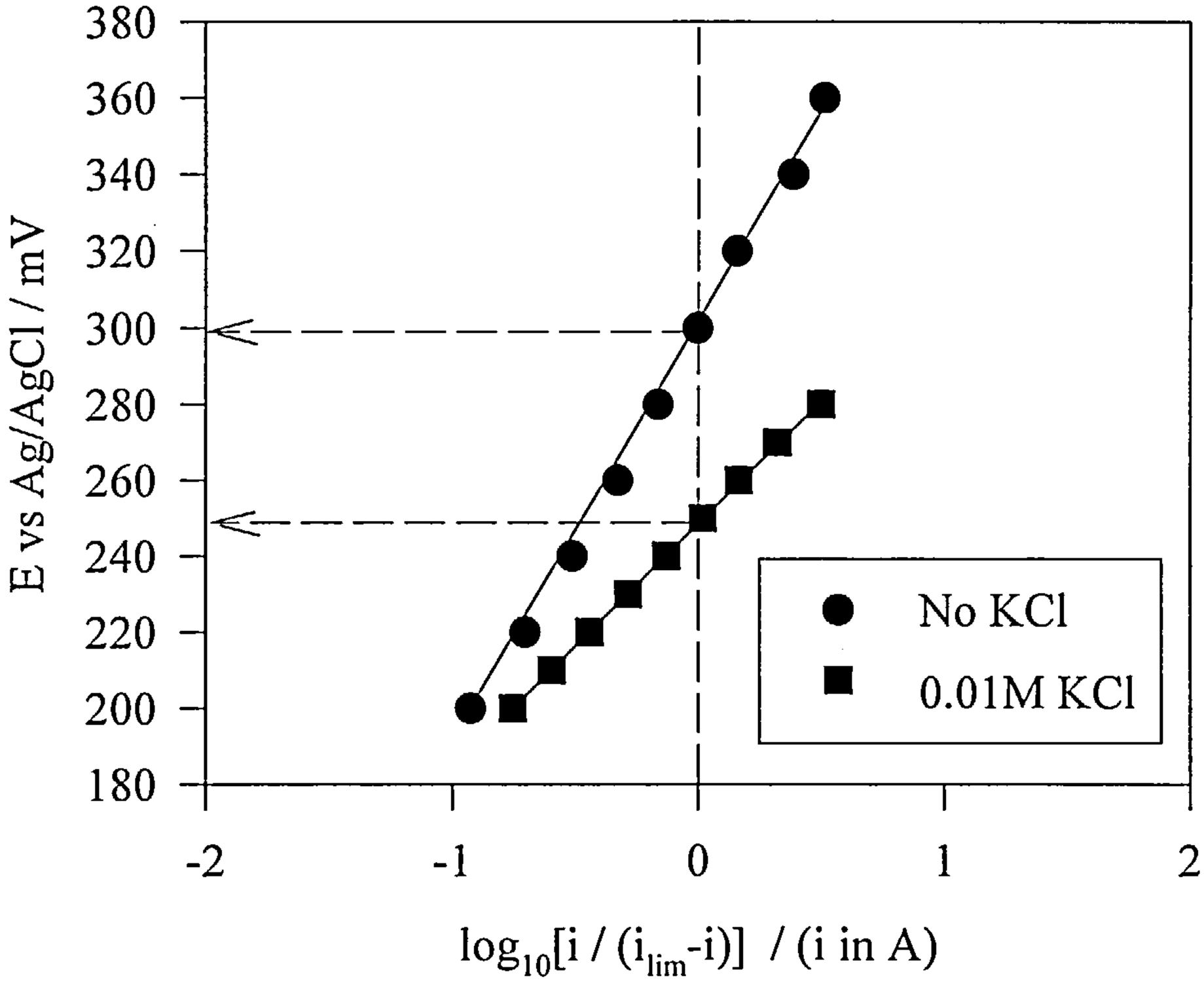

Appendix 3A.iii : Typical RDE voltammograms (0.167 mol dm^{-3} TX-100 + 0.10 mol dm^{-3} KCl 20^{O}C)

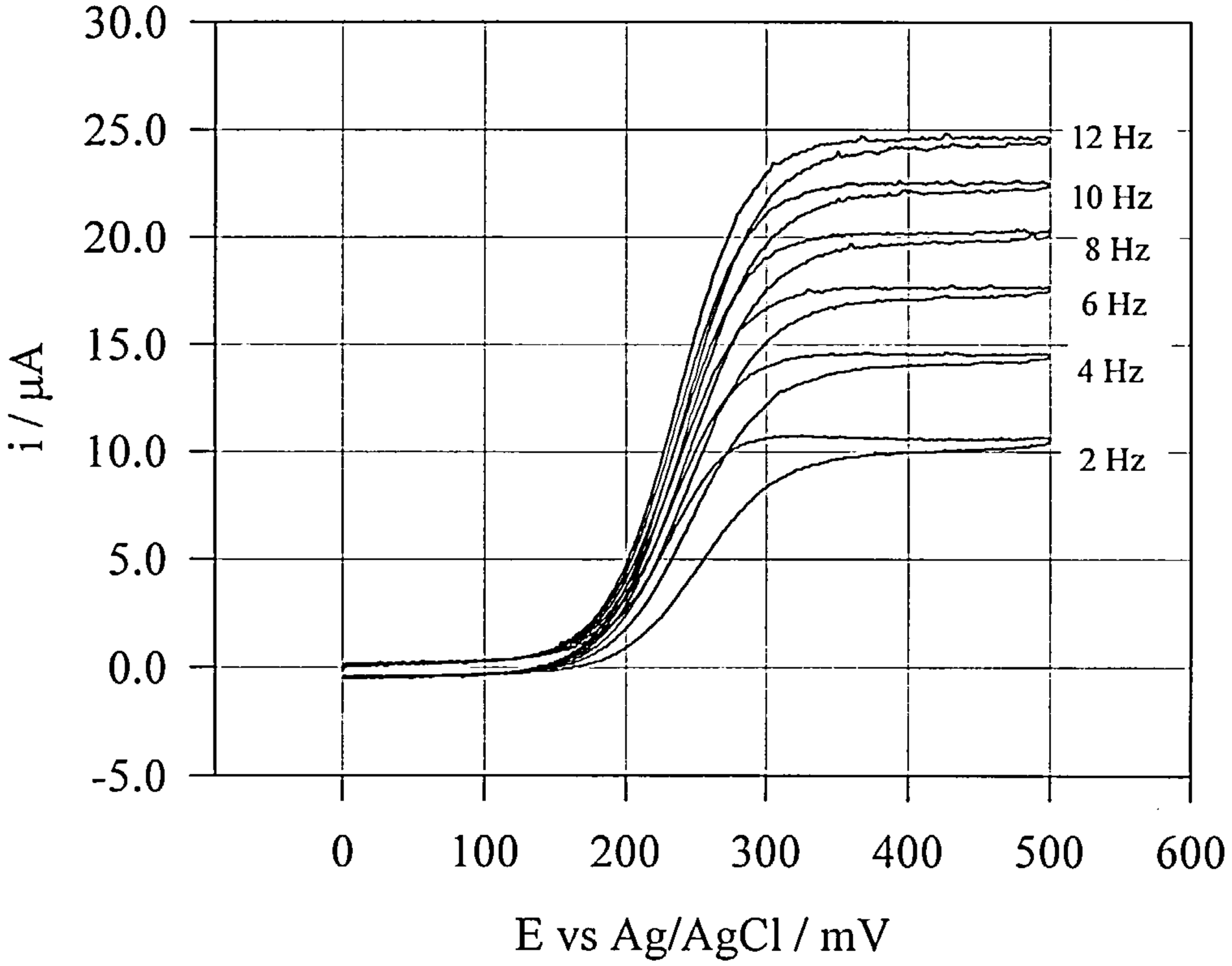

Appendix 3A.iv : Examples of Levich plots (i_{Lim} vs. $\omega^{1/2}$) (TX-100 + 0.1 mol dm^{-3} KCl)

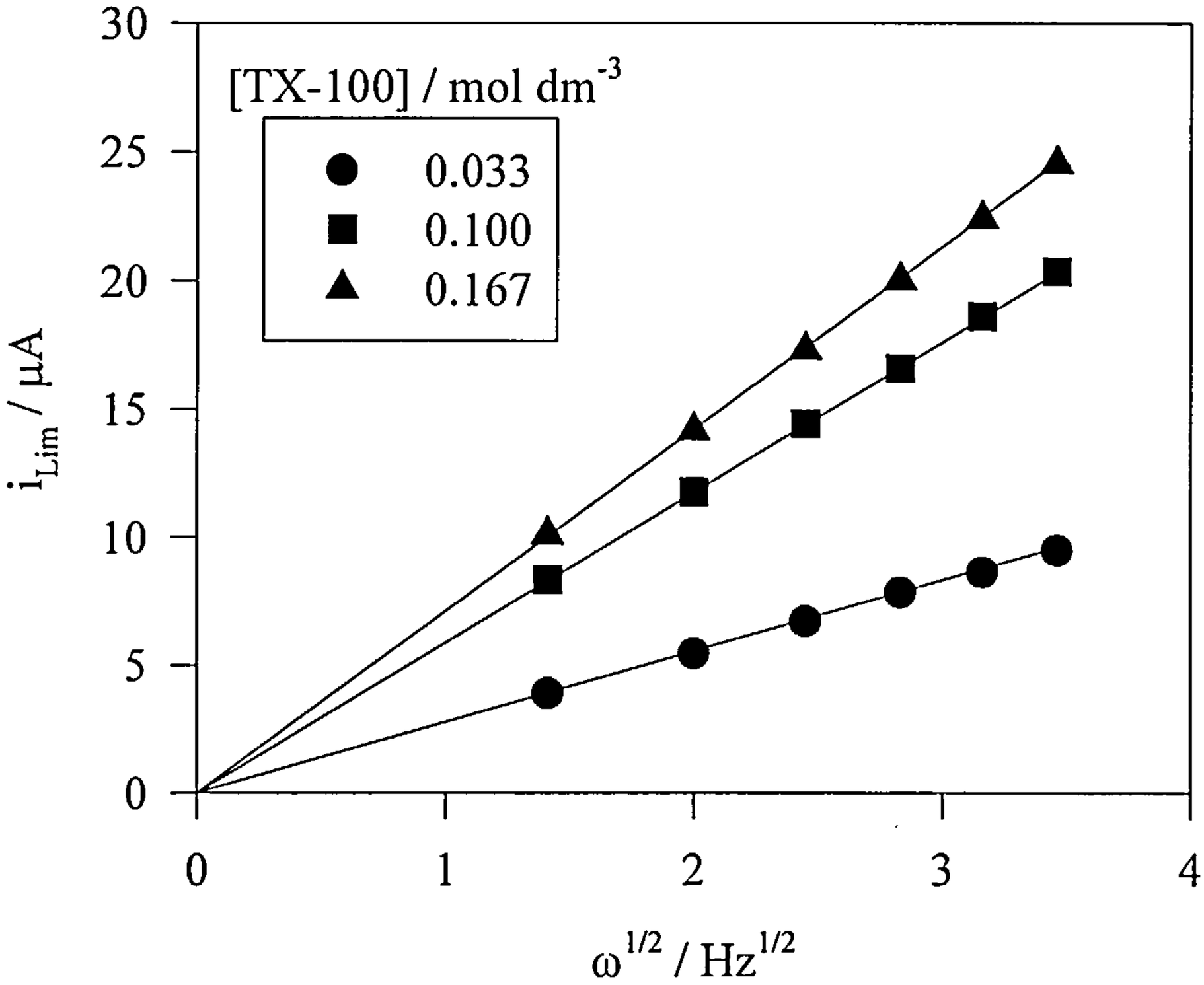

Appendix 3A.v : Diffusion coefficient variation with [KCl]

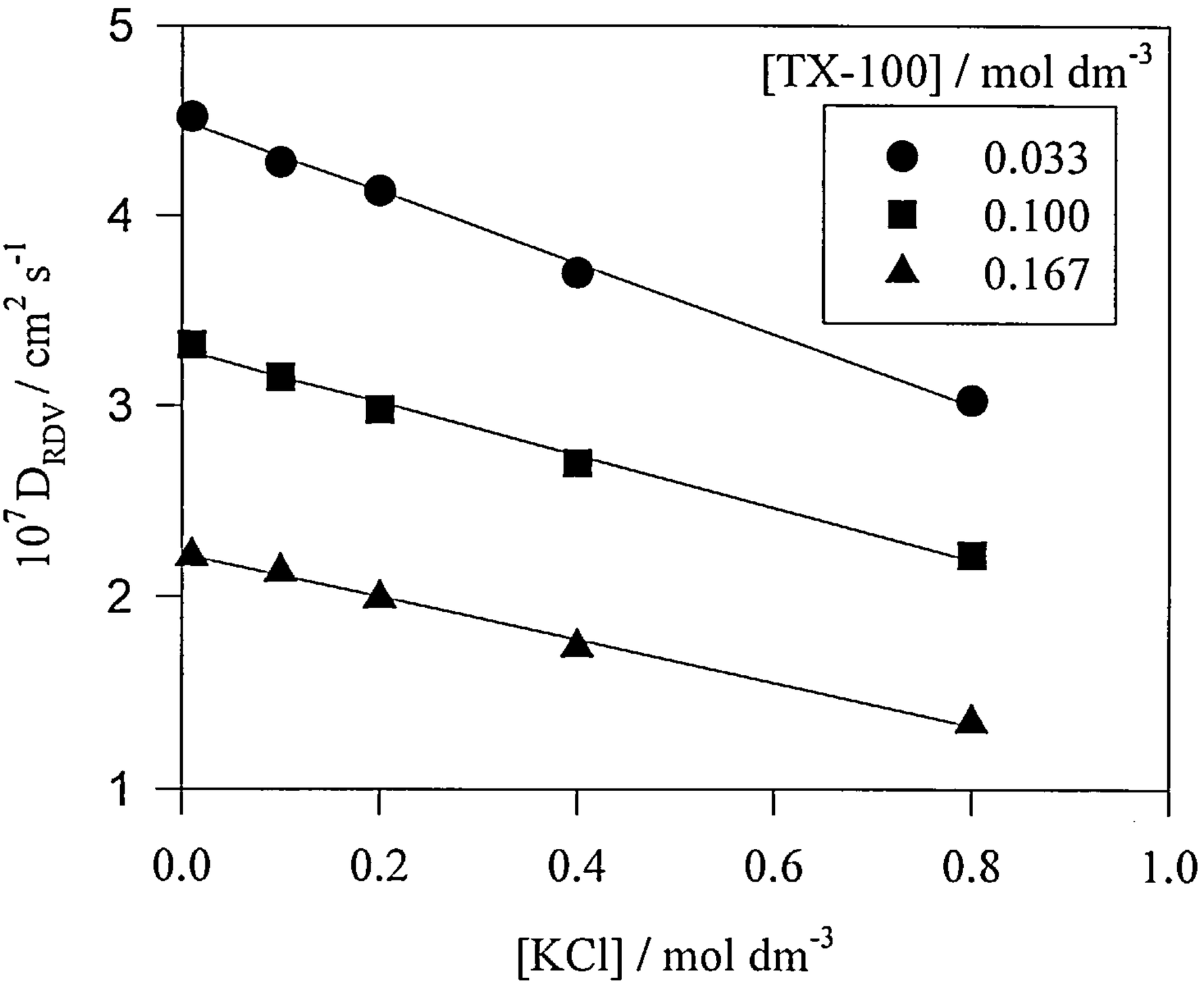

Appendix 3A.vi : Variation of diffusion coefficient with increasing [TX-100]

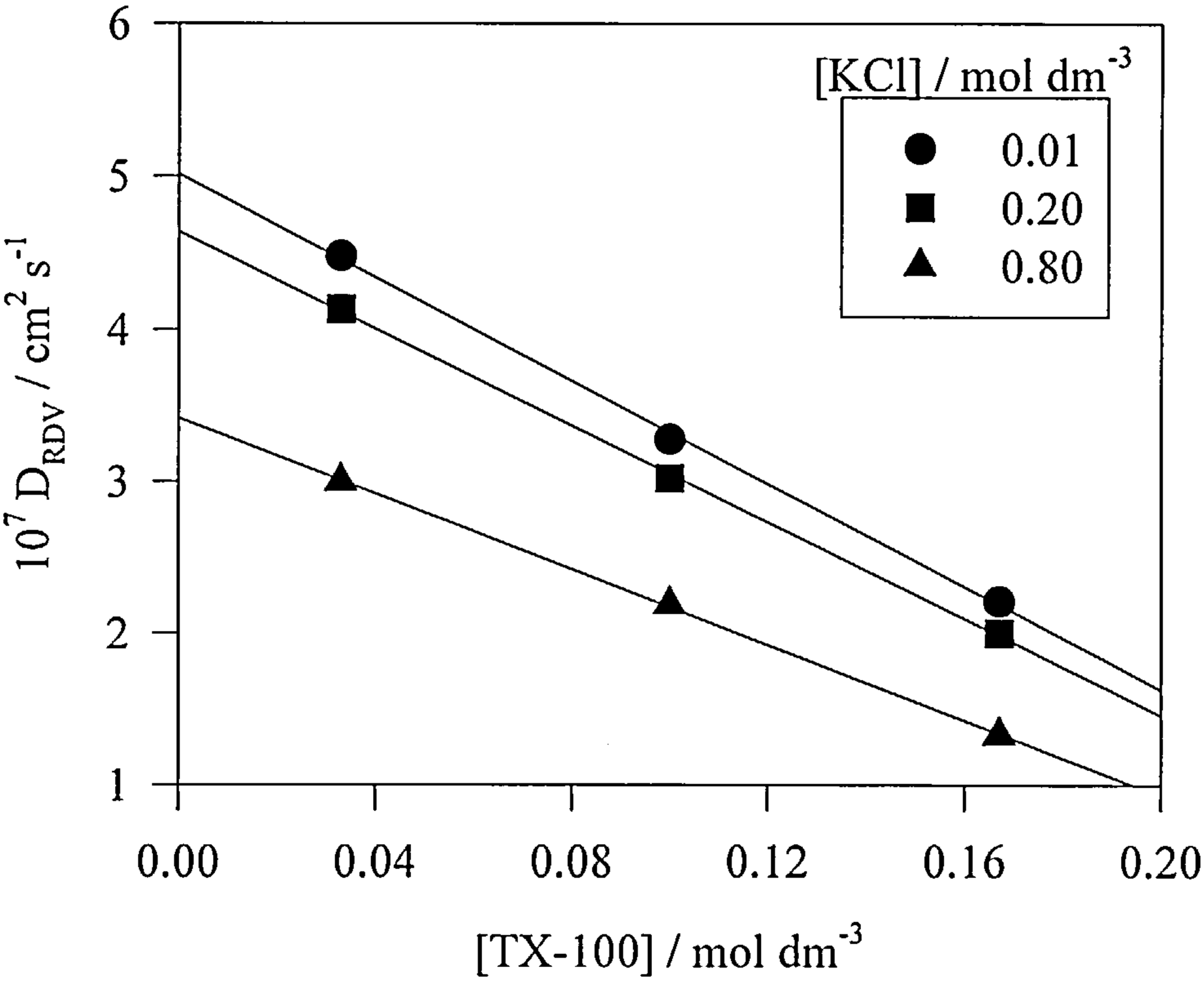

Appendix 3A.vii : Variation of self-diffusion coefficient (at infinite dilution) with added KCl

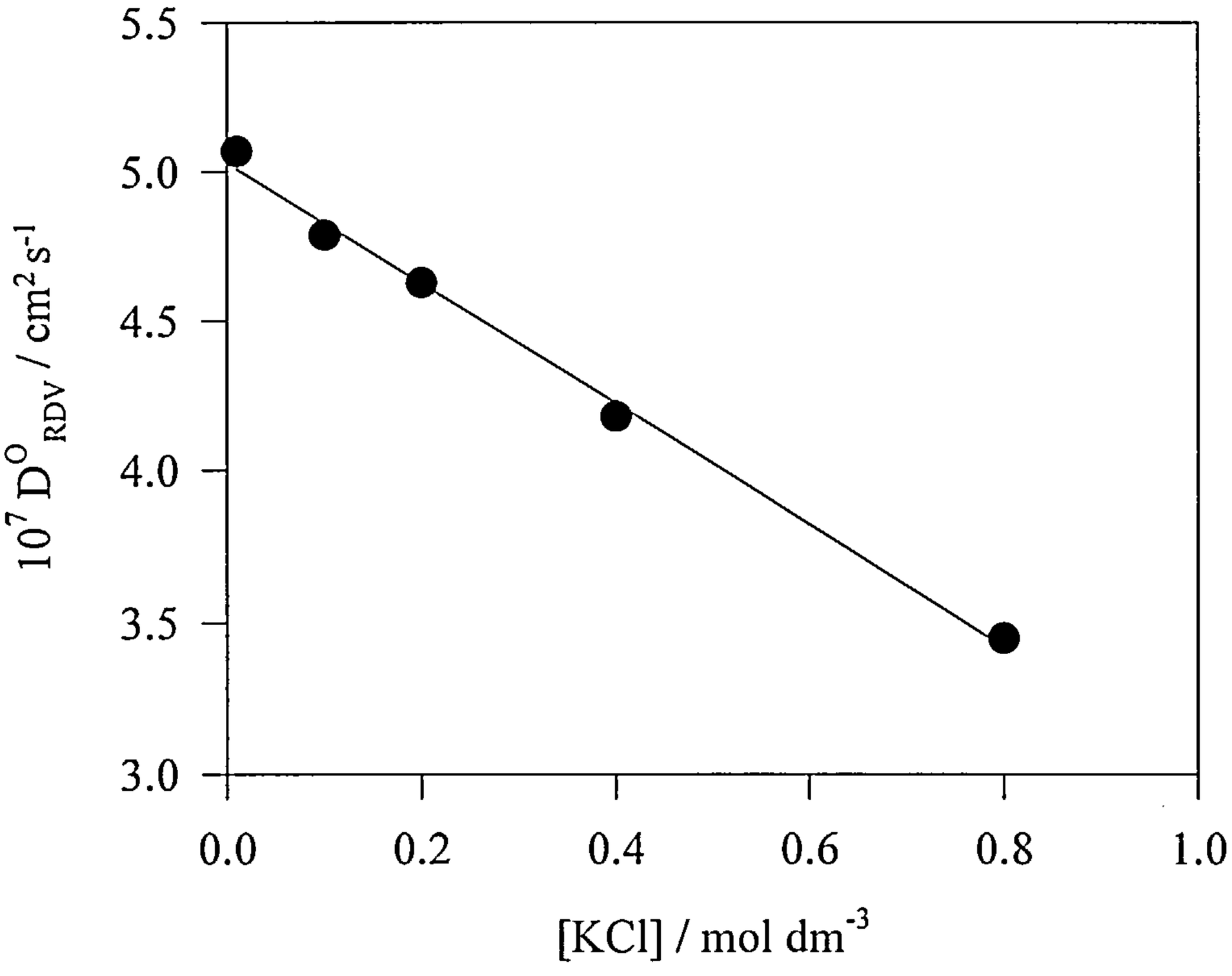

Appendix 3A.viii: Variation of intermicellar interaction parameter with added KCl

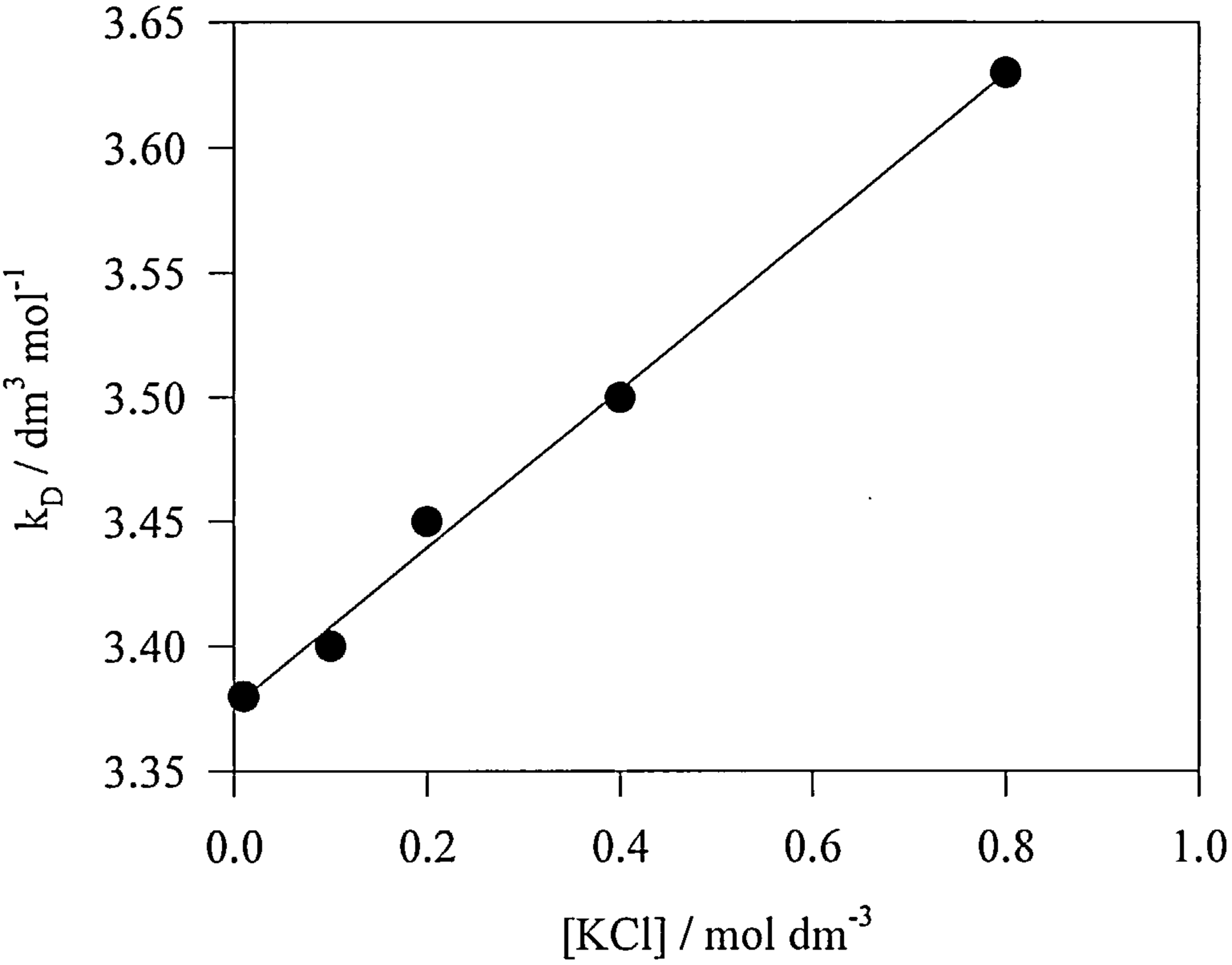

Appendix 3A.ix : Variation of micellar hydrodynamic radius with added KCl

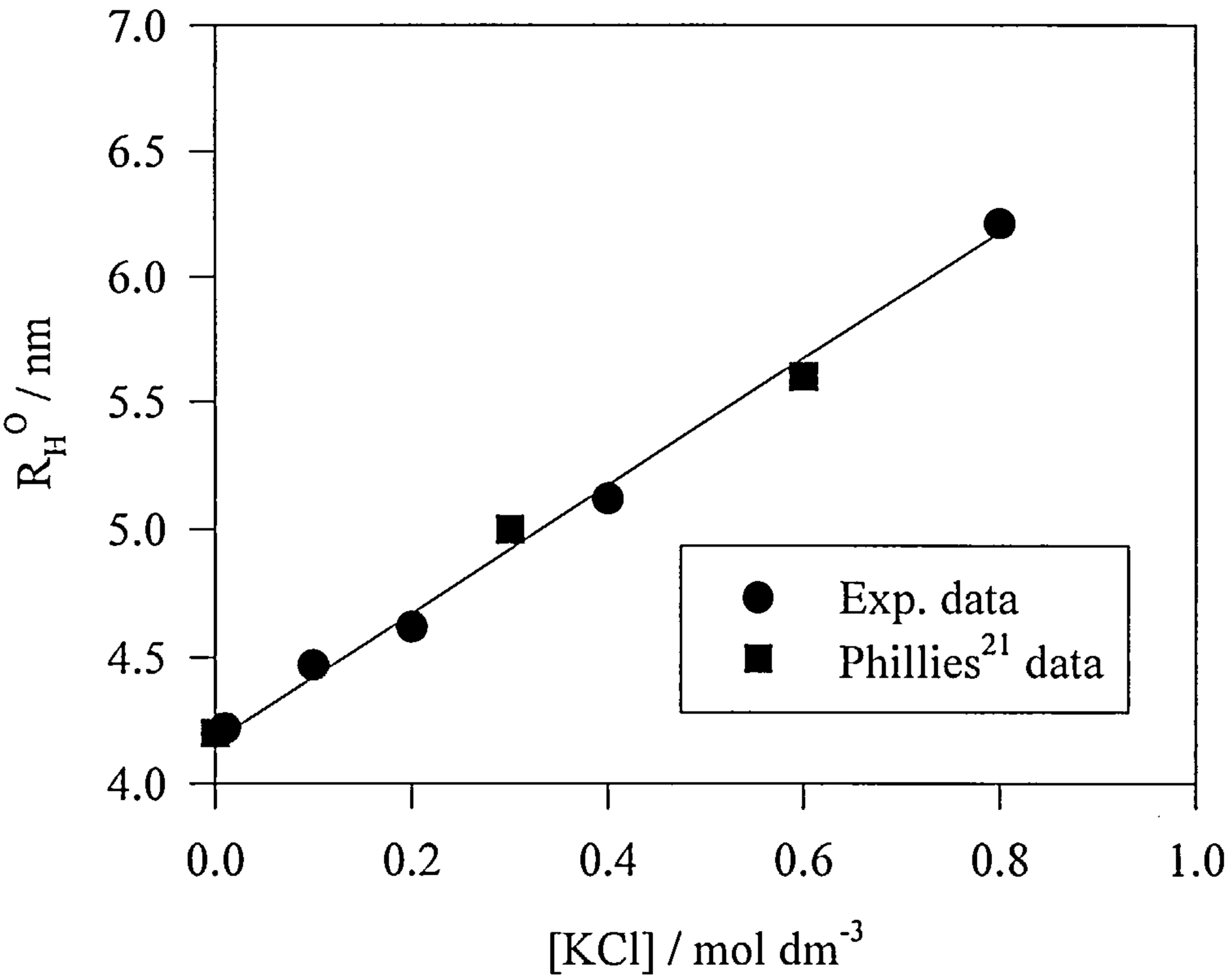

Appendix 3A.x : Variation of micellar hydrodynamic radius with intermicellar interaction parameter

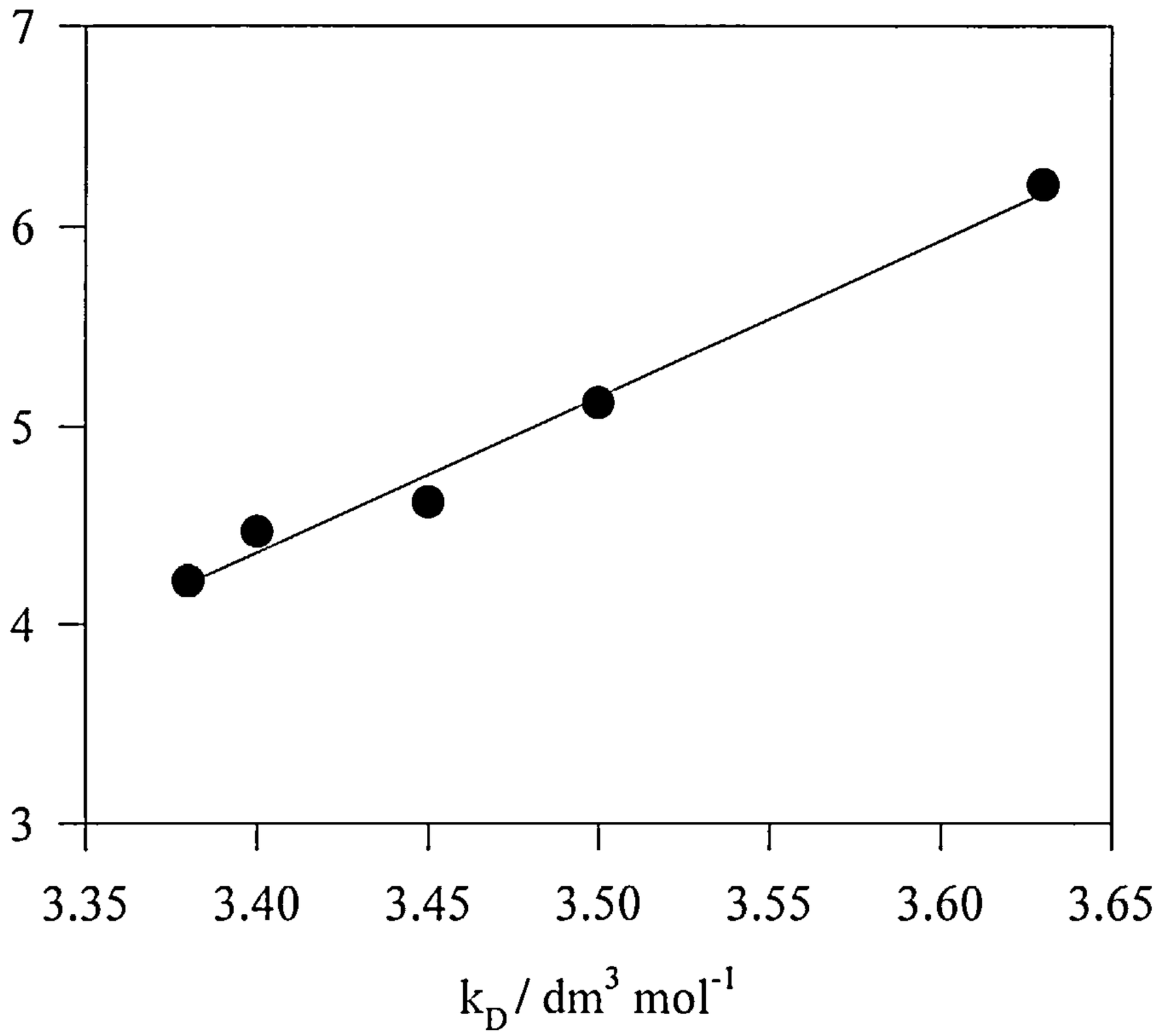

Appendix 3A.xi : Diffusion coefficient variation with added KCl (effect of varying temperature)

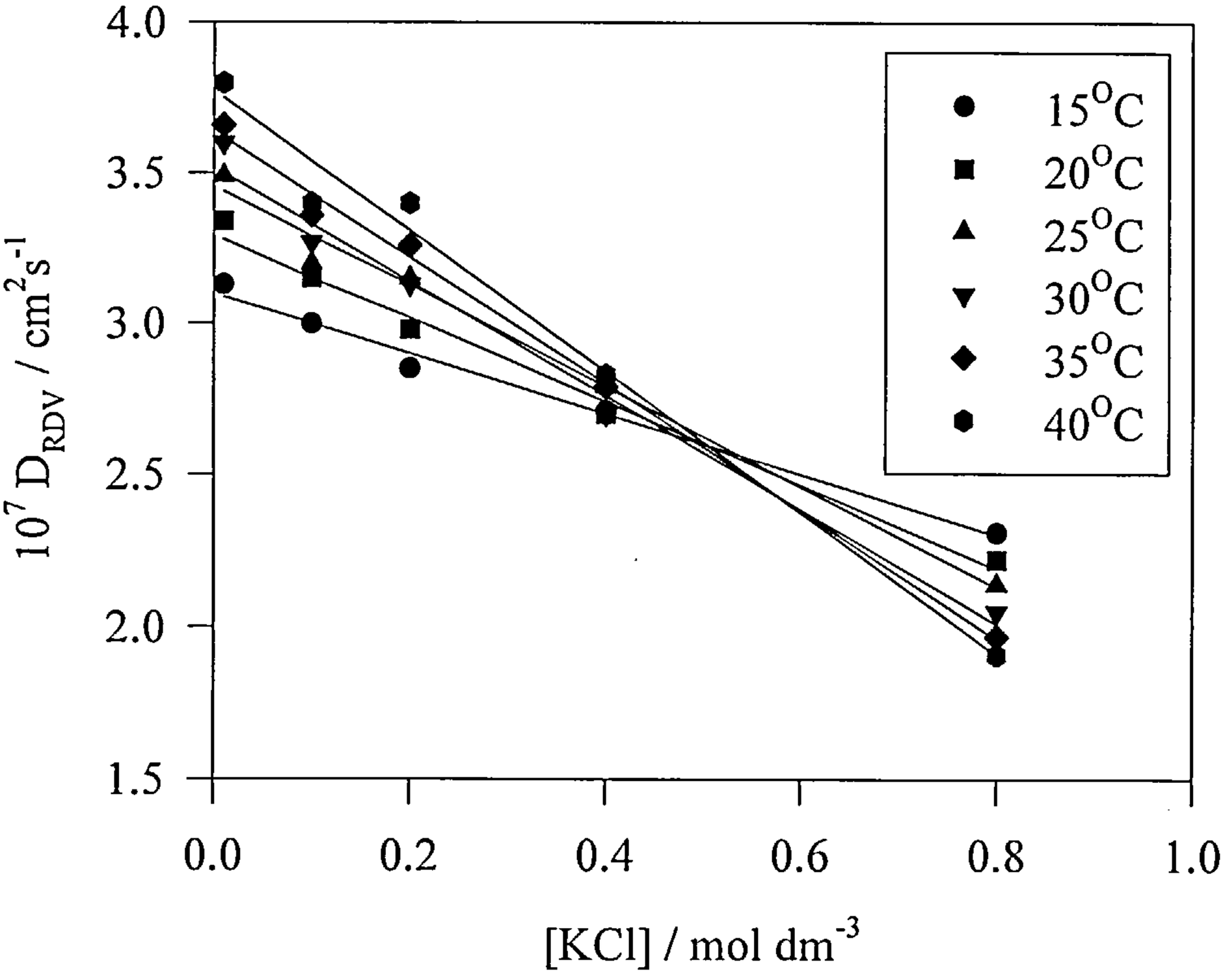

Appendix 3A.xii : Arrhenius plot for temperature dependent diffusion coefficient

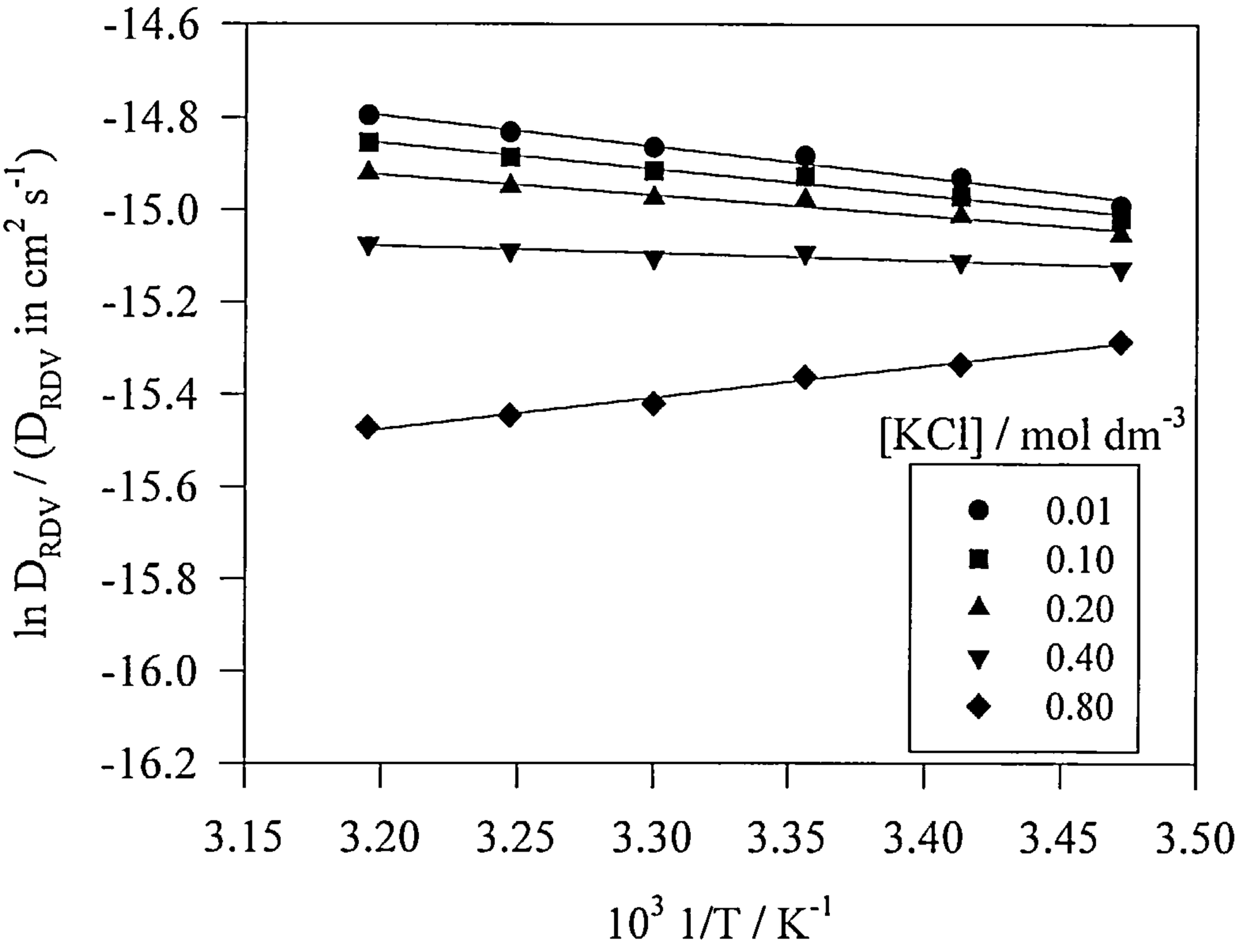

Appendix 3A.xiii : Variation of activation energy from arrenhius plots with added KCl

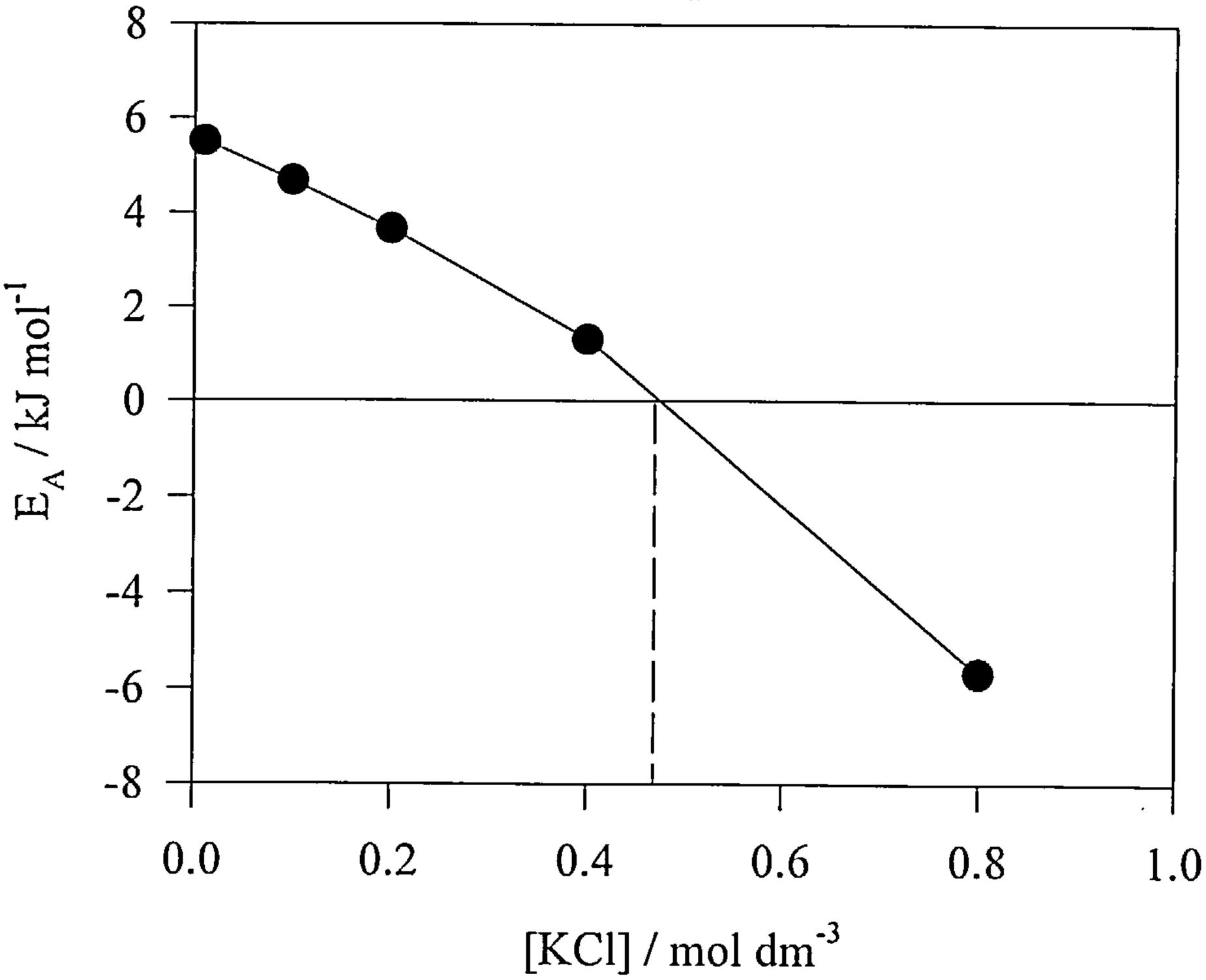

Chapter 3B: Rheology of Triton X-100

3B.1 Introduction

It was noted earlier that nonionic micelles exhibit no electrostatic interactions but rather excluded volume interactions (Ch. 3A.2.2.2). Therefore, inferences from rheological data can lead to properties of non-electrostatic interactions, hydration and micellar growth / shape change. A number of viscosity studies have been carried out on TX-100, the majority analysing the effect of surfactant concentration[3,14,15,16,22]. Few though have extensively examined the combined role of surfactant, electrolyte concentration and temperature. This chapter will explore how the phase behaviour of the TX-100 / water system can be significantly altered by changing the experimental conditions. Results will show how there appears to be a gradual change in the micellar shape dimensions. Some degree of micellar growth / phase transition occurs at a constant temperature difference ('distance') from the lower consolute curve regardless of electrolyte concentration.

3B.2 Results and Discussion

The static viscosities were measured on all of the solutions previously studied by RDV over a range of 0.033 - 0.167 mol dm^{-3} TX-100 and at 0.01, 0.10, 0.20, 0.40, 0.80 mol dm^{-3} KCl.

Experimental results for the viscosity at each [TX-100] are shown in Table 3B.1.

Table 3B.1 : Experimental viscosity results

[KCl] / mol dm^{-3}	$10^2 \eta$ / g cm^{-1} s^{-1}		
	0.033 mol dm^{-3} TX-100	0.10 mol dm^{-3} TX-100	0.167 mol dm^{-3} TX-100
0.01	1.15	1.62	2.49
0.10	1.15	1.65	2.56
0.20	1.15	1.69	2.70
0.40	1.15	1.73	2.86
0.80	1.15	1.83	3.23

Note: standard error = ± 0.01x10^{-2} g cm^{-1} s^{-1}, each measurement was repeated twice.

This data is illustrated in Appendix 3B.i along with lines of best fit. Correlation coefficients >0.998 were obtained, confirming that a linear fit was valid. This correlates well with the D_{RDV} values which displayed a linear dependence on the [KCl].

Table 3B.2: Linearly fitted values

[KCl] / mol dm^{-3}	$10^2 \eta$ / g cm^{-1} s^{-1}		
	0.033 mol dm^{-3} TX-100	0.10 mol dm^{-3} TX-100	0.167 mol dm^{-3} TX-100
0.01	1.15	1.62	2.48
0.10	1.15	1.65	2.57
0.20	1.15	1.67	2.67
0.40	1.15	1.73	2.86
0.80	1.15	1.83	3.24

3B.2.1 Results Analysis

It can be seen that at 0.033 mol dm^{-3} there is no apparent change in the viscosity over the range of KCl concentrations, whereas at 0.167 mol dm^{-3} TX-100 there is an increase of ~30%. This can be explained by the fact that the volume fraction (ϕ) of micelles at 0.167 mol dm^{-3} will be approximately five times greater that at 0.033 mol dm^{-3} as [TX-100] $\propto \phi^{41}$. The interparticle separation will therefore be reduced and

hence the probability of two micelles colliding and possibly combining leads to the observed increase in viscosity with increasing electrolyte concentration. In order to fully interpret the viscosity data, the results must be analysed in terms of a virial expansion. Brown et al.[15] have described the viscosity as a function of surfactant concentration and shape factors where η_{SP} is the specific viscosity $[(\eta/\eta_0) -1]$:-

$$\eta_{SP}/C_S = \nu V + \kappa V^2 C_S + \ldots\ldots \qquad (3B.1)$$

which reduces to:-

$$\eta/\eta_0 = 1 + \alpha V C_S + \beta V^2 C_S^2 \ldots\ldots \qquad (3B.2)$$

To avoid confusion in later analysis, α and β have replaced ν and κ respectively. η_0 is the viscosity at infinite dilution (1.005×10^{-2} g cm^{-1} s^{-1}), V is the micelle specific volume (0.91 cm^3 g^{-1} ≡ 1.76 mol dm^{-3})[47] with α and β representing the shape factors. The viscosity data described by this expansion is shown in Appendix 3B.ii. It can be seen that there is a common intercept at ~1.00 in fitting with expression (3B.2). A quadratic fit of the viscosity data provides values for α and β (Table 3B.3).

Table 3B.3 : Viscosity virial expansion parameters (shape factors)

[KCl] / mol dm^{-3}	α / no units	β / no units
0.01	0.72	13.96
0.10	0.59	15.44
0.20	0.45	17.01
0.40	0.18	20.06
0.80	-0.34	26.09

Values for α and β are seen to vary in a linear fashion with an increase in KCl concentration and are illustrated in Appendix 3B.iii. It is apparent from both plots that a decrease in α corresponds to an increase in β, which would tend to suggest that a change in shape/asymmetry is occurring[15]. If an oblate micelle is assumed, the change in shape factors would relate to increase in the ratio of long dimension semi axis : short dimension semi axis (a/b). This would infer that the micelle is tending

towards a rod shaped micelle, and due to the linear changes in α and β, gradual structural evolution is proposed. This correlates well with the linear increase in the apparent hydrodynamic radius (R_H^O) on [KCl] as calculated from self-diffusion coefficients (Ch. 3A.2.2.3). At a [KCl] ~ 0.50 mol dm^{-3}, it can be seen that the value for α = 0, this corresponds with the activation energy calculations where $E_A = 0$ at the same electrolyte concentration (Ch. 3A.2.3.3). It may be that a negative value for α is indicative of spontaneous micellar growth i.e. a negative value for the free energy (Ch. 3A.2.3.3) though this is contradicted somewhat by the linear relationship of α and β. It could be postulated that if large scale flocculation was occurring a non-linear dependence of α and β would be observed. This hypothesis is confirmed somewhat by the absence of any dramatic increases in viscosity over the KCl range whereas for CTAC a precipitous increase in η was characteristic of a significant structural change i.e. a sphere to rod transition (Ch. 4B.2.1).

It must also be noted that an increase in the micelle size / shape change leads to an alteration in the intermicellar radial distribution function as well as the hydrodynamic interactions[21]. This has the affect of increasing the range of micellar hard core repulsion in comparison to the apparent hydrodynamic radius[21]. So, it is possible that any inference from viscosity data relating to an apparent change in shape may need to consider changes in excluded volume interactions between micelles. However, it is more likely that the change in micellar size (Ch. 3A.2.2.3) attended by a change in shape is accurately illustrated by the α and β relationship[15].

3B.2.1.1 Intrinsic Viscosity

The degree of hydration of TX-100 micelles is a very important factor as it influences shape, size and ethylene oxide chain conformation. From rheological analysis, the easiest way to calculate the degree of hydration is from the intrinsic viscosity [η]. The intrinsic viscosity effectively removes any contributions from intermicellar interactions by extrapolating to infinite dilution. At low concentrations

the viscosity of the micellar solution (η) is related to the viscosity of the solvent (η_0) and surfactant concentration (C_S) by the relationship[57]:-

$$\eta = \eta_0 \{1 + [\eta]C_S + ...\} \qquad (3B.3)$$

The intrinsic viscosity can be said to be a virial coefficient and it follows that it can be measured by taking the limit as $C_S \rightarrow 0$.

$$[\eta] = \lim_{C \rightarrow 0} \{[(\eta/\eta_0) - 1]/C_S\} \qquad (3B.4)$$

Hence, the intrinsic viscosity can be found from the intercept of $[(\eta/\eta_0) - 1]/C_S$ against C_S for each KCl concentration. These plots are shown in Appendix 3B.iv. The $(\eta/\eta_0) - 1$ values are shown in Table 3B.4 as a function of C_S along with the resultant $[\eta]$ values (shown in Appendix 3B.v).

Table 3B.4 : Calculated intrinsic viscosities

[KCl] / mol dm^{-3}	$\{[(\eta/\eta_0) - 1]/ C_S\}$ / $cm^3 g^{-1}$			$[\eta]$ / $cm^3 g^{-1}$
	$C_S = 0.0208$ / g cm^{-3}	$C_S = 0.0624$ / g cm^{-3}	$C_S = 0.104$ / g cm^{-3}	
0.01	6.98	9.84	14.10	6.09
0.10	6.98	10.25	15.00	5.91
0.20	6.98	10.67	15.91	5.73
0.40	6.98	11.51	17.72	5.35
0.80	6.98	13.19	21.34	4.61

Note: For [η] to be in the correct units the surfactant concentration was converted from mol dm^{-3} to g cm^{-3} by multiplying by 624 g mol^{-1} / 1000.

It may be expected that a linear dependence of $[(\eta/\eta_0) - 1]/C_S$ with C_S should be observed. This is only strictly true at lower surfactant concentrations than have been studied here, but the data is still valid as perfect quadratic plots were obtained (See Appendix 3B.iv). Brown et al.[15], also analysed viscosity data using quadratic plots which lead to $[\eta]$ values in agreement with those presented here. There is further

confirmation when the results are compared to published values with [η] varying between 4.5 - 7.3 $cm^3\ g^{-1}$ depending on the temperature[22,27,47].

From Appendix 3B.v it can seen that there is a linear dependence of [η] on the KCl concentration. This can be explained by gradual dehydration of the micelles on the addition of electrolyte as has been discussed earlier (Ch. 3A.2.2.2, Ch. 3A.2.2.3). Brown et al. showed a drop in [η] with an increase in temperature and attributed it to dehydration and/or contraction of the EO chains[15]. As the extension of the an EO chain has been calculated at 1.52-1.72 (Ch. 3A.2.2.3), if any contraction occurred the chains would have to be extremely coiled[44]. Therefore, the observed decrease in [η] can be proposed to be predominately due to dehydration. An electrolyte induced linear increase in micellar size was observed in Ch. 3A.2.2.3 and it follows that a linear plot of R_H^O against [η] (Appendix 3.vi) illustrates the intimate relationship between micellar size, viscosity and (de)hydration.

3B.2.1.2 Degree of Hydration

A number of authors have related the intrinsic viscosity of a micelle solution to the partial specific volumes of TX-100 / water (υ_T, υ_W), the Simha factor (ν) and hydration parameter (δ)[22,27,47]. The partial specific volume represents the volume contribution from 1 g of solute to the solvent.

$$[\eta] = \nu(\upsilon_T + \delta\upsilon_W) \qquad (3B.5)$$

Values for υ_T and υ_W have been given as 0.91 cm^3g^{-1} and 1.0 cm^3g^{-1} respectively[15]. The shape or Simha factor has values of 2.5 for spheres (sp), 2.8 for oblate (ob) ellipsoid and 6.1 for prolate (pr) ellipsoid[47]. The only problem regarding this analysis is that ν and δ are inseparable and prior knowledge of either parameter is required to estimate the other[22,47]. As was stated earlier, the shape of the micelle (and therefore ν) cannot be implicitly stated from either viscosity or diffusion coefficient results.

Hence values for δ are calculated from expression 3B.5 using each of the aforementioned values for ν.

Table 3B.5 : Calculated hydration parameters

[KCl] / mol dm^{-3}	[η] / cm^3g^{-1}	δ (g H_2O / g surfactant)		
		ν = 2.5 (sp)	ν = 2.8 (ob)	ν = 6.1 (pr)
0.01	6.09	1.53	1.27	0.09
0.10	5.91	1.45	1.20	0.06
0.20	5.73	1.38	1.13	0.03
0.40	5.35	1.23	1.00	-0.03
0.80	4.61	0.93	0.74	-0.15

The first observation that can be made is regarding the prolate ellipsoid model. The values for δ are low and are even negative at high [KCl]. This was also observed by Robson et al.[47] and Birdi[27] and both authors concluded that the prolate model was therefore unacceptable for characterising a TX-100 micelle. Both Robson et al. and Birdi proposed that from intrinsic viscosity considerations the oblate model best described the micellar shape[27,47]. However, as the δ values here for spherical and oblate are comparable neither model can be totally discounted.

As was mentioned earlier (Ch. 3A.2.2.2), water molecules are hydrogen bonded to the ether oxygens in the PEO chains, and the degree of hydrogen bonding that determines the shape, size etc. By multiplying δ by the molecular weight of one hydrophilic EO chain, it is possible to estimate the number of water molecules per ethylene oxide chain. Birdi[27] appeared to use the molecular weight of the whole surfactant chain for the calculation which would appear to give the amount of water per TX-100 molecule, but as there will be little solvent penetration into the hydrophobic core this may be misleading[44]. Values for the number of water molecules per EO chain using both the MW of TX-100 (624 g mol^{-1}) and the hydrophilic ethylene oxide part (435 g mol^{-1}) are given in Table 3B.6.

Table 3B.6 : Number of water molecules per EO chain

[KCl] / mol dm^{-3}	Spherical model		Oblate model	
	Whole TX-100 molecule	EO chain only	Whole TX-100 molecule	EO chain only
0.01	53	37	44	31
0.10	50	35	42	29
0.20	48	33	39	27
0.40	43	30	35	24
0.80	32	23	26	17

Values have been reported between 20 and 50 H_2O molecules per EO chain though these most of these studies were carried out at a number of electrolyte concentrations[1,14,17,22,27,44,50]. It must be noted, however, that different techniques employ different definitions of micellar hydration i.e. whether the solvent is specifically bound to the micelle and / or associated with the micelle as a kinetic component[55]. Nevertheless, there is considerable agreement between the experimental values and those in the literature[1,14,17,22,27,44,50] which tends to support the application of electrochemical techniques as tools for probing micellar hydration.

3B.2.1.3 Micellar Structure

The main problem in the analysis of intrinsic viscosity is the associated relationship between the shape factor (ν) and the hydration parameter (δ). It follows that for accurate determination of both quantities, two independent methods are required. Mandal et al.[22] have used Vand's equation[58] to determine the micellar shape parameter:-

$$1/\log \eta_r = 2.303/\nu V_h C_S - 2.303Q/\nu \qquad (3B.6)$$

where $\eta_r = \eta/\eta_0$, V_h is the hydrated specific volume and Q is a constant. Therefore a plot of $1/\log\eta_r$ against $1/C_S$ will yield a gradient of $2.303/\nu V_h$ and an intercept equal to $-2.303Q/\nu$. The only parameter unknown is V_h, which Mandal et al. calculated from conductance measurements[22]. This was used in Vand's equation and with Q

values between ~3.4 - 8.4, subsequent ν values ranged from 3.85 - 4.18. Both these values seem higher than could be expected, since ν for spheres and oblate are 2.5 and 2.8 respectively[47] and Vand has stated that Q = 0.61 for rigid non-solvated spheres. Nevertheless, plots of $1/\log\eta_r$ against $1/C_S$ were constructed (Appendix 3B.vii) and the resultant gradient and intercept found (Table 3B.7).

Table 3B.7 : Vand's equation parameters

[KCl] / mol dm^{-3}	$(1/\log\eta_r)$ / dm^3mol^{-1}			$2.303/\nu V_h$ (slope) / mol dm^{-3}	$-2.303Q/\nu$ (intercept) / no units
	$1/C_S = 30.0$	$1/C_S = 10.0$	$1/C_S = 6.0$		
0.01	16.98	4.81	2.55	0.604	-1.142
0.10	16.98	4.66	2.45	0.609	-1.305
0.20	16.98	4.51	2.36	0.614	-1.461
0.40	16.98	4.25	2.20	0.623	-1.735
0.80	16.98	3.83	1.97	0.637	-2.155

It is expected that the hydrated specific volume of the micelle will decrease on the addition of KCl due to dehydration, and therefore only a ν value at 0.01 mol dm^{-3} (no significant dehydration) can be estimated. A value of $V_h \sim 0.97$ dm^3 mol^{-1} at 20 ^oC can be found from data presented by Mandal et al.[22], which leads to a ν = 3.93. Although this is higher than maybe expected it is in excellent agreement with the reported values[22]. The deviation from values of ν = 2.5 (sphere), 2.8 (oblate), may suggest that the micelle is more of a elongated oblate shape i.e. tending towards a prolate (ν = 6.1). Nevertheless, the results still confirm that the micelles have a shape close to oblate. An illustration of the possible micellar elongation process is shown below.

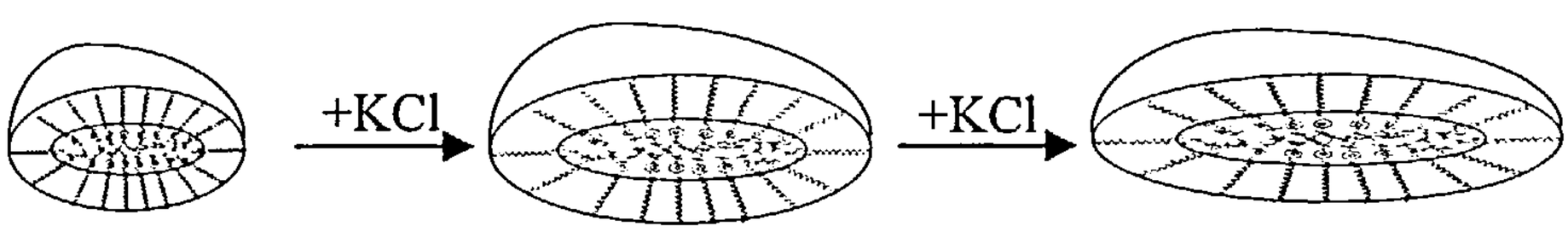

Figure 3B.1 : Elongation process for electrolyte induced growth of TX-100 micelles

The aggregation number (N_{agg}) is one property that is very important in determining the micellar size and shape. For a small value of N_{agg} the micelle is

likely to be close to spherical due to it being the thermodynamically most favoured structure[27]. The nature of the surfactant chain means that there will be a certain value of N_{agg} at which a spherical form becomes unfavourable and a shape change occurs. It has been shown previously (Ch. 3A.2.2.3) that a gradual shape change occurs with an increase in [KCl] and this is primarily due to a dehydration induced increase in aggregation number. Few studies have investigated the affect of electrolyte on the aggregation number of TX-100 micelles. One such study reports an increase in N_{agg} of 79 - 125 over a range of [NaCl] = 0.0 - 0.6 mol dm^{-3}, though it is generally accepted that the aggregation number of TX-100 micelles lies somewhere between 100-140[11,15,20,41,47]. Geetha et al. have reported a relationship between the hydrodynamic radius, intrinsic viscosity and the micellar molecular weight[28].

$$R_H^O = \{3[\eta]M_W / 10\pi N_A\}^{1/3} \qquad (3B.7)$$

which can be rearranged in terms of the aggregation number, as the weight of one surfactant chain is known (624 g mol^{-1}), where $N_{agg} = M_W / 624$:-

$$N_{agg} = 10\pi N_A(R_H^O)^3 / 1872.[\eta] \qquad (3B.8)$$

Values for R_H^O and [η] were determined in Ch. 3A.2.2.1 and 3B.2.1.1 respectively. Table 3B.8 below and Appendix 3.viii show how the aggregation number is affected by an increase in electrolyte concentration.

Table 3B.8 : Variation of Aggregation number with [KCl]

[KCl] / mol dm^{-3}	N_{agg} / no units
0.01	125
0.10	153
0.20	174
0.40	253
0.80	525

It can be seen that at 0.01 mol dm^{-3} KCl, a value of N_{agg} = 125 is in excellent agreement with reported values (N_{agg} = 100 - 140)[11,15,20,41,47]. A subsequent increase in electrolyte concentration causes a massive increase in N_{agg} which shows that a

spherical shape cannot exist and therefore a change in dimensions, and consequently shape, must be occurring. From aggregation numbers alone a transition from an oblate to a rod shape micelle is postulated. The nature of this shape change cannot be proved by the results presented, but the conclusions from micellar intrinsic viscosity, hydration and structure demonstrate that any changes in micellar dimensions are correlated with size changes due to volume packing effects[41].

3B.2.2 Effect of Temperature

A limited number of studies have reported the variation of TX-100 viscosity with temperature, the majority analysing the effect of surfactant concentration. Obviously an increase in the volume fraction of micelles will increase the likelihood of micellar growth, but it is interesting to investigate how the supporting electrolyte will effect the viscosity at a set surfactant concentration. To my knowledge only one report presents viscosity data of a TX-100 / water / electrolyte system at different temperatures[43]. This data has been interpreted as changes in the spontaneity of a micellar sphere-rod transition. Previously in Ch. 3A.2.3, the temperature dependence of the diffusion coefficient was studied over a range of temperatures and KCl concentrations and similar inferences regarding phase changes were proposed. Therefore, studying the viscosity under an identical set of conditions will further enhance knowledge of the TX-100 / water phase behaviour.

Experimental results are shown in Table 3B.9 and illustrated in Appendix 3B.ix.

Table 3B.9 : Experimental results

T / ^{O}C	10^2 η / g cm^{-1} s^{-1} : effect of [KCl] / mol dm^{-3}				
	0.01	0.10	0.20	0.40	0.80
15	1.77	1.82	1.84	1.86	1.90
20	1.62	1.65	1.67	1.73	1.83
25	1.50	1.53	1.57	1.67	1.92
30	1.45	1.50	1.55	1.68	2.05
35	1.43	1.49	1.56	1.74	2.24
40	1.45	1.54	1.64	1.87	2.55

Note: standard error for Table 3B.9 = $\pm 0.01 \times 10^{-2}$ g $cm^{-1}s^{-1}$

The most apparent observation from Appendix 3B.ix is how dramatically the viscosity is affected by a combination of temperature and electrolyte concentration. In Ch. 3B.2.1.1, it was noted that independent increases in both [KCl] and temperature[15] had the effect of decreasing the intrinsic viscosity [η] and increasing the micellar size (Ch. 3A.2.2.3) due to dehydration of ethylene oxide chains. It follows that the associative effect of both quantities should be much greater, as was observed from diffusion coefficient results (Ch. 3A.2.3).

Zhizhen et al.[43] measured the viscosity of TX-100 over a range of electrolyte concentrations ([NaCl] = 0.05 - 0.50 mol dm^{-3}) and observed a monotonic increase in η over a temperature range of 30-50 ^{O}C. The behaviour was such that a set of Arrhenius plots were constructed and values for free energy of activation parameters obtained (ΔG*, ΔH*, ΔS*). It is obvious from Appendix 3B.ix that this expected Arrhenius response is not present, though it is not apparent why a difference should exist between both sets of data although it is possible that the difference in electrolyte cation (Na^+ vs. K^+) may lead to different dehydration characteristics[42,43].

By far the most significant observation from Appendix 3B.ix, is regarding the temperature at the point of minimum viscosity ($T_{\eta,min}$). From Table 3B.10 and Appendix 3B.x, $T_{\eta,min}$ is seen to decrease linearly with an increase in [KCl].

Table 3B.10 : Temperature at minimum viscosity and cloud point variation with [KCl]

[KCl] / mol dm^{-3}	$T_{\eta,min}$ / ^{O}C	T_C / ^{O}C
0.01	35.0	65.0
0.10	32.5	63.5
0.20	30.7	61.8
0.40	26.9	58.7
0.80	19.0	52.1

Note: T_C data from reference 42

If these two temperature range are compared, it can be seen there is a constant difference with $T_C - T_{\eta,min} = 31.4 \pm 1.7$ ^{O}C. This would tend to suggest that there is some micellar growth or shape change at a temperature of 31.4 ^{O}C away from the lower consolute curve regardless of electrolyte concentration. Zana et al. have reported similar behaviour for $C_{12}E_n$ surfactants (n = 6, 8, 9) with micellar aggregation numbers remaining constant till T_C - 35 ^{O}C whereupon the rapid large scale growth occurs[46]. Kato et al. observed a similar phenomenon and suggested that the T_C - 35 ^{O}C dependency was either a factor of increasing micellar weight or a dominance of attractive interactions[29]. However, it has been shown that Triton X-100 exhibits a linearly increasing aggregation number up to 50 ^{O}C[46], which obviously contradicts the experimental results presented here. However, the results are in excellent agreement with those for other surfactants with PEO moieties, of which the dehydration characteristics would be alike, which tends to add credence to the trend observed[29,46].

Below $T_{\eta,min}$ the viscosity is seen to decrease reasonably slowly with increasing temperature, and above a increase is seen which is more dramatic at high [KCl]. A similar observation was noted by Lesemann et al. on a n-dodecyl pentaethylene oxide ($C_{12}E_5$) / D_2O surfactant system[59]. It was seen that the value of $T_{\eta,min}$ shifted to lower temperatures with an increase in the concentration of $C_{12}E_5$ which is analogous to an increase in [KCl]. Below $T_{\eta,min}$ the viscosity was deemed to be due to non-interacting micelles and above deviation from hard sphere behaviour could be expected[59]. The observed increase in viscosity will represent either significant micellar growth or a shape change[19], due to micellar dehydration, but conversely from diffusion coefficient measurements a linear dependence on temperature and [KCl] was seen. It is therefore possible that the viscosity values are influenced by significant van der Waals micelle-micelle interaction[59].

It is obvious from the results presented here, that the Arrhenius relationship observed for the diffusion coefficient is not apparent for viscosity. It is therefore possible that for the nonionic system the viscosity is more sensitive to changes in shape and / or micellar growth. This divergence in behaviour from diffusion

coefficient results highlights the need for complimentary techniques to fully characterise the size, growth and interaction properties of nonionic micellar systems.

3B.3 Summary

The rheological properties of a series of TX-100 micellar solutions have been measured using a cone and plate viscometer over a range of surfactant (0.033 - 0.167 mol dm^{-3}) and electrolyte (0.01 - 0.80 mol dm^{-3}) concentrations. A linear increase in viscosity was seen with increasing [TX-100] which corresponds with the diffusion coefficient results (Ch. 3A.2.2). The linear dependence of viscosity on the increasing KCl concentration indicated gradual micellar growth rather than a sudden change. This was also in agreement with observations from diffusion coefficient data. Analysis of the viscosity virial expansion showed a linear relationship of α, β with KCl concentration. A decrease in α corresponded to a increase in β, again indicating a gradual change of micellar shape from oblate (or quasi spherical) to rod-like. This was a modification of both literature and experimental assumptions that the dimension ratio (a / b) remains constant (Ch. 3A.2.2.3). This has the consequence of altering the interpretation of the R_H^O values and hence the derived micellar growth pattern (Ch. 3A.2.2.3). However, the α and β data was unable to provide a quantitative range of a / b values, but rather provided a different perspective with regards to the micellar growth pattern i.e. oblate expansion (diffusion coefficient) : a / b = constant; sphere - elongated micelle transition (viscosity) : a / b increased.

The intrinsic viscosity [η] has been shown to decrease as the [KCl] increases. Further analysis of [η] lead to a calculation of the hydration parameter (δ), which decreased with [KCl], confirming the theory that KCl will dehydrate the hydrophilic micellar region. δ values correspond to 2 - 5 water molecules per EO unit, which depend on the shape model chosen. This confirmed that δ and ν are intimately associated values. Using an expression to link the intrinsic viscosity and the hydrodynamic radius, the aggregation number was determined. The effect of electrolyte was quite dramatic and shows that a truly spherical micelle is unlikely to

exist even at low [KCl] due to packing requirements. Therefore, the statement that the micelle is likely to be quasi-spherical appeared to be validated.

The use of Vand's equation allowed the calculation of the shape parameter (ν). Although a value of $\nu = 3.93$ at 0.01 mol dm^{-3} KCl appeared high compared to spherical (2.5) and oblate (2.8), it was in excellent agreement with literature measurements. However, from δ values the prolate model was unacceptable (negative δ), which suggested that the micellar shape was close to oblate, though maybe slightly elongated.

The combined effect of both temperature and electrolyte concentration significantly influenced the micellar system phase behaviour. Micellar growth / shape change appeared to occur at lower temperatures when a high electrolyte concentration was present. This was illustrated by a plot of viscosity against temperature which showed an electrolyte dependent minimum in viscosity. The temperature at which this occurred decreased in a linear fashion as [KCl] increased. This temperature remained at a constant value of 31.4 ^{O}C away from the lower consolute curve (which decreased with increasing [KCl]). It became clear that that this temperature difference from the cloud point is indicative of some micellar growth / shape change. This viscosity data due to the combined affect of electrolyte and temperature was not mirrored by the diffusion coefficient results (Ch. 3A.2.3.1). The reason for this was not apparent, but it may be linked to a greater sensitivity of the rheological properties to alterations in the phase behaviour of the system.

Appendix 3B.i : Variation of solution viscosity with added KCl

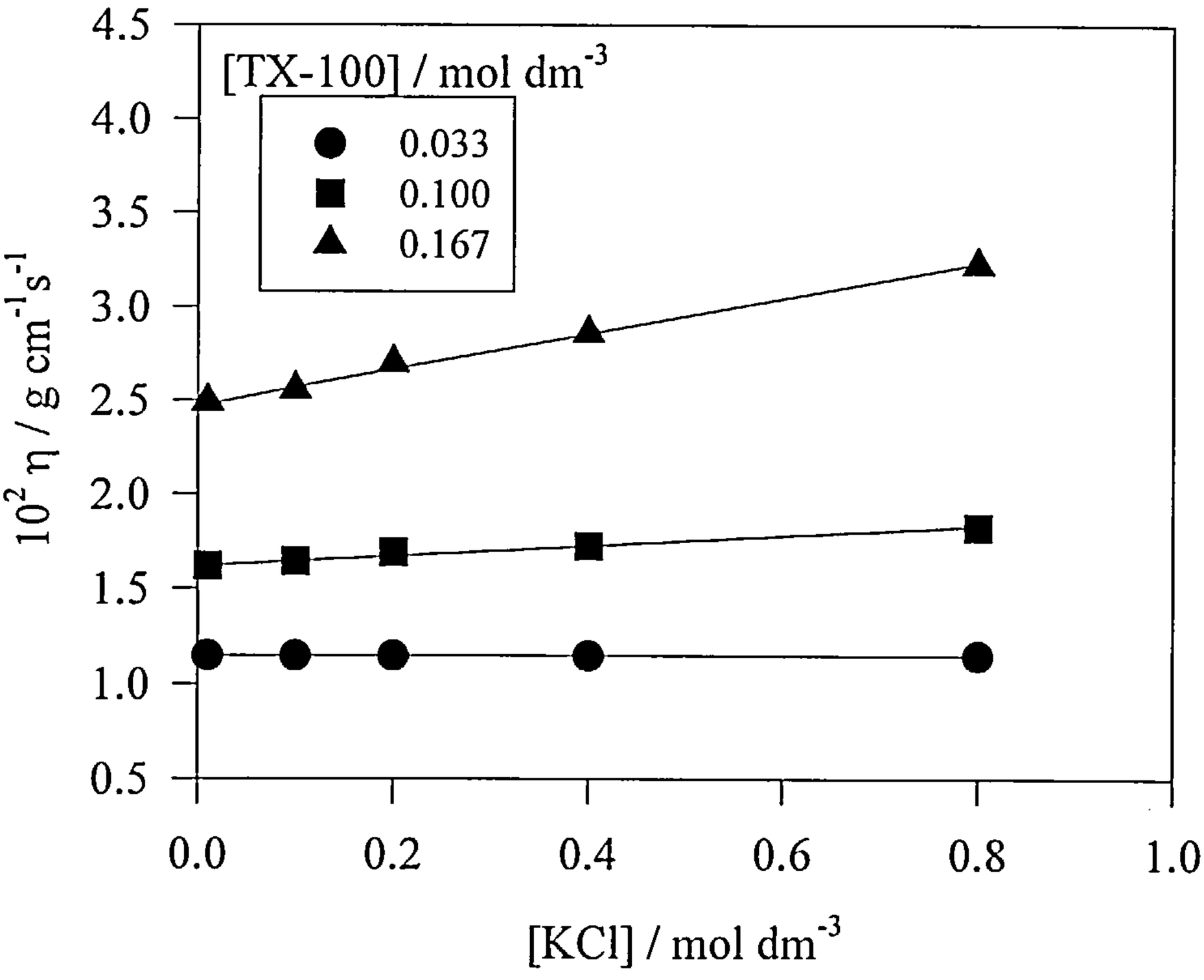

Appendix 3B.ii : Variation of solution viscosity with [TX-100] (effect of added [KCl])

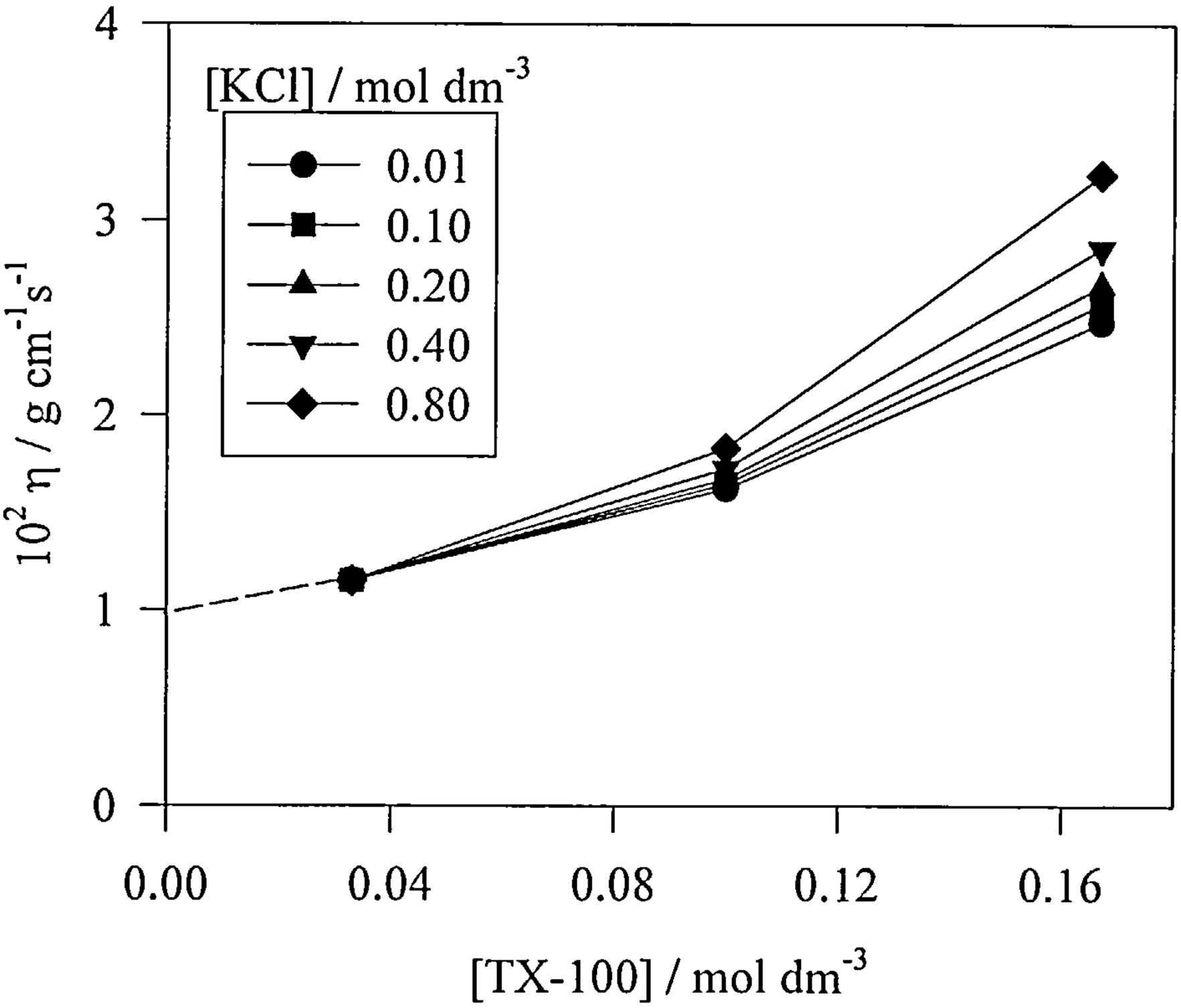

Appendix 3B.iii : Variation of shape parameters (α,β) with added KCl

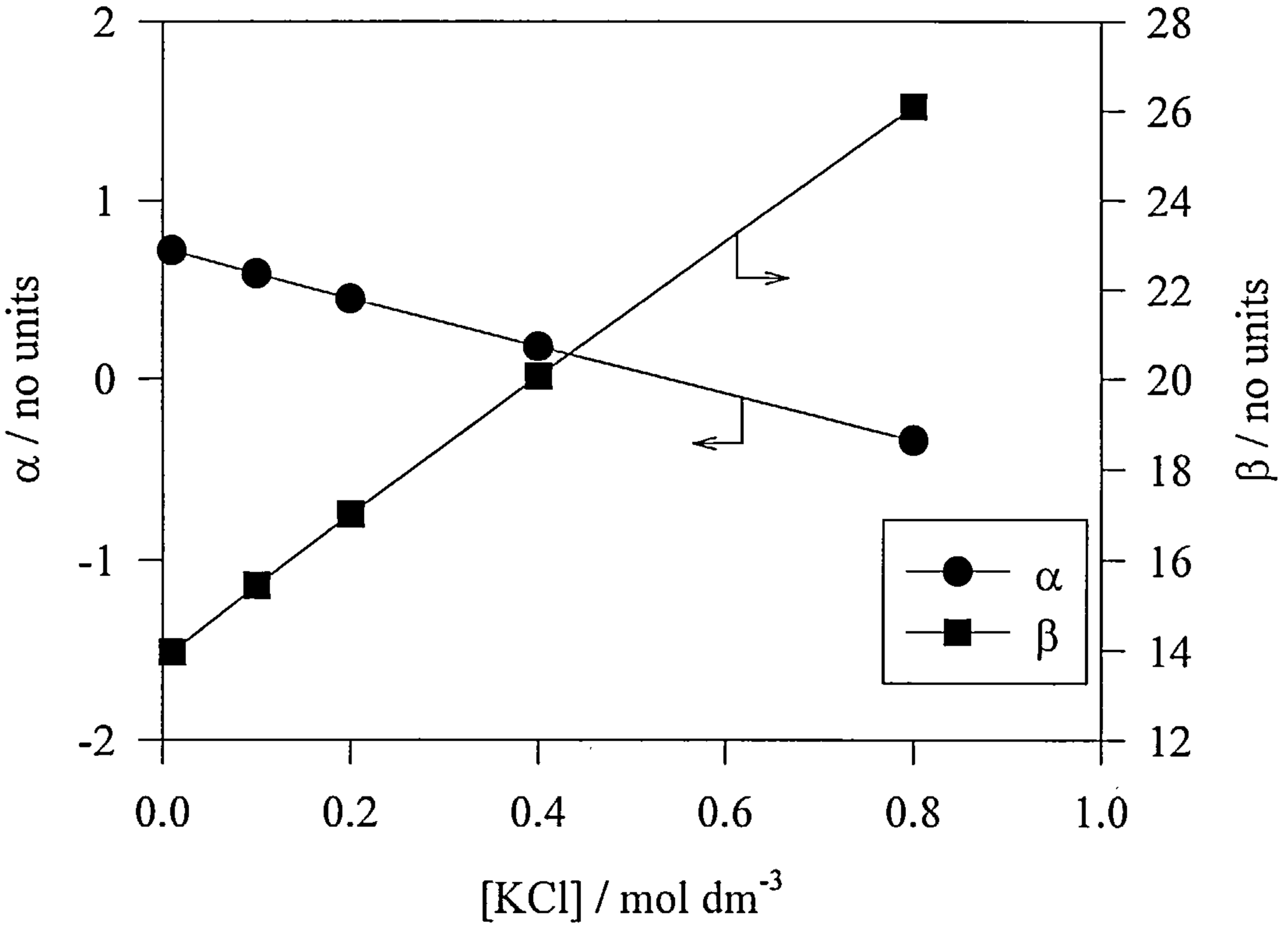

Appendix 3B.iv : Variation of [(η/η_o-1)]/[TX-100] with [TX-100] (effect of added KCl)

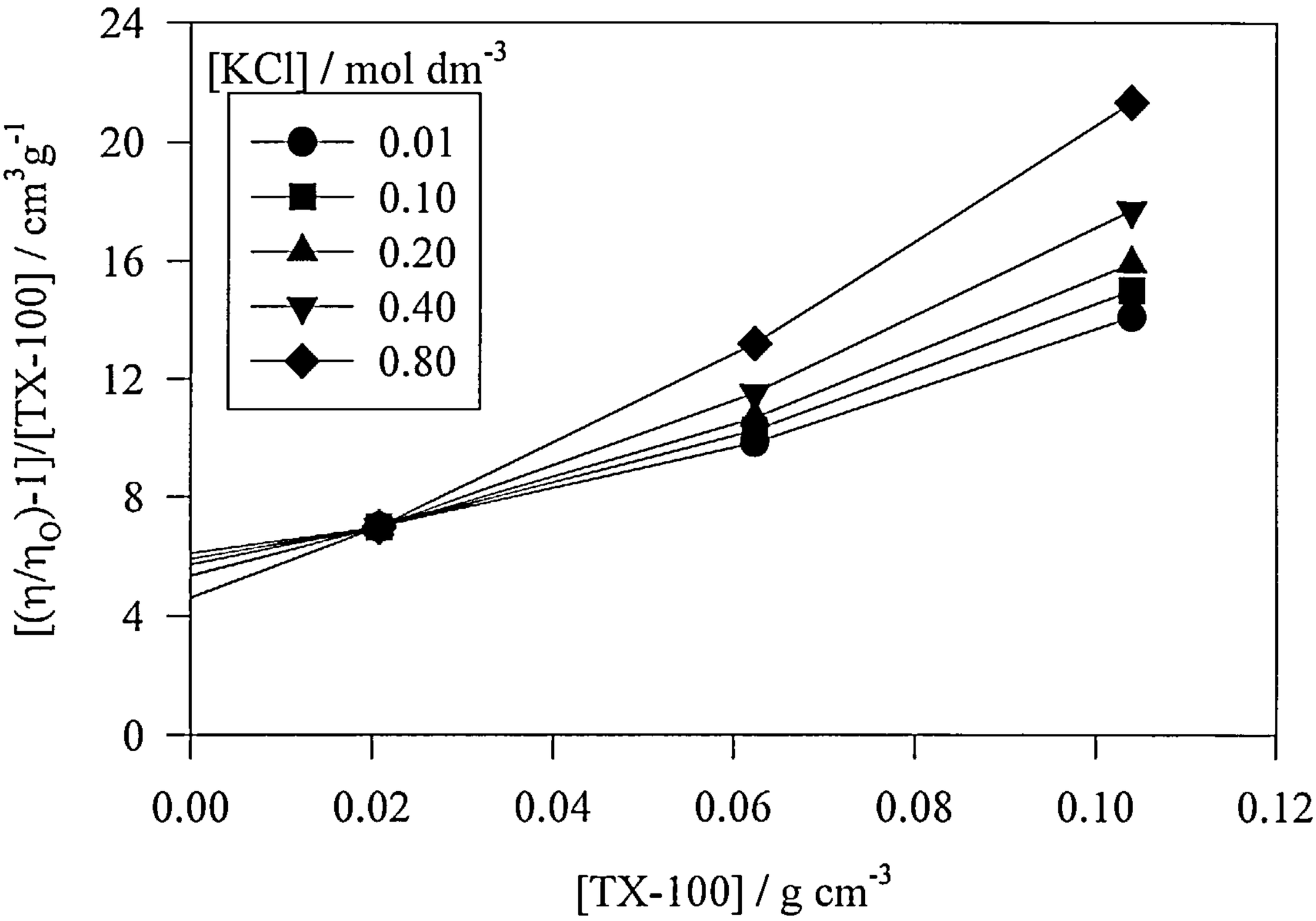

Appendix 3B.v : Variation of intrinsic viscosity with added KCl

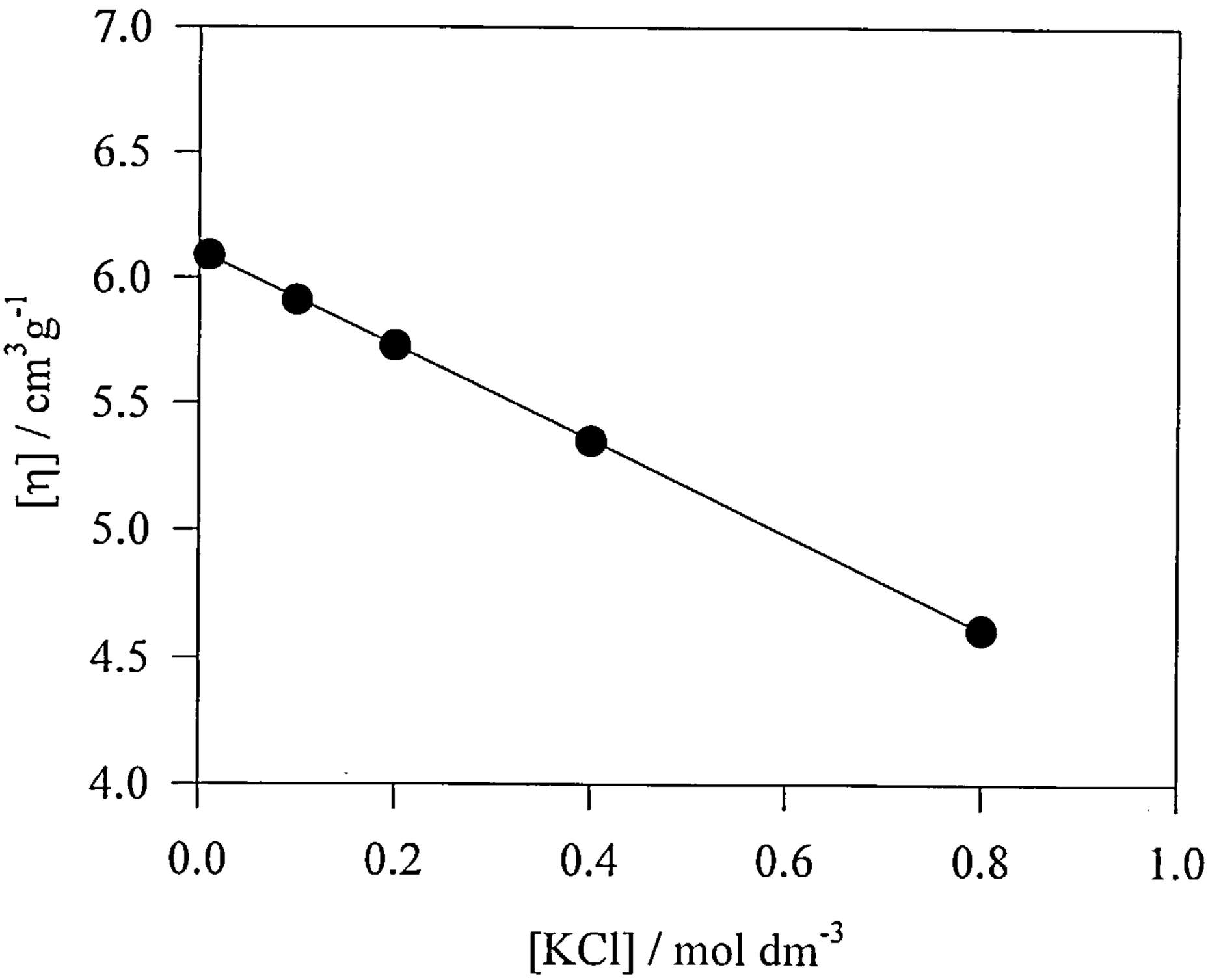

Appendix 3B.vi : Variation of intrinsic viscosity with hydrodynamic radius

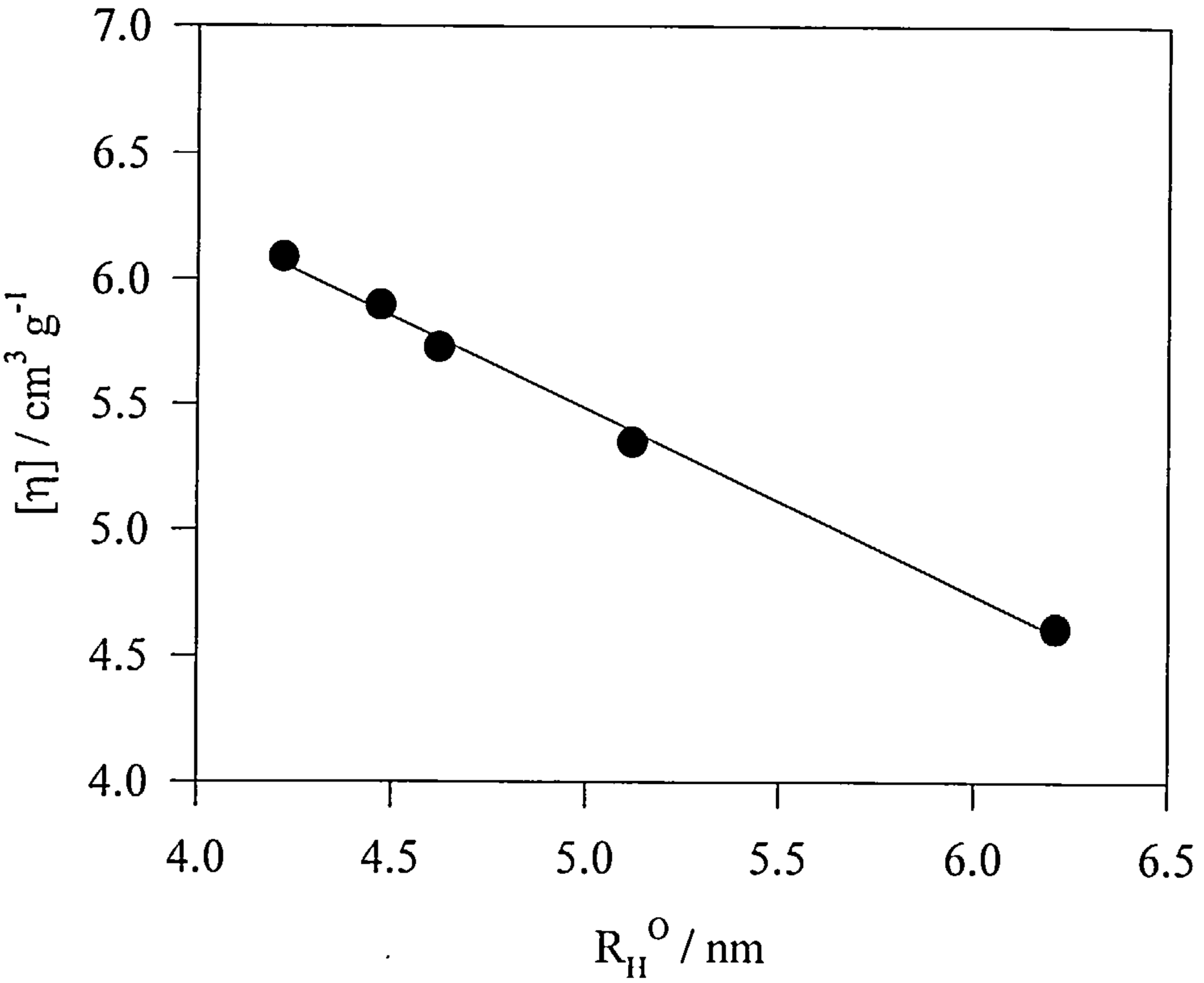

Appendix 3B.vii : Variation of $\log_{10}\eta_r$ with 1/[TX-100]
-Vand's equation- (effect of added KCl)

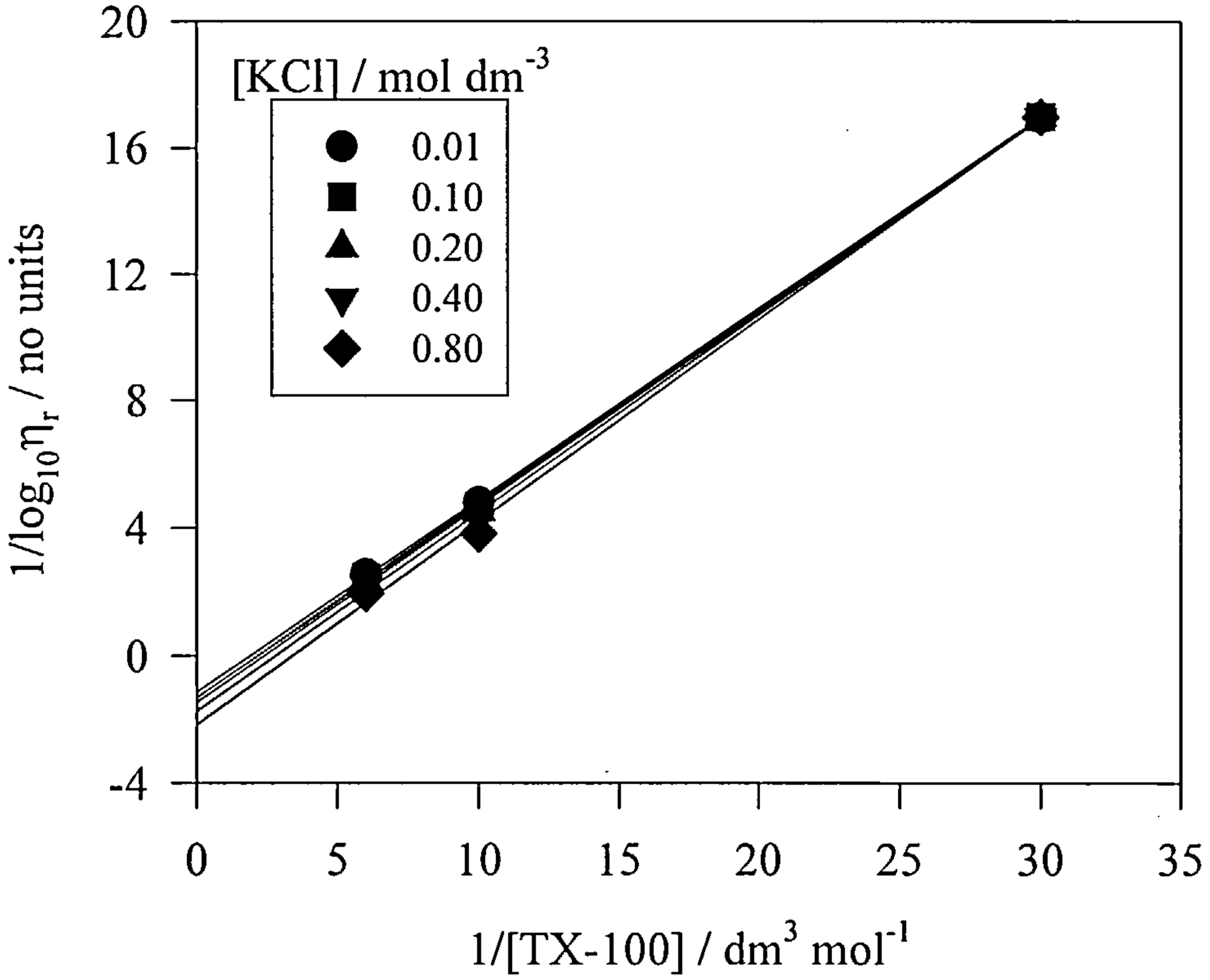

Appendix 3B.viii : Variation of aggregation number with [KCl]

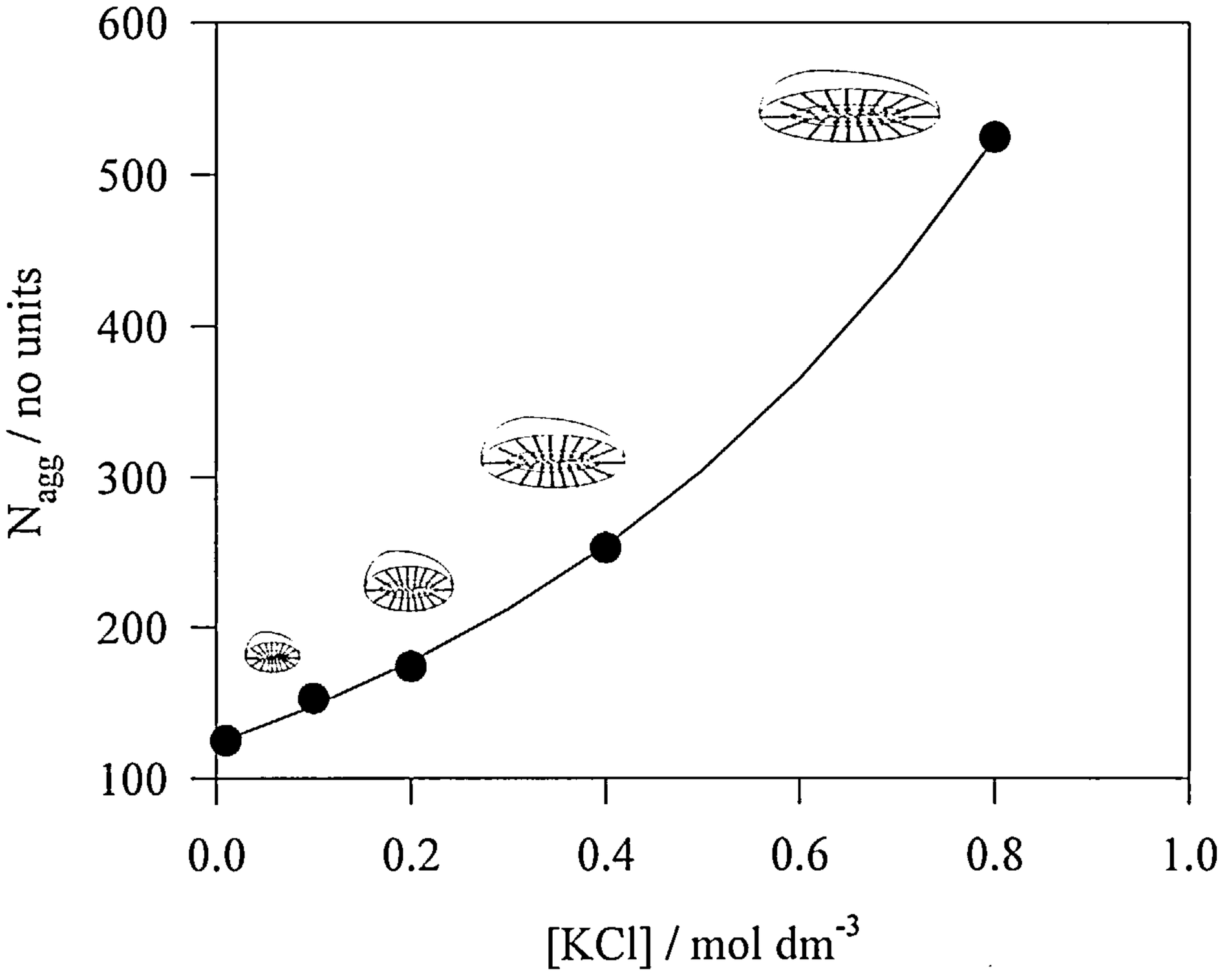

Appendix 3B.ix : Variation of viscosity with temperature (effect of KCl)

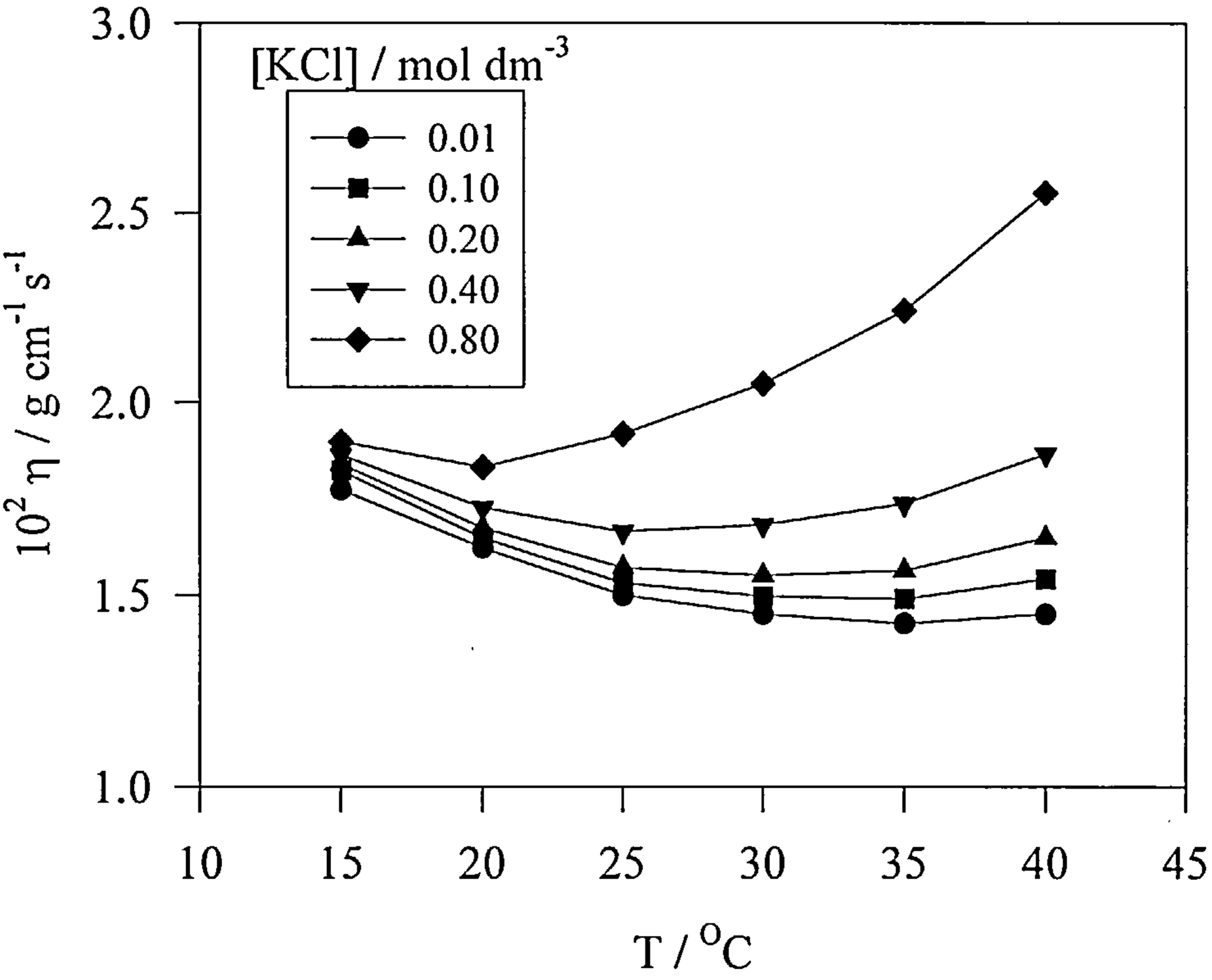

Appendix 3B.x : Temperature of minimum viscosity -variation with [KCl]

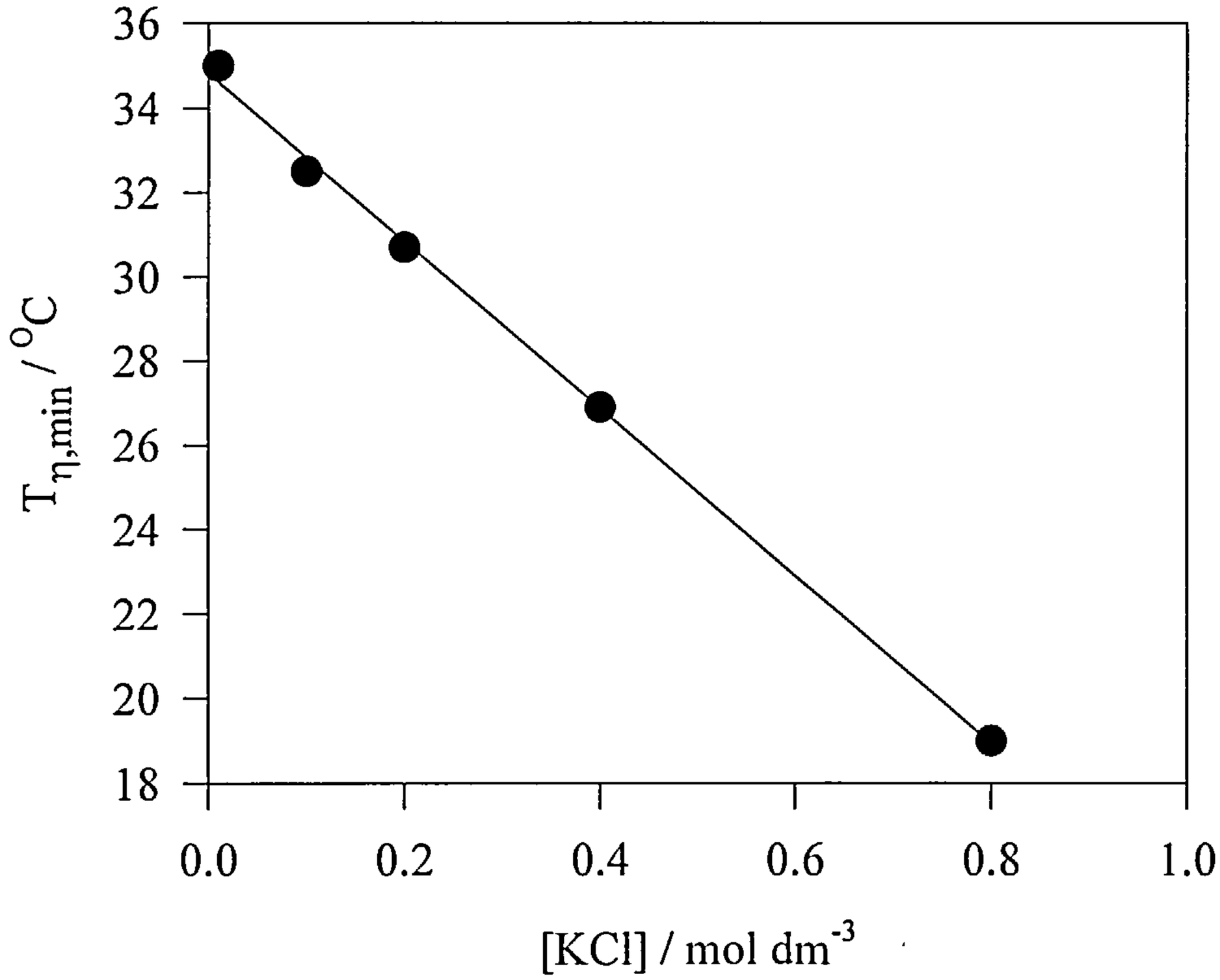

Chapter 3C: Triton X-100 Self Diffusion Coefficients (CV,CA)

3C.1 Introduction

The size, shape and interaction of TX-100 micelles have been characterised previously using rotating disk voltammetry (Ch. 3A) and rheological studies (Ch. 3B). Both of these techniques studied the micellar structure under flow and so it seemed prudent to study the micellar solution under quiescent / stationary conditions. The methods used were cyclic voltammetry (CV) and chronoamperometry (CA), the basis of these have been discussed earlier in Ch. 2.1.3 (CV) and Ch 2.1.4 (CA). Chronoamperometric studies on TX-100 have not appeared previously and there are only limited references to cyclic voltammetry with Triton X-100[5,60].

This chapter will present the first comprehensive study of Triton X-100 using CV over a range of electrolyte and surfactant concentrations. The diffusion coefficients show a quadratic dependence on the TX-100 concentration, as opposed to RDV where a linear relationship was established (Ch. 3A.2.2.1). An explanation for the variation between diffusion coefficient results from hydrodynamic and stationary methods will be proposed. The chronoamperometry results will show that potential step measurements on nonionic micellar systems are possible though with limited experimental accuracy.

3C.2 Results and Discussion

3C.2.1 General Electrochemistry (CV)

The diffusion coefficients of TX-100 micellar solutions were measured between surfactant concentrations 0.067 - 0.167 mol dm^{-3}, and KCl concentrations of 0.01 - 0.80 mol dm^{-3}. From the RDV study (Ch. 3A.2.1) it was seen that solutions without added electrolyte resulted in voltammograms severely distorted by ohmic drop. It followed that the [KCl] range was the same as used in Ch. 3A. Initial experiments at 0.033 mol dm^{-3} TX-100 tended to give irreproducible results due to the low Faradaic currents obtained from $3.3x10^{-4}$ mol dm^{-3} ferrocene. The errors due to the baseline extrapolation of the capacitance currents were more evident at this low ferrocene concentration and so the low concentration limit was increased slightly to 0.067 mol dm^{-3}. Following the RDV experiments it was seen that the half wave potential ($E_{1/2}$) was affected by increases in both the surfactant and electrolyte concentrations (Ch. 3A.2.1). It was therefore necessary to determine whether $E_{1/2}$ was affected in the same way and to the same extent under stationary conditions. $E_{1/2}$ was easily found by the following expression[61]:-

$$E_{1/2} = (E_{Pa} + E_{Pc}) / 2 \qquad (3C.1)$$

where E_{Pa} and E_{Pc} are the anodic and cathodic peak currents respectively. Values for the half wave potentials are shown in Table 3C.1

Table 3C.1 : Variation of $E_{1/2}$ with surfactant and electrolyte concentration

[TX-100] / mol dm^{-3}	$E_{1/2}$ / mV	
	0.01 mol dm^{-3} KCl	0.80 mol dm^{-3} KCl
0.067	237.3	225.8
0.100	243.6	233.9
0.133	249.0	238.4
0.167	252.8	240.8

The same trends that were seen under hydrodynamic conditions (Ch. 3A.2.1) are seen under stationary conditions i.e. $E_{1/2}$ increases with [TX-100] and decreases with [KCl]. Not only are the trends identical but actual values for $E_{1/2}$ are almost equal from RDV analysis. The variation in $E_{1/2}$ with [TX-100] and [KCl] has been explained in Ch. 3A.2.1 as an inhibitory effect on the electron transfer process by the adsorbed surfactant on the electrode. Munoz et al.[31] have observed that the $E_{1/2}$ values of cefazolin reduction varies in a logarithmic fashion with [TX-100], with a slope of ~50 mV decade^{-1}. This was also attributed to inhibition of electron transfer due to adsorbed surfactant on the electrode. This observation is matched by the results presented here and can be seen in Appendix 3C.i. It is apparent that the slope of $E_{1/2}$ vs. $\log_{10}$[TX-100] plot remains constant at ~40 mV decade^{-1} regardless of the KCl concentration, this is in excellent agreement with Munoz et al.[31].

Analysis of the peak-peak separation of a cyclic voltammogram can allow the determination of the heterogeneous rate constant (k^O) for the electron transfer. Using Equation 1.23, an average value was found for $k^O = 0.036 \pm 0.023$ cm s^{-1} and was not seen to change appreciably with electrolyte or surfactant concentration. It must be noted, however, that the peak-peak separation (E_{Pa} - E_{Pc}) remains constant at ~60 mV with increasing potential sweep rate (υ) for each TX-100 concentration. Nevertheless, this range of values was in good agreement with Mandal et al.[60] who recorded $k^O = 0.019$ cm s^{-1} for ferrocene in 0.05 mol dm^{-3} TX-100. Mahanta et al.[63] observed that $k^O = (7.9 - 12.5) \times 10^{-3}$ cm s^{-1} for ferrocene in 2.4% TX-100 in aqueous solution, an order of magnitude lower than in organic solvents demonstrating that ferrocene resides within the micellar interior.

The k^O values are also comparable with those of ferrocene in SDS (0.013 cm s^{-1}) and CTAB (0.020 cm s^{-1}) as determined by CV at a 0.5 mm diameter Pt electrode[62]. Even though the values are generally similar to k^O in a wide range of different solvents, they are appreciably smaller than those determined in short chain alcohols[62] e.g. MeOH, $k^O = 0.178$ cm s^{-1}.

Full calculations will be presented in Ch. 4C.2.1 for CTAC where a change in k^O with electrolyte concentration is noted.

3C.2.2 Diffusion Coefficient Results (D_{CV})

A full set of typical CV plots over a potential sweep range of 20 - 150 mV s^{-1} for 0.167 mol dm^{-3} TX-100 + 0.10 mol dm^{-3} KCl can be seen in Appendix 3C.ii. Randles-Sevcik plots from Equation 1.22 are shown in Appendix 3C.iii and the resultant diffusion coefficient results (D_{CV}) from the Randles-Sevcik analysis are shown in Table 3C.2 over the surfactant and electrolyte ranges.

Table 3C.2 : Experimental D_{CV} results

[KCl] / mol dm^{-3}	$10^7 D_{CV}$ / cm^2 s^{-1}			
	0.067 mol dm^{-3} TX-100	0.100 mol dm^{-3} TX-100	0.133 mol dm^{-3} TX-100	0.167 mol dm^{-3} TX-100
0.01	4.95	3.82	2.80	2.27
0.10	4.77	3.76	2.65	2.16
0.20	4.51	3.36	2.56	2.01
0.40	4.04	3.14	2.37	1.93
0.60	3.61	2.93	2.12	1.72
0.80	3.27	2.47	1.84	1.56

Note: standard error = $\pm 0.09x10^{-7}$ cm^2 s^{-1}

Plots of D_{CV} against [KCl] for each [TX-100] are shown in Appendix 3C.iv along with lines of best fit. Correlation coefficients >0.993 show that the relationship is perfectly linear and hence values for the fitted line are obtained and can be seen in Table 3C.3.

Table 3C.3 : Linearly fitted D_{CV} results

[KCl] / mol dm^{-3}	$10^7 D_{CV}$ / cm^2 s^{-1}			
	0.067 mol dm^{-3} TX-100	0.100 mol dm^{-3} TX-100	0.133 mol dm^{-3} TX-100	0.167 mol dm^{-3} TX-100
0.01	4.92	3.81	2.78	2.23
0.10	4.73	3.66	2.68	2.15
0.20	4.51	3.49	2.56	2.07
0.40	4.08	3.16	2.33	1.90
0.60	3.66	2.84	2.10	1.73
0.80	3.23	2.51	1.87	1.56

By comparing the fitted values to those in Table 3C.2 it can be seen that the biggest deviation is 0.10×10^{-7} cm^2 s^{-1} which can be accounted for by experimental error, showing that the linearly fitted values are valid.

3C.2.2.1 D_{CV} - Results Analysis

As opposed to RDV experiments the diffusion coefficients do not decrease in direct proportion to an increase in [TX-100] and therefore do not adhere to linear interaction theory over 0.067 - 0.167 mol dm^{-3}. Values for D_{CV} are in good agreement with D_{RDV} at 0.167 mol dm^{-3} TX-100 but differ as the [TX-100] is decreased. Examples of the differences between D_{CV} and D_{RDV} are shown in Table 3C.4.

Table 3C.4 : Variation of D_{CV} and D_{RDV} with [TX-100] and [KCl]

[KCl] / mol dm^{-3}	0.100 mol dm^{-3} TX-100		0.167 mol dm^{-3} TX-100	
	10^7 D_{RDV} / cm^2 s^{-1}	10^7 D_{CV} / cm^2 s^{-1}	10^7 D_{RDV} / cm^2 s^{-1}	10^7 D_{CV} / cm^2 s^{-1}
0.01	3.28	3.81	2.21	2.23
0.80	2.19	2.51	1.33	1.56

It can be seen that there is a difference between 0.32 - 0.53 $x10^{-7}$ cm^2 s^{-1} for D_{RDV} and D_{CV} at 0.10 mol dm^{-3} TX-100, this drops to 0.02 - 0.23 $x10^{-7}$ cm^2 s^{-1} at 0.167 mol dm^{-3}. An explanation for the disparity between the results from CV and RDV is not obvious, however, three options are possible, namely two diffusional regimes, probe pre-concentration or anisotropic diffusion.

Recently, Birkin has proposed the presence of two diffusional regimes at different timescales for a stationary electrode[64], similar behaviour may be possible here. It could be suggested that for CV experiments the ferrocene probe is contained within the volume element, when the potential is swept (20-150 mV s^{-1}), the probe diffuses towards the electrode at a rate slower than free ferrocene but faster than free micelle diffusion. However, in RDV, when the electrode is rotated and the potential

scanned slowly (5 mV s^{-1}) the ferrocene in the volume element is completely oxidised, establishing a steady state diffusion layer. Micelles approach the diffusion layer boundary at a rate slower than free ferrocene diffusion in the volume element. As the boundary is reached, the ferrocene within the micelles maybe transferred into the volume element at which point they will diffuse to the electrode (it would seem unreasonable for intact micelles to diffuse faster at the interface). Within this framework, it could be predicted that there are two distinctly different diffusion coefficients since with CV, diffusion through a viscous region in the vicinity of the electrode would be evident whereas with RDV, diffusion of micelles to the boundary layer would be current limiting.

Another concept worth considering is that of ferrocene probe pre-concentration[65]. In Ch. 3A.2.1, it was observed that TX-100 formed an adsorbed surfactant layer at the electrode surface. If this adsorbed layer is in the form of a continuous or bilayer structure[21,29,30], it is conceivable that disproportionate concentrations of ferrocene may reside within the surface aggregates. Since more electroactive species are present at the electrode surface (surface [fc] > bulk [fc]) the Faradaic currents will be higher leading to an overestimation of D_S. Also, as the Randles-Sevcik plots are strictly linear, the ferrocene is not adsorbed on the electrode. Therefore, the observed currents will not be entirely due to micellar diffusion thus attenuating the diffusion coefficients. A high pre-concentration of ferrocene could, in theory, lead to Dahms-Ruff electron self exchange analogous to that observed with redox active polymer films[66], although this is not expected to occur in this case due to the low [fc].

Chung et al., using a NMR pulsed field gradient spin echo (PFGSE) technique, observed two distinct diffusion coefficients in a liquid crystal phase of Triton X-100 / D_2O / dimyristoylphosphatidylcholine (DMPC)[67]. This was attributed to the aligned diskoids hindering diffusion perpendicular to the disk surface but having little affect in the parallel direction. However, the concentration of Triton X-100 was 30 wt%, at least six times higher than those used here. Therefore, the formation of a liquid crystal phase at the electrode is unlikely to be responsible for the observed diffusion coefficient behaviour.

Although each of the possibilities discussed cannot be implicitly stated as the cause for the observed difference between D_{CV} and D_{RDV} they do, however, form a good phenomenological basis for future investigation.

The nature of the D_{CV} data allowed a quadratic plot to be drawn (Appendix 3C.v) at each KCl concentration, however, no inferences with regards to changes in interaction and size can be made. However, if the point at 0.167 mol dm^{-3} TX-100 is omitted the linear interaction theory (Equation 3A.2) can be applied with excellent correlation coefficients > 0.9994. This is represented by a dashed line in Appendix 3C.v. It must be noted that the calculated values for D^{O}_{CV}, k_D and $R_H{}^{O}$ are apparent because they are a function of the analysis range on the quadratic plot.

Values obtained for the analysis over 0.067 - 0.133 mol dm^{-3} TX-100 are shown in Table 3C.5 along with calculated hydrodynamic radii (see Equation 3A.3, Ch 3A.2.2.1).

Table 3C.5 : Linear extrapolation results

[KCl] / mol dm^{-3}	10^7 D^{O}_{CV} / cm^2 s^{-1}	$R_H{}^{O}$ / nm	k_D / dm^3 mol^{-1}
0.01	7.08	3.02	4.58
0.10	6.80	3.15	4.57
0.20	6.47	3.31	4.56
0.40	5.84	3.67	4.54
0.60	5.23	4.09	4.52
0.80	4.60	4.65	4.48

D^{O}_{CV}, $R_H{}^{O}$ and k_D are plotted against [KCl] in Appendices 3C.vi, 3C.vii and 3C.viii respectively along with the corresponding values determined from RDV (Ch. 3A.2.2). It was seen in Chapter 3A.2.2.1 that the values for hydrodynamic radius were in excellent agreement with literature[2,15,16,17,20,41,47]. It can be seen from Appendix 3C.vii that the apparent $R_H{}^{O}$ (CV) are lower than $R_H{}^{O}$ (RDV) and therefore not in agreement with the literature. The difference between the radii of both techniques varies from 1.20 nm to 1.56 nm over the KCl concentration range. CV consistently over estimates D_S, this discrepancy between the values may be a function of the adsorbed surfactant layer behaving in a different fashion under stationary conditions as compared to forced field flow (RDV) although this is not

substantiated by analysis of half wave potentials (Ch. 3A.2.1, Ch. 3C.2.1) and that plots of i_{Lim} vs. $\omega^{1/2}$ are perfectly linear from 0.2 - 50 Hz^{-1}. The results may also suggest that the enhanced currents necessary to over estimate D_S^O is due to pre-concentration of ferrocene at the electrode surface as was discussed previously. It must be noted, however, that the R_H^O (CV) values are dependent on the range over which the linear extrapolation is carried out.

Whereas with R_H^O, there was an agreement in the general trend between CV and RDV, the interaction parameter (k_D) behaviour is inverted. Not only are the values ~ 1.0 dm^3 mol^{-1} higher than those determined from RDV but they also experience the opposite trend to what would be expected for growing nonionic micelles i.e. increasing excluded volume interactions (Ch. 3A.2.2.2). This observation is wholly unexpected with no obvious explanation and therefore any further analysis would be unjustified.

3C.2.3 General Electrochemistry (CA)

As was discussed in Ch. 1.3.3 it is important to ensure that the correct analysis range is used. A number of time ranges were analysed in terms of correlation coefficient, gradient and intercept of the resultant Faradaic current decay (Appendix 3C.ix) for a 0.167 mol dm^{-3} TX-100 solution. The results are shown in Table 3C.6 and Appendices 3C.x, 3C.xi and 3C.xii respectively.

Table 3C.6 : Variation of correlation coefficient, gradient and intercept on time analysis range used

t range / s	Corr. coeff.	10^6 Gradient / A $s^{1/2}$	10^7 Intercept / A
0 - 1	0.9861	5.56	-29.6
1 - 2	0.9897	3.52	-4.69
2 - 3	0.9984	3.30	-3.13
3 - 4	0.9979	3.14	-2.29
4 - 5	0.9965	3.22	-2.64
5 - 6	0.9866	3.10	-2.07
6 - 7	0.9677	3.17	-2.36
7 - 8	0.9547	3.09	-2.07

It can be seen that the correlation coefficient reaches a peak between t = 2-5 s, with the gradient and intercept reaching limiting values over the same range. This justifies the use of the time range 2-5 s, and the resultant Cottrell analysis for the aforementioned solution is seen in Appendix 3C.xiii.

3C.2.4 Diffusion Coefficient Results (D_{CA})

The diffusion coefficients (D_{CA}) were measured over 0.01 - 0.80 mol dm^{-3} KCl and 0.033 - 0.167 mol dm^{-3} TX-100 as in RDV. As mentioned earlier background traces were required, from which the resulting Cottrell analysis over t = 2-5 s yielded the gradients in Table 3C.7 and Appendix 3C.xiv.

Table 3C.7 : Variation of background gradients with [KCl] and [TX-100]

[KCl] / mol dm^{-3}	10^6 Background gradients / A $s^{1/2}$		
	0.033 mol dm^{-3} TX-100	0.100 mol dm^{-3} TX-100	0.167 mol dm^{-3} TX-100
0.01	1.22	1.46	1.53
0.10	2.27	2.27	2.27
0.20	2.66	2.66	2.66
0.40	3.13	3.13	3.13
0.80	3.69	3.69	3.69

Note : standard error in Table 3C.7 = ± 0.16 x 10^{-6} A $s^{1/2}$

From 0.10 - 0.80 mol dm^{-3} KCl, the gradients fell within each others experimental error bars and hence average values are shown above. This shows that the background gradients become invariant to changes in surfactant concentration at [KCl] ≥ 0.10 mol dm^{-3}.

Following the background experiments the experimental traces (with ferrocene) were recorded and the following gradients from the Cottrell analysis obtained. These are shown in Table 3C.8 and Appendix 3C.xv.

Table 3C.8 : Variation of experiment gradients with [KCl] and [TX-100]

[KCl] / mol dm^{-3}	10^6 Experimental gradients / A $s^{1/2}$		
	0.033 mol dm^{-3} TX-100	0.100 mol dm^{-3} TX-100	0.167 mol dm^{-3} TX-100
0.01	2.41	3.88	4.74
0.10	3.24	4.58	5.25
0.20	3.51	4.78	5.45
0.40	3.73	4.96	5.55
0.80	3.90	5.05	5.57

Note : standard error = ± 0.07 x 10^{-6} A $s^{1/2}$

Subtracting the background and aqueous phase ferrocene from the experimental gradients as described in Ch. 2.1.4 leads to the true Faradaic response of the system. These are shown in Table 3C.9 and Appendix 3C.xvi

Table 3C.9 : Variation of true Cottrell gradients with [KCl] and [TX-100]

[KCl] / mol dm^{-3}	10^6 Cottrell gradients / A $s^{1/2}$		
	0.033 mol dm^{-3} TX-100	0.100 mol dm^{-3} TX-100	0.167 mol dm^{-3} TX-100
0.01	1.07	2.30	3.09
0.10	0.85	2.19	2.85
0.20	0.72	2.02	2.67
0.40	0.47	1.70	2.30
0.80	0.08	1.23	1.75

Note : standard error in Table 3C.9 = ± 0.23 x 10^{-6} A $s^{1/2}$

It is apparent that the standard error is substantial when compared to the actual values of the gradients. This is largely due to the additive effects of both the background and experimental gradients. In reality the error may be not be as large as that quoted but, this represents the worst case scenario.

Using the gradients in Table 3C.9 the diffusion coefficients can be determined using Equation 1.24, these are presented in Table 3C.10 and Appendix 3C.xvii.

Table 3C.10 : Experimental D_{CA} results

[KCl] / mol dm^{-3}	10^7 D_{CA} / cm^2 s^{-1}		
	0.033 mol dm^{-3} TX-100	0.100 mol dm^{-3} TX-100	0.167 mol dm^{-3} TX-100
0.01	6.96	3.63	2.35
0.10	4.40	3.28	2.01
0.20	3.20	2.79	1.75
0.40	1.37	1.99	1.30
0.80	0.04	1.04	0.75

Note : standard error = ± 0.8 x 10^{-7} cm s^{-1}

3C.2.4.1 D_{CA} - Results Analysis

Although the standard error may be slightly cautious, the results do show that the technique lacks the precision observed with CV or RDV (errors ~x10 CV, RDV). The diffusion coefficients at 0.033 mol dm^{-3} TX-100 do not even fit in with the expected pattern that was seen with CV and RDV i.e. D_{CA} (0.033 mol dm^{-3}) > D_{CA} (0.100 mol dm^{-3}) > D_{CA} (0.167 mol dm^{-3}). This essentially means that values for R_H^O, D^O and k_D cannot be obtained with confidence. Comparisons between D_{CA}, D_{CV} and D_{RDV} for 0.167 mol dm^{-3} TX-100 are shown in Table 3C.11 and Appendix 3C.xviii.

Table 3C.11 : Comparison of diffusion coefficients from CA, CV and RDV for 0.167 mol dm^{-3} TX-100

[KCl] / mol dm^{-3}	$10^7 D_{CA}$ / $cm^2 s^{-1}$	$10^7 D_{CV}$ / $cm^2 s^{-1}$	$10^7 D_{RDV}$ / $cm^2 s^{-1}$
0.01	2.35	2.27	2.21
0.10	2.01	2.16	2.13
0.20	1.75	2.01	1.99
0.40	1.30	1.93	1.74
0.80	0.75	1.56	1.35

Within experimental error (± $0.80x10^{-7}$ cm^2 s^{-1}) the values for D_{CA} could be viewed as decreasing in a linear fashion with [KCl] as for CV and RDV, though this cannot be stated implicitly due to the limited precision of the technique.

3C.3 Summary

Cyclic voltammetry has been used to precisely determine the diffusion coefficients of TX-100 micelles, with standard errors equivalent to those observed with RDV. Analysis of the cyclic voltammograms demonstrated that the half wave potentials ($E_{1/2}$) for the ferrocene / ferricinium red-ox couple was a function of both electrolyte and surfactant concentration. This was in agreement with findings from RDV and was attributed to an inhibitory affect of adsorbed surfactant on the electron transfer process.

The micellar diffusion coefficient (D_{CV}) was seen to decrease in a linear fashion with increasing [KCl] which concurred with the results from RDV (D_{RDV}). At 0.167 mol dm^{-3} TX-100, values for D_{CV} were almost identical to D_{RDV} but, as the [TX-100] was decreased the results begin to deviate to a greater extent. The results could suggest that the Faradaic currents obtained from CV had a contribution from pre-concentrated ferrocene residing in the adsorbed TX-100 layer on the electrode surface. The possibility also exists of the self-diffusion coefficients being attenuated

by ferrocene in a viscous layer at the electrode such that they reflect motion through the volume element rather than free micelle diffusion.

The results show that D_{CV} decreased in a quadratic fashion with an increase in [TX-100] as opposed to D_{RDV} where a linear relationship was apparent. The linear interaction theory that was utilised for D_{RDV} therefore could not be strictly applied, but was confined to a small concentration range. Analysis of this limited linear extrapolation indicated that the micelles were 1.20 - 1.56 nm smaller than those calculated from RDV and therefore disagree with published values[2,15,16,17,20,41,47]. Obviously the range over which the linear extrapolation was applied to the quadratic plot participates in determining the intercept and gradient, so the resultant D_{CV} and k_D values can only be as apparent.

Values for k_D (CV), the interaction parameter, appear to decrease as the concentration of KCl was increased. This was counter to observations with RDV, where k_D increased due to larger excluded volume interactions. An explanation for this apparent inversion in behaviour was not apparent and further investigation was not undertaken.

Chronoamperometry has been used to determine the diffusion coefficient of TX-100 micelles but with an experimental errors ~ 10 times that of both RDV and CV. The limited experimental accuracy meant that it was impossible to conduct any analysis on the diffusion coefficients (D_{CA}) obtained. However, it is possible that D_{CA} may decrease in a linear fashion with [KCl] as for D_{CV} and D_{RDV} though this could not be stated implicitly.

Appendix 3C.i : Variation of half wave potential ($E_{1/2}$) with $\log_{10}$[TX-100) -effect of added [KCl]-

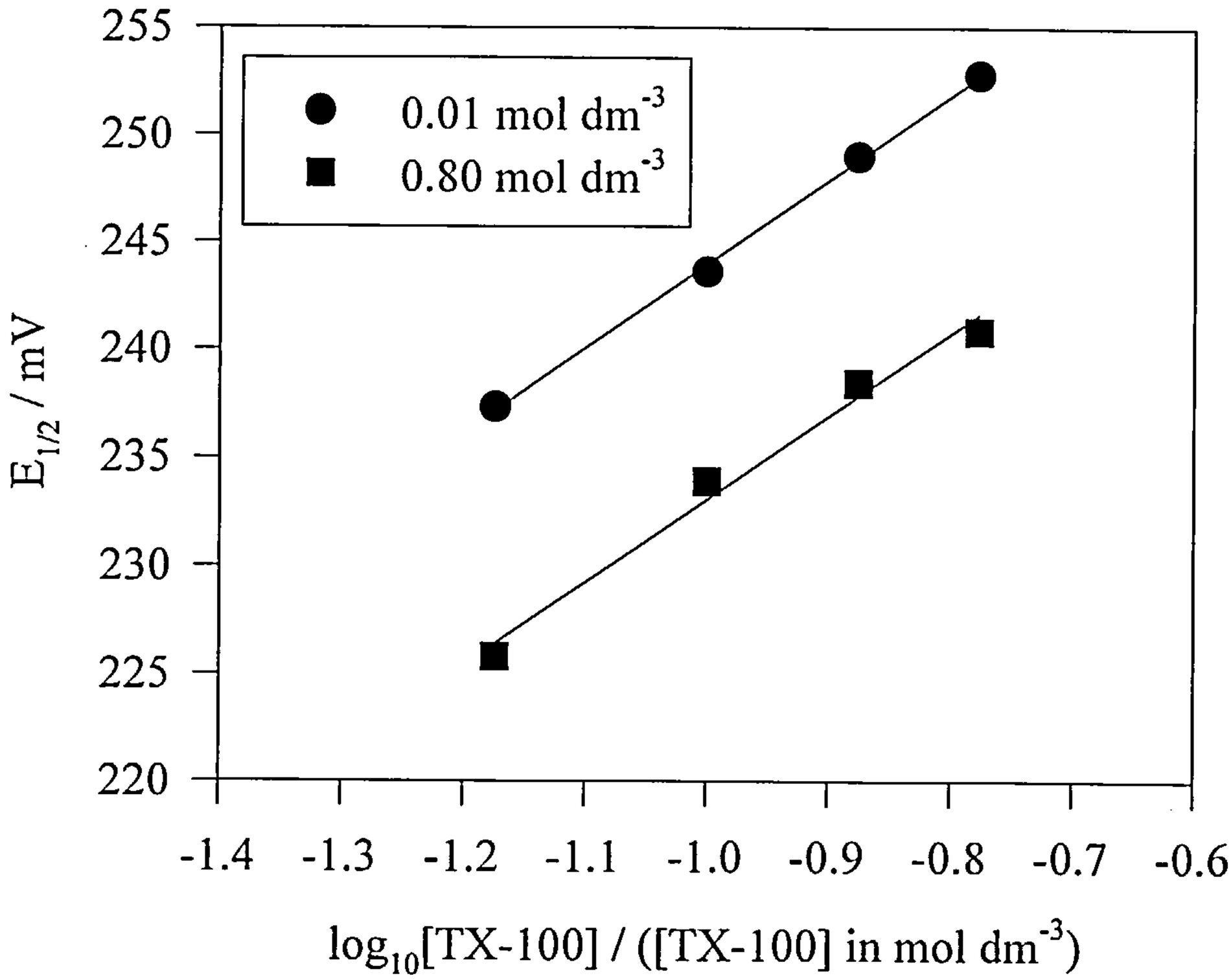

Appendix 3C.ii : Typical cyclic voltammograms @ 20 ^{O}C
(0.167 mol dm^{-3} TX-100 + 0.1 mol dm^{-3} KCl)

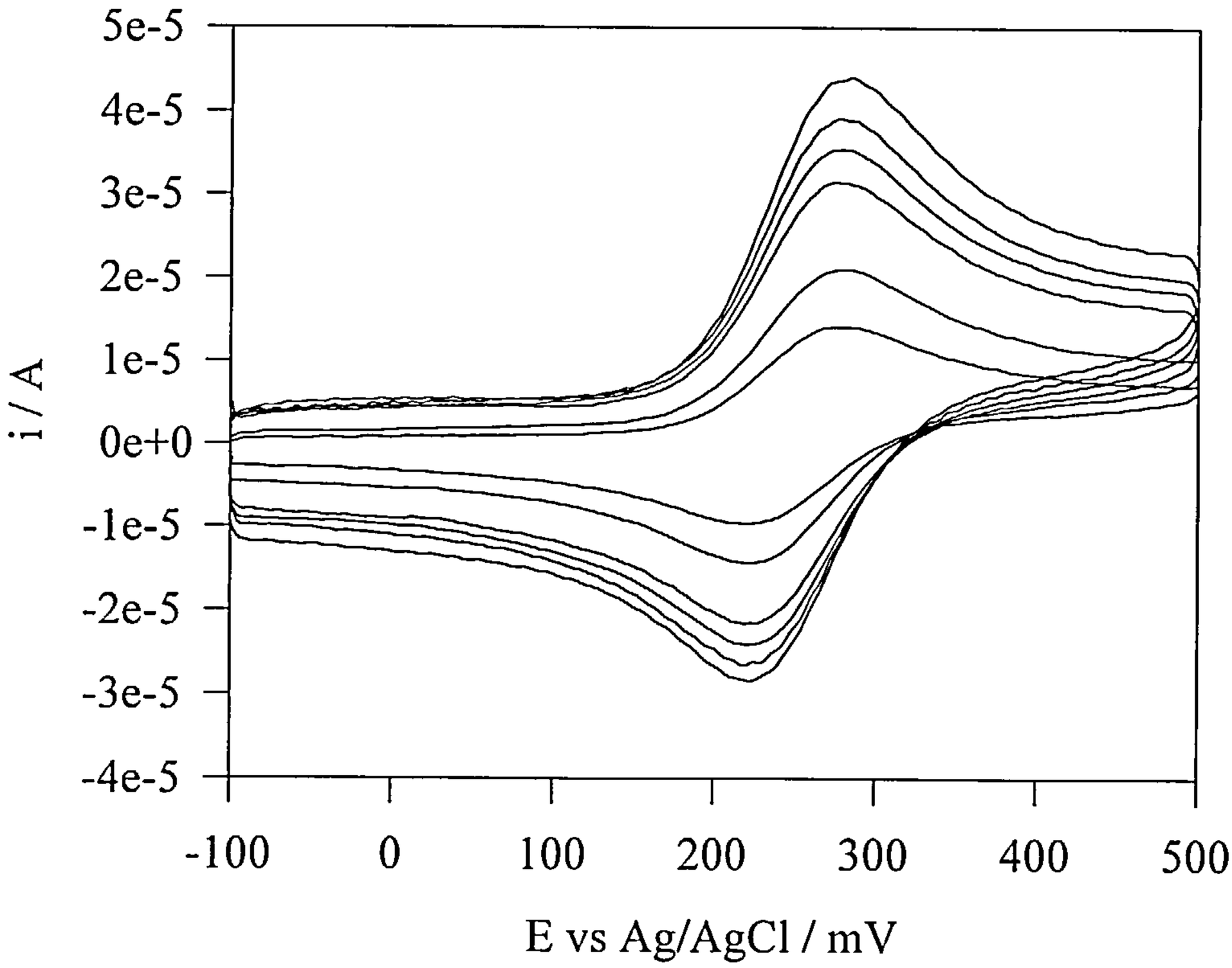

Appendix 3C.iii : Examples of Randles-Sevcik plots (i_p vs $\upsilon^{1/2}$)

(TX-100 + 0.1 mol dm^{-3} KCl)

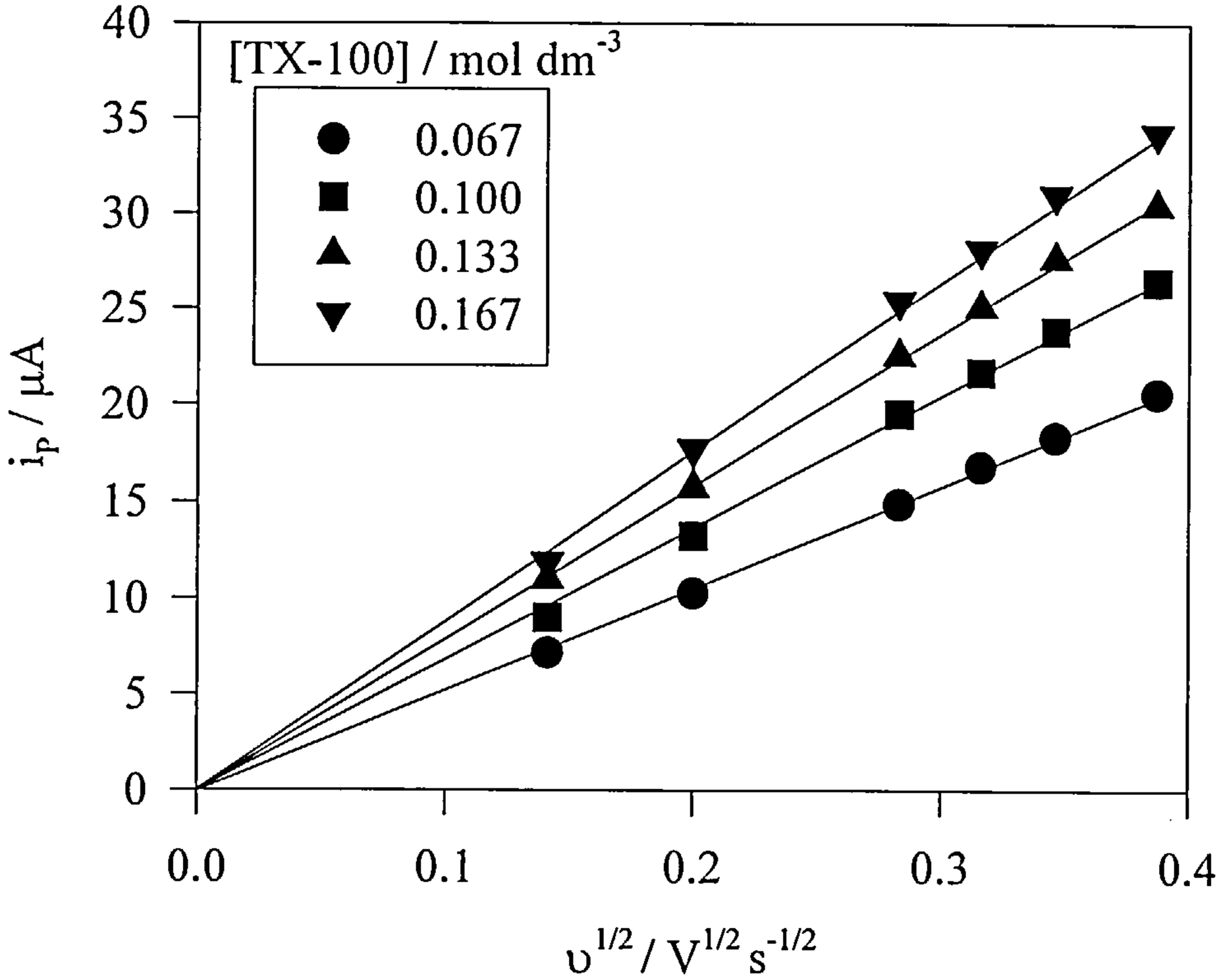

Appendix 3C.iv : Diffusion coefficient (D_{CV}) variation with [KCl]

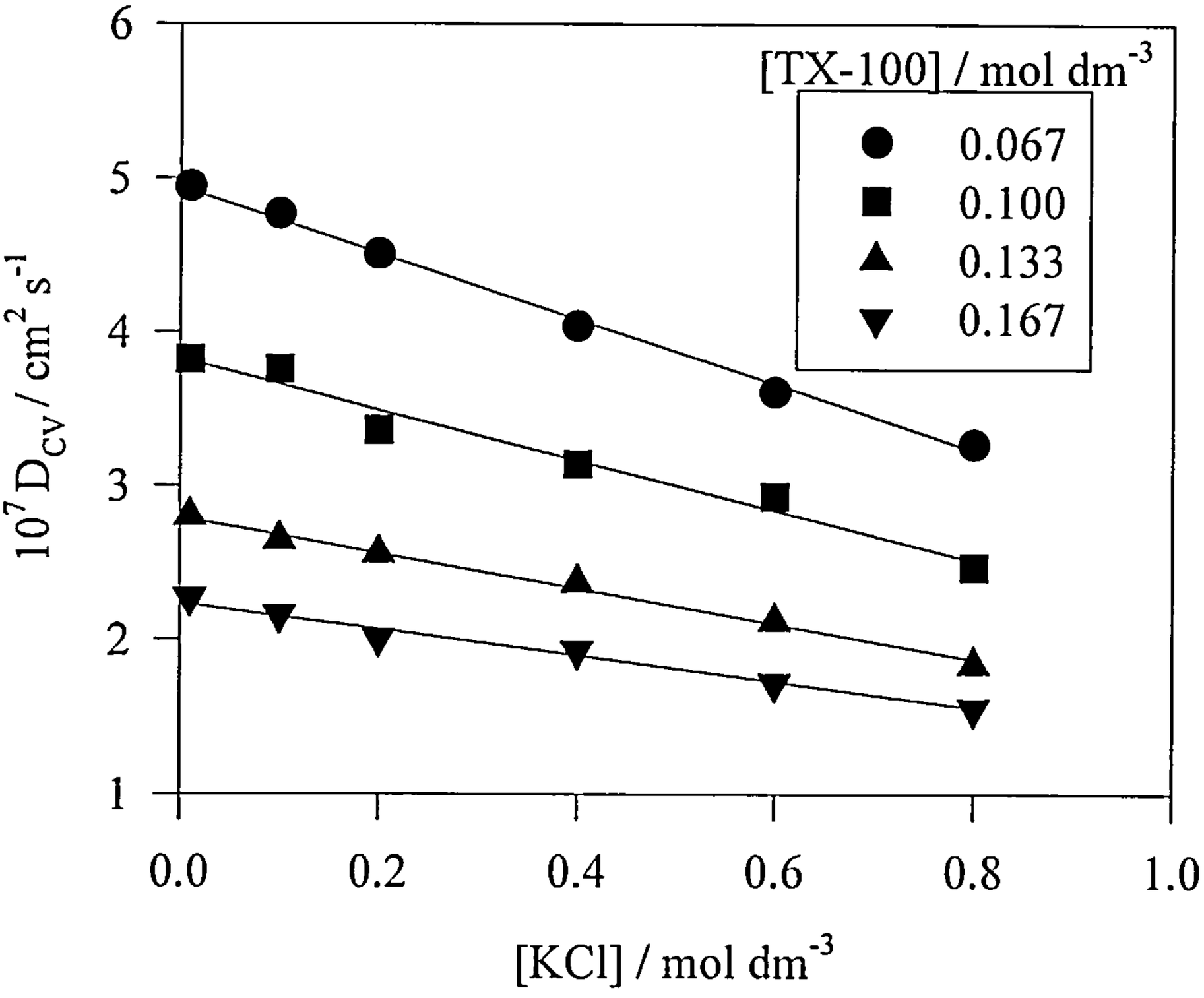

Appendix 3C.v : Diffusion coefficient (D_{CV}) variation with [TX-100] (effect of added KCl)

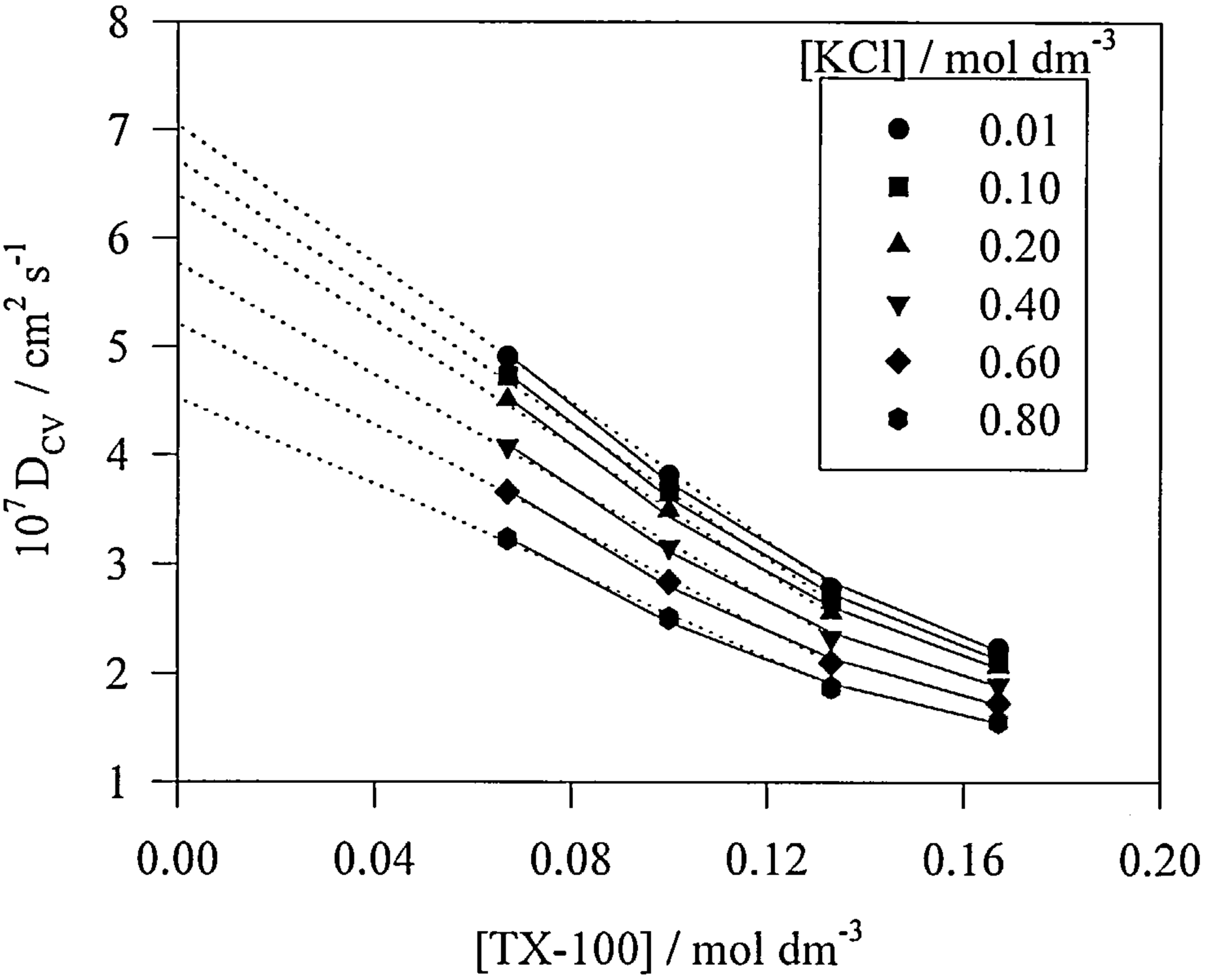

Appendix 3C.vi : Variation of diffusion coefficient at infinite dilution for RDV and CV

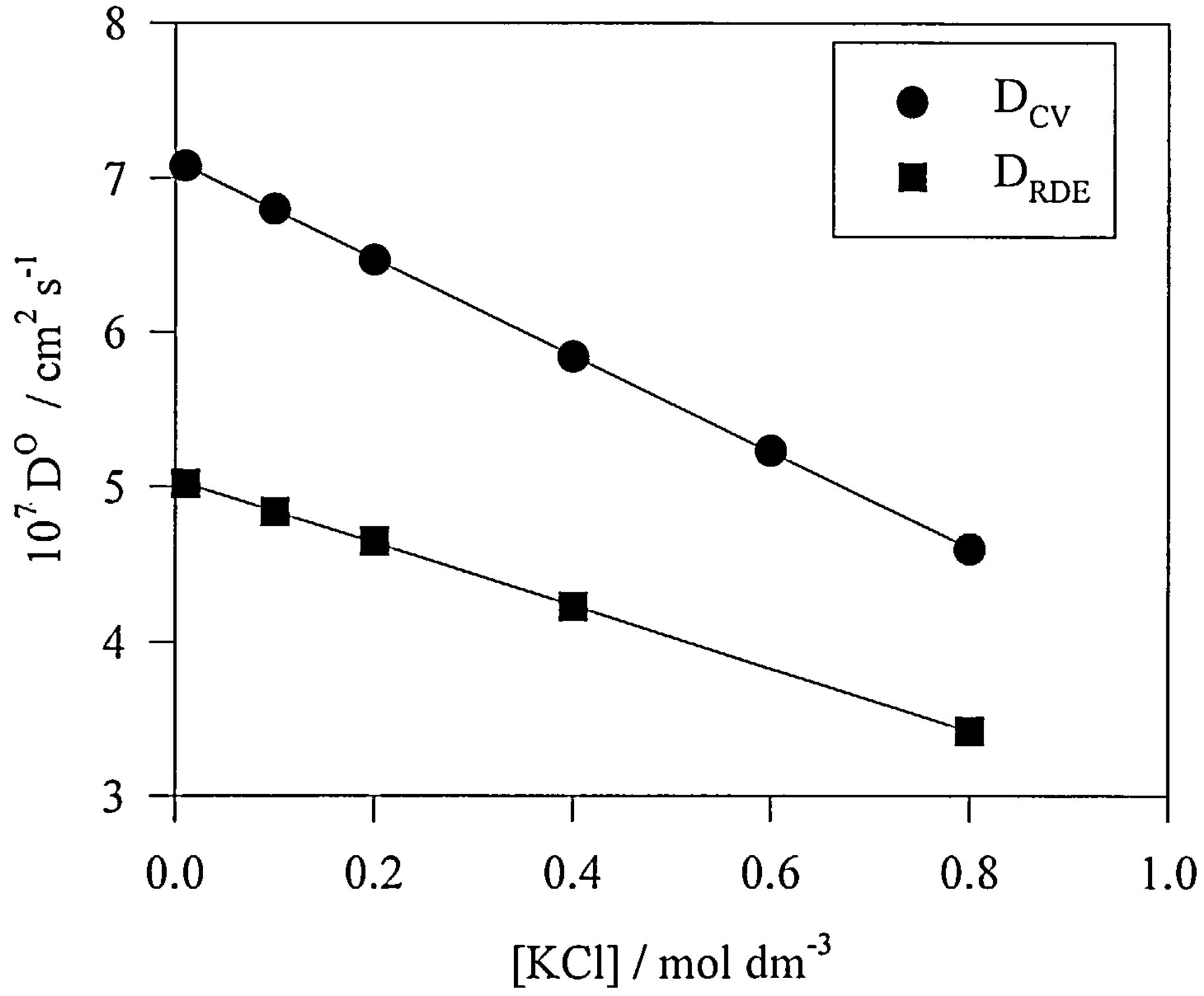

Appendix 3C.vii : Variation of hydrodynamic radius with [KCl] for CV and RDV

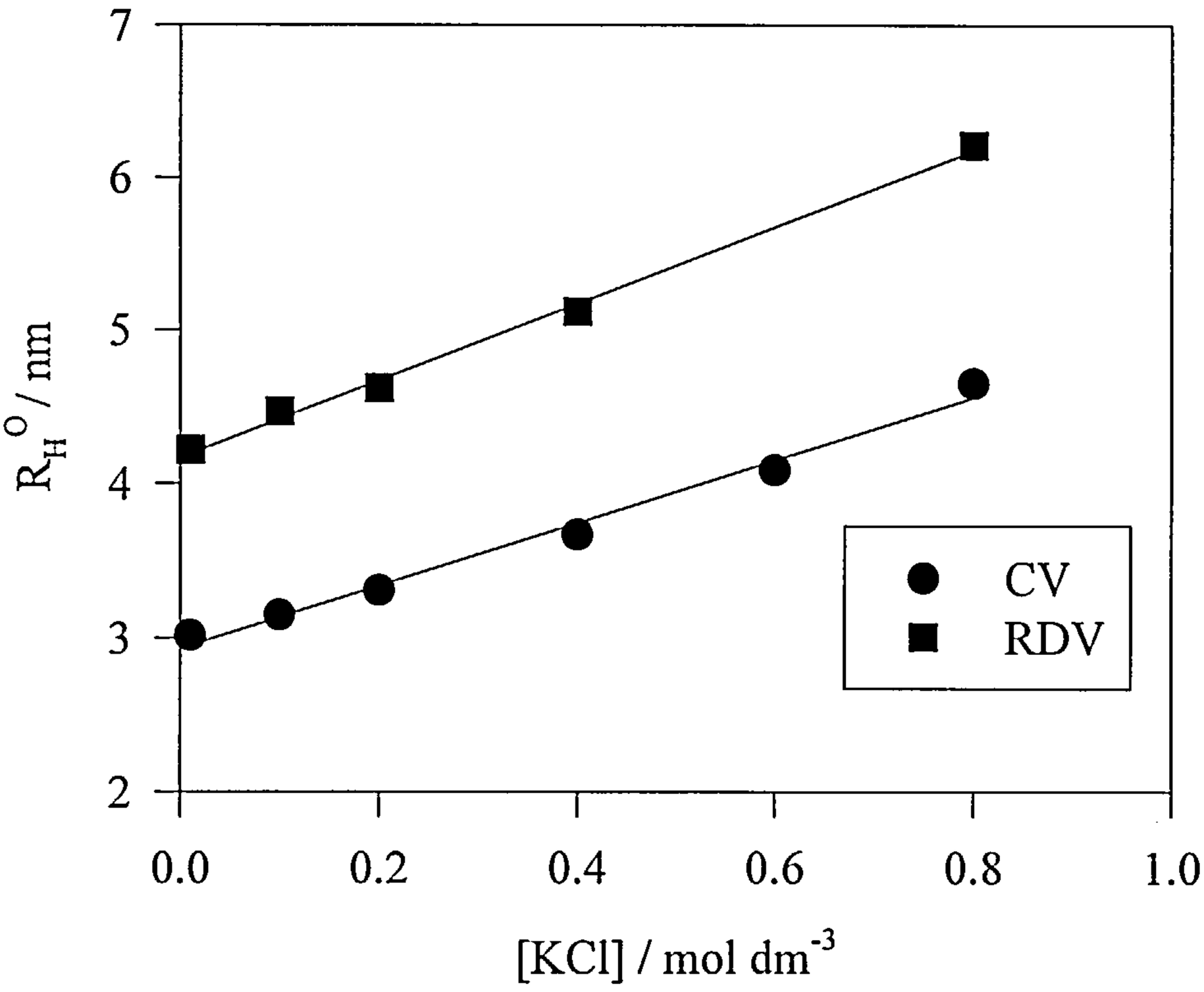

Appendix 3C.viii : Variation of intermicellar interaction parameter for CV and RDV

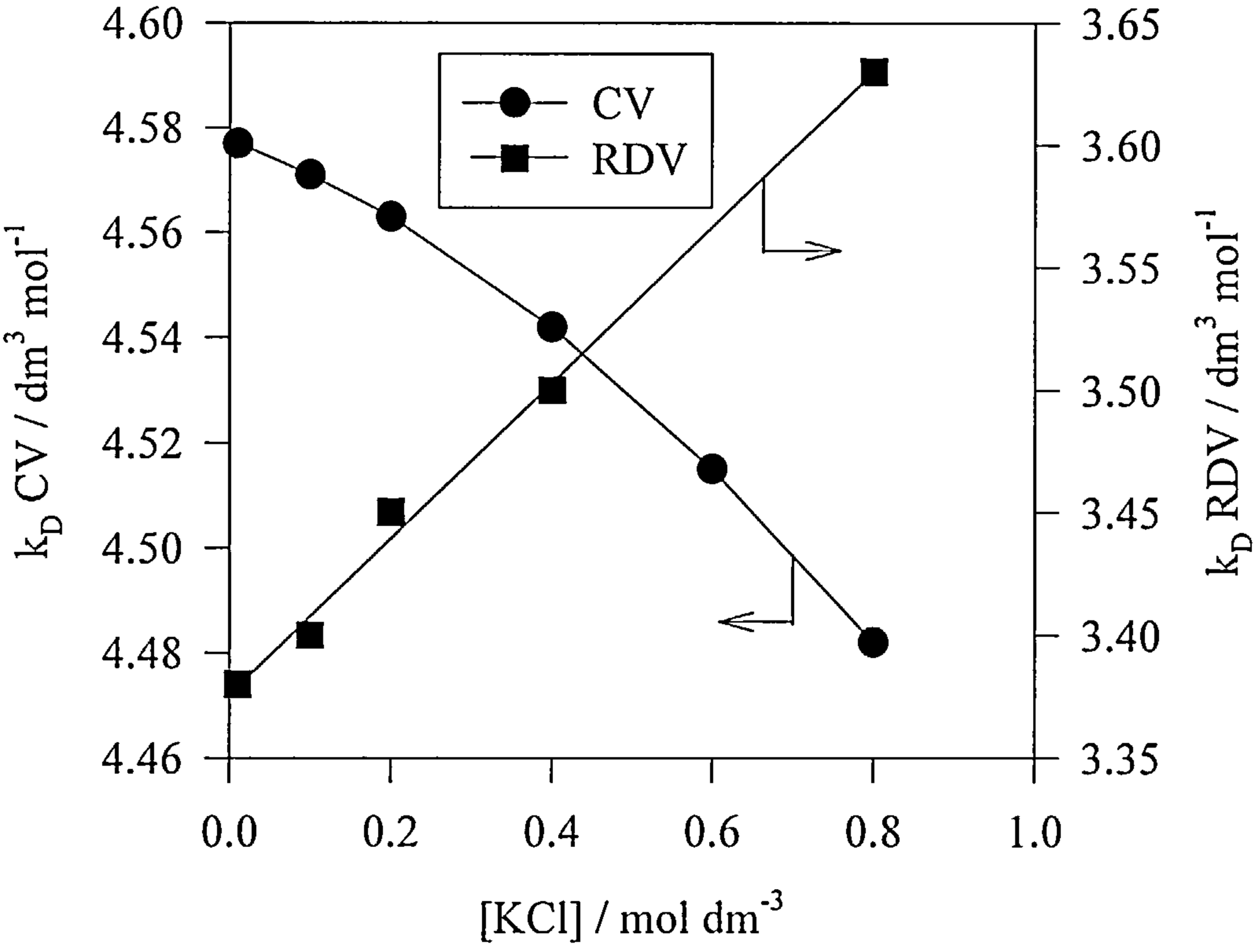

Appendix 3C.ix : Current response after potential step for 0.167 mol dm^{-3} TX-100 + 0.01 mol dm^{-3} KCl

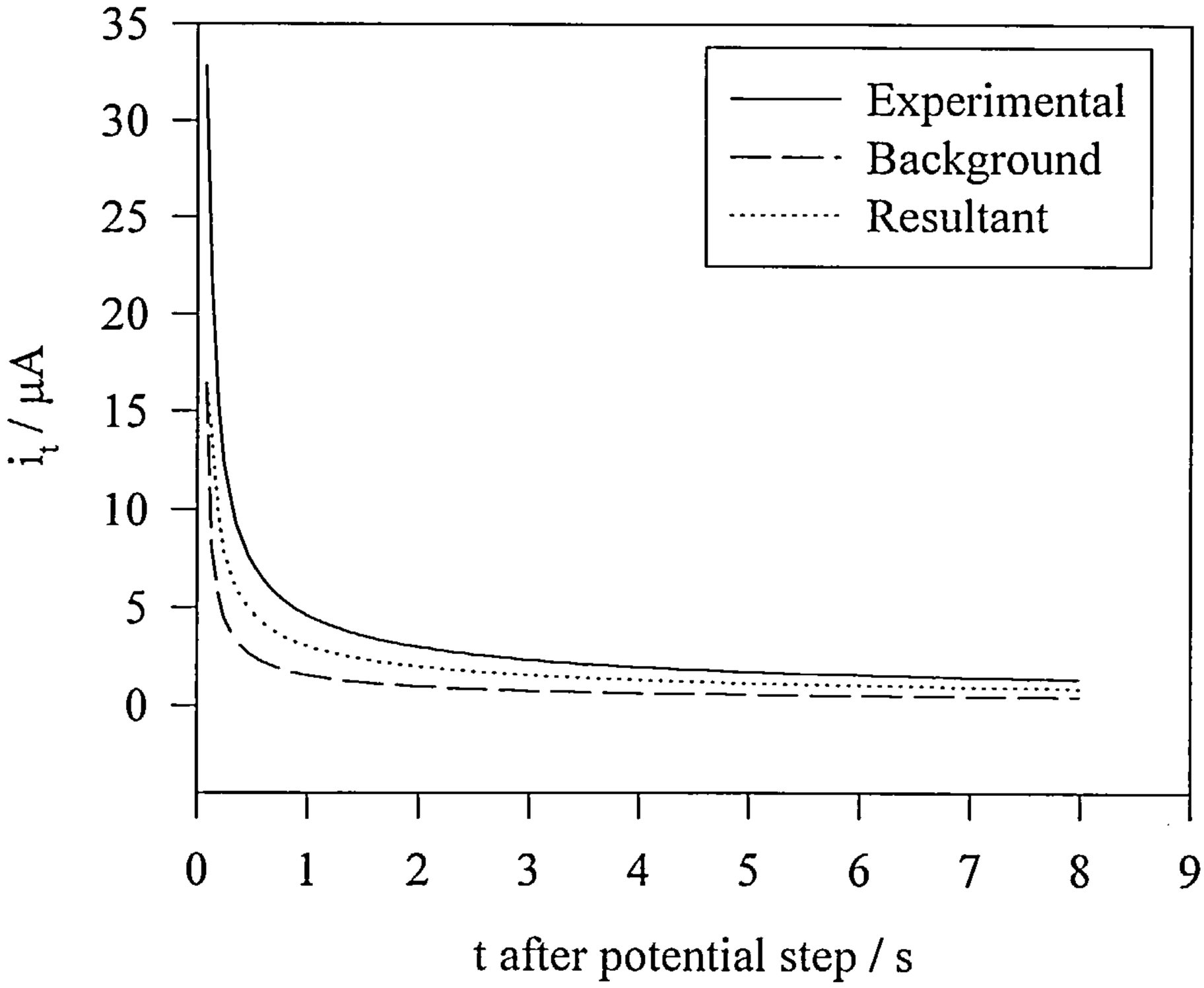

Appendix 3C.x : Variation of correlation coefficient with Cottrell time analysis range

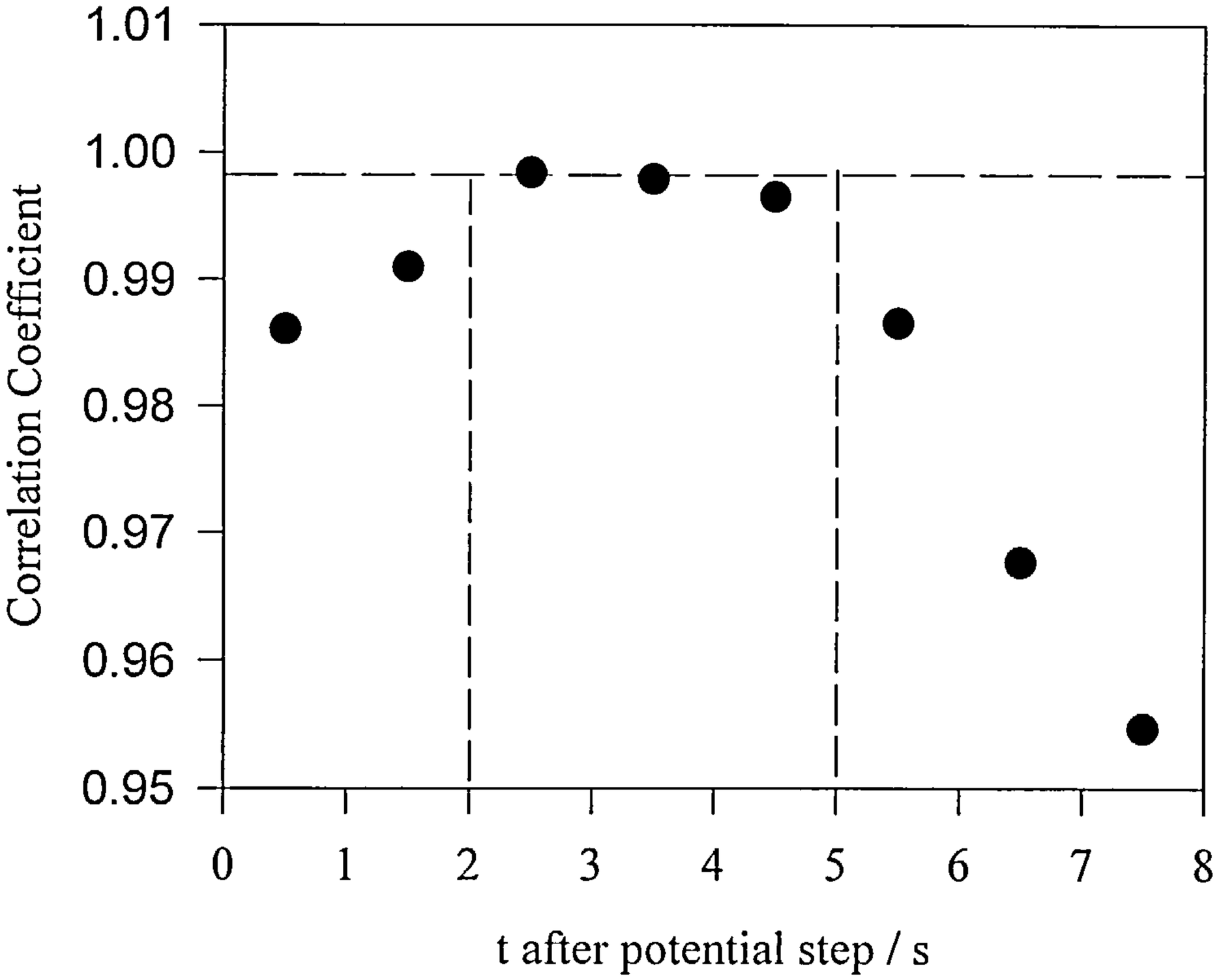

Appendix 3C.xi : Variation of Cottrell gradient with time analysis range

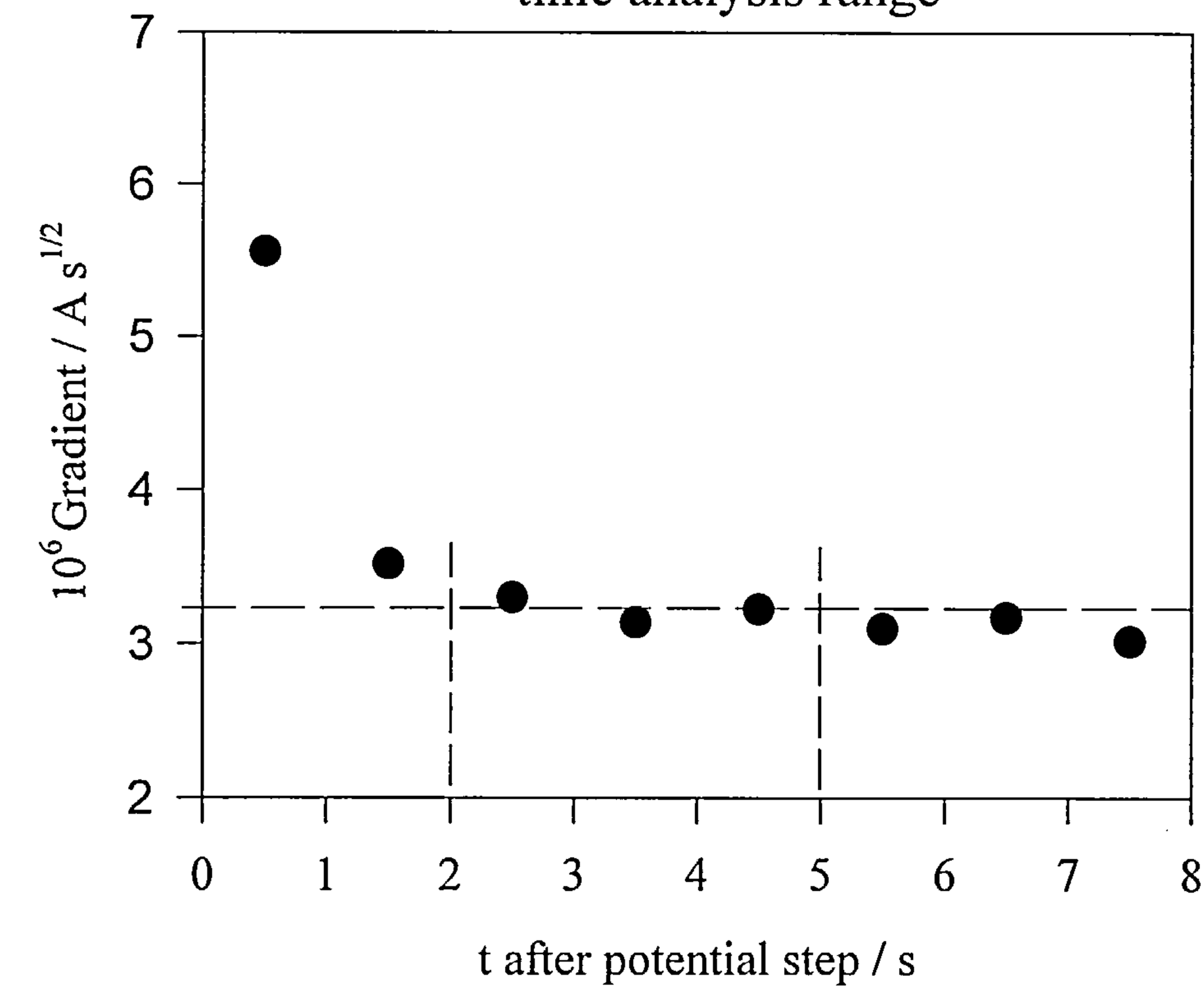

Appendix 3C.xii : Variation of Cottrell intercept with time analysis range

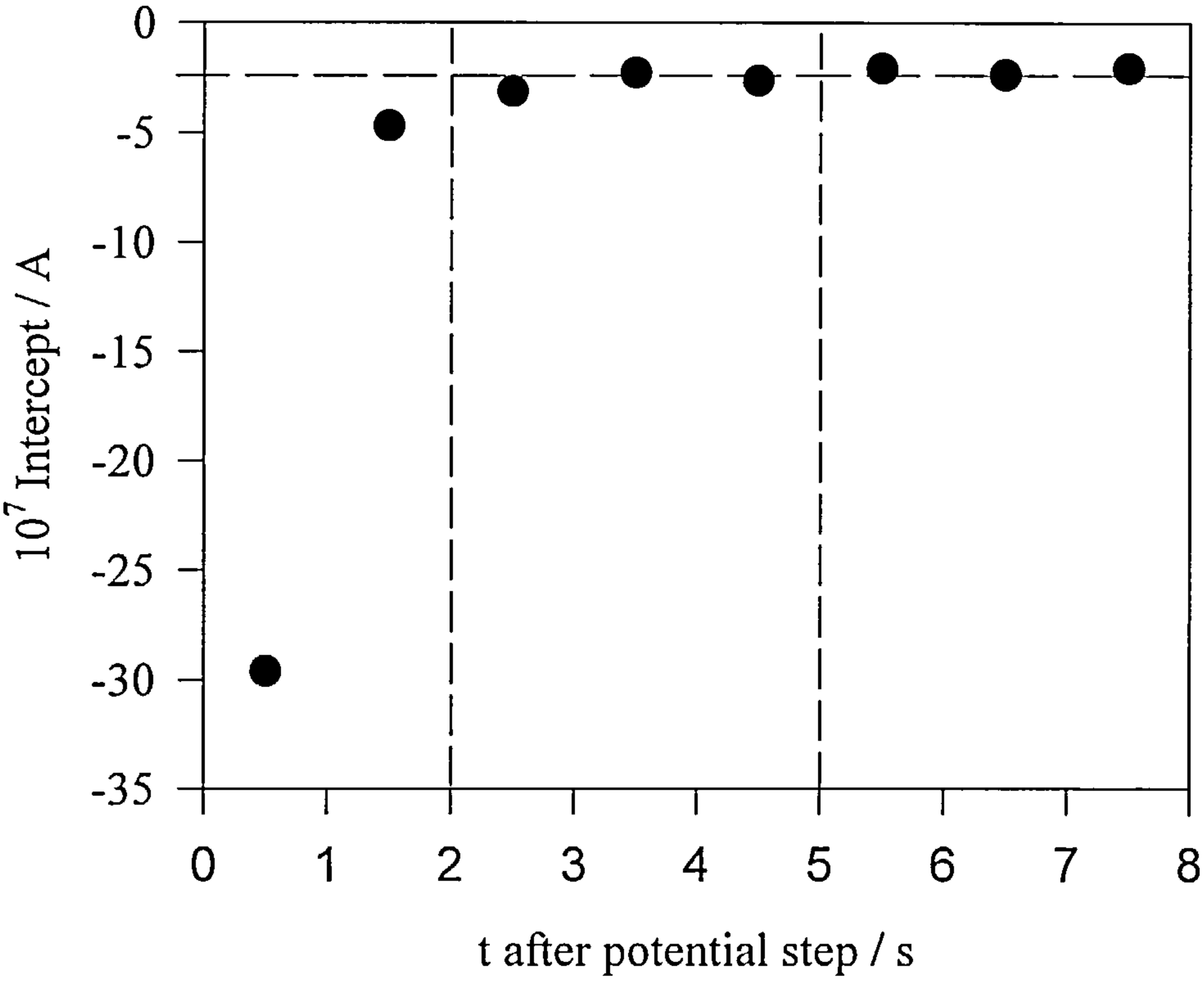

Appendix 3C.xiii : Cottrell plot with chosen analysis range for 0.167 mol dm^{-3} TX-100 + 0.01 mol dm^{-3} KCl

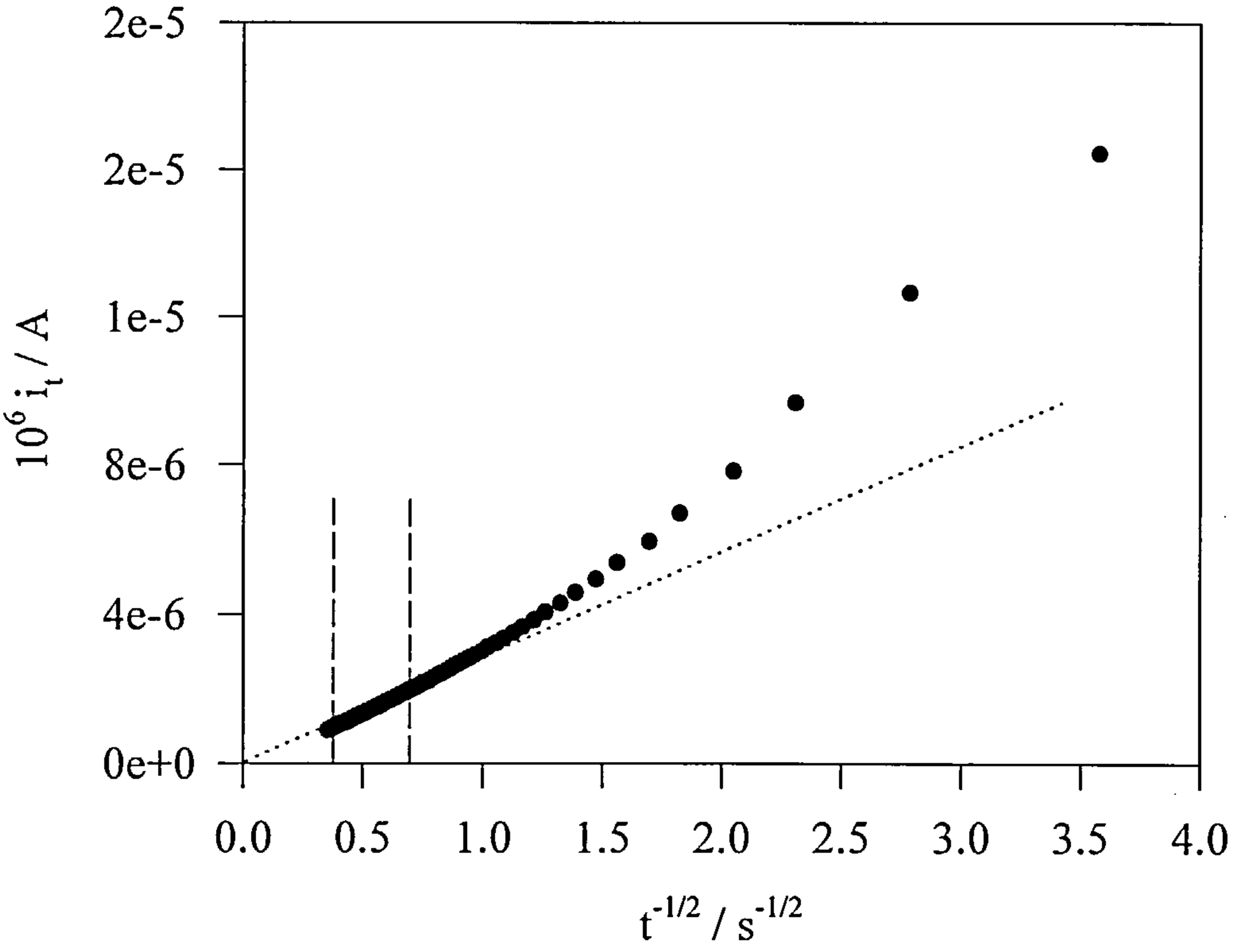

Appendix 3C.xiv : Variation of Cottrell background gradients with [KCl]

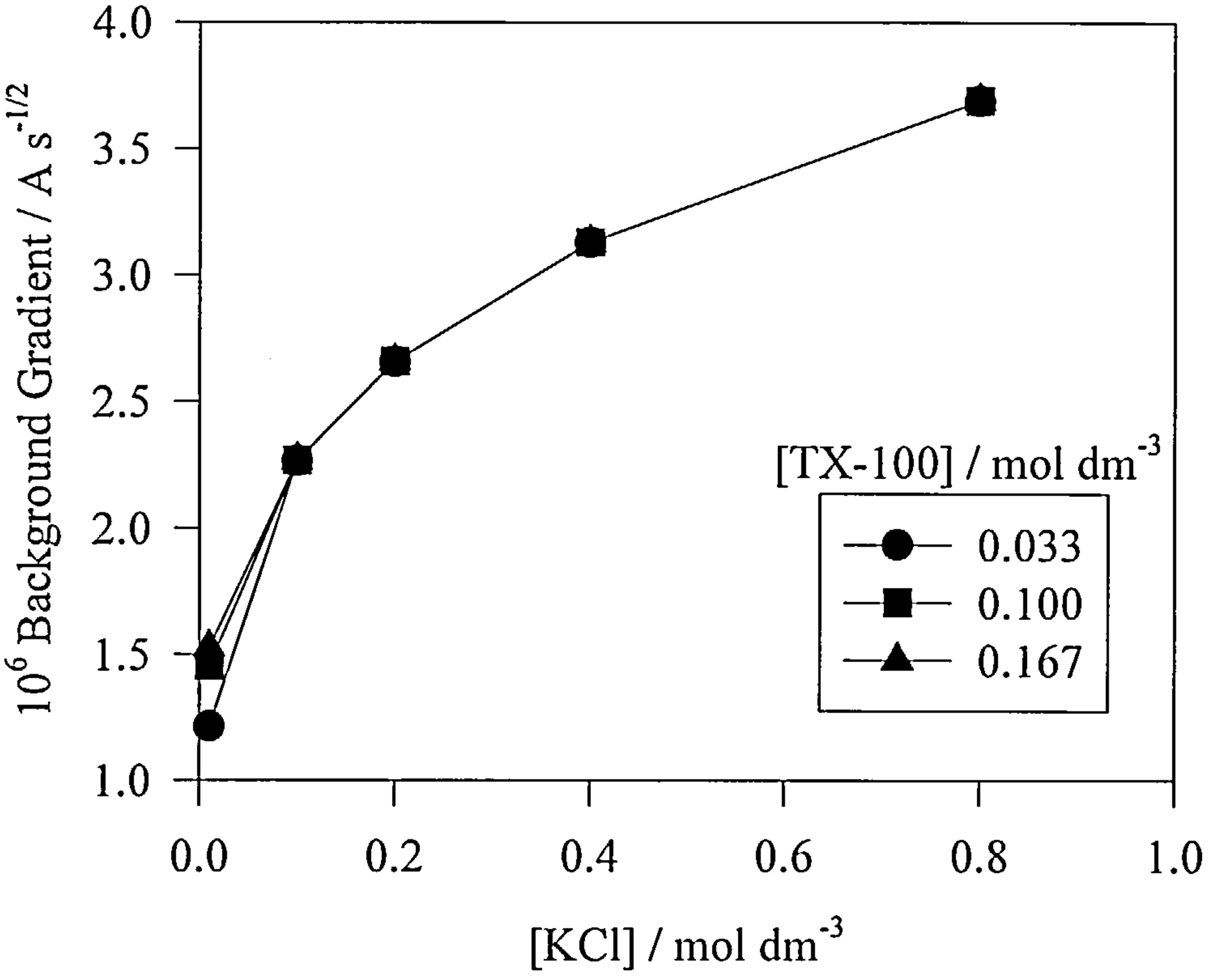

Appendix 3C.xv : Variation of Cottrell experimental gradients with [KCl]

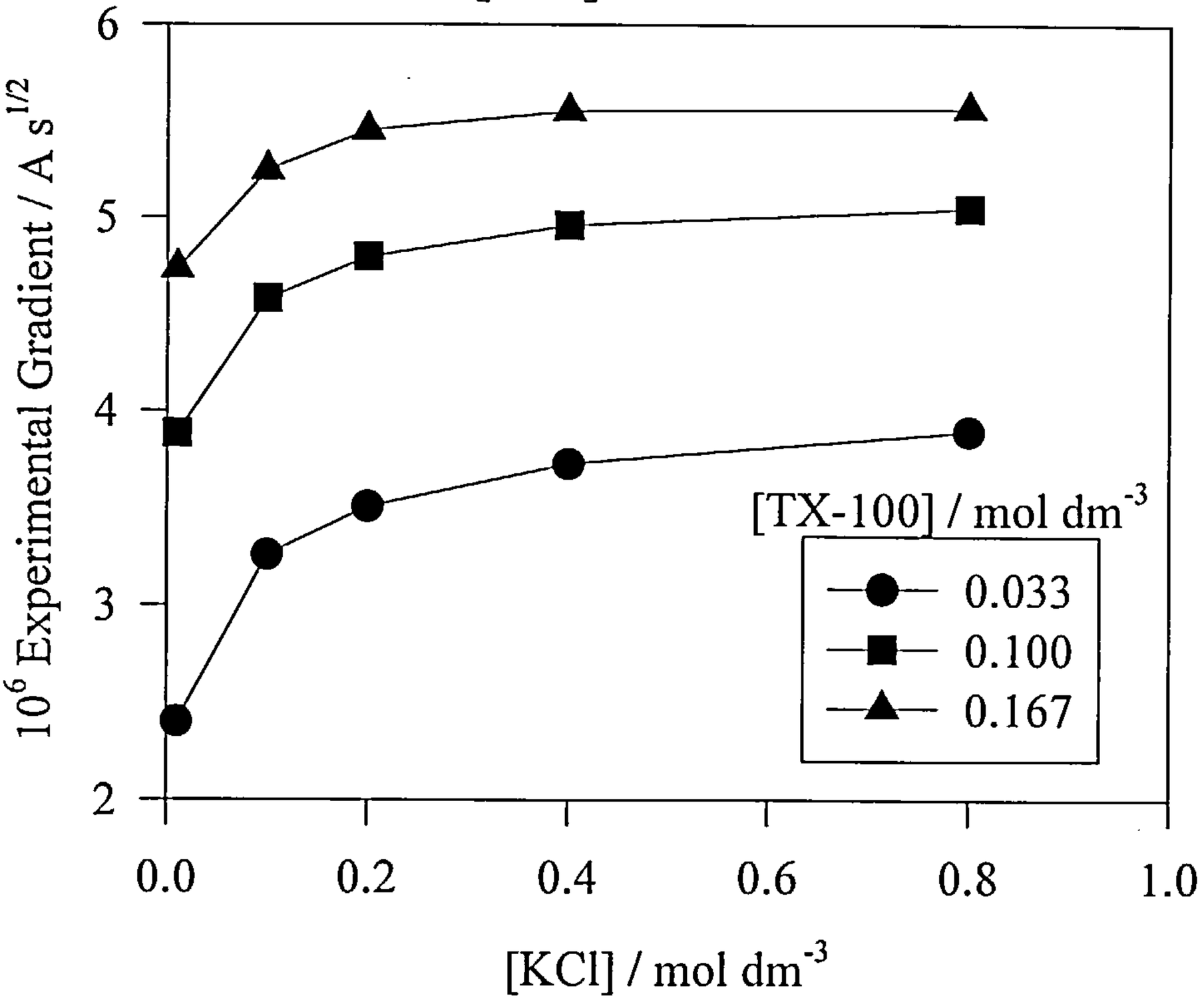

Appendix 3C.xvi : Variation of corrected Cottrell gradients with [KCl]

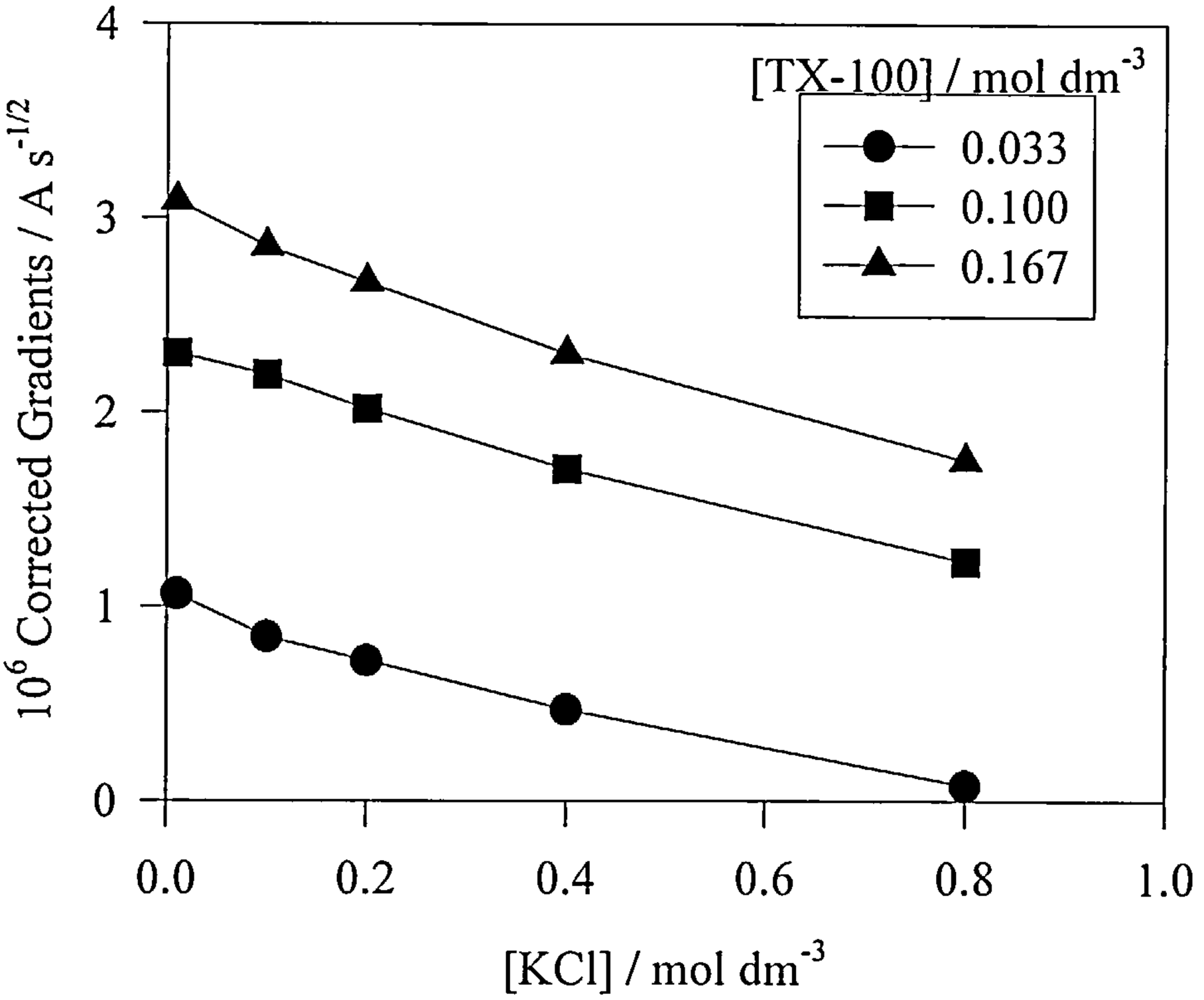

Appendix 3C.xvii : Diffusion coefficient (D_{CA}) variation with [KCl]

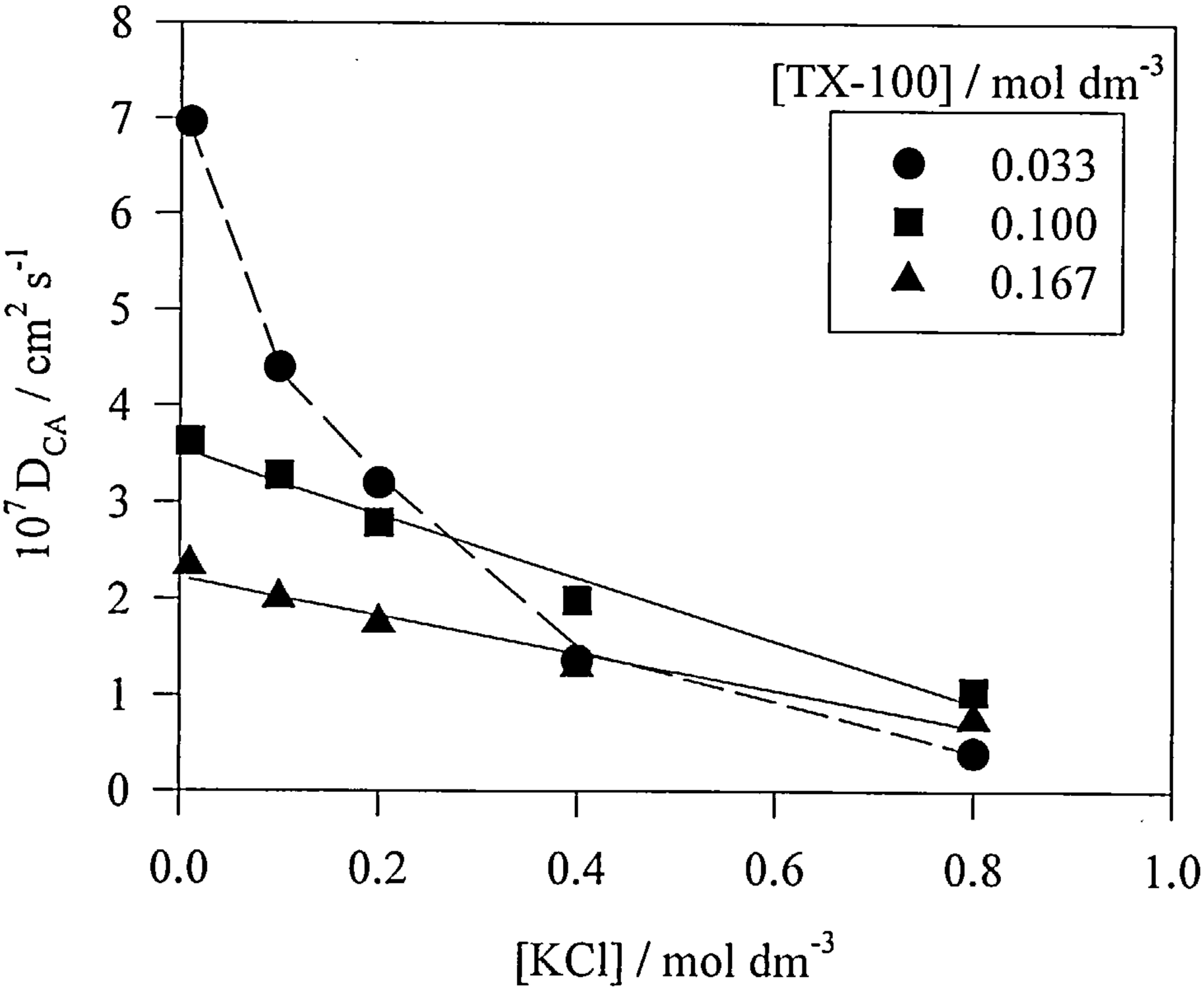

Appendix 3C.xviii : Comparison of diffusion coefficients with technique for 0.167 mol dm^{-3} TX-100

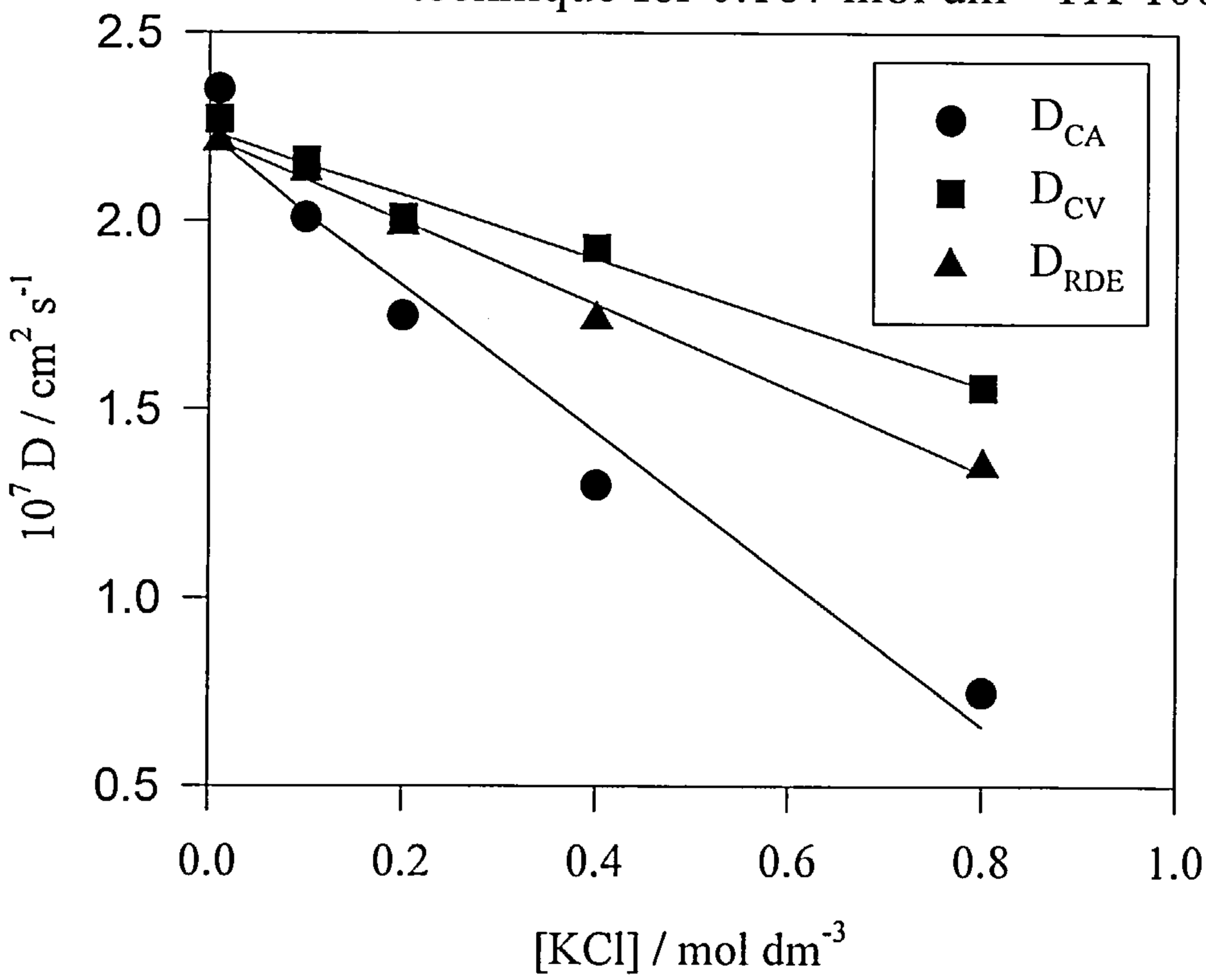

Chapter 3D: Triton X-100 Conclusions

The size, shape and interaction of a non-ionic micellar system has been thoroughly investigated using three electrochemical techniques rotating disk voltammetry, cyclic voltammetry and chronoamperometry in addition to rheological measurements with a cone and plate viscometer. Each of the electrochemical methods yielded easily accessible micellar self diffusion coefficients, however, a high degree of disparity existed between the results. With RDV the application of linear interaction theory allowed the determination of interaction parameters and hydrodynamic radii in excellent agreement with published values[35]. These properties were observed to be controlled by the dehydrating nature of the added electrolyte. For CV, the variation of D_{CV} with surfactant concentration was less straightforward as a quadratic dependence was observed. However, with the careful selection of a concentration range a linear extrapolation could be made. The attenuated D_{CV} values (as compared to D_{RDV}) resulted in lower hydrodynamic radii and interaction parameters that exhibited the opposite trend to what would be expected for growing non-ionic micelles.

An explanation for the observed differences between D_{CV} and D_{RDV} is not readily apparent but, a number of plausible theories have been discussed. The presence of two diffusional regimes at the electrode could lead to an increase in the measured diffusion coefficient by virtue of a contribution from ferrocene diffusing through a viscous volume element close to the electrode surface. If ferrocene was pre-concentrated in a adsorbed surfactant layer the resultant Faradaic currents would be higher due to the increased concentration of electroactive species. Finally the possibility of anisotropic self diffusion has been considered, however, it is believed that at the concentration of surfactant used here (1-5 wt%) would be insufficient to form the liquid crystals required (~30 wt%) to see the observed result[74]. Although none of these theories can be used to explain implicitly the observed behaviour they do offer an excellent basis for the understanding of such a phenomenon.

Rheological measurements were equally important as electrochemical methods for examining the behaviour of the micellar system. Whereas results from self diffusion coefficients illustrated changes in micellar size, viscosity results highlighted structural evolution corresponding to the size change. Analysis of viscosity data using a virial expansion led to α and β shape parameters. These parameters tended to suggest that the micellar shape was gradually shifting from a quasi-spherical to a more elongated micelle.

Measuring the viscosity as a function of electrolyte and temperature indicated that these two parameters were working in tandem to dehydrate the ethylene oxide chains of the micelle. This was characterised by a drop in viscosity at low temperatures followed by a corresponding increase as the temperature increased. These viscosity minima ($T_{\eta,min}$) were a function of the [KCl] and each could be seen to be 31.4^{O}C from the lower consolute curve in the TX-100 phase diagram. The significance of this observation is not fully understood but it is believed to be a function of the onset of some form of increased micellar growth or major shape change which are unable to be detected by voltammetric techniques.

In summary, it has been observed that different electrochemical techniques give different micellar diffusion coefficients. Although this could be viewed as a disadvantage to the methods utilised, it forms an excellent basis for further investigation into diffusion coefficients obtained from transient and hydrodynamic techniques. The possibility of two diffusional regimes and / or probe pre-concentration in micellar systems enhances the rudimentary understanding of self-assembled supramolecular structures at an electrode interface.

A combination of techniques has allowed easily accessible characterisation of Triton X-100 micellar phase behaviour. Whereas electrochemical techniques appear to essentially probe micellar size, interpretation of rheological measurements yield inferences on micellar shape. Therefore, it is evident that complimentary techniques must be used to achieve a full description of non-ionic micellar properties

Triton X-100 (Ch. 3A, 3B, 3C) References:

1. P.S.Goyal, S.V.G.Menon, B.A.Dasannacharya, P.Thiyagarajan, *Physical Review E*, 1995, vol. 51, p. 2308.

2. S.V.G.Menon, P.S.Goyal, B.A.Dasannacharya, P.Thiyagarajan, *Physical Review E*, 1996, vol. 53, p. 6569.

3. L.Qiao, A.J.Easteal, *Colloid and Polymer Science*, 1996, vol. 274, p. 974.

4. A.S.Sadaghiani, A.Khan, *Langmuir*, 1991, vol. 7, p. 898.

5. A.B.Mandal, B.U.Nair, D.Ramaswamy, *Langmuir*, 1988, vol. 4, p. 736.

6. A.Helenius, K.Simons, *Biochim. Biphys. Acta*, 1972, vol. 265, p. 241.

7. S.Razin, *Biochim. Biphys. Acta*, 1975, vol. 415, p. 29.

8. R.A.Deems, B.R.Eaton, E.A.Dennis, *J. Biol. Chem.*, 1975, vol. 250, p. 8003.

9. T.G.Warner, E.A.Dennis, *J. Biol. Chem.*, 1975, vol. 250, p. 9013.

10. E.A.Dennis, *Arch. Biochem. Biophys.*, 1973, vol. 258, p. 485.

11. R.J.Robson, E.A.Dennis, *Biochim. Biphys. Acta*, 1978, vol. 508, 513.

12. E.H.Crook, D.B.Fordyce, G.F.Trebbi, *J. Phys. Chem.*, 1963, vol. 67, p. 1987.

13. A.Ray, G.Nemethy, *J. Am. Chem. Soc.*, 1971, vol. 93, p. 6787.

14. L.M.Kushner, W.D.Hubbard, *J. Phys. Chem.*, 1954, vol. 58, p. 1163.

15. W.Brown, R.Rymden, J. van Stam, M.Almgren, G.Svensk, *J. Phys. Chem.*, 1989, vol. 93, p. 2512.

16. H.H.Paradies, *J. Phys. Chem.*, 1980, vol. 84, p. 599.

17. P.S.Goyal, S.V.G.Menon, B.A.Dasannacharya, P.Thiyagarajan, *Physica B*, vol. 213-214, p. 610.

18. R.M.Weinheimer, D.F.Evans, E.L.Cusler, *J. Colloid and Int. Sci.*, 1981, vol. 80, p. 357.

19. T.R.Carale, D.Blankschtein, *J. Phys. Chem.*, 1992, vol. 96, p. 459.

20. K.Streletzky, G.D.J.Phillies, *Langmuir*, 1995, vol. 11, p. 42.

21. G.J.Phillies, J.E.Yambert, *Langmuir*, 1996, vol. 12, p. 3431.

22. A.B.Mandal, S.Ray, A.M.Biswas, S.P.Moulik, *J. Phys. Chem.*, 1980, vol. 84, p. 856.

23. G.Komaromy-Hiller, N.Calkins, R. von Wandruszka, *Langmuir*, 1996, vol. 12, p. 916.

24. B.Lindman, H.Wennerström, *J. Phys. Chem.*, 1991, vol. 95, p. 6053.

25. T.Imae, *J. Phys. Chem.*, 1988, vol. 92, p. 5721.

26. S.Ikeda, *J. Phys. Chem.*, 1984, vol. 88, p. 2144.

27. K.S.Birdi, *Progress in Colloid and Polymer Sci.*, 1985, vol. 70, p. 23.

28. B.Geetha, A.B.Mandal, *J. Chem. Phys.*, 1996, vol. 105, p. 9649.

29. T.Kato, T.Seimiya, *J. Phys. Chem.*, 1986, vol. 90, p. 3159.

30. A.C.Fisher, *Electrode Dynamics*, Oxford University Press, 1996.

31. E.Munoz, R.Rodriguez-Amaro, J.J.Ruiz, J.L.Avila, L.Camacho, V.Lopez, *J. Electroanal. Chem.*, 1992, vol. 324, p. 359.

32. R.E.Verrall, S.Milioto, A.Giradudeau, R.Zana, *Langmuir*, 1989, vol. 5, p. 1242.

33. R.Guidelli, M.L.Foresti, *J. Electroanal. Chem.*, 1977, vol. 77, p. 73.

34. Z.Kozarac, S.Nikolic, I.Ruzic, B.Cosovic, *J. Electroanal. Chem.*, 1982, vol. 137, p. 279.

35. P.Levitz, H. Van Damme, D.Keravis, *J. Phys. Chem.*, 1984, vol. 88, p. 2228.

36. J.Zhao, W.Brown, *J. Phys. Chem.*, 1996, vol. 100, p. 3775.

37. N.Batina, I.Ruzic, B.Cosovic, *J. Electroanal. Chem.*, 1985, vol. 190, p. 21.

38. A.Szymanski, Z.Lukaszewski, *Analytica Chimica Acta,* 1990, vol. 231. p. 77.

39. A.P.Doherty, K.Scott, *J. Chem. Soc. Faraday Trans.*, 1996, vol. 92, p. 4551.

40. T.Tominaga, M.Nishinaka, *J. Chem. Soc. Faraday Trans.*, 1993, vol. 89, p. 3459.

41. G.D.J.Phillies, J.Stott, S.Z.Ren, *J. Phys. Chem.*, 1993, vol. 97, p. 11563.

42. D.Balasubramanian, P.Mitra, *J. Phys. Chem.*, 1979, vol. 83, p. 2724.

43. H.Zhizhen, L.Xinming, C.Zongqi, *J. Disp. Sci. and Tech.*, 1991, vol. 12, p. 483.

44. P.G.Nilsson, H.Wennerström, B.Lindman, *J. Phys. Chem.*, 1983, vol. 87, p. 4756.

45. M.Zulauf, J.P.Rosenbusch, *J. Phys. Chem.*, 1983, vol. 87, p. 856.

46. R.Zana, C.Weill, *J. Physique Letters*, 1985, vol. 46, L953.

47. R.J.Robson, E.A.Dennis, *J. Phys. Chem.*, 1977, vol. 81, p. 1075.

48. C.Tanford, Y.Nozaki, M.F.Rohde, *J. Phys. Chem.*, 1977, vol. 81, p. 1555.

49. H.Matsuura, K.Fukuhara, K.Takashima, *J. Phys. Chem.*, 1991, vol. 95, p. 10800.

50. N.Kimura, J.Umemura, S.Hayashi, *J. Colloid and Int. Sci.*, 1996, vol. 182, p. 356.

51. R.P.Cooney, C.G.Barraclough, T.W.Healy, *J. Phys. Chem.*, 1983, vol. 87, p. 1868.

52. D.G.Leaist, *J. Solution Chem.*, 1991, vol. 20, no. 2, p. 187.

53. A.K.Wright, *J. Colloid and Int. Sci.*, 1976, vol. 55, p. 109.

54. H.Rau, G.Greiner, H.Hämmerle, *Ber. Bunsenges. Phys. Chem.*, 1984, vol. 88, p. 116.

55. P.G.Nilsson, H.Wennerström, B.Lindman, *J. Phys. Chem.*, 1983, vol. 87, p. 1377.

56. J.Penfold, E.Staples, P.G.Cummins, *Adv. In Colloid and Int. Sci.*, 1991, vol. 34, p. 451.

57. P.W.Atkins, *Physical Chemistry*, Oxford University Press, Oxford, 1985.

58. V.Vand, *J. Phys. Colloid Chem.*, 1948, vol. 52, p. 277.

59. M.Lesemann, A.Martin, L.Belkoura, G.Fleischer, D.Woermann, *Langmuir*, 1997, vol. 13, p. 5289.

60. A.B.Mandal, *Langmuir*, 1993, vol. 9, p. 1932.

61. A.J.Bard, L.R.Faulkner, *Electrochemical Methods*, 1980, John Wiley & Sons, New York.

62. A.P.Abbott, C.L.Miaw, J.F.Rusling, *J. Electroanal. Chem.*, 1992, vol. 327, p. 31.

63. N.Mahanta, O.K.Medhi, *Indian Journal of Chemistry*, 1994, vol. 33A, p. 284.

64. P.Birkin, *Ph.D. Thesis*, University of Southampton, 1995.

65. H.Zhang, J.F.Rusling, *Talanta*, 1993, vol. 40, p. 741.

66. R.J.Forster, J.G.Vos, *Langmuir*, 1994, vol. 10, p. 4330.

67. J.Chung, J.H.Prestegard, *J. Phys. Chem.*, 1993, vol. 97, p. 9837.

Chapters 4A, 4B, 4C - A cationic micellar system

- CTAC -

Chapter 4A: CTAC Self-Diffusion Coefficients (RDV)

4A.1 Introduction

CTAC (cetyltrimethylammonium chloride) is a cationic surfactant consisting of a C-16 hydrocarbon chain and a trimethyl ammonium headgroup. The hydrocarbon chain acts as the hydrophobic micellar interior whilst the charged headgroup forms the hydrophilic exterior surface. Each CTAC micelle has a degree of chloride co-ions associated with the headgroups the magnitude of which is subject to the micellar environment. It is this counter ion binding that essentially determines the critical micelle concentration with values ranging from 1.33×10^{-5} - 1.57×10^{-3} mol dm^{-3} from 0.00 - 1.02 mol dm^{-3} KCl[1].

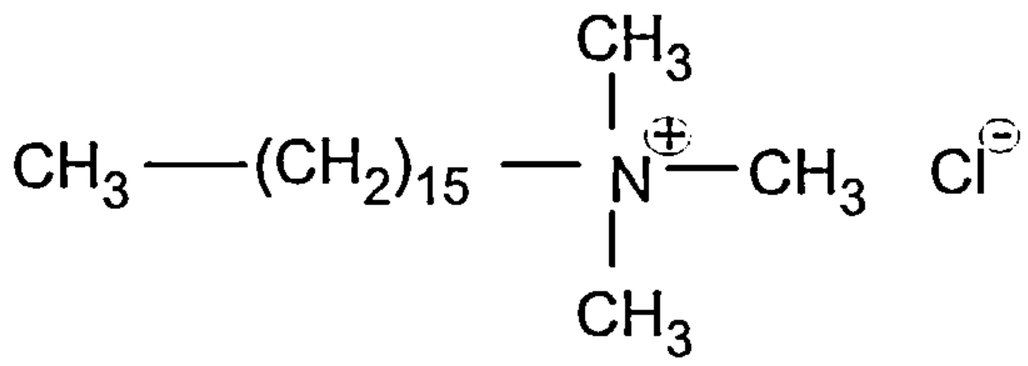

Figure 4A.1 : Structure of CTAC surfactant chain

Alkyl trimethyl ammonium halides ($C_nTA^+X^-$) seem to be the most popular 'family' of cationic surfactants studied. This is mainly due to the fact that varying both the number of carbons (n) and halide (X^-) can lead to inferences on micellar size, growth and counter-ion binding[1,2,3,4]. It appears that the most commonly encountered C_nTAX surfactant is CTAB, with a wide number of studies analysing the effect of electrolyte, temperature and surfactant concentration on the overall micellar phase behaviour. $C_{16}TAX$ micellar systems offer a number of distinct properties that makes them attractive for analysis, for example, low aggregation numbers (N_{agg}) at moderate electrolyte and surfactant concentration. The relative insensitivity of N_{agg} to surfactant concentration (in the low concentration region) suggests that the

micelles retain their spherical shape and exhibit low polydispersity[5]. The low polydispersity is further reinforced as the surfactant concentration is raised, with smaller micellar species growing, hence narrowing the micellar size distribution[6]. It is this property, predominately, which is the main reason for the large number of light scattering (LS) and small angle neutron scattering (SANS) studies that have been carried out[3,4,7,8,9]. It is the wealth of background structural information available for comparison which prompted the use of CTAC here.

The aggregation number of the micellar system is an important parameter as it aids in the evaluation of other factors such as micellar size and growth. A large collection of reported N_{agg} values exist for CTAB and CTAC (bromide and chloride counterions respectively) over a range of temperatures, electrolyte and surfactant concentration[5,6,7,10,11,12,13,14]. The majority of these studies have used fluorescence quenching with pyrene (or a pyrene derivative) as the probe and a range of quenchers[5,6,10,11,12,13,14]. Although the probe-quencher couple can influence the results, a large amount of agreement exists[6,13] and this is thought to be due to CTAX exhibiting dynamic stability on the timescale of fluorescence[13]. On the whole it is widely accepted that at low surfactant and electrolyte concentrations $N_{agg} = 100$ for CTAB and CTAC[3,5,6,7,8,10,11,12,13,14].

The final point to be addressed is which of CTAC and CTAB should be selected for the present study. CTAB can undergo a structural transformation to elongated micelles at [CTAB] ≥ 0.20 mol dm^{-3} [13], whereas CTAC remains spherical to [CTAC] ≤ 1.2 mol dm^{-3} [13]. The difference is due to the nature of the counter ion binding for Br^- and Cl^-. CTAC, therefore, endears itself to use in this case due to well defined aggregation numbers, spherical nature and the lack of precipitous micellar growth at moderate electrolyte and surfactant concentrations.

There are a few studies from light scattering techniques reporting diffusion coefficients of CTAC micelles over a range of electrolyte and surfactant concentrations[3,8]. However, results from electrochemical methods are largely restricted to a single temperature and electrolyte concentration[15,16,17]. This chapter will explore the effect of electrolyte on two main parameters, namely micellar size

and interaction. Inferences on micellar size will lead to the determination of the micellar shear plane location and associated zeta potential. Calculated interaction parameters from voltammetric measurements will be seen to correlate well with theoretical Coulombic potentials. Further to analysis at electrolyte concentrations where micellar growth is limited, the apparent interaction parameter will be determined in an electrolyte range where precipitous micellar elongation occurs which will lead to information on steric (excluded volume) interactions.

4A.2 Results and Discussion

4A.2.1 General Electrochemistry

The micellar self-diffusion coefficients were measured for a series of solutions with CTAC concentrations varying from 0.0313 - 0.1563 mol dm^{-3} (i.e. 1 - 5 % w/v) at 20 ^{O}C. As was discussed previously, at low surfactant concentrations CTAC micelles not only retain their spherical shape but also exhibit a constant aggregation number and therefore micellar size. This meant that any observed changes in the diffusion coefficients would be due to interactions. The added electrolyte (KCl) concentration varied from 0.00 - 1.60 mol dm^{-3}.

With TX-100, the non-ionic nature of the micellar system meant that large iR distortion was present without the addition of electrolyte (Ch. 3A.2.1). However, the nature of the cationic CTAC micelles led to the presence of a finite number of disassociated chloride counter ions in the solution ($CTAC \leftrightarrow CTA^{+} + Cl^{-}$). The solution was therefore of sufficient conductivity to allow a true Faradaic current-voltage response to be obtained. This observation was doubly confirmed by both the shape of the sigmoidal voltammogram and the resultant Nernstian data (i.e. slope ~ 58 mV $decade^{-1}$). Half wave potentials ($E_{1/2}$) were determined over the full range of electrolyte and surfactant concentrations and are shown in Table 4A.1.

Table 4A.1: Half wave potential variation with surfactant and electrolyte concentration

[CTAC] / mol dm^{-3}	$E_{1/2}$ / mV with [KCl] / mol dm^{-3}				
	0.00	0.10	0.80	0.00 - 0.80	1.60
0.0313	203.0	210.1	206.5	206.5	197.9
0.0938	228.0	230.1	234.1	230.7	223.3
0.1563	246.3	244.2	245.6	245.4	233.4

Note : The Nernstian slope remains constant at ~ 58 mV decade^{-1}

The observed increase in $E_{1/2}$ values with surfactant concentration has been seen previously for CTAC[15,17] and CTAB[18]. Eddowes at al. and Georges et al. attributed this to a change in the electroactive probe solubilisation equilibrium[17,18]. It will be seen, however, that $E_{1/2}$ remains unchanged in a solution of fully electrolysed ferrocene i.e. all ferricinium (Ch. 4A.2.2.2). Therefore, it is likely that the increasing $E_{1/2}$ is due to a hindrance of electron transfer[19,20,21] as was discussed for Triton X-100 (Ch. 3A.2.1). An increase in $E_{1/2}$ with electrolyte was seen for TX-100 and was believed to be due to a reduction in the adsorbed surfactant layer thickness as a result of micellar growth in the bulk solution (Ch 3A.2.1). The absence of this effect for CTAC from 0.00 - 0.80 mol dm^{-3} KCl would tend to confirm this conclusion as large scale micellar growth does not occur until [KCl] ≥ 1.20 mol dm^{-3} as will be seen in Ch. 4A.2.3.1 and Ch. 4B.2.1. However, at 1.60 mol dm^{-3} there is a drop of ~10 mV in $E_{1/2}$ as compared to the mean values from 0.00 - 0.80 mol dm^{-3} KCl. This is further evidence of how bulk solution micellar growth influences the half wave potential. The actual mechanism for the adsorption of cationic surfactants exhibits a Frumkin type isotherm at concentrations below the c.m.c.[22,23]. However, this is not of immediate concern here as the [CTAC] >> c.m.c. and therefore the adsorbed layer is likely to be a bilayer structure[24].

In order to further characterise the effect of surfactant and electrolyte concentration a series of background capacitance scans were carried out. In order to give maximum possible surfactant adsorption, the glassy carbon electrode was left stationary in each solution for 30 minutes. The current response of the electrode was then monitored between -200 and +500 mV over a range of applied potential sweep

rates (υ). From the resultant traces the product $2\upsilon C_{dl}$ was found at each sweep rate and a linear plot was constructed. The gradient of this line leads directly to the double layer capacitance. A typical background trace can be seen in Appendix 4A.i, and the variation of $2\upsilon C_{dl}$ with υ is shown below in Table 4A.2 and in Appendix 4A.ii.

Table 4A.2 : Variation of electrode double layer capacitance with surfactant and electrolyte concentration

Sweep rate υ / V s^{-1}	$10^6\ 2\upsilon C_{dl}$ / A			
	No CTAC + 0.10 mol dm^{-3} KCl	5% CTAC + 0.00 mol dm^{-3} KCl	5% CTAC + 0.10 mol dm^{-3} KCl	5% CTAC + 0.80 mol dm^{-3} KCl
0.02	2.938	2.508	2.990	3.106
0.04	5.160	4.880	5.154	5.773
0.08	9.965	8.935	10.38	12.36
0.10	12.23	11.13	12.47	15.07
0.12	14.63	12.71	14.95	17.05
Correlation	0.9994	0.9985	0.9992	0.9982
Gradient (F)	1.202×10^{-4}	1.061×10^{-4}	1.227×10^{-4}	1.458×10^{-4}
$10^5\ C_{dl}$ / F	6.01	5.31	6.14	7.29

It can be seen that there is only a slight increase in the apparent electrode capacitance between the distilled water and the 5% CTAC solutions both of which contained 0.10 mol dm^{-3} KCl supporting electrolyte. A large increase in C_{dl} is apparent from 0.00 - 0.80 mol dm^{-3} KCl. There are two possible explanations for this occurrence. Firstly, the electrolyte may cause the surfactant to be forced onto the electrode surface. Secondly, and more likely, is that there may be an increased degree of chloride ion adsorption on the surface with increasing electrolyte concentration[25,26] (chloride has been observed to adsorb on glassy carbon[27] and platinum[25,26]). Increases in electrode capacitance with specifically adsorbed small ions has been recorded previously[28,29,30]. An increase in the heterogeneous rate constant (k^O) is seen over this [KCl] range (Ch. 4C.2.1), a similar increase in k^O for ferricyanide reduction has been observed by Goldstein et al. with increases in bromide concentration[31].

In contrast to both k^O and C_{dl}, half wave potential ($E_{1/2}$) studies show that they remain constant over this KCl range whereas they increase with increased surfactant concentration for CTAC.

4A.2.2 Electroactive Probe Considerations

Before electrochemical experiments can be carried out with confidence a number of factors regarding the micellar system need to be taken into consideration. It was shown in Ch. 2 that analytical solution preparation and accurate calibration of electrode area were needed to attain precise and accurate diffusion coefficients. The nature of the electroactive probe is also of importance (Ch. 1.2.2) and considering parameters such as concentration and distribution allows the elimination of any uncertainties in relation to the probe.

4A.2.2.1 Probe Concentration Dependence

One interesting point to address is how the concentration of probe affects certain properties of the system e.g. the diffusion coefficient. It is standard practice to use a probe : micelle ratio = 1, where theoretically there is one probe per micelle. What happens if this ratio deviates from unity? Firstly, it is known that ferrocene conforms to the Poisson distribution or pseudo-phase model in which the presence of a probe in a micelle will not affect any further solubilistion[18,32]. So, in theory a large number of ferrocene molecules could be incorporated within the micellar interior as the radius of a ferrocene molecule is much less than a CTAC micellar core (R_{fc}= 0.365 nm)[18]. Georges et al. and Chokshi et al. have stated that both the diffusion coefficient and half wave potential are totally independent of the ferrocene concentration, though it was not clear if correction for aqueous phase ferrocene was made[18,33]. Conversely, it has been seen that multiple occupancy of a micelle results in a reduction of the diffusion coefficient until a limiting value is reached[34,35]. Rusling et al. observed that the D_S value in 0.10 mol dm^{-3} CTAC + 0.10 mol dm^{-3}

NaCl reached this limiting value at ~$1.0x10^{-3}$ mol dm^{-3} which for an aggregation number of 100 leads to a ferrocene : micelle ratio of ~1[35]. As the results of these studies where conflicting, it was necessary to study the effect of the ferrocene / micelle ratio on the system here.

The diffusion coefficients of 0.1563 mol dm^{-3} CTAC solutions at three different electrolyte concentrations were measured by RDV by the standard method. In each case the concentration of ferrocene dissolved into the micellar solution was varied from $1.563x10^{-3}$ mol dm^{-3} to $1.59x10^{-4}$ mol dm^{-3}. This range ensured that there was a transition from multiply occupied micelles to ferrocene deficient micelles. Electrolyte concentrations of 0.80, 1.40 and 1.60 mol dm^{-3} KCl were used as at these high values it is known that large scale micellar aggregation occurs and therefore a greater scope for multiple occupancy exists.

The experimental diffusion coefficients as a function of ferrocene concentration are shown in Table 4A.3 and graphically in Appendix 4A.iii.

Table 4A.3 : Variation of micellar diffusion coefficient with ferrocene concentration

10^3 [fc] / mol dm^{-3}	$10^7 D_{RDV}$ / $cm^2 s^{-1}$		
	[KCl] = 0.80 mol dm^{-3}	[KCl] = 1.40 mol dm^{-3}	[KCl] = 1.60 mol dm^{-3}
0.159	1.84	1.44	0.78
0.313	3.48	2.72	1.74
0.450	3.93	3.22	2.17
0.625	4.31	3.52	2.42
0.780	4.56	3.77	2.55
0.938	4.76	3.79	2.54
1.250	4.86	3.72	2.46
1.563	4.92	3.74	2.49

Note: Increasing [fc] / [micelle] to ~ 2, did not appreciably affect D_{RDV} indicating no probe induced structural changes. Standard errors = $\pm 0.10x10^{-7}$ cm^2 s^{-1} apart from at a ferrocene concentration of $1.59x10^{-4}$ mol dm^{-3}, where the limiting currents are <5 μA making accurate diffusion coefficient determination difficult. It follows that at this concentration errors in the range $0.20\text{-}0.25x10^{-7}$ cm^2 s^{-1} are obtained.

From the results it can be seen that there is a definite dependency of the diffusion coefficient on the concentration of ferrocene and hence the number of ferrocene molecules per micelle. As the concentration of ferrocene is increased the diffusion coefficient reaches a limiting value. The point at which this limiting value is reached depends on the concentration of KCl, the higher the [KCl] the lower the [fc] at which the diffusion coefficient reaches its limiting value. This can be interpreted in terms of the aggregation number of the micelle (N_{agg}). If it is assumed that deviation from the limiting value occurs at a micelle : ferrocene ratio of 1:1 i.e. [micelles] = [fc] then the aggregation number can be calculated.

$$N_{agg} = ([CTAC] - c.m.c.) / [micelles] \equiv [CTAC] / [fc] \qquad (4A.1)$$

Studies by Johnson et al.[1] have shown that values for the critical micelle concentration (c.m.c.) at [KCl] = 1.00 mol dm^{-3} will be of the order $1.0x10^{-5}$ mol dm^{-3}. Therefore, as the concentration of KCl is 0.80 - 1.60 mol dm^{-3} the affect of the c.m.c. will be negligible. From the curves drawn in Appendix 4A.iii, the limiting ferrocene concentration is estimated and hence the aggregation number. These values are shown in Table 4A.4.

Table 4A.4 : Variation of limiting ferrocene concentration and micellar aggregation number with concentration of KCl.

[KCl] / mol dm^{-3}	10^3 $[fc]_{lim}$ / mol dm^{-3}	N_{agg} / no units
0.80	1.10	156
1.40	0.78	200
1.60	0.60	260

The value at 0.80 mol dm^{-3} KCl is in reasonable agreement with literature ($N \sim 175$)[5] though it must be noted that a precise limiting ferrocene concentration is difficult to determine unless a greater number of experimental points are obtained. It can therefore be assumed that at concentrations higher than the limiting ferrocene concentration the micelles are multiply occupied and below there will be a number of micelles without ferrocene molecules. The results can now be interpreted in terms of a pseudo-stochastic process with 'empty' micelles hindering the transport of

micelles containing ferrocene molecules to the electrode surface. Another way of viewing the results is as a probability relationship. If each micelle contained a probe molecule then the probabilities of going in any direction would be equal and therefore every micelle hitting the electrode surface would contain a probe i.e. a limiting diffusion coefficient.

The presented data may lead to inferences in micellar packing and in effect a 3-dimensional model of the micellar structure. Although beyond the scope of this work, the use of Monte-Carlo simulation may yield insightful information.

Nernstian plots were constructed from the redox waves by plotting E against $\log_{10}[i / (i_{Lim} - i)]$, from which the y-axis intercept gives the half wave potential ($E_{1/2}$) and the gradient is the Nernstian slope (theoretically ~58 mV decade^{-1} 20 ^{O}C). It can be seen from Appendix 4A.iv that there is a distinct difference in the slope and intercept as the concentration of ferrocene is altered. The resultant data is presented in Table 4A.5.

Table 4A.5 : Variation of half wave potential and Nernstian slope with ferrocene concentration

10^3 [fc] / mol dm^{-3}	[fc]:[micelle]	Slope / mV decade^{-1}	Exp. $E_{1/2}$ / mV
0.159	<1	68.5	228.3
0.313	<1	62.5	232.9
0.450	<1	60.7	235.1
0.625	<1	60.1	235.0
0.780	≤1	59.5	236.4
0.938	≥1	58.9	236.8
1.250	>1	58.3	237.1

The experimental data is plotted in Appendix 4A.v and 4A.vi.

Variations in half wave potentials have been previously explained in terms of electron transfer at the electrode (3A.2.1, 4A.2.1), with inferences made on the nature of an adsorbed surfactant layer. However, analysis on the basis of electron transfer shows that the results (Table 4A.5) are inconsistent. The observed increase in $E_{1/2}$ suggests that electron transfer is more difficult whereas the drop in Nernstian

slope indicates easier electron transfer. Hence, there must be a more compatible explanation.

The change in half wave potentials can be considered with reference to the Nernst equation (Ch. 1.3.2, Equation 1.19), where $E = E_{1/2}$. If the formal potential (E^O) remains constant then it can be seen that the ratio of $[fc^+]$ / [fc] may decrease to effect an increase in $E_{1/2}$. This correlates with an increase in $E_{1/2}$ from 228 mV to 237 mV with increasing ferrocene concentration.

For a reaction exhibiting a steady state current there is an associated overpotential which consists of contributions from concentration polarisation (or mass transfer overpotential), charge transfer overpotential and reaction overpotential[30]. At low ferrocene concentrations there may be insufficient probe present to maintain the concentration polarisation overpotential and hence the Nernst equilibrium[30]. This could result in 'super' Nernstian responses as are observed in Table 4A.5.

The results presented here highlight the fact that for true diffusion coefficients it is necessary that [fc] / [micelle] $\geq$ 1. It is this procedure that was adopted in the preparation of CTAC and Triton X-100 micellar solutions (Ch. 2.2).

4A.2.2.2 Probe Distribution in Micelles

One aspect of the fc / fc^+ couple in micellar solutions that is somewhat difficult to elucidate is whether the ferrocene and ferricinium remain in the micelle during electron transfer. In certain cases it is believed that the probe leaves the micelle prior to oxidation, but it is not known if this is a general case[34]. Another possibility is that the probe may partition into a surfactant layer on the electrode surface before electron transfer[34]. However, in the electrochemical measurements, diffusion is the current limiting factor and is therefore not affected by whether the ferrocene is inside or outside a micelle prior to electron transfer so long as the process is fast. Nevertheless, it is interesting to consider the probe distribution in order to give a better insight into the electron transfer process.

One factor that may help to explain the mechanism is the solubility of the ferricinium in the aqueous phase and this can be assessed by considering its diffusion coefficient. The diffusion coefficient of ferrocene in water is somewhat difficult to measure due to its limited solubility (1×10^{-5} mol dm^{-3}) and hence the small currents obtained in electrochemical measurements[18,37]. A value of 10.5×10^{-6} cm^2 s^{-1} for ferrocene diffusion in the aqueous phase has been reported[37] and it is obvious that this is at least an order of magnitude higher than ferrocene in micellar solutions[18,32,37]. Georges et al. assumed that ferrocene and ferricinium have identical diffusion coefficients in aqueous solution[18], and concluded that a ferricinium diffusion coefficient larger than ferrocene in a CTAB micellar solution was indicative of some ferricinium residing outside the micelle[18]. This has also been seen in a range of other cationic surfactants[32,34]. However, in polyoxyethylene-23 lauryl ether (Brij 35) and sodium dodecylsulfate (SDS) it has been observed that both the ferrocene and ferricinium are partitioned in the micellar phase[18].

It has been stated earlier that the low solubility of ferrocene in the aqueous phase will not only make electrochemical measurements of the aqueous phase ferrocene diffusion coefficient difficult, but inaccurate. Therefore, rather than attempting to determine the diffusion coefficient of ferricinium in a purely aqueous solution, a solution of 0.1563 mol dm^{-3} CTAC with 1.563×10^{-3} mol dm^{-3} of ferrocene and 0.10 mol dm^{-3} KCl was completely electrolysed and the resulting diffusion coefficient measured by RDV. The electrolysis cell was identical to that as shown earlier (Appendix 2.i) but with a number of slight modifications. The working electrode was a 35 mm x 35 mm platinum grid to ensure faster electrolysis. The counter electrode resided in a small reservoir of the un-electrolysed solution separated from the bulk solution by a ceramic frit, this prevented any reduction of ferricinium back to ferrocene.

Using Coulombs law it is simple to calculate how much charge was required to be passed through the solution for full electrolysis.

$$Q = n.F.N = i.t \qquad (4A.2)$$

Where n is the number of electrons transferred (=1), F is Faraday's constant and N is the number of moles of ferrocene. For a 200 cm^3 sample volume there are $3.126x10^{-4}$ moles of ferrocene and hence the amount of charge (Q) needed is 30.2 C. Therefore if a set constant current is applied to the solution the time required for full electrolysis can be calculated. In order to keep the electrolysis time practical, a high current OxSys potentiostat was used to apply a current of $9.12x10^{-4}$ A. This enabled a micellar solution containing ferricinium (and no ferrocene) to be obtained after ~9½ hours. In order to confirm that the solution had been totally electrolysed, a UV/Vis spectrum was compared to that of the original ferrocene solution. This is shown in Appendix 4A.vii and it can be seen that there is no absorption peak at 440 nm and it follows that no ferrocene remains in the solution.

The presence of a peak at 620 nm suggests that it corresponds to ferricinium (as no ferrocene peak at 440 nm exists), and from knowing the concentration present in the solution ($1.563x10^{-3}$ mol dm^{-3}) the extinction coefficient can be found from the Beer-Lambert law.

$$A_{630nm} = \varepsilon.c.l \qquad (4A.3)$$

where l is the path length (= 1 cm). It follows that $\varepsilon = 366\ dm^3\ mol^{-1}\ cm^{-1}$ which is in excellent agreement with Wilkinson et al.[38] ($\varepsilon = 360\ dm^3\ mol^{-1}\ cm^{-1}$).

Appendix 4A.viii shows the difference in RDV sigmoidal plots between the initial and fully electrolysed solution. From these plots the i_{lim} is plotted as a function of the $\omega^{1/2}$ (Appendix 4A.ix) and hence the diffusion coefficients for both the ferrocene and ferricinium micellar solutions. Table 4A.6 shows the difference in current magnitude between both solutions.

Table 4A.6 : Variation of limiting current with rotation rate for ferrocene and ferricinium in 0.1563 mol dm^{-3} CTAC + 0.1 mol dm^{-3} KCl

Un-electrolysed solution (ferrocene)		Electrolysed solution (ferricinium)	
$\omega^{1/2}$ / $Hz^{1/2}$	10^5 i_{lim} / A	$\omega^{1/2}$ / $Hz^{1/2}$	10^5 i_{lim} / A
1.41	1.80	1.00	5.69
2.00	2.51	1.22	6.81
2.45	3.09	1.41	7.85
2.83	3.57	1.58	8.79
3.16	4.01	1.73	9.69
3.46	4.39	2.00	11.03
10^7 D_{RDV} / cm^2 s^{-1}	5.10	10^7 D_{RDV} / cm^2 s^{-1}	49.0

For ferricinium to be totally partitioned in the aqueous phase the diffusion coefficient would be expected to be $10.5x10^{-6}$ cm^2 s^{-1} [37]. If the ferricinium was totally solubilised in the micellar phase a diffusion coefficient equal to that of the ferrocene ($5.1x10^{-7}$ cm^2 s^{-1}) would be expected. The fact that the measured value is between these two extremes suggests that some, but not all, of the ferricinium is retained in the micellar interior. Georges et al.[18] reported ratios between 7 - 17 for D_{fc+} : D_{fc} in CTAB, these are in excellent agreement with a value of 9.6 from the above results.

Rusling has expressed the diffusion coefficient as a function of the probe fraction residing inside / outside the micelle and the respective diffusion coefficients in the micellar and aqueous phases[34]. This can be applied to the analysis of the ferricinium distribution, where D_{obs}, D_{aq} and D_{mic} are the observed, aqueous and micellar diffusion coefficients respectively; f_{aq} is the fraction of ferricinium in the aqueous phase.

$$D_{obs} = (f_{aq}.D_{aq}^{1/2} + (1-f_{aq}).D_{mic}^{1/2})^2 \qquad (4A.4)$$

Using values of $D_{obs} = 49x10^{-7}$ cm^2 s^{-1}, $D_{aq} = 10.5x10^{-6}$ cm^2 s^{-1} and $D_{mic} = 5.1x10^{-7}$ cm^2 s^{-1}, the fraction of ferricinium in the aqueous phase is found to be 60%, which is in agreement with previous findings[18,32,34]. In the above calculation the value from Mandal et al.[37] has been used here, however, Georges et al. estimated D_{aq} from the

size of a ferrocene molecule and obtained $6.7x10^{-7}$ cm^2 s^{-1}, which when used above results in f_{aq} = 80%. Both of these results show that the majority of ferricinium resides outside the micellar interior.

Another important property to check is the Nernstian response of the system before and after bulk electrolysis. Nernstian data for CTAC micellar solutions has been analysed previously in Ch. 4A.2.1 and Ch. 4A.2.2.1. It was observed that the half wave potentials remained unchanged at $E_{1/2}$ ~ 235 mV and the actual slope also remained constant at ~58 mV $decade^{-1}$ (if [fc] / [micelle] >1). If the ferricinium reduction occurred in the aqueous phase a change in $E_{1/2}$ could be expected, however, it has been shown above that ferricinium resides predominately in the aqueous phase. The consistency in $E_{1/2}$ would tend to suggest that the electron transfer process is occurring in the same environment and this could be possible if the process is occurring in the adsorbed surfactant layer on the electrode. A mechanism of this sort has been discussed by Rusling[24].

4A.2.3 Diffusion Coefficient Results

A full set of typical RDV plots over a rotation rate range of 2-12 Hz for 0.1563 mol dm^{-3} CTAC + 0.10 mol dm^{-3} KCl are shown in Appendix 4A.x. Levich plots (i_{Lim} vs. $\omega^{1/2}$), from which the diffusion coefficients are calculated, are shown in Appendix 4A.xi for three different [CTAC]. Table 4A.7 shows the experimentally determined diffusion coefficients from 0.0313 - 0.1563 mol dm^{-3} CTAC and 0.00 - 1.60 mol dm^{-3} KCl.

Table 4A.7 : Experimental D_{RDV} results

[KCl] / mol dm^{-3}	$10^7 D_{RDV}$ / cm^2 s^{-1}		
	0.0313 mol dm^{-3} CTAC	0.0938 mol dm^{-3} CTAC	0.1563 mol dm^{-3} CTAC
0.00	6.03	5.01	4.11
0.01	6.40	5.46	4.29
0.02	7.05	5.68	4.62
0.05	7.16	5.95	5.01
0.08	7.28	6.13	5.08
0.10	7.26	6.24	5.02
0.20	7.26	6.24	5.18
0.40	6.80	6.01	5.14
0.80	6.36	5.58	4.92
1.00	5.97	5.30	4.67
1.20	5.63	4.98	4.38
1.40	5.32	4.67	3.74
1.60	4.92	3.89	2.49

Note: standard error = $\pm 0.09x10^{-7}$ cm^2 s^{-1}; experiments repeated twice

Plots of D_{RDV} against [KCl] for each [CTAC] are shown in Appendix 4A.xii along with the respective curve fits. The data can essentially be separated into two regions, [KCl] ≤ 0.80 mol dm^{-3} and [KCl] ≥ 1.00 mol dm^{-3}. At [KCl] ≤ 0.80 mol dm^{-3} the data fits a rational function with correlation coefficients ~ 0.99. The data at [KCl] ≥ 1.00 mol dm^{-3} fits a number of mathematical functions, but a simple spline curve of best fit is sufficient.

The rational function is written as:-

$$y = (a + bx) / (1 + cx + dx^2) \qquad (4A.5)$$

where y is the diffusion coefficient, x is the concentration of KCl and a, b, c, d are numerical constants. Values for a, b, c and d are shown below in Table 4A.8.

Table 4A.8 : Rational function; numerical constants

Numerical Constants	[CTAC] / mol dm^{-3}		
	0.0313	0.0938	0.1563
a / cm^2 s^{-1}	$5.99x10^{-7}$	$5.03x10^{-7}$	$4.07x10^{-7}$
b / dm^3 mol^{-1}	$4.10x10^{-5}$	$2.11x10^{-5}$	$1.60x10^{-5}$
c / dm^3 mol^{-1}	53.1	31.3	28.8
d / dm^6 mol^{-2}	14.8	7.89	4.26

The data from the rational fitted curves for each [CTAC] is shown in Table 4A.9. It can be seen that the fitted values only deviates from the experimental data, on average, by a small degree (~$0.05x10^{-7}$ cm^2 s^{-1}) and this can be accounted for by experimental error.

Table 4A.9 : Rational fitted diffusion coefficient data

[KCl] / mol dm^{-3}	10^7 D_{RDV} / cm^2 s^{-1}		
	0.0313 mol dm^{-3} CTAC	0.0938 mol dm^{-3} CTAC	0.1563 mol dm^{-3} CTAC
0.00	5.99	5.03	4.07
0.01	6.59	5.43	4.40
0.02	6.87	5.67	4.60
0.05	7.18	6.01	4.91
0.08	7.26	6.15	5.05
0.10	7.28	6.19	5.10
0.20	7.21	6.22	5.19
0.40	6.91	6.03	5.14
0.80	6.31	5.58	4.92
1.00	5.98	5.31	4.70
1.20	5.65	5.03	4.36
1.40	5.30	4.64	3.75
1.60	4.92	3.89	2.49

The fitted data is used for further analysis (Ch. 4A.2.3.1) and is plotted in Appendix 4A.xii.

4A.2.3.1 Results Analysis

It was seen for Triton X-100 that the effect of surfactant concentration on micellar diffusion coefficients could be analysed using linear interaction theory (Ch. 3A.2.2.1). It is this procedure that is adopted for the study of CTAC micellar diffusion coefficients. With TX-100 the D_{RDV} values exhibited one type of behaviour with added electrolyte i.e. a linear decrease with [KCl]. With CTAC, however, there are three distinct regions with which it is prudent to analyse prior to the use of linear interaction theory.

At low electrolyte concentrations the diffusion coefficients display a steep increase with [KCl]. The addition of electrolyte has two opposing effects, firstly decreased electrostatic drag[2,3,4,9,12,39,40,41,42] and secondly increased micellar hard sphere size[2,5,7]. The predominant effect over this electrolyte range is the increased electrostatic screening due to neutralisation of the surface charge[1,2,3,12,40]. It is known that over 0.00 - 0.10 mol dm^{-3} KCl the surface potential (ψ) drops from 166 mV - 105 mV[1] which explains the decreased repulsion and increased particle mobility. Behaviour of this sort has been observed previously by tracer diffusion measurements[2].

The second region of note is the observed approximate linear decrease in D_{RDV} with [KCl] from 0.10 - 1.00 mol dm^{-3}. Again, as with [KCl] $\leq$ 0.10 mol dm^{-3} the electrolyte effects both the hard sphere micellar size and electrostatic repulsion. The surface potential decreases from 105 mV - 70 mV, which is less of a variation than at [KCl] $\leq$ 0.10 mol dm^{-3}. The absence of any increase in D_{RDV} over this range suggests that micellar growth dominates over electrostatic considerations in determining the particle mobility. It is known that from 0.10 - 1.00 mol dm^{-3} NaCl the micellar aggregation number (N_{agg}) increases from ~ 130 - 180[5], and the fact that linear interaction theory remains valid indicates that radial micellar expansion is occurring. Tominaga et al. also reported behaviour of this sort with C_nTAB (n= 10, 12, 14, 16) and NaBr, this was also characterised as increased micellar aggregation [2].

The third region is the precipitous decrease in D_{RDV} at [KCl] ≥ 1.20 mol dm^{-3}. This can be attributed to large scale structural evolution i.e. sphere - rod transition. This transformation will be confirmed with reference to the interaction parameter (Ch. 4A.2.3.2) and viscosity measurements (Ch. 4B.2.1). The effect is more apparent at 0.1563 mol dm^{-3} CTAC which is not surprising considering the decrease in interparticle separation (l) with increasing surfactant concentration and therefore volume fraction.(ϕ). The interparticle separation can be expressed as a function of ϕ and hydrodynamic radius (R_H^O) from the equation[15]:-

$$l^3 = [8.\pi. / 2^{1/3}].\phi.(R_H^O)^3 \qquad (4A.6)$$

It can be concluded that the addition of electrolyte has three major consequences, firstly reducing electrostatic repulsion, secondly radially expanding micellar aggregates and finally inducing a sphere-rod transition at high concentrations. The results presented are entirely consistent with previously reported data[2,3,4,5,7].

The presented data is analysed by linear interaction theory (Equation 3A.2) to obtain information on micellar size and interaction. It is known that over the chosen surfactant concentration range the micellar shape and aggregation, and hence, size does not change appreciably[13]. It can therefore be assumed that observed changes in D_{RDV} with respect to [CTAC] are purely due to interaction[43].

The c.m.c. term in Equation 3A.2 has little affect on the experimental analysis due to the fact that [CTAC] >> c.m.c. The c.m.c. for CTAC micelle varies from $1.57x10^{-3}$ - $1.33x10^{-5}$ mol dm^{-3} over a concentration range of 0.00 - 1.02 mol dm^{-3} KCl[1]. It is therefore valid for the c.m.c. term to be omitted from the calculation. Plots of D_{RDV} against [CTAC] for 0.00, 0.10, 0.40 and 1.00 mol dm^{-3} KCl are shown in Appendix 4A.xiii.

From 0.00 - 1.00 mol dm^{-3}, the linear interaction theory is observed to apply rigorously with correlation coefficients ≥ 0.9996. As the electrolyte concentration is increased to ≥ 1.20 mol dm^{-3} there is a distinct deviation from linear behaviour corresponding to a decrease in correlation coefficients from 0.9996 - 0.9960 over

[KCl] = 1.20 - 1.60 mol dm^{-3}. The breakdown in linear interaction theory corresponds with the observed precipitous decrease in D_{RDV} and is indicative of a structural transition. It must therefore be noted that the calculated values of k_D and $R_H{}^O$ over this range are purely 'apparent' as linear interaction theory is only strictly applicable to spherical particles.

Calculated values for $D^O{}_{RDV}$, k_D and $R_H{}^O$ are shown in Table 4A.10 and in Appendices 4A.xiv, 4A.xv and 4A.xvi respectively.

Table 4A.10 : Linear extrapolation results

[KCl] / mol dm^{-3}	10^7 $D^O{}_{RDV}$ / cm^2 s^{-1}	k_D / dm^3 mol^{-1}	$R_H{}^O$ / nm
0.00	6.45	2.38	3.32
0.01	7.11	2.46	3.01
0.02	7.42	2.45	2.89
0.05	7.74	2.34	2.77
0.08	7.81	2.26	2.74
0.10	7.83	2.23	2.73
0.20	7.72	2.09	2.77
0.40	7.35	1.93	2.91
0.80	6.65	1.67	3.22
1.00	6.29	1.63	3.40
1.20	5.98	1.73	3.58
1.40	5.73	2.16	3.74
1.60	5.59	3.48	3.83

Note: 0.00 - 1.00 mol dm^{-3}: 'real' values, 1.20 - 1.60 mol dm^{-3}: 'apparent' values

Interpretation of the diffusion coefficient behaviour has been described previously in this chapter, however, the significance of the calculated k_D and $R_H{}^O$ values merits further investigation.

4A.2.3.2 Micellar Interaction

Values for k_D are plotted against [KCl] in Appendix 4A.xv along with the surface potentials (ψ_O) as determined by Johnson et al.[1]. It is important to interpret the interaction parameter relative to the surface potential as it is this property of the

micelle which essentially determines the particle behaviour[7]. It is obvious that for 0.00 mol dm^{-3} KCl the experimental point is slightly anomalous and from the presented curve should be ~2.5 dm^3 mol^{-1}. Over the range 0.00 - 1.00 mol dm^{-3} KCl, k_D decreases in an exponential fashion correlating with the observed drop in surface potential[1]. The reason that the interaction parameter does not tend towards zero is due to the micelles still retaining a degree of surface charge (70 mV)[1]. This has been explained previously as increased electrostatic screening due to neutralisation of the charged micellar headgroups[2,3,4,8,9,39,40,41]. Although an increase in micellar aggregation (N_{agg}) is known to occur over this electrolyte range[5], it will not affect the calculated k_D values. An increase in N_{agg} is likely to occur to the same extent at each surfactant concentration[13] and this will be reflected in the intercept (D^O_{RDV}) rather than the gradient (k_D) from the plot of D_{RDV} vs. [CTAC].

At [KCl] ≥ 1.20 mol dm^{-3}, k_D is seen to rise rapidly with added electrolyte despite the residual surface charge which will exist[1]. This corresponds to the onset of a structural transition from spherical to rod-like micelles. Although k_D over this range is classed as an 'apparent' variable it demonstrates the effect of micellar growth on micellar interaction. The nature of the interaction is likely to be steric (excluded volume) due to elongated micelles as opposed to any electrostatic considerations[44].

The effect of added electrolyte on micellar interaction has been reported previously for different surfactant type[2,3,8,39,40]. Dorshow et al. utilised light scattering to study CTAC micellar diffusion coefficients over a range of NaCl concentrations[3,8]. It was observed that k_D decreased as the electrolyte concentration was increased, eventually passing through zero to yield negative values. This was discussed as being a transition from repulsive Coulombic to attractive van der Waals forces[3,8]. The point at which $k_D = 0$ was attributed to a balancing of attractive and repulsive interactions and was found to occur at [KCl] = 0.50 - 1.00 mol dm^{-3}. The fact that a structural transition has been observed at [KCl] ≥ 1.20 mol dm^{-3} indicates that attractive van der Waals forces are working to a notable extent. However, it is obvious that no such interaction transition has occurred with the k_D values presented here, but it must be recalled that light scattering techniques measure mutual diffusion. The observed contrasts in reported and experimental interaction parameters above 1.00 mol dm^{-3} KCl are likely to be due to the differences in the

modes of diffusion studied i.e. mutual vs. self diffusion as mutual = self diffusion only at the c.m.c. Dickinson reported that at low concentrations Coulombic interactions reduce self diffusion (D_S) but increase mutual diffusion (D_M), whereas when attractive interactions are more evident both D_S and D_M are reduced[45]. It was also reported that the quantitative effects of D_M and D_S were different, which can explain the opposite signs for the k_D values at [KCl] $\geq$ 1.20 mol dm^{-3}.

To further examine the determined interaction parameters it is important to compare k_D to theoretical interaction energies i.e. Coulombic potential {U(r)}. An expression for two identical spherical macro ions is utilised as described by Hayter et al.[46]:-

$$U(r) = \pi.\varepsilon.\varepsilon_O.\sigma^2.\psi_O^2.\ \exp\left[-\kappa\,(r-\sigma)\right] / r, \qquad r > \sigma \qquad (4A.7)$$

where ε is the dielectric constant of the medium (80.37), ε_O is the permittivity of free space, ψ_O is the surface potential, κ is the Debye-Huckel inverse screening length and r is the particle centre-centre distance. σ is the particle diameter and is equivalent to $2.R_H^O$ where R_H^O has been determined previously (Ch. 4A.2.3.1). The centre-centre particle separation can be found from knowledge of ϕ, R_H^O and l.

$$r = 2.R_H^O + l \qquad (4A.8)$$

where l has been defined in Equation 4A.6. Table 4A.11 shows the calculated Coulombic potentials along with the corresponding interaction parameters (k_D) at each electrolyte concentration. There is no U(r) calculable without the presence of electrolyte as $\kappa \rightarrow 0$ i.e. infinite Debye-Huckel screening length.

Table 4A.11 : Variation of Coulombic potential with experimentally determined interaction parameters

[KCl] / mol dm^{-3}	k_D / dm^3 mol^{-1}	k_BT U(r) / J
0.01	2.46	3.170
0.02	2.45	2.020
0.05	2.34	0.900
0.08	2.26	0.520
0.10	2.23	0.370
0.20	2.09	0.116
0.40	1.93	0.018
0.80	1.67	5.42x10-4
1.00	1.63	7.64x10-5
1.20	1.73	8.55x10-6
1.40	2.16	9.55x10-7
1.60	3.48	2.02x10-7

Appendix 4A.xvii shows a plot of U(r) against k_D values corresponding to electrolyte concentrations ≤ 1.00 mol dm^{-3}. It is apparent that the Coulombic potential is directly related to the experimental interaction parameters. This confirms the observation that Coulombic electrostatic interactions are governing the particle mobility over this electrolyte concentration range. At low electrolyte concentrations, as the interaction parameter inclines towards 2.5 dm^3 mol^{-1}, the Coulombic potential can be seen to tend towards infinity and is almost asymptotic in nature. This behaviour emphasises the role of unscreened Coulombic at low electrolyte concentrations which is not surprising considering the extent of micellar surface potential, ~166 mV at 0.00 mol dm^{-3} KCl[1].

As the electrolyte concentration is increased the interaction parameter decreases monotonically as the Coulombic potential approaches zero. This stresses the transition from Coulombic interactions towards screened Coulombic interactions and the associated increase in attractive van der Waals forces. As the [KCl] ≥ 1.20 mol dm^{-3} the Coulombic potential continues towards zero whereas the interaction parameter begins to increase. This is characteristic of an increase in excluded volume interactions due to the growth of elongated micelles[44,47] (i.e. not Coulombic in nature). Excluded volume interactions were shown earlier to be characteristic of

non-ionic Triton X-100 micelles (Ch. 3A.2.2.2) demonstrating their non-electrostatic nature.

4A.2.3.3 Micellar Size

Values for the variation in hydrodynamic radii with electrolyte concentration have been presented in Table 4A.10 and plotted in Appendix 4A.xvi. R_H^O can be observed to decrease sharply to 0.10 mol dm^{-3} KCl prior to a monotonic linear increase up to 1.00 mol dm^{-3} KCl. It was noted earlier that at [KCl] $\geq$ 1.20 mol dm^{-3} there is deviation from linear interaction theory (Ch. 4A.2.3.1). Although 'apparent' values for k_D have been obtained it was explained that the structural transition would manifest itself in the intercept of D_{RDV} vs. [CTAC] rather than the gradient (Ch. 4A.2.3.2). For this reason the R_H^O values at [KCl] $\geq$ 1.20 mol dm^{-3} are neglected for further analysis.

In the study of cationic micellar systems it is commonly assumed that the hydrodynamic radius remains constant with changes in electrolyte concentration when there is no significant micellar growth. Dorshow et al. used light scattering to determine the mutual diffusion coefficients (D_M) of CTAC micelles and observed that plots of D_M vs. [CTAC] collapsed to a single point[3,8]. This in effect yielded constant hydrodynamic radii over a concentration range of 0.02 - 1.00 mol dm^{-3} NaCl[3,8]. Recently electrochemical techniques have been used to determine R_H^O values, although most of these studies were at a single electrolyte concentration[15,37]. Tominaga et al., however, measured hydrodynamic radii of C_nTAB (n = 14, 16) micelles over a range of NaBr concentrations[2]. An observed drop and subsequent increase in R_H^O was reported and attributed to a balance of electrostatic repulsive forces and micellar aggregation[2]. These results tend to support the experimentally determined trend in hydrodynamic radii seen here.

It is important to distinguish between the micellar hard sphere radius (R_{HS}) and the hydrodynamic radius (R_H^O). R_{HS} depends purely on the physical structure of

a micelle i.e. carbon chain length and aggregation number amongst other parameters[2,7]. As well as the micellar structure, R_H^O encompasses substances in the surrounding aqueous environment[48]. Rohde et al. noted that if the stern layer is subtracted from R_H^O the resulting radius can yield information on the aggregation number[41]. It follows that knowledge of R_{HS} and R_H^O can lead to the determination of the shear plane distance (λ). The shear plane thickness essentially consists of a bound layer of ions and solvent which move along with the micelle as a single entity[48,49] and is an important characteristic in colloidal systems[48,49,50,51,52]. An investigation into λ is not only stimulated by the lack of existing data on shear thickness in micellar systems but also the lack of any quantitative association between the shear plane and double layer thickness[48].

The hard sphere radii of CTAC micelles are essentially the template to which R_H^O can be compared and are calculated from structural parameters reported in the literature. Hayter et al. have expressed the hard sphere micellar volume as a function of a number of parameters[7]:-

$$V_M = N_{agg} [V_{CH3} + nV_{CH2} + V_{HG} + \omega_{HG}V_S + (1-\delta) (V_{CI} + V_S)] \qquad (4A.9)$$

where V_M is the micellar volume ($4/3.\pi.R_{HS}^3$), n is the number of CH_2 groups in the chain (=15), V_{CH3} (0.0543 nm^3) and V_{CH2} (0.0248 nm^3) are the volumes of these groups, V_{HG} in the volume of the headgroup (0.1023 nm^3), V_S is the volume of water (0.0299 nm^3), V_{CI} is the volume of the counter ion (0.0289 nm^3) and ω is the degree of hydration (HG = 1, CI = 4)[7]. Values for the aggregation number (N_{agg}) and degree of disassociation (δ) have been obtained from reported literature[1,5] and are shown in Table 4A.12 as a function of electrolyte concentration.

Table 4A.12 : Variation of CTAC aggregation number and degree of counterion disassociation with electrolyte concentration

[KCl] / mol dm^{-3}	N_{agg} / no units	δ / no units
0.00	131	0.40
0.01	132	0.50
0.02	133	0.54
0.05	136	0.58
0.08	139	0.59
0.10	140	0.59
0.20	148	0.61
0.40	160	0.62
0.80	175	0.64

Note: N_{agg} values reproduced from Malliaris et al.[5], δ reproduced from Johnson et al.[1].

It is therefore apparent that the micellar hard sphere radius (R_{HS}) can be determined at each electrolyte concentration. These values are shown in Table 4A.13 along with the corresponding hydrodynamic radii (R_H^O) and the resultant difference ($\lambda = R_H^O - R_{HS}$).

Table 4A.13 : Variation of micellar hard sphere and hydrodynamic radius with electrolyte concentration

[KCl] / mol dm^{-3}	R_H^O / nm	R_{HS} / nm	λ / nm	$R_{HS} + \kappa^{-1}$ / nm
0.00	3.32	2.73	0.59	-
0.01	3.01	2.71	0.30	5.75
0.02	2.89	2.71	0.18	4.86
0.05	2.77	2.72	0.05	4.08
0.08	2.74	2.74	0.00	3.82
0.10	2.73	2.75	-0.02	3.71
0.20	2.77	2.79	-0.02	3.47
0.40	2.91	2.86	-0.05	3.34
0.80	3.22	2.95	-0.27	3.29

Also shown in Table 4A.13 is the parameter $R_{HS} + \kappa^{-1}$ where κ^{-1} is the Debye-Huckel screening length. This will be used in later analysis to characterise the nature of the

initial drop in hydrodynamic radius. Appendix 4A.xviii shows the variation of R_H^O, R_{HS} and $R_{HS} + \kappa^{-1}$ with [KCl].

With the difference, $\lambda = R_H^O - R_{HS}$, being equivalent to the shear plane thickness[41] a number of analogies to colloidal systems can be made. There are many reported studies showing a decrease in hydrodynamic radii of functionalised polystyrene latex spheres with added electrolyte[48,53,54,55]. There are two major theories that are used to describe this behaviour, the hairy[55,56,57,58] and double layer models[48,49,50,60,61]. The hairy layer model predicts decreased repulsion between functionalised 'hairs' as electrolyte is added leading to a shrinkage in the radius[56]. This model is not applicable to the study of micellar systems due to the smoothness of trimethylammonium aggregate surfaces[62]. It is the double layer model which provides the best insight to the mechanism of the hydrodynamic radius fluctuation. As the electrolyte concentration is increased it is well known that the double layer on a charged surface will be compressed[48,49,50,60,61]. It has been noted for polystyrene latex spheres that double layer compression has the consequence of reducing the shear plane thickness i.e. the shear or slipping plane collapses towards the particle surface[48,51,60,61]. It is predicted that the double layer and shear plane are intimately related though the exact relationship is not known[48].

There are a number of important factors that are as yet unresolved, namely, the position of the shear plane, its relationship to the double layer thickness and the associated shear plane potential. Knowledge of the shear plane and double layer thickness along with the micellar surface potential allows these issues to be addressed here.

In Appendix 4A.xviii, it can be seen that a decrease in $R_{HS} + \kappa^{-1}$ is mirrored by a decrease in R_H^O. It is therefore possible to elucidate the relationship between the double layer (κ^{-1}) and shear plane thickness (λ). The double layer thickness is expressed by the well known Debye-Huckel equation[63]:-

$$\kappa^{-1} = [(\varepsilon_O.\varepsilon_R.k_BT) / (e^2.\Sigma_i\, n_i.Z_i^2)]^{1/2} \qquad (4A.10)$$

where $\Sigma_i n_i.Z_i^2$ is equivalent to the electrolyte concentration.

In Appendix 4A.xix, a graph of the change in R_H^O against the change in κ^{-1} is plotted over the range of initial radius decrease. It is evident that from 0.02 - 0.10 mol dm^{-3} a linear relationship exists with a correlation coefficient ≈ 0.999 resulting in the relationship:-

$$\Delta\kappa^{-1} = 0.032 + 5.86.\Delta R_H^O \qquad (4A.11)$$

This confirms the hypothesis that the micellar double layer is larger than the shear plane thickness and responsible for its compression[48]. It must be noted that at ≤ 0.01 mol dm^{-3} there is a deviation from linear behaviour but this is likely to be due to the diffuse nature of the double layer at low electrolyte concentrations ($\kappa^{-1} \rightarrow \infty$).

The Eversole-Boardman equation allows the potential profile as a function of distance from a charged surface to be determined[61,64]:-

$$\ln \tanh (Z.e.\psi_t / 4k_BT) = \ln \tanh (Z.e.\psi_O / 4k_BT) - \kappa t \qquad (4A.12)$$

where ψ_O is the surface potential, Z is the valency of the counterion (=1), κ is the inverse Debye length (= $1/k^{-1}$) and ψ_t is the potential at some distance t. The potential profiles can be simulated as the surface potentials at a range of [KCl] are known[1], these can be seen in Appendix 4A.xx. The shear plane distance (λ) variation with electrolyte concentration has been calculated and presented in Table 4A.13. It is therefore apparent that the shear plane potential (ξ) can be determined i.e. $\psi_t = \xi$ when $t = \lambda$. It is apparent from Appendix 4A.xx that the ξ potentials are independent of electrolyte concentration at 112 mV until the hard sphere radius is reached (R_H^O - R_{HS} = 0). This result is in excellent agreement with values of 100 - 140 mV as determined by a solvatochromic acid-base indicator technique for CTAC micelles[1]. To my knowledge, this is the first reported measurement of the shear plane distance and associated potential in a supramolecular self-assembled system. The results form not only a quantitative model for micellar systems but also a phenomenological basis

for modelling charged particles in solution. Knowledge of the ξ potential enhances the fundamental understanding of properties such as electrokinetic mobility[49,50,56] and frictional forces[65] as well as aiding electrophoretic fingerprinting techniques[58,66]. It also offers applications for the study of membrane mimetics and associated properties[63].

The results presented in this section allows the medium surrounding a micellar aggregate to be elucidated in terms of the shear plane and Debye screening length. A representation of this environment is shown in Figure 4A.2.

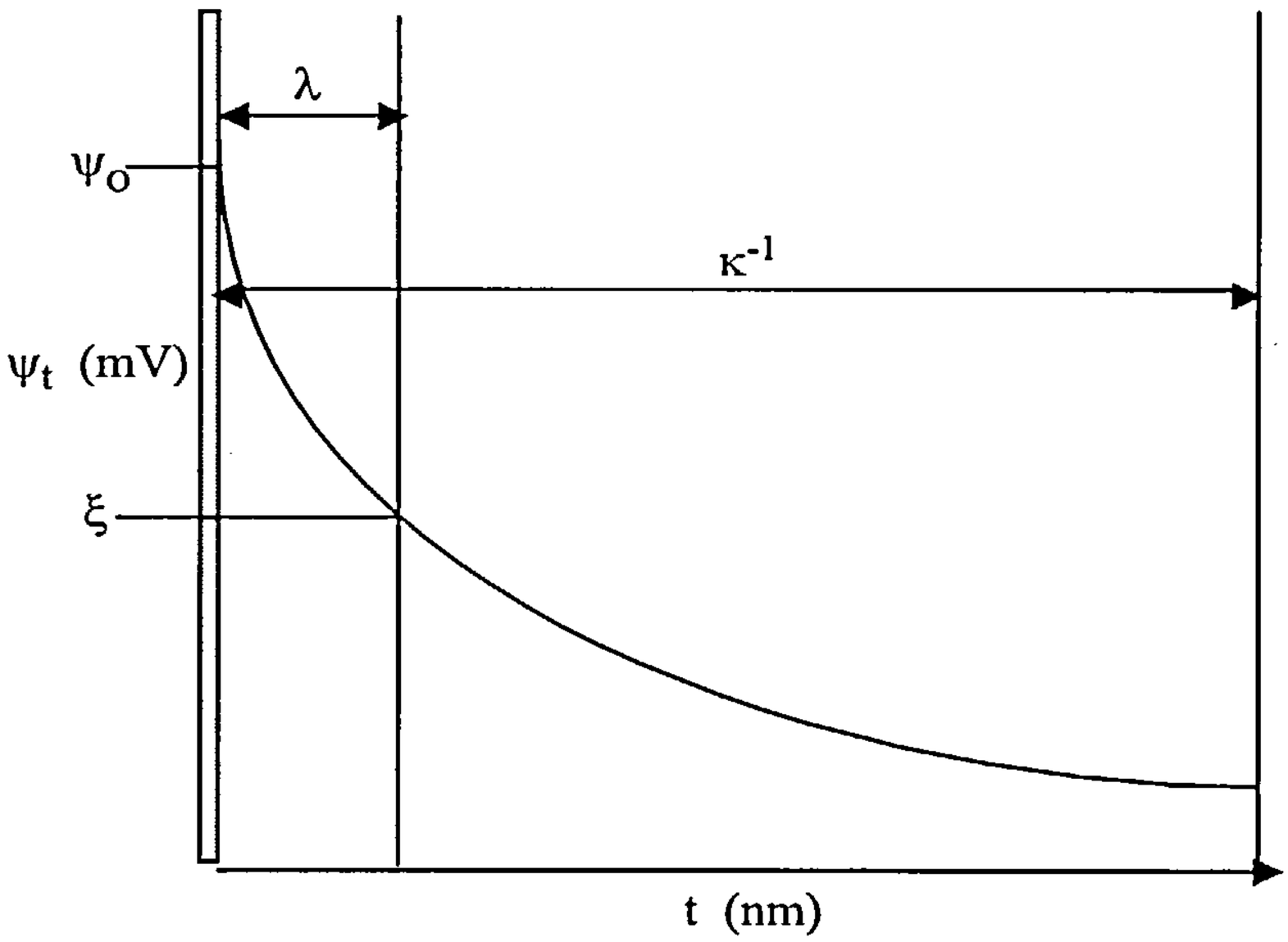

Figure 4A.2 : Representation of shear plane - screening length relationship and associated potential profile

4A.2.4 Effect of Temperature

It was shown that the self diffusion of a non-ionic micellar system could be significantly modified by the combined affect of temperature and electrolyte (Ch. 3A.2.3). For Triton X-100 it was observed that micellar growth, size and shape were a function of electrolyte and temperature induced dehydration. The size and shape of cationic micelles, however, are known to be less sensitive to temperature changes.

The aggregation number (N_{agg}) of CTAC micelles have been observed, by fluorescence quenching, to decrease with increasing temperature[5,6,10,12,14]. As opposed to Triton X-100 where large scale growth was observed (Ch. 3A.2.3), N_{agg} values for CTAC were seen to vary from ~112 - 85 over 25 - 50 ^{O}C[10,14]. This decrease in N_{agg} is mirrored by a linear drop in hydrodynamic radius from ~ 2.9 - 2.6 nm[3,8]. For Triton X-100, Arrhenius behaviour was observed and interpreted as changes in micellar structure, however, the absence of any large scale changes in micellar growth patterns for CTAC allows a greater emphasis towards intermicellar interactions. Therefore, for CTAC micelles, Arrhenius behaviour can be used to highlight interactions rather than structure and results correlated with previously determined k_D values (Ch. 4A.2.3.1).

The CTAC micellar diffusion coefficients were measured at temperatures of 15, 25, 30, 35 and 40 ^{O}C in addition to those at 20 ^{O}C presented earlier (Ch. 4A.2.3) Electrolyte concentrations were chosen that corresponded to different types of behaviour in the D_{RDV} vs. [KCl] plot (Appendix 4A.xii). At 0.00 mol dm^{-3} no micellar surface potential had occurred, 0.02 mol dm^{-3}: electrostatic drag was reduced, 0.10 mol dm^{-3}: shear plane thickness was essentially zero, 0.80 mol dm^{-3}: prior to precipitous micellar growth. All solutions had [CTAC] = 0.0938 mol dm^{-3}. The diffusion coefficient results are shown in Table 4A.14 and plotted as a function of temperature in Appendix 4A.xxi.

Table 4A.14 : Diffusion coefficient variation with temperature and electrolyte concentration ([CTAC] = 0.0938 mol dm^{-3})

T / ^{O}C	10^7 D_{RDV} / cm^2 s^{-1}; with [KCl] / mol dm^{-3}			
	0.00	0.02	0.10	0.80
15	4.67	4.98	5.61	5.14
20	5.01	5.87	6.24	5.58
25	6.23	6.69	7.28	6.57
30	7.14	7.80	8.41	7.48
35	7.94	8.38	9.09	7.67
40	8.80	9.10	10.18	8.48

Note: standard error = ± 0.09x10^{-7} cm^2 s^{-1}; experiments repeated twice.

In Appendix 4A.xxi, the dashed lines show that the D_{RDV} data retains the same behaviour at each of the temperatures studied. The shape of this rational function curve has been explained previously in terms of a balance between the reduction of electrostatic repulsion and increase in micellar aggregation number (Ch. 4A.2.3.1). As the diffusion coefficients are dependent on temperature changes to the same extent, it is possible to analyse the results with an Arrhenius plot. For a true Arrhenius relationship a plot of ln D_{RDV} against 1/T will yield a gradient from which the diffusional activation energy can be determined (E_{AD}). This procedure has been carried out previously for Triton X-100 in Ch. 3A.2.3.3. The relevant data is shown in Table 4A.15 and plotted in Appendix 4A.xxii.

Table 4A.15: Arrhenius data for temperature dependent diffusion coefficient

10^3 1/T / K^{-1}	ln D_{RDV} variation at different [KCl]			
	0.00 mol dm^{-3}	0.02 mol dm^{-3}	0.10 mol dm^{-3}	0.80 mol dm^{-3}
3.195	-13.940	-13.910	-13.798	-13.980
3.247	-14.046	-13.880	-13.911	-14.081
3.300	-14.152	-14.064	-13.989	-14.106
3.356	-14.289	-14.217	-14.253	-14.236
3.413	-14.507	-14.348	-14.287	-14.399
3.472	-14.577	-14.513	-14.395	-14.480
E_{AD} / kJ mol^{-1}	20.19	19.66	18.27	15.41
ln A	-6.17	-6.28	-6.77	-8.04

Note: correlation coefficients ≈ 0.99 were obtained from the Arrhenius plots.

The magnitude of the activation energies are in excellent agreement with $E_A = 20 \pm 4$ KJ mol^{-1} for the quenching reaction of 1-methylpyrene by n-methyl-N-decylaniline in CTAC micelles[14].

It can be seen that E_{AD} decreases as the concentration of electrolyte increases which can be interpreted as a reduction in frictional forces as the double layer collapses i.e. electrostatic drag reduction[2,3,4,9,12,39,40,41,42]. This demonstrates that micellar diffusion, activation energy, and interaction are intrinsically related and it is therefore prudent to compare the activation energies to the previously determined interaction parameters (Ch. 4A.2.3.1).

Table 4A.16: Comparison of diffusional activation energies and intermicellar Interaction Parameters

[KCl] / mol dm^{-3}	k_D / dm^3 mol^{-1}	E_{AD} / kJ mol^{-1}
0.00	2.50	20.19
0.02	2.45	19.66
0.10	2.23	18.27
0.80	1.67	15.41

A graph of E_{AD} against k_D (Appendix 4A.xxiii) yields a linear plot with a correlation coefficient of 0.997. This shows that activation energy and micellar interaction are intimately related i.e. as electrostatic repulsion between micelles is reduced the associated energy required for a micelle to pass from one solution domain to another is subsequently reduced.

4A.3 Summary

Rotating disk voltammetry has been used to accurately and precisely determine CTAC micellar diffusion coefficients over a range of electrolyte and surfactant concentrations. The diffusion coefficient (D_{RDV}) with respect to KCl concentration showed three regions of behaviour; 0.00 - 0.10 mol dm^{-3}: sharp increase in D_{RDV} due to reduction of electrostatic drag; 0.10 - 1.00 mol dm^{-3}: linear decrease in D_{RDV} due to increased micellar aggregation; ≥ 1.20 mol dm^{-3} severe decrease in D_{RDV} due to the onset of a structural transition. At 0.00 - 0.10 mol dm^{-3} KCl the addition of electrolyte caused the partial neutralisation of the charged micellar surface (166 mV - 105 mV), effectively screening micellar Coulombic repulsion. From 0.10 - 1.00 mol dm^{-3} KCl, the Coulombic forces continued to be screened, but, the governing factor over this electrolyte range was increased micellar aggregation. The linear decrease in D_{RDV} suggested that the micelles expand in a radial fashion with the retention of the spherical shape. At [KCl] ≥ 1.20 mol dm^{-3}, Coulombic forces were negligible with attractive van der Waals forces driving micellar growth as a result of reduced surface potential (<70 mV). The diffusion coefficient data was analysed

using linear interaction theory which strictly applies at [KCl] ≤ 1.0 mol dm^{-3}. Values for the interaction parameter (k_D) and hydrodynamic radius (R_H^O) were obtained.

The interaction parameter (k_D) exhibited an exponential type decay with increasing electrolyte concentration up to [KCl] ≤ 1.00 mol dm^{-3}. This was due to the progressive screening of Coulombic forces via the neutralisation of surface potential. At [KCl] ≥ 1.20 mol dm^{-3}, linear interaction did not strictly apply, but for illustrative purposes, still yielded 'apparent' k_D values. The k_D values showed a steep increase that coincided with micellar growth, suggesting that the nature of micellar interactions had become steric or excluded volume in nature. Overall, the interaction parameter showed that transition from Coulombic repulsion via van der Waals attraction to excluded volume interactions.

The hydrodynamic radius (R_H^O) showed a severe fluctuation with increasing electrolyte concentration. R_H^O decreased sharply from 0.00 - 0.10 mol dm^{-3} and was followed by an approximately linear increase to [KCl] ≤ 1.00 mol dm^{-3}. The initial increase was described in terms of compression of the micellar double layer and the increase by increased micellar aggregation. A graph of the change in R_H^O (ΔR_H^O) against the change in Debye screening length ($\Delta\kappa^{-1}$) yielded a linear plot. This indicated that the drop in R_H^O is attributable to collapse of the micellar double layer. The use of literature values for the counterion disassociation and aggregation number as well as other CTAC structural parameters allowed the determination of the hard sphere radius (R_{HS}). The observed difference between R_H^O and R_{HS} was found to be a function of the shear plane thickness (λ). It followed that the shear plane thickness appeared to collapse towards the micellar surface until at 0.08 mol dm^{-3} KCl, $R_H^O - R_{HS} = \lambda = 0$ nm. This finding coupled with that of the linear R_H^O vs. $\Delta\kappa^{-1}$ correlation suggested that the micellar double layer collapse and the shear plane contraction were intimately related.

The use of the Eversole-Boardman equation allowed the simulation of the potential profile from the micellar surface. With the shear plane thickness already

calculated, the shear plane potential (ξ) was determined. ξ was found to be independent of electrolyte concentration at a constant value of 112 mV.
The determination of the shear plane thickness and associated potential has not, to my knowledge, been previously reported for a nano-scale supramolecular system.

The micellar diffusion coefficients were measured over range of temperatures (15 - 40 ^{O}C) and the D_{RDV} vs. [KCl] plot exhibit the same behavioural pattern at each temperature i.e. rational fitted function. Arrhenius analysis of the presented data allowed the determination of the diffusional activation energy (E_{AD}) and was seen to decrease as the electrolyte concentration increased. E_{AD} exhibited a linear dependence on the interaction parameter (k_D) which indicated that the energy needed for a micelle to pass its nearest neighbours is a direct function of intermicellar interactions.

Appendix 4A.i : Background capacitance of glassy carbon electrode (0.1563 mol dm^{-3} CTAC + 0.1 mol dm^{-3} KCl)

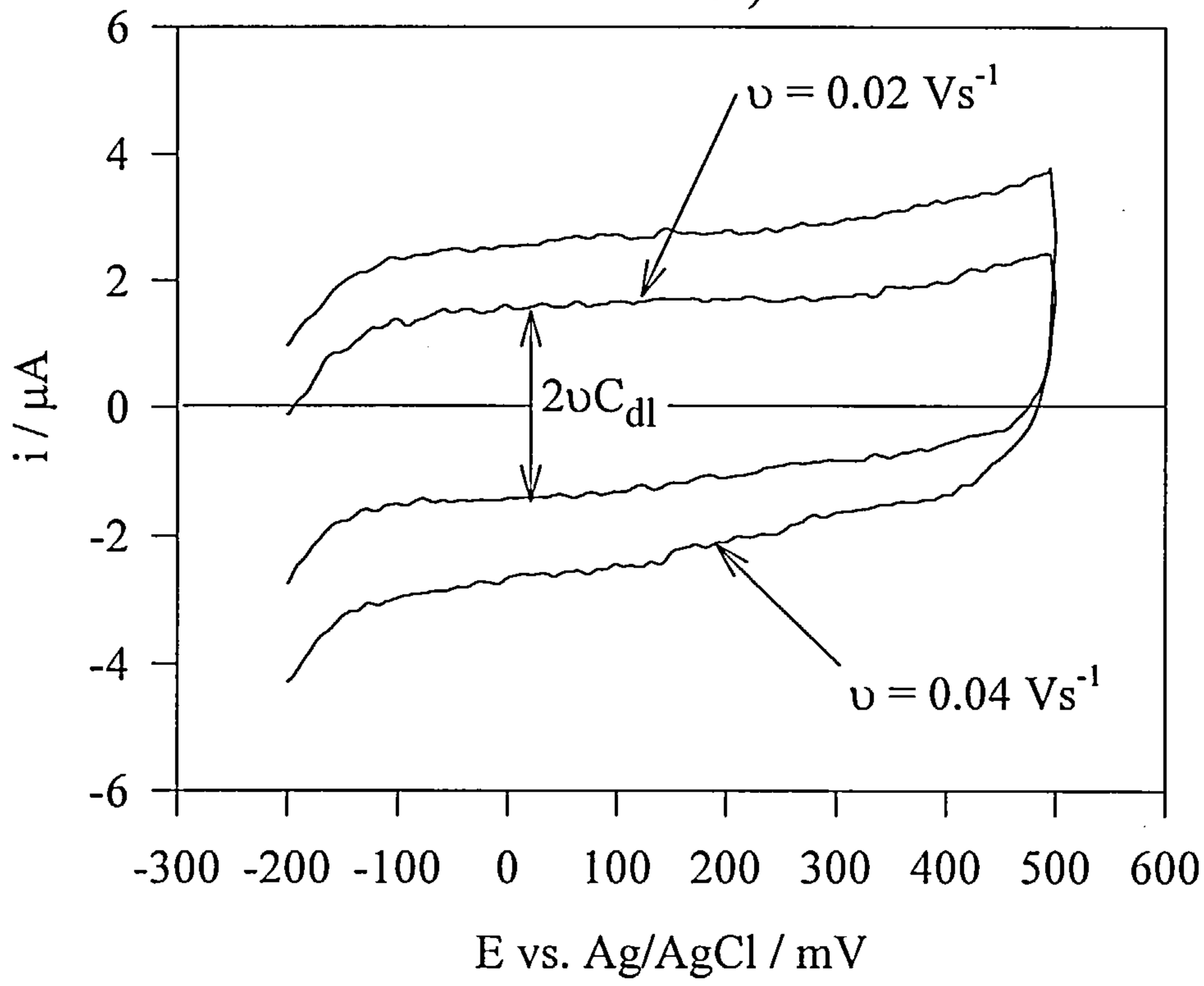

Appendix 4A.ii : Variation of background capacitance current with sweep rate (0.1563 mol dm^{-3} CTAC)

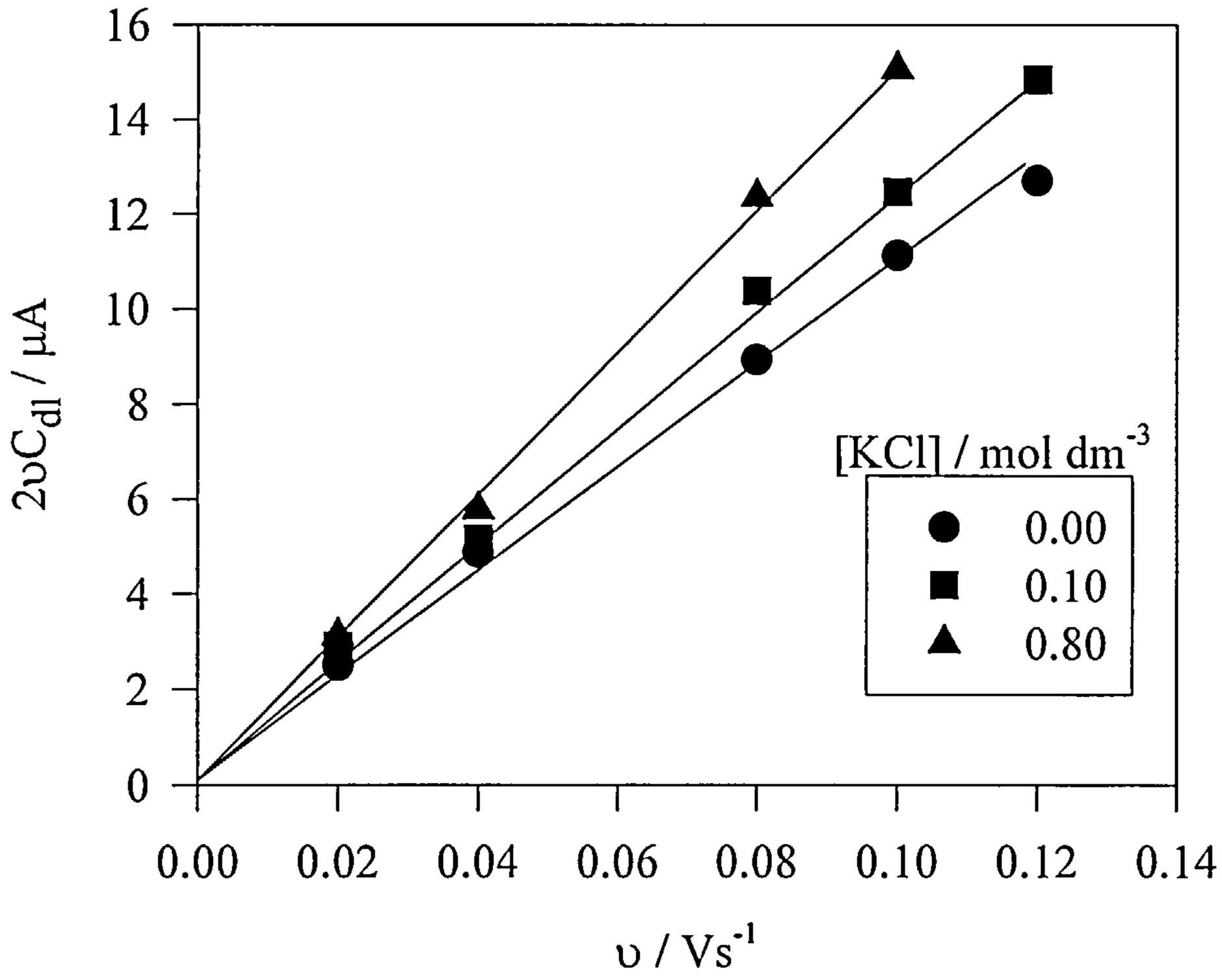

Appendix 4A.iii : Variation of diffusion coefficient (D_{RDV}) with ferrocene concentration

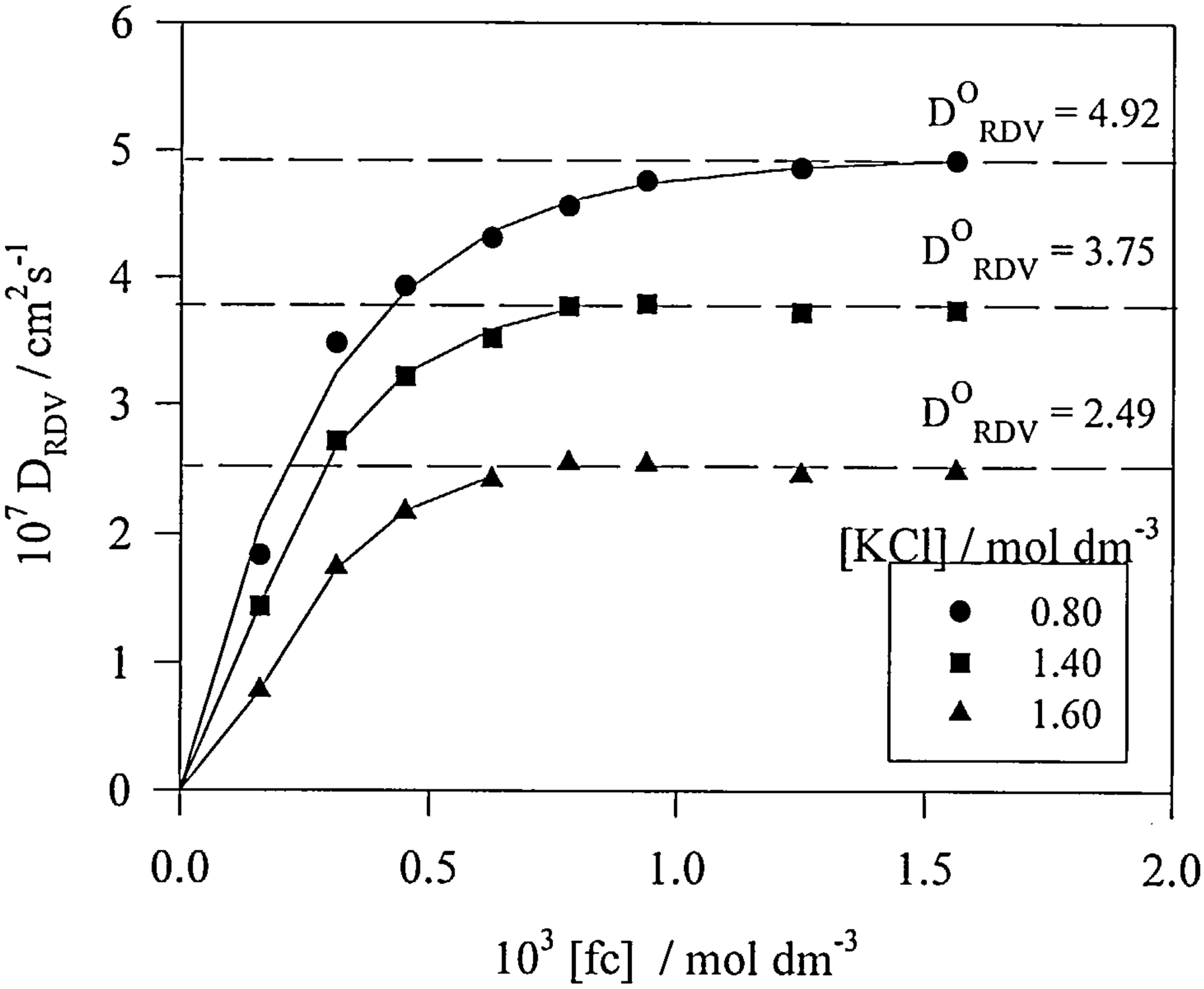

Appendix 4A.iv : Effect of ferrocene concentration on Nernstian plots (0.1563 mol dm^{-3} CTAC + 0.80 mol dm^{-3} KCl)

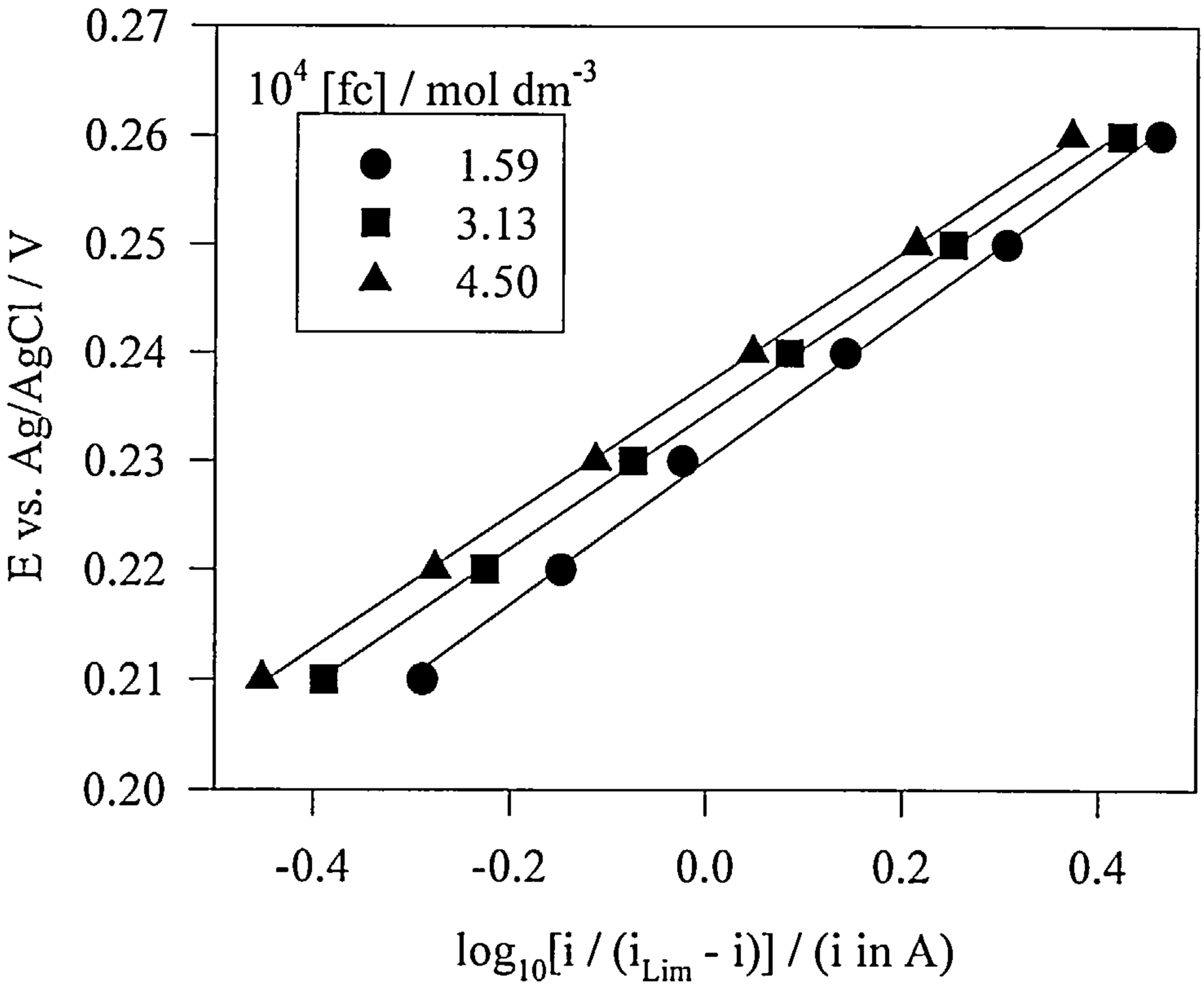

Appendix 4A.v : Variation of half wave potential with ferrocene concentration (in 0.1563 mol dm^{-3} CTAC).

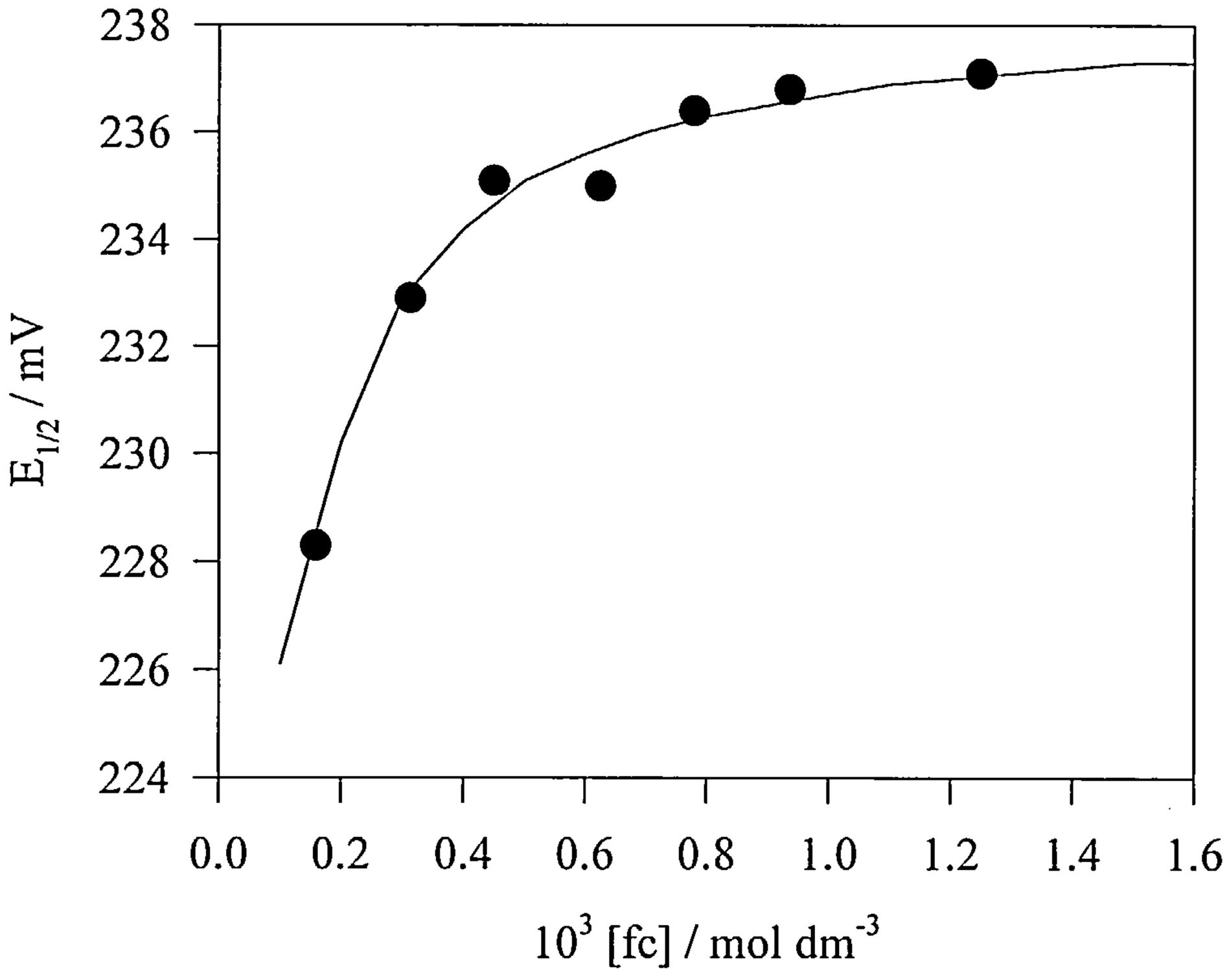

Appendix 4A.vi : Variation of Nernstian slope with ferrocene concentration (in 0.1563 mol dm^{-3} CTAC)

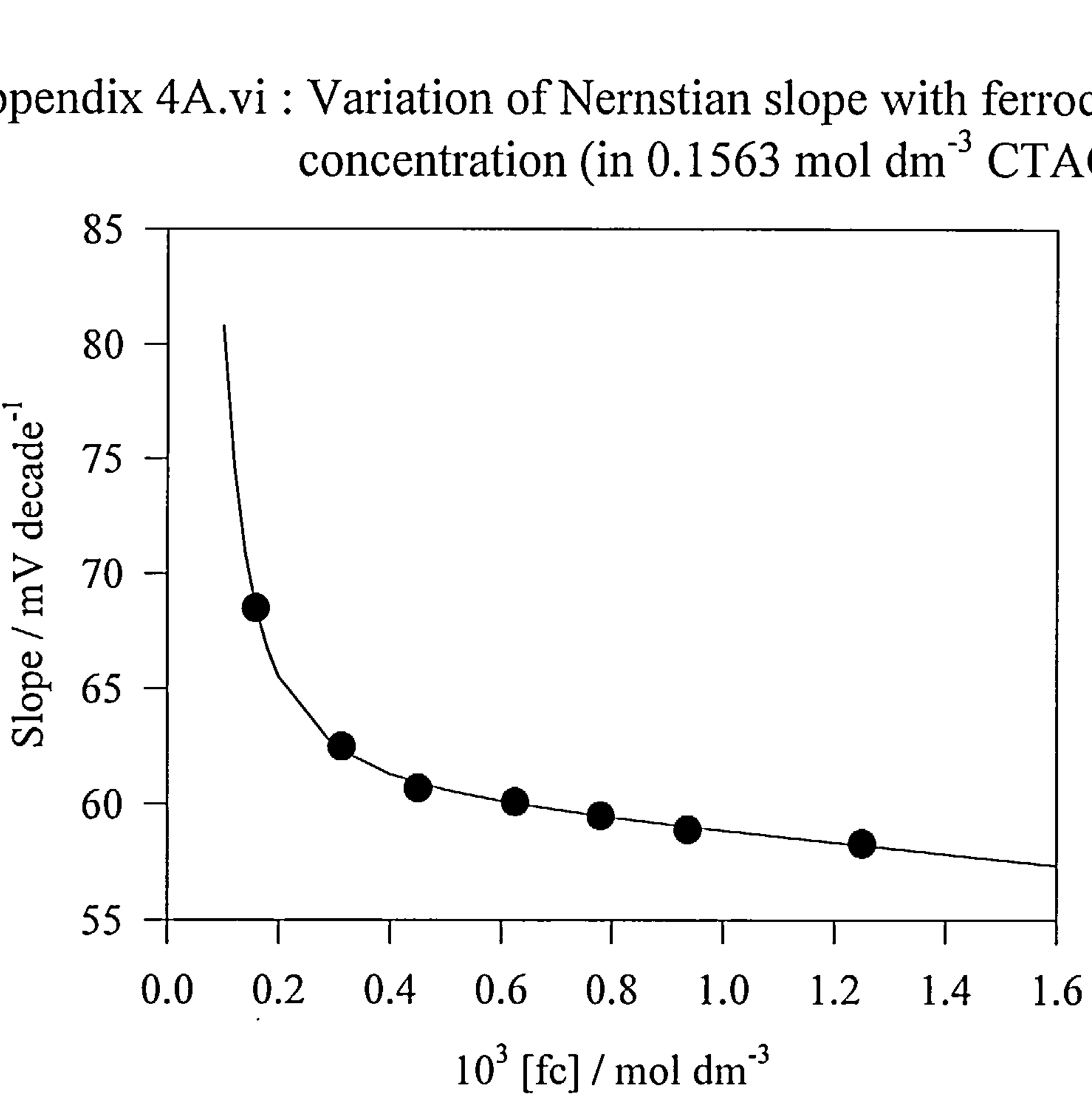

Appendix 4A.vii : UV / Vis spectra of ferrocene / ferricinium in 0.1563 mol dm^{-3} CTAC before and after bulk solution electrolysis

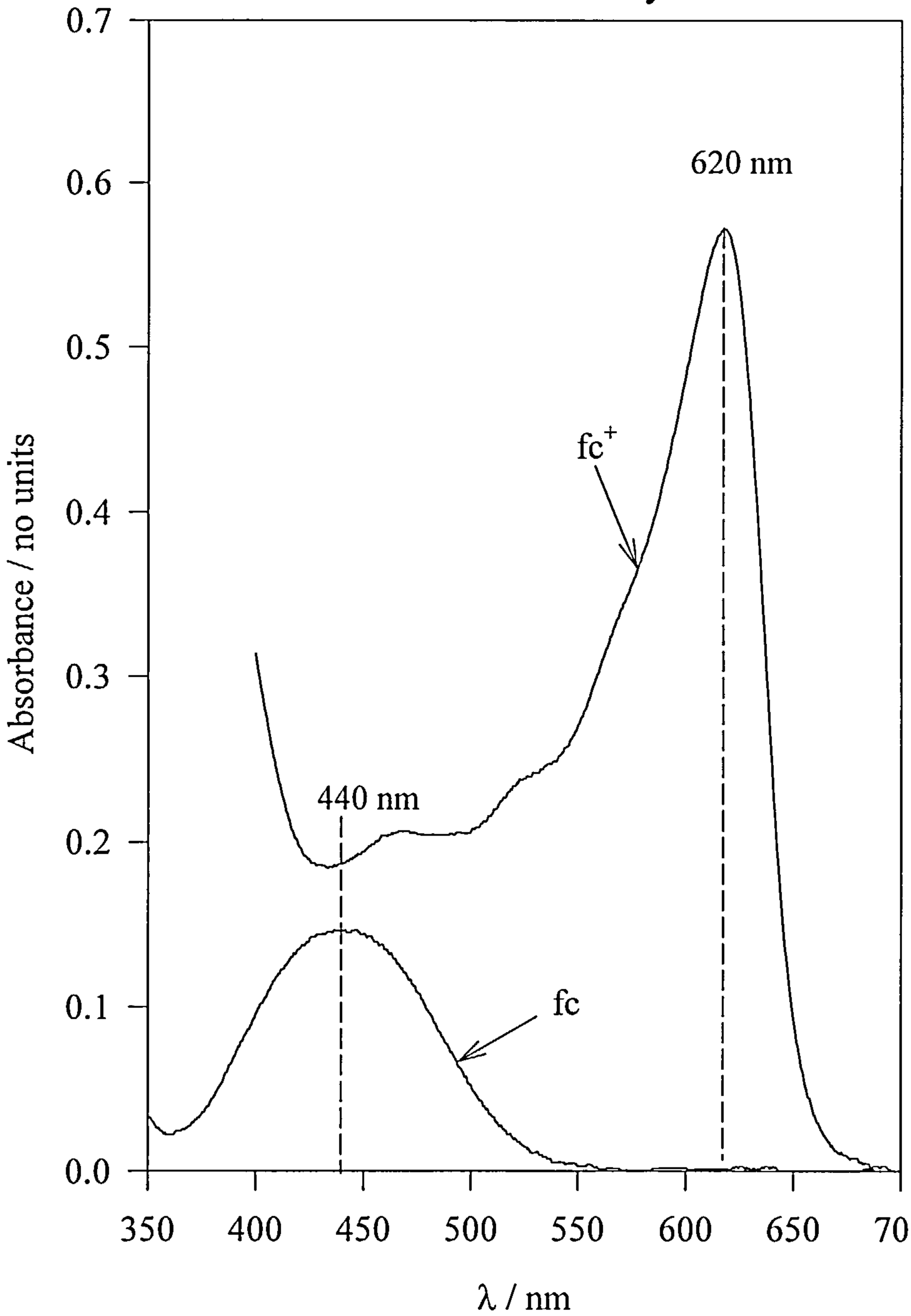

Appendix 4A.viii : RDV sigmoidal traces before and after electrolysis of 1.563×10^{-3} mol dm^{-3} ferrocene in 0.1563 mol dm^{-3} CTAC

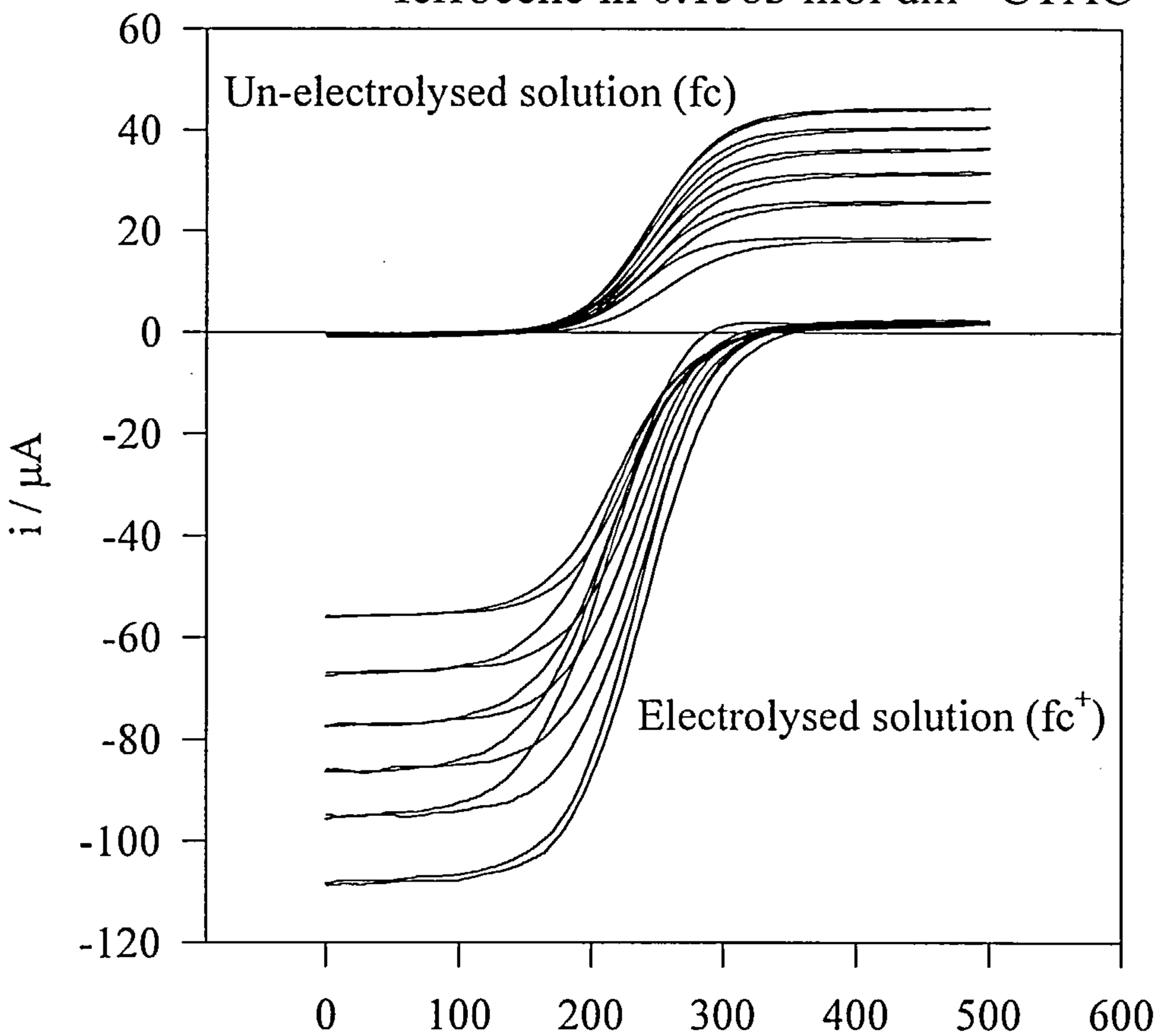

Appendix 4A.ix : Variation of i_{Lim} with $\omega^{1/2}$ before and after electrolysis of the solution

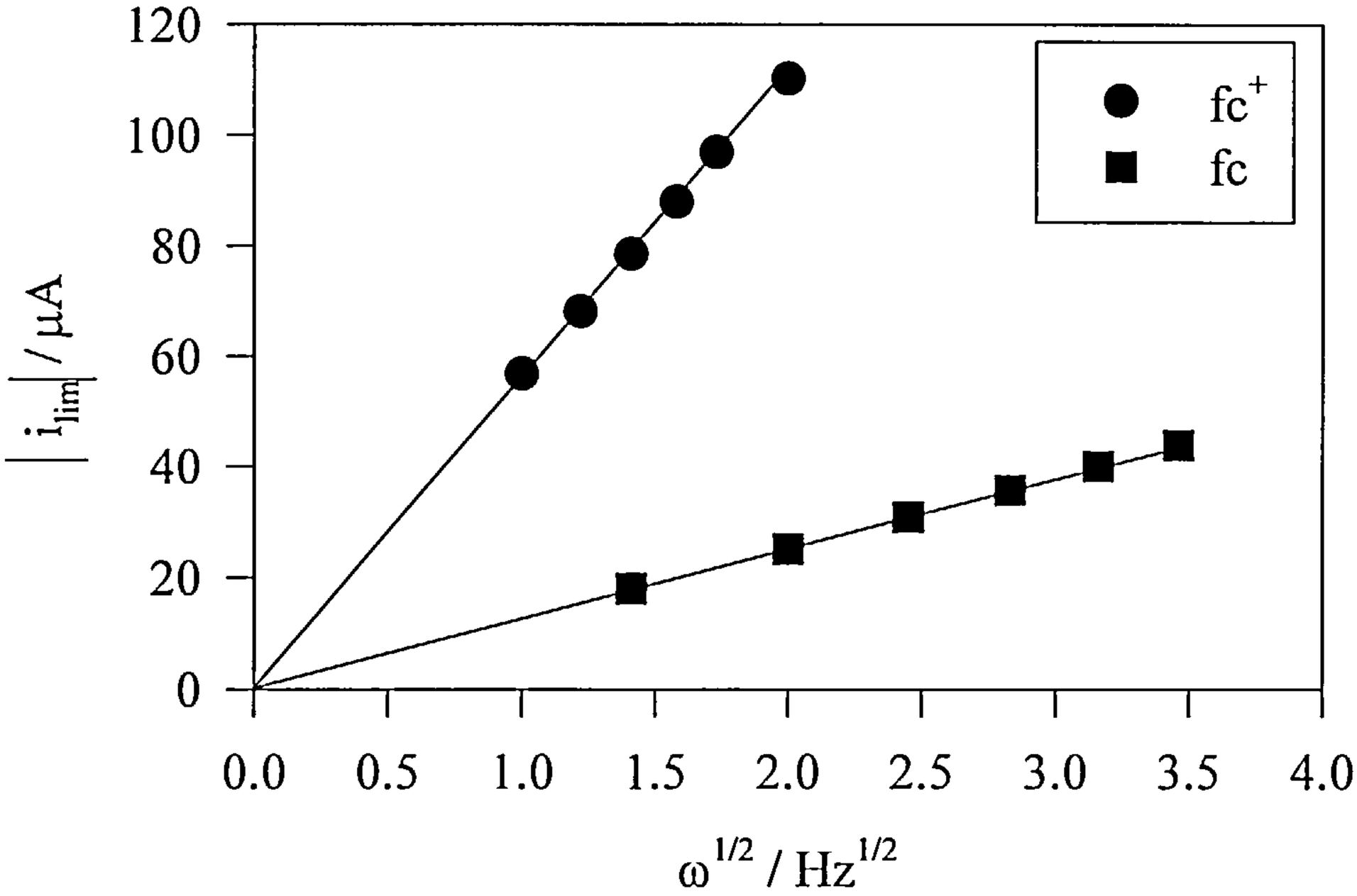

Appendix 4A.x : Typical RDV voltammograms

0.1563 mol dm^{-3} CTAC + 0.10 mol dm^{-3} KCl

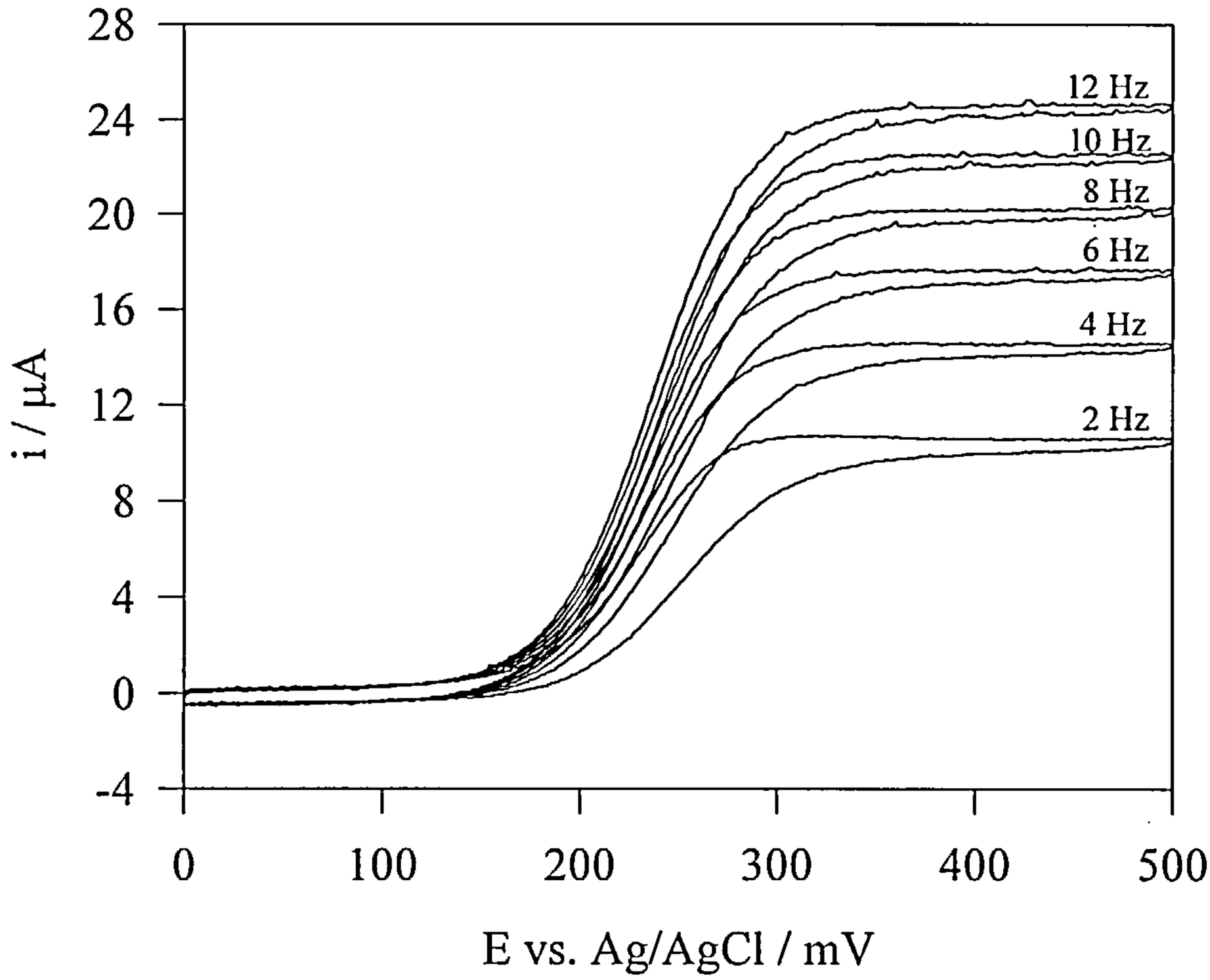

Appendix 4A.xi : Examples of Levich plots (i_{Lim} vs $\omega^{1/2}$)

CTAC + 0.10 mol dm^{-3} KCl

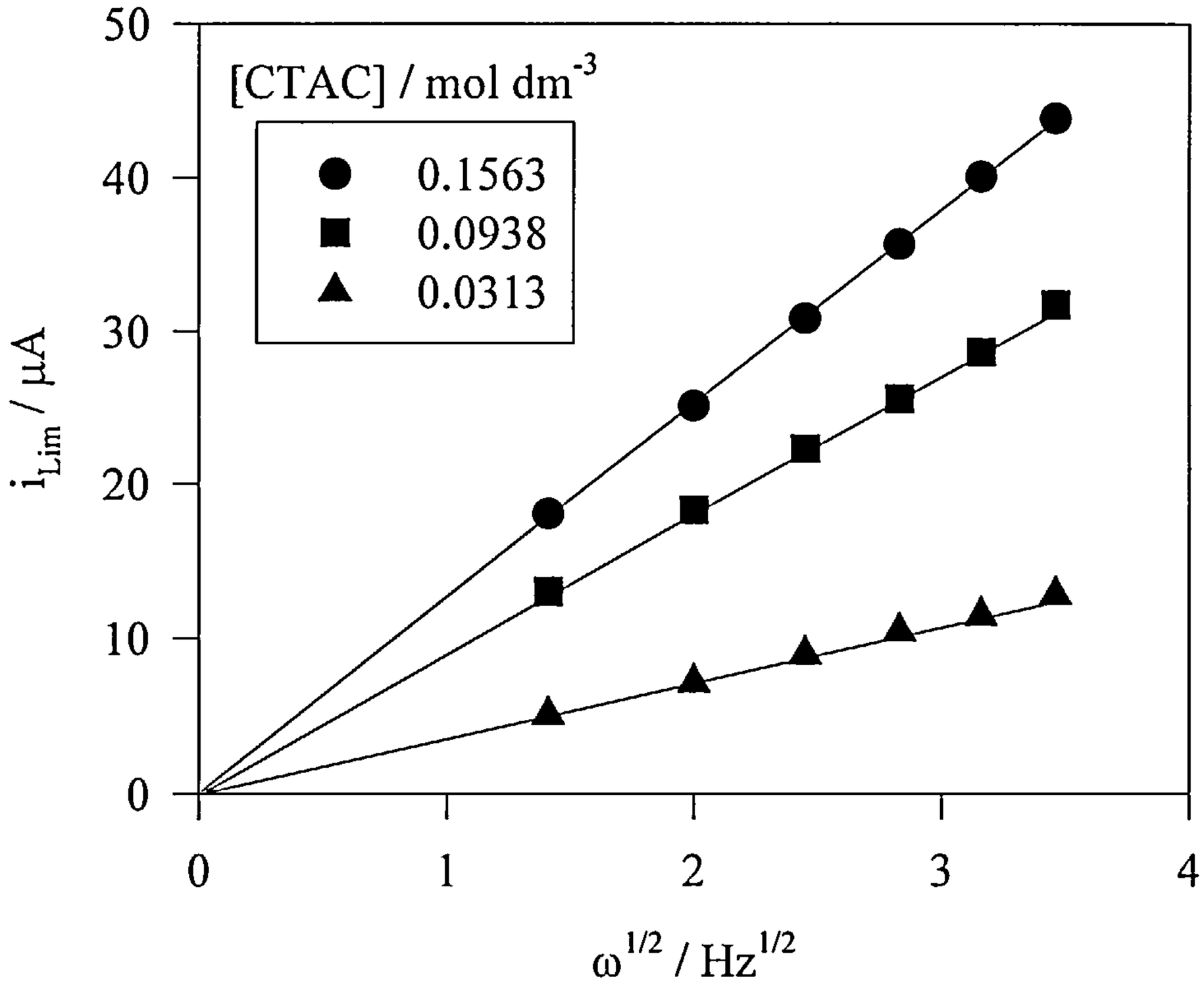

Appendix 4A.xii : Diffusion coefficient variation with [KCl]

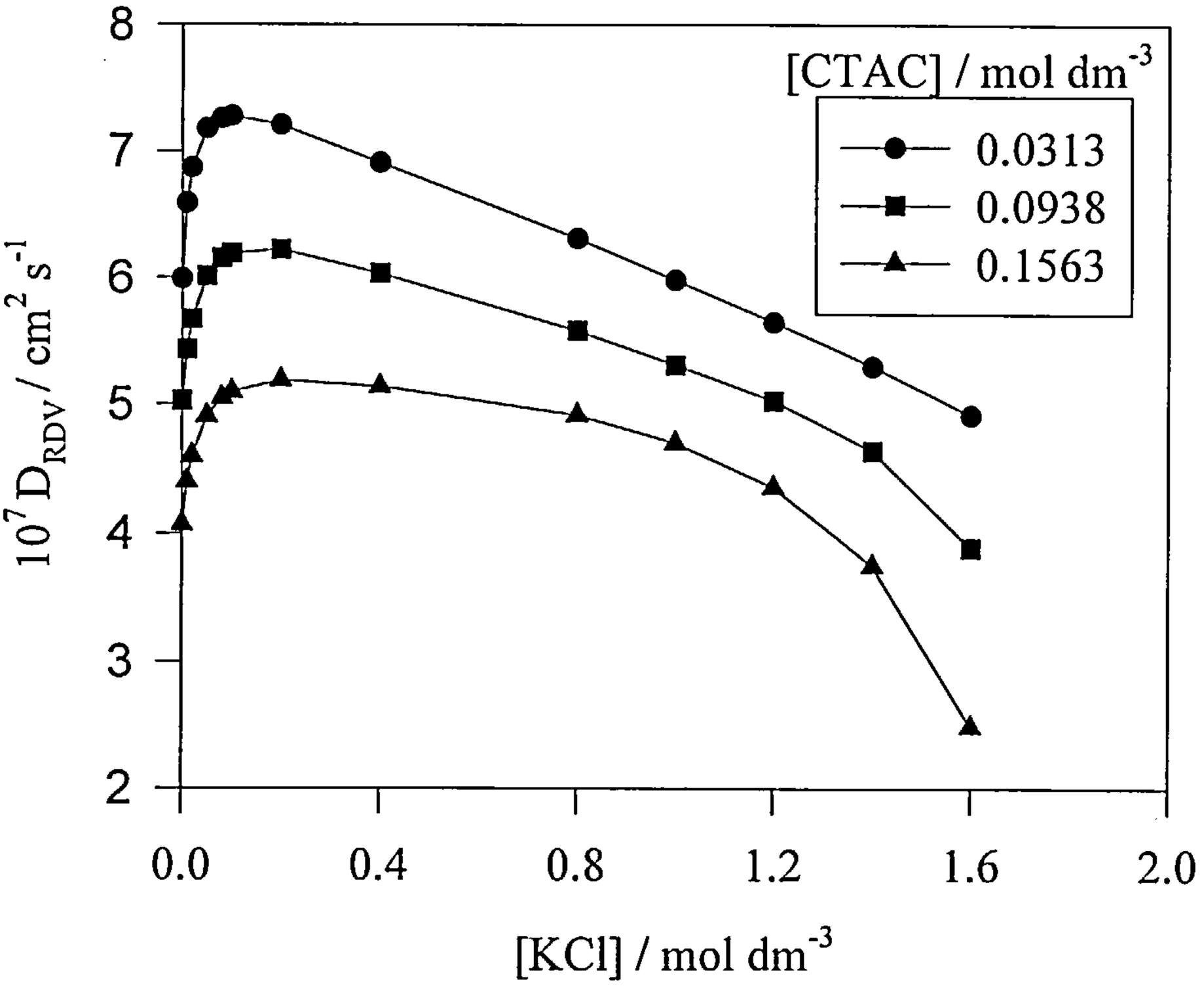

Appendix 4A.xiii : Diffusion coefficient variation with [CTAC]

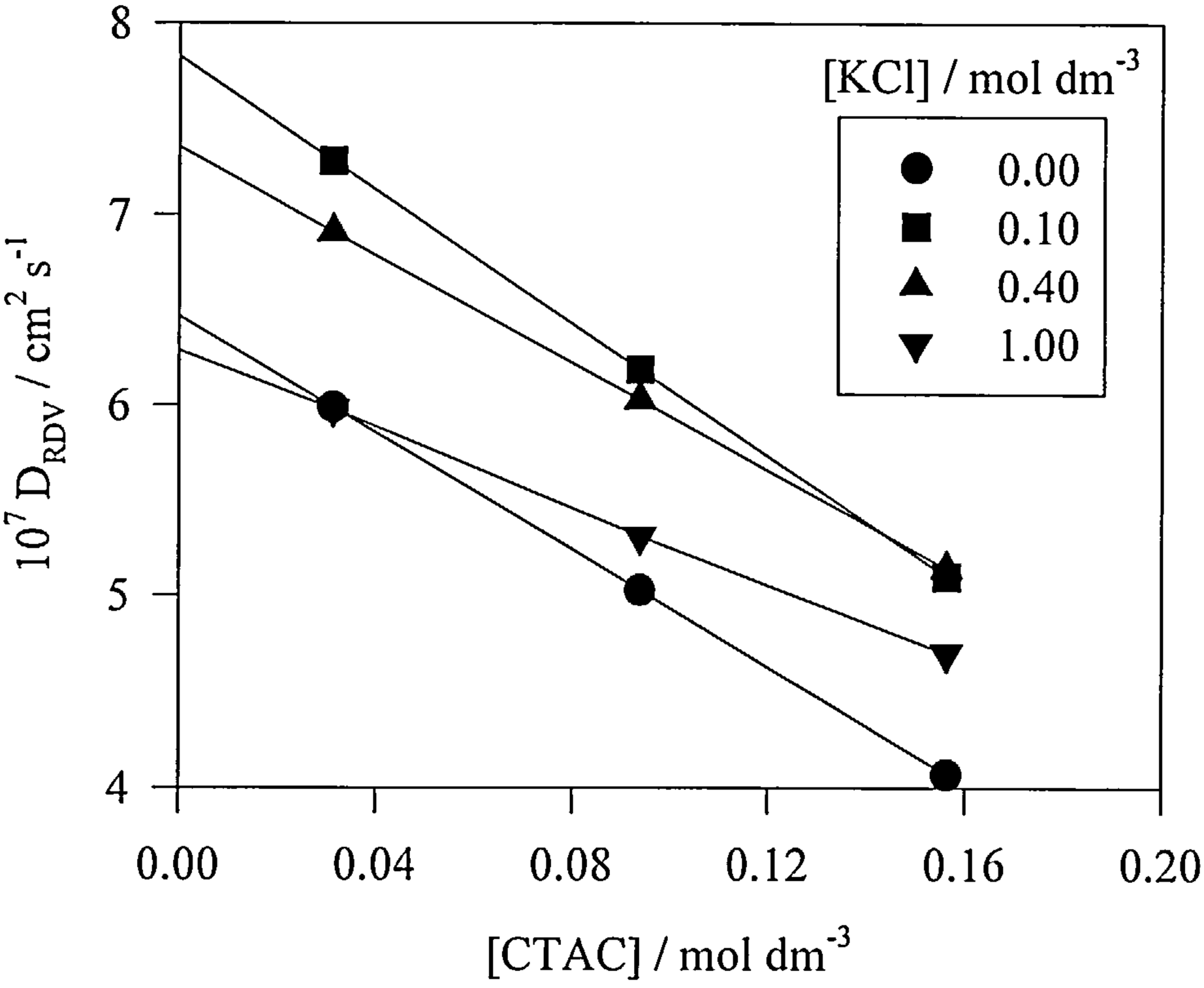

Appendix 4A.xiv : Variation of diffusion coefficient at infinite dilution with added KCl

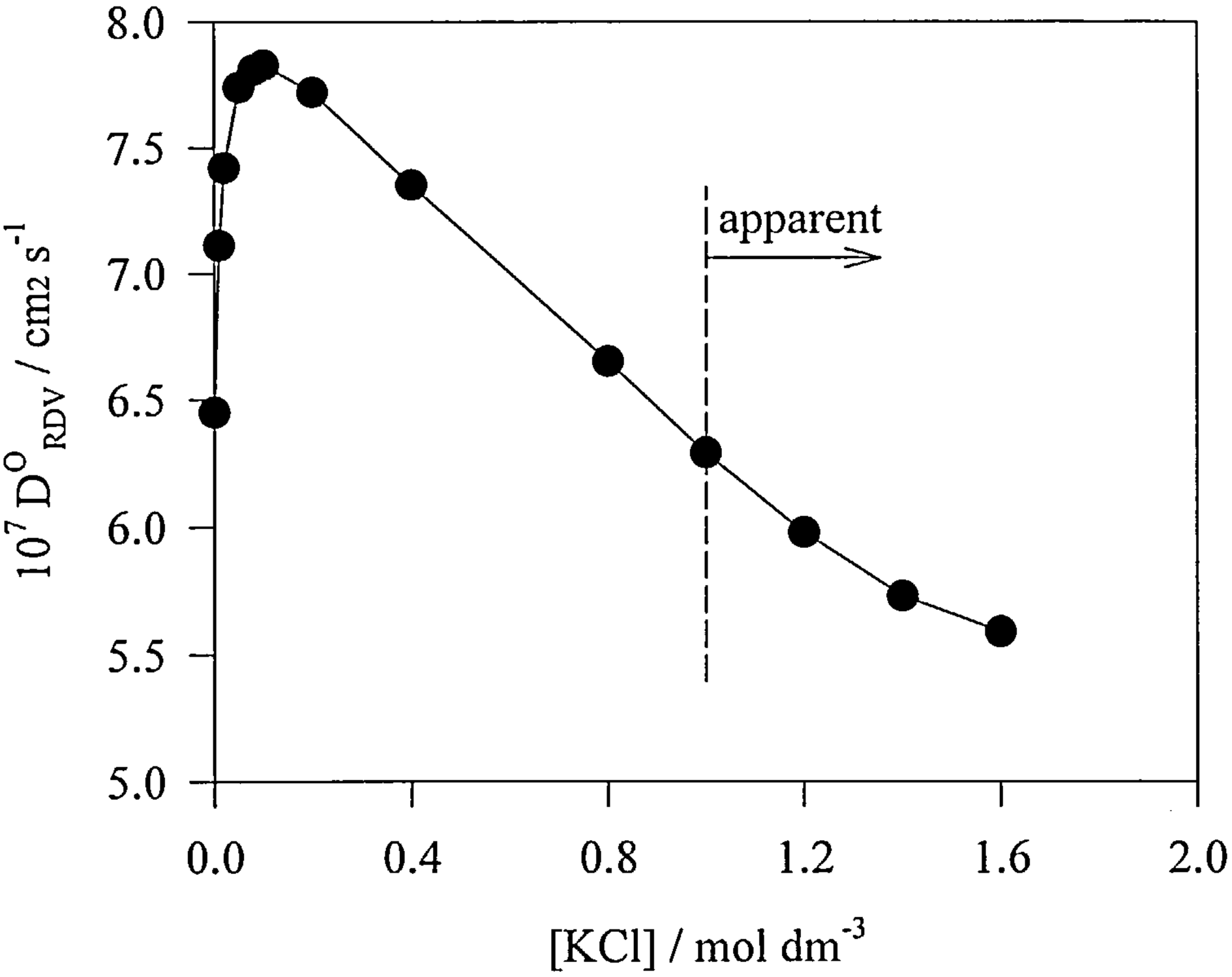

Appendix 4A.xv : Variation of interaction parameter (k_D) and surface potential (inset) with added KCl

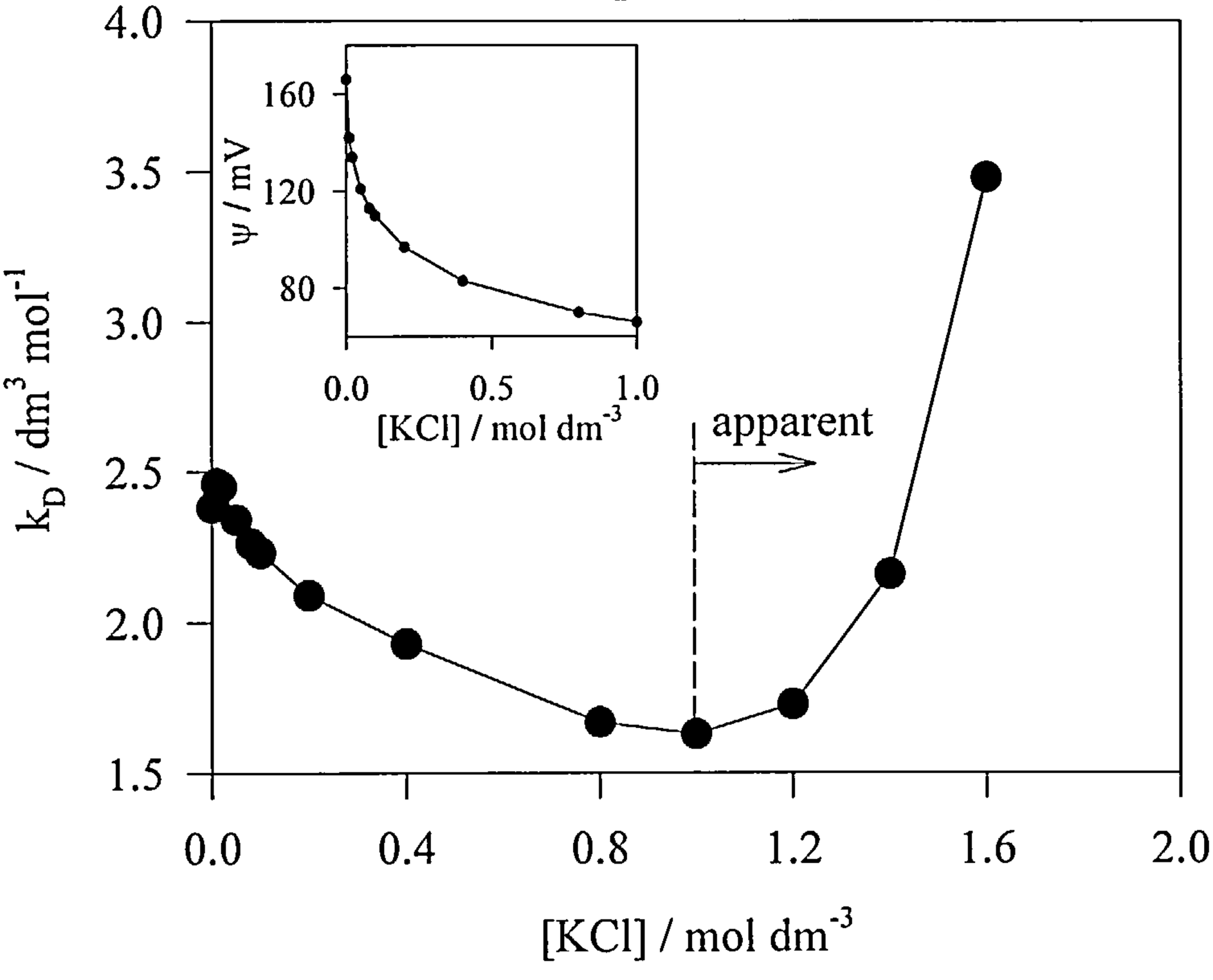

Appendix 4A.xvi : Variation of hydrodynamic radius (R_H^O) with added KCl

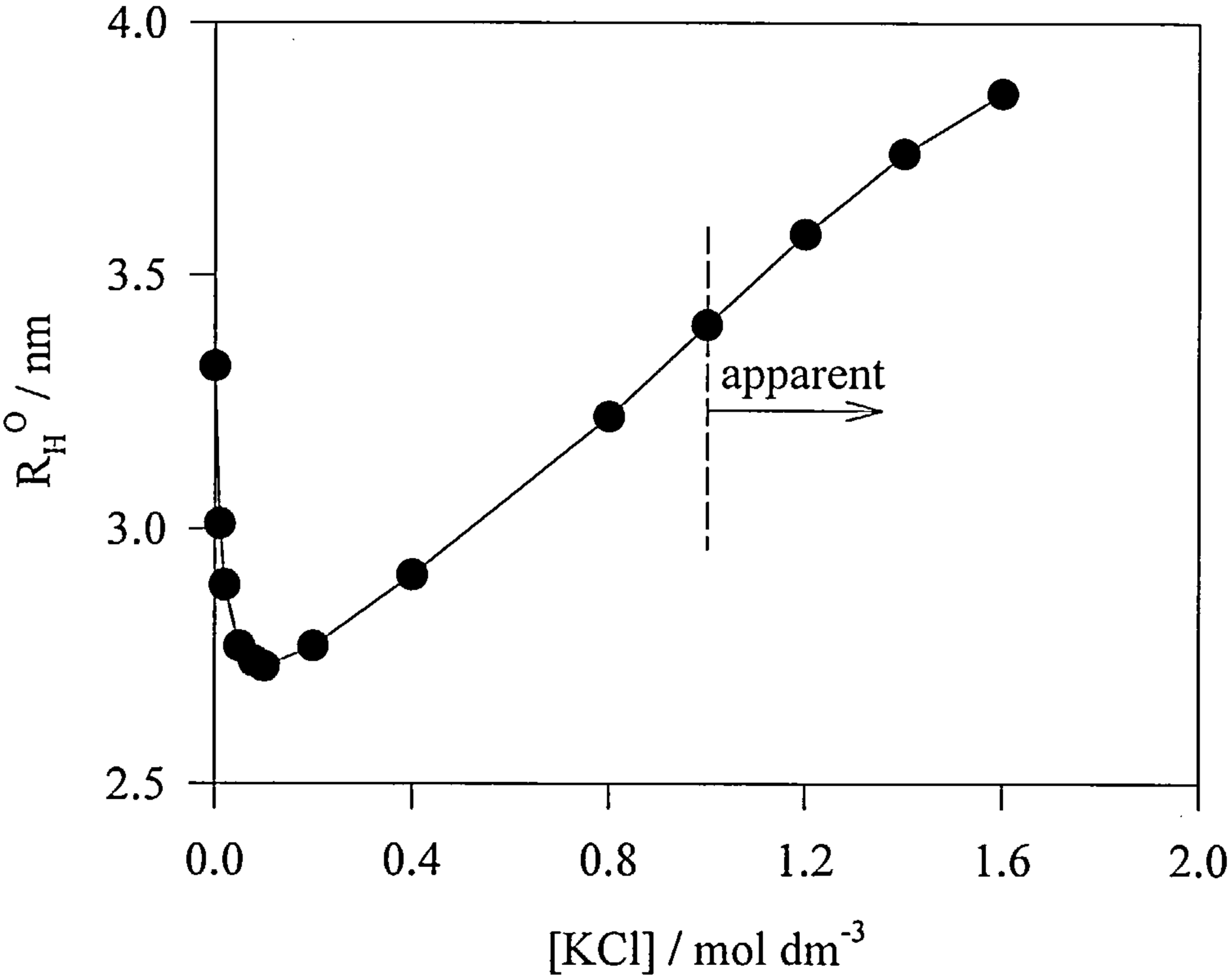

Appendix 4A.xvii : Variation of calculated coulombic potential with experimental interaction parameters

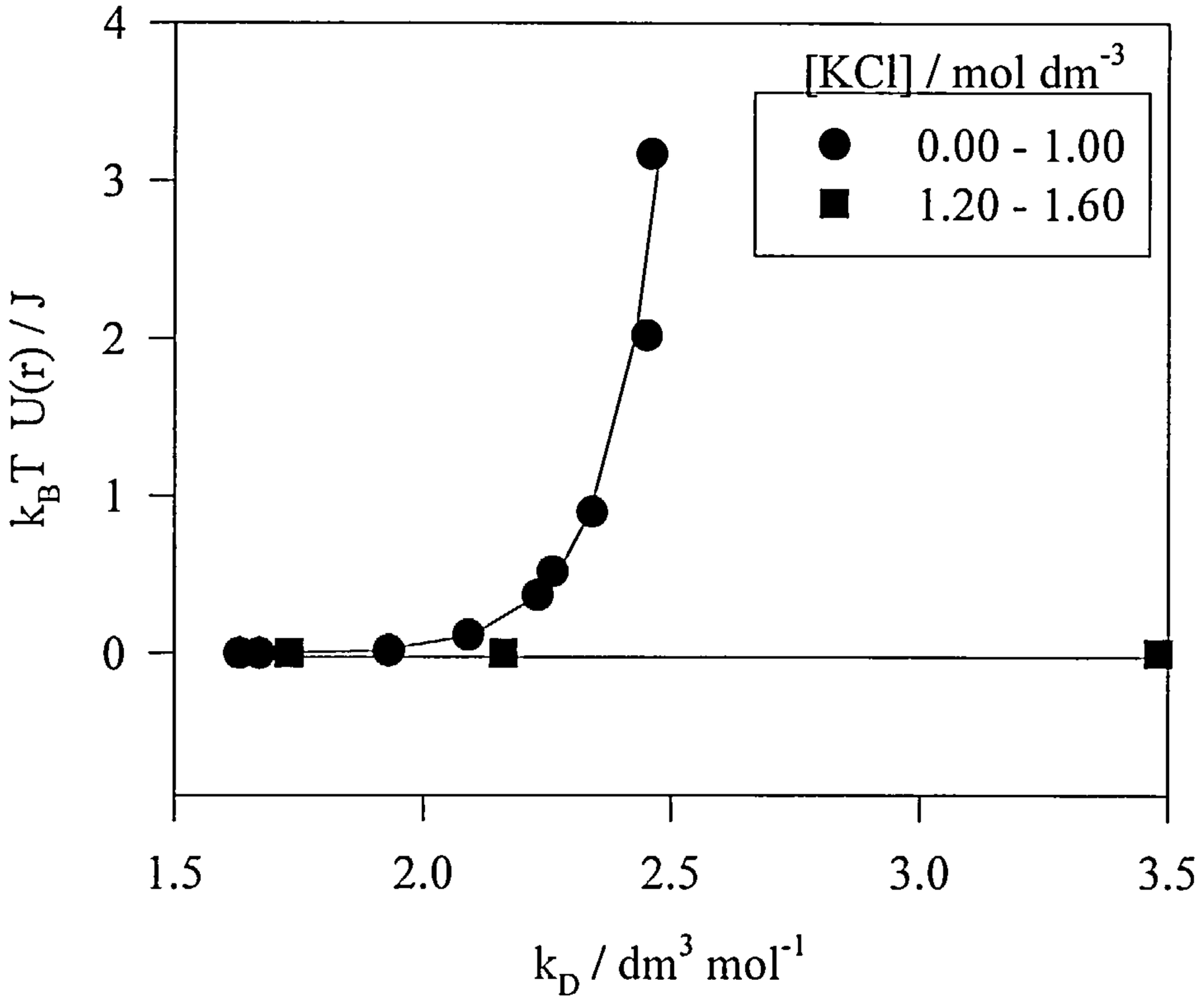

Appendix 4A.xviii : Variation of micellar radii with added KCl

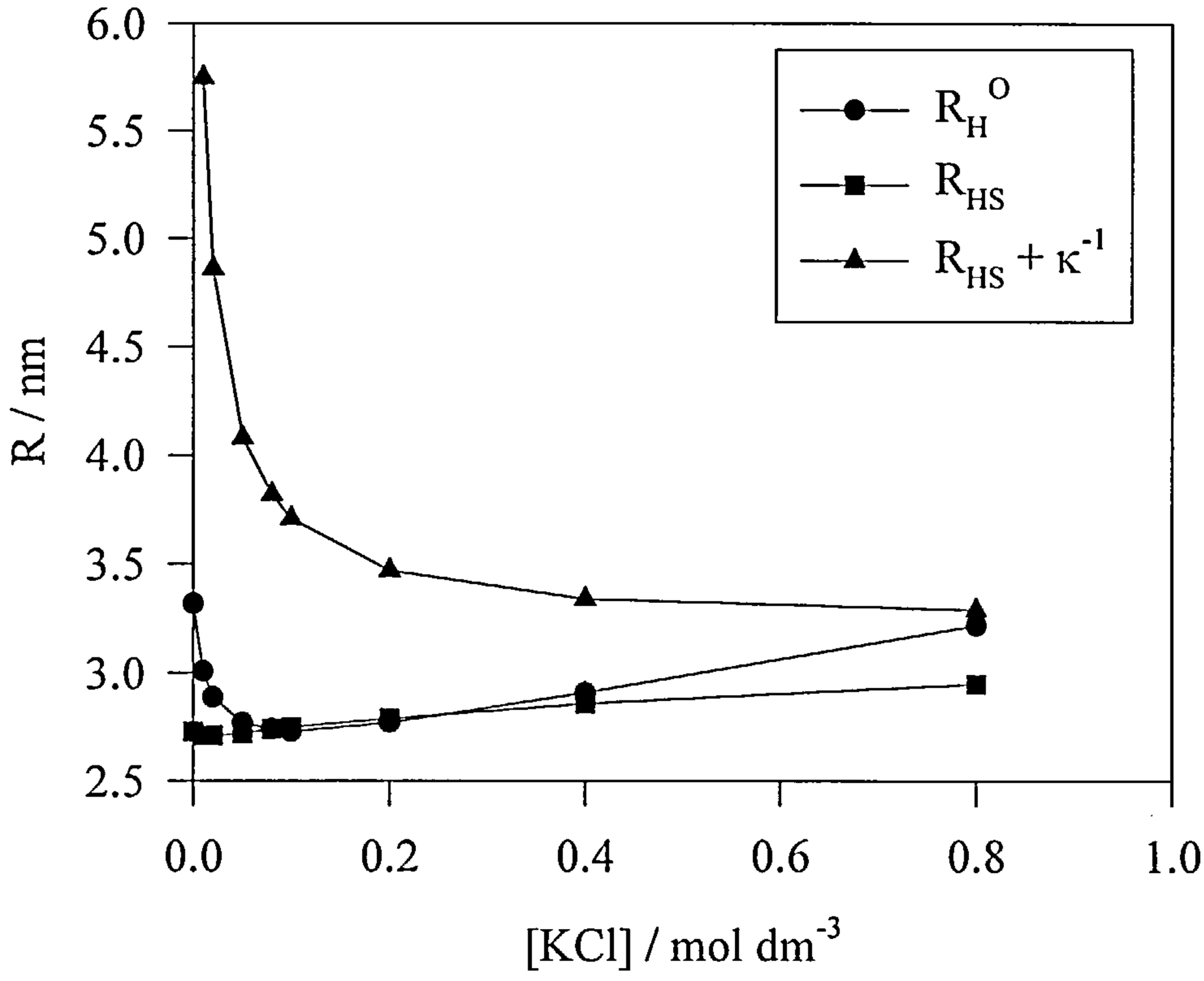

Appendix 4A.xix : Relationship between change in Debye length and change in hydrodynamic radius

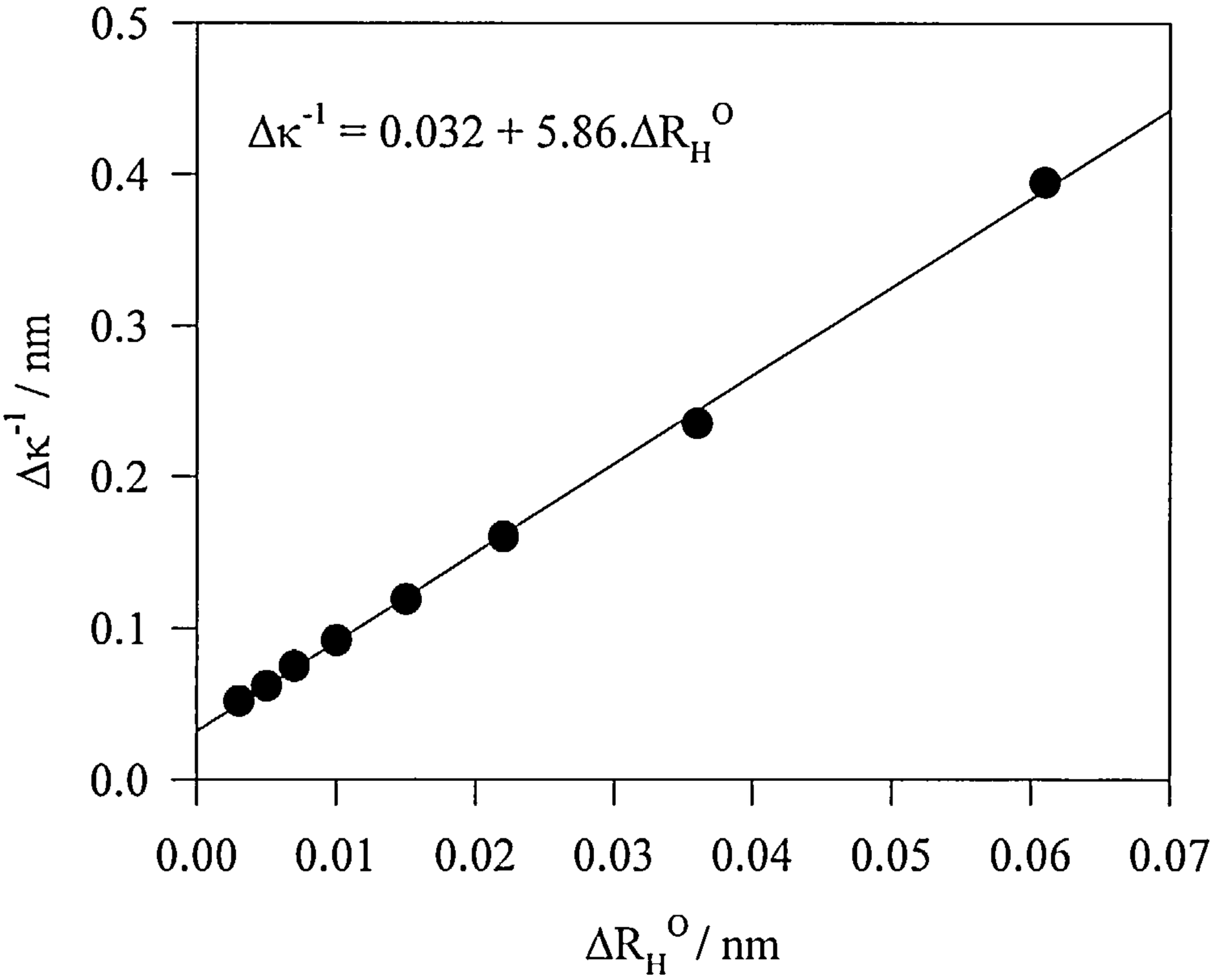

Appendix 4A.xx : Potential profiles from micellar surface; determination of shear plane potential (ξ)

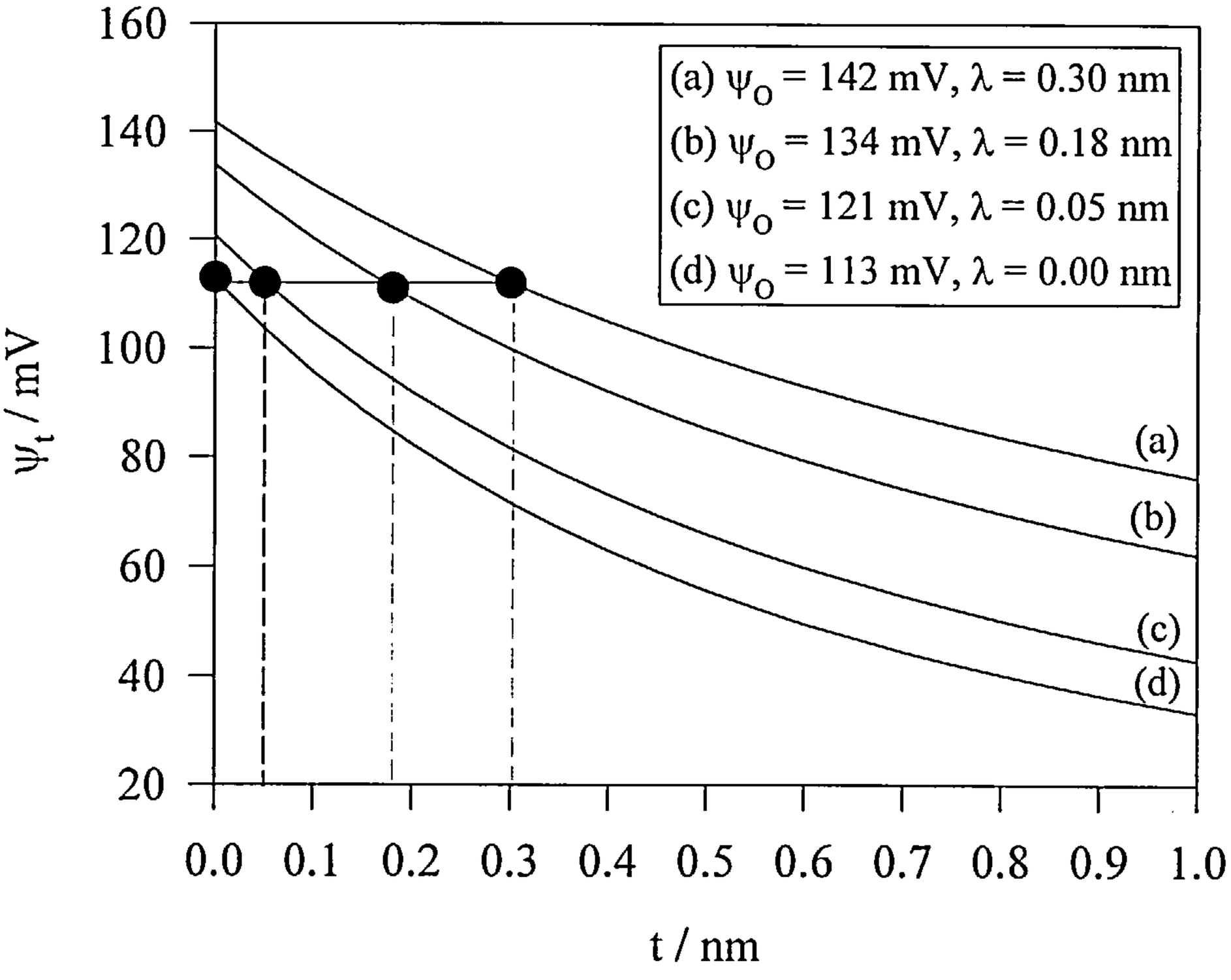

Appendix 4A.xxi : Variation of diffusion coefficient with [KCl] and temperature

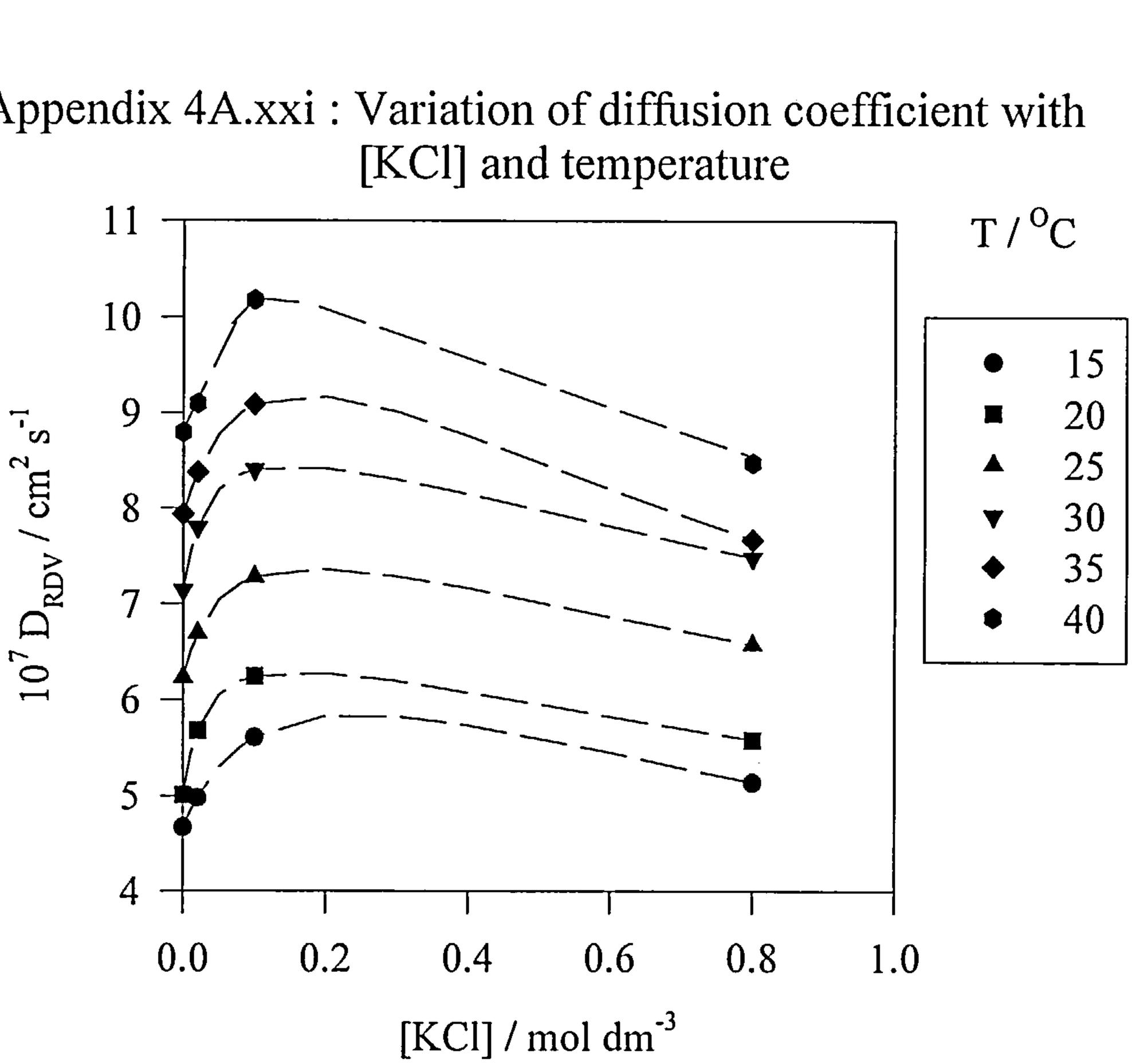

Appendix 4A.xxii : Arrhenius plot for temperature dependent diffusion coefficient

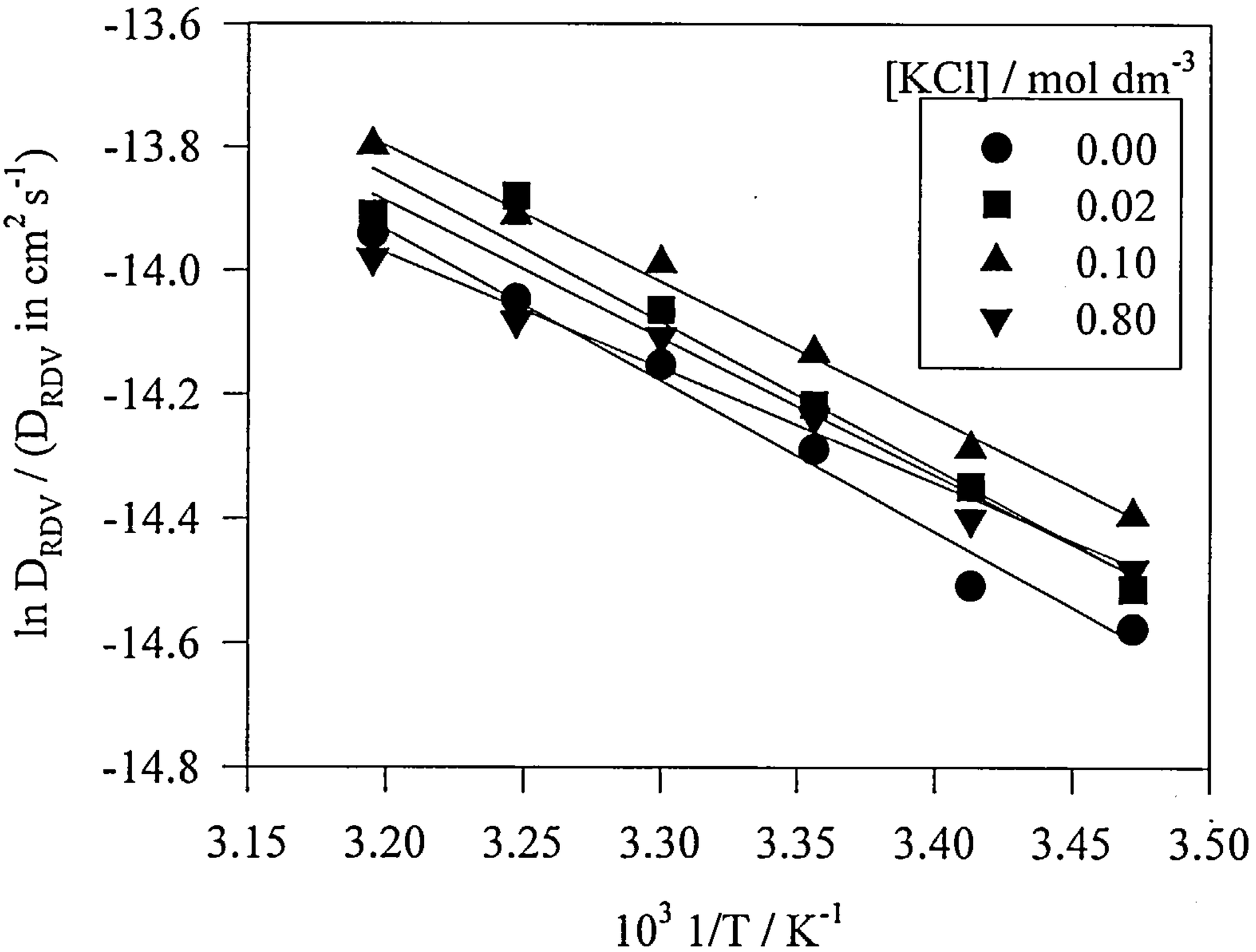

Appendix 4A.xxiii : Relationship between activation energy for diffusion and intermicellar interaction parameter

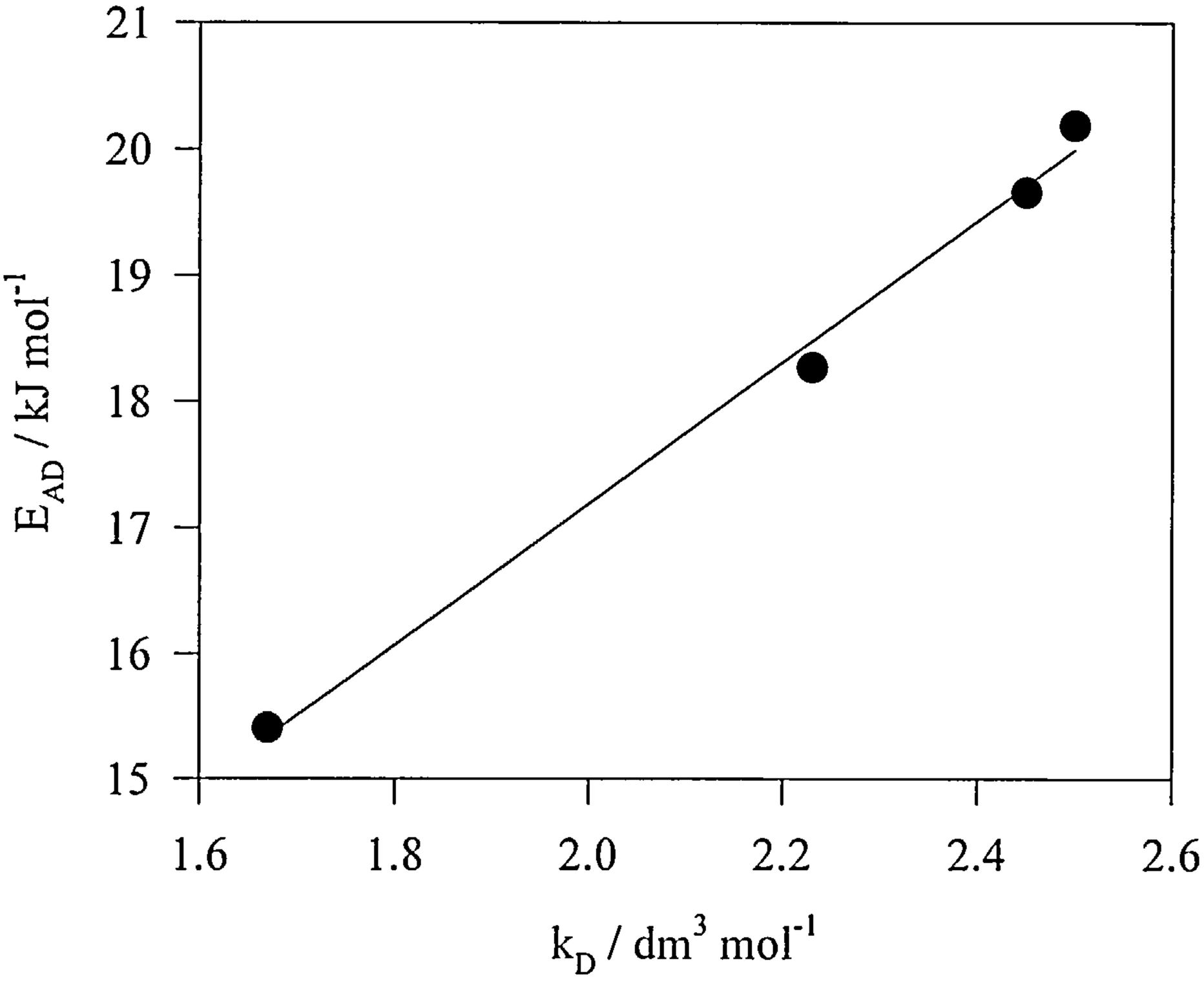

Chapter 4B: Rheology of CTAC

4B.1 Introduction

The rheological behaviour of cationic micellar systems has been well researched in the past. The most popular application of viscosity measurements appears to be the determination of the onset of significant micellar structural transitions[47,59,67,68,69,70]. Many authors have focused on the nature of the micellar growth with changes in halide counterion with inferences been made as to the strength of counterion binding[43,47,67,68,71]. Intermicellar interaction, however, is one physical property that has received little attention. Rheological studies have tended to be limited to a single surfactant concentration which allows no supposition as to interactions. This chapter will explore the behaviour of intermicellar interactions as a function of electrolyte concentration. Further confirmation of structural evolution at high electrolyte concentrations will be presented and compared to D_{RDV} data.

4B.2 Results and Discussion

Viscosity measurements were made on CTAC micellar solutions with electrolyte concentrations identical to those in Chapter 4A i.e. [CTAC] = 0.0313 - 0.1563 mol dm^{-3}, [KCl] = 0.00 - 1.60 mol dm^{-3}.

Table 4B.1 shows the range of viscosity results and these are also plotted in Appendix 4B.i.

Table 4B.1 : Experimental viscosity results

[KCl] / mol dm^{-3}	10^2 η / g cm^{-1} s^{-1}		
	0.0313 mol dm^{-3} CTAC	0.0938 mol dm^{-3} CTAC	0.1563 mol dm^{-3} CTAC
0.00	1.10	1.28	1.50
0.01	1.05	1.20	1.41
0.02	1.03	1.17	1.36
0.05	1.03	1.13	1.30
0.08	1.03	1.12	1.27
0.10	1.03	1.11	1.26
0.20	1.03	1.10	1.23
0.40	1.03	1.09	1.21
0.80	1.03	1.08	1.19
1.00	1.03	1.09	1.25
1.20	1.03	1.12	1.39
1.40	1.03	1.19	1.74
1.60	1.05	1.34	2.37

Note: standard error = $\pm 0.01x10^{-2}$ g cm^{-1} s^{-1}, each measurement repeated twice

The data exhibits behaviour that is inverse to that of the diffusion coefficients (Ch. 4A.2.3.1) ($\eta \alpha 1/D_{RDV}$) thus indicating a possible link between the macroscopic behaviours. The initial drop in viscosity corresponds to the increase in D_{RDV} from 0.00 - 0.10 mol dm^{-3} and it follows that the viscosity data will fit a rational function (Ch. 4A.2.3, Equation 4A.5) at electrolyte concentrations prior to the large precipitous increases at each surfactant concentration.

Table 4B.2 : Rational function; numerical constants

Numerical Constants	[CTAC] / mol dm^{-3}		
	0.0313	0.0938	0.1563
a (g cm^{-1} s^{-1})	$1.097x10^{-2}$	$1.278x10^{-2}$	$1.500x10^{-2}$
b (dm^3 mol^{-1})	2.129	0.804	0.545
c (dm^3 mol^{-1})	208.3	73.58	45.20
d (dm^6 mol^{-2})	-1.430	1.234	1.130

Correlation coefficients > 0.999 were obtained for the rational functions showing that the data is of sufficiently high standard for further analysis.

4B.2.1 Results Analysis

The viscosity data exhibits three regions of behaviour. At low electrolyte concentrations there is a sharp decrease in η corresponding to the neutralisation of micellar surface charge. It is known that weakly bound counterions result in lower viscosity micellar solutions[68], this is reflected in the presented data with reference to increasing chloride disassociation[1]. The decrease in viscosity is mirrored by a decrease in both k_D (Ch. 4A.2.3.3) and R_H^O (Ch. 4A.2.3.3) which suggests that viscosity data is effectively describing changes in interaction and hydrodynamic size i.e. the compression of the micellar shear plane and double layer (Ch. 4A.2.3.3).

At moderate electrolyte concentrations the viscosity is largely insensitive to addition of KCl implying that repulsive forces are effectively screened[1,2,3,12,40], which correlates with the small change in k_D observed over 0.10 - 1.00 mol dm^{-3} KCl (Ch. 4A.2.3.2). However, over this electrolyte concentration, the increase in R_{HS} that was observed by D_{RDV} measurements (Ch. 4A.2.3.3) is not manifested in the viscosity data. This indicates that although the viscosity data can describe small micellar size changes induced by electrostatic screening, it is unable to detect small micellar hard sphere size changes.

For each [CTAC] there is a threshold electrolyte concentration, above which, large increases in viscosity are observed. This precipitous increase is known to be due to sphere to rod transitions in cationic micellar systems[59,67,69] and it is at this point that the repulsive barrier between micelles has been overcome[68]. The threshold concentration has been termed the second critical micelle concentration ($c.m.c._{II}$)[68].

$$mD \leftrightarrow D_m \qquad c.m.c._I \qquad (4B.1)$$

$$nD_m \leftrightarrow D_{mn} \qquad c.m.c._{II} \qquad (4B.2)$$

If $c.m.c._I$ is the formation of spherical micelles (D_m) from m monomeric surfactant chains, $c.m.c._{II}$ is the formation of rod-like micelles (D_{mn}) from n spherical micelles[47]. It is known that rod-like micelles are only formed when the surfactant

concentration is high enough[47] which is reflected in the $c.m.c._{II}$ variation with [CTAC]. Appendix 4B.ii shows that a linear relationship exists between $c.m.c._{II}$ and [CTAC], from which, by linear extrapolation, it can be predicted that $c.m.c._{II} = 0.0$ mol dm^{-3} KCl when [CTAC] ≈ 0.34 mol dm^{-3}. This suggests that rod-like micelles can be formed in the absence of any added electrolyte[47] i.e. surfactant induced structural evolution if the surfactant concentration is high enough.

The highly sensitive nature of the micellar viscosity to increases in electrolyte concentration is a consequence of rod-like micellar extension i.e. significant growth[43,47,70,71,72,73]. Imae et al showed that the aggregation number of CTAC micelles increased from 309-11400 over 1.50 - 4.00 mol dm^{-3} NaCl[72]. This corresponds to massive increases in micellar molecular weight as described by the expression below for rod-like micelles above the threshold electrolyte concentration[43]:-

$$\log_{10}M_{mn} = A_{mn} \log_{10}(c.m.c._I + C_E) + B_{mn} \qquad (4B.3)$$

where M_{mn} is the molecular weight A_{mn} (=3.66) and B_{mn} (=4.31) are constants and C_E is the electrolyte concentration. Using this relationship, aggregation numbers (N_{agg}) of 124, 219 and 356 are obtained at [KCl] = 1.20, 1.40 and 1.60 mol dm^{-3} respectively (where $N_{agg} = M_{mn} / 320$ g mol^{-1}). At these high electrolyte concentrations the rod-like micelles essentially act as neutral polymers due to the shielding of micellar surface charge[68]. The rod-like micelles can therefore entangle together to form semi-flexible highly viscous networks[71,72,74]. It is generally accepted[74,75] that rod-like micellar size increases with [electrolyte]$^{1/2}$, which is in agreement with the observed increase in N_{agg} presented here.

With Triton X-100 the viscosity data was analysed in terms of a virial expansion. The nature of TX-100 micelles mean that inferences were made regarding micellar growth and shape changes (Ch. 3B.2.1). CTAC micelles, however, remain spherical up to 1.20 mol dm^{-3} CTAC[13] and undergo no significant structural changes until high electrolyte concentrations are present. The highly

charged surface of CTAC micelles[1] means that analysis of the virial expansion is made with respect to intermicellar interactions[74,76].

$$\eta / \eta_O = 1 + k_V.C_S + k_V'.C_S^2 \qquad (4B.4)$$

k_V is the viscosity interaction parameter and C_S is the surfactant concentration. A series of plots of η / η_O against [CTAC] for different electrolyte concentrations are shown in Appendix 4B.iii. The data is seen to fit Equation 4B.4 with an average intercept of ~ 1.01 although there is deviation from this point at ≥ 1.00 mol dm^{-3} KCl. From the quadratic fit, a range of values for k_V and k_V' were obtained (Table 4B.3)

Table 4B.3 : Viscosity virial expansion; interaction parameters

[KCl] / mol dm^{-3}	k_V / dm^3 mol^{-1}	k_V' / dm^6 mol^{-2}
0.00	2.22	5.25
0.01	1.41	7.68
0.02	1.22	7.42
0.05	0.67	7.81
0.08	0.50	7.55
0.10	0.43	7.42
0.20	0.29	7.04
0.40	0.16	6.91
0.80	0.00	6.19
1.00	-0.50	11.90
1.20	-1.52	23.68
1.40	-3.41	48.26
1.60	-6.85	92.50

The values for k_V and k_V' are plotted in Appendix 4B.iv and 4B.v respectively. Both parameters show a significant transition at 0.80 - 1.00 mol dm^{-3} KCl. The results suggest that k_V and k_V' are representative of different types of interaction, possibly direct micelle-micelle interactions and hydrodynamic[74]. Hydrodynamic interactions are a result of the flow field generated by particle motion through the solution which affects the movement of any neighbouring particles[40].

The k_V data is comparable with interaction parameters (k_D) determined by rotating disk voltammetry (Ch. 4A.2.3.1). The initial exponential type decay with increasing

electrolyte is characteristic of a reduction in repulsive interactions from gradual neutralisation of surface charge[1,2,3,12,40]. k_V then remains relatively insensitive to changes in electrolyte concentration until it passes through $k_V = 0.00$ at 0.80 mol dm^{-3} KCl. This is indicative of micellar structural evolution and is in excellent agreement with Ikeda[43] and Imae[47] who observed a CTAC sphere-rod transition at 1.18 mol dm^{-3} NaCl. The negative k_V values at $\geq$ 1.00 mol dm^{-3} KCl are evidence of the van der Waals attractive forces necessary for micellar growth[3,8]. Dorshow et al. showed by light scattering that at [NaCl] = 0.50 - 1.00 mol dm^{-3} there is zero nett interaction between micelles prior to micellar growth[3,8], this is confirmed by the k_V data shown here.

With RDV, the diffusion interaction parameter (k_D) was seen to increase at [KCl] $\approx$ 1.20 mol dm^{-3} (Ch. 4A.2.3.2). Although, the actual values of k_V and k_D are not quantitatively comparable at high electrolyte concentrations they do show the effect of significant micellar growth (Appendix 4B.vi). It has been noted, however, that interactions manifest themselves to a greater extent in rheological testing than in diffusion coefficient measurements[76]. This is a possible explanation for the behaviour above 1.00 mol dm^{-3} KCl i.e. $k_V \rightarrow$ negative, $k_D \rightarrow$ positive.

4B.2.2 Effect of temperature

In Ch. 4A.2.4, the activation energies of CTAC micellar solutions were determined over a range of electrolyte concentrations. It was shown that a decrease in activation energy (E_{AD}) was accompanied by a corresponding decrease in intermicellar interaction (k_D). This section will use rheological measurements at different temperatures to determined the viscosity activation energy (E_{AV}). All measurements were carried out on 0.0938 mol dm^{-3} CTAC over a temperature range of 15-40 ^{O}C in addition to those results at 20 ^{O}C previously presented (Ch. 4B.2). Electrolyte concentrations of 0.00, 0.02, 0.10 and 0.80 mol dm^{-3} KCl were chosen for reasons described previously (Ch. 4A.2.4) i.e. different regions on D_{RDV} vs. [KCl] graph.

Table 4B.4 shows the raw viscosity data as a function of temperature and electrolyte concentration.

Table 4B.4 : Viscosity variation with temperature and electrolyte concentration

T / ^{O}C	10^2 η / g cm^{-1} s^{-1}; with [KCl] / mol dm^{-3}			
	0.00	0.02	0.10	0.80
15	1.43	1.30	1.24	1.22
20	1.28	1.17	1.11	1.08
25	1.14	1.04	1.00	0.99
30	1.02	0.94	0.91	0.90
35	0.92	0.84	0.81	0.79
40	0.83	0.76	0.73	0.74

Note: standard error = ±0.01x10^{-2} g cm^{-1} s^{-1}, each measurement repeated twice

In Ch. 3B.2.2, it was seen that Triton X-100 viscosity data did not adhere to normal Arrhenius behaviour due to changes in the micellar structure. In cationic micelles it is known that as temperature increases spherical micelles are favoured[59,67] due to their decrease in volume size[5,6,10,12,14]. Although this may alter micellar size distribution, viscosity is not greatly affected by assumptions of mono or polydispersity[74]. It is therefore not surprising that the viscosity data obeys Arrhenius behaviour[59]:-

$$\eta = A.\exp.(E_{AV}/RT) \qquad (4B.5)$$

By plotting graphs of ln η against 1/T the activation energy of viscous flow (E_{AV}) can be determined. The Arrhenius data is shown below in Table 4B.5 and plotted in Appendix 4B.vii.

Table 4B.5 : Arrhenius data for temperature dependent viscosity

10^3 1/T / K^{-1}	ln D_{RDV} variation at different [KCl]			
	0.00 mol dm^{-3}	0.02 mol dm^{-3}	0.10 mol dm^{-3}	0.80 mol dm^{-3}
3.195	-4.794	-4.872	-4.914	-4.908
3.247	-4.687	-4.775	-4.813	-4.838
3.300	-4.586	-4.668	-4.697	-4.711
3.356	-4.474	-4.566	-4.605	-4.612
3.413	-4.360	-4.451	-4.498	-4.527
3.472	-4.247	-4.342	-4.389	-4.406
E_{AV} / kJ mol^{-1}	16.40	15.96	15.69	15.18
ln A	-11.10	-11.01	-10.93	-10.75

The activation energies for viscosity are in excellent agreement with those reported in the literature for dodecylammonium bromide (DTAB) and sodium dodecylsulfate (SDS)[59] where E_{AV} = 17 kJ mol^{-1}, though they are slightly higher than those determined by Kern et al. where E_{AV} ~ 11 kJ mol^{-1} for CTAC/NaCl[71]. The results are, however, characteristic of aqueous solutions and spherocolloids[59].

In Ch. 4A.2.4, an intimate relationship between the diffusional activation energies and interaction parameters was established, it is therefore logical to compare the viscosity activation energies and interaction parameters. These are shown in Table 4B.6 and plotted in Appendix 4B.viii.

Table 4B.6 : Comparison of viscosity activation energies and intermicellar interaction parameters

[KCl] / mol dm^{-3}	k_V / dm^3 mol^{-1}	E_{AV} / kJ mol^{-1}
0.00	2.22	16.40
0.02	1.22	15.96
0.10	0.43	15.69
0.80	0.00	15.18

From Appendix 4B.viii it can be seen that the same relationship exists as was observed for diffusional data i.e. a linear increase in activation energy with interaction parameter. This was explained in Ch. 4A.2.4 in terms of the energy of a micelle required to pass its nearest neighbour whilst overcoming repulsive interactions (Ch. 4A.2.4). This is supported by the presented data.

As a further comparison, Appendix 4B.ix shows how the activation energy for diffusion (E_{AD}) and activation energy for viscosity (E_{AV}) vary with added electrolyte. It can be seen that there is an initial sharp drop in both E_{AD} and E_{AV} characteristic of a decrease in repulsive forces between micelles due to partial neutralisation of surface charge[1,2,3,12,40]. Although the values are not equal, the qualitative behaviour is the same for both E_{AD} and E_{AV}. An explanation for the divergence of E_{AV} and E_{AD} at low electrolyte concentration is not totally apparent but, it may be that diffusion is more sensitive than viscosity to interaction effects as well as changes in hard sphere micellar size (in the absence of a sphere - rod transition). At 0.80 mol dm^{-3} KCl, however, the values do almost concur with $E_{AD} \sim E_{AV} \sim 15.3$ kJ mol^{-1}. At this high electrolyte concentration Coulombic interactions are highly screened[1,2,3,12,40] suggesting that the effects on diffusion and viscosity are comparable.

4B.3 Summary

The rheological properties of CTAC micellar solutions have been studied over a range of surfactant (0.0313 - 0.1563 mol dm^{-3}) and electrolyte (0.00 - 0.80 mol dm^{-3}) concentrations. The viscosity was observed to decrease in a fashion that corresponded to the previous increase in diffusion coefficient data i.e. $\eta \alpha 1/D_{RDV}$. The viscosity data at [KCl] $\leq$ 0.80 mol dm^{-3} was seen to fit a rational function and was interpreted in terms of a reduction in repulsive forces between micelles due to the screening of charged headgroups. The viscosity exhibited a large increase at threshold concentrations dependent on the surfactant concentration. As the [CTAC] increased the precipitous increase was noted to occur at lower electrolyte concentrations. The large increase in viscosity was typical of a structural transition from sphere to rod-like micelles. This suggested that the sphere to rod-like transformation was dependent on both electrolyte and surfactant concentration and it was predicted that at [CTAC] ~ 0.34 mol dm^{-3} structural evolution would occur in the absence of added electrolyte.

The experimental viscosity data was analysed by a virial expansion from plots of η / η_O against [CTAC]. The expansion led to the determination of two interaction parameters, k_V and k_V'. Although both terms were seen to vary with electrolyte concentration it was the behaviour of k_V that proved of most interest. k_V was observed to decay in an exponential fashion due to the gradual reduction in Coulombic repulsion from 0.00 - 0.80 mol dm^{-3} KCl. As the electrolyte concentration $\geq$ 1.00 mol dm^{-3}, k_V was seen to shift from positive to negative. Corresponding to a sphere-rod like micellar transition, the shift in k_V was indicative of the conversion from repulsive interaction to attractive van der Waals forces.

The viscosities of a series of 0.0938 mol dm^{-3} micellar solutions were measured over a range of temperatures and electrolyte concentrations. The rheological behaviour was seen to adhere to the standard Arrhenius relationship. Plots of ln η against 1/T led to the determination of the activation energy for viscous flow (E_{AV}). As for diffusion activation energy (E_{AD}) data, E_{AV} was observed to increase in a linear fashion with the experimentally determined interaction parameter (k_V). This presented further evidence that the energy of a micelle required to pass its nearest neighbour was intimately related to the intermicellar repulsion. Although, the actual values of both E_{AV} and E_{AD} were not equal they did exhibit the same behaviour i.e. a decrease with an increased electrolyte concentration. This could suggest that E_{AD} was more sensitive to changes in interaction than E_{AV}.

Appendix 4B.i : Viscosity variation with added electrolyte

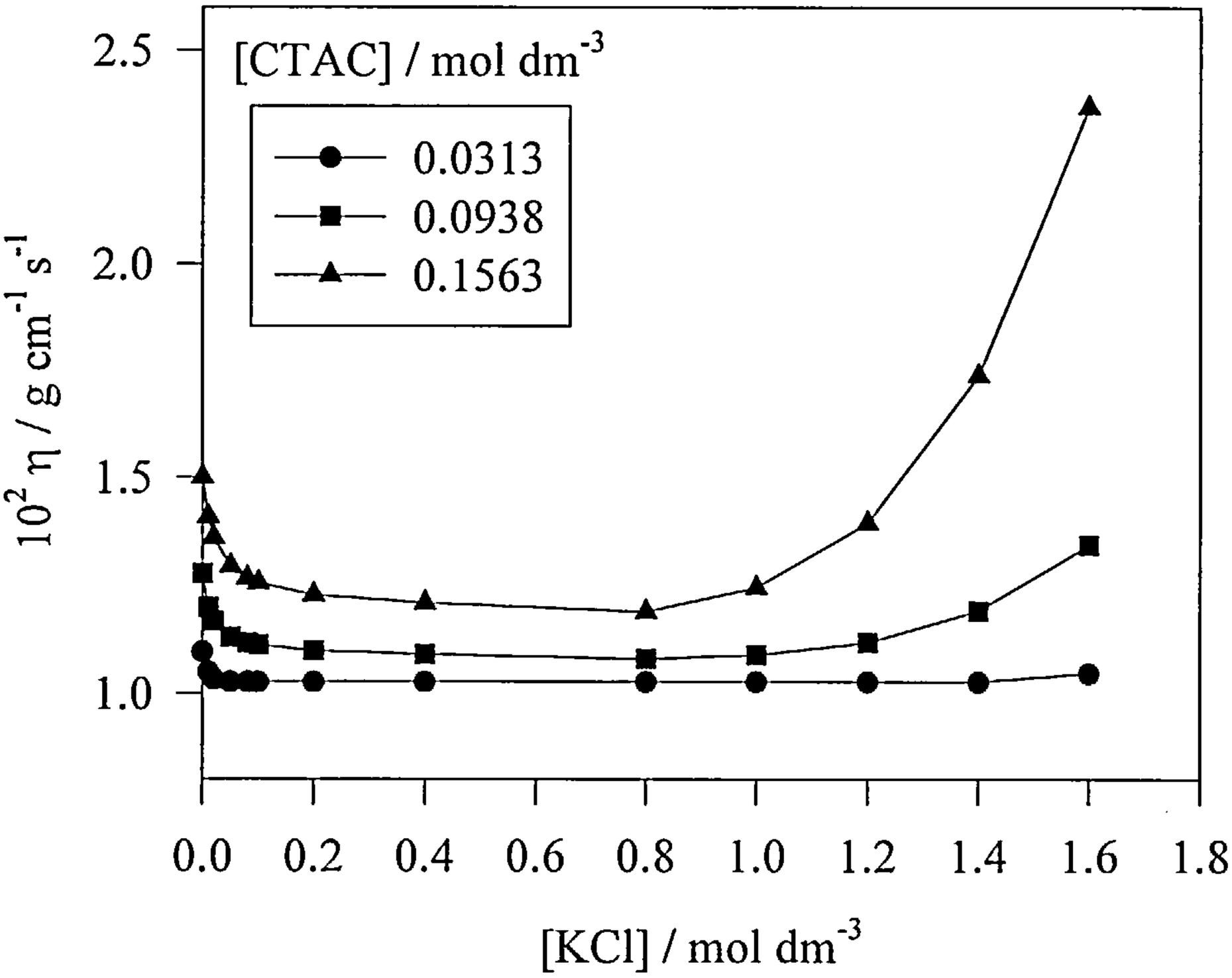

Appendix 4B.ii : Variation of threshold electrolyte concentration ($c.m.c._{II}$) with surfactant concentration

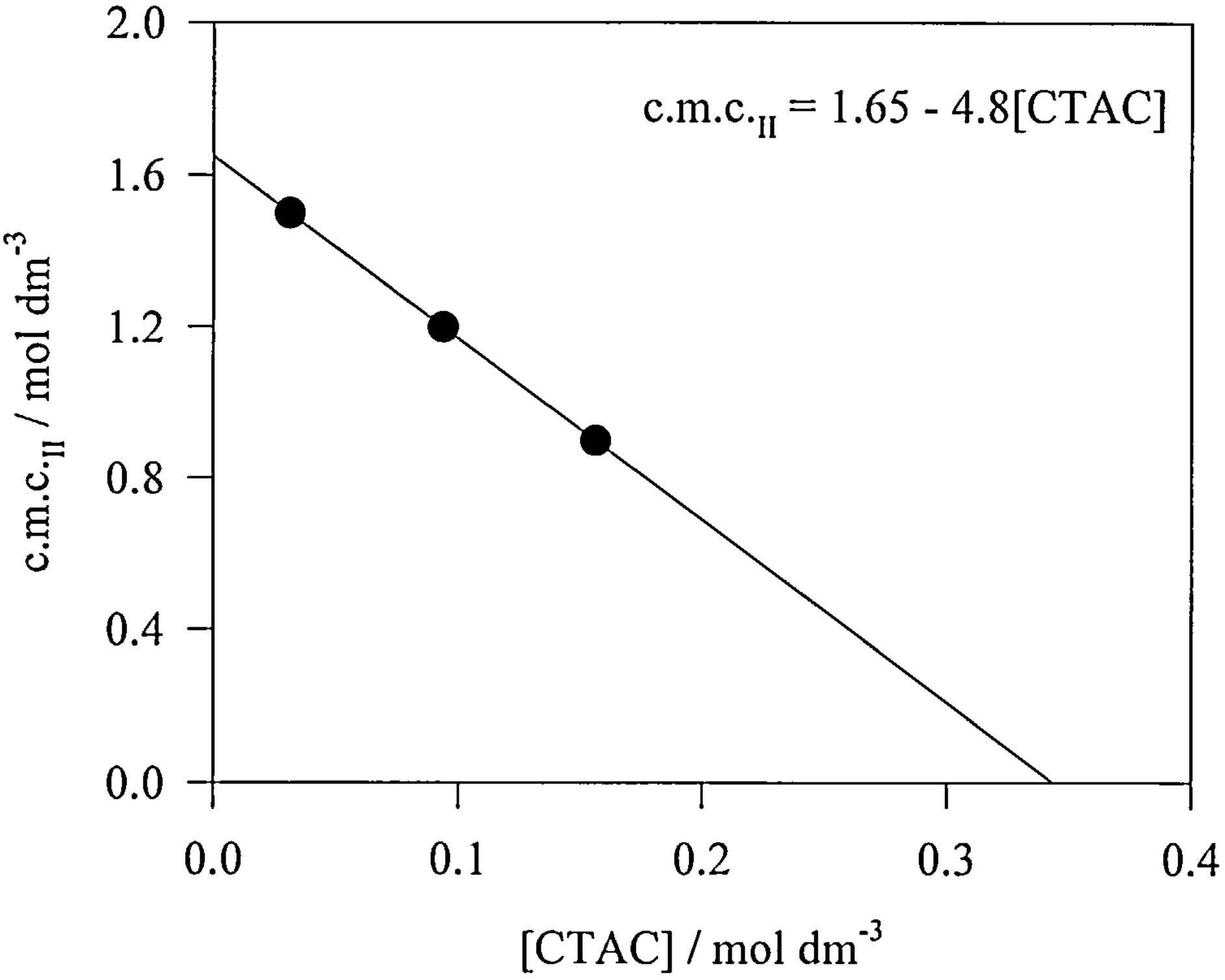

Appendix 4B.iii: Variation of relative viscosity with [CTAC]

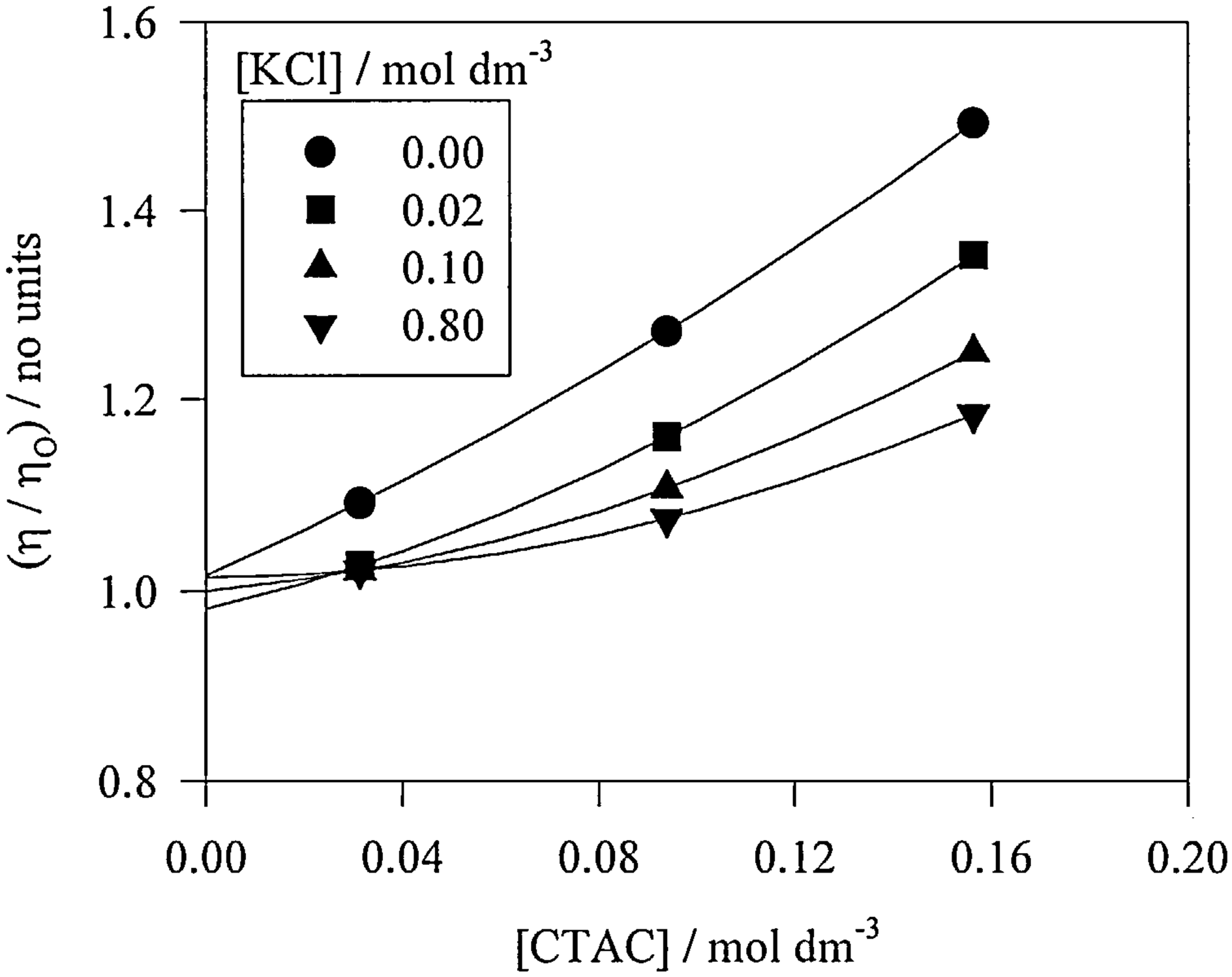

Appendix 4B.iv: Variation of first virial interaction parameter (viscosity) with added electrolyte

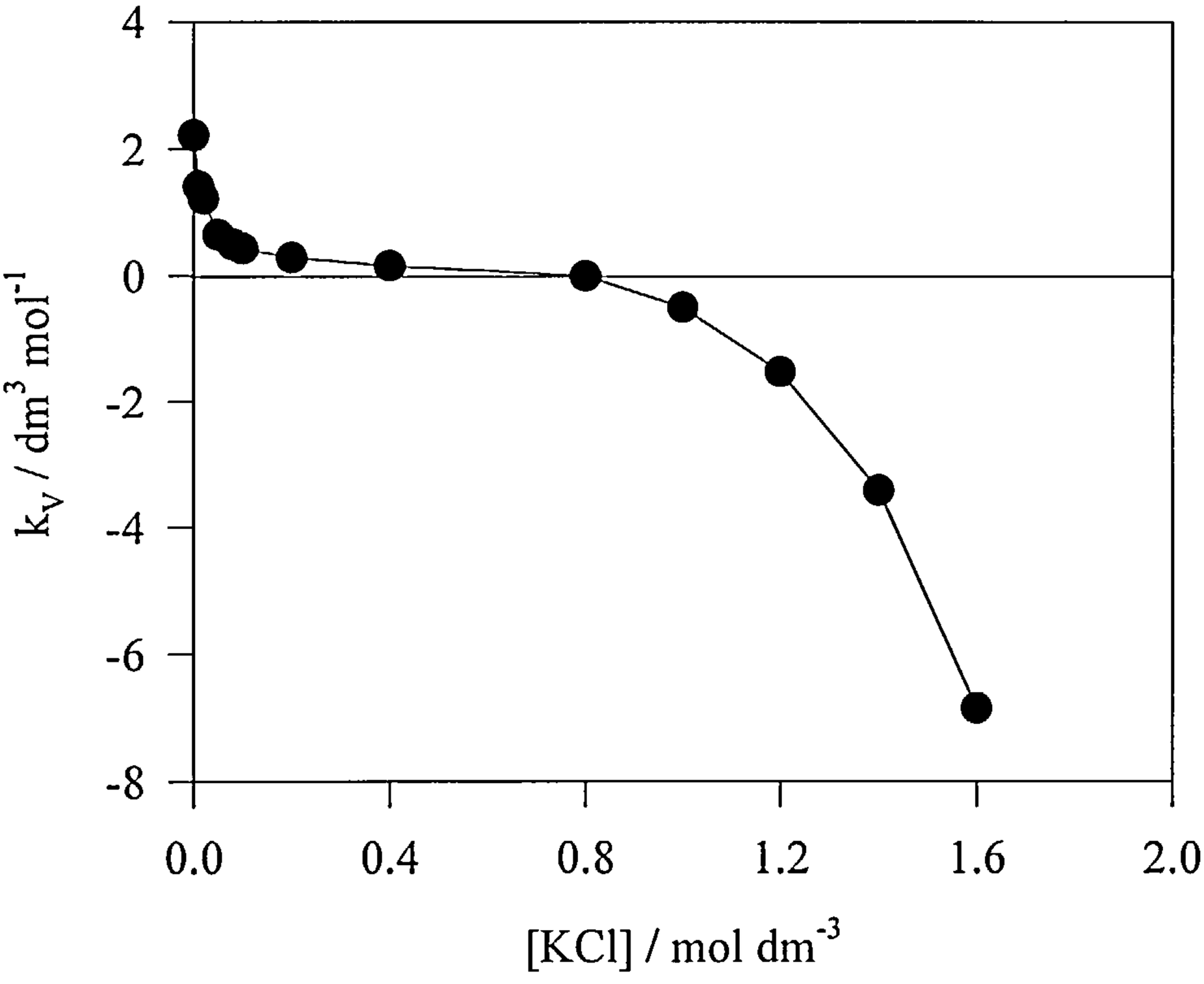

Appendix 4B.v: Variation of second virial interaction (viscosity) parameter with added electrolyte

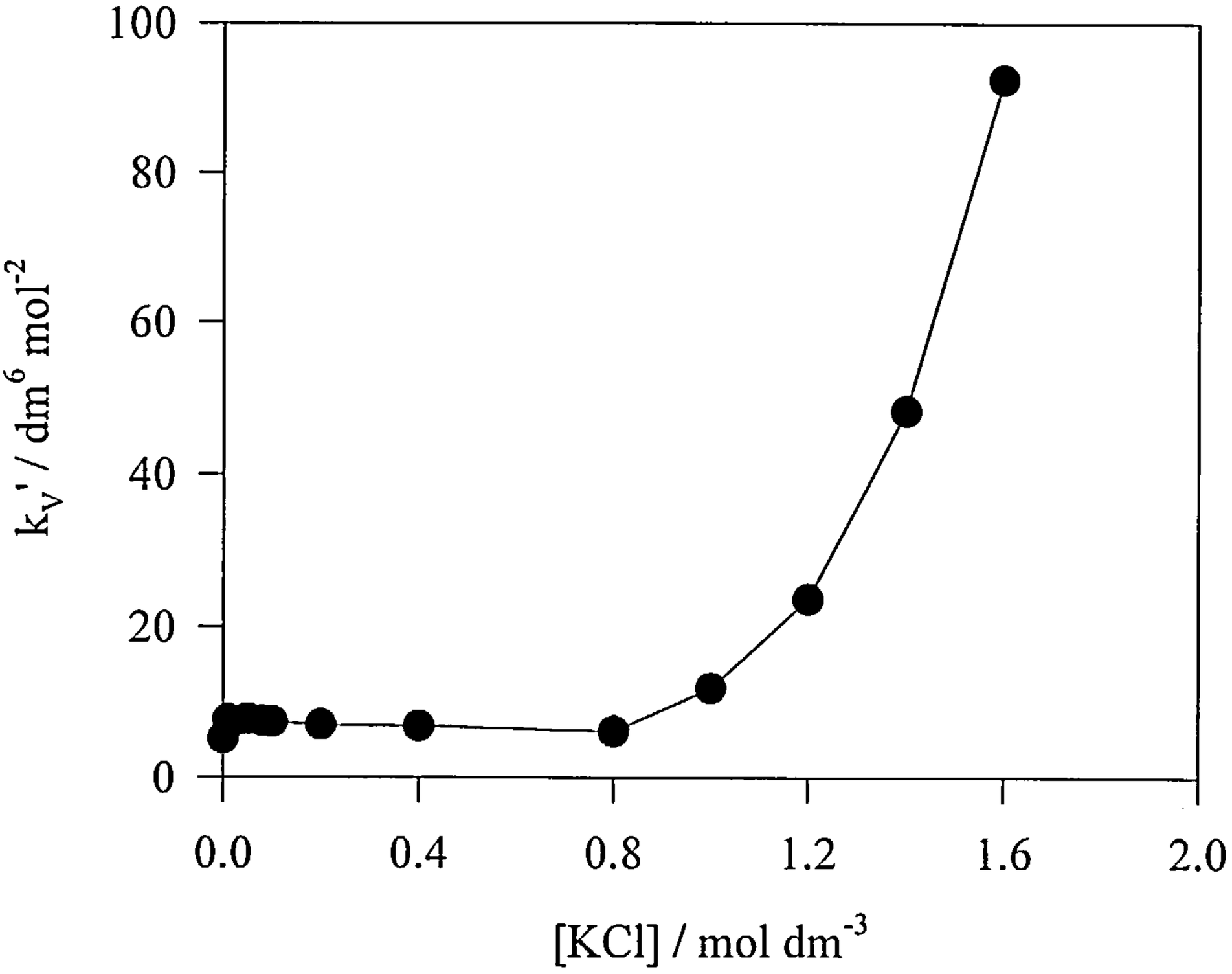

Appendix 4B.vi: Comparison between diffusion and viscosity interaction parameters

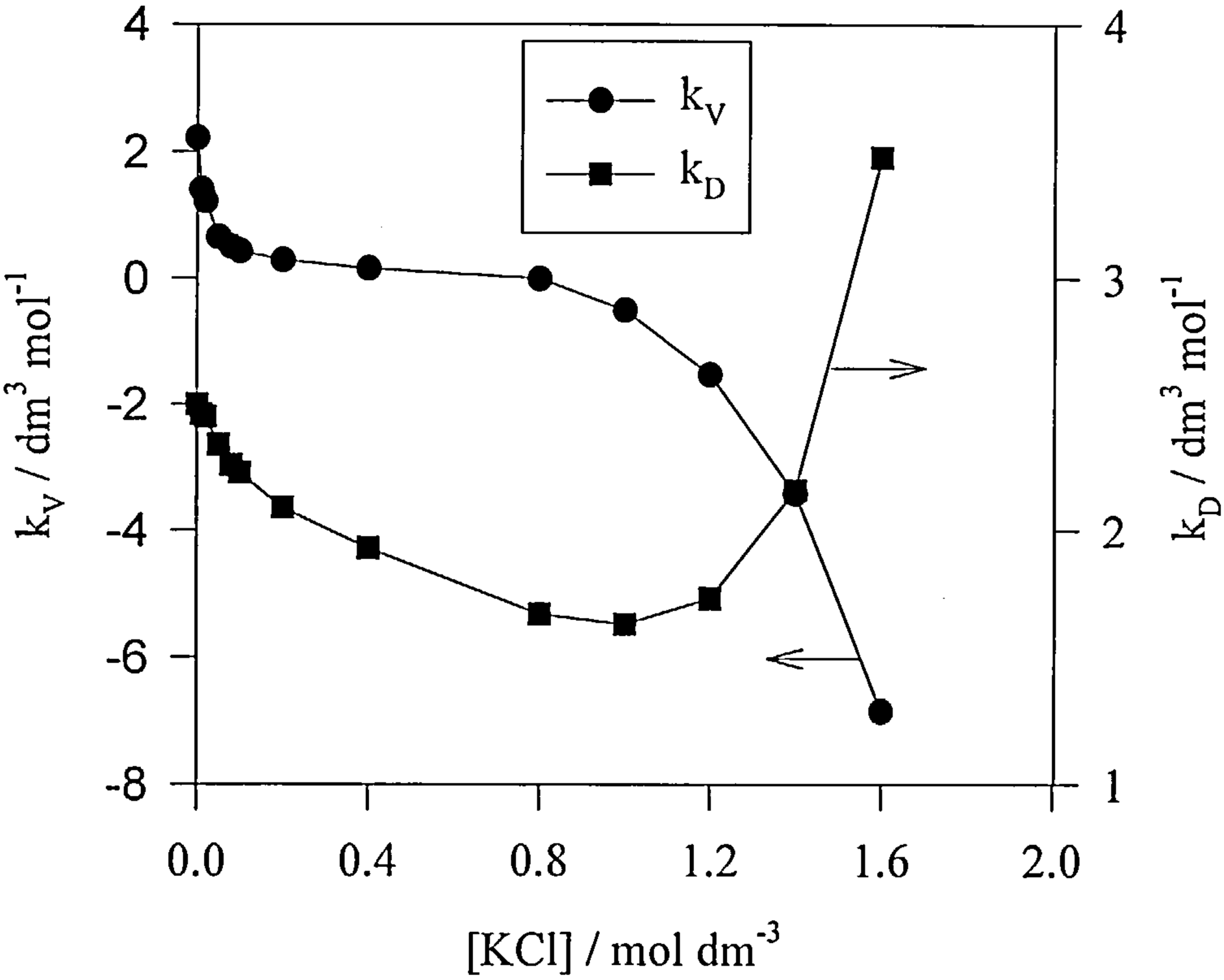

Appendix 4B.vii : Arrhenius plot for temperature dependent viscosity

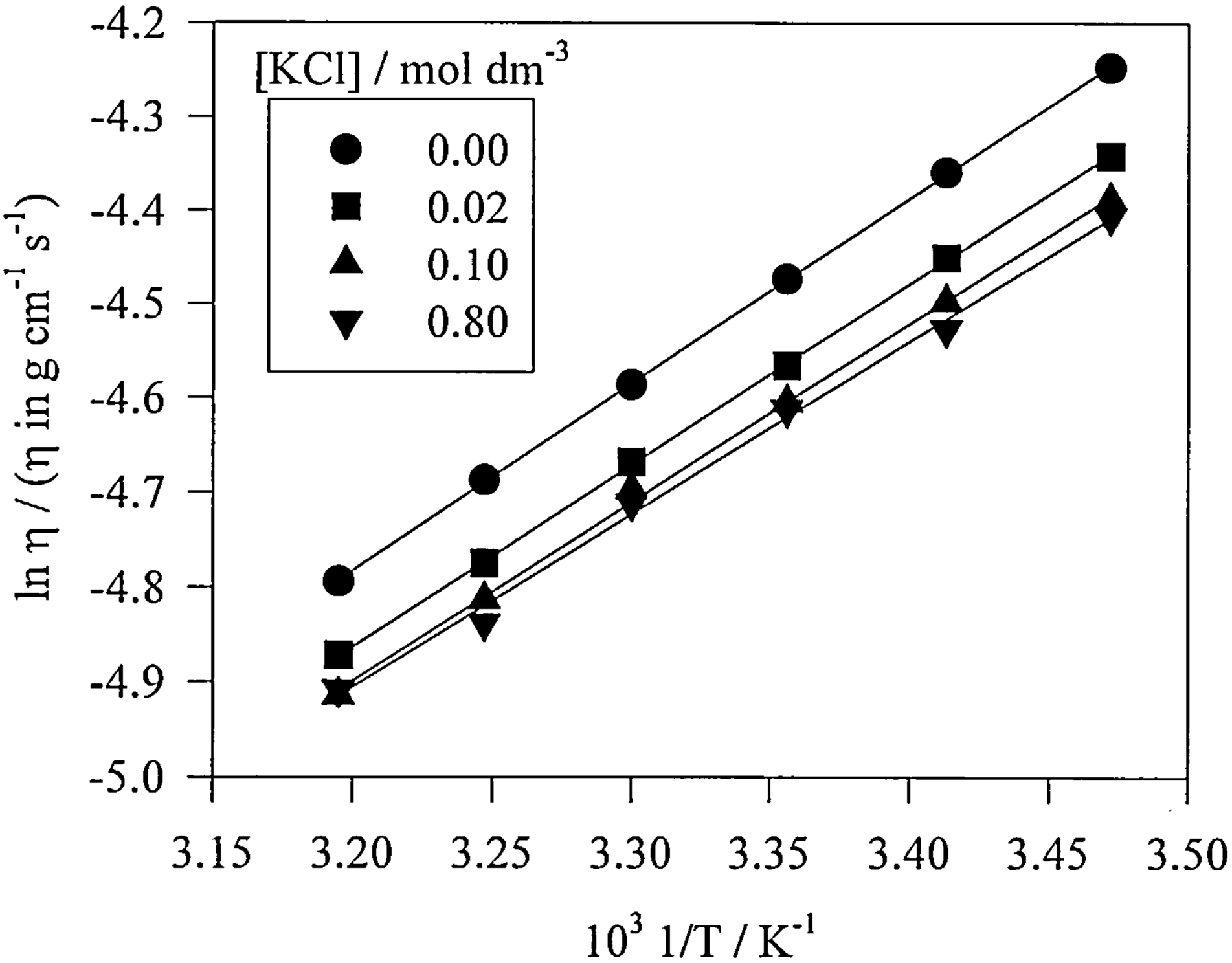

Appendix 4B.viii : Comparison between viscosity activation energy and interaction parameter

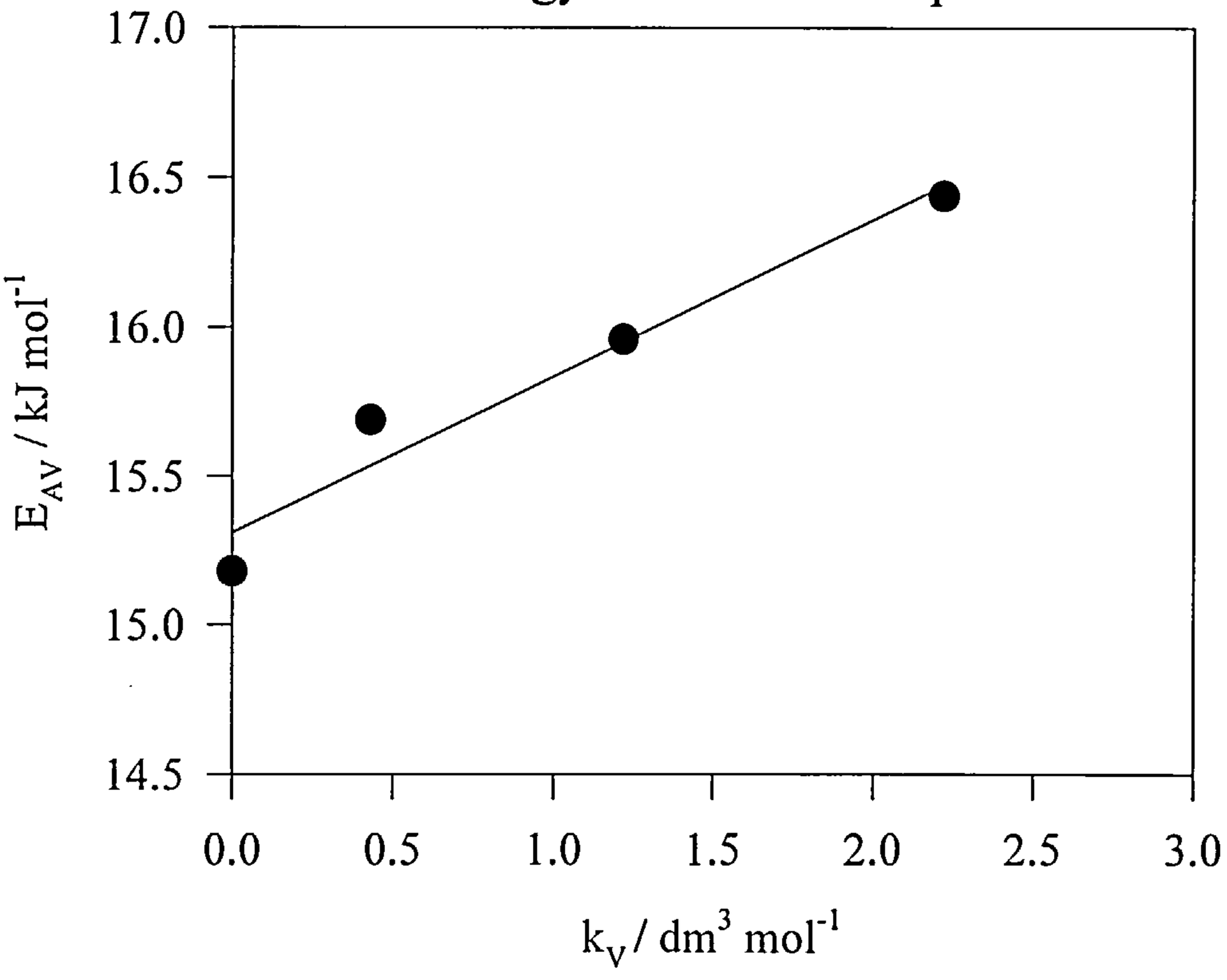

Appendix 4B.ix: Comparison between activation energies (viscosity and diffusion) with added KCl

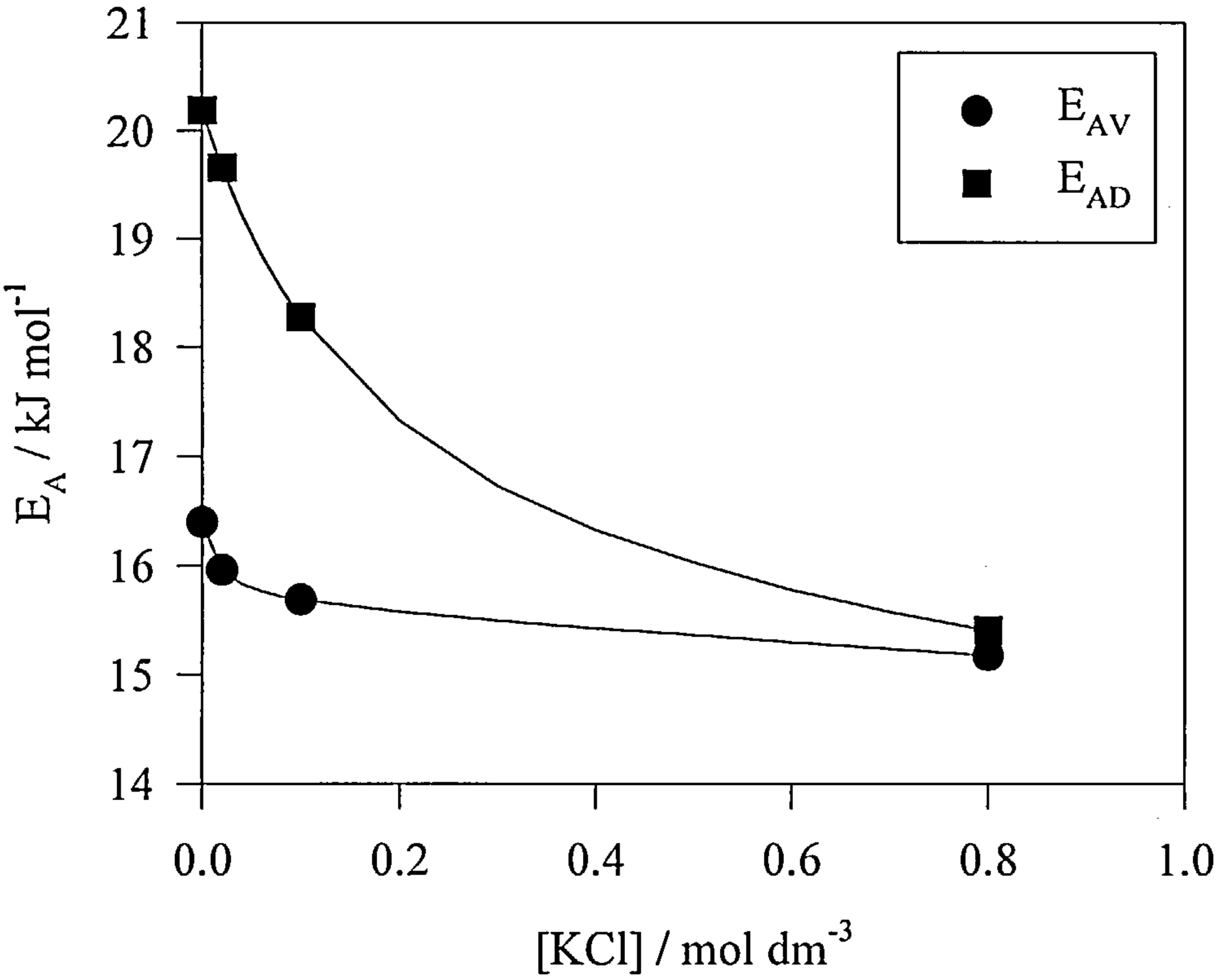

Chapter 4C: CTAC Self-Diffusion Coefficients (CV, CA)

4C.1 Introduction

In Chapter 4A and 4B, CTAC micelles were studied by rotating disk voltammetry and rheology. Inferences from the results led to significant observations on micellar size, growth and different modes of interaction. Both of these methods analysed micellar properties under flow, so it seemed astute to compare the results to those of micelles in a quiescent solution. With Triton X-100, differences in the self-diffusion coefficients were observed between rotating disk voltammetry, cyclic voltammetry and chronoamperometry. It was therefore important to determine whether any deviations were purely a function of the surfactant or if they were due to inherent properties of the technique. Cyclic voltammetry appears to be the most popular electrochemical method for measuring self-diffusion coefficients of CTA^+X^- micelles. Both CTAB[18,37] and CTAC[15,16,17] micellar solutions have been studied using the electroactive probes, ferrocene[15,18,37] and tetrathiofulvalene (TTF)[16,17]. Although a limited number of studies have used linear interaction theory to determine micellar size and interaction[15,37], analysis has been largely restricted to a single electrolyte concentration. Chronoamperometric studies of CTAC micelles, conversely, have not appeared in the literature.

This chapter will present the first exhaustive study of a CTAC micellar system under quiescent conditions over a range of electrolyte and surfactant concentrations. The micellar self-diffusion coefficients from CV and CA show a quadratic dependence on surfactant concentration and it followed that linear interaction theory could not be applied. Diffusion coefficients as determined by chronoamperometry displayed the same phenomenological behaviour with respect to [KCl] as both CV and RDV but with limited experimental accuracy.

4C.2 Results and Discussion

4C.2.1 General Electrochemistry (CV)

The self-diffusion coefficients of CTAC micelles were measured over a surfactant concentration range of 0.0625 - 0.2188 mol dm^{-3}. Initial experimentation at 0.0313 mol dm^{-3} resulted in irreproducible diffusion coefficients with large experimental errors due to the low Faradaic currents obtained from $3.13x10^{-4}$ mol dm^{-3} ferrocene. Therefore, at this low concentration, the extrapolation out of background capacitance currents was more difficult. It followed that the lower limit of the surfactant concentration was raised to 0.0625 mol dm^{-3} which lead to a shifting of the whole range to higher [CTAC]. The electrolyte concentration was varied from 0.00 - 0.80 mol dm^{-3} KCl.

It was observed from the RDV results that the half-wave potentials ($E_{1/2}$) from the voltammetric waves increased with surfactant concentration but were invariant with changes in electrolyte concentration (Ch. 4A.2.1). It was important to see if any major differences existed between $E_{1/2}$ values under stationary conditions compared to hydrodynamic conditions. $E_{1/2}$ is the mid point between the peak cathodic and anodic currents as shown in Ch. 4A.21. The values of $E_{1/2}$ as determined by cyclic voltammetry are shown in Table 4C.1.

Table 4C.1 : Variation of $E_{1/2}$ with surfactant and electrolyte concentration

[CTAC] / mol dm^{-3}	$E_{1/2}$ / mV with [KCl] / mol dm^{-3}			
	0.00	0.10	0.80	0.00 - 0.80
0.0625	221.0	226.5	221.3	222.9
0.0938	236.0	230.0	226.4	230.8
0.1563	239.0	244.0	237.7	240.2
0.2188	246.2	253.0	246.2	248.5

These values are plotted in Appendix 4C.i along with the half-wave potentials as determined by RDV (Ch. 4A.2.1). From Appendix 4C.i, it can be seen that the half-wave potentials are not a function of the technique and hence are not affected by the

absence or presence of hydrodynamic conditions. A similar increase in $E_{1/2}$ with [CTAC] was seen by Eddowes et al, although it was reported that $E_{1/2}$ (CV) > $E_{1/2}$ (RDV) by ~ 10 mV[17]. Nevertheless the experimental results presented here suggests that the interfacial region is not affected by electrode rotation. For Triton X-100 it was seen that a plot of $E_{1/2}$ against [TX-100] yielded a linear graph with a gradient of ~40 mV decade^{-1} (Ch. 3C.2.1). Appendix 4C.ii shows a plot of $E_{1/2}$ against [CTAC] resulting in a gradient of 50 mV decade^{-1}. This value is identical to that reported by Munoz et al. albeit for TX-100[19]. The results tend to confirm the observation that the increase in $E_{1/2}$ is due to increased surfactant adsorption resulting in inhibited electron transfer[19]. This was discussed in more detail in Ch. 3C.2.1. Another possibility is that an increase in $E_{1/2}$ with [CTAC] is due to a shift in the distribution of fc and fc^+, this was discussed in Ch. 4A.2.2.1.

The variation in half-wave potential has been attributed to inhibition of electron transfer from the solution to working electrode[19]. It is therefore of interest to analyse how the hetereogeneous rate constant (k^O) varies over the same electrolyte and surfactant concentrations. Cathodic-anodic peak-peak separations (ΔE_P) in cyclic voltammograms gives the unitless kinetic parameter (ψ) which can be used to determine k^O as a function of potential sweep rate (υ) from the expression[36]:-

$$k^0 = \psi\,[D_{fc}.\pi.\upsilon.(nF/RT)]^{1/2}.\,(D_{fc+}/D_{fc})^{\alpha/2} \qquad (4C.1)$$

D_{fc} and D_{fc+} are the diffusion coefficient of the ferrocene and ferricinium respectively in CTAC micelles and it was seen in Ch. 4A.2.2.2, that $D_{fc+} \approx 9.6\ D_{fc}$. It is usually assumed that the diffusion coefficients of the oxidised and reduced species are equal. However, in this case it is more applicable to use the gross fc^+ diffusion coefficient as the fc^+ quickly partitions to equilibrium concentrations[32] and reflects fc^+ mobility in both aqueous and micellar environments (Ch. 4A.2.2.2). α is the transfer coefficient and is usually assumed = 0.5. Table 4C.2 shows the variation of ψ with ΔE_P[77].

Table 4C.2 : Variation of kinetic parameter with peak-peak separation

ΔE_P / mV	ψ / no units	ΔE_P / mV	ψ / no units
60	19.00	69	2.51
61	11.50	70	2.26
62	8.40	75	1.51
63	6.45	80	1.14
64	5.10	85	0.92
65	4.30	90	0.77
66	3.63	95	0.65
67	3.16	100	0.57
68	2.81	105	0.50

Note : Data reproduced from reference 77

Although the above table shows values of ΔE_P between 60 - 105 mV, the peak-peak separations are typically between 60 - 80 mV. Appendix 4C.iii shows a set of typical cyclic voltammograms at different potential sweep rates from which ΔE_P and subsequently k^O can be calculated. To ensure that calculated values of k^O are real, uncompensated solution resistance, which would distort the voltammograms, must be negligible. As mentioned earlier, this is ensured by the use of a luggin capillary and the iR compensation function on the BAS CV-50W potentiostat. Table 4C.3 shows the calculated heterogeneous rate constants over a range of surfactant and electrolyte concentrations.

Table 4C.3 : Variation of hetereogeneous rate constant with electrolyte and surfactant concentration

[CTAC] / mol dm^{-3}	k^O / cm s^{-1} with [KCl] / mol dm^{-3}		
	0.00	0.10	0.80
0.0625	7.87×10^{-3}	0.028	0.069
0.0938	8.85×10^{-3}	0.040	0.014
0.1563	7.74×10^{-3}	0.023	0.021
0.2188	8.70×10^{-3}	0.040	0.017
Av. k^O / cm s^{-1}	8.29×10^{-3}	0.033	0.030

The general trends are that k^O increases with electrolyte concentration but remains relatively insensitive to surfactant concentration. This disagrees somewhat with reported results in which k^O was seen to increase with decreasing [CTAC][17].

However, Eddowes et al. attributed this behaviour to the partitioning of the tetrathiofulvalene (TTF) probe between micellar an aqueous phases[17] whereas it is known that ferrocene is negligibly soluble in water[15,37].

On increasing the electrolyte concentration from 0.00 - 0.10 mol dm^{-3} KCl, k^O is seen to increase approximately four-fold, yet from 0.10 - 0.80 mol dm^{-3} KCl there is relatively little change. In the absence of electrolyte it is likely that the surfactant is forming a bilayer[24] which is then displaced by the addition of KCl resulting in the increase in k^O.

Goldstein et al noted an increase in k^O for ferricyanide reduction with increasing [KBr] and attributed this to a greater concentration of Br^- adsorption at the electrode surface[31]. This observation may suggest that the invariance of k^O at [KCl] > 0.10 mol dm^{-3} is due to Cl^- ion saturation i.e. surfactant displacement of the electrode surface, in which case any further increase in [KCl] will not affect k^O.

The actual values of k^O, however, are in excellent agreement with literature for CTA^+X^- micelles; CTAB[37] $k^O = 0.018$ cm s^{-1} and CTAC[17] $k^O = 1.5x10^{-3}$ - 0.013 cm s^{-1}. The results, however, are at least an order of magnitude lower than those obtained in methanol by cyclic voltammetry[78]; $k^O = 0.178$ cm s^{-1}.

4C.2.2 Diffusion Coefficient Results (D_{CV})

A full set of cyclic voltammograms for 0.1563 mol dm^{-3} CTAC + 0.10 mol dm^{-3} KCl over a potential sweep rate (υ) of 20-150 mV s^{-1} are shown in Appendix 4C.iii. Appendix 4C.iv shows a series of Randles-Sevcik plots over a range of surfactant concentrations, each with (0,0) intercepts indicating a diffusionally controlled reversible one electron process. The experimental diffusion coefficients (D_{CV}) as determined from the Randles-Sevcik plots are shown in Table 4C.4 over a [CTAC] = 0.0625 - 0.2188 mol dm^{-3} and [KCl] = 0.00 - 0.80 mol dm^{-3}.

Table 4C.4 : Experimental D_{CV} results

[KCl] / mol dm^{-3}	10^7 D_{CV} / cm^2 s^{-1}			
	0.0625 mol dm^{-3} CTAC	0.0938 mol dm^{-3} CTAC	0.1563 mol dm^{-3} CTAC	0.2188 mol dm^{-3} CTAC
0.00	4.81	4.61	4.17	4.07
0.01	5.59	5.32	4.63	4.59
0.02	6.17	5.54	5.13	4.92
0.05	7.24	6.51	5.77	5.38
0.08	8.29	7.21	6.05	5.50
0.10	8.19	7.47	6.31	5.92
0.20	8.29	7.73	6.58	6.13
0.40	8.47	7.79	6.58	6.10
0.80	8.32	7.71	6.57	6.14

Note: standard error = $\pm 0.09x10^{-7}$ cm^2 s^{-1}; experiments repeated twice

Appendix 4C.v shows plots of D_{CV} against electrolyte concentration for each of the surfactant concentrations studied. The behaviour of D_{CV} can be seen to remain the same at each surfactant concentration, and therefore it is possible to mathematically fit the data. For RDV (Ch. 4A.2.3.1), the diffusion coefficient data was seen to fit a rational function, this is not the case here. The D_{CV} data fits a logistic model as described the expression:-

$$y = a / [1 + b.\exp(-cx)] \qquad (4C.2)$$

where y is the diffusion coefficient, x is the concentration of KCl and a, b and c are numerical constants. Excellent correlation coefficients were obtained (>0.994), the numerical constants are shown in Table 4C.5.

Table 4C.5 : Logistic function; numerical constants

Numerical constants	[CTAC] /mol dm^{-3}			
	0.0625	0.0938	0.1563	0.2188
a / cm^2 s^{-1}	$8.39x10^{-7}$	$7.76x10^{-7}$	$6.56x10^{-7}$	$6.11x10^{-7}$
b / no units	0.73	0.66	0.54	0.45
c / dm^3 mol^{-1}	35.97	26.21	27.10	23.26

The logistic fitted data is shown below in Table 4C.6. It can be seen that the fitted values only deviates from the experimental data, on average, by a small degree (~0.08×10^{-7} cm^2 s^{-1}) and this can be accounted for by experimental error.

Table 4C.6 : Logistic fitted diffusion coefficient data

[KCl] / mol dm^{-3}	$10^7 D_{CV}$ / cm^2 s^{-1}			
	0.0625 mol dm^{-3} CTAC	0.0938 mol dm^{-3} CTAC	0.1563 mol dm^{-3} CTAC	0.2188 mol dm^{-3} CTAC
0.00	4.84	4.69	4.25	4.22
0.01	5.53	5.16	4.64	4.51
0.02	6.15	5.59	4.99	4.77
0.05	7.44	6.60	5.75	5.36
0.08	8.03	7.18	6.17	5.72
0.10	8.21	7.41	6.33	5.86
0.20	8.39	7.74	6.54	6.09
0.40	8.39	7.76	6.56	6.11
0.80	8.39	7.76	6.56	6.11

This data is plotted as a curve overlaying the experimental data in Appendix 4C.v.

4C.2.2.1 D_{CV} - Results Analysis

It has been shown in Ch. 4A.2.3 that there is a linear decrease in diffusion coefficient (D_{RDV}) with an increase in surfactant concentration. However, considering Appendix 4C.vi, it can be seen that no such relationship exists for the diffusion coefficient as determined by cyclic voltammetry (D_{CV}). A similar trend was observed for TX-100 where a linear trend was apparent for D_{RDV} (Ch. 3A.2.2.1) but not for D_{CV} (Ch. 3C.2.2.1). Nevertheless linear interaction theory was applied to a small section of the D_{CV} vs. [TX-100] graph, yielding apparent hydrodynamic radii and interaction parameters (Ch. 3C.2.2.1).

For the results presented here no such region is obvious and therefore another method of analysis needs to be applied. In certain cases a reciprocal relationship has been used from which values for R_H^O and k_D were obtained[15,79].

$$D_{CV} = D_{CV}^{O} / [1 + k_D.(C_S\text{-c.m.c})] \qquad (4C.3)$$

If this approach is adopted here, plots of D_{CV}^{-1} against [CTAC] should yield linear relationships as shown in Appendix 4C.vii. Correlation coefficients ≈ 0.98 were obtained, which although may not be as high as desired, still give apparent values for R_H^O and k_D. Table 4C.7 displays these values as a function of electrolyte concentration.

Table 4C.7 : Reciprocal extrapolation results

[KCl] / mol dm^{-3}	10^7 D^O_{CV} / cm^2 s^{-1}	R_H^O / nm	k_D / dm^3 mol^{-1}
0.00	5.13	4.17	1.08
0.01	5.95	3.60	1.58
0.02	6.76	3.17	2.01
0.05	8.48	2.52	2.79
0.08	9.30	2.30	2.99
0.10	9.56	2.24	3.00
0.20	9.79	2.18	2.91
0.40	9.79	2.18	2.87
0.80	9.79	2.18	2.87

Values for the hydrodynamic radii (R_H^O) and interaction parameter (k_D) are plotted along with those corresponding as determined by RDV in Appendices 4C.viii and 4C.ix respectively.

The hydrodynamic radii as determined by CV show the same initial trend as RDV. The decrease in R_H^O is attributed to collapse of the double layer towards the micellar surface as was discussed in Ch. 4A and 4B. As the concentration of electrolyte is increased above ~ 0.05 mol dm^{-3} there is deviation in R_H^O (CV) from R_H^O (RDV). With RDV the increase in R_H^O at [KCl] > 0.10 mol dm^{-3} was seen to be due to radial micellar expansion due to an increase in aggregation number (Ch. 4A.2.3.3). With CV, however, R_H^O remains constant at [KCl] > 0.20 mol dm^{-3} which not only contradicts the results from RDV but is also in disagreement with micellar sizes from surfactant volume considerations[7]. The suggestion is that at [KCl] ≥ 0.05 mol dm^{-3} CV is over estimating D_S^O, which may indicate the presence of pre-

concentrated probe at the electrode surface[80]. This was also evident for the attenuated D_{CV} values in comparison to D_{RDV} for Triton X-100 (3C.2.2.1) leading to differences between R_H^O (CV) and R_H^O (RDV).

Appendix 4C.ix shows a comparison between intermicellar interaction parameters as determined by CV and RDV. The exponential type behaviour for k_D (RDV) is seen to be inverted for k_D (CV) which contradicts the expected trend for decreased electrostatic repulsion on addition of electrolyte[2,3,4,8,9,39,40,41]. With Triton X-100 inverted behaviour was also observed, which suggests that the effect is not confined to one surfactant type. Again, an explanation for the inverted behaviour is totally unclear and therefore further analysis will not be attempted.

The possibility of probe pre-concentration and two diffusional regimes means that cyclic voltammetry is not an appropriate method for determining micellar structural and interaction behaviour.

4C.2.3 Effect of Temperature

In Ch. 4A.2.4, the diffusional activation energies (E_{AD}) of a series of CTAC micellar solutions were determined by Arrhenius analysis. E_{AD} was shown to be linearly related to the diffusional interaction parameter as determined by RDV. Rather than initiating a full study of activation energies from CV measurements, E_{AD} was calculated at a single electrolyte concentration to observe whether agreement between E_{AD} (CV) and E_{AD} (RDV) existed. The diffusion coefficients were measured over 15 - 40 ^{O}C with [CTAC] = 0.1563 mol dm^{-3}, [KCl] = 0.10 mol dm^{-3}; the results are presented in Table 4C.8.

Table 4C.8 : Diffusion coefficient variation with temperature and corresponding Arrhenius parameters

T / ^{O}C	10^{7} D_{CV} / cm^{2} s^{-1}	10^{3} 1/T / K^{-1}	ln (D_{CV}) / (D_{CV} in cm^{2} s^{-1})
15	5.06	3.472	-14.497
20	6.11	3.413	-14.308
25	7.35	3.356	-14.123
30	8.47	3.300	-13.982
35	10.05	3.247	-13.811
40	11.09	3.195	-13.712

Appendix 4C.x shows the Arrhenius plot from which an diffusional activation energy (E_{AD}) = 23.86 kJ mol^{-1} was obtained. This is in comparison with E_{AD} (RDV) = 18.27 kJ mol^{-1}. Although the values are not identical the difference may be explained by the larger concentration of CTAC used in CV than RDV i.e. 0.1563 and 0.0938 mol dm^{-3} respectively. Nevertheless, the experiment shows that Arrhenius behaviour for CTAC micelles is observed under quiescent conditions as well as hydrodynamic flow.

In Ch. 4C.2.1, the heterogeneous rate constant (k^{O}) was seen to be insensitive to changes in surfactant concentration but was affected by an increase in electrolyte concentration. A single surfactant and electrolyte concentration was selected to analyse how k^{O} varied with temperature. Determination of k^{O} was carried out as was described in Ch. 4C.2.1 using Equation 4C.1 over a temperature range of 15 - 40 ^{O}C. It was found that k^{O} = 0.019 ± 0.001 cm s^{-1} and it came of a great surprise that k^{O} appeared to remain constant with temperature. Zhou et al. observed k^{O} to increase by nearly an order of magnitude from 15 - 35 ^{O}C for ferrocene oxidation in PEG.$MClO_4$ (M = cation) polyelectrolyte[81]. The magnitude of the reported k^{O} values ($6x10^{-4}$ - $2x10^{-3}$ cm s^{-1}) suggests that any increase in k^{O} for the micellar solution used here should have been detected[81] in accordance with the expression[36]:-

$$\ln k^{O} = \ln A - E_A / RT \qquad (4C.4)$$

It is known, however, that k^O is sensitive to a number of factors including adsorption of electrolyte anion on the electrode[31] and surfactant adsorption[78], despite these influences an increase in k^O with temperature would still be expected. It is possible that a number of factors are combining to conceal the true heterogeneous rate constant, though nothing can be conclusively stated from the presented results.

4C.2.4 Chronoamperometry

It was noted in Ch. 3C.2.3, that the time range for Cottrell analysis was of paramount importance when determining the diffusion coefficient. A number of ranges were analysed in terms of correlation coefficient, Cottrell gradient (i_t vs. $t^{-1/2}$) and intercept from the Faradaic response of a 0.1563 mol dm^{-3} CTAC solution (Appendix 4C.xi). The results are displayed in Table 4C.9 and in Appendices 4C.xii, 4C.xiii and 4C.xiv respectively.

Table 4C.9 : Variation of correlation coefficient, gradient and intercept with time analysis range used

t range / s	Corr. coeff.	10^6 Gradient / A $s^{1/2}$	10^7 Intercept / A
0 - 1	0.9745	7.94	-41.53
1 - 2	0.9897	4.78	-1.73
2 - 3	0.9989	4.46	+0.60
3 - 4	0.9990	4.38	+1.05
4 - 5	0.9977	4.31	+1.36
5 - 6	0.9960	4.47	+0.64
6 - 7	0.9879	4.51	+0.50
7 - 8	0.9867	4.71	-0.22

It can be seen that the correlation coefficient reaches the highest values between 2 - 5 s with the gradient and intercept achieving limiting values over the same range. This justifies the use of a time range of 2 - 5 s for the Cottrell analysis and is also in agreement with the time range as determined for a Triton X-100 solution (Ch. 3C.2.4). The Cottrell plot for 0.1563 mol dm^{-3} CTAC is shown in Appendix 4C.xv.

4C.2.5 Diffusion Coefficient Results (D_{CA})

The diffusion coefficients (D_{CA}) were measured over 0.0313 - 0.1563 mol dm^{-3} CTAC and 0.00 - 0.80 mol dm^{-3} KCl. As was mentioned in Ch. 2.1.4, two current response traces are required, the experimental and firstly the background. Table 4C.10 and Appendix 4C.xvi shows the background Cottrell gradients as determined from a plot of i_t vs. $t^{-1/2}$ over a time analysis range of 2 - 5 s.

Table 4C.10 : Variation of background gradients with [KCl] and [CTAC]

[KCl] / mol dm^{-3}	10^6 Background gradients / A $s^{1/2}$		
	0.0313 mol dm^{-3} CTAC	0.0938 mol dm^{-3} CTAC	0.1563 mol dm^{-3} CTAC
0.00	1.25	1.42	1.61
0.01	1.36	1.50	1.67
0.01	1.45	1.57	1.72
0.05	1.68	1.76	1.86
0.08	1.85	1.91	1.99
0.10	1.95	1.99	2.07
0.20	2.30	2.31	2.34
0.40	2.73	2.75	2.90
0.80	3.38	3.49	3.76

Note : standard error $\pm 0.04x10^{-6}$ A $s^{1/2}$, except for 0.0313 mol dm^{-3} CTAC + 0.40 - 0.80 mol dm^{-3} KCl where error $\pm 0.45x10^{-6}$ A $s^{1/2}$.

The experimental traces with the presence of ferrocene probe for the above solutions were then recorded. The experimental Cottrell gradients are shown in Table 4C.11 and in Appendix 4C.xvii

Table 4C.11 : Variation of experiment gradients with [KCl] and [CTAC]

[KCl] / mol dm^{-3}	10^6 Experimental gradients / A $s^{1/2}$		
	0.0313 mol dm^{-3} CTAC	0.0938 mol dm^{-3} CTAC	0.1563 mol dm^{-3} CTAC
0.00	2.79	4.40	6.05
0.01	2.91	4.62	6.29
0.02	3.01	4.79	6.47
0.05	3.26	5.11	6.81
0.08	3.44	5.29	7.01
0.10	3.54	5.38	7.11
0.20	3.84	5.68	7.42
0.40	4.35	6.06	7.80
0.80	5.09	6.73	8.45

Note : standard error = ± 0.03 x 10^{-6} A $s^{1/2}$, except for 0.0313 mol dm^{-3} CTAC + 0.40 - 0.80 mol dm^{-3} KCl where error ± 0.12x10^{-6} A $s^{1/2}$.

Subtracting the background and aqueous phase ferrocene (1.247x10^{-7} A $s^{1/2}$) from the experimental gradients leads to the true Cottrell gradients due purely to the Faradaic current response from ferrocene oxidation. These are shown in Table 4C.12 and Appendix 4C.xviii.

Table 4C.12 : Variation of true Cottrell gradients with [KCl] and [CTAC]

[KCl] / mol dm^{-3}	10^6 True Cottrell gradients / A $s^{1/2}$		
	0.0313 mol dm^{-3} CTAC	0.0938 mol dm^{-3} CTAC	0.1563 mol dm^{-3} CTAC
0.00	1.41	2.85	4.31
0.01	1.43	3.00	4.50
0.02	1.44	3.09	4.63
0.05	1.45	3.22	4.83
0.08	1.46	3.26	4.90
0.10	1.46	3.27	4.92
0.20	1.47	3.24	4.90
0.40	1.49	3.18	4.77
0.80	1.59	3.11	4.56

Note : standard error = ± 0.07 x 10^{-6} A $s^{1/2}$, except for 0.0313 mol dm^{-3} CTAC + 0.40 - 0.80 mol dm^{-3} KCl where error ± 0.27x10^{-6} A $s^{1/2}$.

It is obvious that the errors in the gradient measurements are significantly lower than those experienced for Triton X-100 (Ch. 3C.2.4). However, at 0.0313 mol dm^{-3} CTAC and 0.40 - 0.80 mol dm^{-3} KCl, the total error due to the additive affect of both the experimental and background gradients, is approximately twice as large than at other surfactant and electrolyte concentrations. This reasons for this is unclear but is probably a function of the lower Faradaic current obtained due to the proportionally lower ferrocene concentration present i.e. [CTAC] α [fc].

Using the gradients shown in Table 4C.12 the diffusion coefficients can be calculated from Equation 1.24 in Ch. 2.1.2. CA values are shown in Table 4C.13 and plotted against [KCl] in Appendix 4C.xix.

Table 4C.13 : Experimental D_{CA} results

[KCl] / mol dm^{-3}	$10^7 D_{CA}$ / cm^2 s^{-1}		
	0.0313 mol dm^{-3} CTAC	0.0938 mol dm^{-3} CTAC	0.1563 mol dm^{-3} CTAC
0.00	13.75	6.24	5.14
0.01	14.03	6.91	5.60
0.02	14.22	7.34	5.93
0.05	14.57	7.97	6.44
0.08	14.73	8.16	6.63
0.10	14.77	8.20	6.68
0.20	13.82	8.07	6.63
0.40	15.38	7.77	6.31
0.80	17.47	7.42	5.75

Note : standard error = $\pm$ 0.29 x 10^{-7} A $s^{1/2}$, except for 0.0313 mol dm^{-3} CTAC + 0.40 - 0.80 mol dm^{-3} KCl where error $\pm$0.70x10^{-7} A $s^{1/2}$

4C.2.5.1 D_{CA} - Results Analysis

The first point to note from the diffusion coefficient results (Appendix 4C.xix) is that the D_{CA} values for 0.0313 mol dm^{-3} are much higher than might be expected when compared to D_{CA} at 0.0938 and 0.1563 mol dm^{-3} CTAC (see Table 4C.13). This can be partly explained by the large experimental errors that exist at 0.40, 0.80

mol dm^{-3} KCl and that the *percentage* errors will be approximately 3 - 5 times higher than at the other [CTAC]. Nevertheless, the diffusion coefficients at 0.0938 and 0.1563 mol dm^{-3} CTAC exhibit the same behaviour that was seen with D_{RDV} (Ch. 4A.2.3). Once again, the initial increase is attributed to decreased electrostatic repulsion[1,2,3,12,40] and the increase to spherical micellar expansion[2,5,7]. However, despite the lack of experimental precision, it is surprising how well the data fits the same mathematical expression that was used to model D_{RDV} data (a rational function). D_{CA} data function at 0.0938 and 0.1563 mol dm^{-3} CTAC is fitted to a rational function (Ch. 4A.2.3, Equation 4A.5) with the resulting numerical constants shown in Table 4C.14.

Table 4C.14 : Rational function; numerical constants

Numerical Constants	[CTAC] / mol dm^{-3}	
	0.0938	0.1563
a / cm^2 s^{-1}	6.20×10^{-7}	5.11×10^{-7}
b / dm^3 mol^{-1}	3.90×10^{-5}	2.23×10^{-5}
c / dm^3 mol^{-1}	44.59	30.18
d / dm^6 mol^{-2}	10.52	10.93

This rational function fitted data is plotted is Appendix 4C.xx along with the respective diffusion coefficients as determined by RDV (Ch. 4A.2.3) and CV (Ch. 4C.2.2) for 0.1563 mol dm^{-3} CTAC. With both D_{RDV} and D_{CA} exhibiting behaviour that fits a rational function it seemed prudent to check if the data was related to any extent. Doherty et al. related diffusion coefficient data as determined by CV and RDV by using the following expression which is adapted here[15]:-

$$D_{CA} = D_{RDV} \{1 + k_h [CTAC]\} \qquad (4C.5)$$

where k_h is defined as the hydrodynamic interaction parameter. Ratios of D_{CA} / D_{RDV} are found to be constant at 1.29 ± 0.06 for each electrolyte concentration. This is an excellent correlation considering the experimental error that exists for D_{CA} measurements. This ratio leads to k_h = 13.75 and 8.25 dm^3 mol^{-1} at 0.0938 and

0.1563 mol dm^{-3} CTAC respectively, these values are in good agreement with literature[15].

The relationship between D_{CA} and D_{RDV} may suggest that there are two diffusional regimes occurring at the electrode surface causing an attenuation of D_{CA} data[82]. Dr. P.Birkin is currently analysing the presented data to check whether it conforms to his theoretical model[83].

4C.3 Summary

Cyclic voltammetry has been used to accurately / precisely determine the self-diffusion coefficients of CTAC micelles over a range of electrolyte an surfactant concentrations. Analysis of the cyclic voltammograms yielded the half-wave potentials ($E_{1/2}$) for the ferrocene / ferricinium redox couple as a function of [CTAC] and [KCl]. $E_{1/2}$ was seen to increase with surfactant concentration with values identical to those determined by RDV and was attributed to an inhibitory affect on the electron transfer process. $E_{1/2}$ remained constant with changes in [KCl] which, as for RDV, indicated that no significant micellar growth other than radial micellar expansion. Analysing the peak-peak separation of cyclic voltammograms over a range of potential sweep rates led to the determination of the heterogeneous rate constant (k^O). k^O was observed to remain invariant with changes in surfactant concentration but was modified by electrolyte. At 0.00 - 0.10 mol dm^{-3} KCl, k^O increased approximately four-fold yet remained insensitive from 0.10 - 0.80 mol dm^{-3} KCl. This was believed to be due to a saturation process occurring when the Cl^- concentration reached maximum value at 0.10 mol dm^{-3}.

The micellar diffusion coefficients (D_{CV}) were seen to behave in a similar fashion to those determined by RDV. D_{CV} increased sharply from 0.00 - 0.10 mol dm^{-3} but remained constant above 0.20 mol dm^{-3} KCl, which suggested a reduction in Coulombic repulsion but no spherical micellar expansion. The D_{CV} data fits a

logistic function rather than the rational function as in D_{RDV}. The data could not be interpreted in terms of linear interaction theory as no such linear D_{CV} vs. [CTAC] plot was obtained. However, a reciprocal relationship was applied and yielded approximately linear graphs resulting in apparent values for R_H^O and k_D.

Values for R_H^O as determined from CV were found to exhibit the same initial drop as seen with R_H^O (RDV). Whereas with R_H^O (RDV) a subsequent increase was observed due to micellar expansion, no such increase was seen for R_H^O (CV). The interaction parameter (k_D) behaviour was seen to be inverted when compared to k_D (RDV). As well as contradicting the RDV findings, k_D (CV) also counter theory in which k_D should decrease due to a reduction in electrostatic repulsion on addition of electrolyte.

The diffusional activation energy of a CTAC micellar solution was calculated using diffusion coefficient measurements from CV. E_{AD} (CV) was seen to be higher than E_{AD} (RDV), but this was believed to be due to the higher surfactant concentration used in CV than in RDV (0.1563 vs. 0.0938 mol dm^{-3} CTAC). The data, however, showed that CTAC micellar solutions exhibited Arrhenius behaviour both under stationary and hydrodynamic conditions.

Chronoamperometry was used to determine CTAC micellar self-diffusion coefficients but with errors greater than those from CV and RDV. D_{CA} values at 0.0313 mol dm^{-3} CTAC were much higher than expected when compared to the other two surfactant concentrations. However, the D_{CA} values at 0.0938 and 0.1563 mol dm^{-3} CTAC exhibited behaviour that was analogous to D_{RDV} with increasing electrolyte concentration. It followed that the D_{CA} values were simulated by fitting with a rational function. Comparing D_{CA} to D_{RDV} showed that D_{CA} was constantly higher than D_{RDV} by a factor of ~ 1.30 over all electrolyte concentrations. Using a virial expansion hydrodynamic interaction parameters (k_h) were found to be 13.75 and 8.25 dm^3 mol^{-1} at 0.0938 and 0.1563 mol dm^{-3} CTAC respectively.

Appendix 4C.i : Variation of half-wave potential with [CTAC]

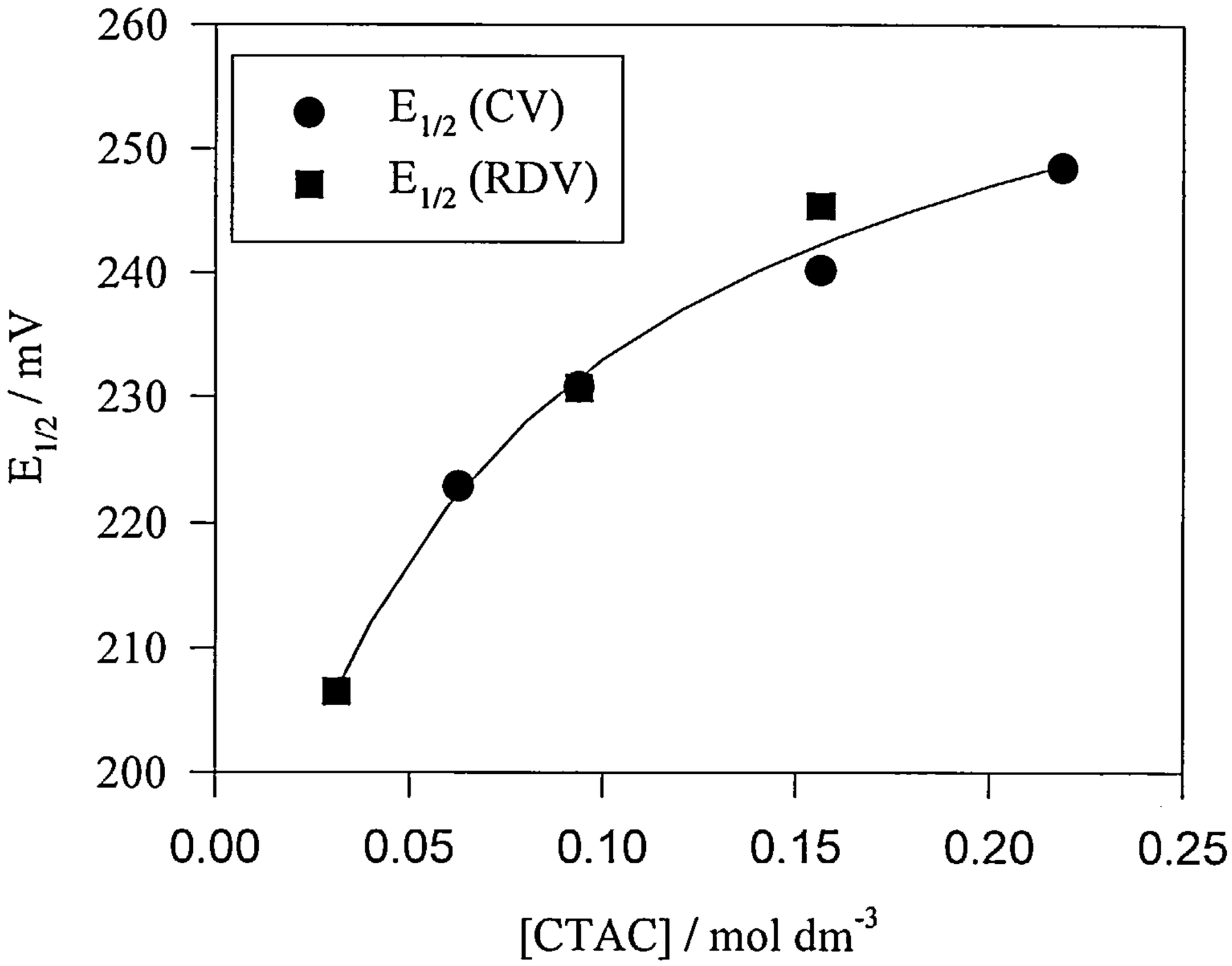

Appendix 4C.ii : Variation of half-wave potential with $\log_{10}$[CTAC]

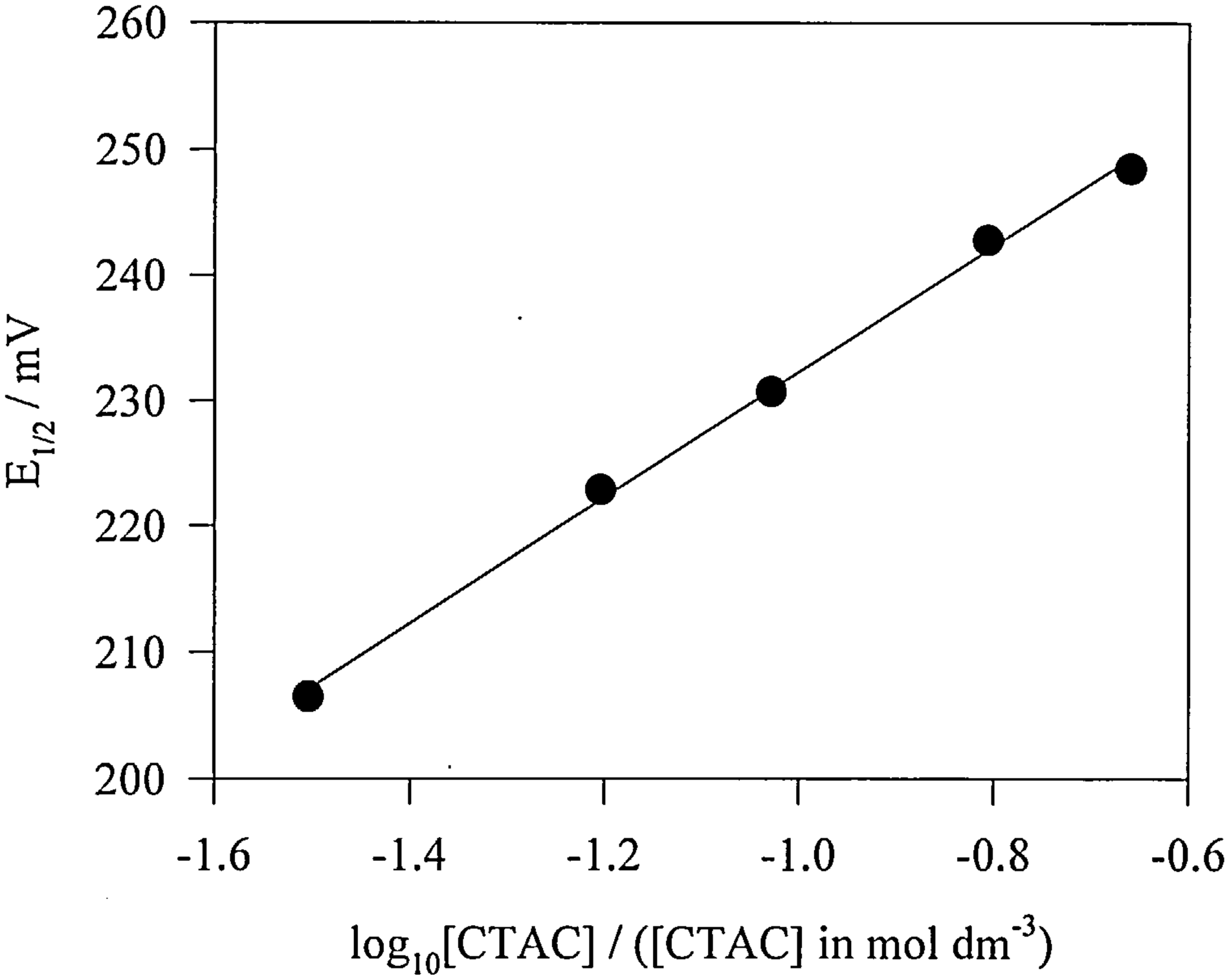

Appendix 4C.iii : Typical cyclic voltammograms @20^{o}C
(0.1563 mol dm^{-3} CTAC + 0.10 mol dm^{-3} KCl)

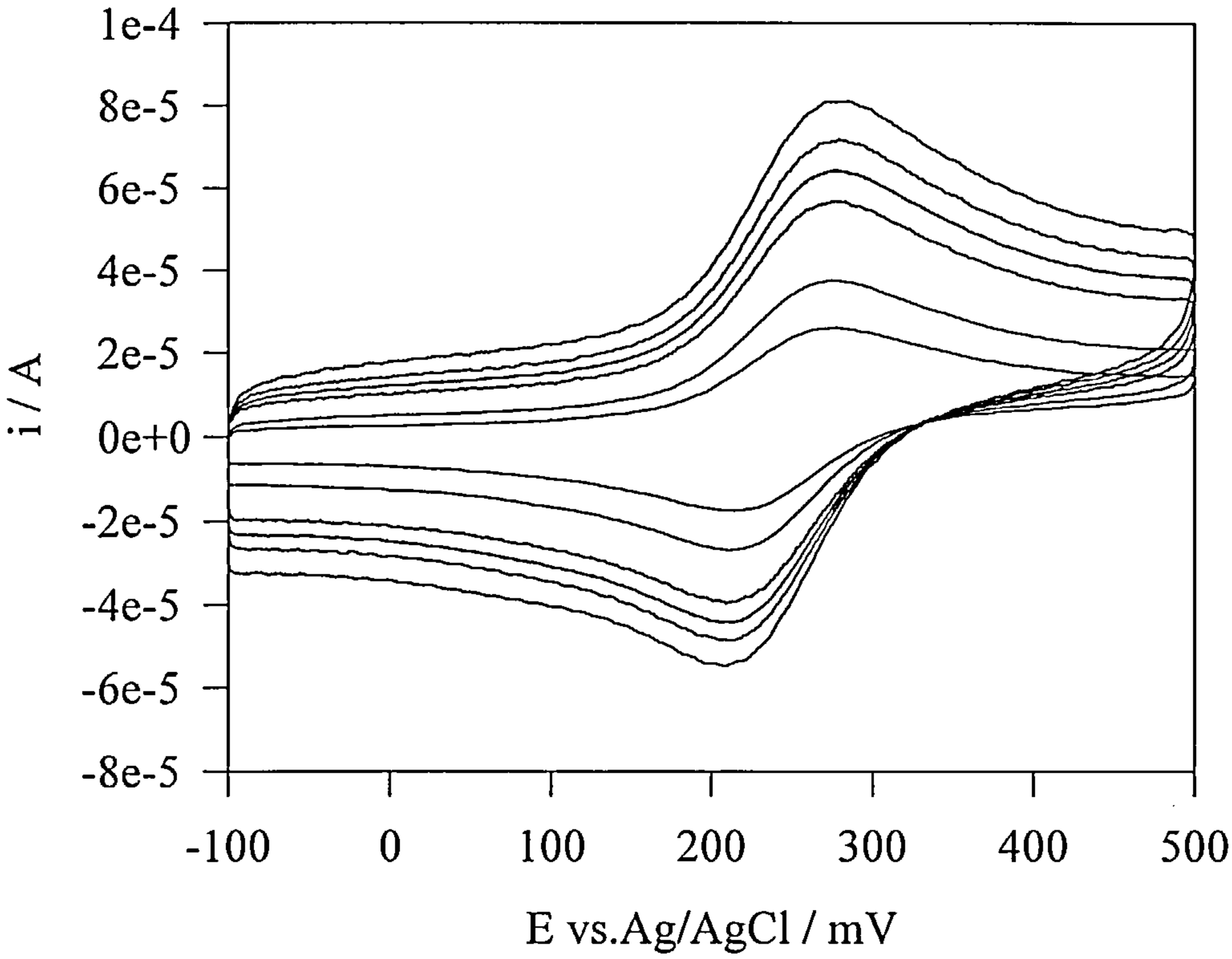

Appendix 4C.iv : Examples of Randles-Sevcik plots (i_p vs $\upsilon^{1/2}$)
(CTAC + 0.10 mol dm^{-3} KCl)

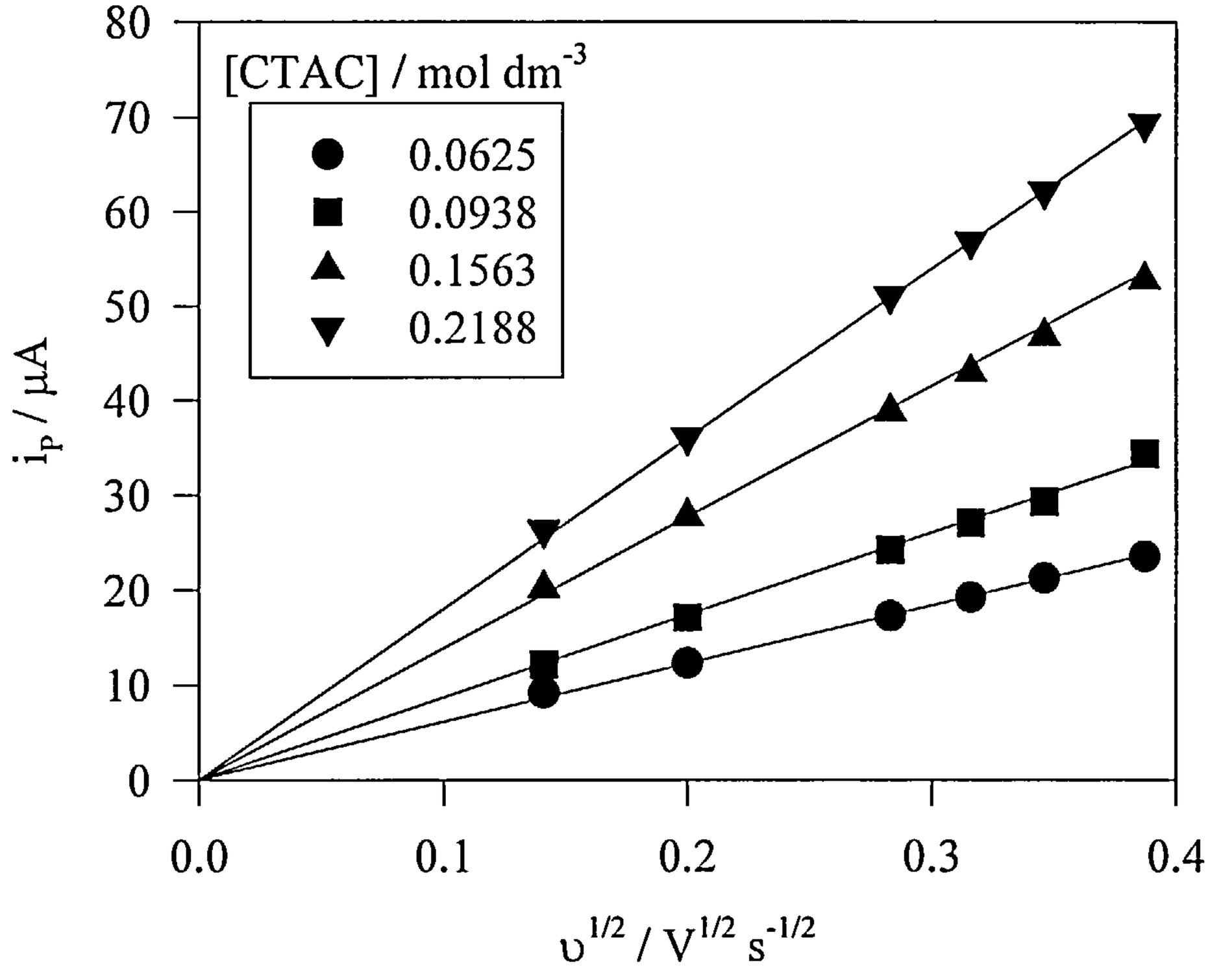

Appendix 4C.v: Diffusion coefficient variation with [KCl]
(Experimental data + fitted logistic curve)

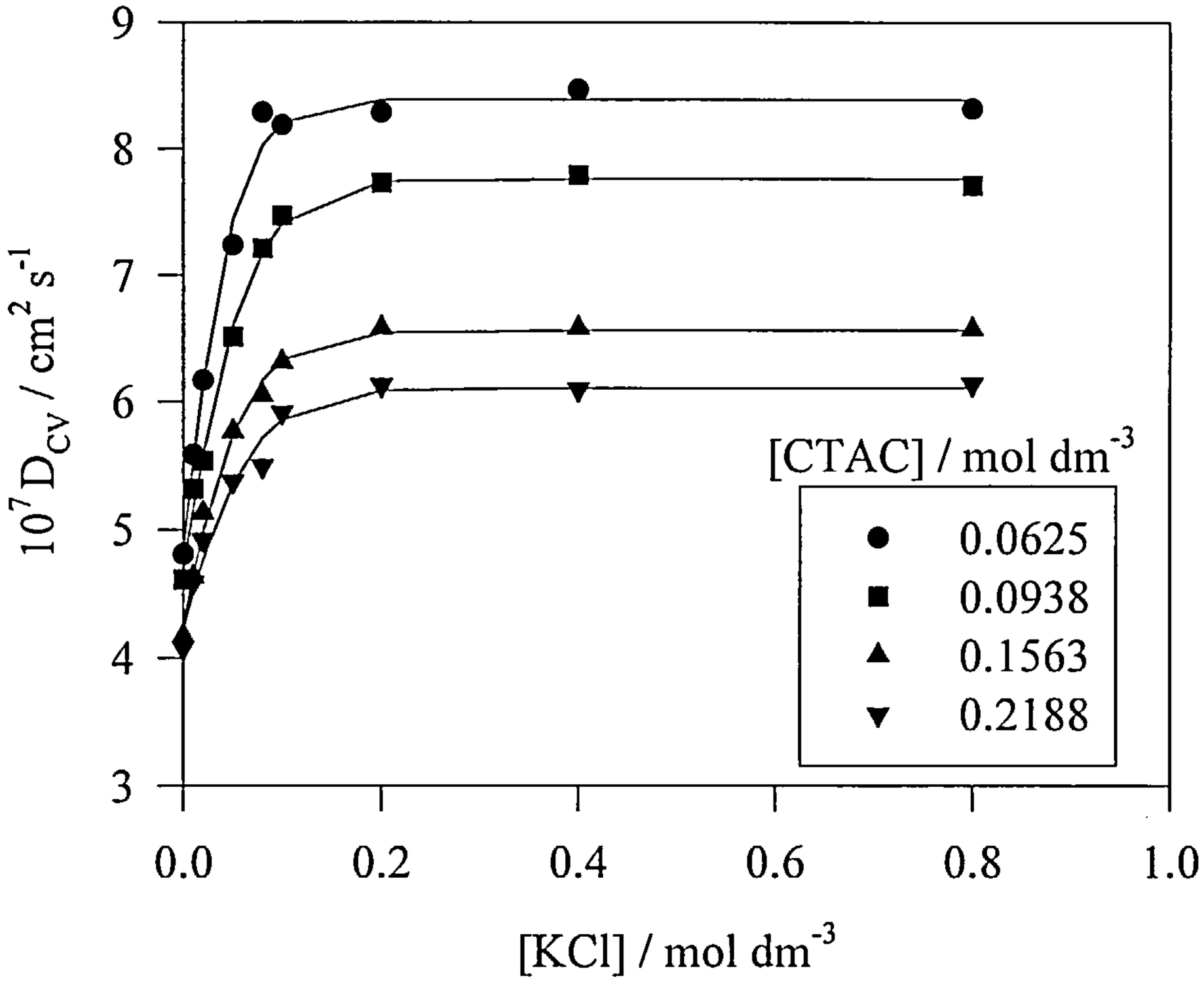

Appendix 4C.vi : Diffusion coefficient variation with CTAC
-effect of added KCl-

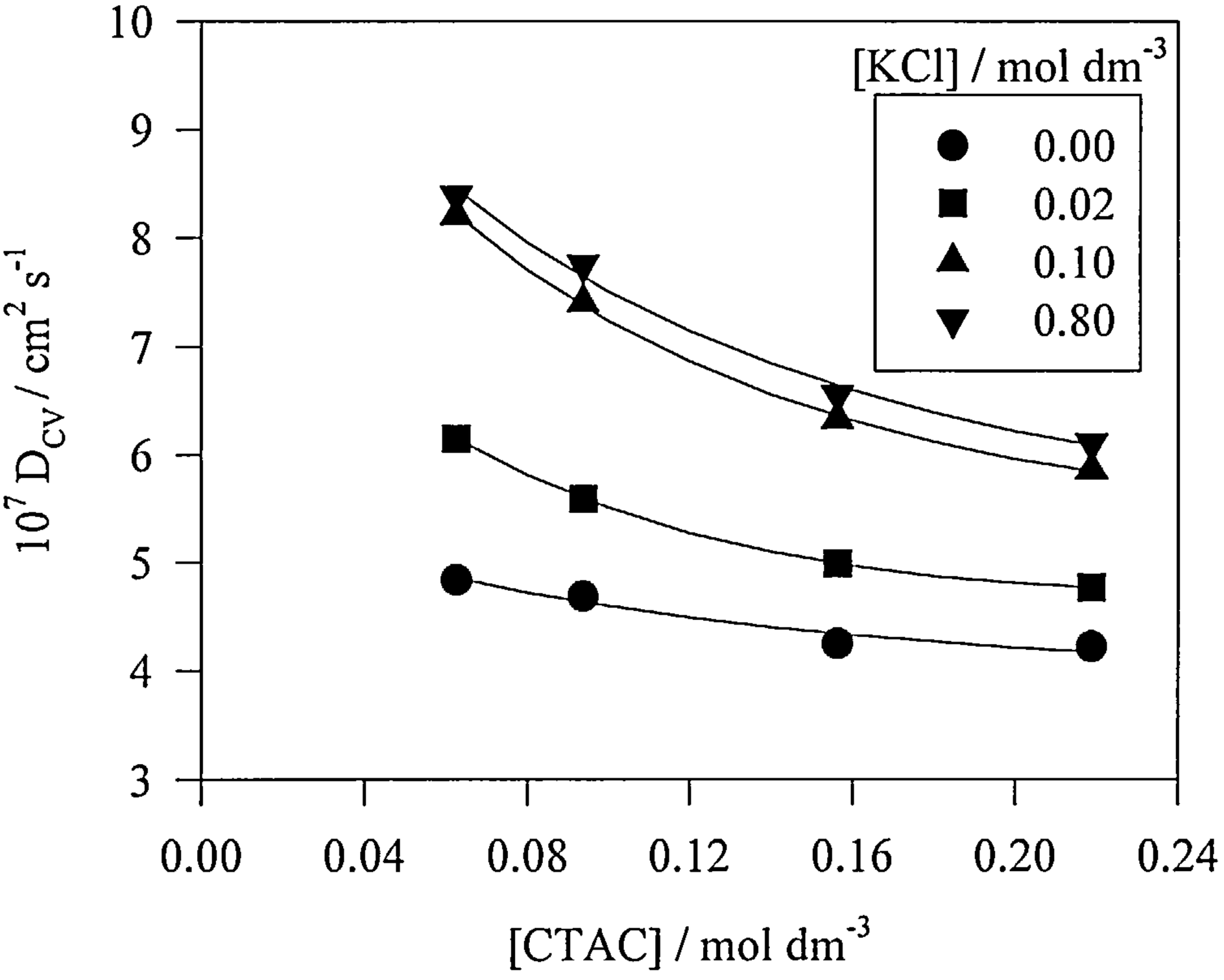

Appendix 4C.vii : Reciprocal diffusion coefficient variation with surfactant concentration

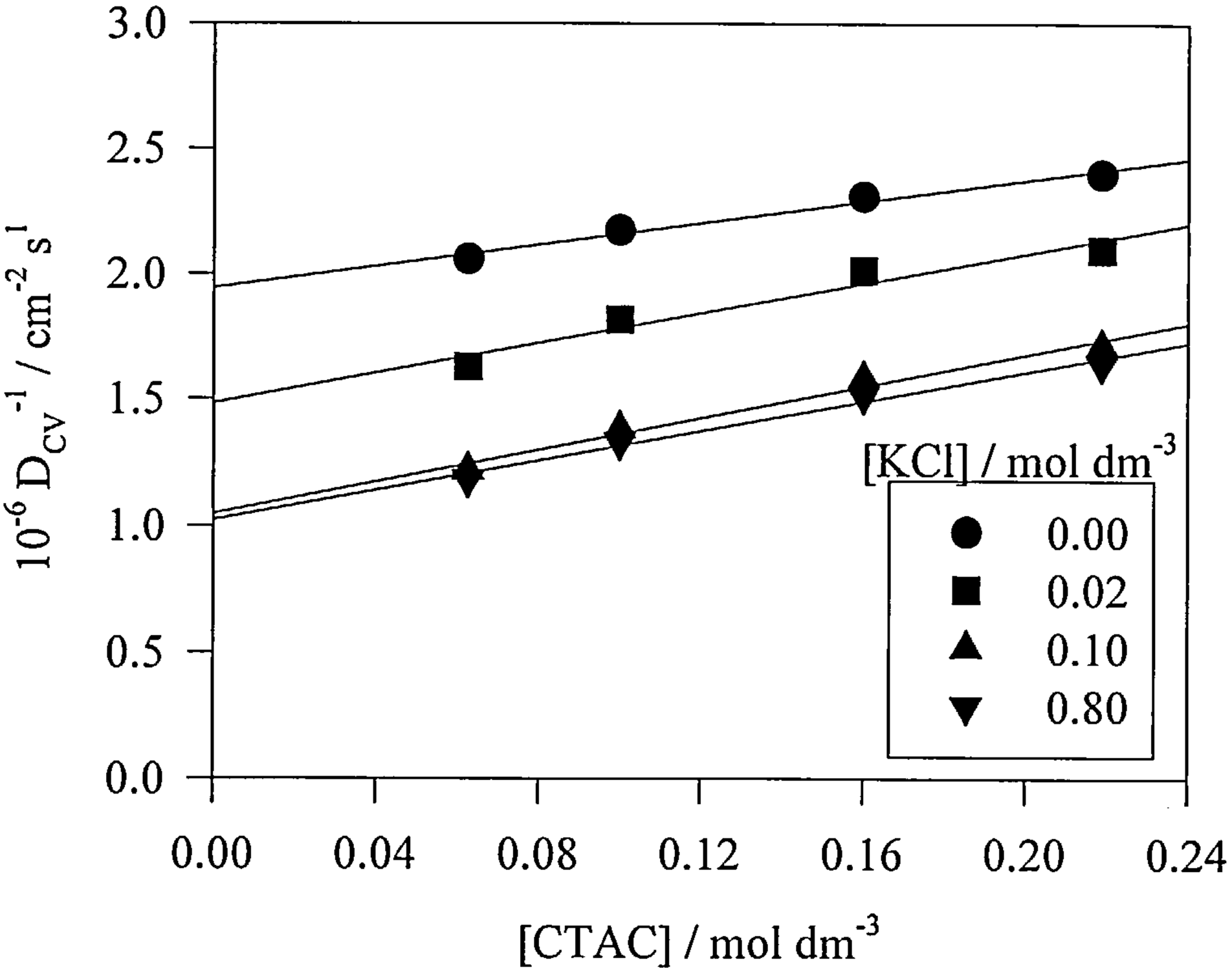

Appendix 4C.viii : Variation of hydrodynamic radius with [KCl] for CV and RDV

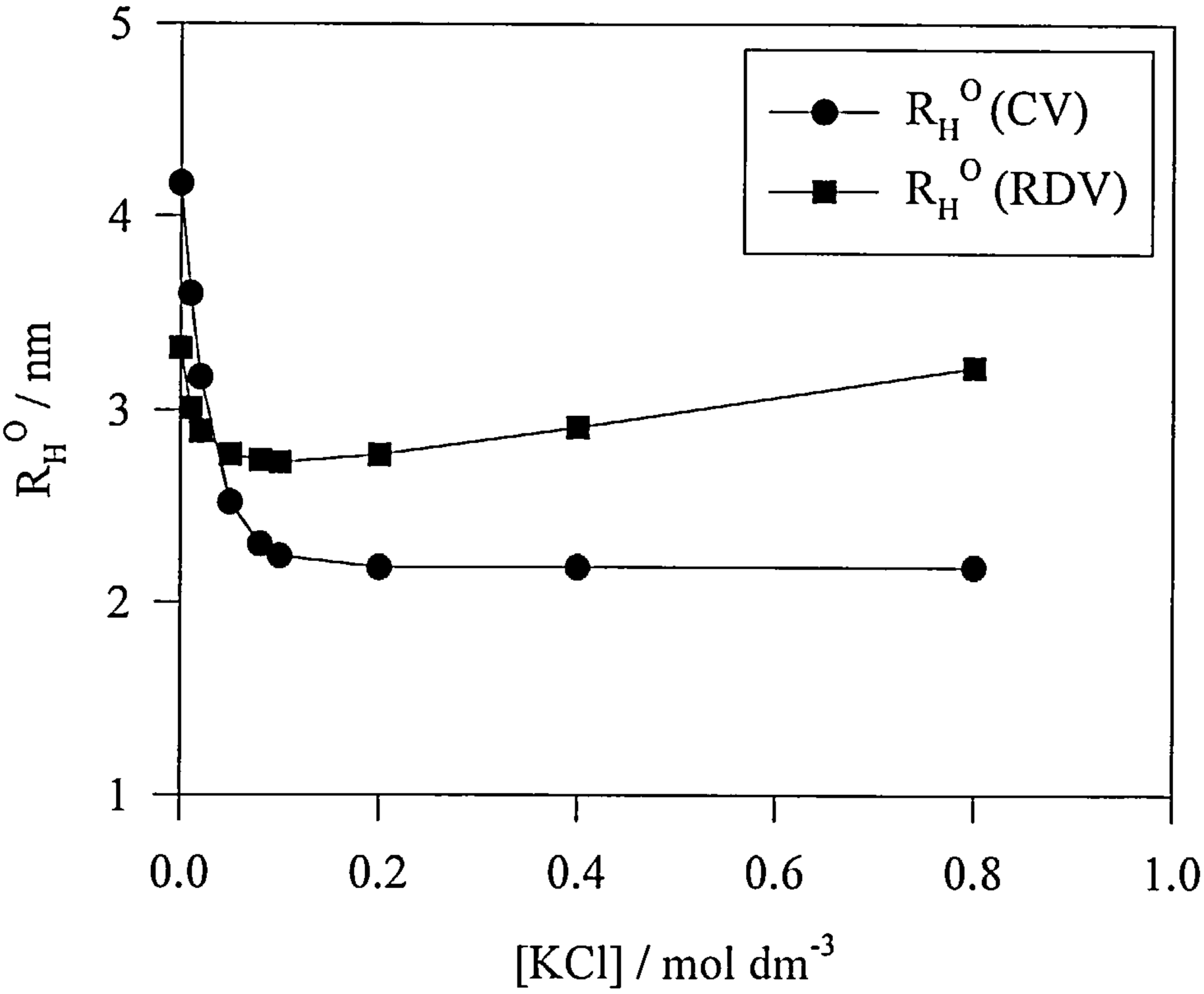

Appendix 4C.ix : Variation of interaction parameter with [KCl] for CV and RDV

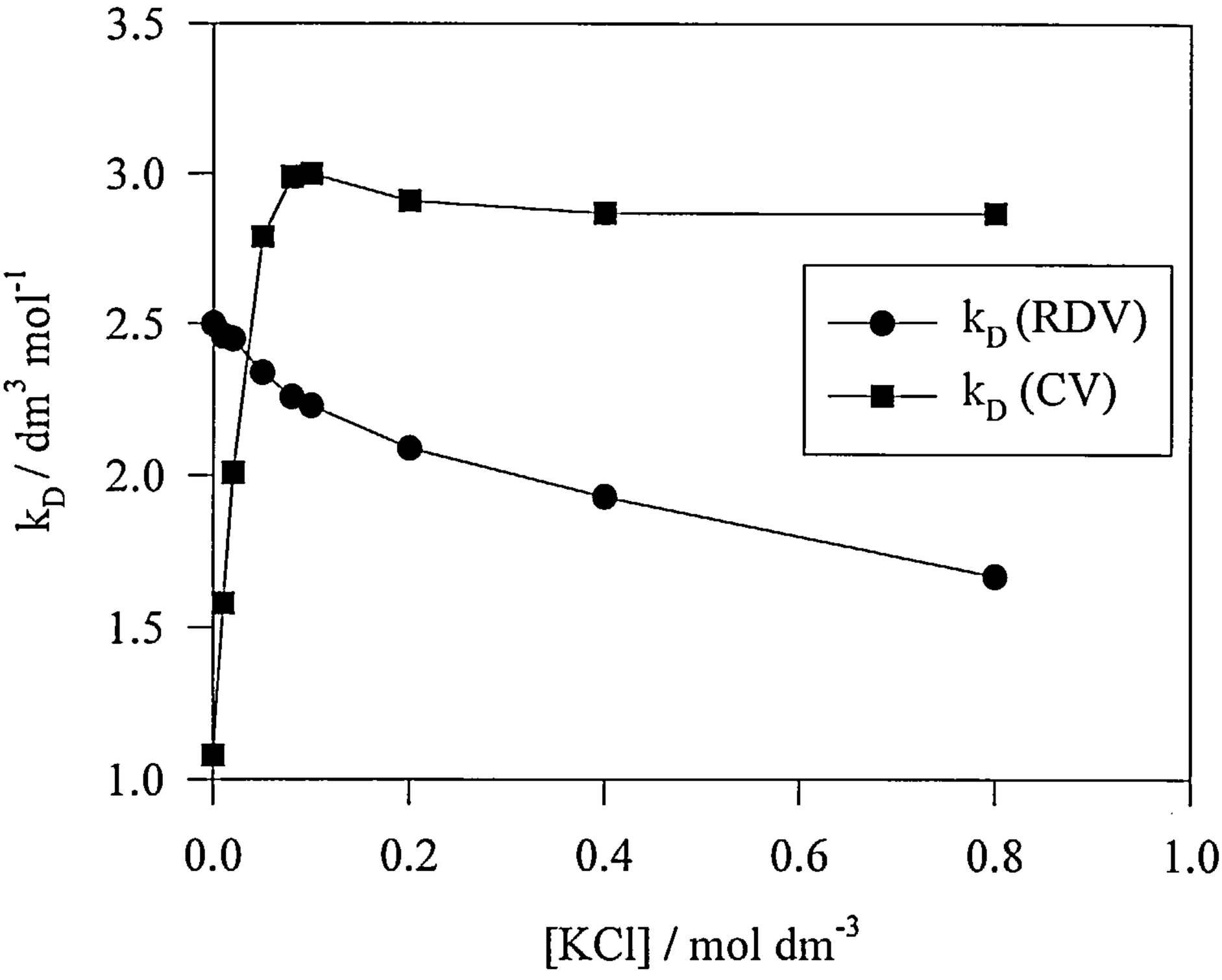

Appendix 4C.x : Arrenhius plot for temperature dependent diffusion coefficient (0.1563 mol dm^{-3} CTAC + 0.10 mol dm^{-3} KCl)

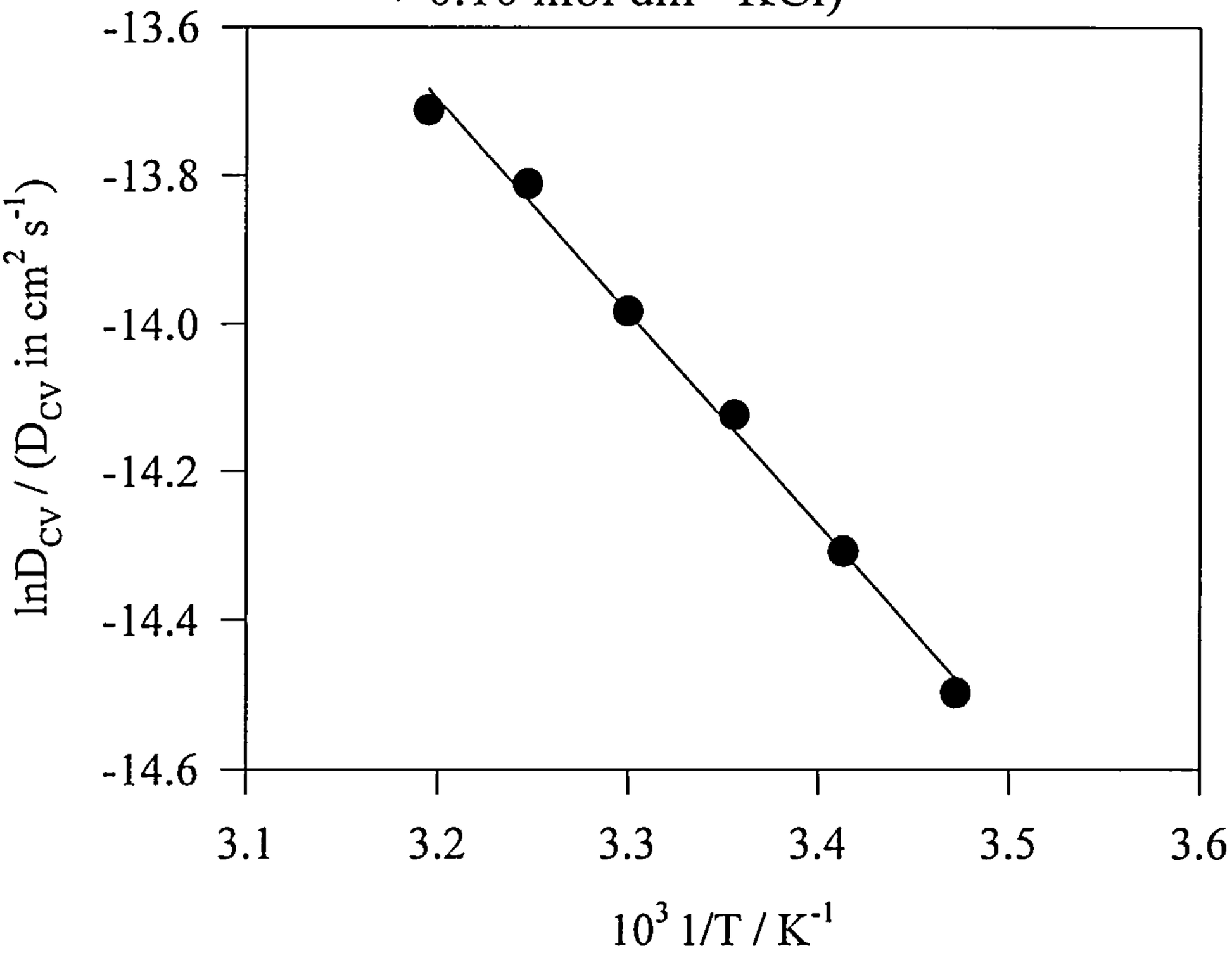

Appendix 4C.xi : Current response after potential step for 0.1563 mol dm^{-3} CTAC + 0.01 mol dm^{-3} KCl

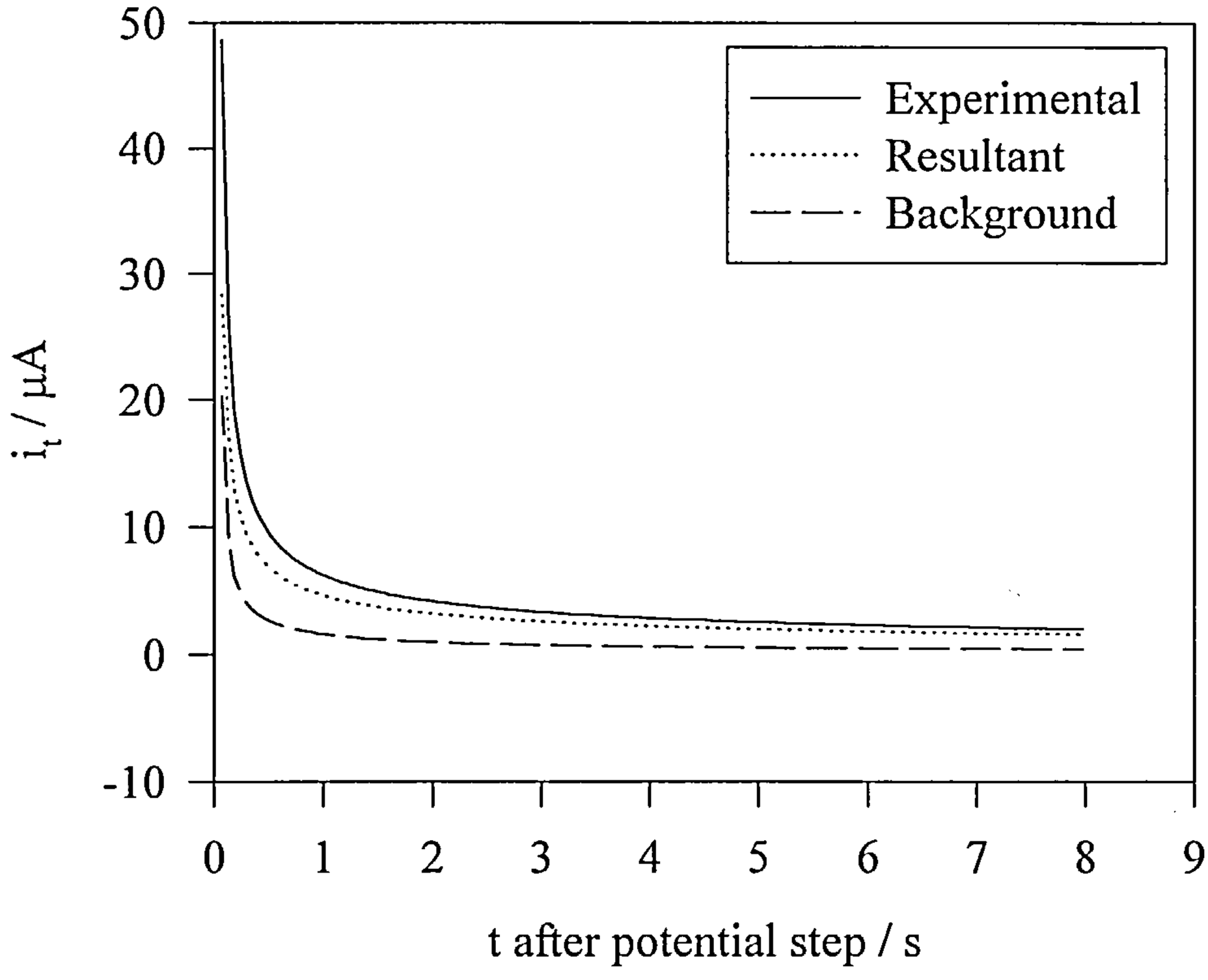

Appendix 4C.xii : Variation of correlation coefficient with Cottrell time analysis range

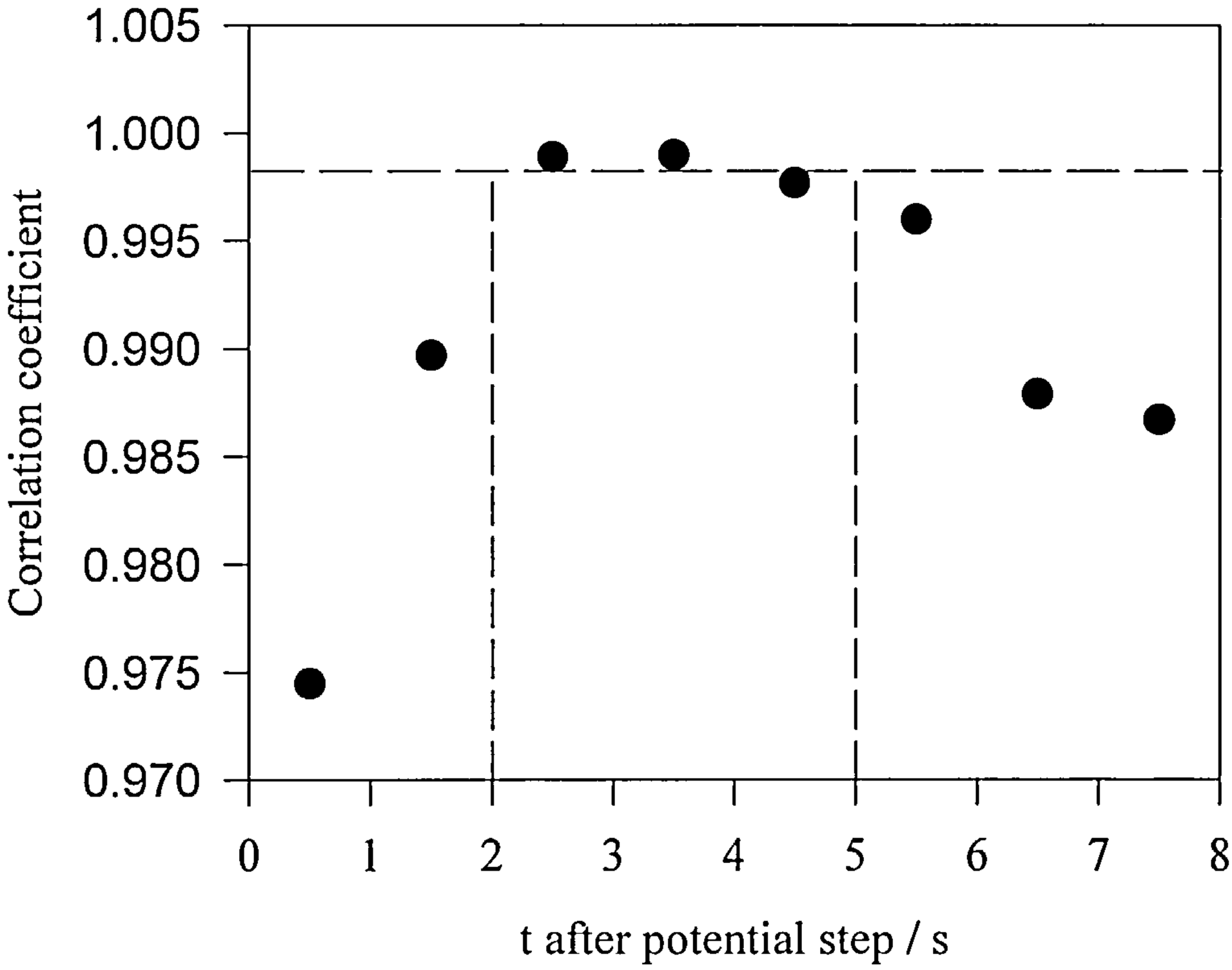

Appendix 4C.xiii : Variation of Cottrell gradient with time analysis range

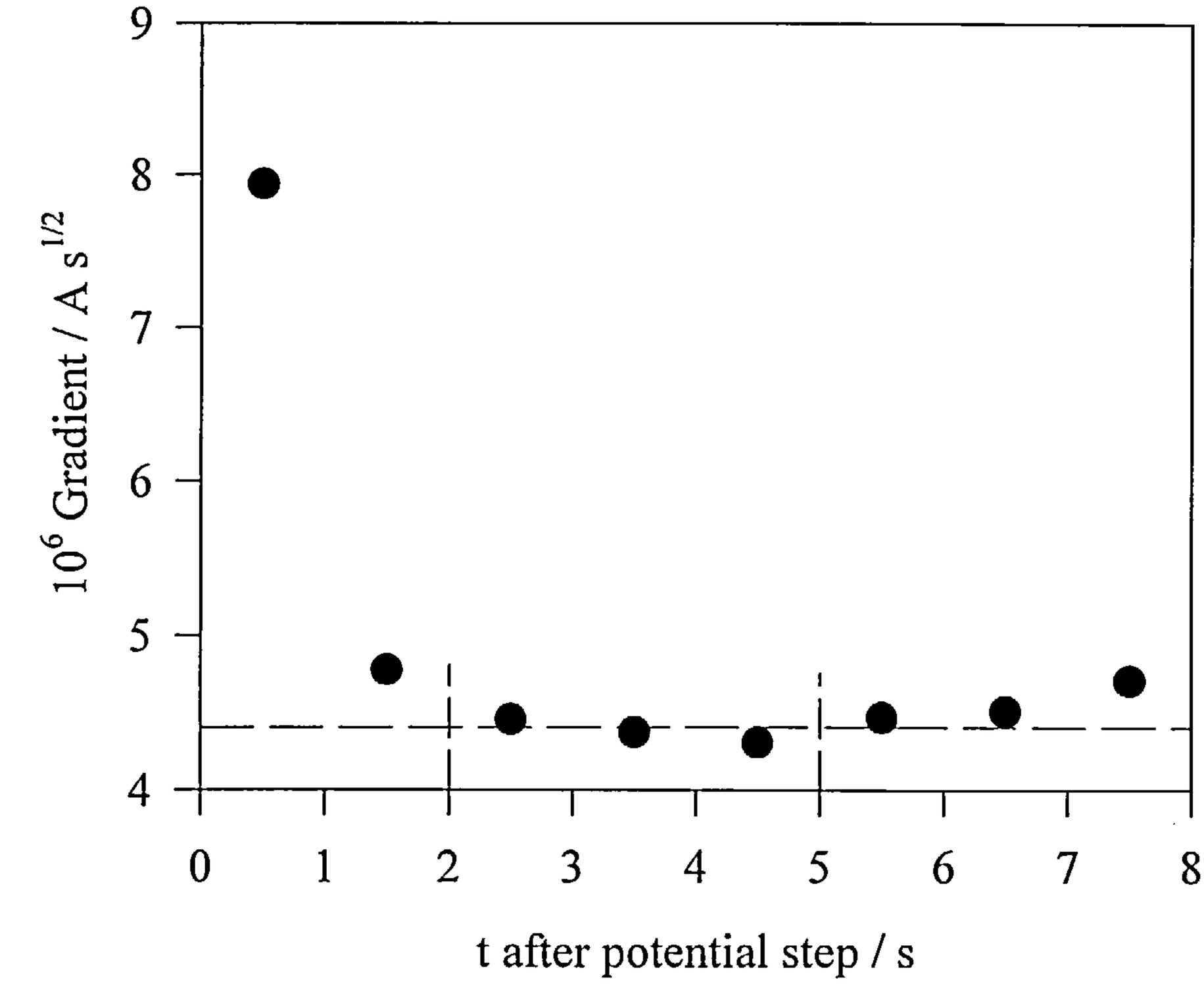

Appendix 4C.xiv : Variation of Cottrell intercept with time analysis range

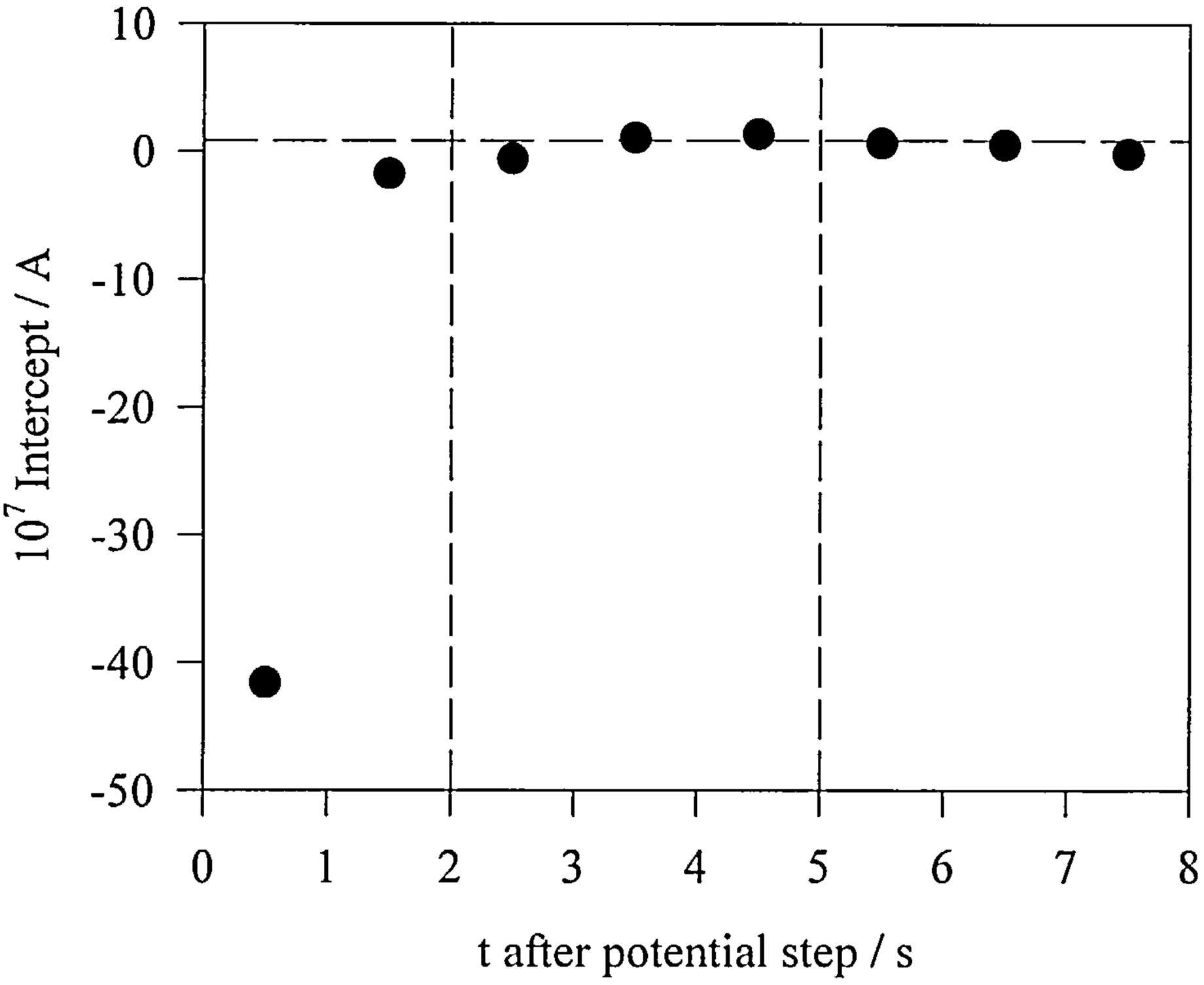

Appendix 4C.xv : Cottrell plot with chosen analysis range for 0.1563 mol dm^{-3} CTAC + 0.01 mol dm^{-3} KCl

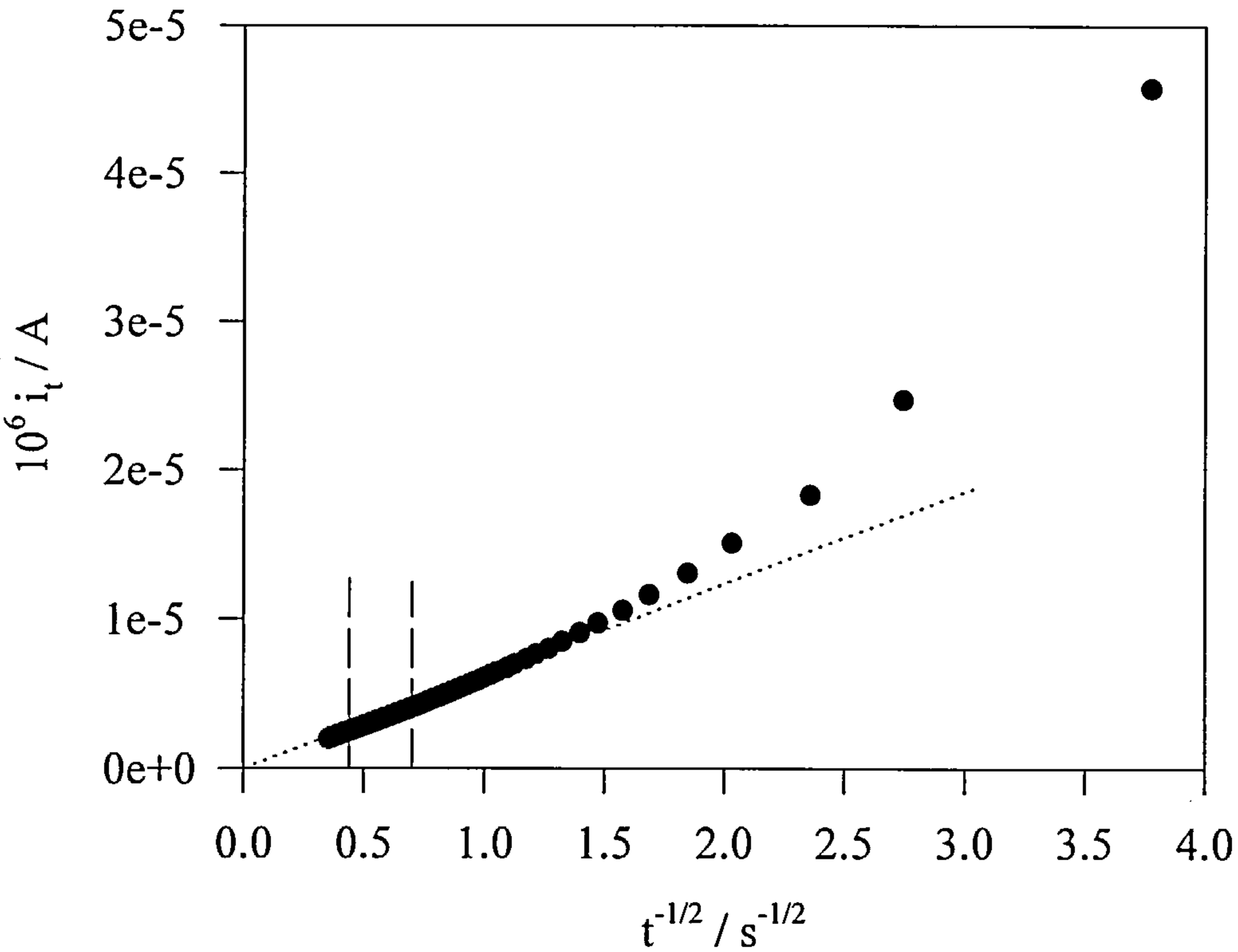

Appendix 4C.xvi : Variation of Cottrell background gradients with [KCl]

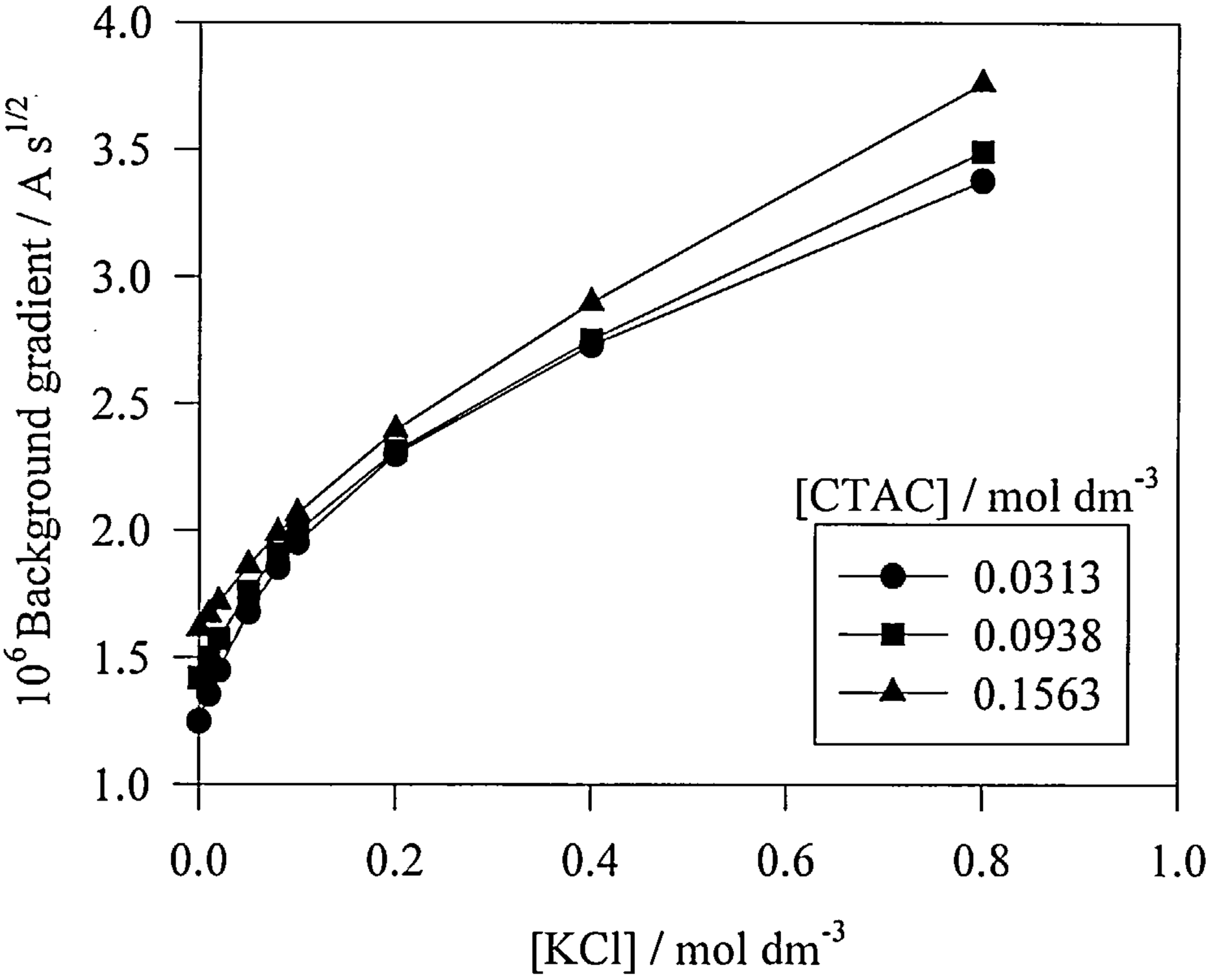

Appendix 4C.xvii : Variation of Cottrell experimental gradients with [KCl]

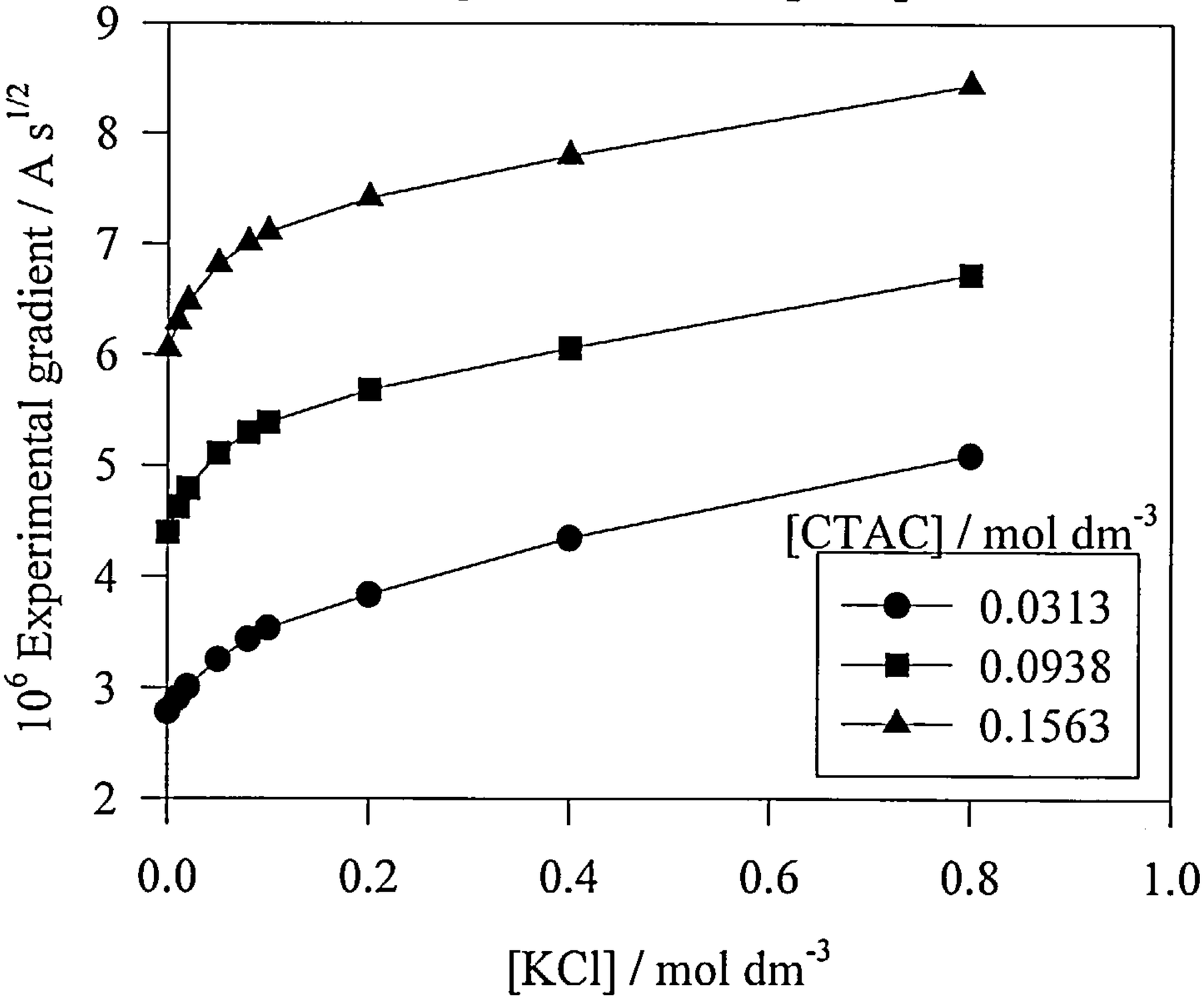

Appendix 4C.xviii : Variation of corrected Cottrell gradients with [KCl]

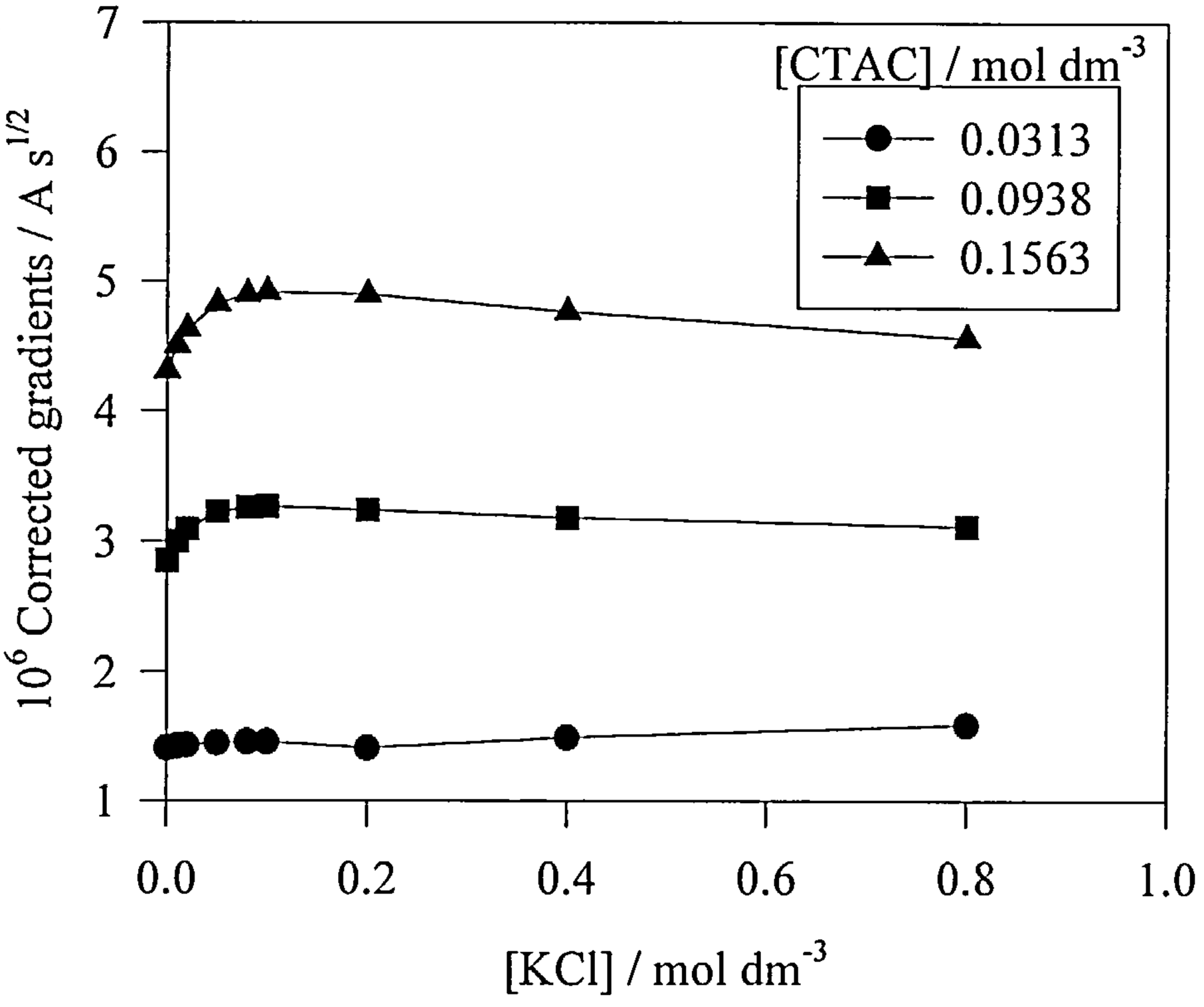

Appendix 4C.xix : Diffusion Coefficient variation with [KCl]

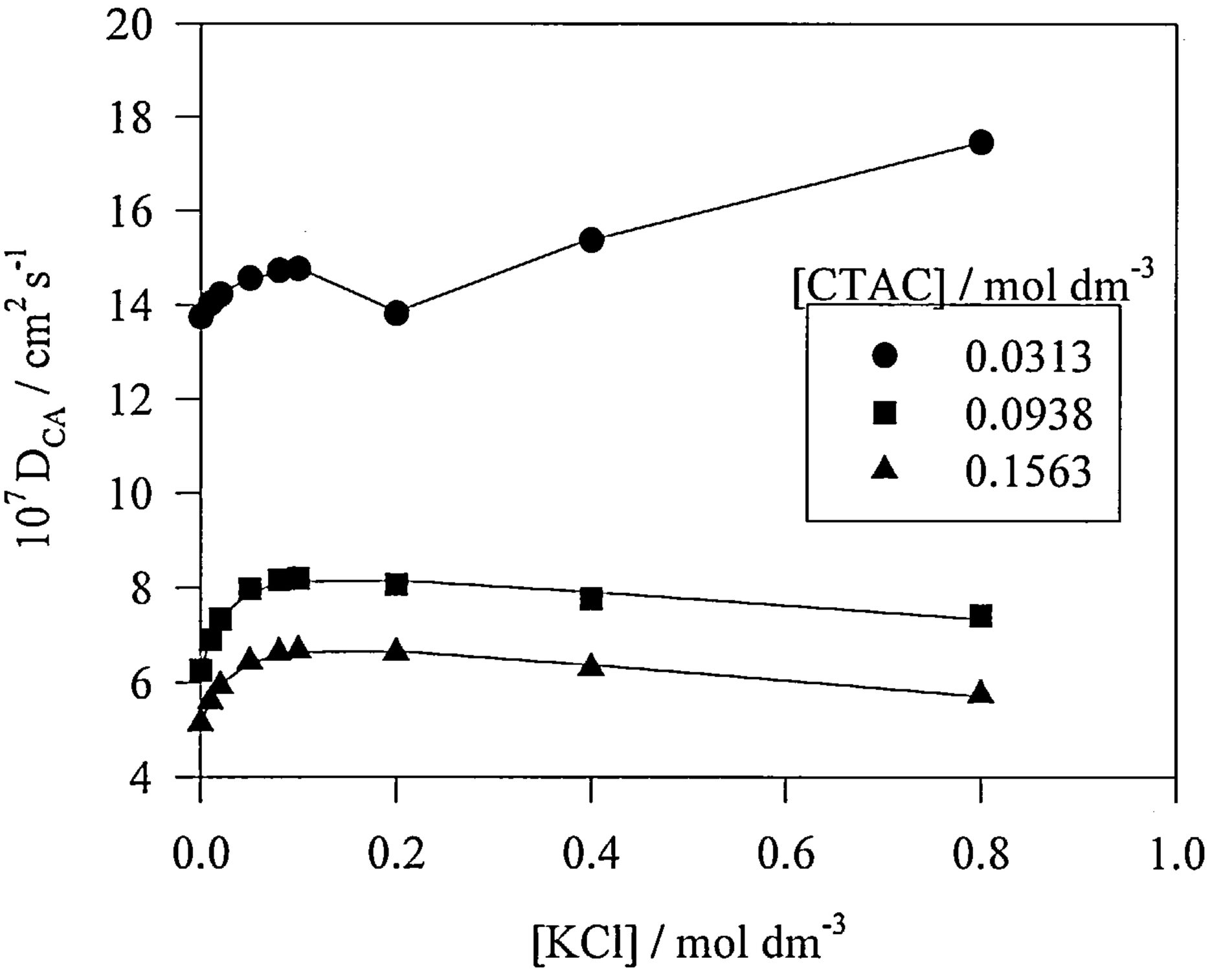

Appendix 4C.xx : Comparison of diffusion coefficients with technique for 0.1563 mol dm^{-3} CTAC

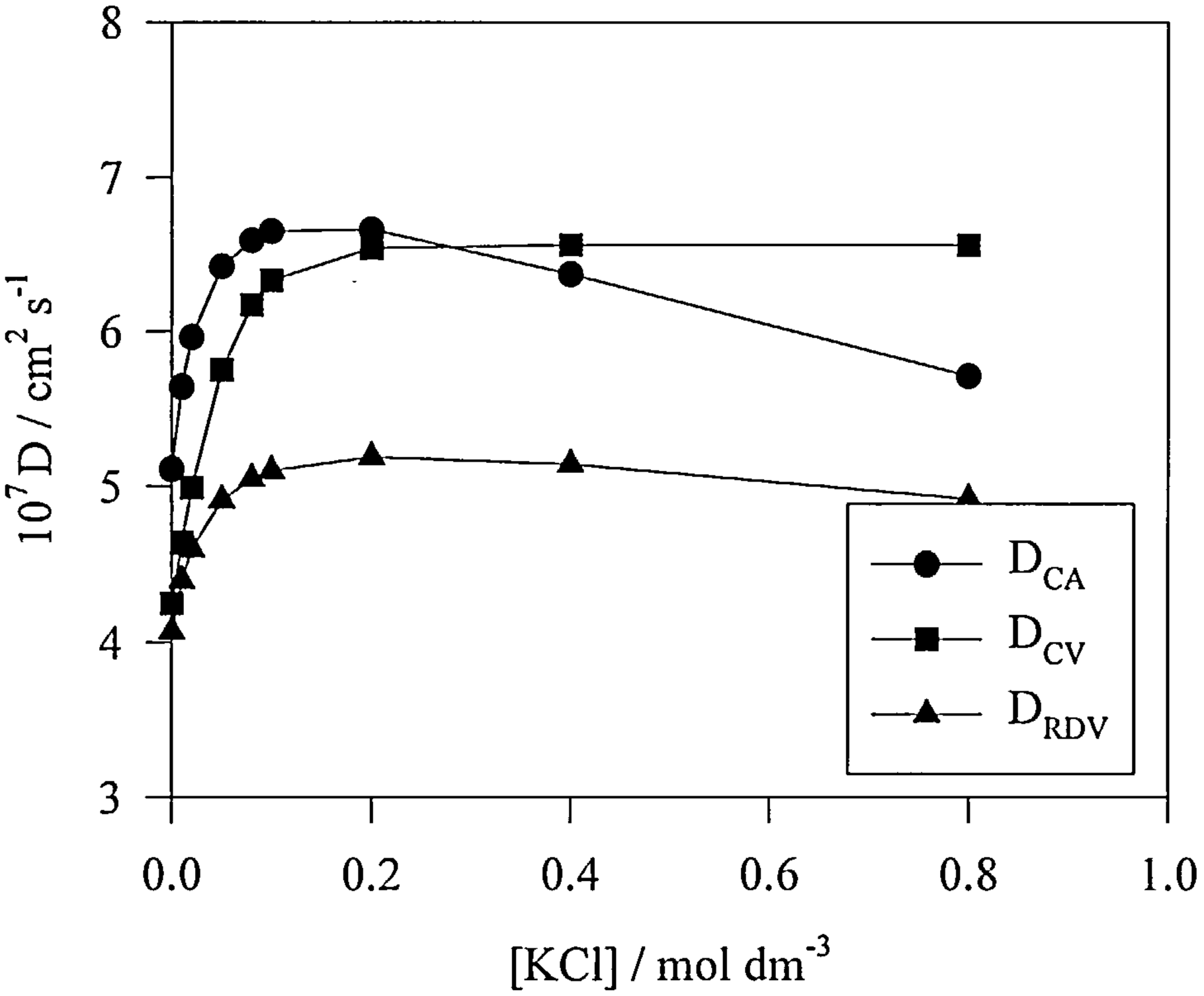

CHAPTER 4D: CTAC Conclusions

The size, interaction and structural evolution characteristics of a cationic micellar system (CTAC) have been examined using three electrochemical methods, rotating disk voltammetry, cyclic voltammetry and chronoamperometry in addition to rheological measurements with a cone and plate viscometer.

RDV provided the greatest amount of interpretable diffusion coefficient data, which on the application of linear interaction theory yielded some significant results. The interaction parameter was shown to describe micellar structural evolution by virtue of a transition from Coulombic repulsion to van der Waals attraction on the addition of electrolyte. Analysis of the hydrodynamic radii allowed the determination of the micellar shear plane and zeta potential. In addition to these, the first elucidation of the double layer - shear plane relationship has been obtained. These parameters are important principles in understanding the fundamental behaviour of charged supramolecular species in solution. This work provides a significant quantitative and phenomenological basis for modelling, amongst others, colloidal and membrane mimetic systems.

In previous studies rheological measurements have been used to detect changes in the structural behaviour of micellar solutions[59,67,69]. As well as using the raw viscosity to observe a sphere to rod transition, further analysis of the experimental data has allowed the transformation from Coulombic repulsion to van der Waals attraction to be followed. Although there was good qualitative agreement between k_D and k_V, the quantitative differences suggest that intermicellar interaction is manifested to a greater extent in rheological results than diffusion coefficients[76].

For both rheological and diffusion coefficient measurements micellar solutions were seen to exhibit Arrhenius behaviour. In both cases there was a good qualitative relationship between activation energy and interaction parameter, indicating the inherently linked nature of diffusion, viscosity and interaction.

As for Triton X-100, there was disparity between the results as determined by electrochemical techniques. Both CV and CA yielded diffusion coefficients that were higher than those as determined by RDV. These attenuated D_{CV} and D_{CA} values were believed to be a result of either pre-concentrated ferrocene and / or two diffusional regimes at a stationary electrode. This was confirmed somewhat by the constant D_{CA} / D_{RDV} ratio that was observed, despite D_{CA} lacking the precision that was apparent for D_{RDV} and D_{CV}.

In summary, the results that have been presented for CTAC can be assessed from two perspectives namely experimental technique and macroscopic solution behaviour. For the full elucidation of micellar solution structure and interaction, a number of complimentary techniques must be used as each highlight different properties. The macroscopic solution behaviour of a micellar system can be successfully determined by the combination of different techniques. From the application of relatively simple electrochemistry and subsequent analysis, previously undetermined properties (e.g. micellar shear plane thickness) can be easily calculated.

CTAC (Ch. 4A, 4B, 4C) References:

1. S.B.Johnson, C.J.Drummond, P.J.Scales, S.Nishimura, *Colloids and Surfaces A: Physicochem. and Eng. Aspects*, 1995, vol. 103, p. 195.

2. T.Tominaga, M.Nishinaka, *J. Chem. Soc. Faraday Trans.*, 1993, vol. 89, p. 3459.

3. R.B.Dorshow, C.A.Bunton, D.F.Nicoli, *J. Phys. Chem.,* 1983, vol. 87, p. 1409.

4. V.K.Aswal, P.S.Goyal, S.V.G.Menon, B.A.Dasannacharya, *Physica B*, 1995, vol. 213&214, p. 607.

5. A.Malliaris, J.Lang, R.Zana, *J. Phys. Chem.*, 1986, vol. 90, p. 655.

6. S.Reekmans, D.Bernik, M.Gehlen, J. van Stam, M. Van der Auweraer, F.C.De Schryver, *Langmuir,* 1993, vol. 9, p. 2289.

7. J.B.Hayter, J.Penfold, *Colloid and Polymer Sci.*, 1983, vol. 261, p. 1022.

8. D.F.Nicoli, R.B.Dorshow, *Physics of Amphipiles: Micelles, Vesicles and Microemulsions,* (eds. V.Degiorgio, M.Corti), Societa Italiana di Fiscia, Bologna, 1985, p. 429.

9. P.S.Goyal, S.V.G.Menon, B.A.Dasannacharya, V.Rajagopalan, *Chem. Phys. Letters*, 1993, vol. 211, p. 559.

10. A.Malliaris, J.Le Moigne, J.Sturm, R.Zana, *J. Phys. Chem.*, 1985, vol. 89, p. 2709.

11. P.Lianos, M-L.Viriot, R.Zana, *J. Phys. Chem.*, 1984, vol. 88, p. 1098.

12. E.Roelants, F.C.De Schryver, *Langmuir*, 1987, vol. 3, p. 209.

13. A.Malliaris, J.Lang, R.Zana, *J. Chem. Soc. Faraday Trans.,* 1986, vol. 82, p. 109.

14. E.Roelants, E.Gelade, J.Smid, F.C.De Schryver, *J. Colloid and Int. Sci.,* 1985, vol. 7, p. 337.

15. A.P.Doherty, K.Scott, *J. Chem. Soc. Faraday Trans.*, 1996, vol. 92, p. 4541.

16. M.J.Eddowes, M.Gratzel, *J. Electroanal. Chem.*, 1983, vol. 152, p. 143.

17. M.J.Eddowes, M.Gratzel, *J. Electroanal. Chem.,* 1984, vol. 163, p. 31.

18. J.Georges, S.Desmettre, *Electrochimica Acta*, 1984, vol. 29, p. 521.

19. E.Munoz, R.Rodriguez-Amaro, J.J.Ruiz, J.L.Avila, L.Camacho, V.Lopez, *J. Electroanal. Chem.*, 1992, vol. 324, p. 359.

20. R.E.Verrall, S.Milioto, A.Giradudeau, R.Zana, *Langmuir*, 1989, vol. 5, p. 1242.

21. Z.Kozarac, S.Nikolic, I.Ruzic, B.Cosovic, *J. Electroanal. Chem.*, 1982, vol. 137, p. 279.

22. S.J.Dong, Y.C.Shui, C.J.Cheng, *Langmuir*, 1991 vol. 7, p. 389.

23. A.Yehia, A.A.Atia, B.G.Ateya, *Adsorption Science and Tech.*, 1998, vol. 16, p. 431.

24. J.F.Rusling, *Colloids and Surfaces A: Physicochem. and Eng. Aspects*, 1997, vol. 123-124, p. 81.

25. G.Horanyi, E.M.Rizmayer, *J. Electroanal. Chem.,* 1977, vol. 83, p. 367.

26. R.F.Lane, A.T.Hubbard, *J. Phys. Chem.*, 1975, col. 79, p. 808.

27. G.Carreno, E.Sosa, I.Gonzales, C.Ponce-de-Leon, N.Batina, M.T.Oropeza, *Electrochimica Acta*, 1999, vol. 44, p. 2633.

28. R.Parsons, *Solid State Ionics*, 1997, vol. 94, p. 91.

29. A.G.Volkov, D.W.Deamer, D.L.Tanelian, V.S.Markin, *Prog. in Surface Sci.*, 1996, vol. 53, p. 1.

30. G.Valette, A.Hamelin, R.Parsons, *Z. Phys. Chem. N.F.,* 1978, vol. 113, p. 71.

31. E.L.Goldstein, M.R. Van De Mark, *Electrochimica Acta*, 1982, vol. 27, p. 1079.

32. Y.Ohsawa, A.Aoyagui, *J. Electroanal. Chem.*, 1982, vol. 136, p. 353.

33. K.Chokshi, S.Qutbuddin, A.Hussam, *J. Colloid and Int. Sci.*, 1989, vol. 129, p. 315.

34. J.F.Rusling, *Electroanal. Chem., A Series of Advances*, (ed. A.J.Bard), 1993, vol. 18, Dekker, NY, p. 1.

35. J.F.Rusling, C-N Shi, T.F.Kumosinki, *Anal. Chem.,* 1988, vol. 60, p. 1260.

36. A.J.Bard, L.R.Faulkner, *Electrochemical Methods*, Wiley, New York, 1980.

37. A.B.Mandal, *Langmuir,* 1993, vol. 9, p. 1932.

38. G.Wilkinson, M.Rosenblum, M.C.Whiting, R.B.Woodward, *J. Am. Chem. Soc.*, 1952, vol. 74, p. 2125.

39. G.D.J.Phillies, *J. Colloid and Int. Sci.*, 1987, vol. 119, p. 528.

40. M.Corti, V.Degiorgio, *J. Phys. Chem.,* 1981, vol. 85, p. 711.

41. A.Rohde, E.Sackmann, *J. Phys. Chem.,* 1980, vol. 84, p. 1598.

42. I.D.Morrison, *Langmuir*, 1991, vol. 7, p. 1920.

43. S.Ikeda, *Colloid and Polymer Sci.*, 1991, vol. 269, p. 49.

44. S.Q.Wang, *Macromolecules*, 1992, vol. 25, p. 1153.

45. E.Dickinson, *Ann. Rev. Prog. Chem.*, 1983, (c), p. 3.

46. J.B.Hayter, J.Penfold, *Molecular Physics*, 1981, vol. 42, p. 109.

47. S.Ikeda, S.Ozeki, M-A.Tsunoda, *J. Colloid and Int. Sci.*, 1980, vol. 73, p. 27.

48. R.Xu, *Langmuir*, 1998, vol. 14, p. 2593.

49. C.F.Zukoski, S.A.Saville, *J. Colloid and Int. Sci.,* 1986, vol. 114, p. 32.

50. B.M.Verdegan, M.A.Anderson, *J. Colloid and Int. Sci.*, 1993, vol. 158, p. 372.

51. B.R.Midmore, R.J.Hunter, *J. Colloid and Int. Sci.*, 1988, vol. 122, p. 521.

52. B.Siffert, A.Jada, J.E.Letsango, *J. Colloid and Int. Sci.*, 1994, vol. 163, p. 327.

53. S.Sasaki, *Colloid and Polymer Sci.,* 1984, vol. 262, p. 406.

54. J.W.S.Goossens, A.Zembrod, *J. Disp. Sci. and Tech.,* 1981, vol. 2, p. 255.

55. M.R.Gittings, D.A.Saville, *Colloids and Surfaces A: Physicochem. and Eng. Aspects*, 1998, vol. 141, p. 111.

56. A.G.Van der Put, B.H.Bijsterbosch, *J. Colloid and Int. Sci.,* 1983, col. 92, p. 449.

57. J.H.Prescott, S-J.Shiau, R.L.Rowell, *Langmuir*, 1993, vol. 9, p. 2071.

58. B.J.Marlow, R.L.Rowell, *Langmuir*, 1991, vol. 7, p. 2970.

59. E.Ljosland, A.M.Blokhus, K.Veggeland, S.Backlund, H.Hoiland, *Progress in Colloid and Polymer Sci.*, 1985, vol. 70, p. 34.

60. A.M.Pandou, B.Siffert, *J. Colloid and Int. Sci.*, 1984, vol. 102, p. 138.

61. F.J.de las Nieves, E.S.Daniels, M.S.El-Aasser, *Colloids and Surfaces*, 1991, vol. 662 p. 107.

62. J.B.Hayter, *Physics of Amphipiles: Micelles, Vesicles and Microemulsions,* (eds. V.Degiorgio, M.Corti), Societa Italiana di Fiscia, Bologna, 1985, p. 59.

63. J.Marra, M.L.Hair, J. *Colloid and Int. Sci.,* 1989, vol. 128, p. 511.

64. F.J.Carrion, A. De la Maza, J.L.Parra, *J. Colloid and Int. Sci.*, 1994, vol. 164, p. 78.

65. G.A.Schumacher, T.G.M.van der Ven, *Faraday Discuss. Chem. Soc.*, 1987, vol. 83, p. 75.

66. J.H.Prescott, S-J.Shiau, R.L.Rowell, *Langmuir*, 1993, vol. 9, p. 2071.

67. L.Sepulveda, C.Gamboa, *J. Colloid and Int. Sci.*, 1987, vol. 118, p. 87.

68. L.Sepulveda, C.Gamboa, *J. Colloid and Int. Sci.*, 1986, vol. 113, p. 566.

69. P.Ekwall, L.Mandell, P.Solyom, *J. Colloid and Int. Sci.*, 1971, vol. 35, p. 519.

70. F.Kern, F.Lequeux, R.Zana, S.J.Candau, *Langmuir*, 1994, vol. 10, p. 1714.

71. F.Kern, R.Zana, S.J.Candau, *Langmuir*, 1991, vol. 7, p. 1344.

72. T.Imae, S.Ikeda, *Colloid and Polymer Sci.*, 1987, vol. 265, p. 1090.

73. S.J.Candau, E.Hirsch, R.Zana, M.Adam, *J. Colloid and Int. Sci.*, 1988, vol. 122, p. 430.

74. R.Nagarajan, *J. Colloid and Int. Sci.*, 1982, vol. 90, p. 477.

75. P.Mukerjee, *J. Phys. Chem.*, 1972, vol. 76, p. 565.

76. E.Hirsch, S.Candau, R.Zana, *J. Colloid and Int. Sci.*, 1984, vol. 97, p. 318.

77. J.Heinze, *Ber. Bunsenges. Phys. Chem.*, 1981, vol. 85, p 1096.

78. A.P.Abbott, C.L.Miaw, J.F.Rusling, *J. Electroanal. Chem.*, 1992, vol. 327, p. 31.

79. A.B.Mandal, B.U.Nair, *J. Phys. Chem.*, 1991, vol. 95, p. 9008.

80. H.Zhang, J.F.Rusling, *Talanta*, 1993, vol. 40, p. 741.

81. H.Zhou, S.Dong, *Electrochimica Acta*, 1997, vol. 42, p. 1801.

82. P.Birkin, *Ph.D. Thesis*, Southampton University, 1995.

83. P.Birkin, *Private Communication.*

Chapter 5 - A reverse micellar system

- Aerosol-OT -

Chapter 5: Electrochemistry in Aerosol-OT Reverse Micelles

5.1 Introduction

Aerosol-OT (sodium bis-2-ethylhexylsulfosuccinate) is an anionic surfactant that can form reverse micellar or microemulsion systems on the addition of a non-polar solvent. Aerosol-OT is an attractive surfactant due to its ability to solubilise large amounts of polar solvent (typically water)[1,2]. This property essentially results in the thermodynamic stability of such dispersions[1] and therefore there is no need for any co-surfactant[3]. The typical range of the critical micelle concentration (c.m.c.) is within $5x10^{-4}$ - $5x10^{-3}$ and is solvent dependent[4,5,6]. Aerosol-OT (AOT) has two alkyl chains connected via a sulfonate headgroup with a sodium counter ion and has a molecular weight of 444.5 g mol^{-1}.

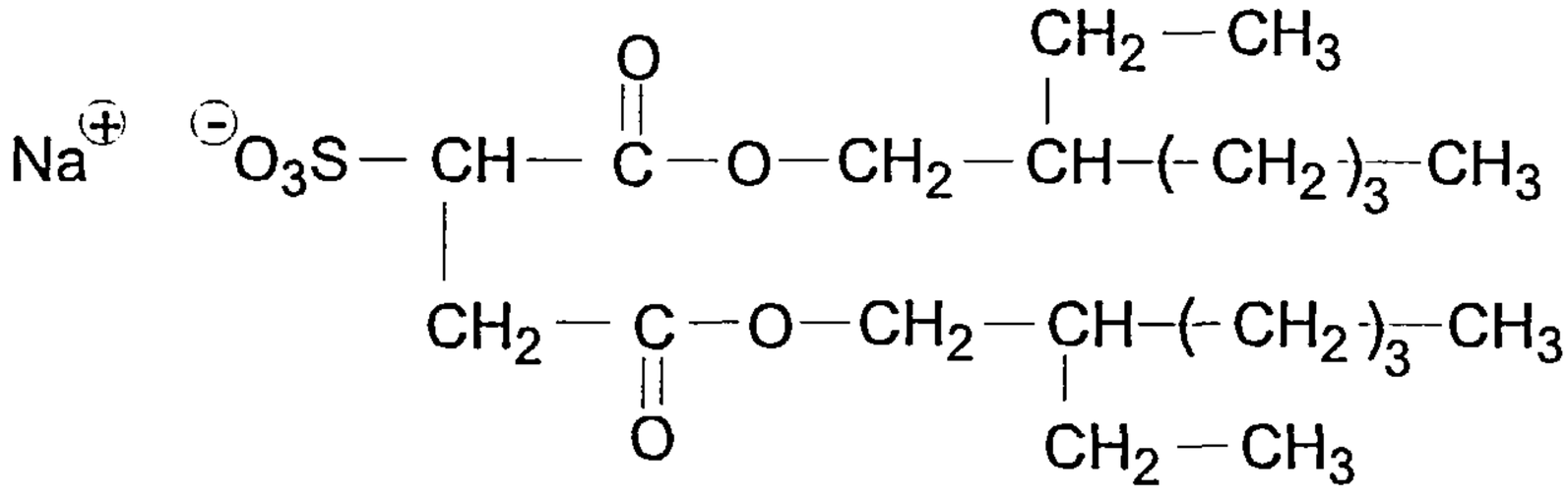

Figure 5.1 : Structure of Aerosol-OT

In a reverse micelle structure the polar sulfonate headgroups orientate inwards towards the polar solvent, with the alkyl chains extending outwards into the bulk solution (non-polar solvent) as illustrated in Figure 5.2. The shape of these aggregates are essentially spherical[1,7,8,9,10], but the size can be highly dependent on the concentration of each of the constituents[1]. The aggregate size is typically characterised by the concentration ratio of water to AOT (W = $[H_2O]$ / [AOT]) rather than the actual concentrations[1]. A clear distinction must be made between reversed micellar microemulsion systems like those encountered in the literature and

the reversed micellar system presented in this study. It is well documented that the micellar aggregate size will increase with a larger W ratio[3,7,11,12,13] until a microemulsion (i.e. free water exists) is formed at approximately W > 15[11]. This study is restricted to W = 10 when the system is of a true reversed micellar nature with each aggregate behaving as rigid macromolecules[4]. For the purpose of this study a microemulsion will refer to those solutions with W > 15, with reverse micelle structures with W ≤ 10 termed 'nanoemulsions'. As a further classification, a nanoemulsion can be described by a reverse micelle system with a finite amount of bound interfacial water[4,11,14,15].

It is known that at a ratio of W = 10 the aggregate size is independent of the solution preparation process i.e. sonication, shaking etc., and insensitive to changes in temperature[4].

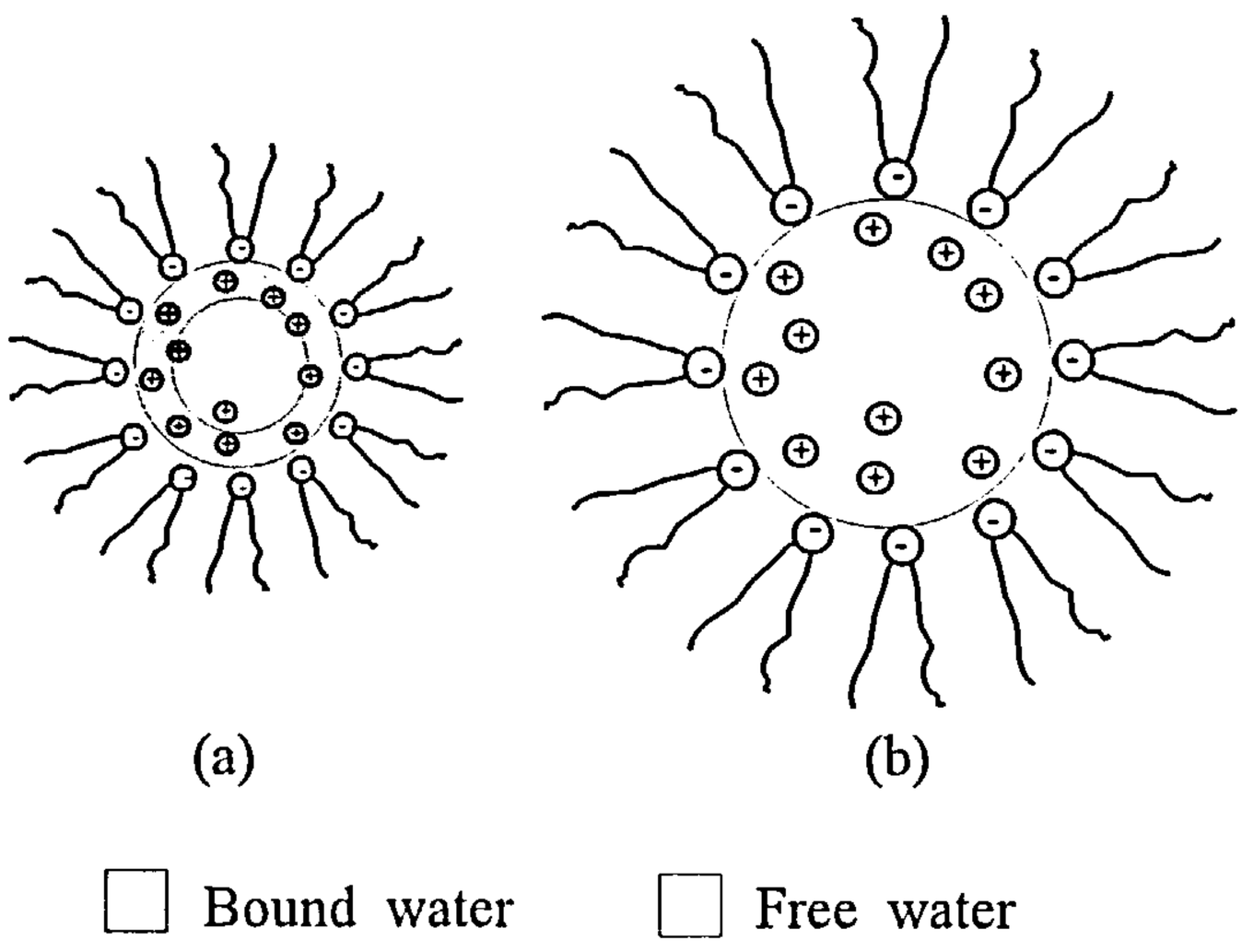

Figure 5.2 : Structures of reverse micelles for (a) nanoemulsion, (b) microemulsion

A number of advantages for reversed micellar nanoemulsions (as to opposed to microemulsions) are beginning to be utilised. At low [H_2O] there is a fixed layer of water which appears to be bound to the sulfonate headgroups[2,4,11,6,14,16,17,18,19,20,21] which becomes more mobile as the W ratio is increased[2,4,22,23,24]. At W = 10, it is likely that there is some bound water and some 'free' water with properties corresponding to bulk water[4,11,14,15]. Therefore, a reverse micelle nanoemulsion can be used to mimic water close to biological membranes and proteins[17,22]. The polar

nature of the micellar interior has been used previously as a nano-reactor for polymerisations[17], ester hydrolysis[25], electrocatalysis[21] and as a host for enzyme kinetic studies[26]. The highly rigid structures of reverse micellar nanoemulsions have also been used as reactors to produce size controlled nano-particles of metals[27] and alloys[28,29].

It is therefore important to have the dimensions of the micelle fully characterised. As for 'normal' micellar systems the majority of studies have used light scattering[1,10,23], neutron scattering[19,30,31] and fluorescence[2,3,22,32]. The assumptions which these techniques employ and subsequent disadvantages have been discussed earlier (Ch. 1). Electrochemical techniques offer a quick, simple and cheap way of obtaining structural information. The majority of electrochemical studies to date have been carried out on microemulsion systems[21,33,34,35,36]. This is due to the fact that the high water content results in media with sufficient conductivity for electrochemistry to be practised. AOT reversed micellar nanoemulsion systems, however, are poorly conducting (20 - 100 nS cm^{-1})[7] leading to large solution resistance, a property which significantly affects electrochemical measurements. However, the advent of microelectrodes has allowed electrochemical studies to be carried out in low conductivity media[37,38,39]. The properties and advantages of microelectrodes have been discussed in Ch. 1.3.4. Owlia et al. have used a carbon fibre microelectrode to study an AOT reversed micellar system, however, it must be noted that that $[H_2O]$ / [AOT] = 20 and is therefore strictly speaking a microemulsion[21].

The microelectrode offers a way of obtaining electrochemical data from a reversed micellar system. This chapter will present the first (to the authors knowledge) microelectrode study of a reversed micellar nanoemulsion system as opposed to a microemulsion.

5.2 Quasi-Reference Electrode

The choice of reference electrode in non-aqueous systems is of great importance and frequently must be different from those used in aqueous media due to the inconsistent reference potentials that maybe obtained. For example, the use of a Ag/AgCl reference electrode may result in precipitation of the electrolyte onto the ceramic frit leading to changes in the liquid junction potential[40,41] or to blocking of the frit. Typically, non-aqueous reference electrodes consist of a wire (usually Pt or Ag) immersed in a solution of the chosen solvent containing dissolved organic electrolyte (e.g. tetraethylammonium chloride). The absence of electrolyte in the system under study meant that this was not viable. Firstly, testing focused on using simply a silver wire immersed in the bulk solution i.e. a pseudo reference electrode, but initial experiments proved earlier findings that a reproducible potential was difficult to obtain[41]. The inability of the silver wire to produce good voltammograms was likely to be due to a pale yellow layer that coated the surface during the experiment.

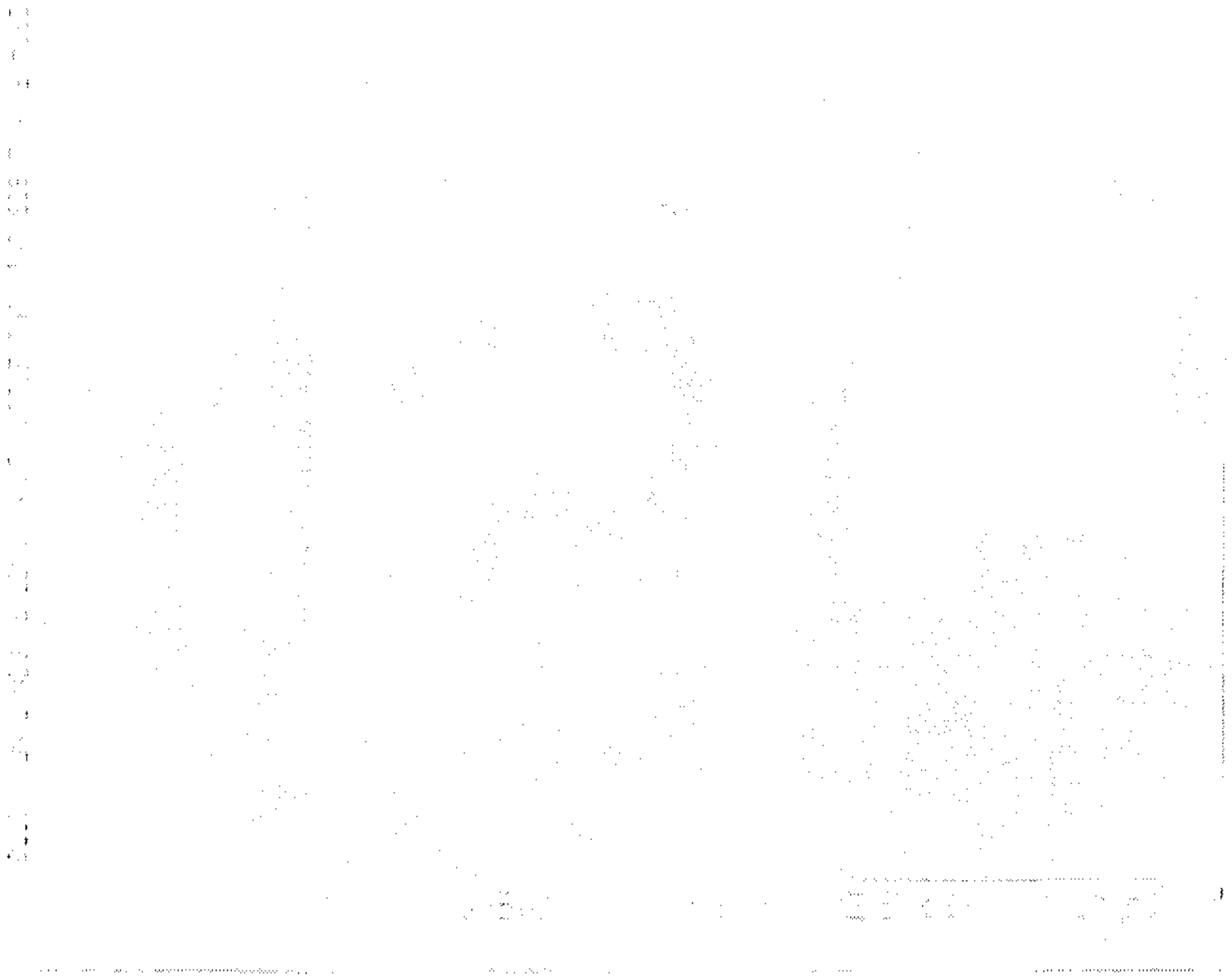

Figure 5.3 : Image showing coating on silver wire

The use of energy dispersion analysis of x-rays (EDAXS) allowed the composition of the coating to be identified. The EDAXS spectrum in Appendix 5.i shows that as well as the silver wire there was a high proportion of oxygen, sulfur and sodium. This would suggest that not only are the Na^+ counterions precipitating onto the silver surface but also the SO_3^-, indicating adsorption of AOT on the silver wire surface, which is not surprising given the tendency of surfactants to adsorb at surfaces. AOT has been observed to form bilayer structures at a mercury electrode with the SO^{3-} groups adjacent to the electrode surface with the hydrocarbon tails extended into solution[42], this tends to support the presented EDAXS data.

It has been noted that a platinum wire covered with a copolymer of pyrrole and ferrocene N-substituted pyrrole provides a stable reference electrode in a non-aqueous system environment[43,44]. Oyama et al. using poly-4-vinylpyridine to attach ruthenium complexes to graphite electrodes have found fast and easy polymer attachment with the coating possessing a long lifetime[45]. It seemed prudent that a similar procedure should be adopted in this case. A silver wire was dip coated with $[Os(bipy)_2(PVP)_{10}Cl]Cl$ where bipy = 2,2'-bipyridyl and PVP = poly-4-vinylpyridine.

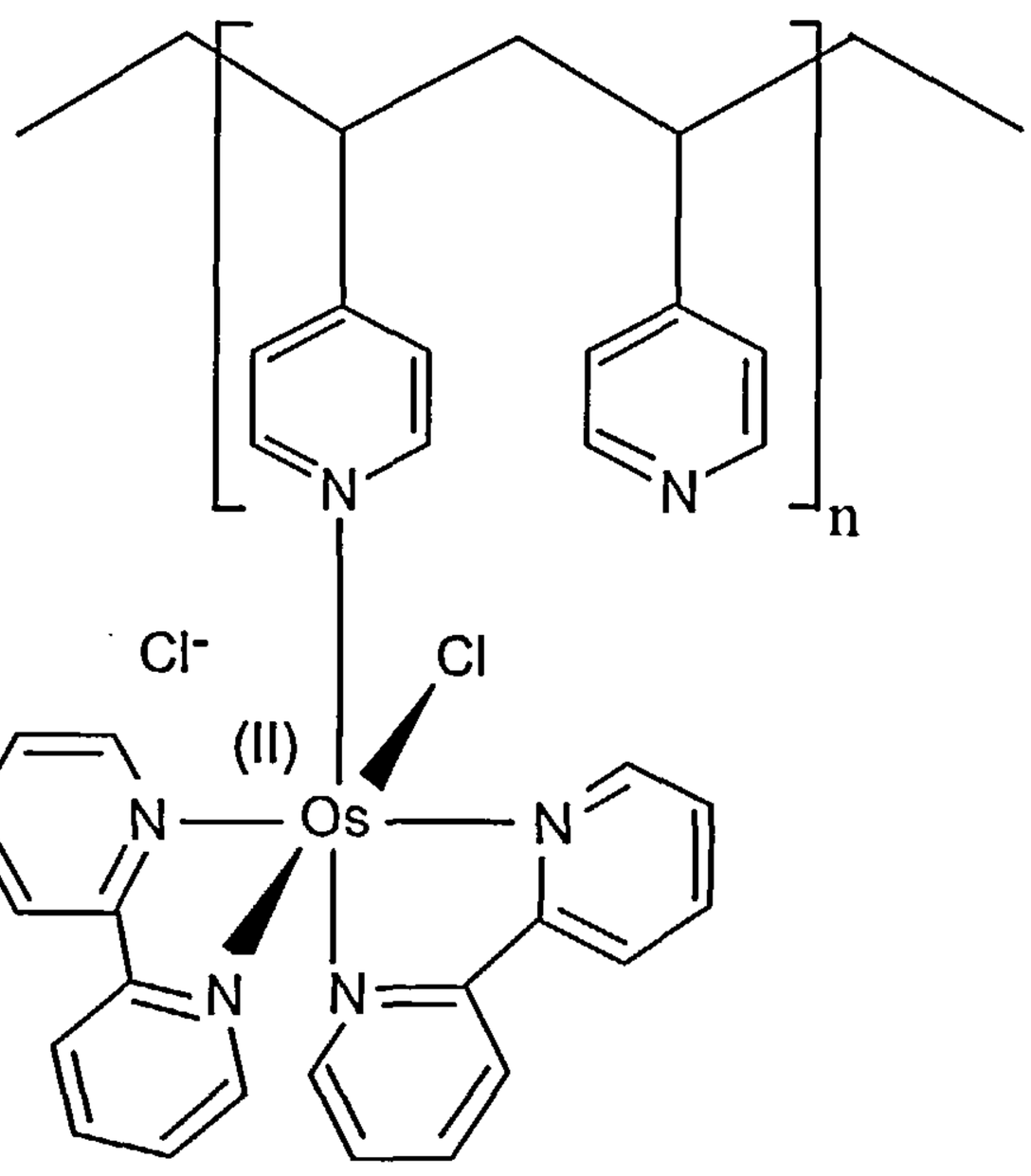

Figure 5.4 : Structure of $[Os(bipy)_2(PVP)_{10}Cl]Cl$ for coating of silver wire for reference electrode

Testing showed that the pale yellow covering apparent with an unmodified silver wire was prevented with the polymer coated wire. This provided a reference electrode potential of -150 mV vs. SCE in a test solution of 1.0 mol dm^{-3} KCl in water. A potential difference of ~0 mV between a $[Os(bipy)_2(PVP)_{10}Cl]Cl$ coated and uncoated silver wire indicates that the polymer is not actively involved in the electrode process but rather behaves as a protective layer.

5.3 General Electrochemistry

It is very important to assess the reversibility of the ferricyanide / ferrocyanide couple from the observed voltammetric responses. For this purpose, the Nernst equation was used again as for Triton X-100 (Ch. 3A.2.1) and CTAC (Ch. 4A.2.1). A plot of E vs. $\log_{10}[i / (i_{Lim} - i)]$ is shown in Appendix 5.ii, and resulted in a slope of ~59 mV $decade^{-1}$ and a half wave potential ($E_{1/2}$) = 141 mV vs. Ag/Ag^+ (no change was observed with changes in the solution composition). Typical values of the Nernstian slope varied from 50 - 70 mV $decade^{-1}$ but showed no correlation with the solution composition. The absence of any significant iR drop is confirmed by the fact that there is no notable decrease in the value of the Nernstian slope from the theoretical value (~58 mV $decade^{-1}$)[46].

The half wave potential compares with $E_{1/2}$ = 185 mV vs. Ag/Ag^+ in aqueous solution (Ch. 2.3.4, Appendix 2.iv) which shows a negative shift in potential due to the reverse micelle system. A shift of ~40 mV ($E_{1/2}$ = 141 mV $\rightarrow$ 100mV vs. SCE) for ferricyanide has also been seen on transition from aqueous solution to a microemulsion of CTAB / hexadecane/ 1-butanol / water[33]. This not only demonstrates the sensitivity of a microelectrode to the solvent media, but may also illustrate a change in pH of the microenvironment surrounding the probe. The reduction potential (E^O) of ferricyanide is known to be sensitive to changes in pH, varying from 460 mV in 0.01 mol dm^{-3} NaOH (pH =12) to 690 mV in 1 mol dm^{-3} H_2SO_4 (pH = -0.3)[47], which corresponds to a change of -18.7 mV pH^{-1}. If this is translated to the $E_{1/2}$ decrease of 45 mV from aqueous (185 mV) to reverse micelle

(141 mV), then this implies an increase in pH of ca. 2.4 i.e. pH 7 (water) to pH 9.4 (reverse micelle). It is known that in reverse micelles with low W, the water molecules can become polarised, like a hydroxide ion, leading to higher basicity[15] e.g. at W = 1.5 - 2.0, pH ≈ 9[15]. An apparent increase in pKa of ca. 2 units has been observed for 7-hydroxycoumarin in comparison to bulk water[48] which concurs with the results presented here.

5.4 Results and Discussion

The self diffusion coefficients were measured on a series of AOT / iso-octane / H_2O reversed micellar nanoemulsions at three different AOT concentrations and at a set temperature of 25 ^{O}C. In each case the volume of water was varied to ensure that W = [H_2O] / [AOT] = 10 remained constant. It is common to express the solution composition in terms of micellar volume fraction (ϕ_{mic}), a simplified expression has been stated by Cassin et al.[14]:-

$$\phi_{mic} = (V_{H2O} / V_0) [1 + (21 / W)] \qquad (5.1)$$

where V_{H2O} is the volume of water in the solution of total volume V_0. AOT concentrations = 0.15, 0.20 and 0.25 mol dm^{-3} are therefore expressed as ϕ_{mic} = 0.084, 0.112 and 0.140 respectively.

It was shown earlier that the ferrocene probe concentration profoundly affected the diffusion coefficient and was analysed as being a hindrance effect of 'empty' micelles (Ch. 4A.2.2.1). It has also been reported that the diffusion coefficient is increased as the probe concentration is decreased in microemulsion systems[21,33]. Therefore, it is necessary to measure the limiting currents and hence the diffusion coefficients as a function of probe concentration as well as [AOT].

From knowledge of the aggregation number (N_{agg}) it is possible to calculate the number of probe molecules per micelle. An AOT reversed micellar system

depends on a number of parameters to determine N_{agg} such as W ratio, [AOT], solvent and temperature. Consequently, the number of literature values for N_{agg} at an explicit solution specification are limited. Values of N_{agg} for W = 10 at moderate [AOT] and temperatures have been found to vary between 70 - 200, though the solvent systems varied between such solvents as heptane[2,3], cyclohexane[1], chlorobenzene[1] and iso-octane[4,18]. Although it has been reported that that there is no appreciable deviation in micellar size between iso-octane and n-alkanes[2,10], it was apparent that a difference in N_{agg} existed. So, it followed that only the data for iso-octane could be used confidently (N_{agg} = 75)[4,18]. The concentration of micelles can be easily found using [AOT] / N_{agg}.

Voltammetric studies were conducted on 0.15, 0.20 and 0.25 mol dm^{-3} AOT (ϕ_{mic} = 0.084, 0.112, 0.140), it is known that in this concentration range the micellar size and aggregation number essentially remain constant at constant W[1,2,8,9]. For each [AOT] the concentration of $K_3Fe(CN)_6$ was varied between [micelle] : [probe] = 0.5 - 1.5 as calculated from [AOT] / N_{agg}. Examples of the responses obtained from AOT / iso-octane / H_2O reversed micelles are shown in Appendix 5.iii over a range of probe concentrations at ϕ_{mic} = 0.084. Table 5.1 shows the limiting currents obtained over the micelle volume fraction and probe concentration ranges. In each case the voltammetric measurements were repeated until reproducible values for the limiting currents were obtained, this was typically achieved after 4-5 experiments. Deviation at the earlier measurements was probably due to the activity of the microelectrode surface not reaching a constant level till after 4-5 experiments. Avranas et al. noted a time dependence for the adsorption of AOT onto a mercury electrode[42] and this process could essentially be the cause of inconsistent limiting currents in initial experiments. Typically, i_{Lim}, was reproducible to ± 3%.

Table 5.1 : Limiting currents from microelectrode voltammograms for AOT / iso-octane / H_2O reversed micellar system

10^3 [$K_3Fe(CN)_6$] / mol dm^{-3}	10^9 i_{lim} / A		
	$\phi_{mic} = 0.084$	$\phi_{mic} = 0.112$	$\phi_{mic} = 0.140$
1.403	0.134	-	-
1.831	0.173	-	-
2.545	0.237	-	-
3.131	0.284	-	-
1.762	-	0.155	-
3.171	-	0.274	-
4.368	-	0.369	-
1.880	-	-	0.155
3.192	-	-	0.261
4.140	-	-	0.335
5.072	-	-	0.410

Note: standard error $\pm 0.05 \times 10^{-9}$ *A*

With the knowledge of the limiting currents and the fact that the electrode radius has been found to be 5.2 μm (Ch. 2.3.4), then the diffusion coefficients can be determined (Ch. 2.3.4, Equation 2.3).

Table 5.2 : Diffusion coefficients (D_{RM}) for ferricyanide in an AOT / iso-octane / H_2O reversed micellar nanoemulsion system

10^3 [$K_3Fe(CN)_6$] / mol dm^{-3}	10^7 D_{RM} / cm^2 s^{-1}		
	$\phi_{mic} = 0.084$	$\phi_{mic} = 0.112$	$\phi_{mic} = 0.140$
1.403	4.75	-	-
1.831	4.71	-	-
2.545	4.64	-	-
3.131	4.52	-	-
1.762	-	4.39	-
3.171	-	4.30	-
4.368	-	4.21	-
1.880	-	-	4.10
3.192	-	-	4.08
4.140	-	-	4.03
5.072	-	-	4.03

Note : standard error $\pm 0.08 \times 10^{-7}$ cm^2 s^{-1}

The diffusion coefficients are an order of magnitude lower than that for ferricyanide in aqueous solution ($7.63x10^{-6}$ cm^2s^{-1})[49] indicating the location of the probe in the micellar interior. The results also suggest that the probe is in a small particle, the diffusion of which results in i_{Lim}. If the probe was in a large microemulsion it would behave, diffusionally at least, as a probe in free water phase. Therefore, D_{PROBE} = D_{RM}, where D_{RM} is the diffusion coefficient of the reversed micelle. A plot of the diffusion coefficient variation with probe concentration can be viewed in Appendix 5.iv

5.4.1 Results Analysis

We have seen that [probe] does not affect the diffusion coefficient if one or more probe is solubilised within each micelle (Ch. 4A.2.2.1). However, here if the variation of the diffusion coefficient (D_{RM}) with probe concentration is considered, it can be seen that there is a linear relationship at each micellar volume fraction. Exponential type decreases in diffusion coefficients at with increasing probe concentrations have been seen previously in microemulsions[21,33] although these systems are not directly comparable with a reverse micelle nanoemulsion. Owlia et al. attributed this effect to probe induced growth of micellar aggregates[21]. Unfortunately, due to the low limiting currents that were achieved here, it was very difficult to obtain reproducible voltammograms at low probe concentrations and hence accurate determination of D_{RM} was futile below [probe] ~ $1.0x10^{-3}$ mol dm^{-3}. Therefore, it is not apparent whether the predicted linear relationship exists at probe concentration lower than those considered here. However, for the purpose of further analysis the diffusion coefficients are extrapolated to $[K_3Fe(CN)_6] = 0$. This effectively eliminates the effect of the probe molecules on micellar size and therefore the resultant diffusion coefficient. Values for the extrapolated diffusion coefficients (D_{RM}') at zero probe concentration are shown in Table 5.3 and plotted against ϕ_{mic} in Appendix 5.v.

Table 5.3 : Variation of diffusion coefficient in absence of any probe (D_{RM}') with micellar volume fraction (ϕ_{mic})

ϕ_{mic} / no units	10^7 D_{RM}' / cm^2 s^{-1}
0.084	4.94
0.112	4.51
0.140	4.14

The results show a linear relationship between D_{RM}' and ϕ_{mic}, which is not unexpected considering the similar observation for Triton X-100 (Ch. 3A.2.3) and CTAC (Ch. 4A.2.3). As for these previous cases, it is possible to extrapolate the diffusion coefficient values to $\phi_{mic} = 0$. This yields the diffusion coefficient in the absence of intermicellar interactions (D^O_{RM}) according to the following expression[50]:-

$$D_{RM}' = D^O_{RM} (1 - k_D.\phi_{mic}) \qquad (5.2)$$

A value for $D^O_{RM} = 6.13x10^{-7}$ cm^2 s^{-1} was determined, and the gradient of the plot yielded the intermicellar interaction parameter (k_D) = 2.33. It was seen that for CTAC and Triton X-100 that hydrodynamic radii could be calculated using D^O in the Stokes-Einstein relationship (Equation 3A.3). The same principle is applied here, where the viscosity (η) is that of pure iso-octane and was determined using a cone and plate viscometer. A value of $\eta = 0.475x10^{-2}$ g cm^{-1} s^{-1} led to a hydrodynamic radius (R_H^O) = 7.49 nm.

5.4.2 Micellar Size

The main theme of the discussion originates form the fact that the calculated hydrodynamic radius is approximately twice as large (7.49 nm) as that expected from theoretical[3,12] and experimental considerations[1,2,3,4,8,23]. The hydrodynamic radius has been found, by numerous methods, to be related to W ($[H_2O]$ / [AOT]) according to the expression[3,12,51]:-

$$R_H^O = 1.5 + 0.175.W \qquad (5.3)$$

At W = 10, Equation 5.3 predicts that R_H^O = 3.25 nm, which agrees with published values between 3.1-3.8 nm calculated from methods such as fluorescence[2,3], electron spin resonance[8], photo correlation spectroscopy[4], viscosity[1] and osmotic compressibility[23]. An explanation for the observed difference is postulated in terms of probe perturbation / interaction, micellar coalescence and migration

5.4.2.1 Probe Perturbation

Concentrating on the affect of perturbation by the probe, ferricyanide has been incorporated within the hydrophilic interior due to its insolubility in iso-octane. It is known that probe or solute molecules can affect the size of the hydrophilic interior and hence the overall micellar size[10,17,21,36,52,53]. This affect is more apparent at lower W when the water pool radius (R_W) is small. At W = 10, $R_W \approx 1.5$ nm[2,9,52], which although may be large enough to incorporate a ferricyanide molecule (r ~ 0.5 nm), may be of insufficient size to eliminate probe induced perturbation. In any case, the diffusion measurements were made at series of probe concentrations, in an attempt to extrapolate out the influence of the probe on micellar structure. As was mentioned earlier, however, this linear relationship may not strictly be true at low probe concentrations[21,33], in which case the diffusion coefficients will appear lower than they really are.

The influence of probe is more apparent when comparing deviations between quasi-elastic light scattering and polarography data at lower water contents in CTAB / hexadecane/ 1-butanol / water microemulsions, where the radii in the presence of a probe were larger than those without a probe[36]. Owlia et al. used a microelectrode to study AOT microemulsions with [H_2O] / [AOT] = 20[21]. Using cobalamine (vitamin B_{12}) as an electroactive probe, the measured hydrodynamic radius was found to be ~50% larger than previously reported values[4] and was attributed to probe induced formation of larger aggregates[21]. Other techniques that utilise probes have

determined reverse micellar radii that are in agreement with non-probe methods. However, fluorescence techniques, for example, use very low [probe] with a ratios to [micelle] of between 1:100 - 1:500[2,32].

If the probe is inducing an increase in micellar size, is the effect purely due to the size of the probe or related to interaction with the micellar interface?. Belletete et al. noted that highly polar probes perturb micellar size at lower water concentrations[22]. The anionic probe sodium fluorescein (NaFl) has been observed to reside in the central region of the internal water pool[32] and therefore with ferricyanide possessing a charge of -3, perturbation due to some degree of electrostatic repulsion with the sulfate headgroups is a distinct possibility. In contrast, Lossia et al. showed that Cu^{2+} cations were immobilised due to ligation with the sulfonate groups[52]. Similar effects (e.g. complexation or ion-association) do not occur with ferricyanide as confirmed by the fact that the UV / Vis peak adsorption maximum remains unchanged from an aqueous to reversed micellar media (Appendix 5.vi). A probe induced increase in AOT micellar volume has been observed previously using laser-induced optoacoustic spectroscopy (LIOAS)[53]. The size perturbation was noted to be a function of the transition in hydrogen bonding between the probe, $Ru(bpy)(CN)_4^{2-}$, and the solubilising water[53]. At W<10, the majority of the water is immobilised at the micellar interface, however, as the $[H_2O]$ / [AOT] is increased the water behaves as 'free' water[4,11,14]. A micellar volume change was apparent when there was a finite amount of bound water (W<10), whereas when the micellar interior consisted of free water a volume change was not evident[53]. For the study presented here it can be assumed that there is bound water present[4,11,14] and therefore the reverse micelle will be susceptible to probe induced increase in size.

Bound water at the interfacial region is known to manipulate the electron transfer from aqueous to lipidic phase[54]. Therefore, the interaction between the probe and micellar interface has implications for the electron transfer process at the electrode. For example, the reduced mobility or change in the solvation shell of the probe[54] by interaction with bound interfacial water may induce a change in the energy required to transfer the probe across the micellar membrane[54]. The actual

mechanism of electron transfer in reverse micellar systems has not been fully elucidated, though two theories have been proposed[55]. A probe containing micelle can collide with the electrode surface forming a hemimicelle prior to electron transfer or a micelle approaches a pre-existing surface hemimicelle with the probe diffusing through the AOT interfacial region to the electrode[55]. Considering that AOT will probably adsorb on the electrode surface[42,56] there would appear to be more likelihood of the second mechanism being dominant.

5.4.2.2 Micellar Coalescence

It is known that measured diffusion coefficients will depend on micellar size distribution as well as the probe distribution amongst aggregates[36]. Light scattering in microemulsions often assume that the size distribution is monodisperse with any variance exhibited a result of polydispersity[36]. So, it may be that a change in diffusion coefficient with probe concentration is due to modifications of the size distribution (i.e. polydispersity) rather than the specific micellar size when a monodispersed system is assumed[3].

A change in the micellar polydispersity can occur if micelles coalesce together to form larger aggregates[20]. Goto et al. observed, using cryo-transmission electron microscopy (TEM), that in 5% w/v AOT/ iso-octane at W = 20, there were particles ranging in diameter from ~ 15 nm to 200 nm, and suggested that this was indicative of small particles clustering together[20]. Further evidence was attained by SANS where the observation of prolate particles was explicated as the aggregation of two spherical particles[30] which is not surprising as AOT micelles have highly deformable walls[57]. This would tend to support the presented results where R_H^O ~ 7.5 nm is twice as large as literature values[1,2,3,4,8,23]. Therefore, as the microelectrode measures *long time* self-diffusion, the lower than expected D_{RM} values may reflect the effect of cumulative micelle-micelle encounters.

The sticky hard sphere (SHS) model has been used previously to interpret clustering in microemulsion systems[58], where attractive interactions between reverse

micelle species are large enough to overcome repulsive (e.g. excluded volume) interactions[59]. These attractive interactions have been observed to be at least an order of magnitude greater than van der Waals[30,59] and are believed to be a consequence of overlap and intersolvation of the hydrophobic surfactant chains[59]. An increase in the overall attractive potential can cause a resultant increase in microemulsion droplet size[59] and is often characterised by phase separation at high water contents (W > 50)[59].

Huruguen et al.[7] noted that stronger attractive interactions were induced when the protein cytochrome C was solubilised in AOT reverse micelles and coupled this observation with an increase in polydispersity[7]. Although many authors have considered the addition of electrolytes to the water pool interior there appears to be disagreement as to the overall effect[2,60,61,62]. Garcia-Rio et al. proposed that the addition of chloride salts would cause a reduction in the effective surfactant headgroup area, an increase in interface curvature and a reduction in the water solubilising ability of the reverse micelle[60]. The combined affect of these led to a decrease in both droplet size and interdroplet attraction[60,61]. Conversely, it has been observed by neutron scattering that the droplet radius increases on the addition of electrolyte[62] and by fluorescent polarisation that the size remains constant[2,61].

Antalek et al.[63] have noted that observed AOT reverse micelle diffusion (D_{OBS}) can be described as a fraction (x) of 'faster diffusing' micelles (D_C) and 'slower diffusing', acrylamide induced, swollen micelles (D_{MIC}).

$$D_{OBS} = x D_C + (1-x) D_{MIC} \qquad (5.4)$$

Although this equation may not be directly adaptable to the results presented here it is further evidence that diffusion coefficients are susceptible to changes in the system polydispersity.

Although, there is clear evidence than the solubilisation of a charged species within the aqueous phase may influence micellar size[21,36,60,61,62] the contributions

from a reduction in headgroup repulsion[60] and probe - interface repulsion[52,53] is difficult to assess.

5.4.2.3 Migration

It has been noted that the micellar diffusion coefficients are lower than expected resulting in a hydrodynamic radius higher than those reported in the literature. The lower diffusion coefficients are a result of lower currents than may be expected. Decreased limiting currents due to migration have been observed in non-polar media with the absence of any deliberately added electrolyte[37,38]. A popular example to demonstrate the migratory effect is the that of a species undergoing successive electron transfer[37,38]:-

$$A \leftrightarrow A^{+} + e^{-} \qquad (5.5a)$$

$$A \leftrightarrow A^{2+} + e^{-} \qquad (5.5b)$$

The observation of unequal limiting currents is due to the compressed second wave from migration of A^{2+} into the bulk solution. When the comproportionation reaction, $A^{2+} + A \leftrightarrow 2A^{+}$, occurs the A^{2+} migrating into solution reacts with the approaching species A, effectively lowering their concentrations[37,38]. This concentration reduction effectively leads to a compression in the observed limiting currents[37,38]. Oldham et al. have shown that a reduction in limiting currents for charged species undergoing oxidation is characterised by a increase in the normalised slope from the voltammetric wave[64]. The absence of this effect in the experimental data present here suggests that migration is not an influential factor as the Nernstian slopes remain between 50-70 mV decade^{-1}.

In summary, the results tend to suggest that the deviation in the hydrodynamic radius from reported values is due to perturbation of the micellar structures by the ferricyanide probe or micellar coalescence rather than any

complexation between the probe and sulfonate headgroups. Migration can also be ruled out due to the absence of any substantial increase in the Nernstian slopes.

5.5 Summary

An AOT reverse micellar nanoemulsion system has been investigated in the absence of supporting electrolyte using the microelectrode technique. By solubilising an electroactive probe, ferricyanide, within the aqueous micellar interior reversible electrochemistry was obtained using a 10.4 μm diameter carbon fibre microelectrode. A quasi-reversible reference electrode has been used with a redox polymer coating $\{[Os(bipy)_2(PVP)_{10}Cl]Cl\}$ acting as protecting film for a silver wire.

Typical currents ranged from between (0.1 - 0.4) $x10^{-9}$ A and yielded diffusion coefficients (D_{RM}) an order of magnitude lower than that obtained in bulk aqueous solution. By studying D_{RM} as a function of both probe concentration and micellar volume fraction allowed the determination of D^{O}_{ME} at the c.m.c. Using the Stokes-Einstein equation a value was found for the hydrodynamic radius (R_H^{O}) = 7.49 nm. This was approximately twice as much as would be expected from both theoretical calculations and experimentally determined values from a range of other techniques. The reason for the observed difference was not explicit, though effects due to migration were ruled out as the Nernstian slope of the voltammograms varied from 50 - 70 mV $decade^{-1}$ i.e. in agreement with theory 58 mV $decade^{-1}$. Two remaining theories, micellar coalescence and size perturbation, were suggested. Micellar coalescence could have occurred by virtue of the *long time* diffusion coefficient detecting cumulative micellar encounters or by a probe induced increase in attractive interactions. Size perturbation relies on the ferricyanide residing in the micellar water pool and electrostatically repelling negatively charged AOT headgroups or disrupting the structured water around these headgroups. Despite that the effect of probe concentration was extrapolated out, this assumes a linear relationship as [probe] $\rightarrow$ 0, which as previous findings have shown, is not

necessarily the case. Therefore effects due to the probe may not have been eliminated.

It has been shown that the microelectrode offers a fast, cheap and simple way of obtaining micellar diffusion coefficients in reverse micellar systems at low water concentrations. Although limited studies have used electrochemical techniques to measure diffusion coefficients in high water content microemulsions, no research on electrochemistry in true (low water content) reversed micellar systems is apparent. Although deviation of R_H^O from the literature was apparent, the technique offers a means of analysing the reversed micellar size as a function of a solubilised molecules. This offers a great advantage is using the micellar interior as a template for the growth of nano-particles of controlled size.

Appendix 5.i : EDAXS spectrum of adosorbed coating on silver wire

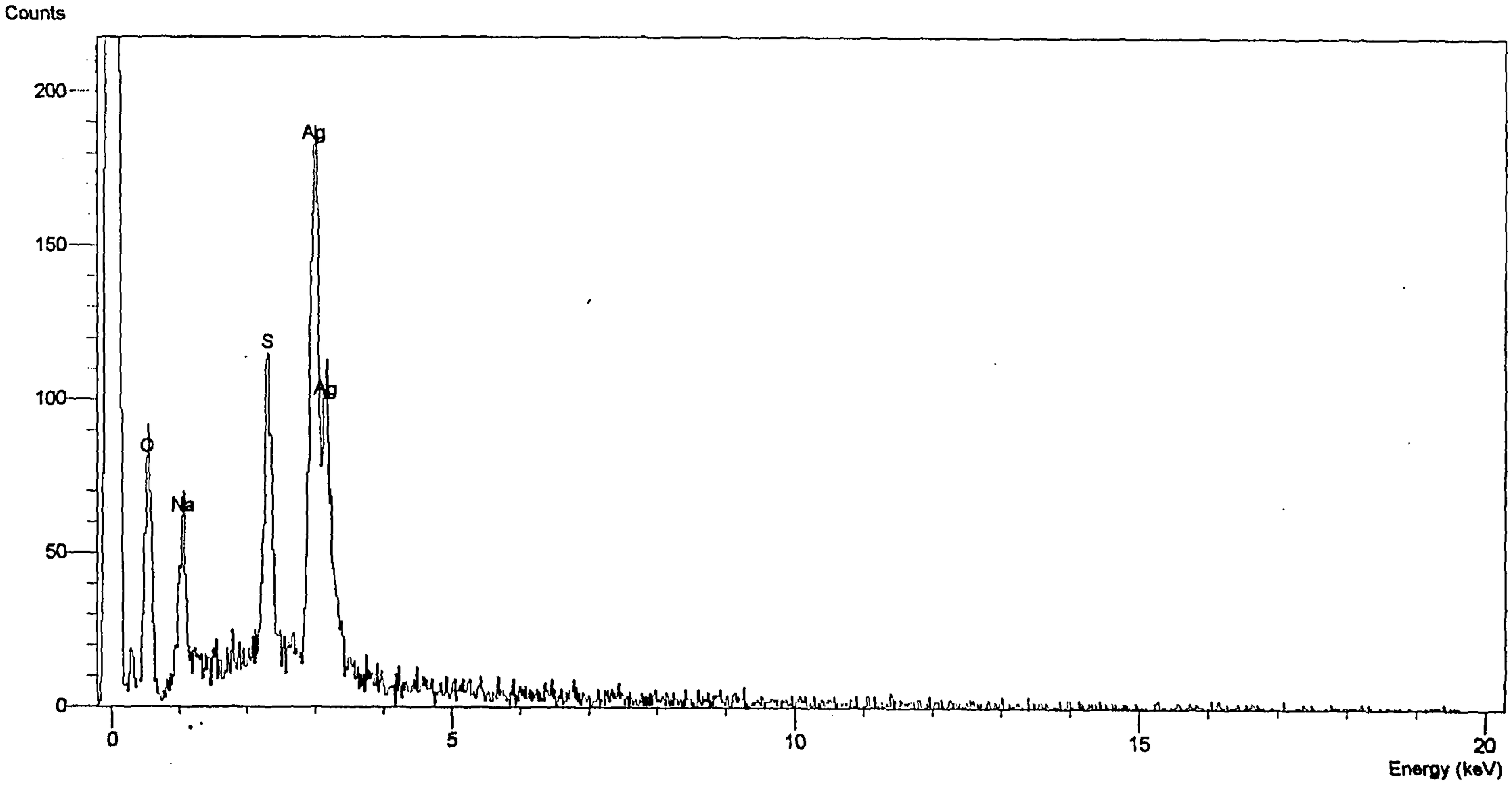

Appendix 5.ii : Nernstian plot for $\phi_{mic} = 0.084$,
$[K_3Fe(CN)_6] = 1.403x10^{-3}$ mol dm^{-3}

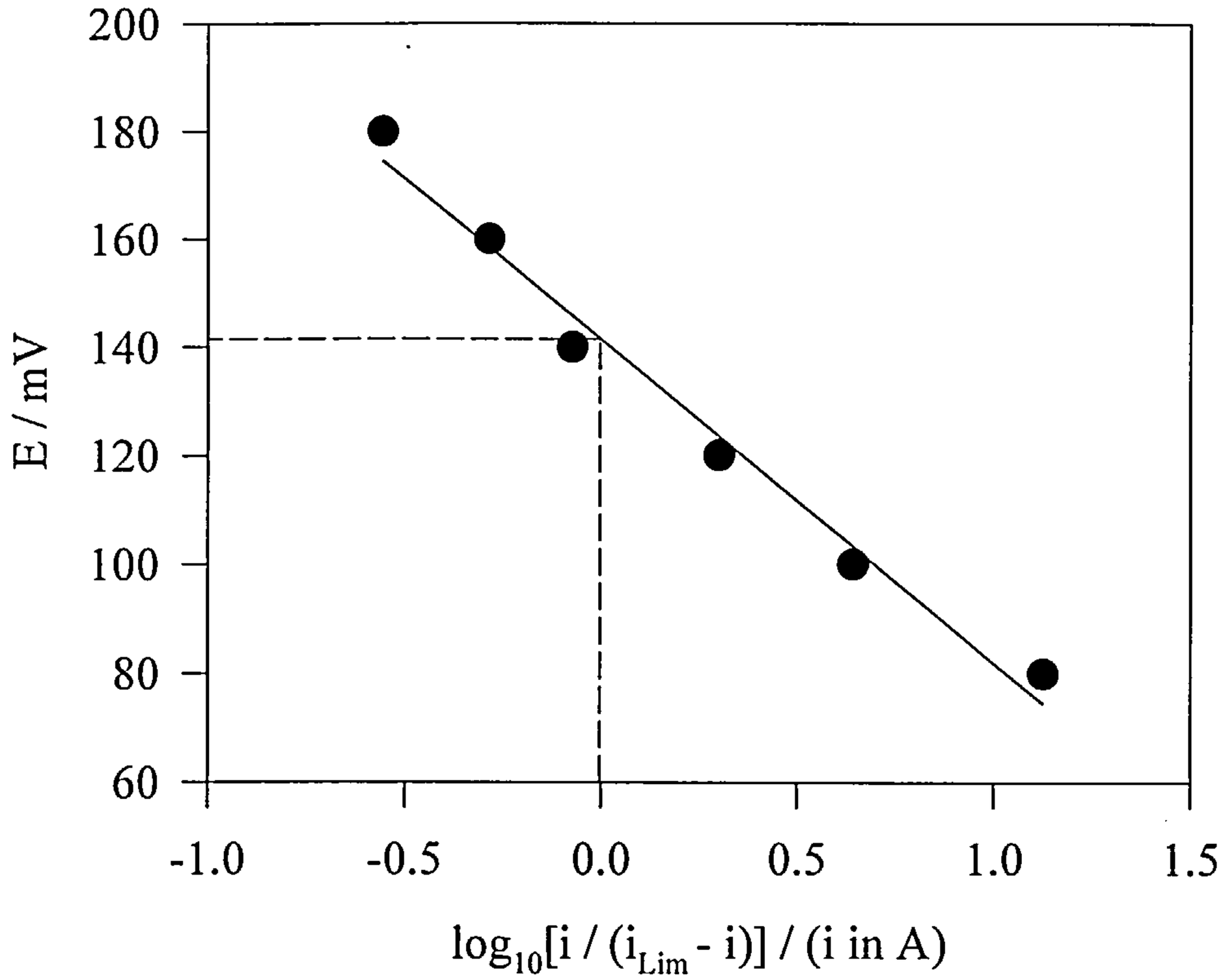

Appendix 5.iii : Voltammograms for AOT / H_2O / i-octane reverse micelles (W = 10, $\phi_{mic} = 0.084$)

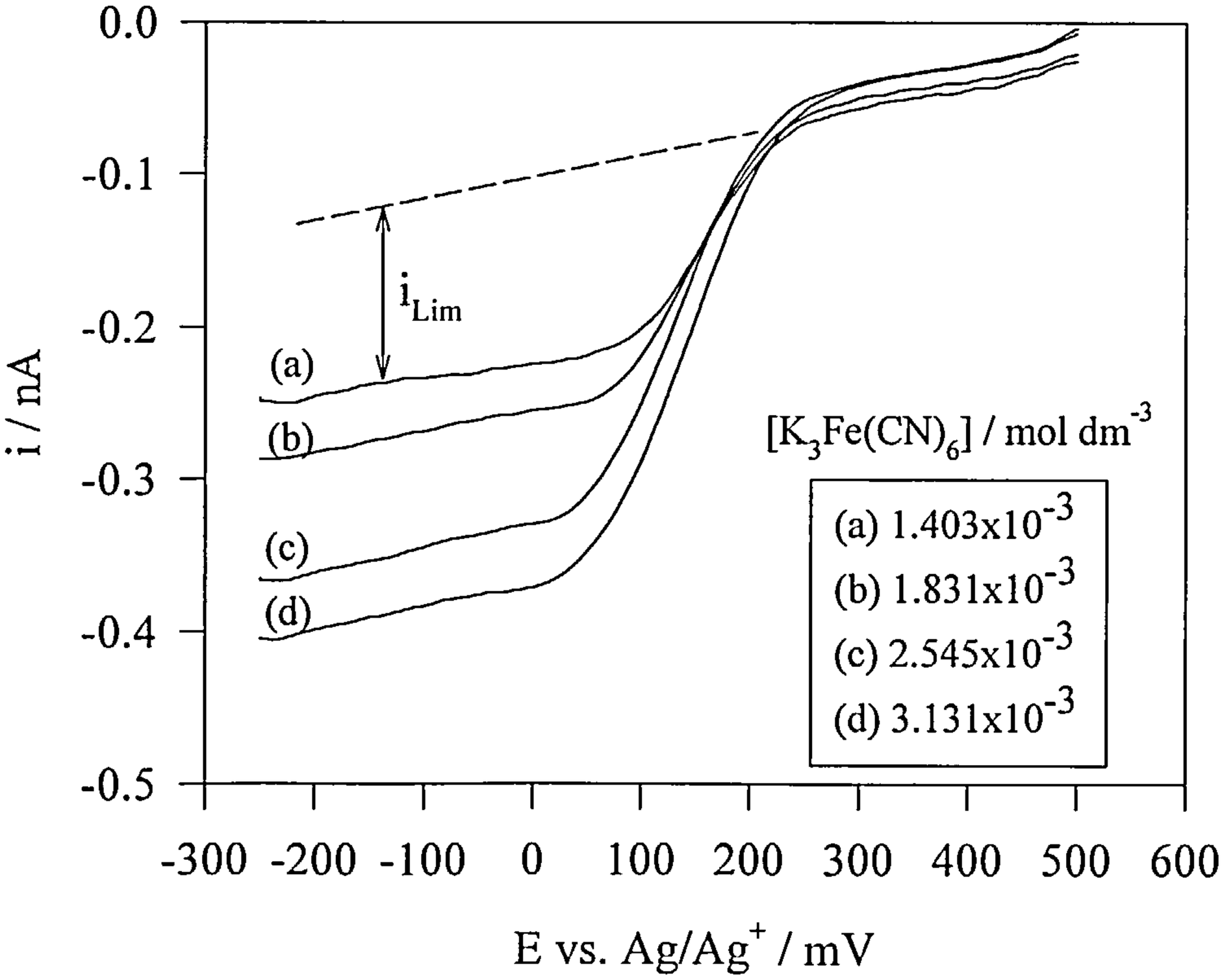

Appendix 5.iv : Diffusion coefficient dependence on probe concentration (effect of volume fraction)

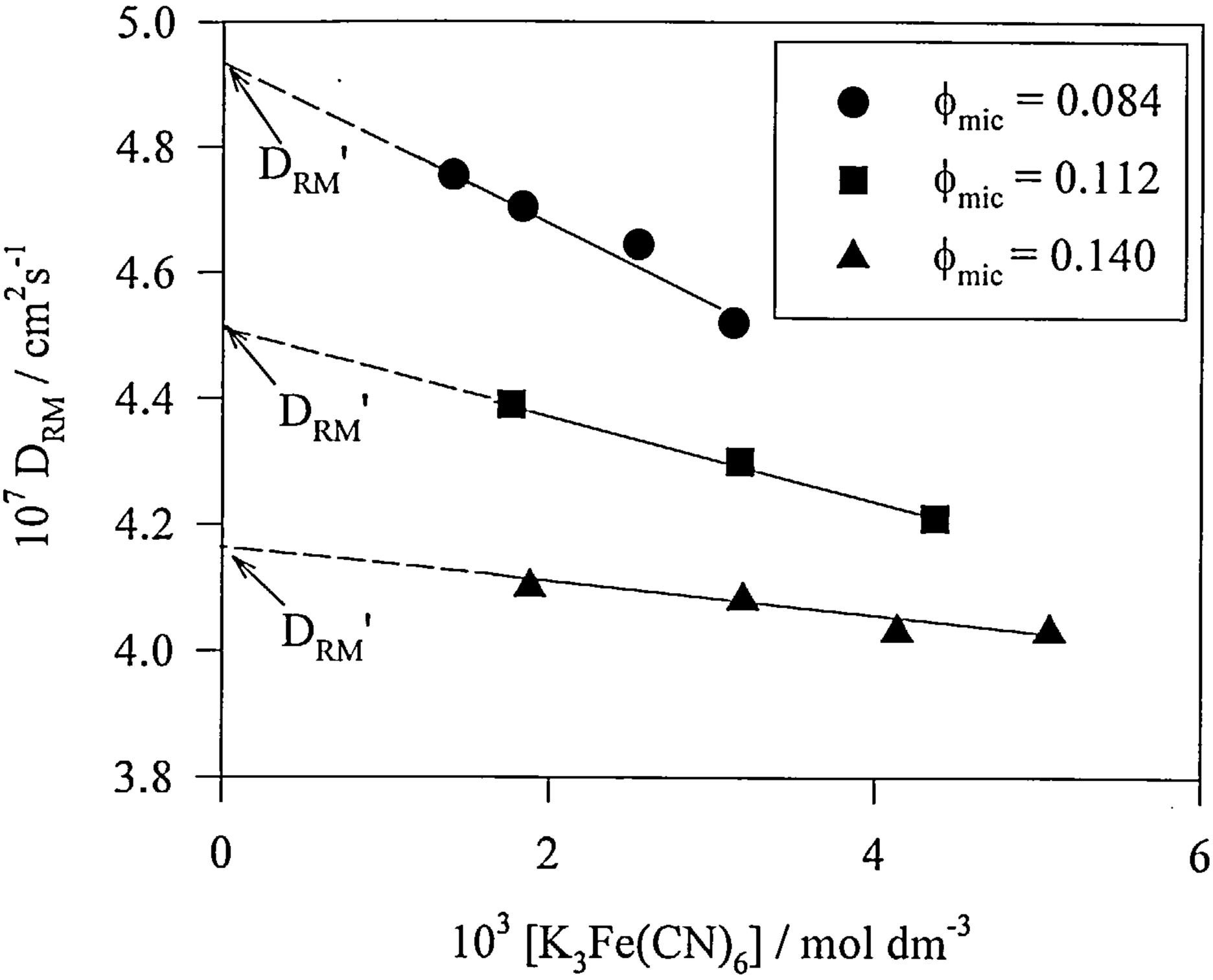

Appendix 5.v : Variation of D_{RM}' (as $[K_3Fe(CN)_6] \longrightarrow 0$) with micellar volume fraction (ϕ_{mic})

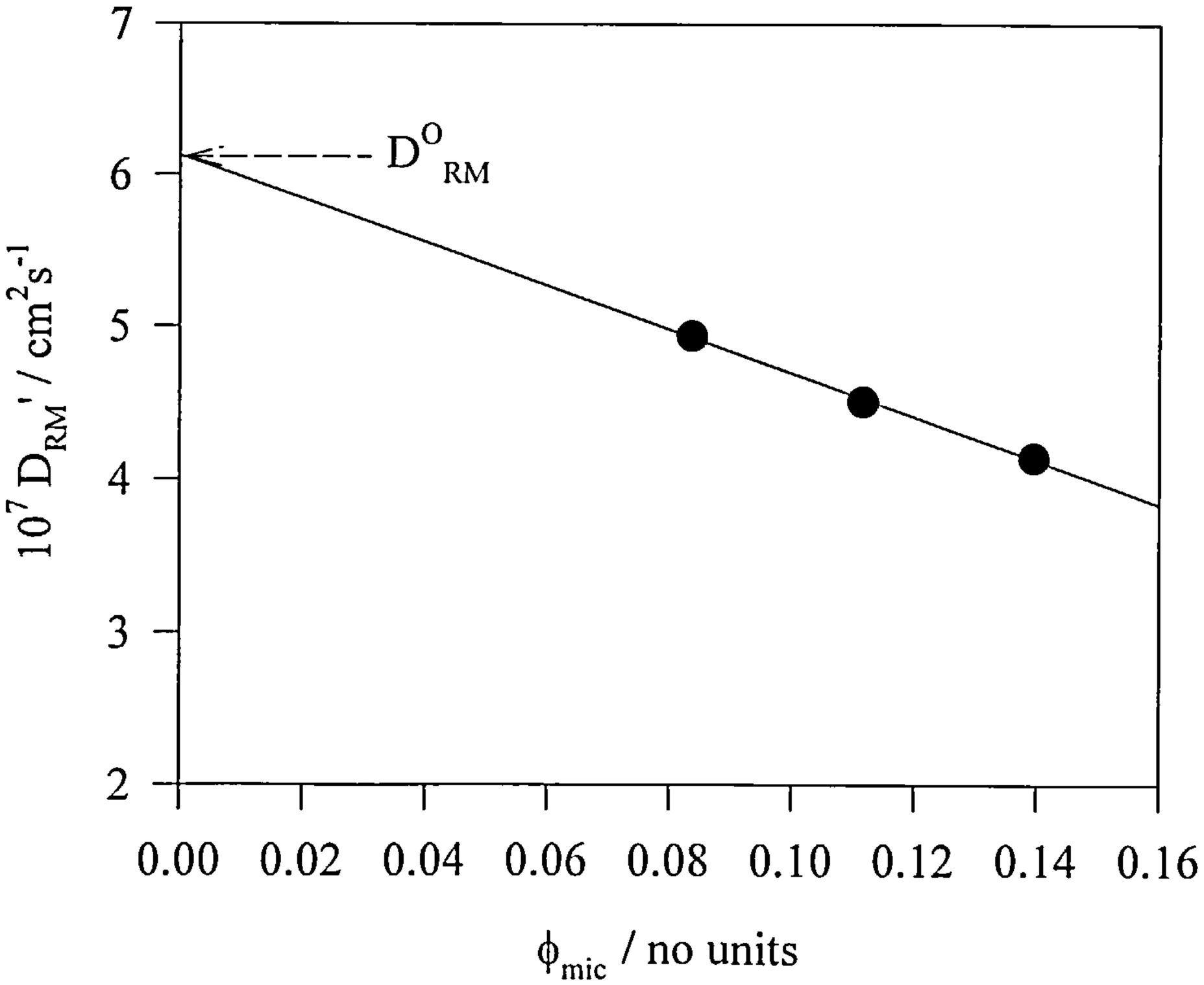

Appendix 5.vi : Effect of solvent media on absorption characteristics of ferricyanide

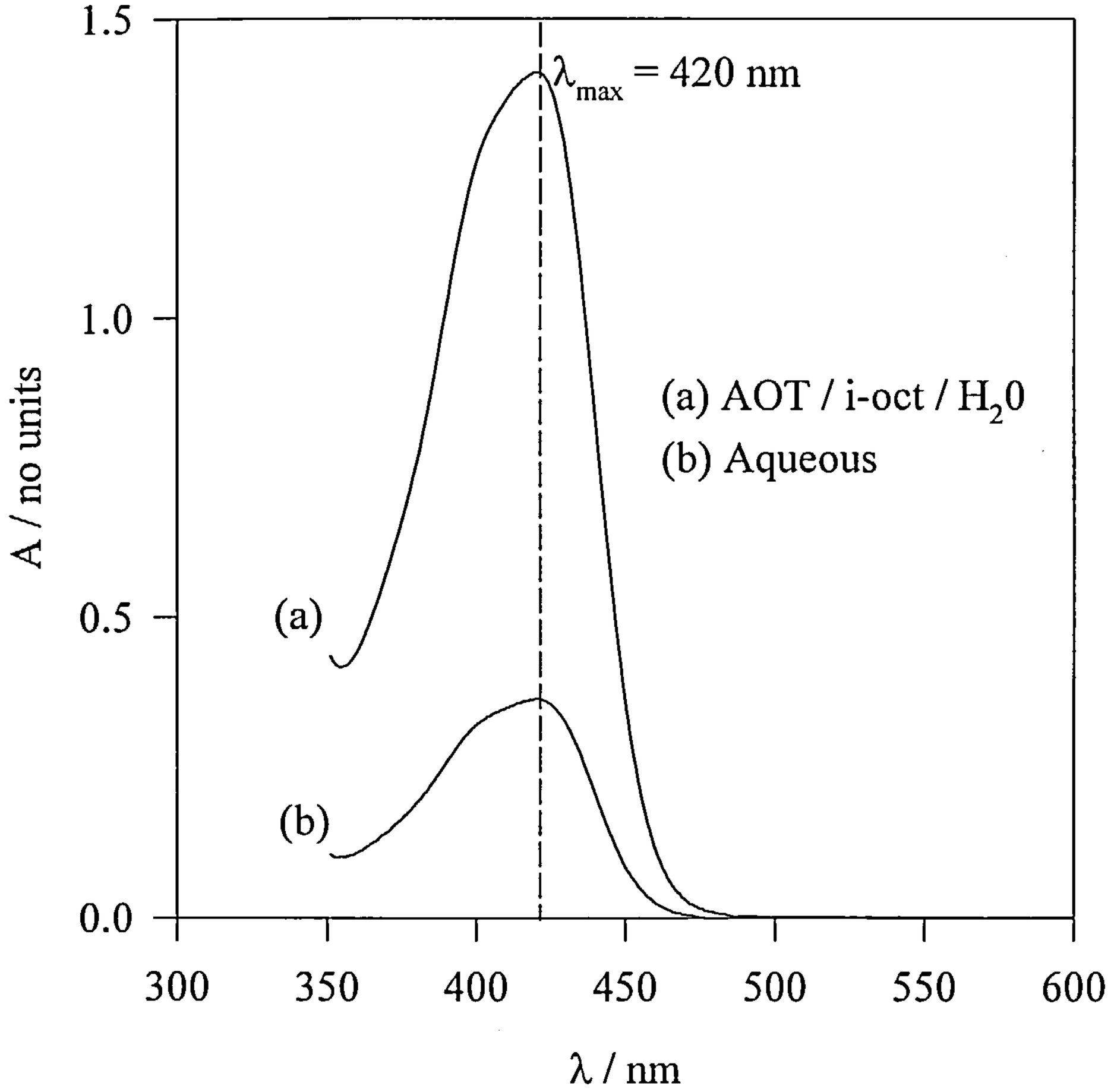

Aerosol-OT (Ch. 5) References:

1. R.A.Day, B.H.Robinson, J.H.R.Clarke, J.V.Doherty, *J. Chem. Soc. Faraday Trans.*, 1979, vol. 75, p. 132.

2. E.Keh, B.Valeur, *J. Colloid and Polymer Sci.*, 1981, vol. 79, p. 465.

3. A.J.W.G.Visser, K.Vos, A. van Hoek, J.S.Santema, *J. Phys. Chem.*, 1988, vol. 92, p. 759.

4. M.Zulauf, H-F.Eicke, *J. Phys. Chem.*, 1979, vol. 83, p. 480.

5. B.Lindman, P.Stilbs, *J. Colloid and Int. Sci.*, 1984, vol. 99, p. 290.

6. K.Mukerjee, S.P.Moulik, D.C.Mukherjee. *Langmuir*, 1993, vol. 9, p. 1727.

7. J.P.Huruguen, M.Authier, J.L.Greffe, M.P.Pileni, *Langmuir*, 1991, vol. 7, p. 243.

8. N.J.Turro, I.V.Khudyakov, *J. Phys. Chem.*, 1995, vol. 99, p. 7654.

9. J.H.Fendler, *Membrane Mimetic Chemistry*, 1982, J. Wiley & Sons Inc. and references therein.

10. J.B.Peri, *J. Colloid and Int. Sci.*, 1969, vol. 29, p. 6.

11. P.Baglioni, H.Nakamura, L.Kevan, *J. Phys. Chem.*, 1991, vol. 95, p. 3856.

12. J.Eastoe, B.H.Robinson, A.J.W.G.Visser, D.C.Steytler, *J. Chem. Soc. Faraday Trans.*, 1991, vol. 87, p. 1899.

13. H.R.Rabie, J.H.Vera, *Fluid Phase Equilibria*, 1996, vol. 122, p. 169.

14. G.Cassin, J.P.Badiali, M.P.Pileni, *J. Phys. Chem.*, 1995, vol. 99, p. 12941.

15. J-W.Xie, J-G.Xu, G-Z.Chen, *Analytica Chimica Acta*, 1995, vol. 312, p. 337.

16. H.Fabre, N.Kamenka, N.Lindman, *J. Phys. Chem.*, 1981, vol. 85, p. 3493.

17. J.H.Fendler, *Acc. Chem. Res.*, 1976, vol. 9, p. 153.

18. M.Ueda, Z.A.Schelly, *Langmuir*, 1988, vol. 4, p. 653.

19. M.Kotlarchyk, J.S.Huang, S-H. Chen, *J. Phys. Chem.*, 1985, vol. 89, p. 4382.

20. A.Goto, Y.Kuwahara, A.Suzuki, H.Yoshioka, R.Goto, T.Iwamoto, T.Imae, *J. Molecular Liquids*, 1997, vol. 72, p. 137.

21. A.Owlia, Z.Wang, J.F.Rusling, *J. Am. Chem. Soc.*, 1989, vol. 111, p. 5091.

22. M.Belletete, M.Lachapelle, G.Durocher, *J. Phys. Chem.*, 1990, vol. 94, p. 5337.

23. B.Bedwell, E.Gulari, *J. Colloid and Int. Sci.*, 1984, vol. 102, p. 88.

24. M.D'Angelo, D.Fioretto, G.Onori, I.Palmieri, A.Santucci, *Physical Rev. E*, 1996, vol. 54, p. 993.

25. F.M.Menger, J.A.Donohue, R.F.Williams, *J. Am. Chem. Soc.*, 1973, vol. 95, p. 286.

26. P.L.Luisi, Angew. *Chem. Int. Ed. Engl.*, 1985, vol. 24, p. 439 and references therein.

27. M.Boutonnet, J.Kizling, P.Stenus, *Colloids and Surfaces*, 1982, vol. 5, p. 209.

28. G.X.Cheng, F.Shen, L.F.Yang, L.R.Ma, Y.Tang, K.D.Yao, P.C.Sun, *Materials Chem. and Phys.*, 1998, vol. 56, p. 97.

29. J.H.Fendler, *Chem. Rev.*, 1987, vol. 87, p. 877.

30. R.Ober, C.Taupin, *J. Phys. Chem.*, 1980, vol. 84, p. 2418.

31. N.Gorski, Y.M.Ostanevich, *J. de Physique IV*, 1993, vol. 3, p. 149.

32. M.Hasegawa, T.Sugimura, Y.Shindo, A.Kitahara, *Colloids and Surfaces A : Physicochem. And Eng. Aspects*, 1996, vol. 109, p. 305.

33. R.A.Mackay, S.A.Myers, L.Bodalbhai, A.Brajter-Toth, *Anal. Chem.*, 1990, vol. 62, p. 1084.

34. A.B.Mandal, B.U.Nair, *J. Chem. Soc. Faraday Trans.*, 1991, vol. 87, p. 133.

35. K.Chokshi, S.Qutubuddin, A.Hussam, *J. Colloid and Int. Sci.*, 1989, vol. 129, p. 315.

36. R.Mackay, N.S.Dixit, R.Agarwal, R.P.Seiders, *J. Disp. Sci and Tech.*, 1983, vol. 4, p. 397.

37. R.J.Forster, *J. Chem. Soc. Rev.*, 1994, vol. 23, p. 289.

38. A.M.Bond, *Analyst*, 1994, vol. 119, p. R1.

39. J.Heinze, *Angew. Chem. Int. Ed. Engl.*, 1993, vol. 32, p. 1268.

40. *BAS Electroanalytical Handbook*, Bioanalytical Systems Inc., 1997.

41. P.J.Peerce, A.J.Bard, *J. Electroanal. Chem.*, 1980, vol. 108, p. 121.

42. A.Avranas, N.Papadopoulos, S.Sotiropoulos, *Colloid and Polymer Sci.*, 1994, vol. 272, p. 1252.

43. E.Barendrecht, *J. Appl. Electrochem.*, 1990, vol. 20, p. 175.

44. A.Haimerl, A.Merz, *Angew. Chem. Int. Ed. Engl.*, 1986, vol. 25, p. 180.

45. N.Oyama, F.C.Anson, *J. Am. Chem. Soc.*, 1979, vol. 101, p. 739.

46. J.O.Howell, R.M.Wightman, *Anal. Chem.*, 1984, vol. 56, p. 524.

47. *CRC Handbook of Chemistry and Physics*, 53rd Edition. R.C.Weast (Ed.), Chemical Rubber Co., 1972-1973.

48. M.Caselli, A.Mangone, A.Traini, *Annali di Chimica*, 1998, vol. 88, p. 299.

49. D.E.Weisshaar, D.E.Tallman, *Anal. Chem.*, 1983, vol. 55, p. 382.

50. T.Tominaga, M.Nishinaka, *J. Chem. Soc. Faraday Trans.*, 1993, vol. 89, p. 3459.

51. J.D.Nicholson, J.H.R.Clarke, In *Surfactants in Solution*, K.L. Mittal, B.Lindman, Eds., Plenum, New York, 1984.

52. S.A.Lossia, S.G.Flore, S.Nimmala, H.Li, S.Schlick, *J. Phys. Chem.*, 1992, vol. 96, p. 6071.

53. C.D.Borsarelli, S.E.Braslavsky, *J. Phys. Chem. B*, 1997, vol. 101, p. 6036.

54. D.Grand, *J. Phys. Chem. B*, 1998, vol. 102, p. 4322.

55. E.Garcia, J.Texter, *J. Colloid. Int. Sci.*, 1994, vol. 62, p. 262.

56. E.Garcia, S.Song, L.E.Oppenheimer, B.Antalek, A.J.Williams, J.Texter, *Langmuir*, 1993, vol. 9, p. 2782.

57. G.Bakale, G.Beck, J.K.Thomas, *J. Phys. Chem.*, 1992, vol. 96, p. 2328.

58. G.J.M.Koper, D.Bedeaux, *Physica A*, 1992, vol. 187, p. 489.

59. J.M.Tingey, J.L.Fulton, R.D.Smith, *J. Phys. Chem.*, 1990, vol. 94, p. 1997.

60. L.Garcia-Rio, J.R.Leis, J.C.Mejuto, M.E.Pena, *Langmuir,* 1994, vol. 10, p. 1676.

61. J.Lang, A.Jada, A.Malliaris, *J. Phys. Chem.*, 1988, vol. 92, p. 1946.

62. C.Cabos, P.Delord, *J. Phys. Lett.*, 1980, vol. 41, p. L-455.

63. B.Antalek, A.J.Williams, J.Texter, *Physical Review E*, 1996, vol. 54, p. R5913.

64. K.B.Oldham, T.J.Cardwell, J.H.Santos, A.M.Bond, *J. Electroanal. Chem.*, 1997, vol. 430, p. 39.

Chapter 6: Conclusions

This thesis has demonstrated the ease of application of electrochemical techniques to microheterogeneous solutions consisting of self-assembled supramolecular species. The conclusions from the presented work can essentially be divided into three parts: (i) the favourable agreement of micellar structure with qualitative and experimental models from previously published values, (ii) the further characterisation of micellar species using 'in depth' analysis and (iii) the organisation of micellar aggregates and electroactive probes in the environment close to the electrode surface.

The solubilisation of an electroactive probe within a micellar interior can be used to obtain self-diffusion coefficients precisely. Although a simple measurement, a wealth of information, such as size and interaction, can be obtained by subsequent analysis. For example, in Ch. 4A further investigation allowed determination of the micellar zeta potential and the relationship between shear plane and double layer thickness was explicated. In previous reports an extensive range of techniques were required to obtain such structural information, whereas a simple electrochemical measurement forms the foundation for the elucidation of an expansive range of structural and physical properties. The applicability and benefit of this work has potential implications in a wide range of disciplines from membrane mimetics and colloidal systems to revolutionary new controlled drug release methods.

Micellar interaction has also been thoroughly investigated over a wide range of electrolyte concentration and a clear, quantifiable transition from repulsive to attractive forces has been observed. This work forms an excellent basis for flocculation (coagulation) phenomena in a diversity of systems including fermentation, agrochemical, cosmetic and food formulations.

The fundamental understanding of supramolecular aggregates at an electrode surface has been expanded by comparing diffusion coefficients from stationary and hydrodynamic techniques. The proportionally higher diffusion coefficients from cyclic voltammetry and chronoamperometry were interpreted as either the presence

of two diffusional regimes or pre-concentration of the electroactive probe at the electrode surface. The phenomenological basis that these results form merit further investigation and at the present time Dr. P.Birkin (University of Southampton) is modelling the data to theoretical predictions.

Investigations into the micellar properties of CTAC and Triton X-100 were carried out in a polar, conducting medium, however, the versatility of electrochemical methods in 'exotic' media was demonstrated in Ch. 5. The use of a microelectrode allowed an electrochemical response to be obtained in low conductivity iso-octane and prompted the study of a reverse micelle 'nanoemulsion'. The observation of micellar size / interaction perturbation may inspire further work into the mechanism of such an effect.

From a series of simple electrochemical measurements considerable insights have been made to micellar size, structural evolution and interaction. The results do not only fit with theoretical predictions but also confirm previous experimental findings. In addition to simply changing the surfactant and electrolyte system, the amount of future work that could be undertaken is extensive. A series of suggestions are made as to further routes of investigation:-

- Use of higher surfactant concentrations to further analyse the difference in results from hydrodynamic and stationary techniques
- Study of anisotropic micellar diffusion in liquid crystal phases
- Characterisation of organised multilayer assemblies at an electrode surface
- Application of the presented work to the use of functionalised electroactive colloids
- Changing the nature of the probe (size and charge) to give implications in the nucleation and growth of nanoparticles in a reverse micelle nanoreactor

Publications :

I.D.Charlton, A.P.Doherty, "Electrochemistry in true reverse micelles", *Electrochem. Comm.*, 1999, vol. 1, no. 5, 176-179.

I.D.Charlton, A.P.Doherty, "Locating the micellar shear-plane and its relationship with the Debye screening length", *J. Phys. Chem. B*, 1999, vol. 103, no. 24, 5081-5083.

I.D.Charlton, A.P.Doherty, "Voltammetric measurement of intermicellar interaction parameters; correlation with predicted interaction energies", *Langmuir*, in press.

I.D.Charlton, A.P.Doherty, "Voltammetry as a tool for monitoring micellar structural evolution?", *Anal. Chem.*, in press.

I.D.Charlton, A.P.Doherty, "Simultaneous observation of attractive interactions, depletion forces and 'sticky' encounters between AOT reverse micelles in iso-octane using microelectrode voltammetry", submitted to *J. Phys. Chem.*